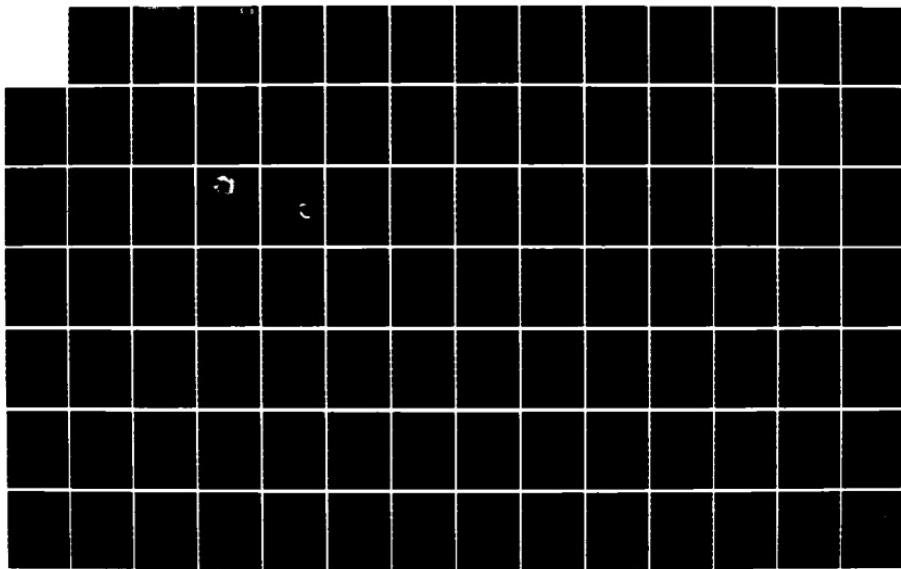


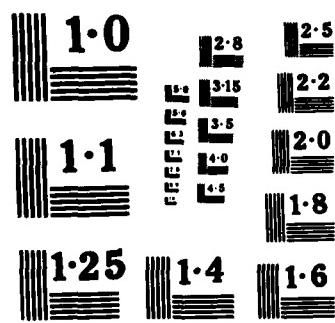
RD-A163 196 FORECASTERS HANDBOOK FOR THE SOUTHERN AFRICAN CONTINENT 1/4  
AND ATLANTIC/INDI. (U) NAVAL ENVIRONMENTAL PREDICTION  
RESEARCH FACILITY MONTEREY CA. F R WILLIAMS ET AL.

UNCLASSIFIED NOV 84 NEPRF-TR-84-88

F/G 4/2

NL





NATIONAL BUREAU OF STANDARDS  
MICROCOPY RESOLUTION TEST CHART

HAYENVPREDRSCHFAC  
TECHNICAL REPORT  
TR 84-08

AD-A163 196



FORECASTERS HANDBOOK  
FOR THE  
SOUTHERN AFRICAN TERRITORY

NOVEMBER 1984

APPROVED FOR PUBLIC RELEASE BY COMINT

86 111 008

UNCLASSIFIED

SECURITY CLASSIFICATION OF THIS PAGE

DTIC  
SELECTED

JAN 21 1980

S

A

D

## REPORT DOCUMENTATION PAGE

1a REPORT SECURITY CLASSIFICATION UNCLASSIFIED		1b RESTRICTIVE MARKINGS S A	
2a SECURITY CLASSIFICATION AUTHORITY		3 DISTRIBUTION/AVAILABILITY OF REPORT Approved for public release; distribution is unlimited	
2b DECLASSIFICATION/DOWNGRADING SCHEDULE			
4 PERFORMING ORGANIZATION REPORT NUMBER(S) TR 84-08		5 MONITORING ORGANIZATION REPORT NUMBER(S)	
6a NAME OF PERFORMING ORGANIZATION Department of Meteorology Naval Postgraduate School	6b OFFICE SYMBOL (if applicable) Code 63Wf	7a. NAME OF MONITORING ORGANIZATION Naval Environmental Prediction Research Facility	
6c ADDRESS (City, State, and ZIP Code) Monterey, CA 93943-5000		7b. ADDRESS (City, State, and ZIP Code) Monterey, CA 93943-5006	
8a. NAME OF FUNDING/SPONSORING ORGANIZATION Naval Air Systems Command	8b OFFICE SYMBOL (if applicable) AIR-330	9. PROCUREMENT INSTRUMENT IDENTIFICATION NUMBER Doc. no. N6685684WR84107	
8c ADDRESS (City, State, and ZIP Code) Department of the Navy Washington, DC 20361		10 SOURCE OF FUNDING NUMBERS	
		PROGRAM ELEMENT NO 62759N	PROJECT NO WF59-551
		TASK NO n/a	WORK UNIT ACCESSION NO n/a
11. TITLE (Include Security Classification) Forecasters Handbook for the Southern African Continent and Atlantic/Indian Ocean Transit			
12 PERSONAL AUTHOR(S) Williams, F.R.; Renard, R.J.; Jung, G.H.; Tomkins, R.D.; Picard, R.R.			
13a TYPE OF REPORT Final	13b TIME COVERED FROM FY83 to FY84	14 DATE OF REPORT (Year, Month, Day) 1984 November	15 PAGE COUNT 325
16 SUPPLEMENTARY NOTATION Qualified requestors may obtain additional copies from the Defense Technical Information Center. All others should apply to the National Technical Information Service.			
17 COSATI CODES		18 SUBJECT TERMS (Continue on reverse if necessary and identify by block number) Southern Hemisphere West Indian Ocean (continued) South Atlantic Ocear Mozambique Channel on Southern Africa Malagasy Republic reverse)	
FIELD 04	GROUP 02		
08	10		
19 ABSTRACT (Continue on reverse if necessary and identify by block number)  This handbook describes the analysis and forecasting of atmospheric and oceanic conditions important to air/sea operations over and near the southern African continent, to include Kenya, Tanzania, Mozambique, Republic of South Africa, and Namibia. Weather over the Malagasy Republic (formerly Madagascar), Mauritius and Reunion (the Mascarene Islands) and Seychelles Islands is also addressed. Included are descriptions of such coastal phenomena as fog, gale frequency, and onshore/offshore winds, as well as an in-depth review of the Agulhas and Benguela near-shore oceanic currents. Southern Hemisphere climatological data also are given for seasonal tracks of cyclones and anticyclones, atmospheric frontal positions, wave heights, sea surface temperatures, and other parameters. Three case studies describe tracks and speeds of extratropical cyclones affecting the -- continued on reverse --			
20 DISTRIBUTION AVAILABILITY OF ABSTRACT <input checked="" type="checkbox"/> UNCLASSIFIED UNLIMITED <input type="checkbox"/> SAME AS RPT <input type="checkbox"/> DTIC USERS		21 ABSTRACT SECURITY CLASSIFICATION UNCLASSIFIED	
22a NAME OF RESPONSIBLE INDIVIDUAL R.W. Fett, contract monitor		22b TELEPHONE (Include Area Code) (408) 646-2823	22c OFFICE SYMBOL NEPRF WU NPS-4

- UNCLASSIFIED

SECURITY CLASSIFICATION OF THIS PAGE

Block 18, Subject Terms, continued.

Satellite meteorology	Berg wind
Cape rollers	Tropical cyclone
Agulhas Current	Benguela Current

Block 19, Abstract, continued.

South Atlantic and western Indian Oceans during the Southern Hemisphere winter.) The studies further verify the usefulness of operational U.S. Navy global meteorological analyses, comparing them with regional Republic of South Africa surface analyses and global U.S. National Meteorological Center 500 mb analyses. Cyclone positions are obtained using imagery from polar-orbiting and geostationary satellites.

-Another case study describes the anomalously high seas "Cape Rollers" found near the 100 fathom contour when high ocean waves, driven by strong southwesterly winds, oppose the Agulhas Current flowing from the northeast near the southeastern coast of the Republic of South Africa. The study includes seasonal frequencies of occurrence, as well as tracks and weather associated with tropical cyclones moving through the Mozambique Channel and over the southwest Indian Ocean east of the Malagasy Republic.

-Further literature search provides two additional cases describing easterly waves and Saharan dust outbreaks, to assist fleet units transiting between the tropical Atlantic and Indian Oceans.

Accesion For	
NTIS	CRA&I
DTIC	TAB
Una	Obj ed
Justification	
By _____	
Distrib tio /	
Availability Codes	
Dist	Avail d/or Special
A-1	

UNCLASSIFIED

SECURITY CLASSIFICATION OF THIS PAGE

## CONTENTS

<b>Foreword . . . . .</b>	<b>xv</b>
<b>Preface . . . . .</b>	<b>xvii</b>
<b>Acknowledgments . . . . .</b>	<b>xviii</b>
Section	
	page
<b>1. GENERAL INTRODUCTION AND SOUTHERN HEMISPHERE METEOROLOGY . . . . .</b>	<b>1-1</b>
1.1 General Introduction . . . . .	1-1
1.2 Southern Hemisphere Meteorology . . . . .	1-3
1.2.1 Climatology . . . . .	1-3
1.2.2 Forecasting 'Thumb Rules' for the Southern Hemisphere . .	1-17
<b>2. SOUTHERN AFRICA . . . . .</b>	<b>2-1</b>
2.1 Topography . . . . .	2-1
2.2 Significant Weather Systems . . . . .	2-2
2.2.1 Winter (June, July, August) . . . . .	2-4
2.2.2 Summer (December, January, February) . . . . .	2-10
2.2.3 All Seasons . . . . .	2-18
2.3 Special Parameters . . . . .	2-20
2.3.1 Fog . . . . .	2-20
2.3.2 Thunderstorms . . . . .	2-23
2.4 Upper-Level Winds and Turbulence . . . . .	2-24
<b>3. MALAGASY REPUBLIC &amp; MOZAMBIQUE . . . . .</b>	<b>3-1</b>
3.1 Topography . . . . .	3-1
3.1.1 Malagasy Republic . . . . .	3-1
3.1.2 Mozambique . . . . .	3-1
3.2 Significant Weather Systems . . . . .	3-1
3.2.1 Malagasy Republic . . . . .	3-1
3.2.2 Mozambique . . . . .	3-15
<b>4. TROPICAL CYCLONES AND THE MASCARENE &amp; SEYCHELLES ISLANDS . . . . .</b>	<b>4-1</b>
4.1 Tropical Cyclones . . . . .	4-1
4.2 Weather Associated with Tropical Cyclones . . . . .	4-8
4.2.1 Tropical Cyclones East of the Malagasy Republic . . . . .	4-8
4.2.2 Tropical Cyclones in the Mozambique Channel . . . . .	4-12

4.3 The Islands of Mauritius and Reunion, and the Seychelles . . .	4-24
4.3.1 Mauritius and Reunion (Islands east of Malagasy Republic). . . . .	4-24
4.3.2 Seychelles Islands (Islands northeast of Malagasy Republic) . . . . .	4-25
4.3.3 Thunderstorms (Mauritius, Reunion and the Seychelles) . . . . .	4-25
4.3.4 Tropical Cyclones affecting the Islands . . . . .	4-26
<b>5. KENYA AND TANZANIA . . . . .</b>	<b>5-1</b>
5.1 Topography . . . . .	5-1
5.2 Surface Winds . . . . .	5-2
5.2.1 Kenya. . . . .	5-2
5.2.2 Tanzania . . . . .	5-3
5.3 Temperature. . . . .	5-3
5.4 Significant Weather Systems . . . . .	5-4
5.4.1 Austral Summer . . . . .	5-4
5.4.2 Austral Winter . . . . .	5-5
5.4.3 Transition Periods (April-May and October-November) . . . . .	5-6
5.4.4 Thunderstorms . . . . .	5-7
5.5 Upper-Air Winds and Turbulence . . . . .	5-8
5.5.1 Kenya. . . . .	5-8
5.5.2 Tanzania . . . . .	5-10
<b>6. CASE STUDIES AND OCEANIC WEATHER . . . . .</b>	<b>6-1</b>
6.1 Case I - Easterly Waves (24 - 28 August 1983) . . . . .	6-1
6.1.1 General Discussion . . . . .	6-1
6.1.2 Synoptic Description . . . . .	6-4
6.1.3 Forecast Rules/Aids . . . . .	6-12
6.1.4 Satellite Imagery 'Clues' . . . . .	6-12
6.2 Case II - Saharan Dust Outbreaks (2 - 3 May 1983) . . . . .	6-12
6.2.1 General Discussion . . . . .	6-12
6.2.2 Saharan Air Characteristics . . . . .	6-14
6.2.3 Large Scale Movement of Saharan Air Dust . . . . .	6-16
6.2.4 Forecast Rules/Aids . . . . .	6-20
6.2.5 Satellite Imagery 'Clues' . . . . .	6-20
6.3 Case III - Cape Rollers (Abnormal Waves) (21 - 26 Sept. 1973) . . . . .	6-21
6.3.1 General Discussion . . . . .	6-21
6.3.2 Geophysical Background. . . . .	6-23
6.3.3 Case History . . . . .	6-24
6.3.4 Forecast Rules . . . . .	6-27
6.4 Cases IV, V and VI - Winter Storms (July/August 1983) . . . . .	6-29
6.4.1 Introduction. . . . .	6-29
6.4.2 Case Study IV (5 - 9 July 1983) . . . . .	6-30
6.4.3 Case Study V (19 - 23 July 1983) . . . . .	6-55
6.4.4 Case Study VI (3 - 7 August 1983) . . . . .	6-83
6.4.5 Forecast Rules/Hints . . . . .	6-116

6.5 Average Oceanic Weather . . . . .	6-118
6.5.1 Introduction. . . . .	6-118
6.5.2 Atlantic (Equator - 35°S and 15°W - West African Coast) .	6-118
6.5.3 Atlantic & Indian Oceans (35°S - 50°S and 15°W - 60°E). .	6-122
6.5.4 Indian Ocean (Equator - 35°S and 20°E - 60°E) . . . . .	6-127
<b>7. COASTAL OCEANOGRAPHIC INFLUENCES . . . . .</b>	<b>7-1</b>
7.1 Introduction . . . . .	7-1
7.2 Monsoon Circulation Patterns, Western Indian Ocean . . . . .	7-8
7.3 The Agulhas Current . . . . .	7-14
7.4 Cape Rollers, Unusually High Swell Off South Africa . . . . .	7-25
7.5 Southern Ocean Area . . . . .	7-29
7.6 The Benguela Current, 15°S to 35°S. . . . .	7-38
7.7 Equatorial Atlantic Region . . . . .	7-47
<b>8. REFERENCES . . . . .</b>	<b>8-1</b>

## TABLES

Table	page
3.1. Distribution of Thunderstorm Days for the Malagasy Republic . . .	3-11
4.1. Mean Position of Origin of Cyclonic Storms in the South Indian Ocean . . . . .	4-1
4.2. Average Latitude of the Point of Recurvature of Tropical cyclones in the South Indian Ocean . . . . .	4-2
7.1. Comparison of Boundary Current Systems . . . . .	7-3
7.2. Volume Transport of the Agulhas Current . . . . .	7-21
7.3. Wave Height Return Values . . . . .	7-27
7.4. Percentage Frequency of Observations of Waves with Gentle Breeze or Calmer, and Gales . . . . .	7-27
7.5. Characteristics of Three Water Types off the Cape. . . . .	7-43

## FIGURES

Figure	page
1.1. Countries of the Southern African Continent . . . . .	1-2
1.2. Topography of the Southern African Continent . . . . .	1-2
1.3. Mean pressure (mb) at sea level in July . . . . .	1-3
1.4. Mean pressure (mb) at sea level in January . . . . .	1-3
1.5. Mean height (dm) of the 500-mb surface in July . . . . .	1-4
1.6. Mean height (dm) of the 500-mb surface in January . . . . .	1-4
1.7. Mean monthly frequency of anticyclones: August . . . . .	1-5
1.8. Mean monthly frequency of anticyclones: February . . . . .	1-5
1.9. Mean monthly storm tracks: August . . . . .	1-6
1.10. Mean monthly storm tracks: February . . . . .	1-6
1.11. Mean monthly number of atmospheric fronts: August . . . . .	1-7
1.12. Mean monthly number of atmospheric fronts: February . . . . .	1-7
1.13. Frequency of surface fronts during winter and summer . . . . .	1-8
1.14. (A) 5-day-averaged mosaic, November 10-14, 1969 (B) Location of 700-mb troughs . . . . .	1-10
1.15. Major cloud band axes for different seasons . . . . .	1-11
1.16. The Streten-type classification for frontal vortices . . . . .	1-12
1.17. Mean distribution of the "early development" (W, A, B) vortices for the five winters 1973-1977 . . . . .	1-14
1.18. Mean distribution of the "mature" (C) vortices for the five winters 1973-1977 . . . . .	1-14
1.19. Mean distribution of the frontless "cut-off" (F/G) vortices for the five winters 1973-1977 . . . . .	1-15

1.20.	Mean (five-winter) distribution of vortex types as a function of latitude . . . . .	1-16
1.21.	Initial point of wave (W) and "inverted comma" (A) cyclogenesis for all latitudes south of 20°S . . . . .	1-16
1.22.	Distribution of cyclogenesis during the IGY . . . . .	1-19
1.23.	Tracks of surface cyclones for July 1957 . . . . .	1-21
1.24.	Tracks of 500-mb geopotential "minima", July 1957 . . . . .	1-21
1.25.	Frequency distributions of speeds of movement of lows. . . . .	1-22
2.1.	Station locations of Southern Africa . . . . .	2-1
2.2.	Monthly mean surface streamlines . . . . .	2-3
2.3.	RSA surface/850 mb analysis: 1200 GMT 24 August 1973 . . . . .	2-5
2.4.	RSA surface/850 mb analysis: 1200 GMT 18 August 1973 . . . . .	2-5
2.5.	RSA surface/850 mb analysis: 1200 GMT 15 August 1973 . . . . .	2-6
2.6.	RSA surface/850 mb analysis: 1200 GMT 16 August 1973 . . . . .	2-7
2.7.	RSA surface/850 mb analysis: 1200 GMT 17 August 1973 . . . . .	2-7
2.8.	RSA surface/700 mb analysis: 0600 GMT 18 June 1964 . . . . .	2-9
2.9.	RSA surface/850 mb analysis: 1200 GMT 20 December 1973 . . . . .	2-10
2.10.	RSA surface/850 mb analysis: 1200 GMT 21 December 1973 . . . . .	2-11
2.11.	RSA surface/850 mb analysis: 1200 GMT 23 December 1973 . . . . .	2-11
2.12.	RSA surface/850 mb analysis: 1200 GMT 7 January 1973 . . . . .	2-13
2.13.	RSA surface/850 mb analysis: 1200 GMT 12 November 1973 . . . . .	2-13
2.14.	RSA surface/700 mb analysis: 0600 GMT 19 December 1960 . . . . .	2-15
2.15.	RSA surface/850 mb analysis: 1200 GMT 10 December 1973 . . . . .	2-16
2.16.	RSA surface/850 mb analysis: 1200 GMT 11 December 1973 . . . . .	2-17
2.17.	RSA surface/850 mb analysis: 1200 GMT 12 December 1973 . . . . .	2-17
2.18.	RSA surface/850 mb analysis: 1200 GMT 28 December 1973 . . . . .	2-18
2.19.	RSA surface/850 mb analysis: 1200 GMT 29 December 1973 . . . . .	2-19
2.20.	RSA surface/850 mb analysis: 1200 GMT 30 December 1973 . . . . .	2-19

2.21.	Mean monthly frequency of fog occurrence (%): July . . . . .	2-21
2.22.	Mean monthly frequency of fog occurrence (%): October . . . . .	2-21
2.23.	Mean monthly frequency of fog occurrence (%): January . . . . .	2-22
2.24.	Mean monthly frequency of fog occurrence (%): April . . . . .	2-22
2.25.	Average annual number of days with thunder . . . . .	2-23
2.26.	Average annual number of days with hail . . . . .	2-24
2.27.	Mean 200 mb flow over the African Continent: January . . . . .	2-26
2.28.	Mean 200 mb flow over the African Continent: July . . . . .	2-27
2.29.	Mean 500 mb flow over the African Continent: January . . . . .	2-28
2.30.	Mean 500 mb flow over the African Continent: July . . . . .	2-29
2.31.	Mean 700 mb flow over the African Continent: January . . . . .	2-30
2.32.	Mean 700 mb flow over the African Continent: July . . . . .	2-31
3.1.	Station locations of Malagasy Republic . . . . .	3-2
3.2.	Station locations of Mozambique . . . . .	3-2
3.3.	RSA surface/850 mb analysis: 1200 GMT 12 August 1973 . . . . .	3-3
3.4.	RSA surface/850 mb analysis: 1200 GMT 22 January 1972 . . . . .	3-4
3.5.	RSA surface/850 mb analysis: 1200 GMT 23 January 1972 . . . . .	3-5
3.6.	RSA surface/850 mb analysis: 1200 GMT 13 January 1974 . . . . .	3-6
3.7.	RSA surface/850 mb analysis: 1200 GMT 14 January 1974 . . . . .	3-6
3.8.	RSA surface/850 mb analysis: 1200 GMT 15 January 1974 . . . . .	3-7
3.9.	RSA surface/850 mb analysis: 1200 GMT 16 January 1974 . . . . .	3-7
3.10.	RSA surface/850 mb analysis: 1200 GMT 11 November 1973 . . . . .	3-8
3.11.	RSA surface/850 mb analysis: 1200 GMT 12 November 1973 . . . . .	3-9
3.12.	RSA surface/850 mb analysis: 1200 GMT 13 November 1973 . . . . .	3-9
3.13.	RSA surface/850 mb analysis: 1200 GMT 16 November 1978 . . . . .	3-10
3.14.	Monthly positions of the low-level cross-equatorial jet . . . . .	3-13
3.15.	1 km Flow for August over the Arabian Sea/Indian Ocean . . . . .	3-14

3.16.	RSA surface/850 mb analysis: 1200 GMT 6 September 1973 . . . . .	3-16
3.17.	RSA surface/850 mb analysis: 1200 GMT 7 September 1973 . . . . .	3-16
3.18.	RSA surface/850 mb analysis: 1200 GMT 8 September 1973 . . . . .	3-17
4.1.	Tropical cyclone tracks east of the Malagasy Republic . . . . .	4-3
4.2.	Tropical cyclone tracks in the N. Mozambique Channel . . . . .	4-4
4.3.	Tropical cyclone tracks in the S. Mozambique Channel . . . . .	4-5
4.4	RSA surface/850 mb analysis: 1200 GMT 24 February 1975 . . . . .	4-6
4.5	RSA surface/850 mb analysis: 1200 GMT 25 February 1975 . . . . .	4-7
4.6.	NOAA 4 visible satellite imagery: 0600 GMT 25 February 1975 . . .	4-7
4.7.	RSA surface/850 mb analysis: 1200 GMT 21 January 1976. . . . .	4-9
4.8.	NOAA 4 visible satellite imagery: 0600 GMT 21 January 1976 . . .	4-9
4.9.	RSA surface/850 mb analysis: 1200 GMT 22 January 1976. . . . .	4-10
4.10.	NOAA 4 visible satellite imagery: 0600 GMT 22 January 1976 . . .	4-10
4.11.	RSA surface/850 mb analysis: 1200 GMT 24 January 1976. . . . .	4-11
4.12.	RSA surface/850 mb analysis: 1200 GMT 15 January 1975. . . . .	4-12
4.13.	RSA surface/850 mb analysis: 1200 GMT 16 January 1975. . . . .	4-13
4.14.	NOAA 4 visible satellite imagery: 0600 GMT 16 January 1975 . . .	4-13
4.15.	RSA surface/850 mb analysis: 1200 GMT 17 January 1975. . . . .	4-14
4.16.	NOAA 4 visible satellite imagery: 0600 GMT 17 January 1975 . . .	4-14
4.17.	RSA surface/850 mb analysis: 1200 GMT 26 January 1976. . . . .	4-15
4.18.	RSA surface/850 mb analysis: 1200 GMT 27 January 1976. . . . .	4-16
4.19.	RSA surface/850 mb analysis: 1200 GMT 28 January 1976. . . . .	4-16
4.20.	RSA surface/850 mb analysis: 1200 GMT 8 February 1972 . . . . .	4-17
4.21.	RSA surface/850 mb analysis: 1200 GMT 12 February 1972 . . . . .	4-18
4.22.	RSA surface/850 mb analysis: 1200 GMT 14 February 1972 . . . . .	4-18
4.23.	RSA surface/850 mb analysis: 1200 GMT 5 January 1973 . . . . .	4-20
4.24.	RSA surface/850 mb analysis: 1200 GMT 6 January 1973 . . . . .	4-20

4.25.	RSA surface/850 mb analysis: 1200 GMT 7 January 1973 . . . . .	4-21
4.26.	RSA surface/850 mb analysis: 1200 GMT 8 January 1973 . . . . .	4-21
4.27.	RSA surface/850 mb analysis: 1200 GMT 18 January 1975. . . . .	4-22
4.28.	RSA surface/850 mb analysis: 1200 GMT 19 January 1975. . . . .	4-23
4.29.	RSA surface/850 mb analysis: 1200 GMT 20 January 1975. . . . .	4-23
5.1.	Station locations of Kenya and Tanzania . . . . .	5-2
5.2.	Mean northeasterly monsoon flow. . . . .	5-5
5.3.	Mean southwesterly or southeasterly monsoon flow . . . . .	5-5
5.4.	Equatorial duct . . . . .	5-7
6.1.	An ATS-3 view of an inverted V cloud pattern . . . . .	6-2
6.2.	Proposed modification of Frank's schematic relationship between lower tropospheric flow and the inverted V pattern . .	6-3
6.3.	An analysis of relative vorticity for 20 August 1972 . . . . .	6-5
6.4.	Mean sea-surface isotherms, the distribution of initial tropical storm fixes, and the mean position of the 700-mb wave axis . .	6-6
6.5.	Visible imagery (METEOSAT) of an inverted V, 24 August 1983 .	6-7
6.6.	Visible imagery (METEOSAT) of an inverted V, 25 August 1983 .	6-8
6.7.	Visible imagery (METEOSAT) of an inverted V, 26 August 1983 .	6-9
6.8.	Visible imagery (METEOSAT) of an inverted V, 27 August 1983 .	6-10
6.9.	visible imagery (METEOSAT) of an inverted V, 28 August 1983 .	6-11
6.10.	Visible imagery (METEOSAT) of dust outbreak, 2 May 1983 . .	6-13
6.11.	Visible imagery (METEOSAT) of dust outbreak, 3 May 1983 . .	6-14
6.12.	Idealized sounding for dust-laden Saharan air outbreak . . . .	6-15
6.13.	Superimposed serrated line indicating dust front. . . . .	6-17
6.14.	Schematic model of a dust plume moving off Africa. . . . .	6-19
6.15.	Saharan dust plume fallout over Atlantic. . . . .	6-19
6.16.	Chart of SE coast of RSA showing the continental shelf, Agulhas Current & positions of encountered abnormal waves .	6-21

6.17.	Typical great circle paths followed by swell generated at Latitude 55°S by (A) westerly and (B) southwesterly gales . . .	6-22
6.18.	RSA surface/850 mb analysis: 1200 GMT 21 September 1973 . . .	6-23
6.19.	RSA surface/850 mb analysis: 1200 GMT 22 September 1973 . . .	6-25
6.20.	RSA surface/850 mb analysis: 1200 GMT 23 September 1973 . . .	6-25
6.21.	RSA surface/850 mb analysis: 1200 GMT 24 September 1973 . . .	6-26
6.22.	RSA surface/850 mb analysis: 1200 GMT 25 September 1973 . . .	6-26
6.23.	RSA surface/850 mb analysis: 1200 GMT 26 September 1973 . . .	6-27
6.24.	RSA surface/850 mb analysis: 1200 GMT 5 July 1983 . . . . .	6-30
6.25.	Visible METEOSAT imagery, 1155 GMT on 5 July 1983 . . . . .	6-31
6.26.	FNOC sea-level pressure analysis, 1200 GMT on 5 July 1983 . . .	6-32
6.27.	RSA surface/850 mb analysis: 1200 GMT 6 July 1983 . . . . .	6-33
6.28.	Visible METEOSAT imagery, 1155 GMT on 6 July 1983 . . . . .	6-34
6.29.	FNOC sea-level pressure analysis, 1200 GMT on 6 July 1983 . . .	6-35
6.30.	NOAA 7 visible imagery, 1238-1243 GMT on 6 July 1983 . . . . .	6-36
6.31.	NMC 500 mb analysis, 1200 GMT on 6 July 1983 . . . . . . .	6-37
6.32.	FNOC 500 mb analysis, 1200 GMT on 6 July 1983. . . . . . .	6-38
6.33.	RSA surface/850 mb analysis: 1200 GMT 7 July 1983 . . . . .	6-39
6.34.	Visible METEOSAT imagery, 1255 GMT on 7 July 1983 . . . . .	6-40
6.35.	Infrared METEOSAT imagery, 1255 GMT on 7 July 1983 . . . . .	6-41
6.36.	FNOC sea-level pressure analysis, 1200 GMT on 7 July 1983 . . .	6-42
6.37.	FNOC 500 mb analysis, 1200 GMT on 7 July 1983. . . . . . .	6-43
6.38.	RSA surface/850 mb analysis: 1200 GMT 8 July 1983 . . . . .	6-44
6.39.	Visible METEOSAT imagery, 1155 GMT on 8 July 1983 . . . . .	6-45
6.40.	FNOC sea-level pressure analysis, 1200 GMT on 8 July 1983 . . .	6-46
6.41.	NMC 500 mb analysis, 1200 GMT on 8 July 1983 . . . . . . .	6-47
6.42.	FNOC 500 mb analysis, 1200 GMT on 8 July 1983. . . . . . .	6-48

6.43.	RSA surface/850 mb analysis: 1200 GMT 9 July 1983 . . . . .	6-49
6.44.	Visible METEOSAT imagery, 1155 GMT on 9 July 1983 . . . . .	6-50
6.45.	FNOC sea-level pressure analysis, 1200 GMT on 9 July 1983 . . .	6-51
6.46.	NOAA 7 visible imagery, 1201-1206 GMT on 9 July 1983 . . . . .	6-52
6.47.	NMC 500 mb analysis, 1200 GMT on 9 July 1983 . . . . . . .	6-53
6.48.	FNOC 500 mb analysis, 1200 GMT on 9 July 1983. . . . . . .	6-54
6.49.	RSA surface/850 mb analysis: 1200 GMT 19 July 1983 . . . . .	6-55
6.50.	Visible METEOSAT imagery, 1155 GMT on 19 July 1983. . . . .	6-56
6.51.	RSA surface/850 mb analysis: 1200 GMT 20 July 1983 . . . . .	6-57
6.52.	Visible METEOSAT imagery, 1155 GMT on 20 July 1983. . . . .	6-58
6.53.	FNOC sea-level pressure analysis, 1200 GMT on 20 July 1983 . .	6-59
6.54.	NOAA 7 visible imagery, 1309-1314 GMT on 20 July 1983 . . . . .	6-60
6.55.	NOAA 7 visible imagery, 1450-1458 GMT on 20 July 1983 . . . . .	6-61
6.56.	RSA surface/850 mb analysis: 1200 GMT 21 July 1983 . . . . .	6-62
6.57.	Visible METEOSAT imagery, 1155 GMT on 21 July 1983. . . . .	6-63
6.58.	Infrared METEOSAT imagery, 1155 GMT on 21 July 1983 . . . . .	6-64
6.59.	FNOC sea-level pressure analysis, 1200 GMT on 21 July 1983 . .	6-65
6.60.	NMC 500 mb analysis, 1200 GMT on 21 July 1983. . . . . . .	6-66
6.61.	FNOC 500 mb analysis, 1200 GMT on 21 July 1983 . . . . . . .	6-67
6.62.	DMSP visible imagery, 1635 GMT 21 July 1983 . . . . . . .	6-68
6.63.	DMSP infrared imagery, 1635 GMT 21 July 1983 . . . . . . .	6-69
6.64.	RSA surface/850 mb analysis: 1200 GMT 22 July 1983 . . . . .	6-71
6.65.	Visible METEOSAT imagery, 1155 GMT on 22 July 1983. . . . .	6-72
6.66.	FNOC sea-level pressure analysis, 1200 GMT on 22 July 1983 . .	6-73
6.67.	NOAA 7 visible imagery, 1244-1250 GMT on 22 July 1983. . . . .	6-74
6.68.	NMC 500 mb analysis, 1200 GMT on 22 July 1983. . . . . . .	6-75
6.69.	FNOC 500 mb analysis, 1200 GMT on 22 July 1983 . . . . . . .	6-76

6.70.	RSA surface/850 mb analysis: 1200 GMT 23 July 1983 . . . . .	6-77
6.71.	Visible METEOSAT imagery, 1155 GMT on 23 July 1983. . . . .	6-78
6.72.	FNOC sea-level pressure analysis, 1200 GMT on 23 July 1983 . .	6-79
6.73.	NOAA 7 visible imagery, 1231-1237 GMT on 23 July 1983 . . . .	6-80
6.74.	NMC 500 mb analysis, 1200 GMT on 23 July 1983. . . . . . .	6-81
6.75.	FNOC 500 mb analysis, 1200 GMT on 23 July 1983 . . . . . . .	6-82
6.76.	RSA surface/850 mb analysis: 1200 GMT 3 August 1983 . . . . .	6-83
6.77.	Visible METEOSAT imagery, 1155 GMT on 3 August 1983 . . . . .	6-84
6.78.	FNOC sea-level pressure analysis, 1200 GMT on 3 August 1983. .	6-85
6.79.	NOAA 7 visible imagery, 1158-1203 GMT on 3 August 1983 . . . .	6-86
6.80.	NMC 500 mb analysis, 1200 GMT on 3 August 1983 . . . . . . .	6-87
6.81.	FNOC 500 mb analysis, 1200 GMT on 3 August 1983 . . . . . . .	6-88
6.82.	RSA surface/850 mb analysis: 1200 GMT 4 August 1983 . . . . .	6-91
6.83.	Visible METEOSAT imagery, 1155 GMT on 4 August 1983 . . . . .	6-92
6.84.	FNOC sea-level pressure analysis, 1200 GMT on 4 August 1983. .	6-93
6.85.	NOAA 7 visible imagery, 1327-1333 GMT on 4 August 1983 . . . .	6-94
6.86.	NMC 500 mb analysis, 1200 GMT on 4 August 1983 . . . . . . .	6-95
6.87.	FNOC 500 mb analysis, 1200 GMT on 4 August 1983 . . . . . . .	6-96
6.88.	RSA surface/850 mb analysis: 1200 GMT 5 August 1983 . . . . .	6-99
6.89.	Visible METEOSAT imagery, 1155 GMT on 5 August 1983 . . . . .	6-100
6.90.	FNOC sea-level pressure analysis, 1200 GMT on 5 August 1983. .	6-101
6.91.	NOAA 7 visible imagery, 1315-1320 GMT on 5 August 1983 . . . .	6-102
6.92.	FNOC 500 mb analysis, 1200 GMT on 5 August 1983 . . . . . . .	6-103
6.93.	RSA surface/850 mb analysis: 1200 GMT 6 August 1983 . . . . .	6-104
6.94.	Visible METEOSAT imagery, 1155 GMT on 6 August 1983 . . . . .	6-105
6.95.	FNOC sea-level pressure analysis, 1200 GMT on 6 August 1983. .	6-106
6.96.	DMSP visible imagery, 1602 GMT 6 August 1983 . . . . . . . .	6-107

6.97.	NMC 500 mb analysis, 1200 GMT on 6 August 1983 . . . . .	6-108
6.98.	FNOC 500 mb analysis, 1200 GMT on 6 August 1983 . . . . .	6-109
6.99.	RSA surface/850 mb analysis: 1200 GMT 7 August 1983 . . . . .	6-110
6.100.	Visible METEOSAT imagery, 1155 GMT on 7 August 1983 . . . . .	6-111
6.101.	FNOC sea-level pressure analysis, 1200 GMT on 7 August 1983. .	6-112
6.102.	DMSP visible imagery, 0423 GMT 7 August 1983 . . . . .	6-113
6.103.	NMC 500 mb analysis, 1200 GMT on 7 August 1983 . . . . .	6-114
6.104.	FNOC 500 mb analysis, 1200 GMT on 7 August 1983 . . . . .	6-115
6.105.	Gales, June - South Atlantic Ocean . . . . .	6-119
6.106.	Air temperature, September - South Atlantic Ocean . . . . .	6-120
6.107.	Air temperature, March - South Atlantic Ocean . . . . .	6-120
6.108.	Frequency of wave heights, August - South Atlantic Ocean . .	6-121
6.109.	Gales, July - Western Indian Ocean . . . . .	6-123
6.110.	Air temperature, August - South Atlantic Ocean . . . . .	6-125
6.111.	Air temperature, August - Western Indian Ocean . . . . .	6-125
6.112.	Frequency of wave heights, August - W. Indian Ocean . . . .	6-126
7.1.	Southern African continent and adjacent ocean areas . . . . .	7-2
7.2.	Distribution of surface isotherms, February . . . . .	7-4
7.3.	Distribution of surface isotherms, May . . . . .	7-4
7.4.	Distribution of surface isotherms, August . . . . .	7-5
7.5.	Distribution of surface isotherms, November . . . . .	7-5
7.6.	Distribution of surface isohalines, N. H. summer and winter . .	7-7
7.7.	Distribution of high and low pressures in January & July . .	7-8
7.8.	Limit of the monsoon system . . . . .	7-9
7.9.	Surface winds and currents in southwest & northeast monsoon .	7-11
7.10.	Surface currents, Indian Ocean, (August - September) . . . .	7-12
7.11.	Surface currents, Indian Ocean, (February - March) . . . . .	7-13

7.12.	Broad outline of bottom topography of Southern Ocean area . . .	7-15
7.13.	On Sigma-t surface 25.1, isolines are shown for: (a) salinity, (b) oxygen and (c) acceleration potential . . . . .	7-16
7.14.	Surface dynamic height with reference to the 1000-dbar level. Heavy dots indicate track of satellite tracked buoy 1116 . . . . .	7-18
7.15.	Station dispositions superimposed on the bathymetry off southern Africa. . . . .	7-18
7.16.	Acceleration potential contours on the 25.6-sigma-t level. Heavy dotted line indicates track of satellite tracked buoy EOLE . . . . .	7-19
7.17.	(a) Enhanced NOAA-5 satellite infrared image of the southern African coast, August 4, 1976. (b) Line-drawn representation showing a large meander of the Agulhas Current. . . . .	7-19
7.18.	Location chart of sections across the Agulhas Current . . . . .	7-20
7.19.	Monthly mean and peak speeds in core of Agulhas Current. . . . .	7-22
7.20.	The coastal bathymetry off Natal . . . . .	7-24
7.21.	Sea surface temperatures from an airborne radiation thermometer (ART) flight on 30 November 1967. . . . .	7-24
7.22.	Coast of South Africa. The sea area in white is the region for which the wave observations were summarized. . . . .	7-26
7.23.	Synoptic weather chart shows LOW off the southeastern coast of RSA that wrought the damage to ill-fated WILSTAR. . . . .	7-26
7.24.	Mean southerly current speed parallel to the coast in m/s . . . . .	7-28
7.25.	A conceptual image of the main features of the circulation in the ocean areas adjacent to South Africa . . . . .	7-29
7.26.	Conceptual representation of the circulation in the Agulhas Current and Agulhas Return Current . . . . .	7-30
7.27.	The terminal region of the Agulhas Current south of South Africa. . . . .	7-31
7.28.	The Agulhas Current reverses off Africa's tip . . . . .	7-32
7.29.	The 1899 track of the WAIKATO. . . . .	7-33
7.30.	Depth of the 26.20 sigma-t surface during March 1969 for the ocean areas adjoining South Africa . . . . .	7-34

- 7.31. The disposition of clouds and ocean currents in the vicinity of South Africa on 16 December 1977. . . . . 7-35
- 7.32. The advection of warm (darker) water masses of Agulhas Current origin into the South Atlantic . . . . . 7-36
- 7.33. Global mesoscale sea height variability measured by the SEASAT altimeter, 15 September to 10 October 1978 . . . . . 7-37
- 7.34. Surface temperature ( $^{\circ}$ C) distribution (from ART data) of the southern Benguela Current during upwelling, 14 January 1973 . 7-40
- 7.35. Synoptic weather map of southern Africa showing typical summer atmospheric pressure system . . . . . 7-42
- 7.36. Synoptic weather map of southern Africa showing typical winter atmospheric pressure system . . . . . 7-42
- 7.37. A diagram of the relation of the water types found off the Cape Peninsula during upwelling . . . . . 7-44
- 7.38. Idealization of main structural features of the Benguela region between  $29^{\circ}$  and  $32^{\circ}$ S. . . . . 7-46
- 7.39. Idealization of frontal behaviour in the development of a 'centre of upwelling' . . . . . 7-46
- 7.40. Ocean surface currents in February-March. The thick arrows indicate especially strong currents . . . . . 7-48

## **FOREWORD**

The Forecasters Handbook for the Southern African Continent and Atlantic/Indian Ocean Transit was developed under the continuing effort of the Naval Environmental Prediction Research Facility (NEPRF) to improve the quality of naval environmental support in all parts of the world.

While several sources exist concerning the environment of the Southern Hemisphere, (including the Southern African Continent, the eastern South Atlantic and western Indian Ocean), the purpose of this document is to accumulate the most pertinent information available for use by Fleet forecasters who are unfamiliar with the region.

It is intended that this document be responsive to current requirements of U. S. Navy operating forces; therefore, it has been assembled in loose-leaf form. Users are urged to submit to this Command their comments and suggestions regarding contents and changes thereto.

The Forecasters Handbook for the Southern African Continent and Atlantic/Indian Ocean Transit was prepared through the combined efforts of CDR Forrest R. Williams (USN, Ret.), Adj. Professor of Meteorology, and Drs. Robert J. Renard and Glenn H. Jung of the Naval Postgraduate School (NPS), Monterey California; LT Randolph D. Tomkins, USN (while a student at NPS); and Mr. Roland R. Picard of NEPRF. Mr. Robert W. Fett (NEPRF) served as Project Coordinator. The Handbook was tasked and funded by the Commander Naval Oceanography Command to meet Fleet requirements.

L. J. Pingel  
Captain, U. S. Navy  
Commanding Officer

## PREFACE

This handbook is published to provide meteorological (and oceanographic) guidance to naval personnel embarked in Fleet units transiting between the Atlantic and Indian Oceans, as well as to provide regional familiarization to personnel supporting naval operations involving the Southern African Continent.

In the event of limited planning/preparation time prior to operations, it is recommended that forecasters first read Section 1 (Southern Hemisphere meteorology and climatology), Section 6 (case studies of mid-latitude cyclones), Subsections 4.1 and 4.2 (tropical cyclones in the western Indian Ocean and Mozambique Channel) and Section 7 (oceanographic influences including Cape Rollers (unusually high swell), the Agulhas Current and the Benguela Current). Note that the first two case studies of Section 6 concern the tropical Atlantic, while the remaining case studies depict the behavior of migratory cyclones affecting operations in the more poleward, southern latitudes. The potential effects of Cape Rollers, unusually high wave heights found when strong winds from the southwest oppose the Agulhas Current flowing from the northeast, on ships passing along the southeastern coast of the Republic of South Africa cannot be overemphasized.

Since the Navy's global prediction model has been operational for more than three years, it is expected that statistics and indepth analysis of systematic model errors in the Southern Hemisphere will be forthcoming shortly. Thus, it is anticipated that additional sections for this handbook will be available in the future.

Ships and stations with sufficient notice may wish to obtain a copy of the *Climates of the Oceans* (van Loon, 1984) published after the initial work of this handbook was completed.

## ACKNOWLEDGMENTS

Appreciation is extended to Dr. Harry van Loon, climatologist at the National Center for Atmospheric Research (NCAR) in Boulder, Colorado, for both his valuable counsel and provision of countless references concerning the meteorology of the Southern Hemisphere and of the Southern African Continent.

Additionally, the authors are indebted to Dr. J. J. Taljaard of the Weather Bureau of the Republic of South Africa (RSA) for his taking the time necessary to review the initial thesis, offer detailed recommendations and finally provide RSA surface analyses.

Thanks to Dr. Michael Garstang, University of Virginia and to Dr. Henry van de Boogaard, NCAR, for their presentation of motivational seminars at the commencement of the initial research.

The generous provision of METEOSAT imagery through the auspices of John Morgan of the European Space Agency, Darmstadt, Germany is acknowledged.

The authors are indebted also to Michael McDermet, laboratory supervisor/draftsman, Meteorology Department, Naval Postgraduate School, for his reliable and expert assistance including preparation of several figures and maps.

## Section 1

### GENERAL INTRODUCTION AND SOUTHERN HEMISPHERE METEOROLOGY

#### 1.1 GENERAL INTRODUCTION

This handbook describes the analysis and forecasting features of both atmospheric and oceanic conditions important to air/sea operations over the Southern African Continent and surrounding ocean areas. The report includes case studies utilizing satellite imagery relevant to vessels making transit between the Atlantic and Indian Oceans around Southern Africa.

The Southern African Continent, as addressed in this report, includes the following nations along and south of the equator: Kenya, Tanzania, Mozambique, Republic of South Africa (RSA) and Namibia (Figs. 1.1, 1.2). Weather over the Malagasy Republic (formerly known as Madagascar), Mauritius and Reunion (the Mascarene Is.), the Seychelles Is., and the South Atlantic and Indian Ocean areas between 15°W and 60°E from the equator to 50°S is also addressed.

Intense frontal cyclones pass through the ocean waters southwest, south and southeast of the RSA throughout the year. Due to their high frequency of occurrence and the intensity of the associated weather, these storms represent a significant threat to safe and effective operations in the region. The provision of information concerning extra-tropical frontal cyclones is a valuable aid to weather forecasting.

During the months of November through April tropical cyclones move through the Mozambique Channel and over the southwest Indian Ocean east of the Malagasy Republic. The sustained winds in these storms frequently exceed hurricane force (65 kt). A study of seasonal frequencies of occurrence, storm tracks and weather associated with these atmospheric systems is included.

This handbook includes descriptions of coastal weather phenomena (e.g., coastal fog, gale frequency, onshore/offshore winds, etc.) as well as the effects of near-shore oceanic currents and African topography on weather forecasting.

Following a brief discussion regarding weather analysis and forecasting in the Southern Hemisphere, specific continental and oceanic regions are considered in terms of regional topography and climatology. Synoptic-scale weather systems affecting each sub-region are described, including direction of movement of the systems and large-scale weather effects. The associated mesoscale weather phenomena are then discussed. Brief comments concerning significant upper atmospheric weather features are addressed as well.

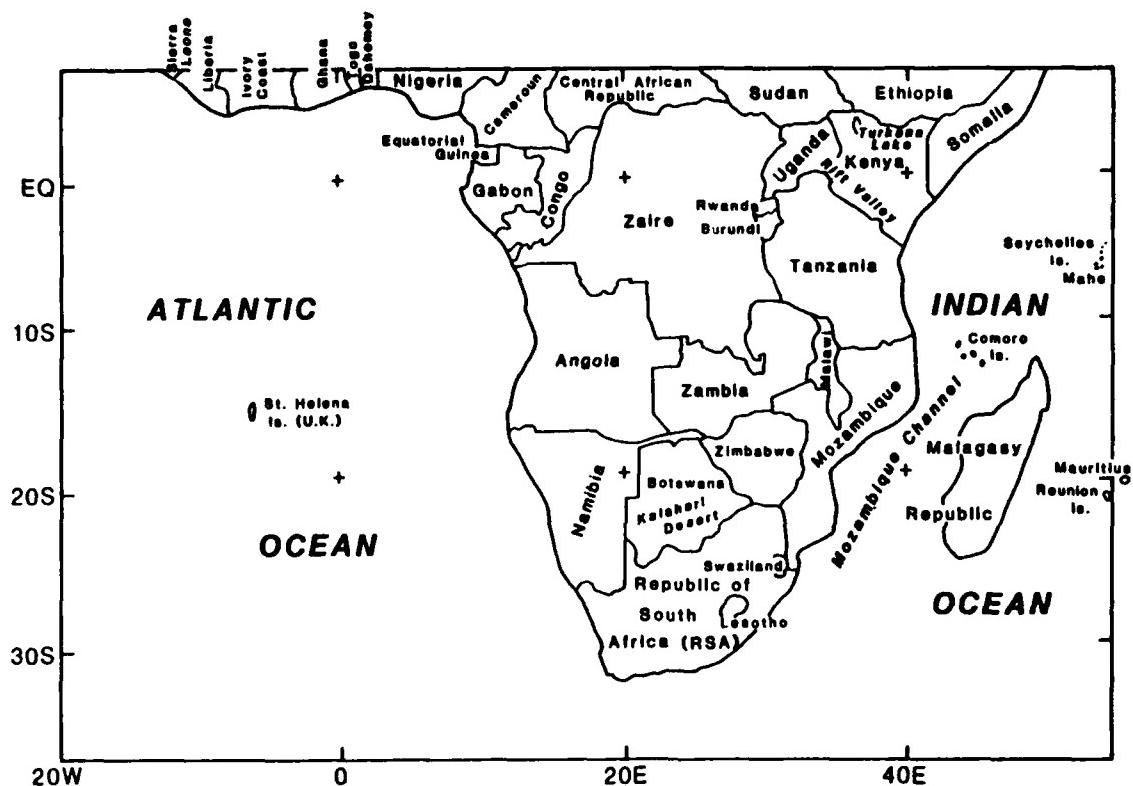


Fig. 1.1. Countries of the Southern African Continent

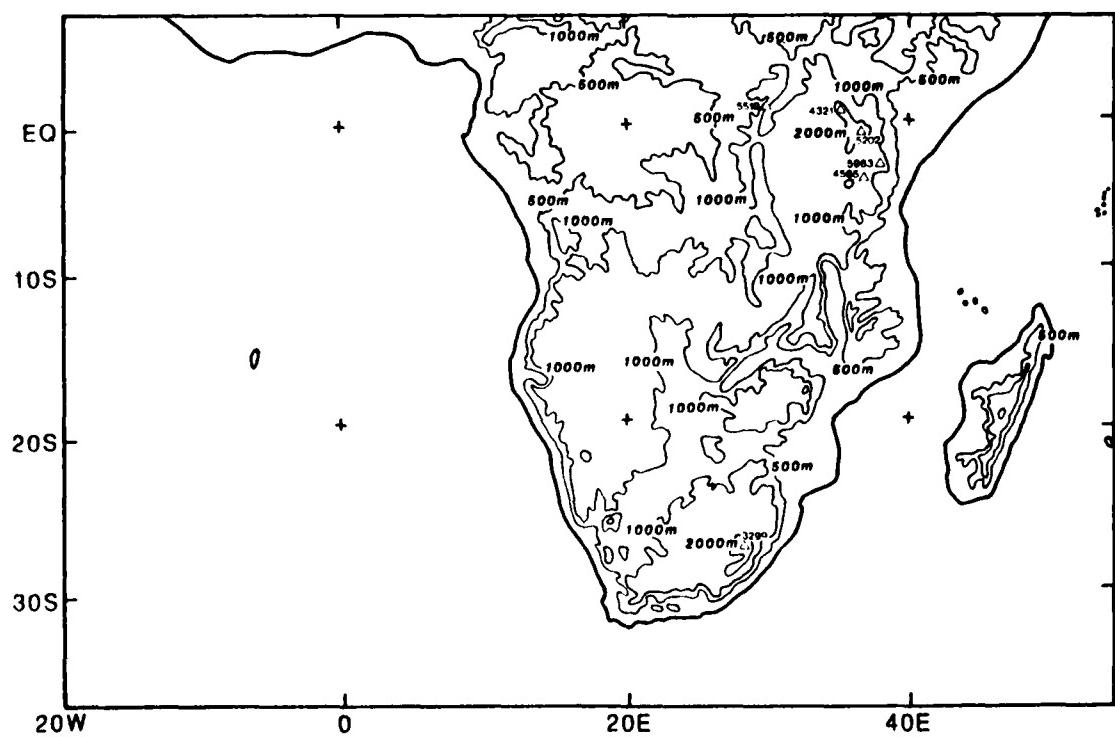


Fig. 1.2. Topography of the Southern African Continent

## 1.2 SOUTHERN HEMISPHERE METEOROLOGY

### 1.2.1 Climatology

Figs. 1.3 and 1.4 from Taljaard et al. (1969) depict mean sea-level pressure in July (winter) and January (summer), respectively. Similarly, Figs. 1.5 and 1.6 depict the mean height of the 500-mb surface for both winter and summer.

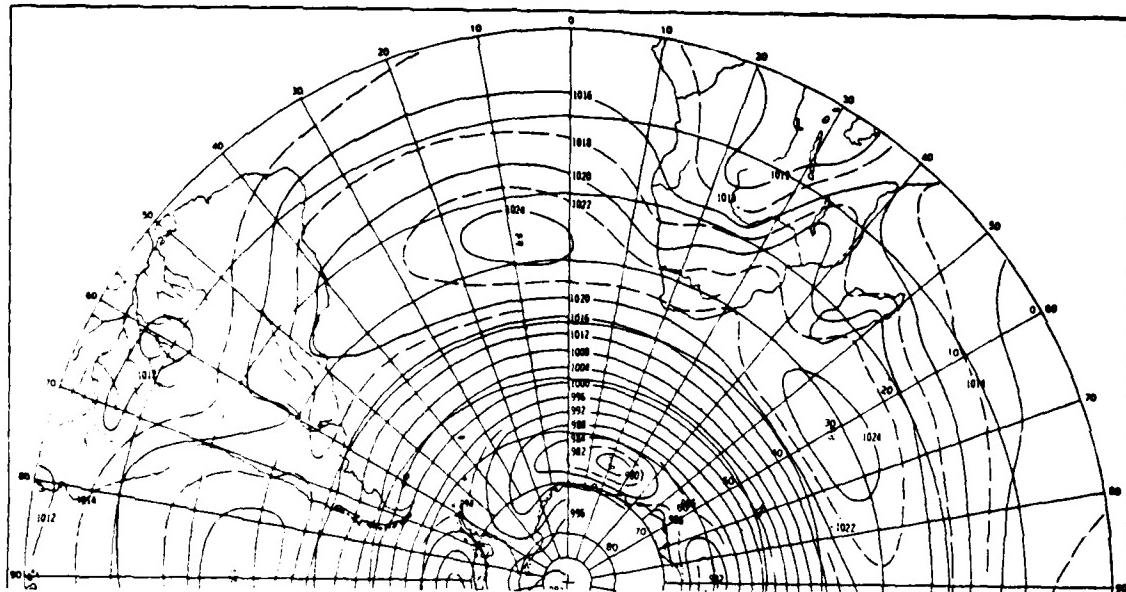


Fig. 1.3. Mean pressure (mb) at sea level in July. (From Taljaard et al., 1969)

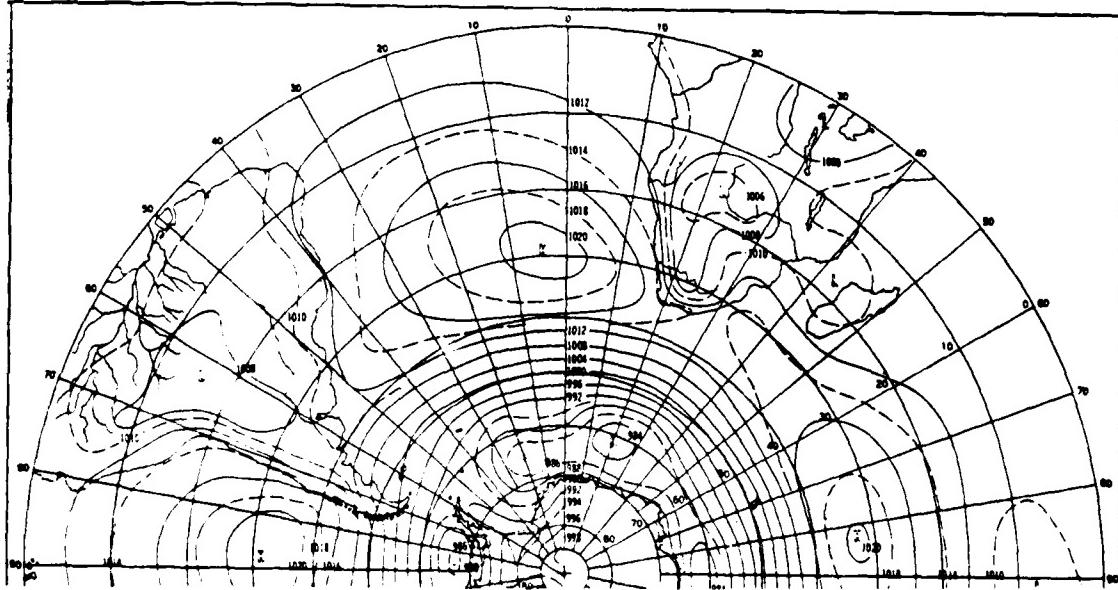
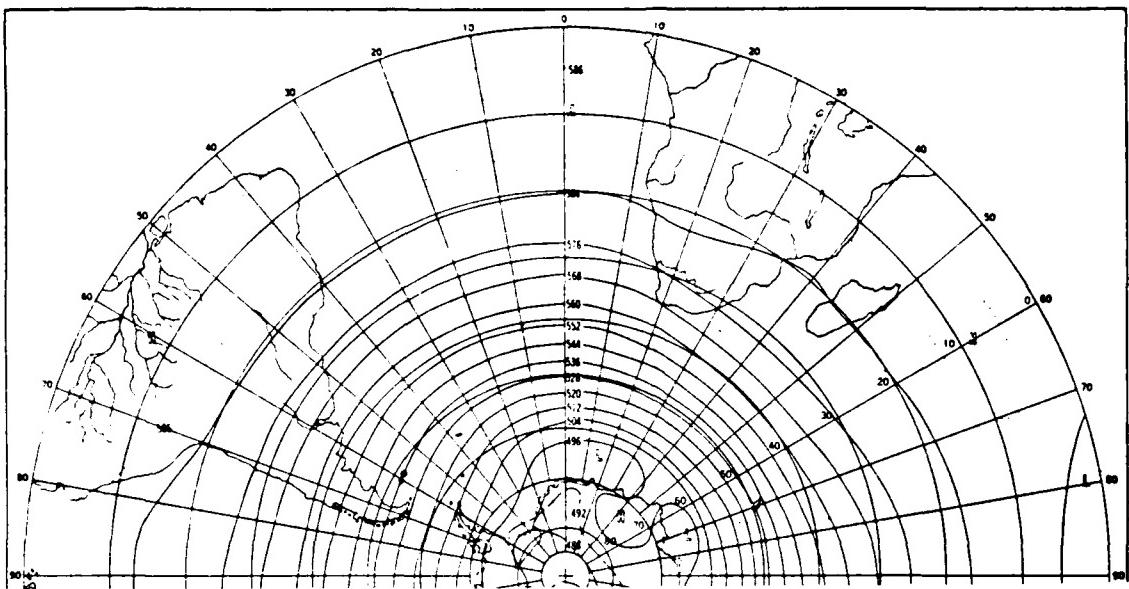


Fig. 1.4. Mean pressure (mb) at sea level in January. (From Taljaard et al., 1969)



Strong migrating anticyclones affect the South Atlantic and Indian Oceans on either side of Southern Africa throughout the year. Figs. 1.7 and 1.8 show the frequency of occurrence of anticyclones over these ocean areas for August and February, respectively.

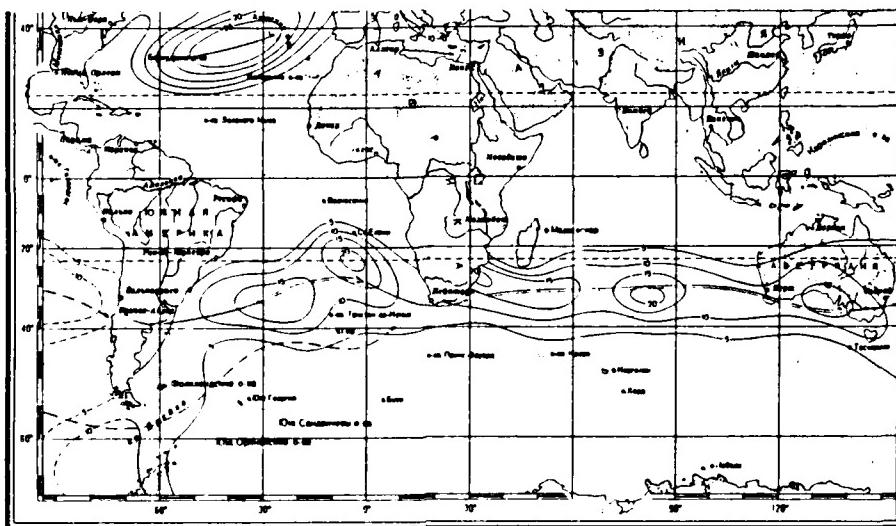


Fig. 1.7. Mean Monthly Frequency of Occurrence (%) of Anticyclones: August (Union of Soviet Socialist Republics Ministry of Defense, 1979)

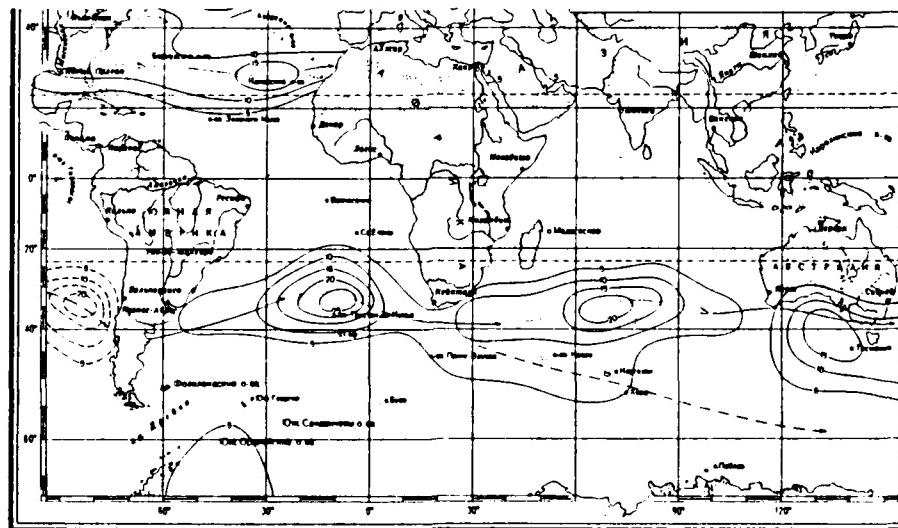


Fig. 1.8. Mean Monthly Frequency of Occurrence (%) of Anticyclones: February (Union of Soviet Socialist Republics Ministry of Defense, 1979)

Mature frontal cyclones also affect the Southern African region, mostly during the winter months as indicated in Figs. 1.9 and 1.10, for August and February. The mean storm tracks over the Atlantic and Indian Oceans in this area are also shown in these figures. The solid double and triple track lines define principal storm tracks over the oceans, the latter representing the primary tracks.

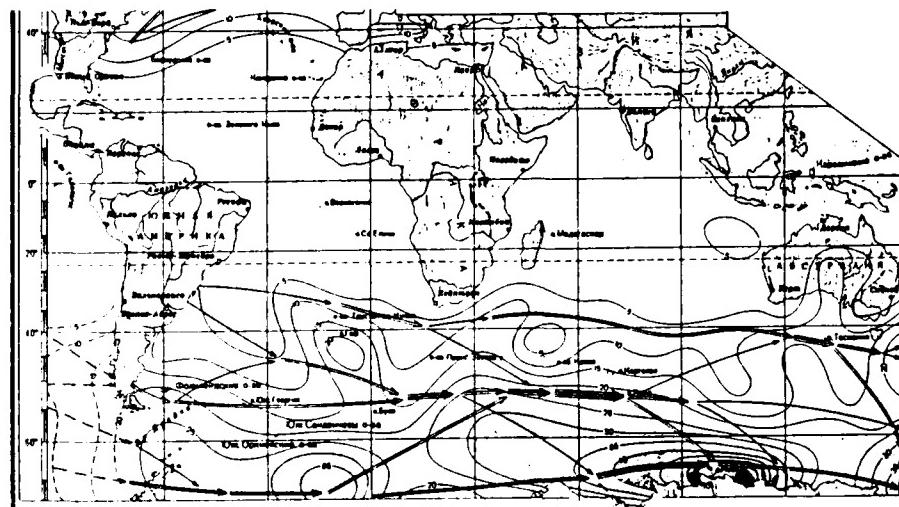


Fig. 1.9. Mean Monthly Storm Tracks: August. Isolines depict the mean Frequency of Occurrence (%) of cyclones. (Union of Soviet Socialist Republics Ministry, 1979)

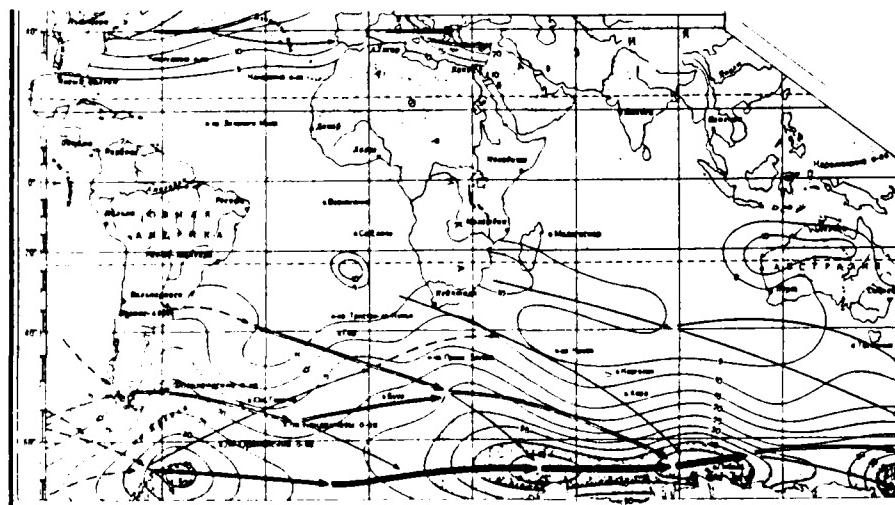


Fig. 1.10. Mean Monthly Storm Tracks: February. Isolines depict the Mean Frequency of Occurrence (%) of cyclones. (Union of Soviet Socialist Republics Ministry of Defense, 1979)

Figs. 1.11 and 1.12 depict the mean monthly occurrences of surface fronts for August and February (U.S.S.R. Ministry of Defense, 1979).

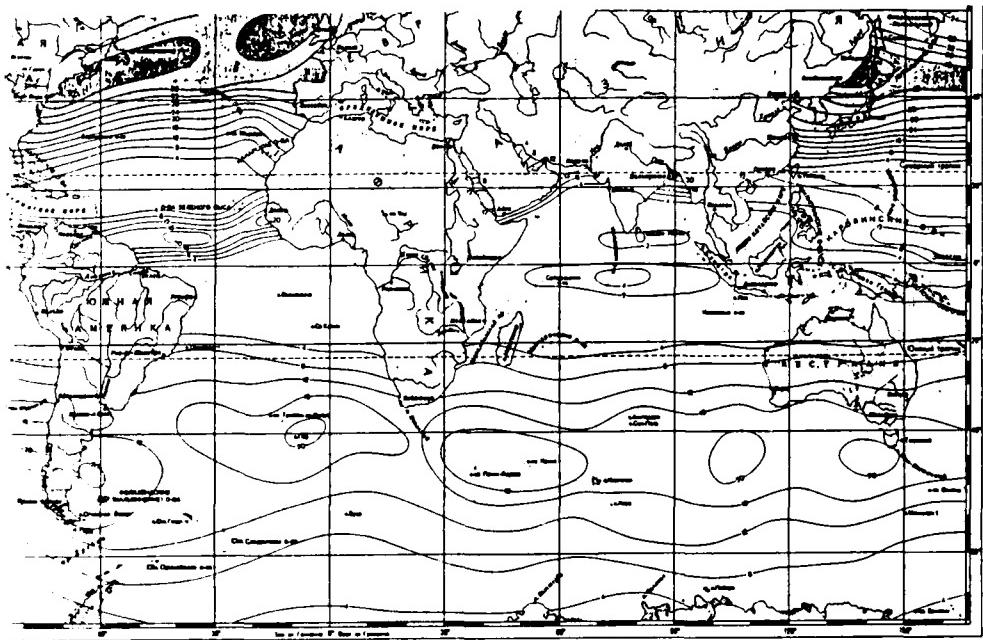


Fig. 1.11. Mean Monthly Number of Atmospheric Fronts: August (Union of Soviet Socialist Republics Ministry of Defense, 1979)

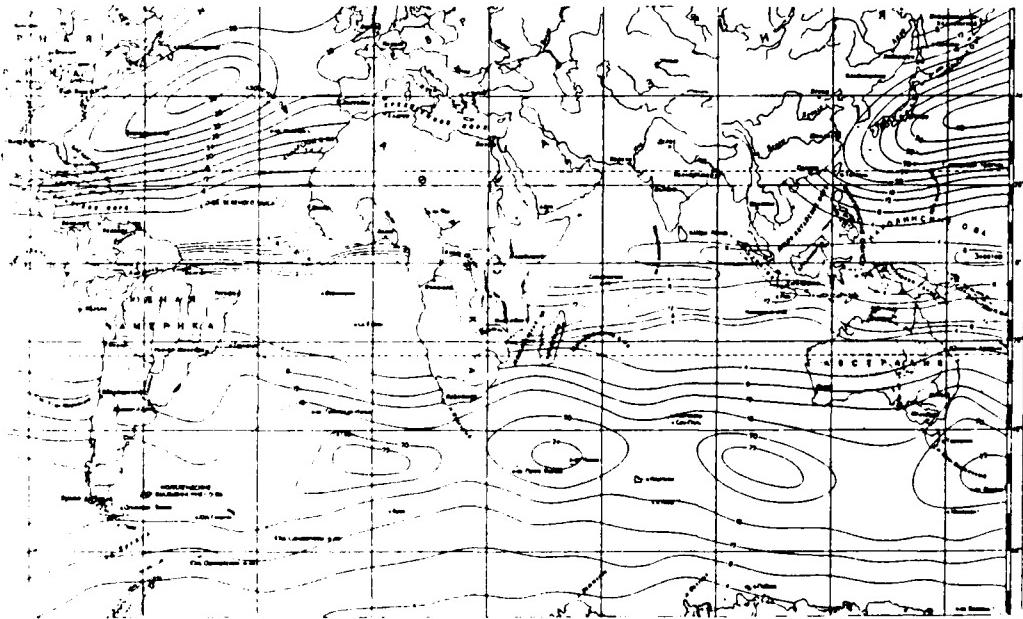


Fig. 1.12. Mean Monthly Number of Atmospheric Fronts: February (Union of Soviet Socialist Republics Ministry of Defense, 1979)

The axis showing maximum frequency of surface fronts during the winter and summer from the International Geophysical Year (IGY) (1957-1958) (see Fig. 1.13 from van Loon (1965)) must be used carefully since the average frontal location is produced by numerous daily fronts which are *seldom* aligned with a circle of latitude.

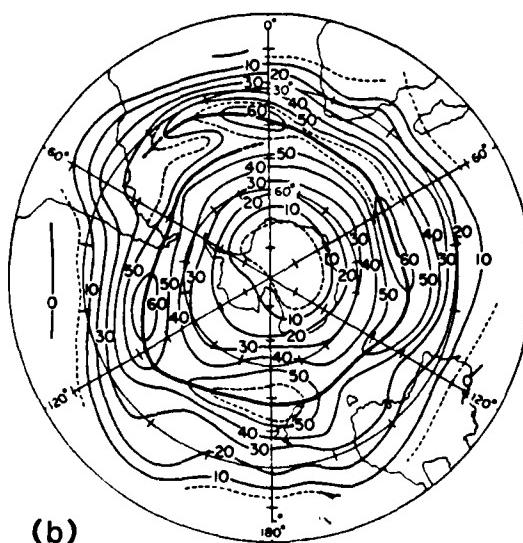
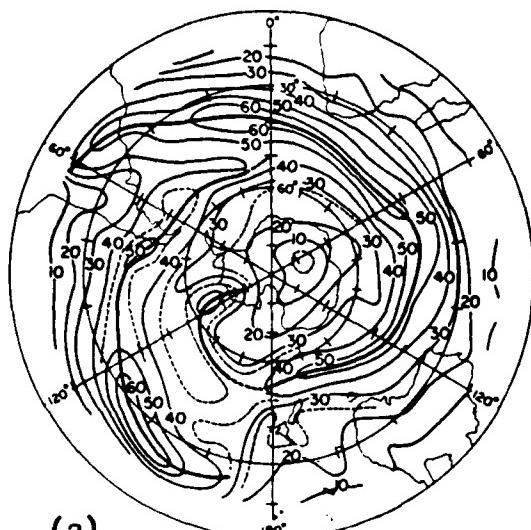


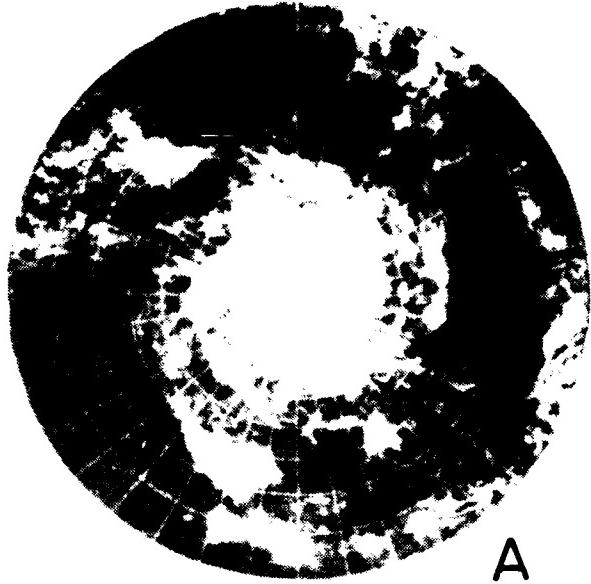
Fig. 1.13. Frequency of surface fronts during (a) July, August and September, 1957 (winter) and (b) January, February and March, 1958 (summer). Frequency represents the number of times in 100 days when part of a front was situated within a unit area of 400,000 km<sup>2</sup>. 30°S and 60°S latitude circles are provided. (van Loon, 1965)

Bright bands on daily visual satellite imagery, within the extratropics, usually represent either frontal clouds or elongated regions of low or midtropospheric convergence lying between midlatitude anticyclones. (Existence of stratocumulus/stratus in the vicinity of anticyclones can be identified on imagery by relatively warm cloud top temperatures.) Streten (1973) viewed averaged "photographs" over a number of days. Fig. 1.14 displays the association of 5-day-averaged visual imagery with long wave 700-mb troughs, when wave number 3 dominates (i.e., three troughs exist around the Southern Hemisphere). Streten found that extratropical bright band patterns display a high frequency of wave numbers 3 and 4. When viewed on averaged photographs over a number of days, the satellite banding is thought to be related to a particular feature or to repetitive events. Synoptic experience supports acceptance of NW-SE oriented satellite bands being located close to the upper-air, long-wave troughs in the lower atmosphere (Streten, 1973).

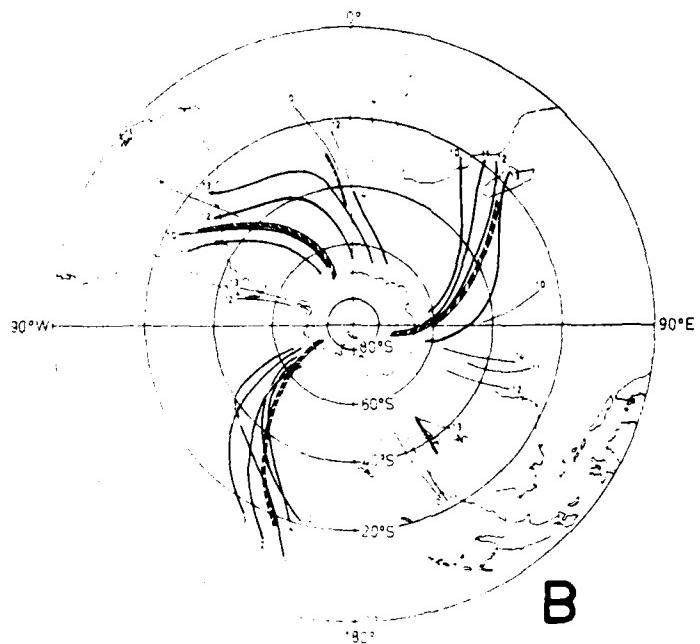
Streten investigated brightness bands found in 200 5-day-averaged brightness mosaics covering the Southern Hemisphere (November 1968 - October 1971). Only cloud bands at least  $20^{\circ}$  latitude in length and  $5^{\circ}$  latitude in width were included. Fig. 1.15 (Streten, 1973) displays the frequency of 5-day-averaged mosaics having axes of major cloud bands within  $5^{\circ}$ -latitude by  $10^{\circ}$ -longitude areas based on three years of data. Streten identified the following features (among others):

- In regard to the entire Southern Hemisphere, a distinct triple maxima exists in summer, with a more complicated pattern in other seasons, although annually a triple maxima prevails.
- A secondary maxima appears off Angola in winter associated with stratus and fog forming in the region of the cold Benguela Current (located just offshore of Angola and Namibia, the current is described in Section 7).
- Very low band frequencies (i.e., less cloudy conditions) are found over southwest Africa.

While Streten found that there was a "general" eastward movement of the averaged bands, westward displacement is more frequent in early autumn and winter. (Of course his findings contain a certain subjective element, since often when no *distinct* band pattern was evident, no clear movement could be assessed.)



A



B

Fig. 114. (A) 3-day averaged mosaic Nov. 10-14, 1969 and (B) location of 700-mb troughs in the long-wave, scale separated components for corresponding indicated dates. Heavy lines represent well-defined troughs, fine lines represent minor troughs, and striped lines represent troughs in the mean 5-day field. (Streten, 1973)

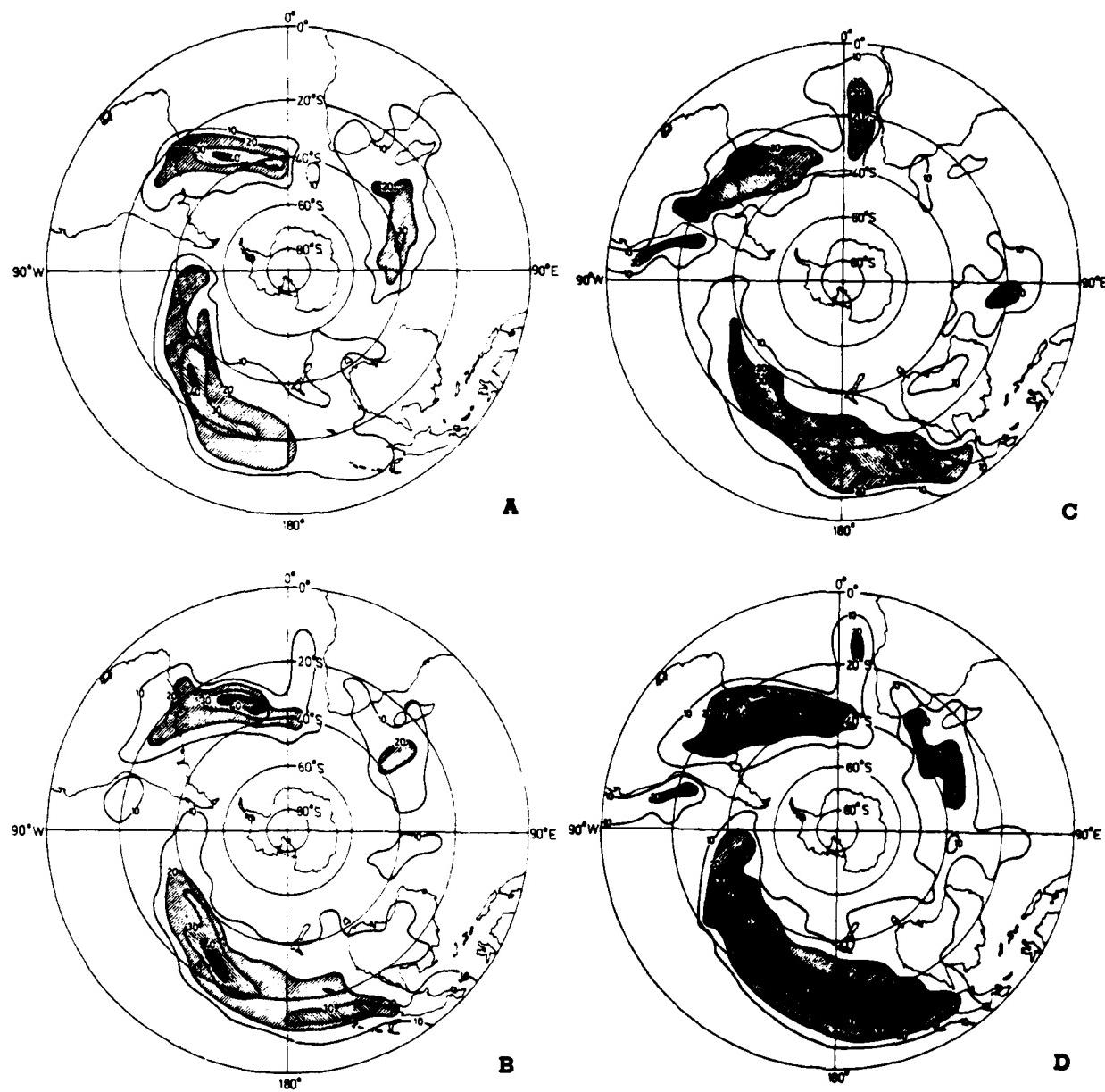


Fig. 1.15. Percentage frequency of 5-day-averaged mosaics having axes of major cloud bands within a  $5^{\circ}$ -latitude by  $10^{\circ}$ -longitude area for (A) summer (December-March), (B) intermediate season (April, May, October, November), (C) winter (June-September) and (D) annual. Data based on period November 1968-October 1971. (Streten, 1973)

Using the vortex cloud classification depicted in Fig. 1.16, Carleton (1979) expanded the study of satellite imagery by studying twice-daily infrared satellite imagery, from polar-orbiting platforms for the winters (June to September) of 1973-1977, to investigate cyclonic activity over the Southern Hemisphere.

SOUTHERN HEMISPHERE SATELLITE-OBSERVED VORTICES  (after Streten & Troup and Streten & Mullas)	STRETEL-TYPE CLASSIFICATION	DESCRIPTIVE COMMENTS
	W	Wave on a frontal band, either marked by change in orientation and/or bulging of the band.
	A	'Inverted comma' cyclone in isolation, without a clear slot.
	B	Developing vortex with slot of clear air; either in isolation or on frontal band.
	C	Vortex at maximum dev- elopment with spiral of clear air around centre.
	D <sub>1</sub>	Dissipating vortex with heavy vertical cloud; no spiralling. Cloud band not asymmetric.
	D <sub>1</sub>	Dissipating vortex with little central cloud; cloud band not asymmetric.
	D <sub>2</sub>	Dissipating vortex with heavy cloud and marked asymmetry of frontal band; normally hook- shaped.
	D <sub>2</sub>	Dissipating vortex with little central cloud and marked asymmetry of frontal band.

Fig. 1.16. The Streten-type classification scheme for frontal cloud vortices appearing on Southern Hemisphere satellite imagery. (Carleton, 1979)

Figs. 1.17, 1.18 and 1.19 depict the mean distribution of "early development" (W, A, B) vortices, "mature" (C) vortices and frontless "cut-off" (F/G)<sup>1</sup> vortices, respectively for the five winters. In Fig. 1.17, axes of vortex maxima extend from southeastern South America into the South Atlantic and in the Indian Ocean from south-west of Australia toward the Malagasy Republic (compare with cloud bands in Fig. 1.15 C), although location of the axis in the complex Pacific Ocean is not attempted.

The figure depicting the location of "dissipating" (D) vortices is not reproduced, however the major regions for weakening of cyclonic circulation (i.e., *cyclolysis*) cluster in high latitudes, not distant from Antarctica. This is confirmed by frame D of Fig. 1.20 which indicates that dissipating vortices are prevalent between 55°-70°S. Whereas Fig. 1.20 presents vortex percentages around the entire Southern Hemisphere, Fig. 1.21 permits the identification of specific *longitudes* where wave (W) and "inverted comma" (A) cyclogenesis occur. Fig. 1.21 emphasizes the predominance of wave (W) cyclogenesis near South America (+65% deviation from the five-year mean). On the other hand, while Fig. 1.21 indicates a small positive deviation (+15%) for "inverted comma" (A) cyclogenesis near the longitude of Southern Africa (20°E), Fig. 1.20 indicates the preference of (A) cyclogenesis for latitudes south of 45°S (i.e., 900 n mi south (or poleward) of Africa).

The areal distribution of the quasi-stationary, "cut-off" (F/G) cyclones shown in Fig. 1.19 indicates the likelihood, though indeed quite small, of cut off lows near Southern Africa. Upper-air cut-off lows are addressed in the Southern Africa section.

Carleton (1979) summarizes (regarding Southern Hemisphere winter):

- High frequency of wave (W) cyclogenesis exists at lower-middle latitudes and high frequency of inverted comma (A) cyclogenesis exists at high latitudes (See Fig. 1.20). This cyclogenesis tends to correspond with the locations of the major hemispheric long wave troughs.
- Increasing cyclonic development generally occurs with increasing latitude in the vicinity of the major frontal axes.
- Cyclolysis (weakening of cyclonic circulation) reaches a maximum in Antarctic coastal waters.
- Quasi-stationary frontless "cut-off" cyclones are more common at lower latitudes (See Fig. 1.20). Their rarity at high latitudes probably reflects the stronger zonal circulation at high latitudes.

---

<sup>1</sup> Fig. 1.16 does not include graphical representation for satellite images of F/G cut-off vortices which are typically circular or concentric.

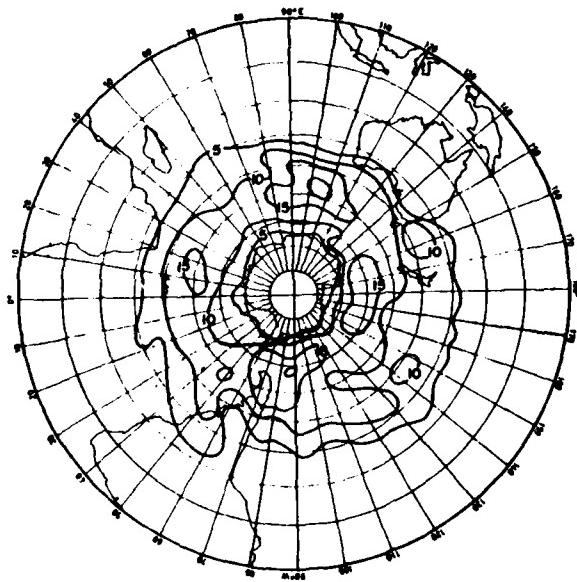


Fig. 1.17. Mean distribution of the "early development" (W, A, B) vortices for the five winters 1973-1977. Isopleth values refer to normalized vortex frequencies in each  $5^{\circ}$  latitude by  $10^{\circ}$  longitude area. (Carleton, 1979)

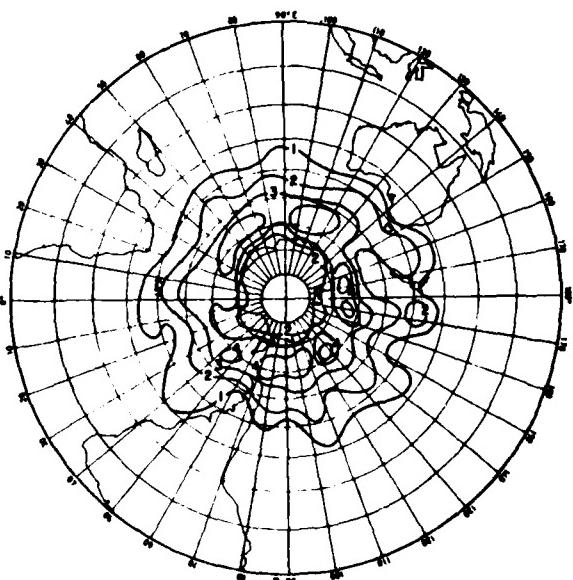


Fig. 1.18. Mean distribution of the "mature" (C) vortices for the five winters 1973-77. Isopleth values refer to normalized vortex frequencies in each  $5^{\circ}$  latitude by  $10^{\circ}$  longitude area. (Carleton, 1979)

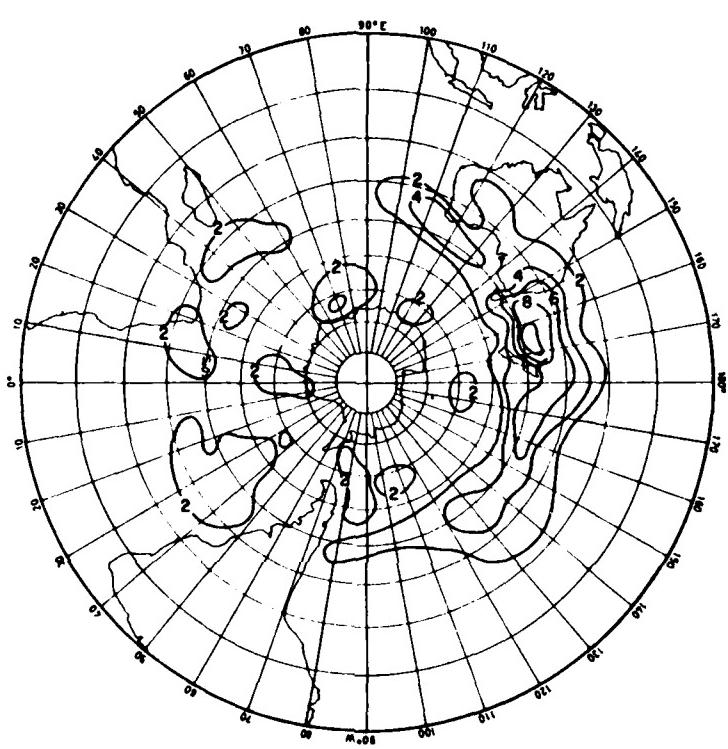


Fig. 1.19. Mean distribution of the frontless "cut-off" (F/G) vortices for the five winters. Isopleth values refer to normalized frequencies in each 5° latitude by 10° longitude area. (Carleton, 1979)

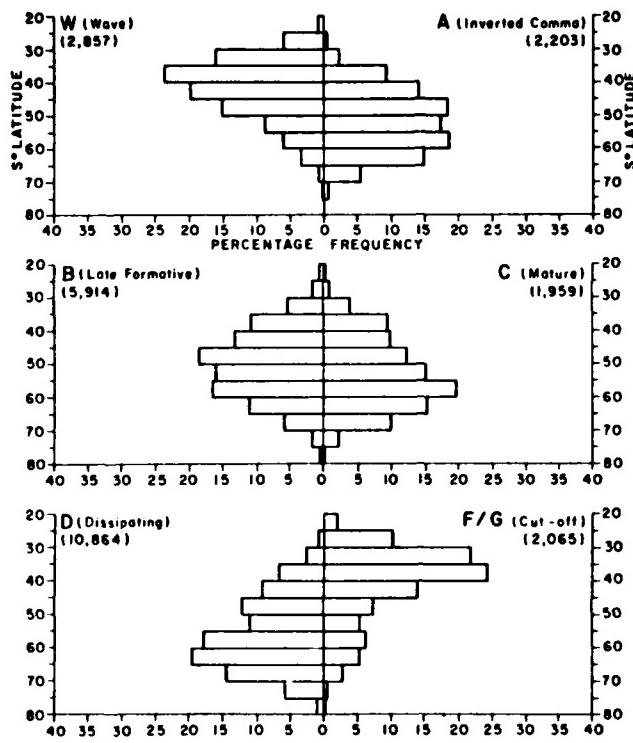


Fig. 1.20. Mean (five-winter) distribution of vortex types as a function of latitude. Frequencies of each  $5^{\circ}$  latitude band are represented as the percentage of the total for that type over all latitudes. Figures in brackets give the total numbers of cyclones for the five winters studied. (Carleton, 1979)

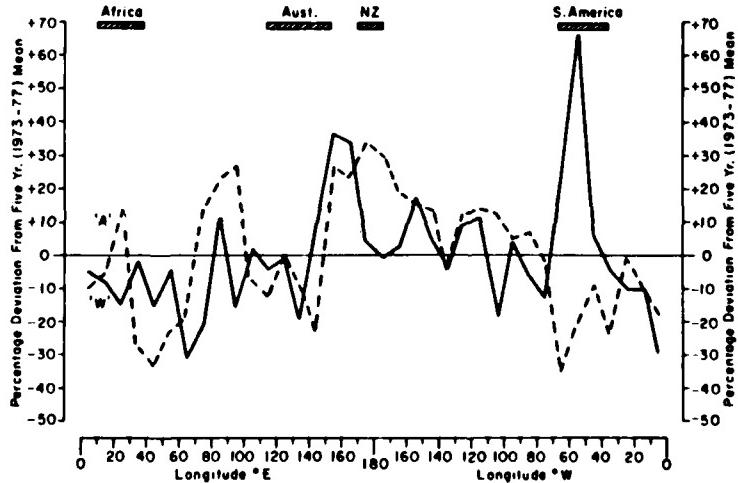


Fig. 1.21. Initial point of wave (W) and "inverted comma" (A) cyclogenesis for all latitudes south of  $20^{\circ}$ S. Vortex frequencies are presented as the percentage departure in each  $10^{\circ}$  longitude band from the mean (five-winter) hemispheric average for each cyclogenetic type. (Carleton, 1979)

### 1.2.2 Forecasting 'Thumb Rules' for the Southern Hemisphere

Assuming that all readers will not be expert in Southern Hemisphere meteorology, the following 'thumb rules' are presented to emphasize differences from the Northern Hemisphere. (Unless indicated otherwise, the material has been taken from Taljaard (1972).)

Low pressure (or cyclonic) systems are associated with *clockwise* rotation in the Southern Hemisphere. Quoting from the American Meteorological Society (1959), p. 151:

Cyclonic - Having a sense of rotation about the local vertical the same as that of the earth's rotation: that is, as viewed from above...clockwise in the Southern Hemisphere...

- Warm fronts may be expected to *not* fit well into systems moving eastward rapidly in the strong zonal flow of the Southern Hemisphere; moreover, similar to the Northern Hemisphere experience, satellite imagery does not assist in locating warm fronts in the extensive cloudiness which normally precedes vortices and cold fronts.
- Regarding anticyclonic centers which are so important in establishing large pressure gradients on their periphery within the Southern Hemisphere oceans:
  1. The core of highest anticyclonic activity moves latitudinally about four degrees equatorward from summer to winter.
  2. Within the Southern Hemisphere region surrounding Southern Africa, the core of highest frequency of anticyclonic centers is farthest equatorward in the Atlantic between  $0^{\circ}$  -  $15^{\circ}$ W.
  3. There is a clear tendency for the strongest anticyclones in the Southern Hemisphere to occur well *south* of the subtropical ridge, with the very strongest anticyclones occurring  $10^{\circ}$  south of the average ridge axis in winter.
  4. Strong anticyclones poleward of  $40^{\circ}$ S are of two types:
    - a) Cold systems forming in the intensifying ridges consisting of surges of cold air in the rear of the last members of cyclone families, usually advancing rapidly with an equatorward component of movement; however systems extending southward tend to slow and form blocking systems.
    - b) Warm blocking systems intensifying as they extend to higher latitudes from the subtropical ridge.
  5. Movement of anticyclones during a life cycle of a few days to several weeks experiences many variations with some advancing along smooth paths (most common of cold systems), while

slow-moving warm systems, particularly those north of the mean tracks, have extremely unpredictable tracks.

6. The mean movement of anticyclones is eastward with a small *northward* (equatorward) component; consequently, more new cells form south of the mean tracks while more old cells dissipate north of the mean tracks. (However, southward (poleward) movement of anticyclones frequently occurs as they approach the southwest coast of Southern Africa, followed by a return to a northward component along the southeast coast of Africa.)
7. Winds produced by pressure gradients created by the proximity of anticyclones to cyclones, dictate that the Southern Hemisphere forecaster be familiar with the behavior of anticyclones, as well as cyclones. The mean *zonal* component of movement of anticyclones (between 40°-50°S and 80°W eastward to 180°E) was described by Meinardus (1928, 1929) as follows:

a) Summer	22.2 kt
b) Autumn	21.1 kt
c) Winter	23.0 kt
d) Spring	21.6 kt
8. The process of splitting or "budding" of anticyclones past the Southern African coast occurs in the 25°-35°S zone when anticyclones extend elongated ridges over or past the "obstacle" (Southern African Continent) in their way. Closed isobars (new cells) then form in the forward part of the ridge, and concurrently the parent cell often retracts to the west.

- In regard to cyclogenesis,<sup>2</sup> during the IGY (see Fig. 1.22):
    1. Taljaard (1972) found that cyclogenesis was most frequent between  $35^{\circ}$  and  $55^{\circ}$ S with some exceptions.

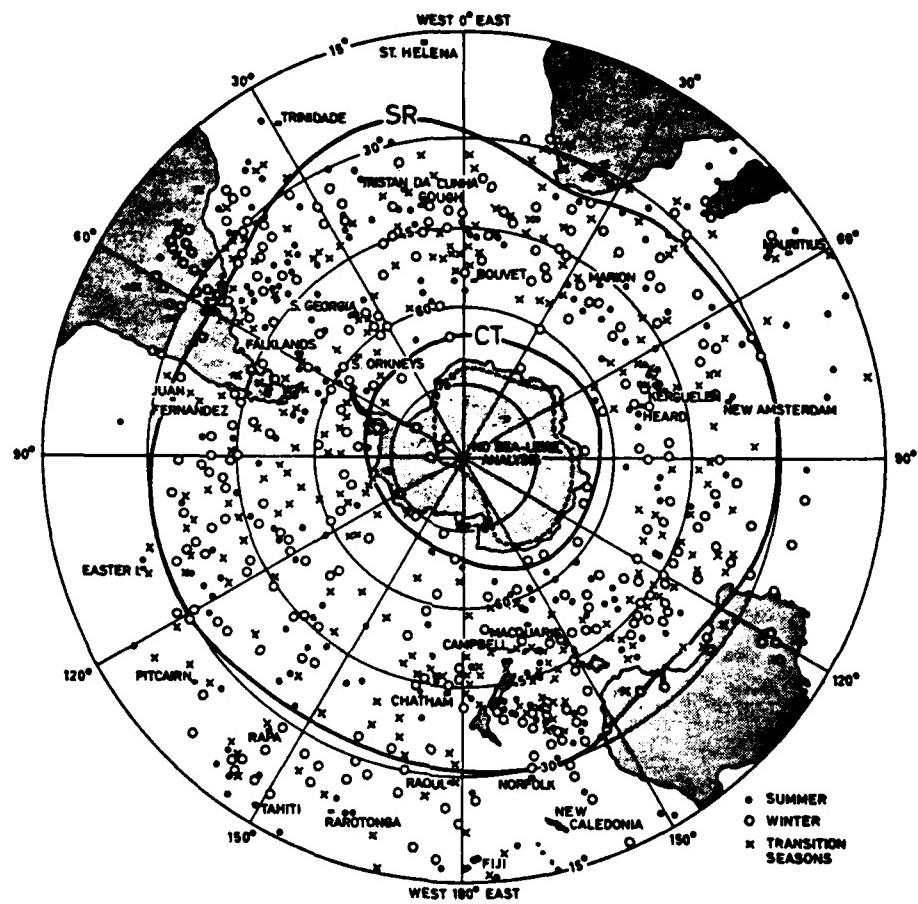


Fig. 1.22. Distribution of cyclogenesis (individual cases) during the IGY. SR is subtropical ridge and CT circum polar trough. (Taljaard, 1972)

2. Cyclogenesis was equally frequent over the sea and land in winter, but more frequent over the sea during the other seasons.

<sup>2</sup> The term *cyclogenesis* as used here denotes the formation of new low pressure systems, not the deepening of existing cyclones.

3. Cyclogenesis was noted equatorward of the subtropical ridge (SR) over Southern Africa particularly during the transitional months.
  4. During the summer, cyclogenesis was noted in the Mozambique Channel and near Mauritius; however, some of these cases are the first appearances of tropical cyclones entering from the north.
- While Figs. 1.9 and 1.10 present mean monthly storm tracks for August and February, showing that tracks of storms (lows) near Southern Africa are generally toward the east or southeast, cyclones tend to move with an *equatorward* component in the extreme southwest Atlantic between 30° and 70°W.

- Figs. 1.23 and 1.24 show surface and 500-mb cyclone tracks during July 1957. During this winter month, cut-off lows are frequently well developed at upper levels over Southern Africa, yet are reflected only as troughs at the surface.

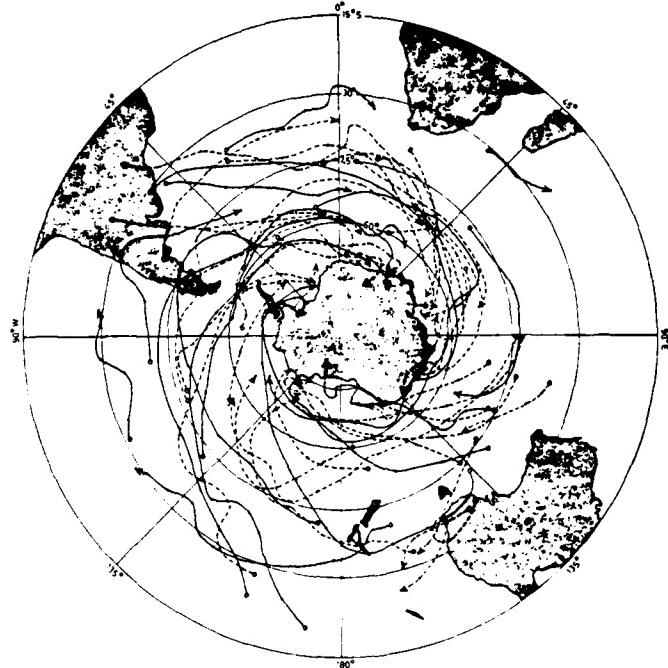


Fig. 1.23. Tracks of surface cyclones for July 1957. (From Taljaard and van Loon, 1962)

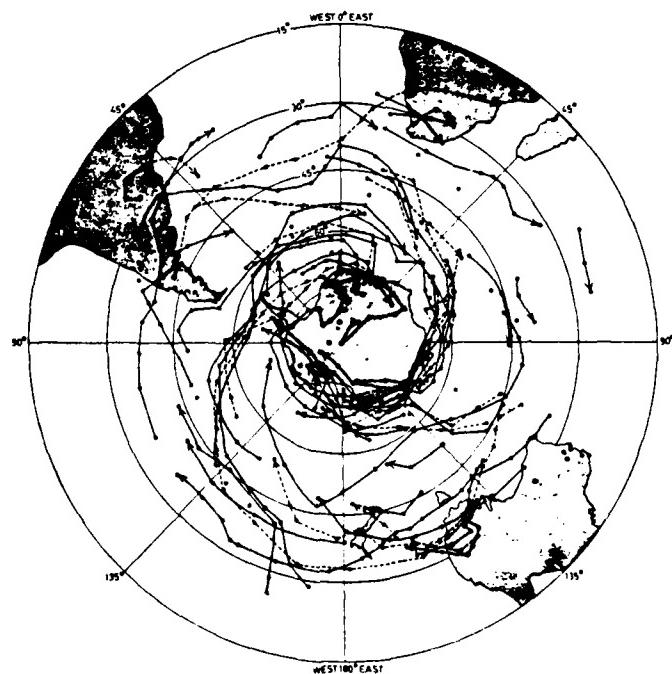


Fig. 1.24. Tracks of 500-mb geopotential "minima" (i.e., closed lows or strong cyclonic vorticity maxima) during July 1957. (From Taljaard and van Loon, 1962)

- Meinardus (1929) compiled zonal (i.e., east-west flow) components of the speed of cyclones, or pressure troughs, in the  $40^{\circ}$ - $50^{\circ}$ S zone from  $0^{\circ}$ - $180^{\circ}$ E:

1. Summer	24.6 kt
2. Winter	24.3 kt

(Assuming an average of 30 degrees between cyclone track and latitude circle, the true speed of the cyclones would be near 29 kt.)

(However, van Loon (1967), using IGY data, found speeds of cyclone movement slightly *faster* during winter. Indeed his zonal index, too, is 9% *lower* during the winter months, but his meridional (i.e., north - south flow) index is 17% higher in winter than in summer.)

- Fig. 1.25 (van Loon, 1967) gives the frequency distribution of the speed of cyclones (around the entire Southern Hemisphere) during the IGY for winter and summer combined.

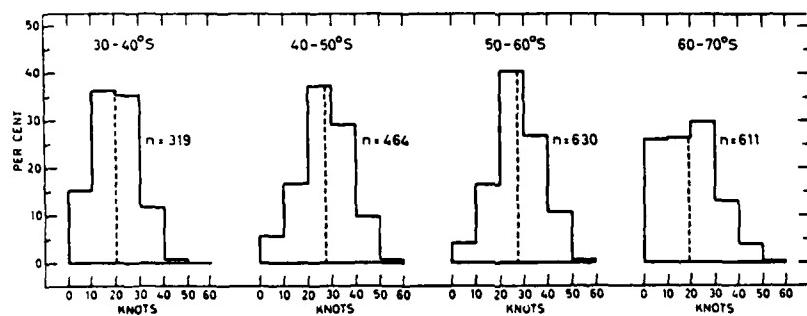


Fig. 1.25. Frequency distributions of speeds of movement (kt) of lows between  $30^{\circ}$  and  $70^{\circ}$ S, in winter 1957 and summer 1958 combined.  
(van Loon, 1967)

- Quoted from Taljaard (1972), p. 182:

It is common experience in the west-wind zones of both hemispheres that weather systems move rapidly and follow each other in quick succession during *some* periods but are slow-moving during *other* periods. Circumpolar maps show that the conditions of rapid or slow propagation of systems occasionally extend almost around a hemisphere, but normally there are distinct regions on any day where the pressure patterns favor either rapid or slow movement of the systems.

(Thus, zonal and meridional circulation indices used so extensively earlier are not ideal for describing the intensity of circulation on a hemispheric basis, but nevertheless they give useful information.)

1. Despite previous claims that blocking (of otherwise zonal west-east flow in the upper air) is rare in the Southern Hemisphere, van Loon (1956) documented its occurrence in the vicinity of Marion and Crozet Islands (SE of Southern Africa). It also occurs over the South Atlantic Ocean, although more prominently over the South Pacific Ocean.
2. For the period 1952-1958, the sea-level mean meridional index (i.e., the north-south flow) was higher in winter than in summer at  $30^{\circ}$  and  $45^{\circ}$ S, while the 500-mb mean meridional index was also found to be higher in winter at  $35^{\circ}$ S during the IGY.
3. Some data from the IGY support the likelihood of Southern Hemispheric blocks (highs) located, in the average, in lower middle latitudes, a contrast to the higher middle latitude blocks of the Northern Hemisphere.
4. The normal frequency of cut-off lows is less than one per month over the Southern African region.

## Section 2

### SOUTHERN AFRICA

(Republic of South Africa (RSA), Namibia and Botswana)

#### 2.1 TOPOGRAPHY (SCHULZE, 1972) (FIGS. 1.1, 1.2 AND 2.1)

The main topographical features of Southern Africa are an interior plateau rising from 1000 m to varying elevations below 1500 m and coastal mountains in Namibia and the Republic of South Africa (RSA). Lying approximately 300 km from the south and east coasts are the ranges collectively known as the Great Escarpment. These mountains rise to over 3000 m northeast of Lesotho. Near the Namibian coast the escarpment forms a discontinuous barrier of mountainous highlands.

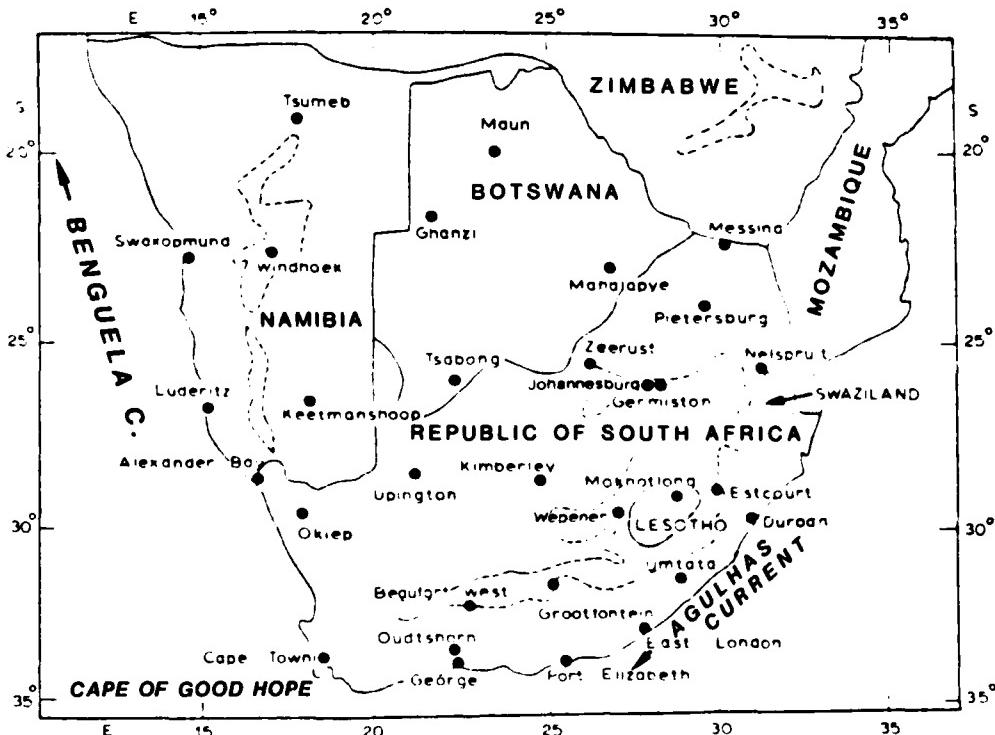


Fig. 2.1. Station Locations of Southern Africa. Continuous lines: international boundaries, broken lines: 1500 m contour. (After Schulze, 1972)

Seaward of the escarpment is the Namibian Desert to the west which transitions into the south coastal regions of the RSA. A coastal plain north of Durban broadens to the north and extends to the Mozambique border.

Inland, the extreme western portion of Lesotho (Figs. 1.1, 1.2) opens onto the highest portion of the interior plateau. This extends northward to Johannesburg. North of Johannesburg the terrain descends into northeastern RSA. Elevations in the extreme northeastern RSA are below 500 m. West of Lesotho and the northern plateau the terrain gradually descends into a semi-arid region (southeastern Botswana, north and northeastern RSA) and finally down to the lowest portion of the interior plateau, the Kalahari Desert (north central and south central Botswana, northwestern RSA). West of the Kalahari Desert the land ascends into the Namibian highlands.

## 2.2 SIGNIFICANT WEATHER SYSTEMS

The following is a discussion of typical synoptic weather patterns in the Southern African summer and winter months. In the spring (September-November) and autumn (March-May) transition periods, synoptic situations typical of either winter or summer can be expected. Winter-type synoptic patterns generally dominate from May through October although 'winter' in Southern Africa is best defined from June through August. Fig. 2.2 (Krishnamurti, 1979) shows the mean monthly surface flow over the African Continent. In winter, northerly/northwesterly flow dominates over much of the RSA interior, although again this is the *mean* flow. In summer, the rainy season over the Southern African interior, easterly flow often penetrates over the RSA interior, i.e., note the mean easterly flow depicted in January over RSA in Fig. 2.2.

In the following subsections, examples of atmospheric circulation over the continent and ocean areas are from the Republic of South Africa (RSA) Weather Bureau analyses.

It should be noted on these 'surface charts' that the pressure analysis is actually the height analysis at the 850 mb level over continental Africa. This is necessary since elevations generally exceed 1000 m over Southern Africa south of 15°S. The analysis represents sea-level pressure over the ocean areas. This bi-level analysis results in otherwise unexplained discontinuities in the analyzed pressure field over all of the Southern African coastal region.

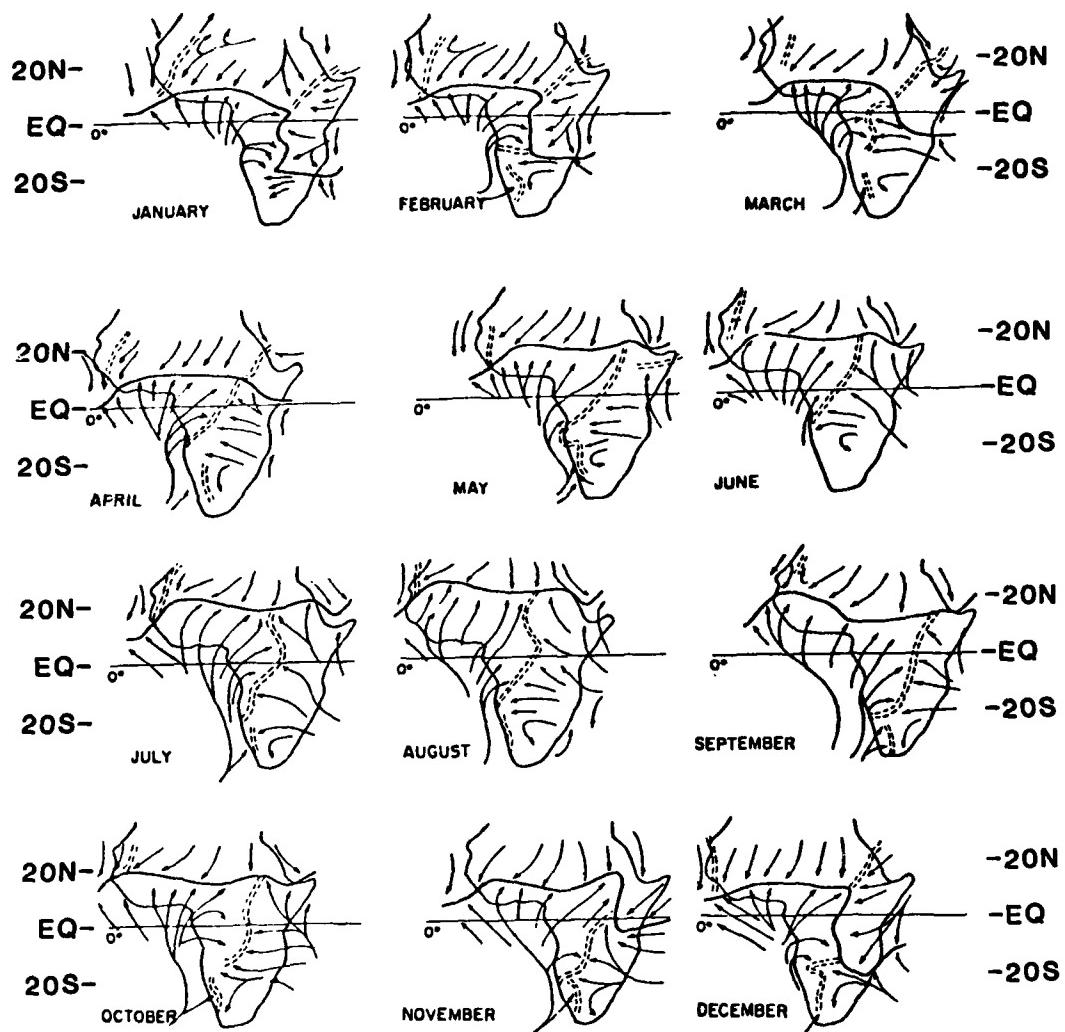


Fig. 2.2. Monthly Mean Surface Streamlines. Heavy and dashed lines indicate significant wind shear lines. (Krishnamurti, 1979)

### 2.2.1 Winter (June, July, August)

#### a. Anticyclone over Continent

The most common winter pattern is exemplified on 24 Aug 1973 (Fig. 2.3). In this situation, the circulation associated with a high cell (or two high cells as shown in Fig. 2.3) is dominating weather over all of Namibia, Botswana and the RSA. Due to subsidence the southeast coastal region and the interior experience warm, dry weather. The anticyclonic flow over the interior can persist for several days or up to two weeks.

A phenomenon frequently experienced with this pattern is the 'berg' wind. This is an abnormally hot, dry wind which flows down-slope from the interior plateau to the coast. Conditions favorable for a berg wind are: (1) strong anticyclonic circulation over the Southern African interior, and (2) approach of a trough or cold front toward the southern coastal region (southern Namibia and coastal RSA). The approach of a trough or cold front from the west or southwest enhances the pressure gradient from the interior plateau to the coastal areas (see southeast coast of RSA in Fig. 2.4). This results in strengthening of the downslope flow. The air warms adiabatically while sinking from the plateau to the coastal region and a hot dry offshore wind develops over the affected coastal areas.

Development of an intense anticyclone over the continental interior favors a strong (occasionally up to 40 kt) berg wind. The magnitude of the wind is a function of the plateau-to-coast pressure gradient, and the berg wind can continue for several days until a cold frontal passage changes the wind flow to southwesterly. This wind shift results in abrupt temperature falls in the coastal regions accompanied by fog and the development of low stratus clouds. Berg winds can also be enhanced by the presence of a migratory coastal low (as seen on Fig. 2.5; see paragraph 2.2.3.a). Berg winds are most common in winter but can occur in fall or spring. All of the Southern African coast from the central Namibian coast to extreme southern Mozambique is susceptible to berg winds.

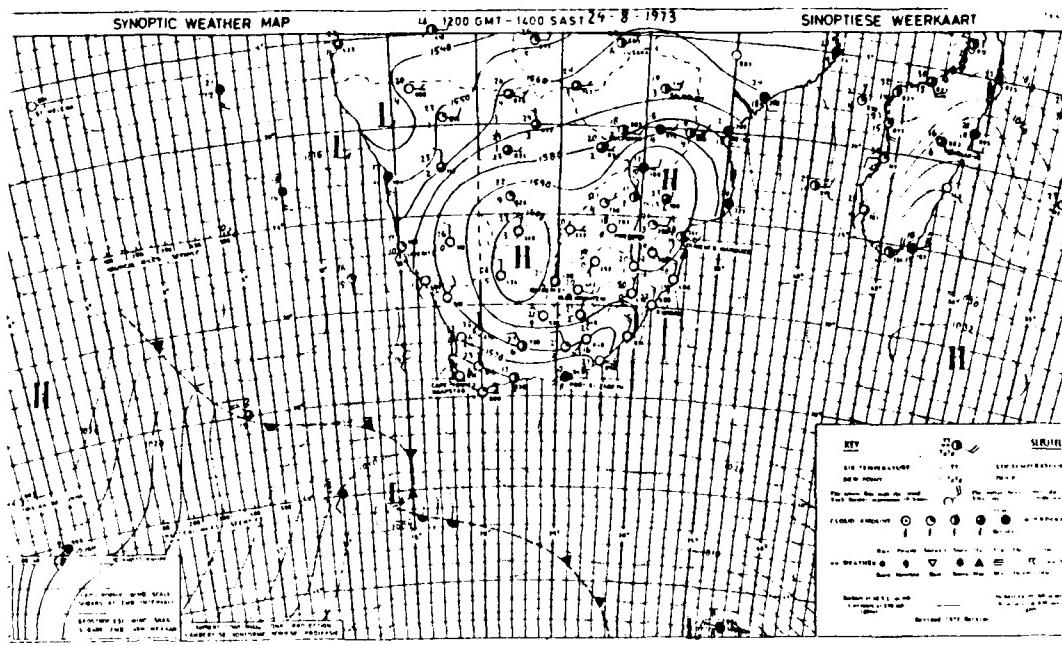


Fig. 2.3. Republic of South Africa Weather Bureau Surface (over Ocean) and 850 mb (over Continent) Analysis: 1200 GMT 24 August 1973

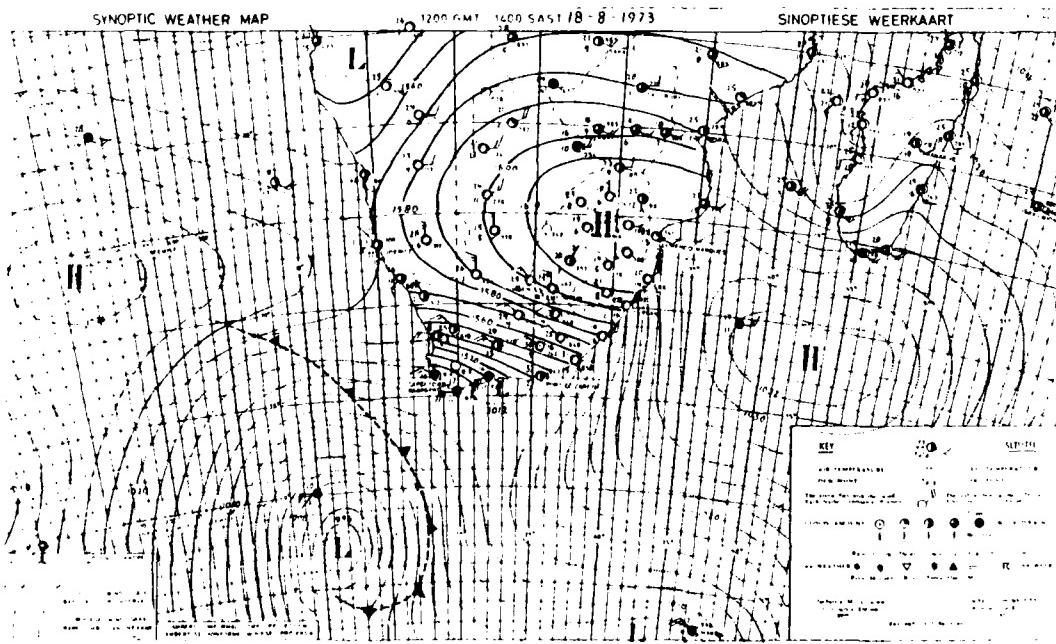


Fig. 2.4. Same as Fig. 2.3 except for 1200 GMT 18 August 1973

### b. Cold Front Penetration over RSA

Cold fronts penetrate RSA most frequently in mid-winter. Southwest of the Cape of Good Hope (Fig. 2.1), unstable frontal waves in the westerlies occasionally mature to deep frontal low pressure systems (Figs. 2.5-2.7). These systems move rapidly eastward and the centers commonly pass within ten degrees latitude of the RSA coast. Gale force north to northwesterly winds with pre-frontal rain showers are common in the southwest, south and southeast coastal areas. Rain showers are likely to follow the frontal passage over the south and southwest Cape coastal region and interior with rapid clearing from the west (Hayward and Steyn, 1967). Onshore flow present in advance of the following anticyclone is associated with orographically produced low clouds and drizzle over the east and southeast coastal regions (Schulze, 1972).

In late winter and early spring these unstable waves develop farther south. In the western and southwestern coastal regions, gale force northwesterly winds precede the arrival of the cold front. Weather associated with these late winter cold fronts does not penetrate as far north and the northerly interior of the Southern Africa region experiences clear conditions. Over the coastal waters east of the RSA (vicinity of Durban, Fig. 2.1), strong convection and occasional thunderstorm activity are observed following a cold air outbreak. An unstable situation develops when the cold maritime air behind an eastward moving cold front passes over the warm Agulhas Current (Fig. 2.1). This causes development of lines of cumulonimbus clouds and occasionally thunderstorms over the near-shore ocean waters. This is most common over the southeast coastal waters from Port St. Johns (100 miles south of Durban) to ~220 n mi northward on the RSA coast (Hayward and Steyn, 1967).

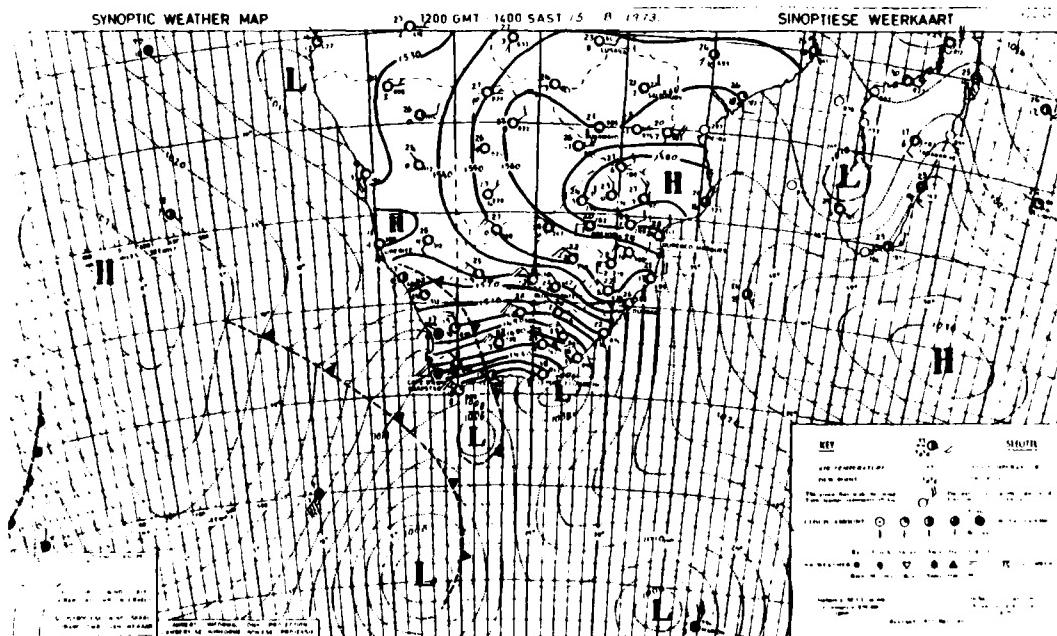


Fig. 2.5. Same as Fig. 2.3 except for 1200 GMT 15 August 1973

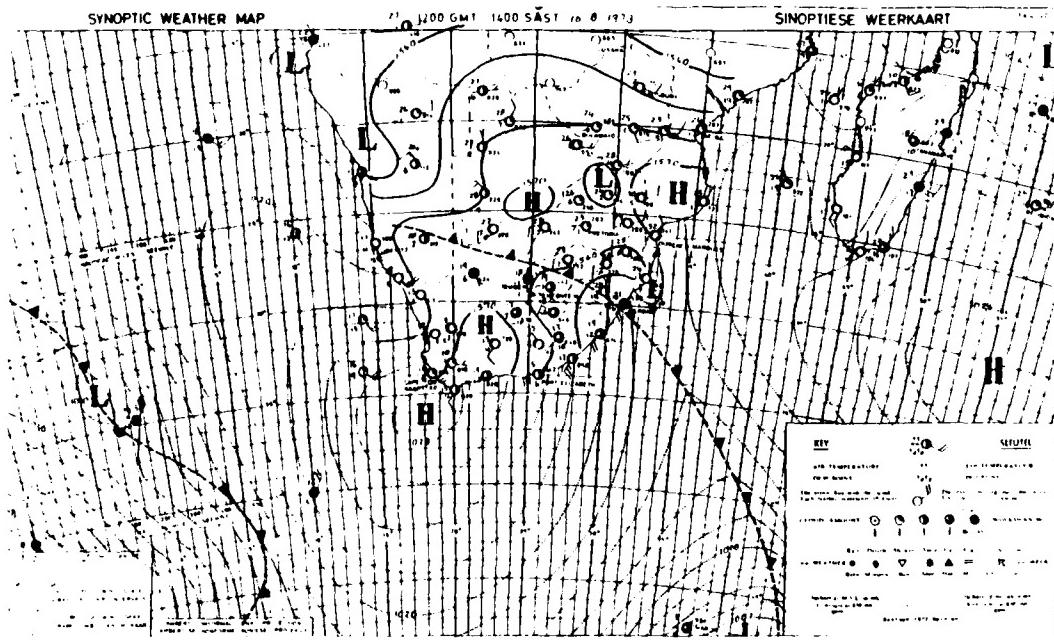


Fig. 2.6. Same as Fig. 2.3 except for 1200 GMT 16 August 1973

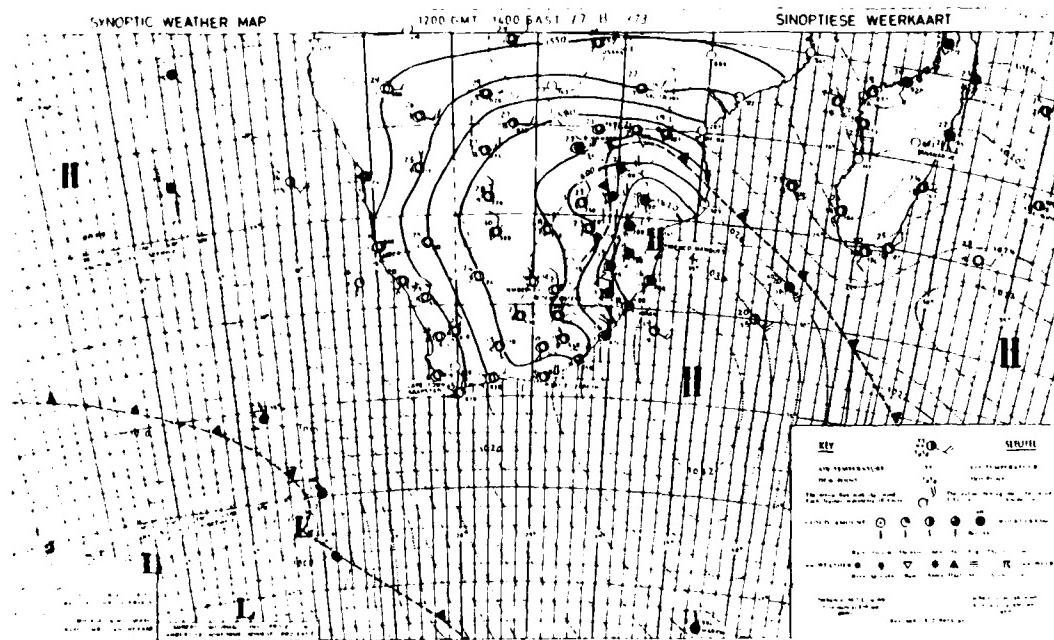


Fig. 2.7. Same as Fig. 2.3 except for 1200 GMT 17 August 1973

When cold air penetrates over the RSA interior, the upper-air (at and above 700 mb) low may become cut-off (Fig. 2.8). Northerly flow on the east side of the system brings warm moist tropical air over the RSA interior. Rainshower activity, occasionally heavy, is likely over the southeast and south RSA in this case. If a wave forms on the polar front to the southeast, strong onshore flow is likely to develop over the southeast and east RSA coast. Heavy rain shower activity occurs over the south and southeast RSA interior and coastal regions (Hayward and Steyn, 1967).

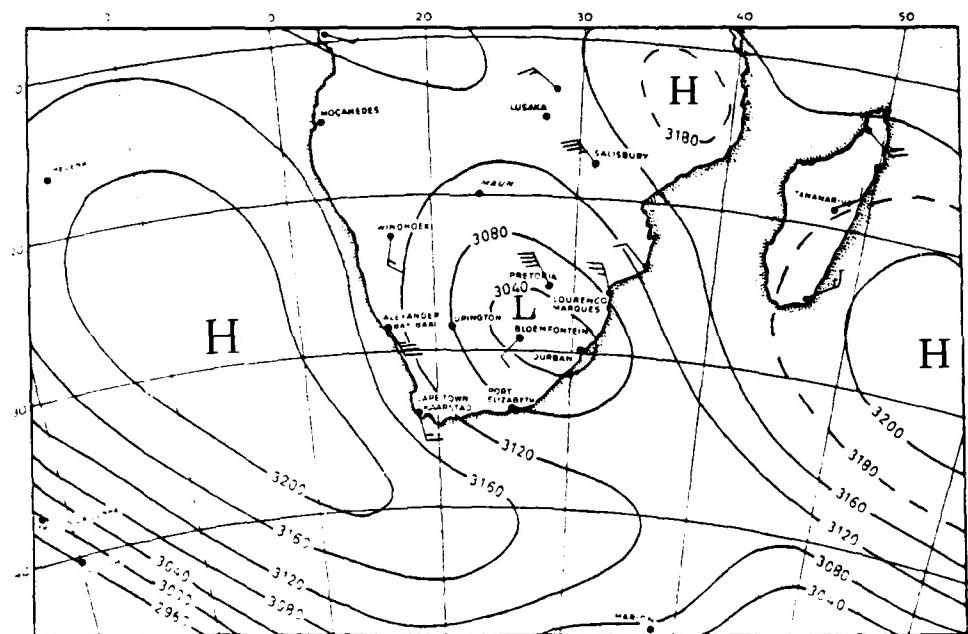
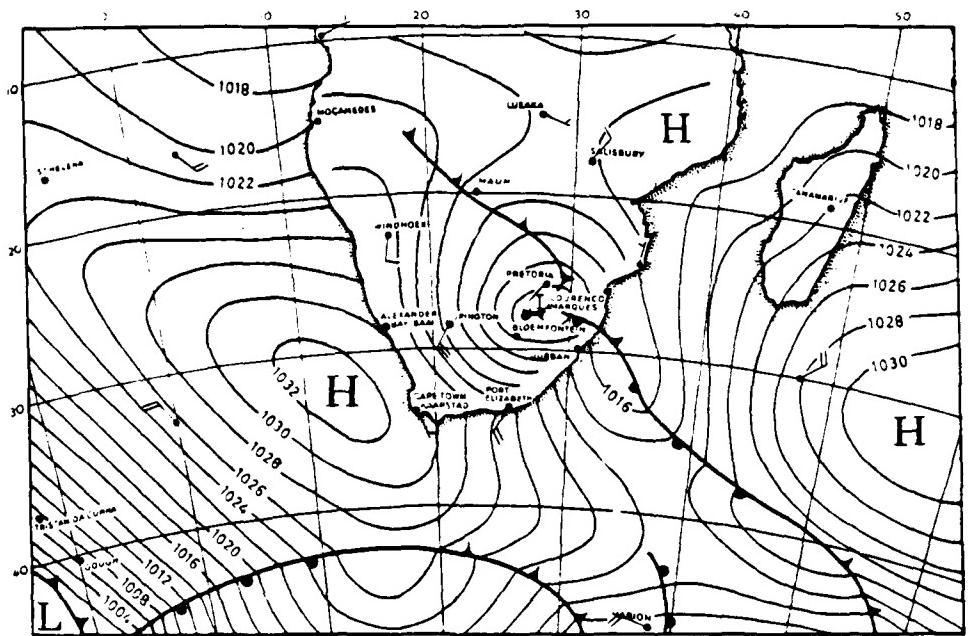


Fig. 2.8. Republic of South Africa Weather Bureau Surface and 700 mb Analyses:  
0600 GMT 18 June 1964 (Hayward and Steyn, 1967)

## 2.2.2 Summer (December, January, February)

### a. Subtropical/Tropical Trough

The most typical summer pattern is displayed in Figs. 2.9-2.11. A trough, extending southward from the low-level subtropical/tropical low over the continent, penetrates into the RSA and may remain quasi-stationary over the western interior while low-level maritime high pressure cells move around the coast. The subtropical trough over the interior frequently persists for a week, and occasionally up to two weeks. Warm moist air from the tropical Indian Ocean penetrates into the RSA interior when this synoptic pattern dominates. Such flow is often associated with high instability and thunderstorm activity over the central and northeast RSA. Continuous, heavy rain shower activity occurs over the northeastern RSA due to orographic lifting and convergence. Occasionally, a tropical low center develops in the trough over central Africa (northern Botswana, Zambia, southern Zaire). Interaction between this weather system and temperate troughs passing south of the RSA is associated with the development of cloud bands and convective rain shower activity over the RSA interior. Harangozo and Harrison (1983) have found that coupling (or co-existence) of tropical lows (over the continent) with midlatitude troughs appears to be a necessary condition for cloud band formation (i.e., rainy conditions) over Southern Africa. Drier conditions exist on the continent when continental tropical low centers are farther eastward and northward, i.e., more distant from the midlatitude trough to the south. Additionally, applying the Walker circulation and Southern Oscillation (not discussed here), Harrison (1983) has proposed that:

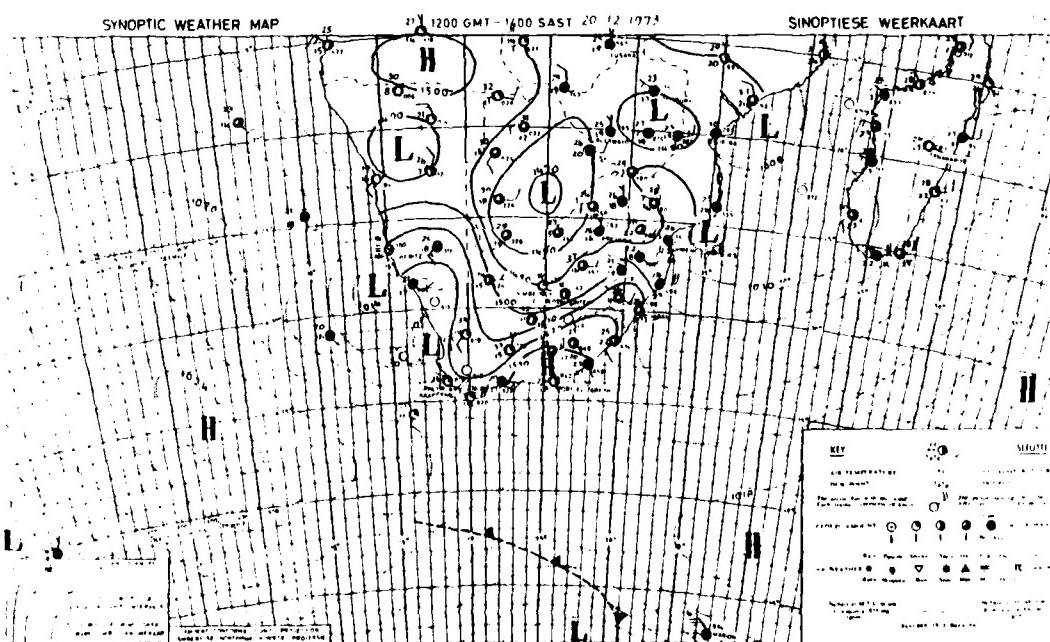


Fig. 2.9. Same as Fig. 2.3 except for 1200 GMT 20 December 1973

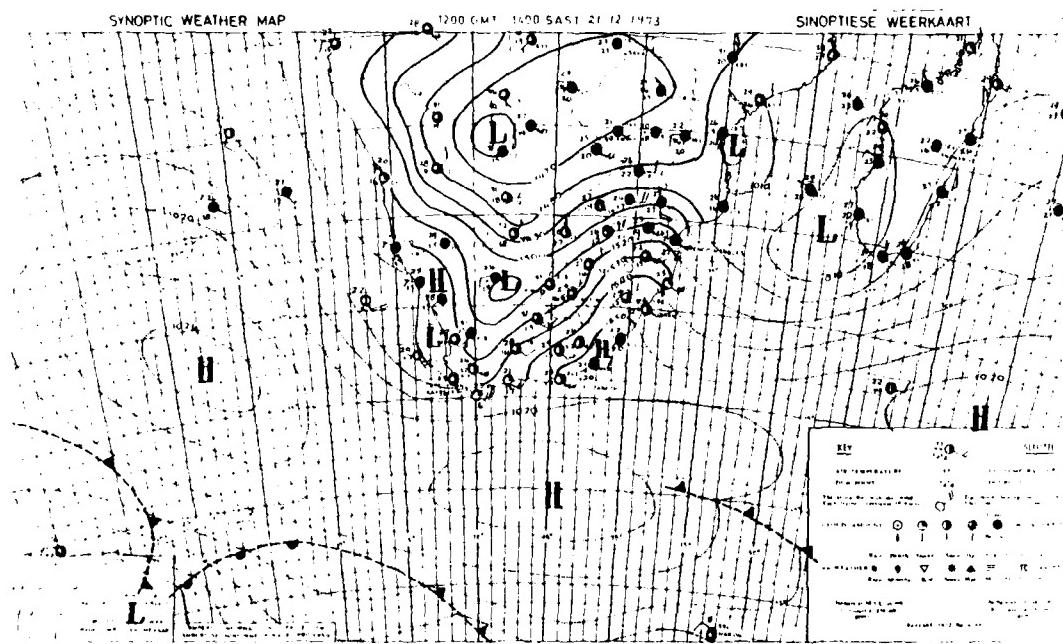


Fig. 2.10. Same as Fig. 2.3 except for 1200 GMT 21 December 1973

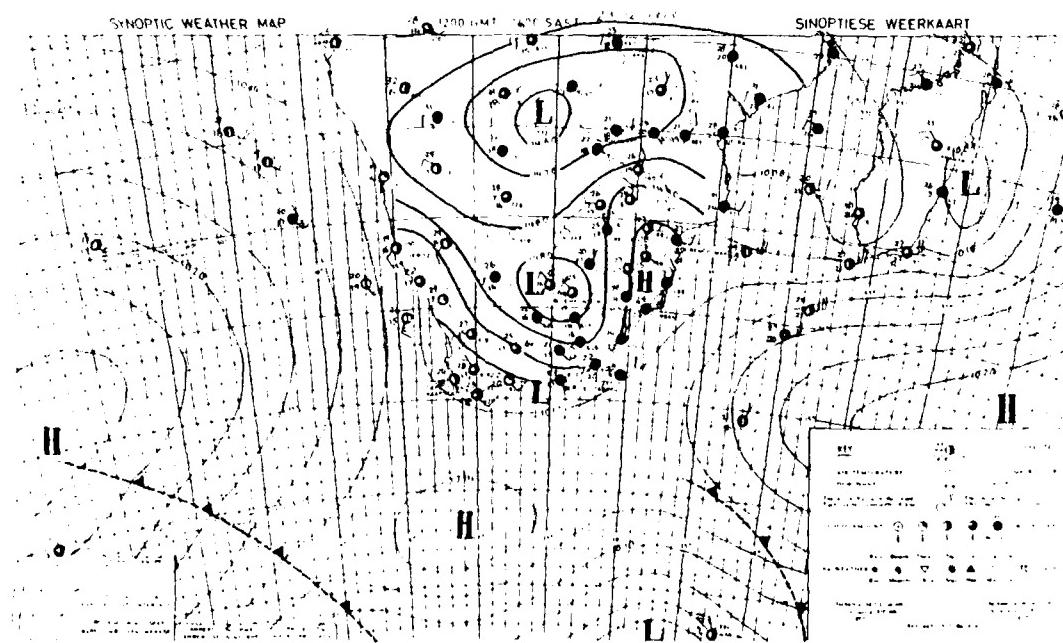


Fig. 2.11. Same as Fig. 2.3 except for 1200 GMT 23 December 1973

1. Increased 200-mb easterlies over Zimbabwe are associated with increased surface low (vortex) formation and increased rainfall over South Africa, while
2. weaker 200-mb easterlies over Zimbabwe indicate a shift of the cloud bands toward the Malagasy Republic with drier conditions in South Africa.

With the existence of a tropical low over the RSA interior, the remaining portions of the regional (northern Namibia and Botswana, and the southwest RSA) interior and coastal areas experience hot, humid weather but little rainfall. Strong winds (up to gale force) develop over the southwest coastal area with this pattern if the trough over Southern Africa deepens or if a strong anticyclone approaches from the southwest.

A wind phenomenon referred to as the 'black southeaster' can develop when a well-defined low pressure center is present over south or southwest RSA with an anticyclone off the south RSA coast. However, over the Cape Peninsula (vicinity of Cape Town, Fig. 2.1) this wind is occasionally *southwesterly*. The wind is normally southeast or east-southeast and affects the RSA south coast from the region surrounding Cape Town to east of Port Elizabeth. The onshore flow undergoes orographic lifting, and low cloud decks and light rain develop over the affected coastal region. Flying conditions are very poor. The strength of the wind depends on the intensities of the low pressure center and anticyclone. The wind and associated weather can last up to several days.<sup>3</sup>

---

<sup>3</sup> Quoted from Taljaard (1984):

The black southeaster is developed at best when an upper cut-off, or cold pool, is located over the western Cape Province (the Cape Province includes the western half of the RSA) or slightly off the west coast. If the cut-off is located further to the east, but still over the land (as in Fig. 2.12), the area southwest of the characteristic coastal pressure minimum gets the onshore blast and the heavy rain even though this would then happen along the southeast coast (Port Elizabeth to Durban). The situation is then absolutely similar to the black southeaster of the south coast...Cut-off lows are least frequent in midwinter and midsummer...

Taljaard added that the 700-mb pattern of the cut-off low in Fig. 2.8 for winter is similar to that developing aloft over the black southeaster during the summer.

*Fairweather* southeasterly flow also occurs in summer and should not be confused with the black southeaster. Southeasterly flow is typical over the RSA southern coastal areas when an anticyclone, present to the southwest or south, dominates the regional weather (Fig. 2.13). Stable subsiding flow occurs in this case. Fine weather with some orographic cloud development is typical of this type of flow, yet the wind is often strong, averaging between 16 and 30 kt over 30% of the time and lasting as long as several days. Note that Port Elizabeth is almost clear in Fig. 2.13 contrasted with its overcast condition in Fig. 2.12.

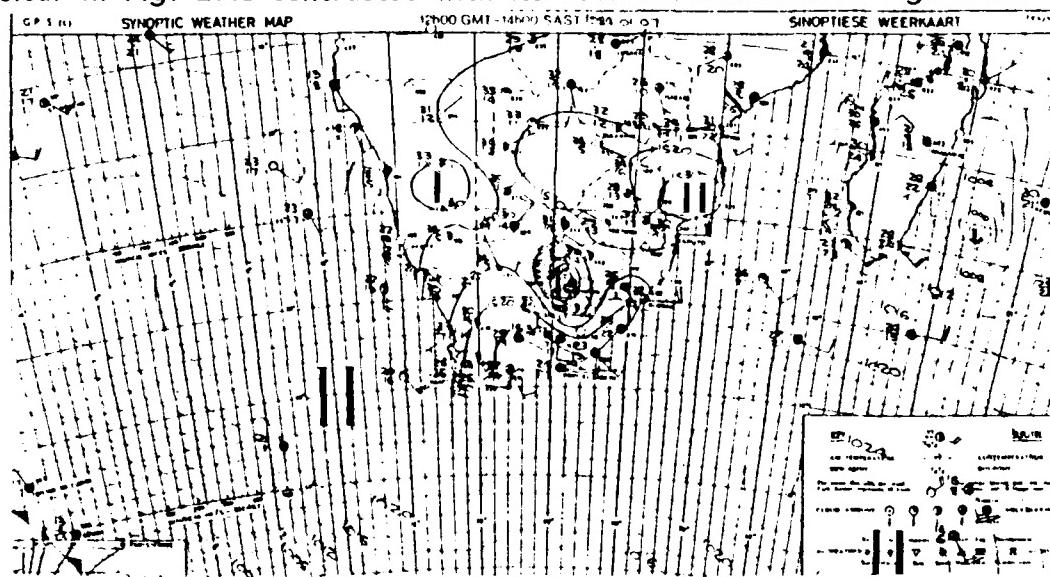


Fig. 2.12. Same as Fig. 2.3 except for 1200 GMT 7 January 1984

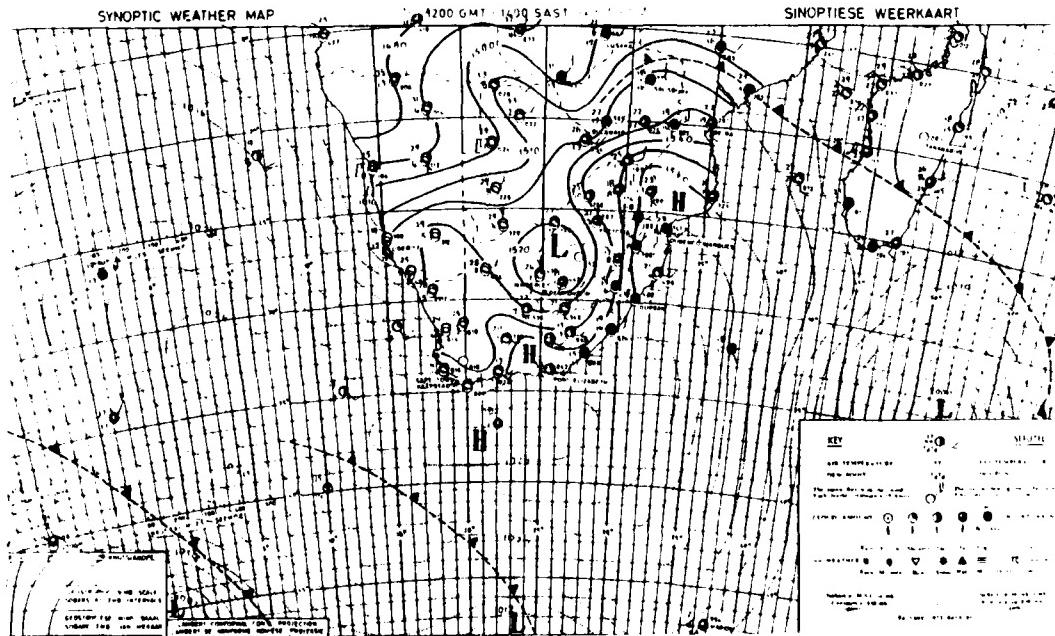


Fig. 2.13. Same as Fig. 2.3 except for 1200 GMT 12 November 1973

b. Cut-off Low

In summer, wave disturbances in the westerlies may develop into cut-off low centers over the southwest RSA (Fig. 2.14). The flow on the east side of the system brings warm moist tropical air over the nation's interior. Orographic lifting and convergence of this cyclonic flow is associated with heavy rain shower activity over most of the RSA. Along the eastern RSA coast rain shower activity occurs frequently in this pattern. Summer cut-off lows over the RSA last for approximately two to three days (Hayward and Steyn, 1967).

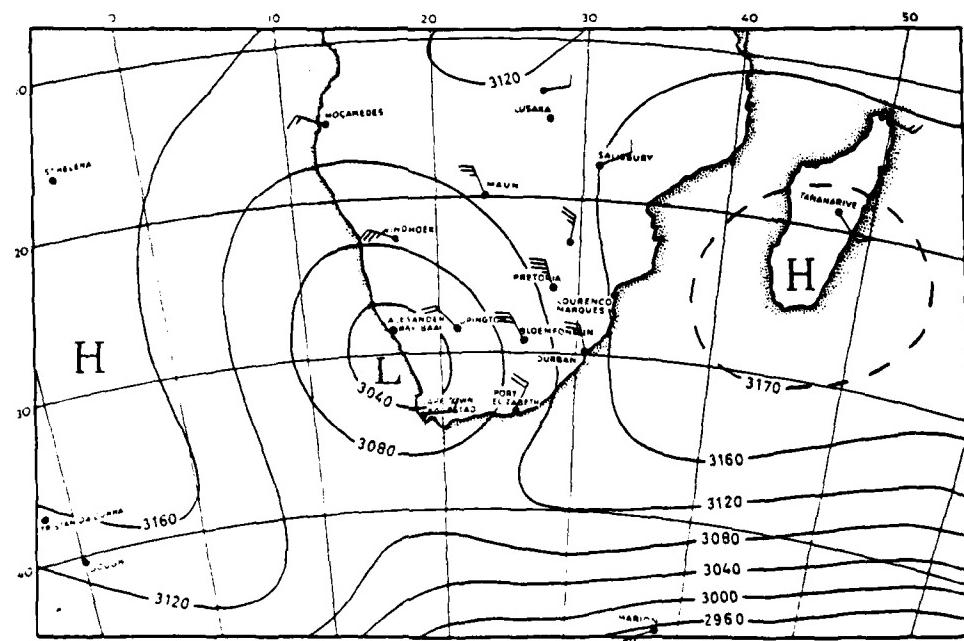
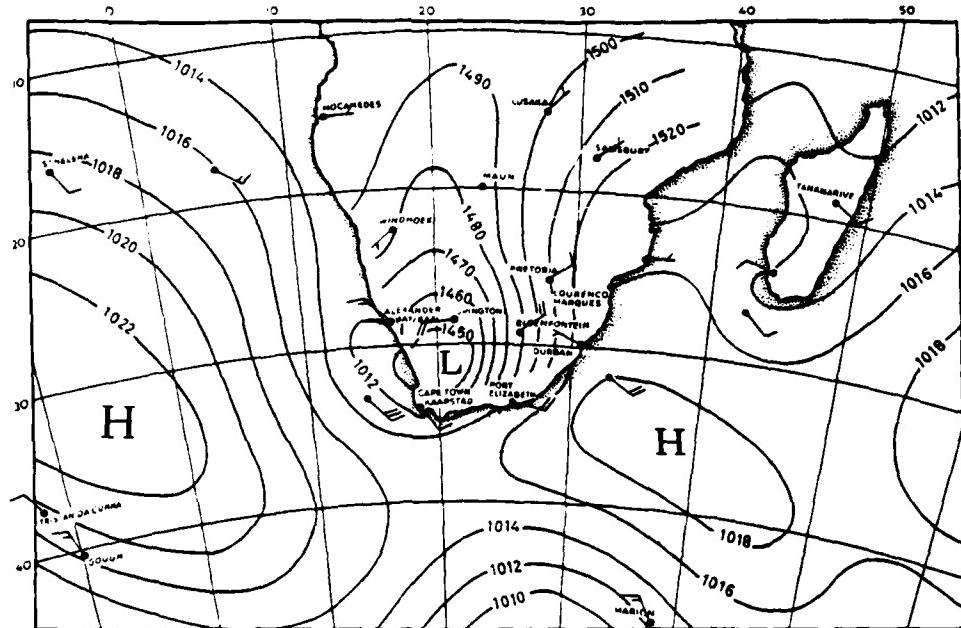


Fig. 2.14. Republic of South Africa Weather Bureau Surface and 700 mb Analyses: 0600 GMT 19 December 1960 (Hayward and Steyn, 1967)

### c. High Cell over Southern Africa

The development of anticyclonic flow over the Southern African interior (Figs. 2.15-2.17) occurs occasionally during the summer months. This produces hot, dry weather and drought conditions over most of the region (Namibia, Botswana and RSA). Cloud development in the coastal regions and interior is severely suppressed as is thunderstorm development even in the mountainous RSA interior. However, in this sequence the southeasterly flow is bringing rain to northeastern RSA in Fig. 2.15 and the cyclonic flow, centered over Angola, is bringing isolated showers to northern Botswana in Fig. 2.16.

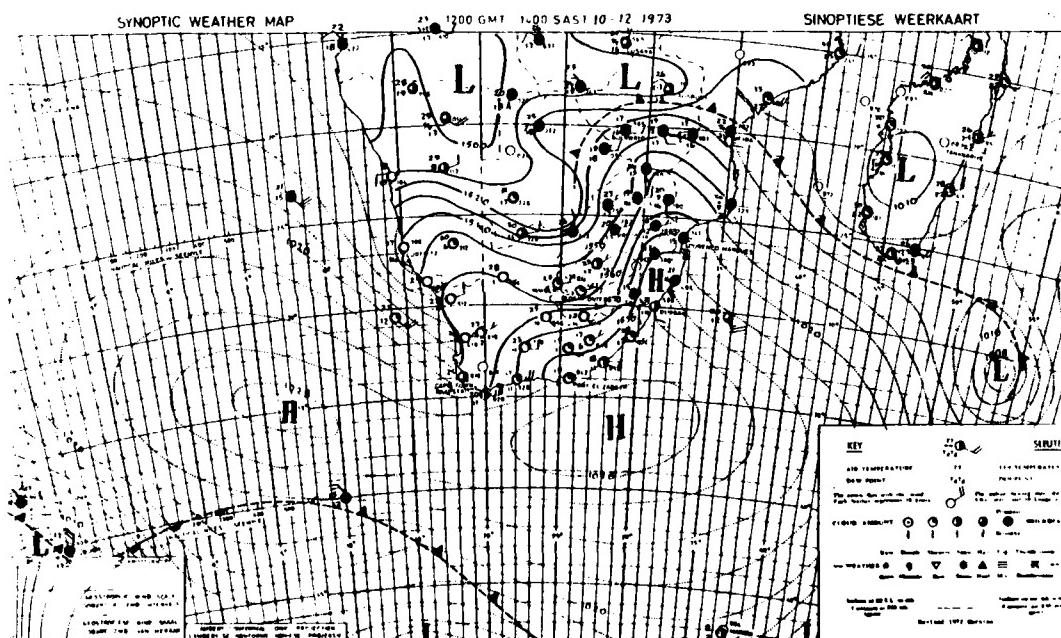


Fig. 2.15. Same as Fig. 2.3 except for 1200 GMT 10 December 1973

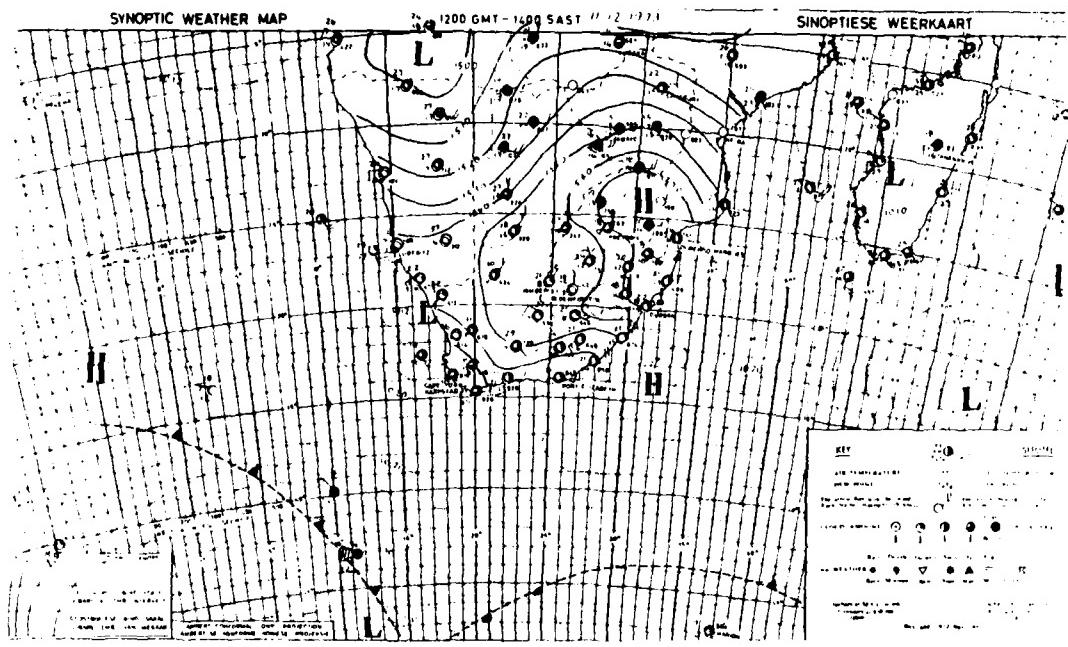


Fig. 2.16. Same as Fig. 2.3 except for 1200 GMT 11 December 1973

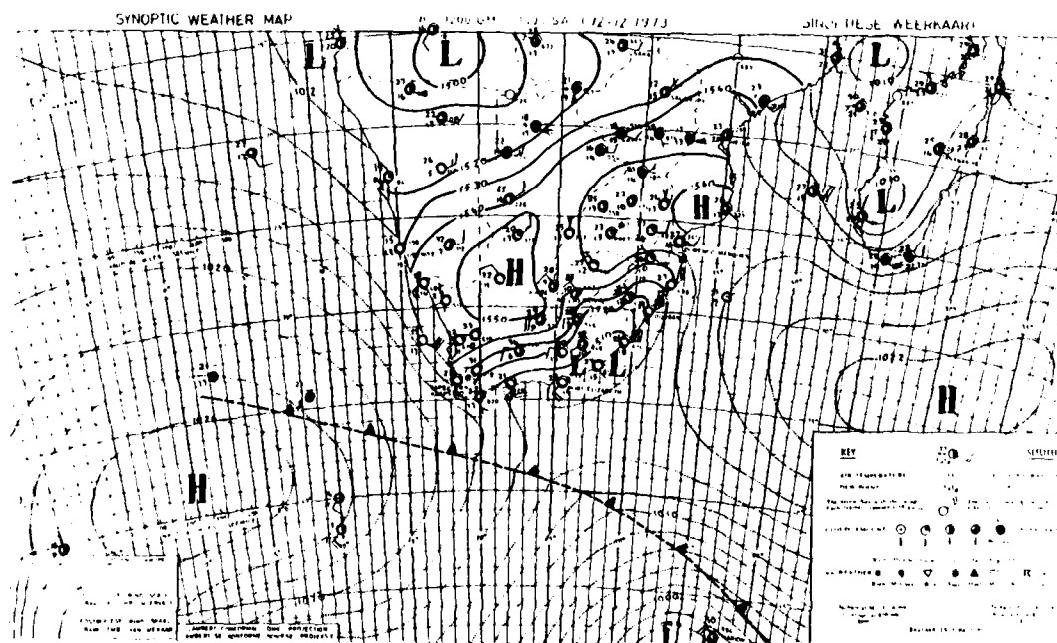


Fig. 2.17. Same as Fig. 2.3 except for 1200 GMT 12 December 1973

### 2.2.3 All Seasons

#### a. Migratory Coastal Low

Frequently, low pressure centers develop over the Southern African coastal regions when an oceanic trough or cold front approaches from the west or southwest (Figs. 2.18-2.20). These pressure minima are termed coastal lows and move from north to south on the western coasts (Namibia, west coastal RSA) and northeast along the southeast coast of RSA in advance of an approaching midlatitude trough or cold front. Uncertainty exists as to whether or not these systems are all closed low centers (Hayward and Steyn, 1967). Strong (25 kt, occasionally 35 kt) offshore 'berg' winds often precede the coastal low in spring, winter and autumn (see Paragraph 2.2.1.a). Following the low, a strong onshore flow often develops. Such flow is generally west to southwest on the Namibian and southwest RSA coasts. These onshore winds are frequently strong (20 kt, sometimes greater) on the south and southeast RSA coasts. On the Namibian and southwest and south RSA coasts, such wind is often associated with rapid development of low clouds or fog. The temperature falls significantly when the berg winds are replaced with onshore flow (Hayward and Steyn, 1967). Occasionally, these lows are accompanied by intense squall line activity over the southeast coastal waters.

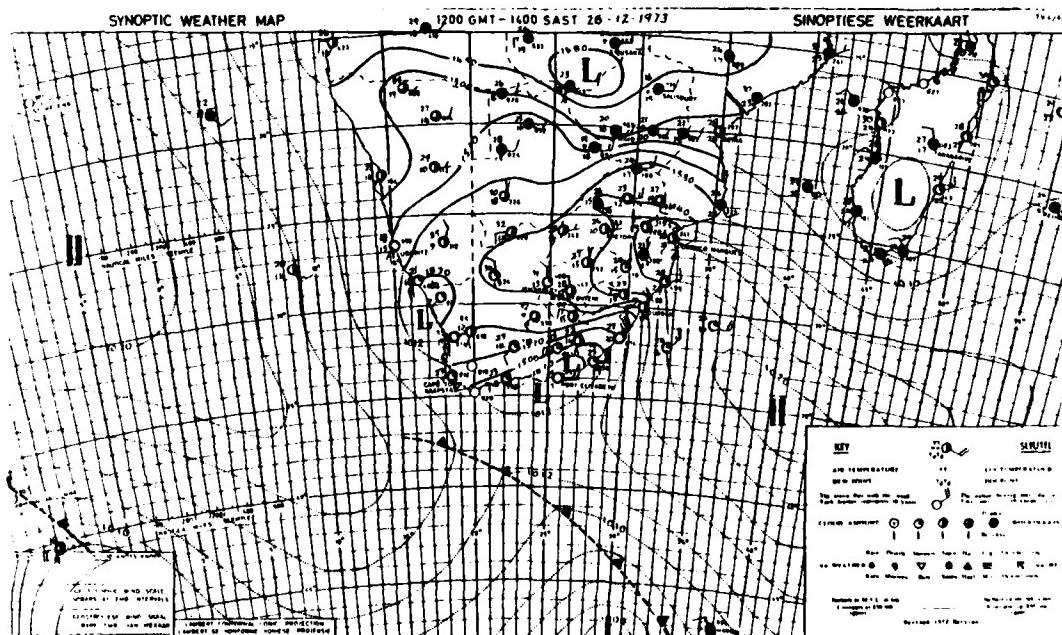


Fig. 2.18. Same as Fig. 2.3 except for 1200 GMT 28 December 1973

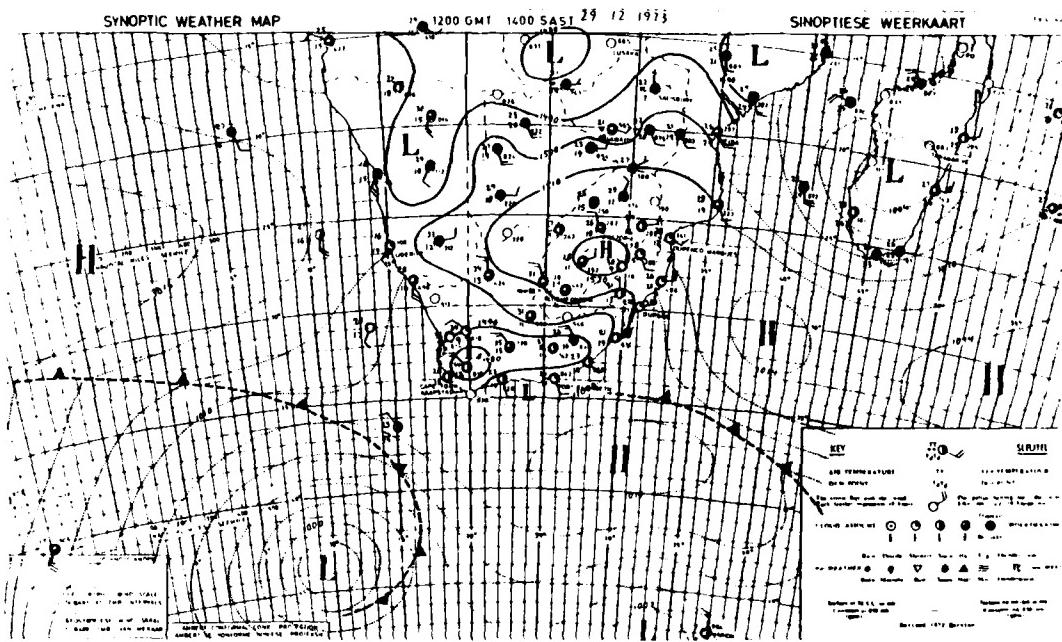


Fig. 2.19. Same as Fig. 2.3 except for 1200 GMT 29 December 1973

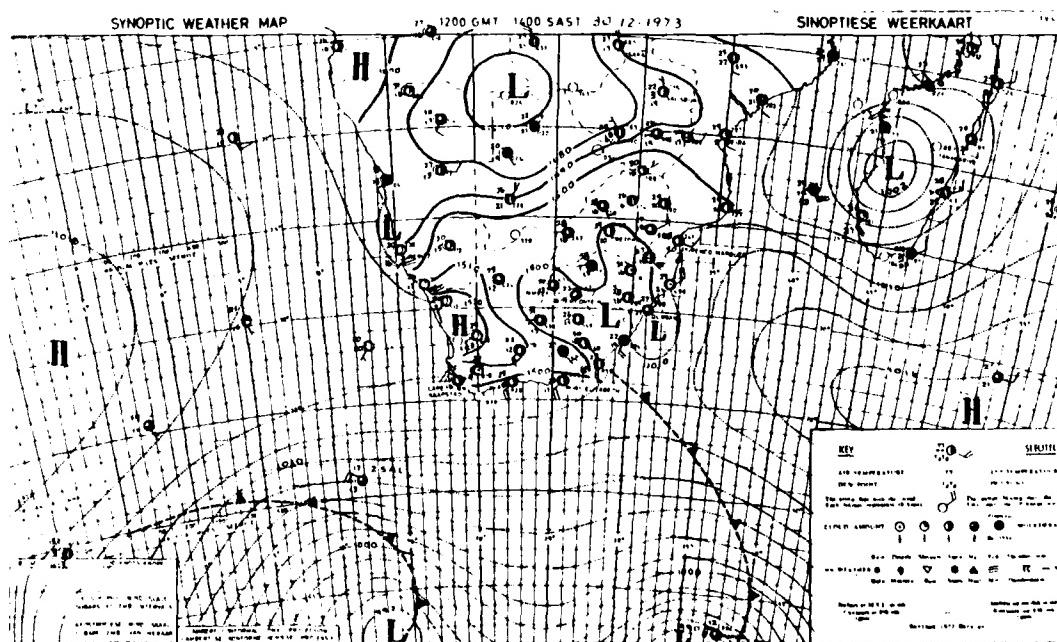


Fig. 2.20. Same as Fig. 2.3 except for 1200 GMT 30 December 1973

## 2.3 SPECIAL PARAMETERS

### 2.1 Fog

Fog occurs most frequently in Southern Africa on the Namibian coast and on the west and southwest coasts of the RSA (Figs. 2.21 - 2.24) (Naval Weather Service, 1978). Fig. 2.24 shows a maximum of 10% in mean monthly frequency of fog occurrence just north of the Cape of Good Hope near 32°S in April. This maximum is supported by the statement that fog occurs most often on the west coast near the Cape of Good Hope from March through July (Hayward and Steyn, 1967). (However, the lower percentages of fog near the Cape in July (Fig. 2.21) is not in agreement with this statement of Hayward and Steyn that fog occurs often in July.) The maxima of 20% on the southern coast of Namibia (near 28°S) in summer (Fig. 2.23) is supported by the statement of Hoflich (1984) that the probability of fog is high predominantly along the *south* coast of Namibia in *summer*. Hoflich continues that the probability of fog is high along the *north* coast of Namibia in *winter*. Indeed, this claim by Hoflich is given credence by the greater cloudiness just offshore of northern Namibia during the winter (near 20°S) depicted in Fig. 1.15 C. Most fog on the west coast of Southern Africa is of the advective type. Warm moist air from the northwest or north moves southeastward over the cold Benguela Current (see Fig. 2.1). The low-level air is cooled and condenses into fog, not unlike occurrences on the west coast of the United States where fog is predominant in the summer, although often present during the late spring and early fall as well. These advection fogs are likely to occur when northwesterly flow is present over the west coastal region (Namibia and RSA west coast). Such flow is generally present behind migrating coastal low centers (see paragraph 2.2.3.a).

On the *south* RSA coast in the vicinity of Port Elizabeth, fog occurs only occasionally. Fog is most likely when light easterly flow brings warm moist air over land. This occurs most frequently in late summer. Such fogs occur at night and seldom extend beyond the mid-morning hours. Fog on the *southeast* RSA coast occurs seldom and is a local phenomenon. Typically, fog over this region occurs when easterly winds advect moist air over the cool land surface. Flow in the forward portions of migrating anticyclones passing east and southeast of the RSA is onshore (*southeasterly*). This occasionally results in development of coastal fog and low stratus. Coastal fog also develops occasionally following passage of coastal low centers. Fog on the southeast coast, though infrequent, is observed most often in late summer during night time hours and seldom lasts beyond mid-morning (Hayward and Steyn, 1967).

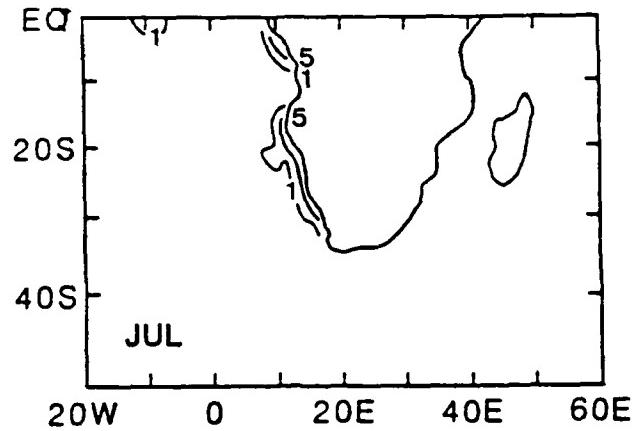


Fig. 2.21. Mean Monthly Frequency of Fog Occurrence (%): July (Naval Weather Service, 1978)

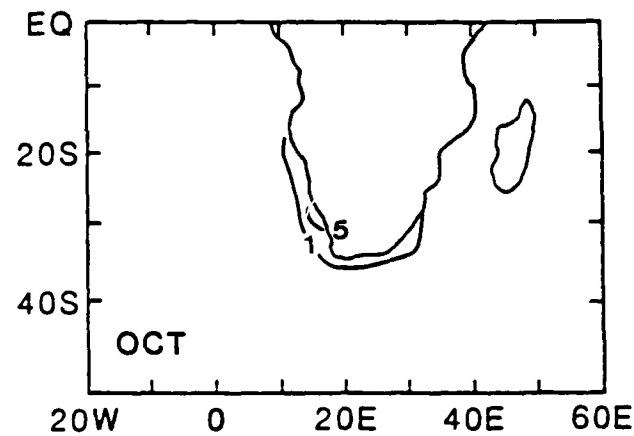


Fig. 2.22. Mean Monthly Frequency of Fog Occurrence (%): October (Naval Weather Service, 1978)

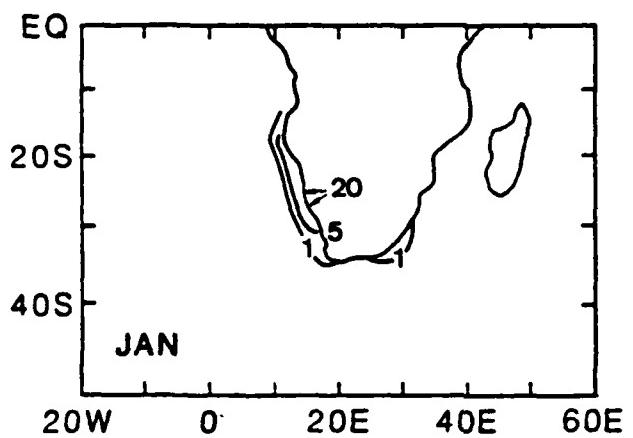


Fig. 2.23. Mean Monthly Frequency of Fog Occurrence (%): January (Naval Weather Service, 1978)

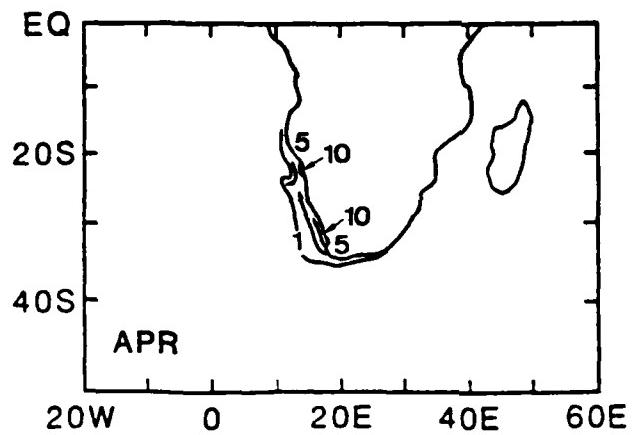


Fig. 2.24. Mean Monthly Frequency of Fog Occurrence (%): April (Naval Weather Service, 1978)

### 2.3.2 Thunderstorms

The thunderstorm 'season' in the Southern African interior is from November through April. The highest frequency of occurrence is in January and February when deep easterlies are established over the interior. In November, low-level easterlies become established over Southern Africa while well defined westerly flow is still present aloft (500 mb). The flow of cold, dry westerly air over the warm, moist easterlies creates high instability over the RSA interior, central and southern Botswana and central and southeast Namibia. Thunderstorms in November frequently produce hail. This suggests that these storms may be more severe than those occurring in later months. Thunderstorm activity is most frequent over the northeastern and central RSA (Fig. 2.25) and may be accompanied by hail (Fig. 2.26) (Schulze, 1972).

Thunderstorm activity over Southern Africa coastal waters is rare. The maximum frequency of occurrence is on the northeast coast of the RSA, during the months of March and April. The interior convection is most likely to build toward the coastal regions during these months. Thunderstorm activity over the western coastal waters is virtually non-existent. Over most of the coastal region, particularly the northeast RSA coast, thunderstorm activity is greatest in March and April when convection from the interior most likely extends to the ocean.

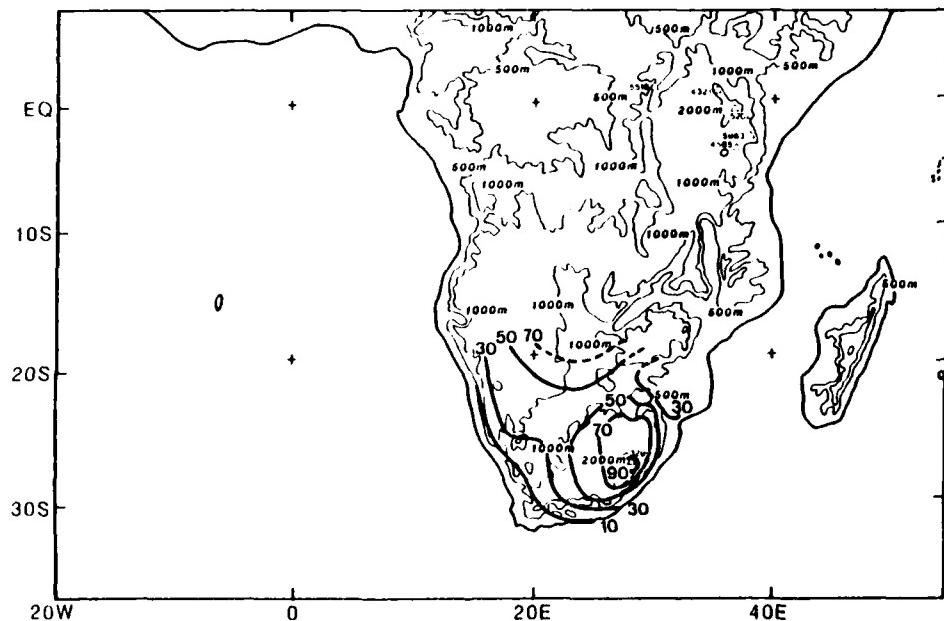


Fig. 2.25. Average Annual Number of Days with Thunder (After Schulze, 1972)

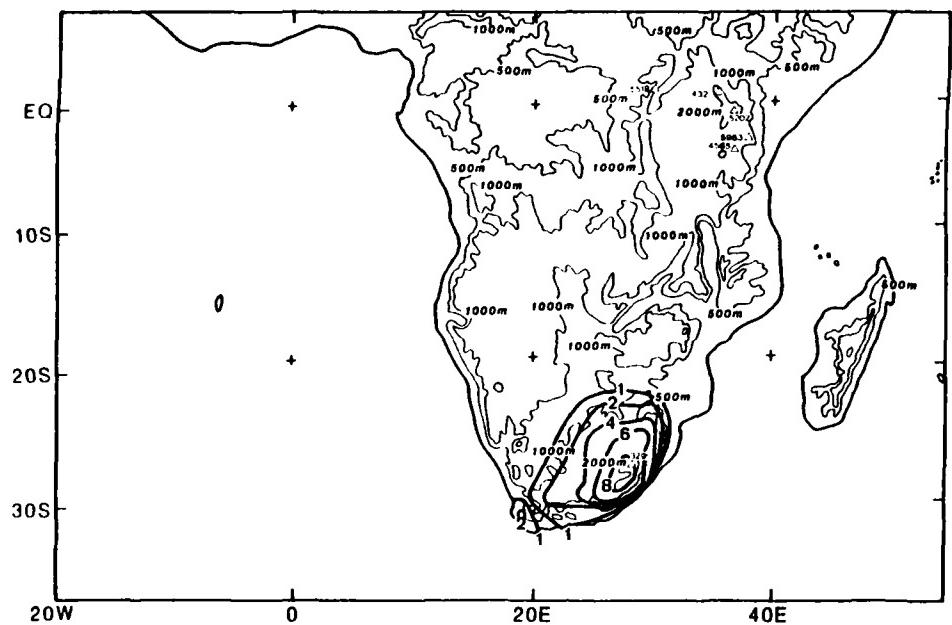


Fig. 2.26. Average Annual Number of Days with Hail (After Schulze, 1972)

#### 2.4 UPPER-LEVEL WINDS AND TURBULENCE

Upper-level winds\* over Southern Africa have significant seasonal variation. Figs. 2.27 and 2.28 show the mean 200 mb wind fields over Southern Africa for the months of January and July respectively (Dean, 1972). South of 25°S, flow is nearly always westerly. During the months of November through March anticyclonic circulation over central Namibia dominates the flow. The resulting flow over northern and central Namibia and Botswana and the northeastern RSA is weak and variable, occasionally easterly. Flow aloft over all of Southern Africa is generally westerly from May through September (October and April are transition periods). Strong flow occurs from June through September,

\* Figs. 2.27 - 2.32 from Dean (1972) present mean upper-air parameters from monthly climatic data for the year, 1970, as being typical of the large-scale structure of systems over Africa. The user must realize that not only will deviations occur from these patterns in different years, but individual, daily wind magnitudes will often exceed these mean values.

due to northward penetration of the polar front during these months.<sup>5</sup> Mean winds of 60-70 kt dominate at the upper (200-300 mb) levels over the southern RSA in winter. Penetration of mid-latitude storms into Southern Africa frequently results in the northward movement of the jet stream over the continent. Upper-level winds frequently develop strong components from the southwest. This is particularly the case with a winter deep low penetration. Jet stream winds flow across the northern portions of these surface disturbances as they move across the southern interior. Clear air turbulence is likely north of these deep surface lows in association with the jet stream. Jet stream activity and clear air turbulence also occur in association with cut-off low centers (summer and winter).

The 500 mb flow (mean) over Southern Africa is westerly south of 25°S during the entire year (Figs. 2.29, 2.30). The westerlies become strongest in winter (40-50 kt). In summer, the westerlies weaken significantly to 10 kt over the southern African interior and 30 kt over the southern RSA in connection with an anticyclone over Namibia. Between summer and the following winter, the anticyclone migrates northward to northern Namibia/southern Angola.

Figs. 2.31 and 2.32 show the mean flow at 700 mb over Southern Africa in January and July. In summer, anticyclonic flow is present over central Namibia, Botswana and the northeast RSA. Weak (5-15 kt) northwesterly flow is present over the southern Namibian coast, increasing to 20 kt over the southern RSA. In winter (July), the anticyclone is displaced northward over northern Botswana and west-northwesterly flow (10-30 kt) dominates virtually all of the RSA.

---

<sup>5</sup> Taljaard (1984) states:

This condition is not simply due to northward penetration of the polar front in winter, but to...the intensification and broadening of the belt of upper westerlies in winter.

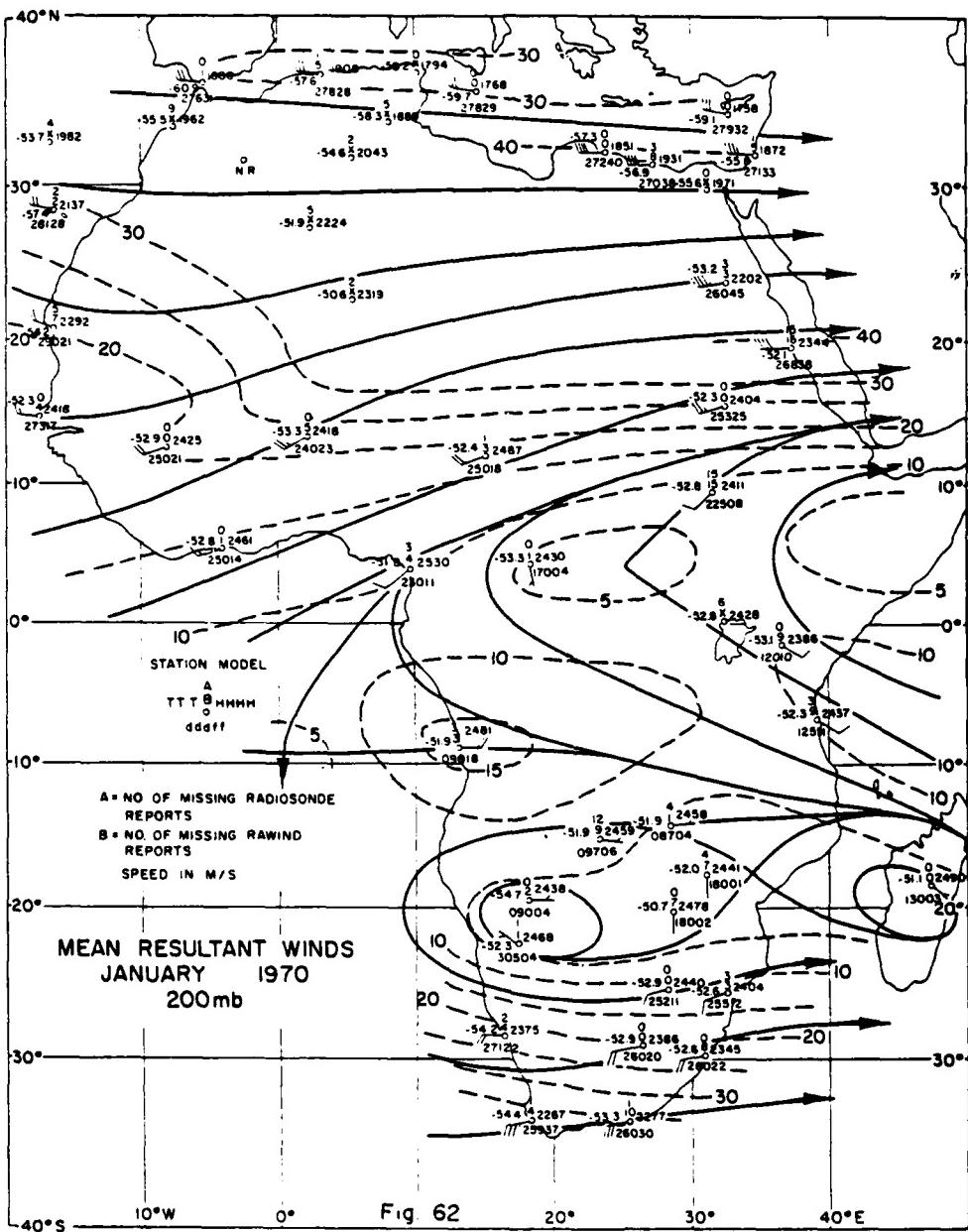


Fig. 2.27. Mean 200 mb Flow over the African Continent: January (Dean, 1972)

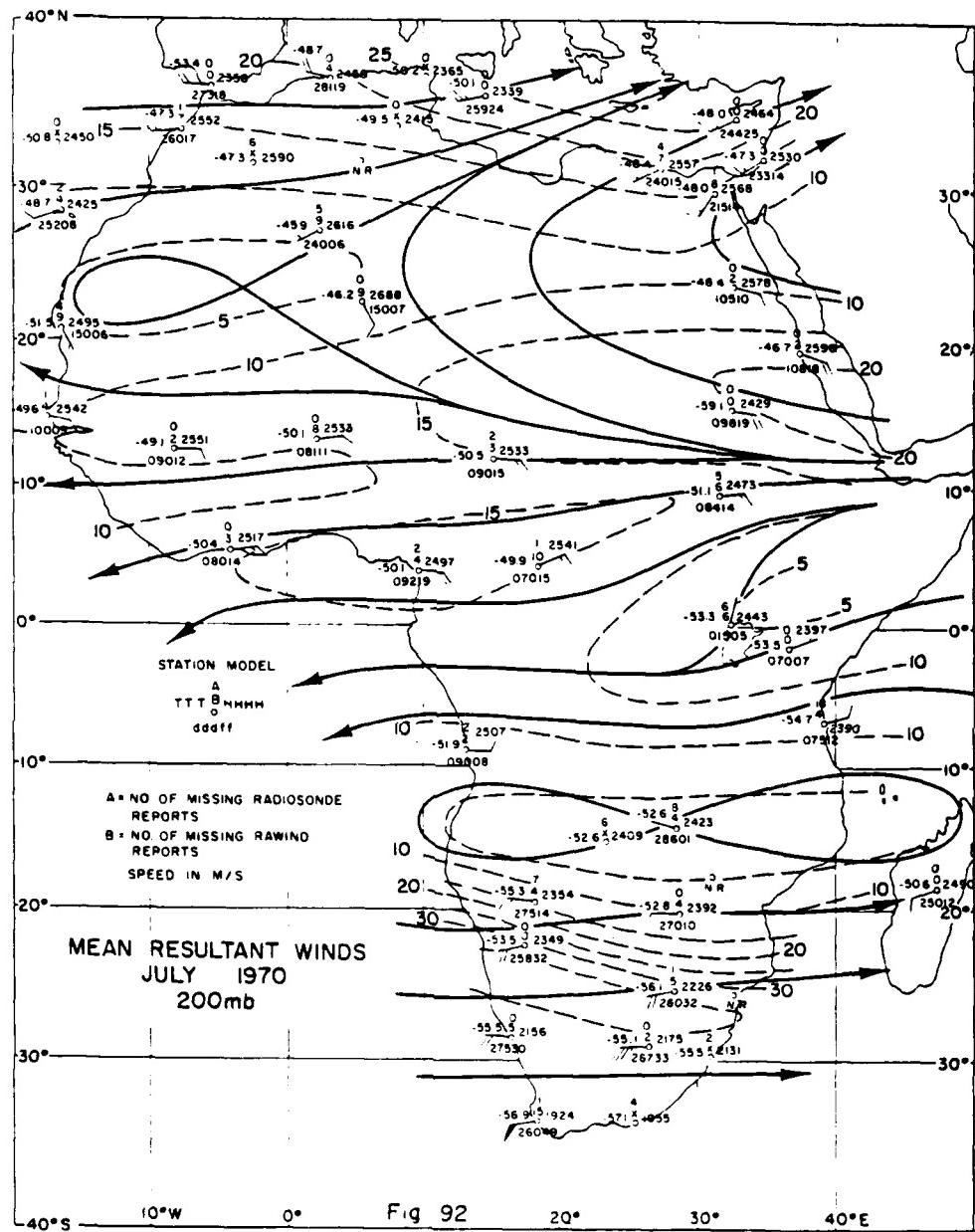


Fig. 2.28. Mean 200 mb Flow over the African Continent: July (Dean, 1972)

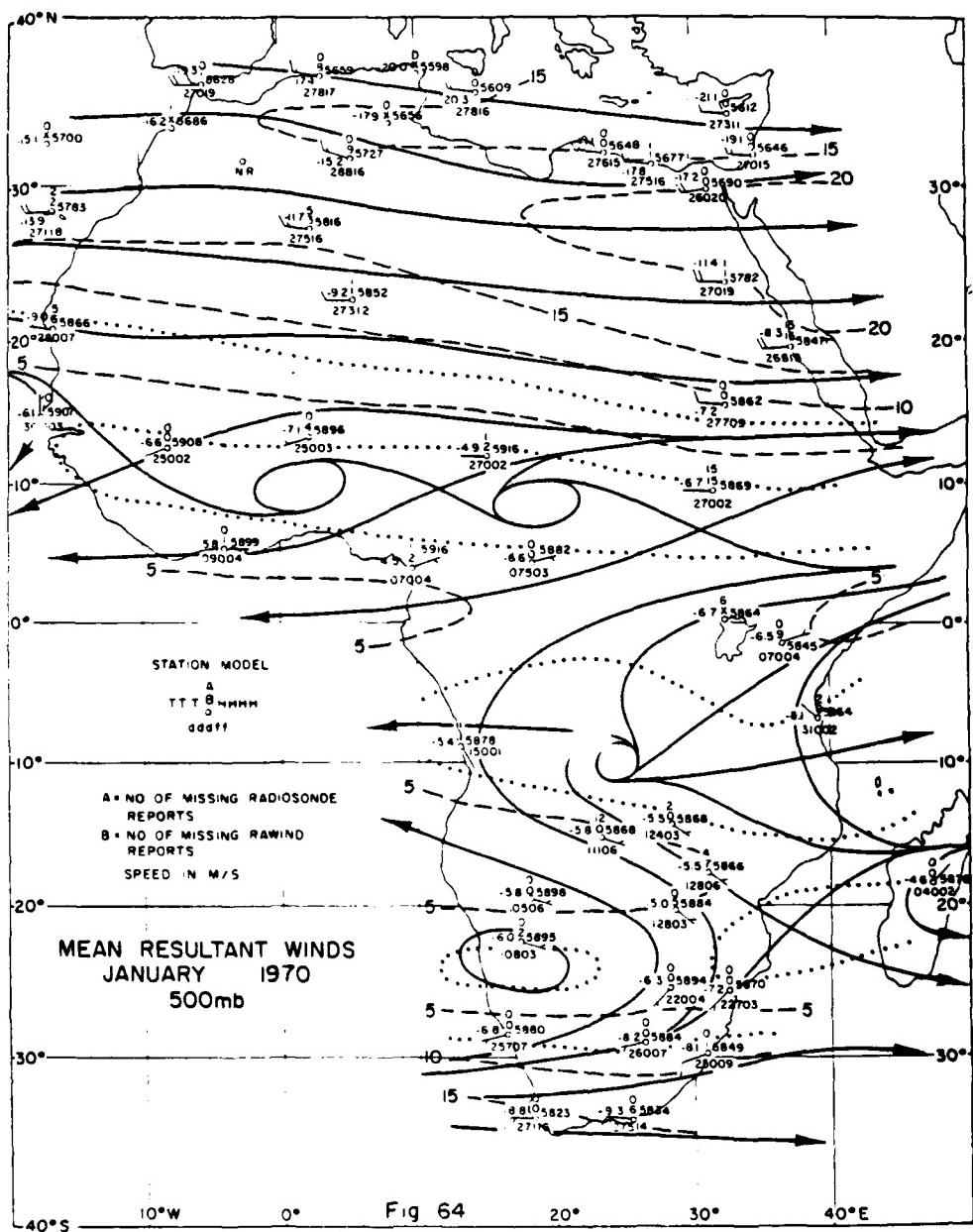


Fig. 64

Fig. 2.29. Mean 500 mb Flow over the African Continent: January (Dean, 1972)

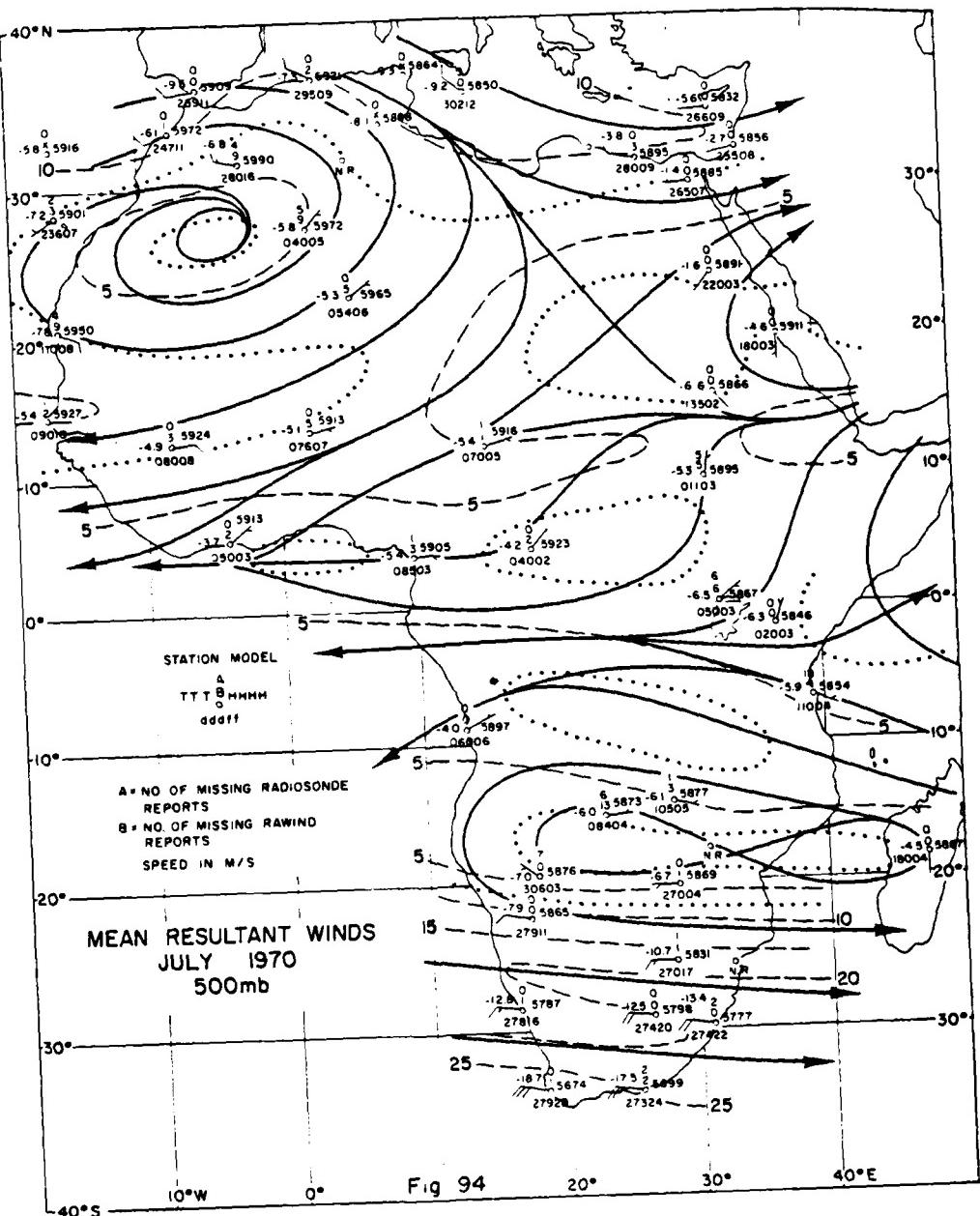


Fig. 2.30. Mean 500 mb Flow over the African Continent: July (Dean, 1972)

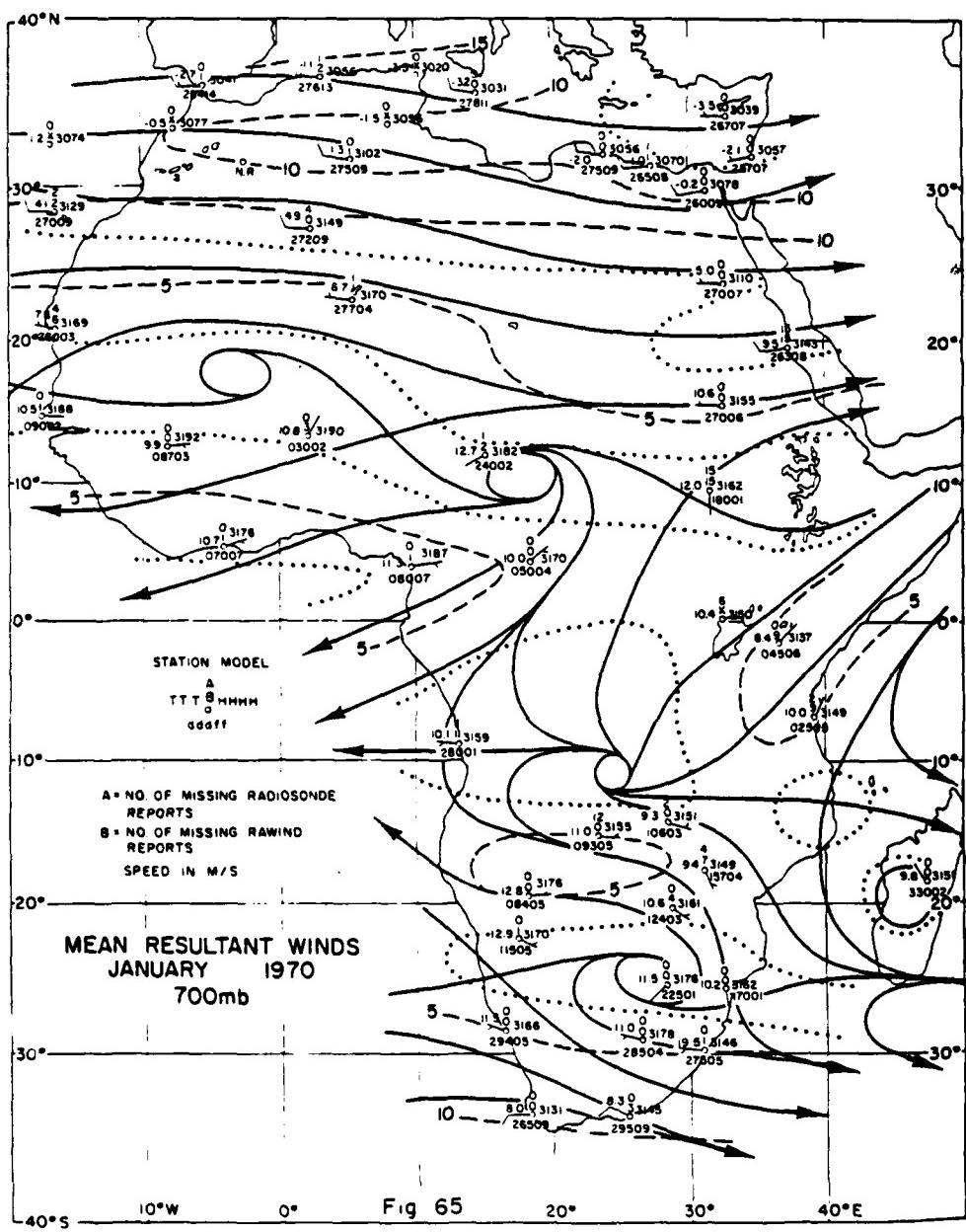


Fig. 2.31. Mean 700 mb Flow over the African Continent: January (Dean, 1972)

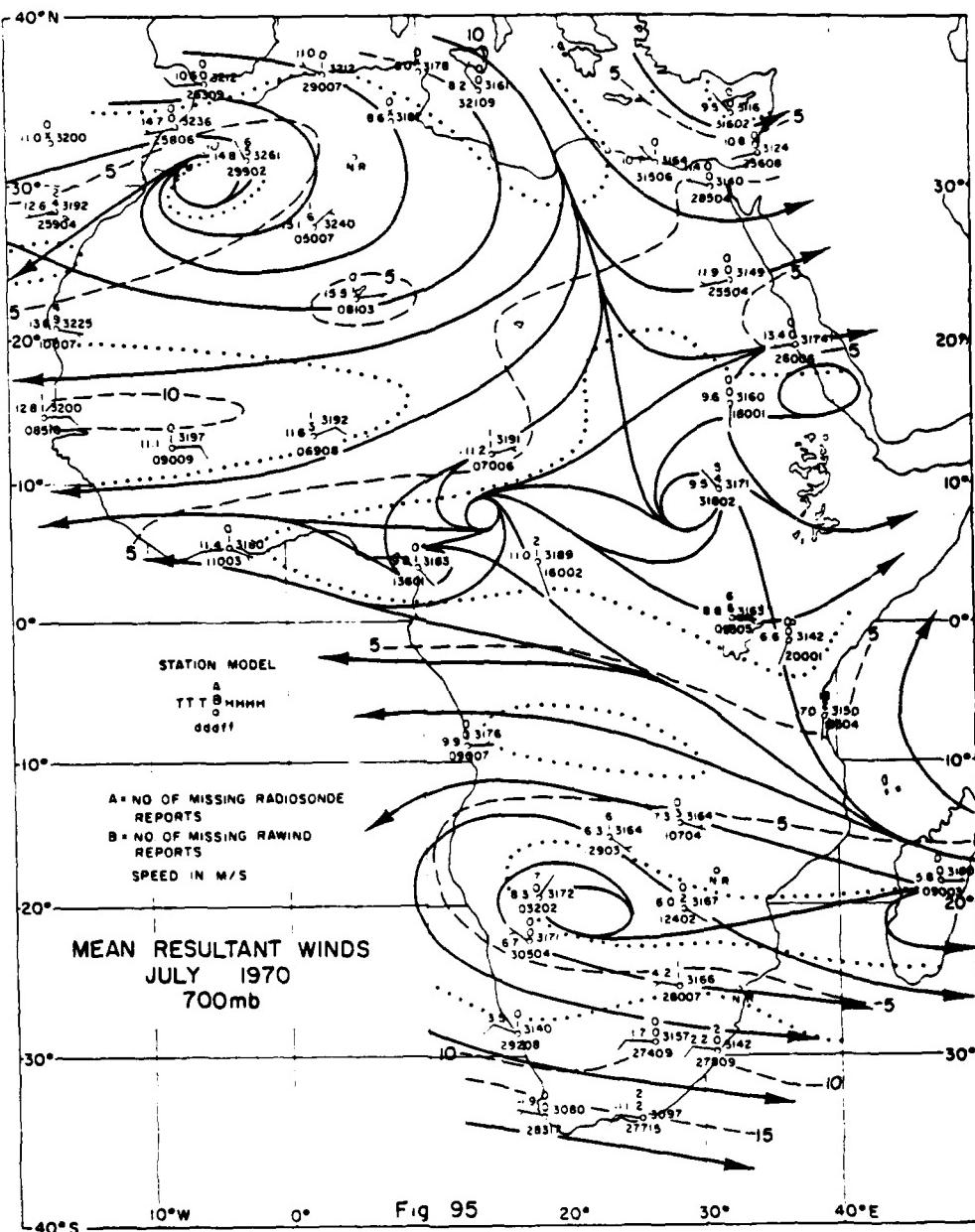


Fig. 2.32. Mean 700 mb Flow over the African Continent: July (Dean, 1972)

## Section 3

### MALAGASY REPUBLIC & MOZAMBIQUE

#### 3.1 TOPOGRAPHY

##### 3.1.1 Malagasy Republic

The main topographical feature is a 1200-1500 m mountain range running the length of the island (Figs. 1.1, 1.2 and 3.1). Three isolated massifs extend to over 2600 m elevation. A narrow coastal plain extends along the east coast. The western portions of the country are mostly low lying. Mangrove swamps are found on much of the west coast (Griffiths and Ranaivoson, 1972).

##### 3.1.2 Mozambique

Mozambique is divided roughly into two parts by the Zambezi River (Figs. 1.1, 1.2 and 3.2). To the north there is a large plateau of 500 m elevation ascending to over 1500 m in small areas. South of, and including the Zambezi River basin, much of the land is low lying (below 200 m), with intermittent lakes and swamplands. A broad coastal plain narrows significantly on the northeastern coast (Griffiths, 1972).

#### 3.2 SIGNIFICANT WEATHER SYSTEMS

##### 3.2.1 Malagasy Republic

Weather over the Malagasy Republic is dominated by trade winds. Passage of tropical cyclones and frontal weather represent the only significant synoptic-scale events which disturb trade wind flow over the Malagasy Republic. The island experiences only two seasons, winter and summer.

###### a. Winter (May - October)

Southeasterly trade winds dominate weather over the Malagasy Republic during the winter months. Over the southern portions of the east coast, wind is diverted to southwest due to the effect of the topography of the island. The wind has a strong diurnal variation especially over the northeast coast, with the strongest winds occurring in the afternoon hours. In Diego Suarez (Fig. 3.1), an August afternoon

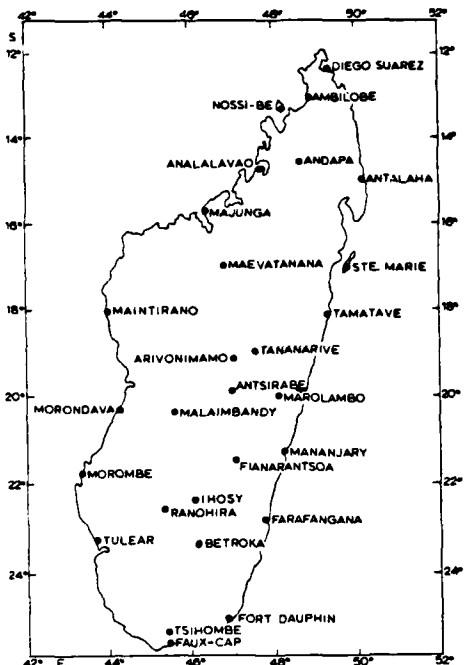


Fig. 3.1. Station Locations of Malagasy Republic (Griffiths and Ranaivoson, 1972)

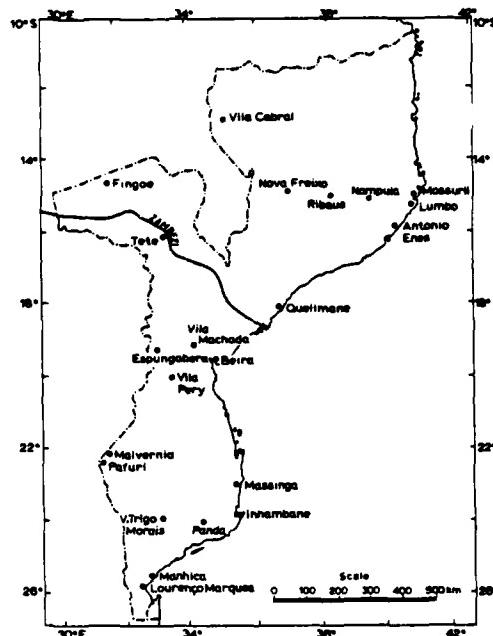


Fig. 3.2. Station Locations of Mozambique (Griffiths, 1972)

wind of 35 to 40 kt is common while the morning wind averages about 15 kt.

Clouds and rain showers are likely to develop over the eastern coast and interior during the morning hours and dissipate in the afternoon. Over the western interior and coastal regions, cloud development and rain showers seldom occur in winter, however, they are more likely during the afternoon. Tropical cyclones seldom occur during the winter months. Significant weather over the Malagasy Republic is limited to the passage of fronts and strong ridging over the southern portion of the island.

#### (1) Frontal Passage.

Often during the winter months a deep mid-latitude low pressure system or cut-off low center passes close to the southern portion of the Malagasy Republic. These weather systems generally approach from the southwest, having reached maximum intensity south of the RSA. The low center and particularly the associated cold front is generally weakening while moving northeastward. The cold air behind the front is

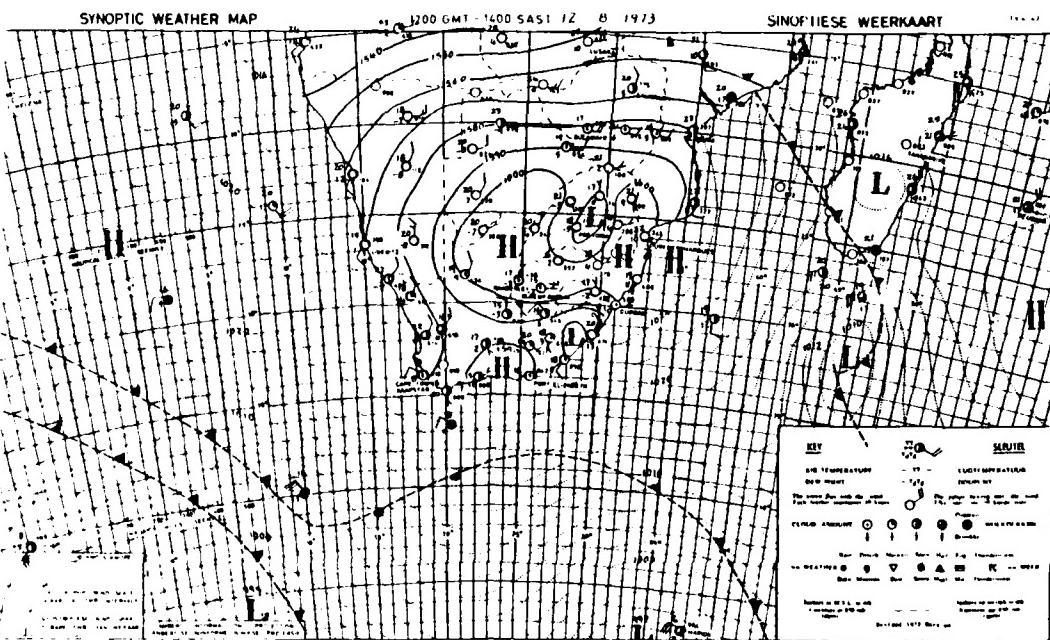


Fig. 3.3. Republic of South Africa Weather Bureau Surface (over Ocean) and 850 mb (over Continent) Analysis: 1200 GMT 12 August 1973

modified by the warm Agulhas Current (see Fig. 2.1) and associated frontolysis occurs, often rapidly. Frequently, only the upper-level trough is evident north of 23°S (Naval Environmental Prediction Research Facility, 1980a). Moderate to strong westerly flow is likely, even preceding the arrival of a cold front on the southwest coast. Dense cloud cover and heavy rain shower activity is likely at and following frontal passage over the southern end of the Malagasy Republic. Following frontal passage, moderate to occasionally strong southerly flow is likely over the southern coast and interior. If the cyclone associated with the cold front is deep or intensifying (not often the case) strong southwesterly flow becomes established following the frontal passage (Fig. 3.3). Even in this case, southeasterly flow is generally reestablished over the area within 24 h. Clear weather conditions develop over the southern Malagasy Republic after frontal passage when the following anticyclone moves over the southern interior. Occasionally, the Indian Ocean high pressure system (east of the advancing cold front) blocks the frontal advance and the cold front stalls over the Malagasy Republic. Broken/overcast conditions and occasional rain shower activity can continue for two to three days in this situation.

#### b. Summer (November - April)

The semi-permanent subtropical anticyclone over the Indian Ocean is weaker in summer and often divides over the western portion.

Southeast trade winds are weaker over the Malagasy Republic. Land/sea breeze cycles occur over the coastal regions and are pronounced over the western coasts. The intertropical convergence zone (ITCZ) and associated convective shower activity move southward over the northern Malagasy Republic as the summer progresses.

### (1) Ridging over the Northern Mozambique Channel

Ridging occurs often over the northern Mozambique Channel (north of  $15^{\circ}$ S) during the summer months. Westerly (onshore) winds develop over the northern and central coast and interior (Fig. 3.4). Also, in the summer a low is often present just off the central coast of Mozambique between  $17^{\circ}$ S and  $21^{\circ}$ S (Figs. 3.4, 3.5). Such low centers occasionally deepen and move toward the Malagasy Republic. The associated flow over northwestern Malagasy Republic is then west-northwesterly. The tropical air flowing over the Republic from the west-northwest is unstable. Convergence of this flow with easterlies over the northern Malagasy Republic is associated with enhanced convective activity in the ITCZ. Convective cloud development, showers and thundershowers are typical.

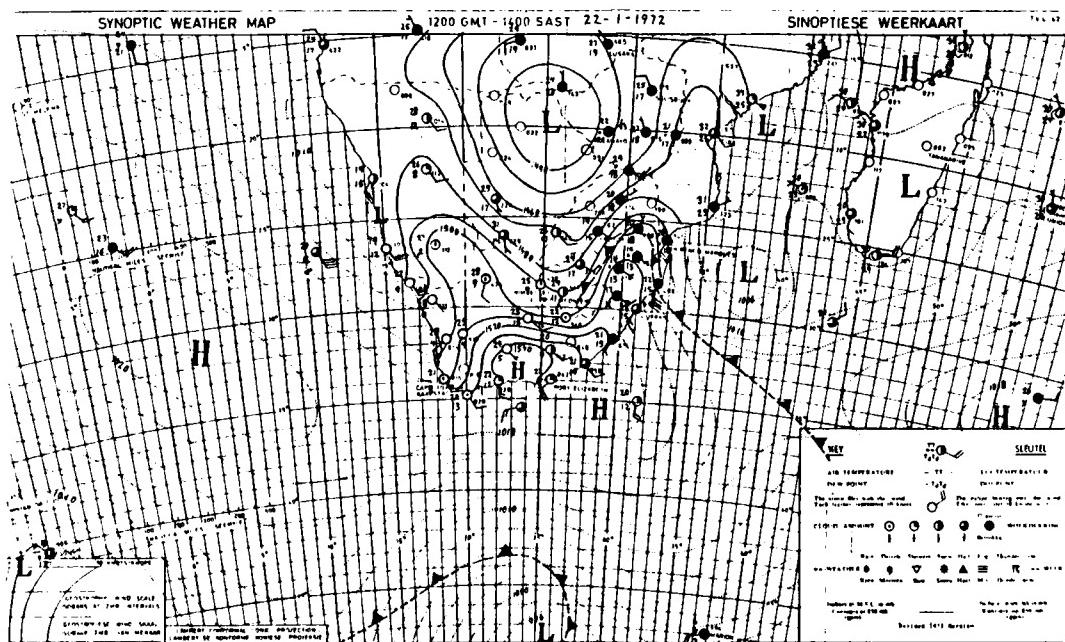


Fig. 3.4. Same as Fig. 3.3 except for 1200 GMT 22 January 1972

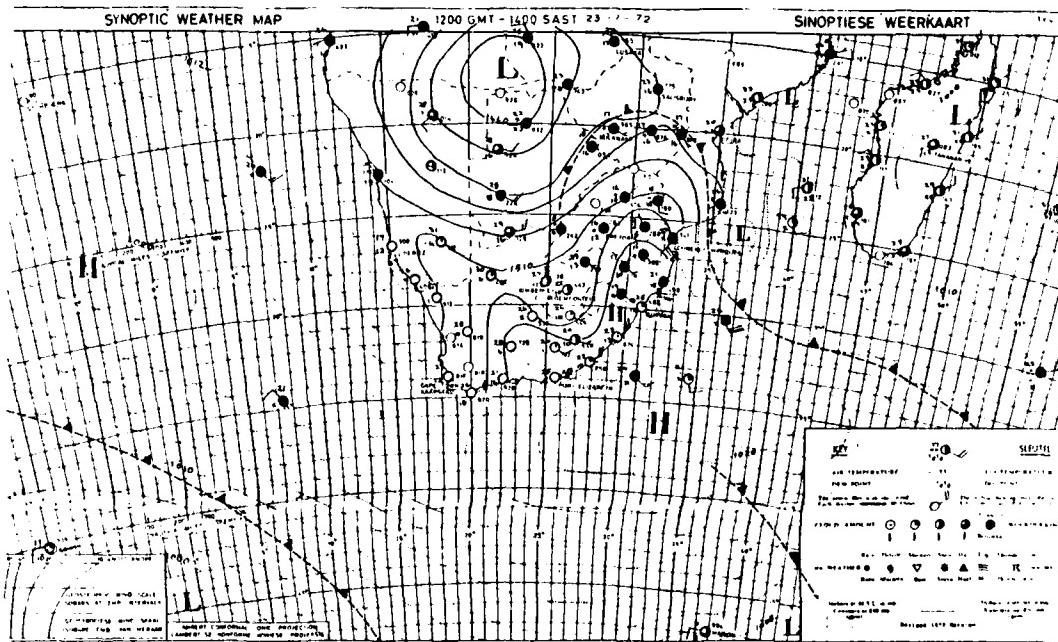


Fig. 3.5. Same as Fig. 3.3 except for 1200 GMT 23 January 1972

Weather over the southern Malagasy Republic is affected by migrating anticyclones and cold frontal passages (discussed in the following paragraph). During the summer period a semipermanent lee trough is present over the western side of the country and frequently a low center develops over the southwestern interior. The strength of the wind near the southern Malagasy Republic is a function of both the pressure in the lee trough and the magnitude of the anticyclone east or south of the Malagasy Republic (Figs. 3.6 - 3.9). Occasionally, the lee trough deepens during passage of a cold front to the south. A strong pressure gradient develops over the southeast Mazambique Channel if a strong anticyclone, ridging northward, follows the front. In this case strong southeasterly flow develops over the southeast Mozambique Channel. These conditions develop with greater intensity early and late in the summer period.

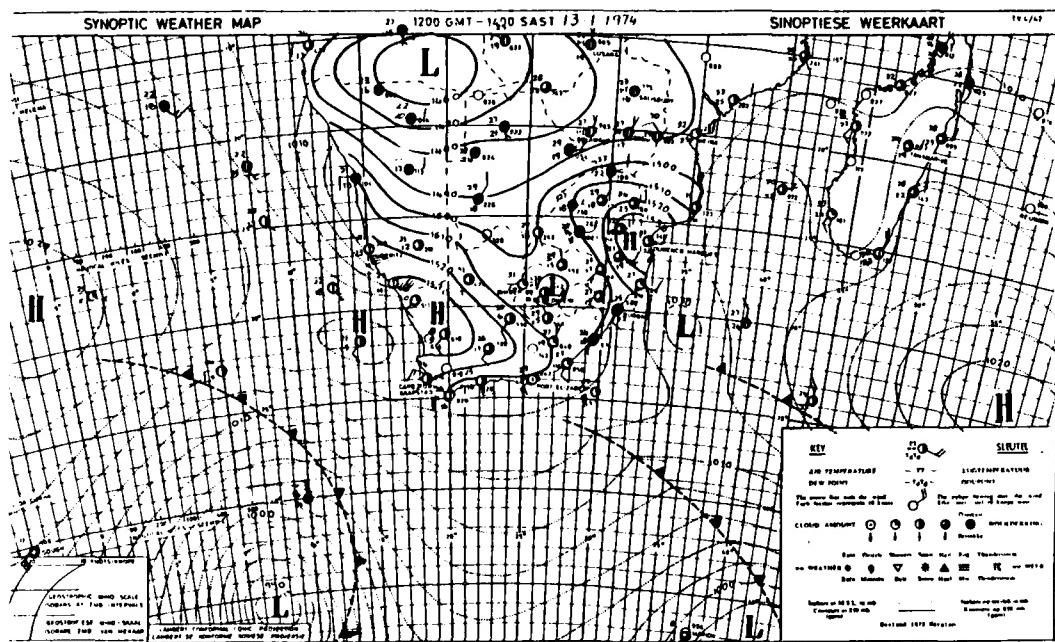


Fig. 3.6. Same as Fig. 3.3 except for 1200 GMT 13 January 1974

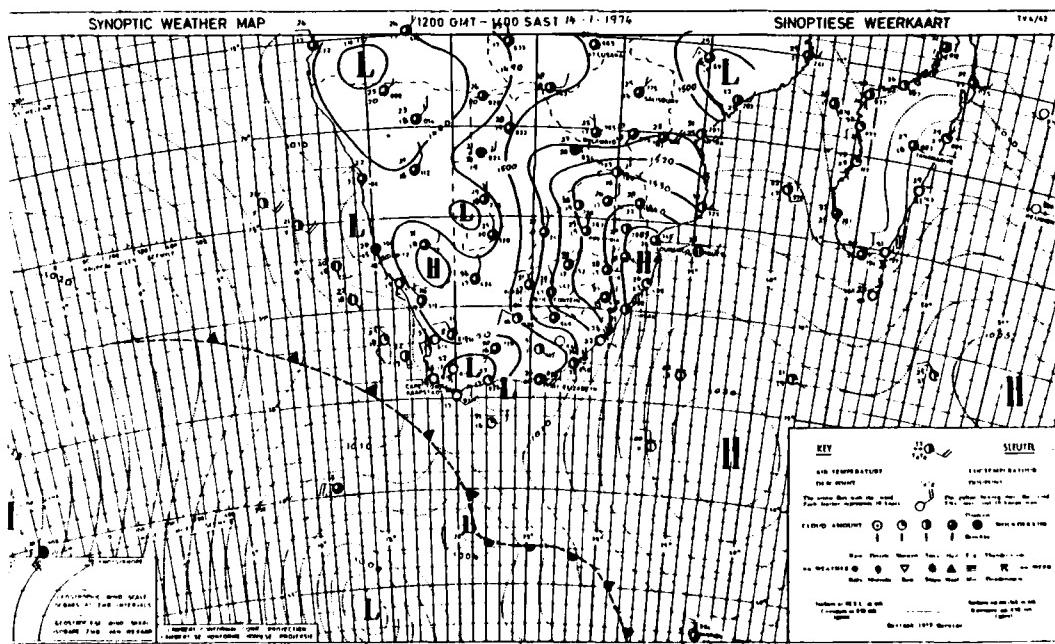


Fig. 3.7. Same as Fig. 3.3 except for 1200 GMT 14 January 1974

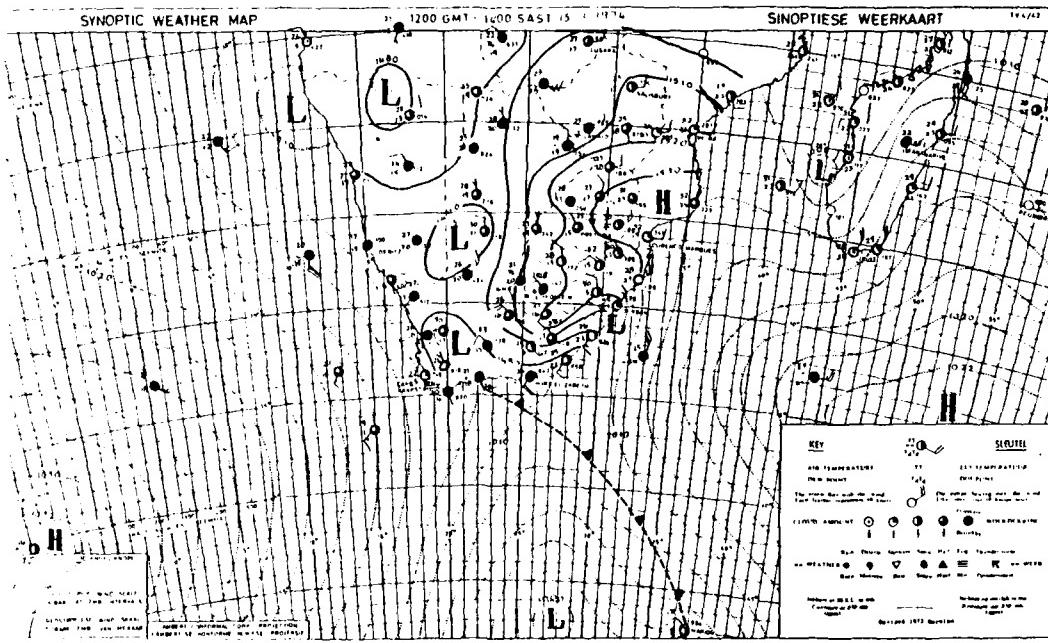


Fig. 3.8. Same as Fig. 3.3 except for 1200 GMT 15 January 1974

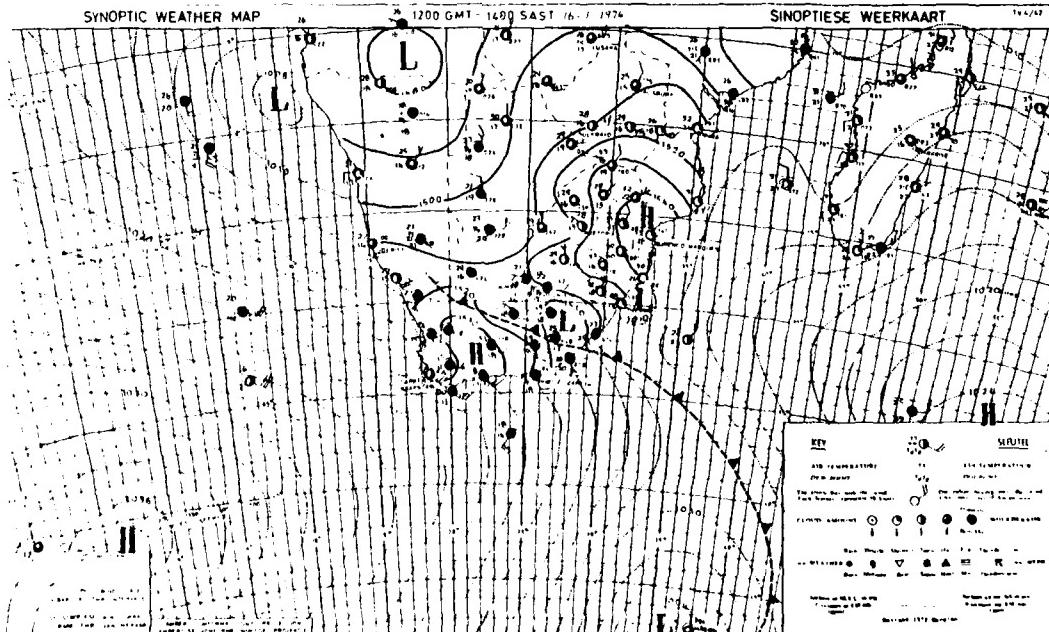
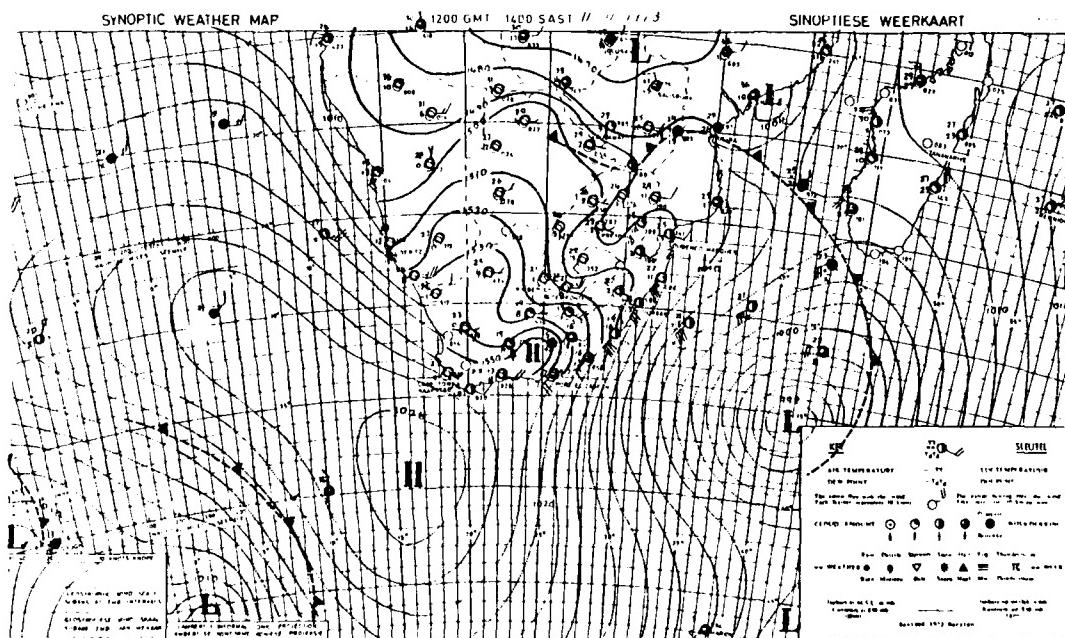


Fig. 3.9. Same as Fig. 3.3 except for 1200 GMT 16 January 1974

## (2) Frontal Passage over the Southern Malagasy Republic

Frontal passage over the southern Malagasy Republic is a rare occurrence in summer. In the seven-year period 1972-1978, only one instance was noted for the months of January and February. However, the likelihood increases significantly early and late in the summer period when deep low centers track farther north. Cold fronts approach the Republic from the southwest. The effect of an advancing cold front over the southern coastal regions varies depending on the strength of the front and proximity of the associated low center to the southeast. If the front is active and if the associated low is deep (Fig. 3.10), winds preceding the frontal passage become moderate to strong northerly over the extreme southern coastal region.



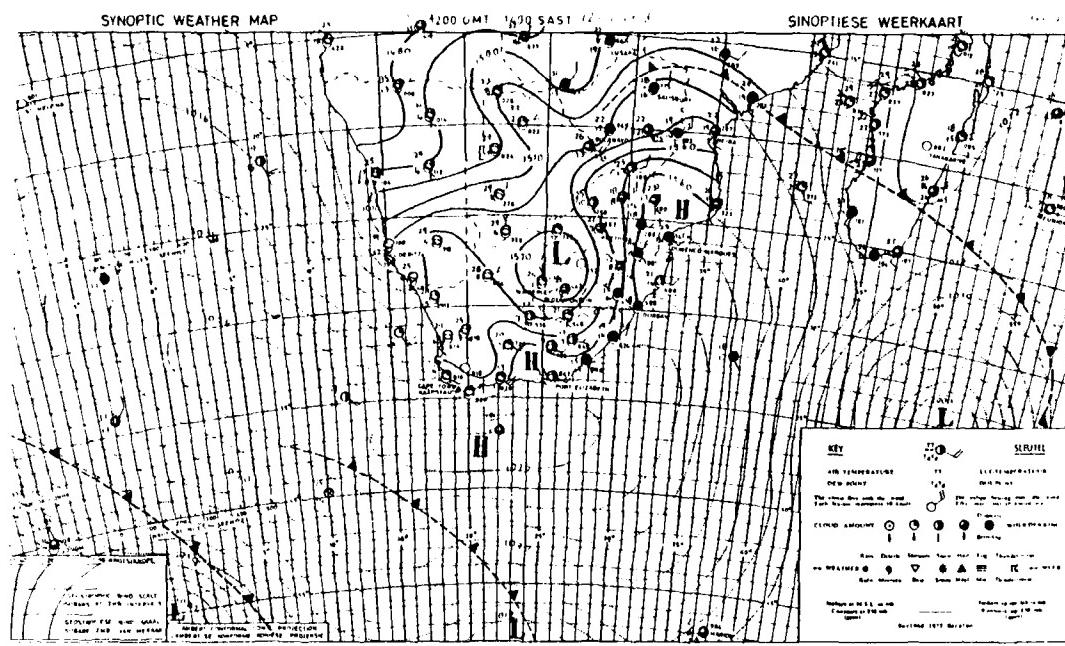


Fig. 3.11. Same as Fig. 3.3 except for 1200 GMT 12 November 1973

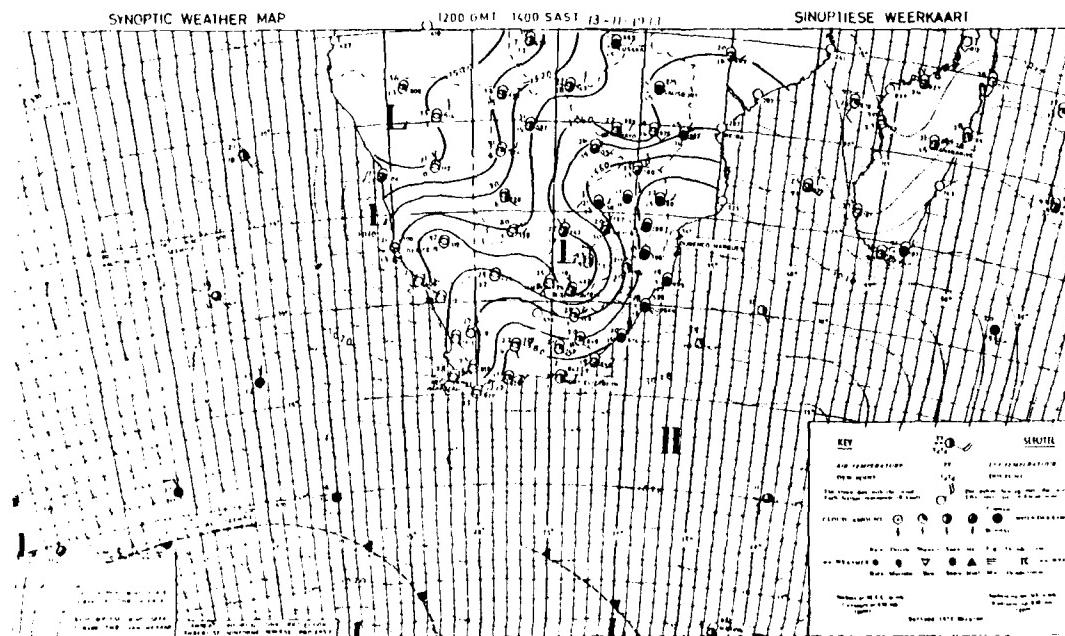


Fig. 3.12. Same as Fig. 3.3 except for 1200 GMT 13 November 1973

If the front is weak or dissipating, southerly winds are likely ahead of the system at the surface. However, in advance of a more intense front, gradient winds over the Indian Ocean south of the Malagasy Republic become strong (25-35 kt) northwesterly. Broken/overcast cloud conditions develop ahead of the cold front. Occasionally, thunderstorm activity over the southwest coast precedes the arrival of the front. After the frontal passage, the wind shifts to southerly over the southwest coast (Fig. 3.11). Associated rain shower activity is generally light. Frequently, the only effect of a cold frontal passage is a shift and temporary increase in the wind. The 24-h temperature change is generally less than ten degrees Celsius. If the front is weak or dissipating, south coastal winds are not significantly affected as the front advances. Following frontal passage, the wind shifts to southerly (light to moderate) over the south and southwest coasts, and easterly (light to moderate) (Fig. 3.12) over the southeast coast. Broken/overcast cloud conditions precede and follow frontal passage. Rain shower activity is light or absent.

Occasionally, the lee trough over the western Malagasy Republic deepens during the frontal passage. Strong southerly winds are likely to develop over the southeastern Mozambique Channel when such deepening occurs. The likelihood increases if a strong anticyclone is advancing from the southwest (Fig. 3.13).

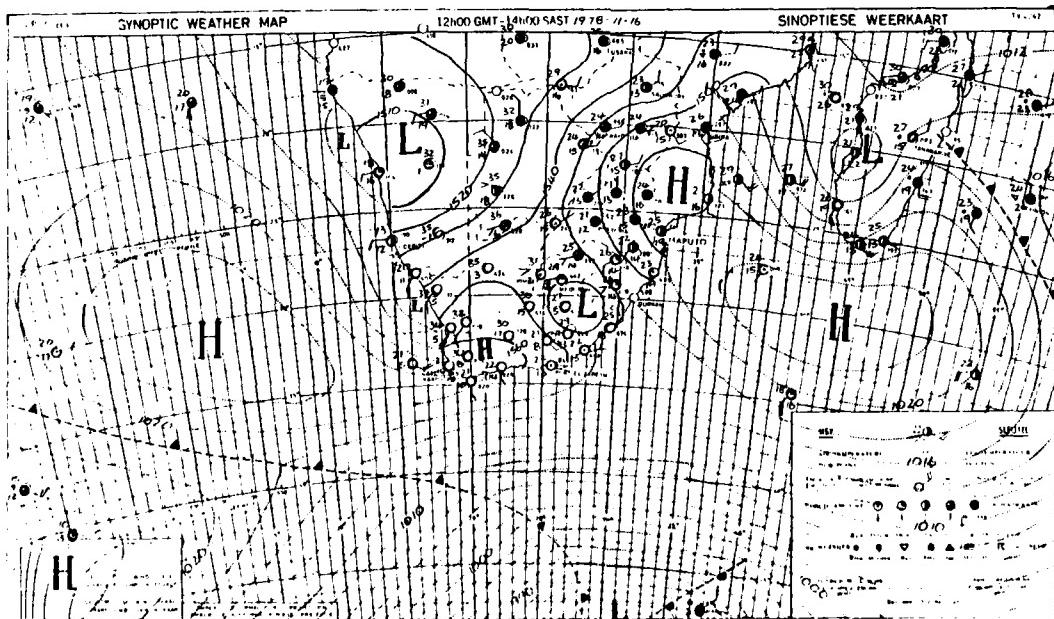


Fig. 3.13. Same as Fig. 3.3 except for 1200 GMT 16 November 1978

### c. Thunderstorms

Thunderstorm activity over the Malagasy Republic is most frequent from December through March over the western central plateau region (Fig. 3.1 and Table 3.1). Much of the activity over the northwest and central western Republic is associated with northwesterly flow into the ITCZ. This flow is enhanced when ridging occurs over the northern Mozambique Channel. This occurs frequently during the summer months. Over the eastern coastal regions, thunderstorm activity occurs less frequently and is associated with easterly (onshore flow). During the winter months, thunderstorm activity is rare, particularly in the period from May through September. Weak convergence aloft and strong directional divergence in the low-level easterlies tend to inhibit convective activity (Griffiths and Ranaivoson, 1972).

TABLE 3.1  
Distribution of Thunderstorm Days for the  
Malagasy Republic (Griffiths and Ranaivoson, 1972)

Station	Alt. (10 m)	Jan.	Feb.	Mar.	Apr.	May	June	July	Aug.	Sept.	Oct.	Nov.	Dec.	Total
Diego-Suarez	11	16	15	14	6	1	0	0	0	0	1	4	13	70
Nossi-Be	1	12	15	13	7	2	0	0	0	0	2	8	16	75
Analalava	6	22	19	18	10	1	0	0	0	0	3	12	21	106
Antalaha	1	12	19	19	11	2	0	0	0	0	3	7	15	98
Majunga	2	22	21	21	11	2	0	0	0	1	6	14	22	120
Maevatanana	8	24	22	20	9	1	0	0	1	1	9	16	23	126
Sainte-Marie	0	11	12	11	6	1	0	0	0	0	2	5	12	60
Maintirano	2	24	23	22	11	1	1	0	1	3	10	19	24	139
Tamatave	1	20	18	20	7	1	1	1	1	2	11	17	20	47
Tananarive	131	22	17	19	12	3	1	1	2	2	14	18	21	132
Antsirabe	151	15	12	12	8	2	0	1	0	1	11	16	16	94
Marolambo	40	15	14	13	8	2	1	1	0	1	7	13	17	92
Morondava	1	21	20	16	4	1	0	0	1	1	6	13	21	104
Malambandy	16	23	20	18	8	2	0	1	1	2	11	20	24	130
Mananjary	1	9	9	9	6	2	1	1	0	0	3	6	11	57
Fianarantsoa	111	14	11	8	6	2	0	1	2	1	6	13	15	79
Morombe	1	21	10	16	4	2	1	1	0	2	4	8	17	92
Ihosy	80	14	10	9	5	2	0	0	0	1	7	11	15	74
Farafangana	1	8	10	9	7	3	1	1	0	1	3	8	11	62
Betroka	80	18	12	11	7	3	1	1	2	1	7	15	18	96
Tulear	1	19	15	13	6	3	2	1	1	1	5	11	17	94
Fort Dauphin	1	11	10	9	5	4	3	2	2	1	5	8	10	70
Tsihombe	6	12	10	6	4	2	2	1	1	1	3	8	10	60

#### d. Upper-Level Winds<sup>6</sup> and Turbulence

Strong (greater than 20 kt) upper-level flow is only occasionally experienced over the Malagasy Republic. In winter months cut-off low centers and polar lows occasionally pass within ten degrees latitude south of the island. The associated jet stream and westerly flow (strongest between 300-200 mb) north of these systems occasionally penetrate over the southern Malagasy Republic. Clear-air turbulence occasionally develops in association with these strong upper-level westerlies. Upper-air (300-200 mb) flow is strongest over the island from May through August (see Figs. 2.27, 2.28). At these levels westerly winds dominate flow over the southern portion of the island and weak anticyclonic flow dominates over the northern portions. Winds at 200 mb are consistently strong (40-60 kt) in winter over the southern portion of the island. At 500 mb anticyclonic flow affects the central portion of the country throughout the year (see Figs. 2.29, 2.30). Over the southern portion of the island the 500 mb wind is westerly and the mean wind is near 25 kt in winter. The 700 mb wind is divergent and southeasterly over most of the northern portions of country in winter (5-10 kt mean) (see Figs. 2.31, 2.32). This flow becomes westerly over the southern portion of the island. In summer the 700 mb wind is weak and cyclonic over most of the island. Weak (5-10 kt) divergent easterly flow is dominant over the southern portion (Dean, 1972).

##### (1) Low-Level Jet

In February and March a low-level jet stream (1 km elevation) is present in the southeasterly flow over the extreme northern Malagasy Republic. The jet axis migrates northwestward from February through June and remains stationary through August (Fig. 3.14). In winter the jet axis migrates back toward the southeast. Wind in this flow is strong in mid-winter, as shown in Fig. 3.15. Strength of the wind field depends on the intensity of the subtropical anticyclone over the southeast Indian Ocean. Clear-air turbulence is possible at low levels in the vicinity of the jet axis. Turbulence, at lower and upper levels, is also likely over the Republic's central and northwest interior in association with thunderstorm activity (Krishnamurti, 1979).

Earlier work by Findlater (1969) indicates the possibility of *multiple* (i.e., horizontally side by side) low-level jet streams as well as instances with *southerly* jets emanating from the Mozambique Channel. Using data sets from the Global Atmospheric Research Program (GARP) Monsoon Experiment (MONEX), Krishnamurti et al. (1981) found that while in Fig. 3.15 the low-level jet along the southeast trades is oriented southeast to northwest over the southern Indian Ocean, in the MONEX analysis it possesses a nearly *zonal* (i.e., easterly wind) orientation along 10°S. While there were several other differences identified, the others were far distant from eastern Africa.

---

<sup>6</sup> See footnote 4 on page 2-24 regarding upper-air wind analyses.

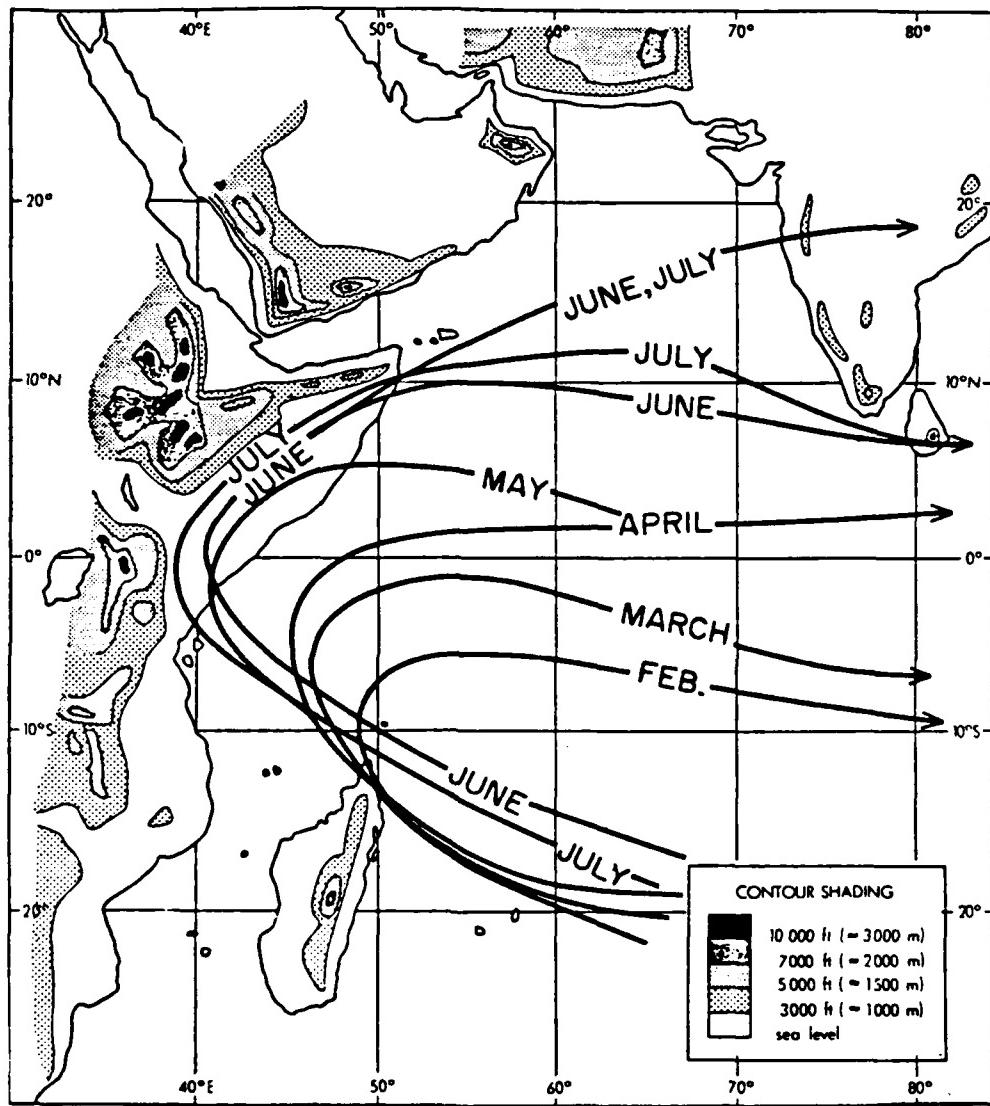


Fig. 3.14. Monthly Positions of the Low Level Cross-Equatorial Jet (Krishnamurti, 1979)

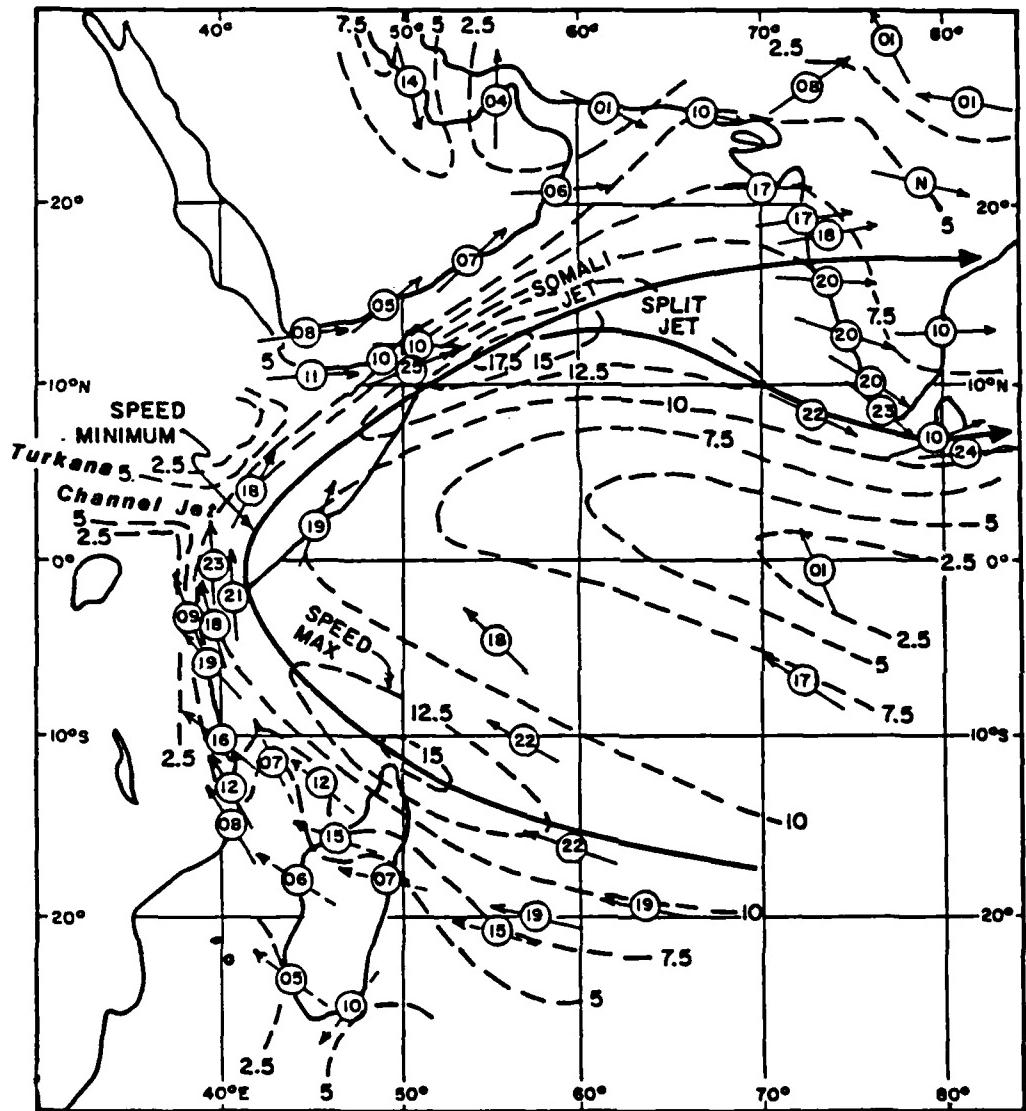


Fig. 3.15. 1 km Flow for August over the Arabian Sea/Indian Ocean region based on Findlater (1971). Speed lines are in  $\text{m s}^{-1}$ . Station values within circles are in knots. The solid line indicates the axis of the low-level jet. (After Krishnamurti, 1979)

### 3.2.2 Mozambique

Synoptic weather over Mozambique is strongly affected by the southeasterly trades throughout the year. Over the area north of 15°S northwesterly flow breaks this pattern in the summer months (Dec-Feb) when an anticyclone is present over the northern Mozambique Channel. Other synoptic phenomena affecting Mozambique are the ITCZ, migrating high and low pressure systems, and tropical cyclones. Due to the geographical location of Mozambique only two seasons occur, winter and summer.

#### a. Winter (April - October)

During winter months the Indian Ocean anticyclone is farther north (30°S) (Griffiths, 1972) than in summer. The high also extends farther west in winter, occasionally linking with the high over the Southern African interior. Associated wind flow over Mozambique is moderate to occasionally strong southeasterly from April until October, when the strongest easterlies develop. The southeasterly flow is occasionally broken by migrating high and low pressure centers. Coastal low centers occasionally affect the extreme southern coast of Mozambique (Figs. 3.16, 3.17).

##### (1) Anticyclone over Mozambique

During the winter months anticyclones are often present over south and central Mozambique. Subsiding air over most of the country is associated with rainless conditions. Moderate southeasterly to easterly (onshore) flow and associated low cloudiness are typical over the northern and central coasts. Northeasterly flow often dominates over the south coast. Cloudiness decreases inland.

##### (2) Cold Frontal Passage

Cold fronts penetrate over the southern and central Mozambique coastal regions in winter (Figs. 3.17, 3.18). North of 23°S these systems are usually only evident aloft. Moderate, often strong (20 kt) northerly winds precede arrival of the cold front. Broken to overcast cloud conditions with little or no rainfall are likely to accompany the frontal passage. In general, moderate to strong northeasterly flow develops over Mozambique when a cold front is present over the southeast RSA coast. Strong winds develop when there is a coastal low center ahead of the advancing cold front, such as in Fig. 3.17. Coastal lows generally precede advancing cold fronts on the southeast RSA coast and seldom advance northward beyond the extreme southern Mozambique coastal region. These small coastal disturbances are often associated with strong surface winds. Strong (20-30 kt) northeasterlies (occasionally offshore flow) can develop over the southern Mozambique coast north of the advancing coastal low center. Behind (south of) the low center strong (20-30 kt) southwesterly flow (often with an onshore component) is likely. Low stratus, and occasionally fog, develops along the affected coast with this onshore flow.

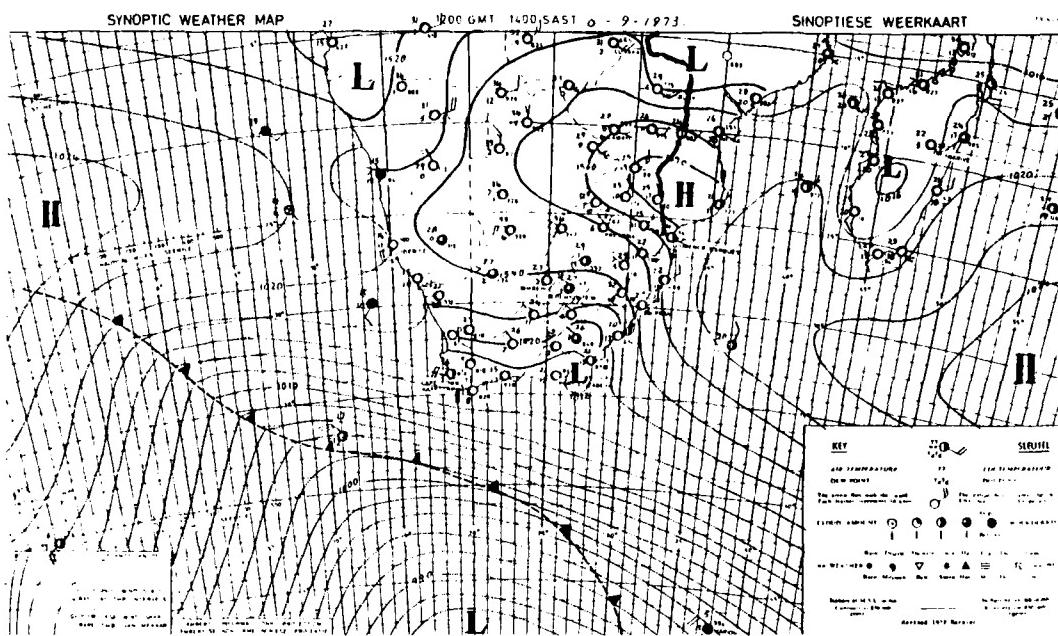


Fig. 3.16. Republic of South Africa Weather Bureau Surface (over Ocean) and 850 mb (over Continent) Analysis: 1200 GMT 6 September 1973 (western boundary of Mozambique is marked with a heavy black line)

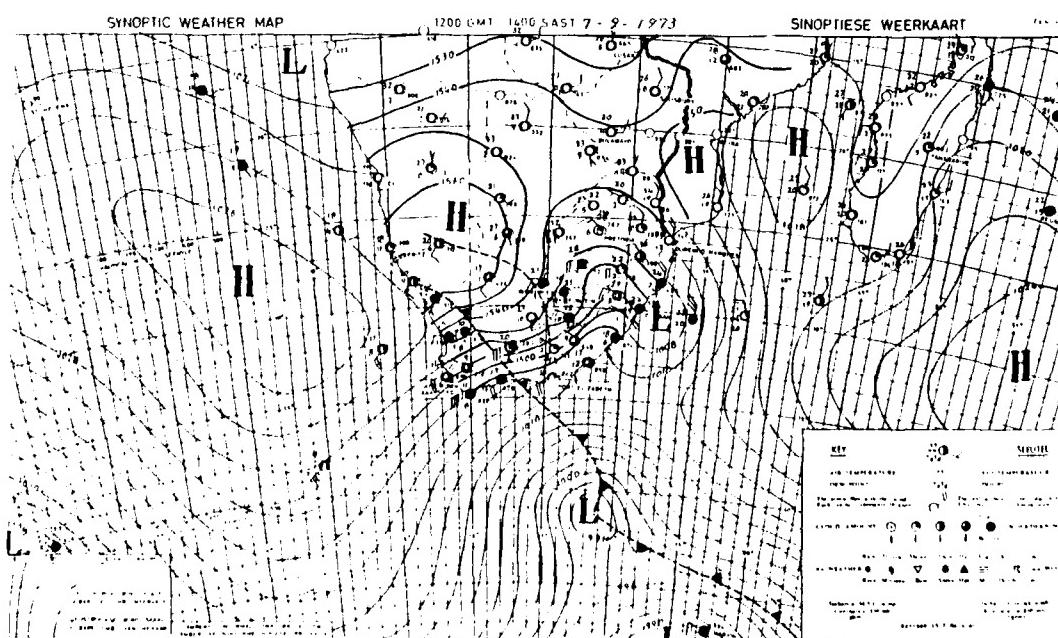


Fig. 3.17 Same as Fig. 3.16 except for 1200 GMT 7 September 1973

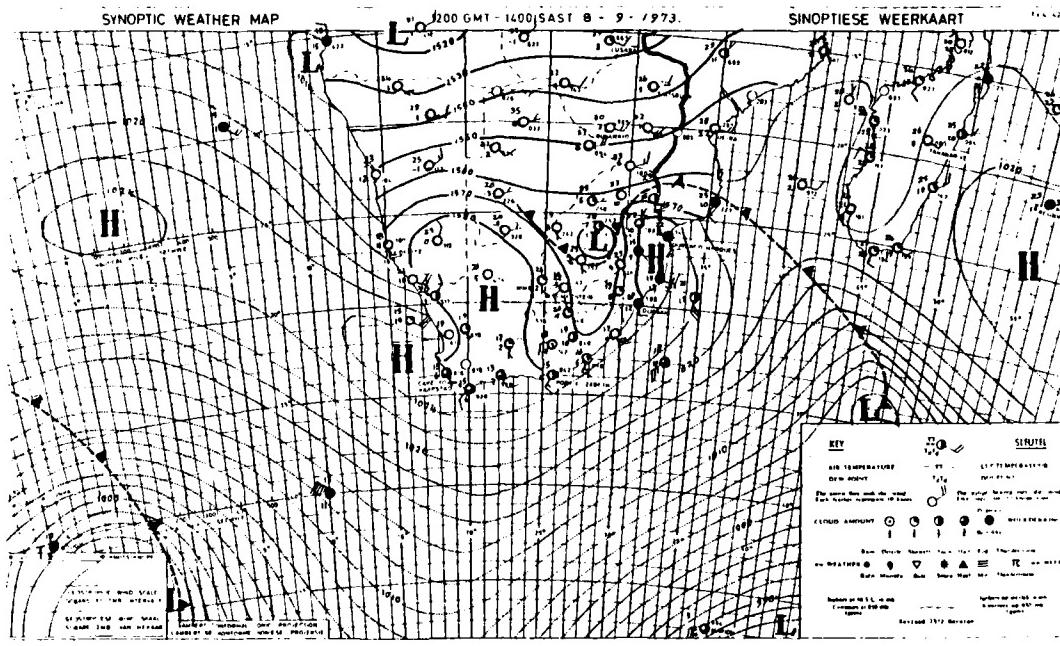


Fig. 3.18 Same as Fig. 3.16 except for 1200 GMT 8 September 1973

### b. Summer (November - March)

Summer is the rainy season in Mozambique. The southeasterly trades are weakened over the country. The Asian anticyclone is strong during the austral summer months and airflow out of this system and the Arabian anticyclone affects weather over northern Mozambique. Ridging over the northern Mozambique Channel occurs frequently. The associated northeasterly flow often replaces weak southeasterly flow over the northern half of the country. Weather is also affected by the intertropical convergence zone (Para. 3.2.2.e) and by tropical cyclones in the Mozambique Channel (Para. 4.2.2).

#### (1) Ridging over the Northern Mozambique Channel

In summer, ridging over the northern Mozambique Channel is associated with northeasterly flow of unstable tropical air over northern Mozambique. Orographic lifting and convective cloud development occur often in this case. Additionally, the northeasterly flow converges with the southeasterlies over northern and central Mozambique. This convergence is associated with increased convection and rainshower activity in the ITCZ (Fig. 2.2). Thunderstorm activity is likely over the northern portions of the country in this situation. Also, in the summer months a semipermanent low is present over the Southern African interior. This low occasionally extends as a trough eastward to the Mozambique coast. An associated weak low often develops over the Mo-

zambique coast between 17°S and 21°S (observed on weather analyses, 1972 - 1978). This coastal low varies in intensity and occasionally enhances onshore flow (20 kt) over the central Mozambique coast.

#### c. Thunderstorms

The thunderstorm season in Mozambique extends from November through March. The highest frequency of occurrence is in northern Mozambique where thunderstorm activity occurs in association with the ITCZ. The southernmost penetration of the ITCZ is in December/January when it lies over north central Mozambique (Fig. 2.2) (Krishnamurti, 1979). ITCZ activity intensifies when strong northeasterly flow develops over northern portions of the country. In this case convective clouds and thunderstorm activity often develop over northern and central Mozambique. The southern portions of the country also experience thunderstorms due to the presence of southeasterly (onshore) flow during this period (Fig. 2.2). Presence of a high pressure cell, with its attendant subsidence, will naturally inhibit thunderstorm activity.

#### d. Upper-level Winds<sup>7</sup> and Turbulence

Winds aloft over Mozambique seldom build to strong ( $\geq 40$  kt) intensity. Even in winter months, when upper-air wind is strongest, the jet stream and associated strong westerlies generally remain south of Mozambique. The exception to this rule is the equatorward penetration of a deep low center or cut-off low over extreme southern Mozambique. In this case jet stream activity (and its attendant clear-air turbulence, 300-200 mb) only affects flow over the southern portions of the country.

During the summer at 200 mb, the flow is weak easterly and diverging over extreme northern Mozambique (see Fig. 2.27), while over southern Mozambique, moderate (10-20 kt) westerly flow prevails. The seasonal change finds the upper (200 mb) westerly winds strengthened to 40-60 kt over the southern portions of the country (see Fig. 2.28). This increase is attributed to the increased influence of passing mid-latitude storms. Over the northern portion, wind is generally weak (10-15 kt) and anticyclonic.

Also in the summer at 500 mb (see Fig. 2.29), the flow is weak east-southeasterly over the north and weak south-southwesterly (5-10 kt) over the south. However, in the winter (see Fig. 2.30), 15 to 40 kt westerly flow is present over southern Mozambique, with weak anticyclonic flow over the central portion of the country, and weak (5-15 kt) southeasterly flow over the northern portion of the country.

Finally, in summer at low levels (700 mb) the wind is weak south-easterly over central and southern Mozambique (see Fig. 2.31), while over the north, the mean flow is variable/northeasterly. In winter at low levels (700 mb) the flow is weak southeasterly and diverging over northern and central Mozambique becoming westerly to the south (see Fig. 2.32).

---

<sup>7</sup> See footnote 4 on page 2-24 regarding upper-air wind analyses.

Turbulence over Mozambique is more likely to be associated with convective storms than with synoptic systems. Thunderstorms occur most frequently in summer months over northern Mozambique, mostly in association with the ITCZ.

e. Intertropical Convergence Zone (ITCZ)

The intertropical convergence zone (ITCZ) affects the northern Malagasy Republic, Mozambique and the Mozambique Channel from November through March. The ITCZ mean monthly positions are shown in Fig. 2.2 (Krishnamurti, 1979). Note that the ITCZ does not advance into southern Mozambique. The ITCZ advances southward over northern Mozambique in January and a rapid retreat northward occurs in March. Motion of the ITCZ is determined by movement and intensification of subtropical high pressure centers on either side of the equator. Southward migration of both subtropical anticyclones is associated with the southward advance of the ITCZ in early summer. Activity in the ITCZ is intensified when a ridge extends southward over the northern Mozambique Channel. This occurs most frequently from December through February. The associated flow pattern draws in unstable tropical air from the north. Over central and northern Mozambique, convergence of tropical northeasterly flow with southeasterly flow intensifies ITCZ convective activity. Cumulonimbus and towering cumulus clouds in squall line activity, frequent and heavy rain shower activity, and thunderstorms typify the associated weather.

## Section 4

### TROPICAL CYCLONES AND THE MASCARENE & SEYCHELLES ISLANDS

#### 4.1 TROPICAL CYCLONES

Tropical disturbances which develop in the South Indian Ocean off the east coast of the RSA are referred to by all regional weather services as tropical cyclones or tropical storms regardless of the stage of development. Therefore, a classification of 'tropical storm' is not an indication of the system's intensity. Warnings are issued by various weather services, including the Joint Typhoon Warning Center (JTWC) on Guam, and the Mauritian Weather Service, both of which issue position and movement information on these tropical systems. JTWC Guam issues 12-, 24- and 48-h forecasts of the movement and intensity of these systems, and these forecasts are updated every 12 hours.

The tropical cyclone season is from November through April, the highest frequency of occurrence being in January and February. Early in the season (November) these systems generally develop and track east of the Malagasy Republic, often passing near the islands of Mauritius and Reunion (see Fig. 1.1 for location of islands). As the season progresses (Dec - Jan) the source region for these systems shifts westward (Table 4.1).

TABLE 4.1

Mean Position of Origin of Cyclonic Storms in the South Indian Ocean  
(Naval Environmental Prediction Research Facility, 1980a)

	Nov.	Dec.	Jan.	Feb.	Mar.	Apr.	May
Latitude S.	..	13.0°	13.8°	13.9°	14.6°	14.4°	13.9°
Longitude E.	..	66.8°	62.8°	61.8°	62.6°	63.0°	66.0°

The potential for storms developing in or passing into the Mozambique Channel is greatest in January and February while the possibility exists throughout the season. Also, by January, storms penetrate farther south before recurving to the southeast (Table 4.2).

TABLE 4.2

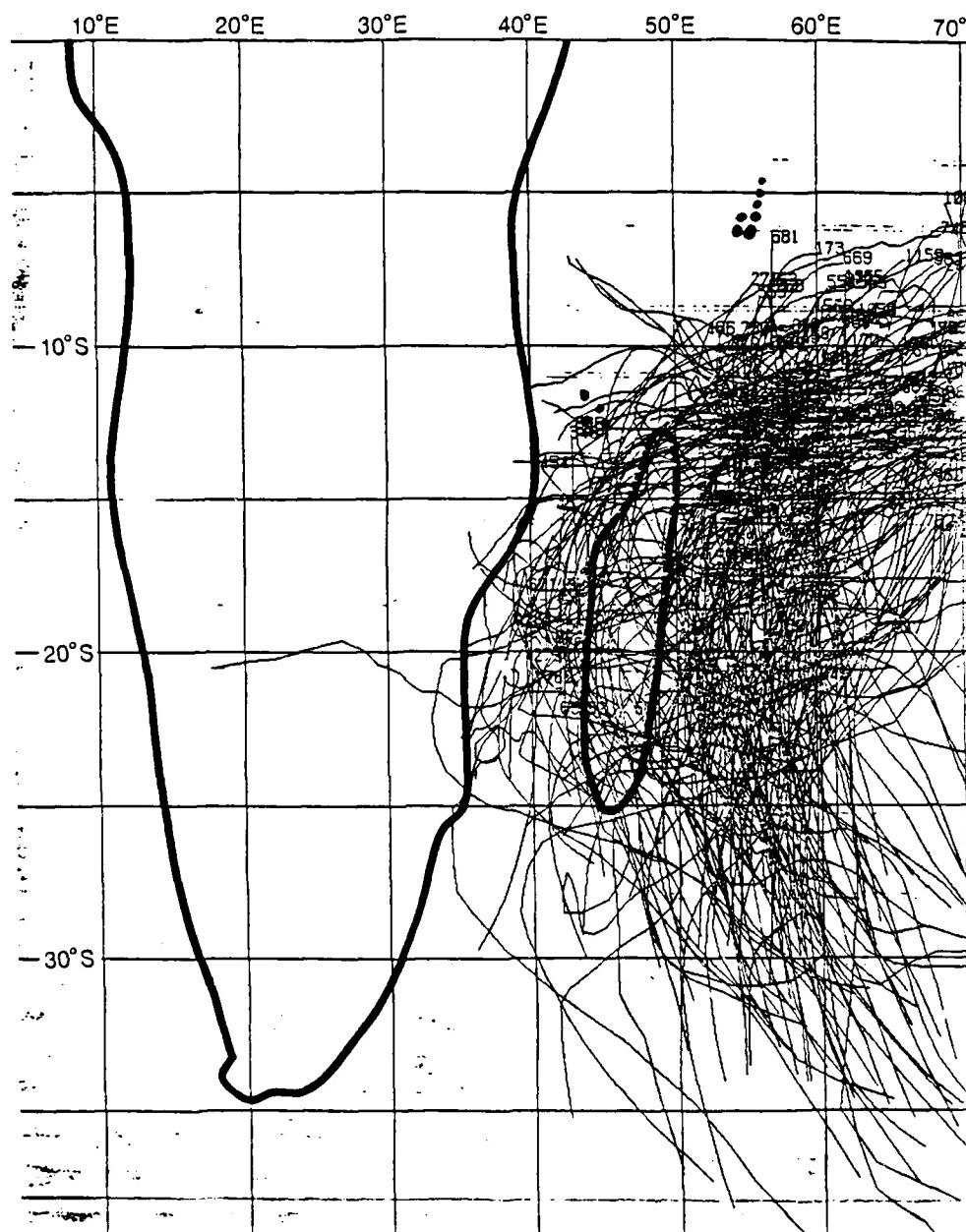
Average Latitude of the Point of Recurvature of  
 Tropical Cyclones in the South Indian Ocean  
 (Naval Environmental Prediction Research Facility, 1980a)

No. of storms .. ..	Nov.	Dec.	Jan.	Feb.	Mar.	Apr.	May
Mean south latitude of recurvature .. ..	17.0°	17.0°	22.2°	22.2°	20.8°	15.0°	14.0°

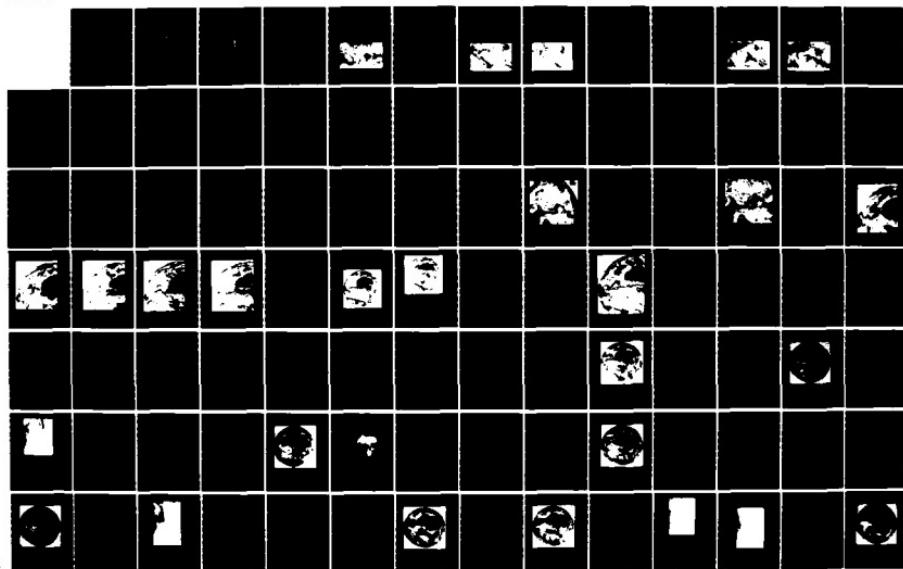
In February the tropical cyclone source region and tracks begin to shift back toward the *east* (Table 4.1), and in March, recurvature occurs farther *north* (Table 4.2). April storms generally pass east of the Malagasy Republic and often well east of Mauritius (Naval Environmental Prediction Research Facility, 1980a).

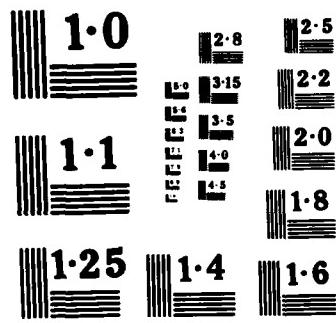
Mean storm tracks have been determined for tropical cyclones which developed over the southwest Indian Ocean from 1950 through 1980. This information, provided by Dr. Ted Tsui of the Naval Environmental Prediction Research Facility (NEPRF), is shown in Figs. 4.1, 4.2 and 4.3. Figure 4.1 depicts a density plot of storm tracks for storms passing east of the Malagasy Republic. Figures 4.2 and 4.3 provide the same information for tropical cyclones passing through the northern and southern Mozambique Channel. Average speed of motion is between six and eight knots, however speed of motion is variable throughout a storm's history. Speed of advance often exceeds these values (speeds occasionally exceed 15 kt) before and after recurvature. Storm motion often slows significantly at recurvature. Storms pass east of the Malagasy Republic more frequently than to the west (i.e., in the Mozambique Channel).

When passing east of the Malagasy Republic the systems generally recurve rapidly toward the southeast. Systems developing in or moving into the Mozambique Channel move more slowly toward the south then, generally, recurve rapidly toward the southeast after passing through the channel. Tropical cyclones in the southwest Indian Ocean are generally small systems compared to North Pacific Ocean typhoons and not so intense. The maximum winds average 68 kt (based on data from seventeen storms) for tropical storms passing east of the Malagasy Republic and 56 kt (based on data from five tropical storms) for the systems in the Mozambique Channel. These values were obtained using data provided by NEPRF.



AD-A163 196 FORECASTERS HANDBOOK FOR THE SOUTHERN AFRICAN CONTINENT 2/4  
AND ATLANTIC/INDI. (U) NAVAL ENVIRONMENTAL PREDICTION  
RESEARCH FACILITY MONTEREY CA. F R WILLIAMS ET AL.  
UNCLASSIFIED NOV 84 NEPRF-TR-84-08 F/G 4/2 NL





NATIONAL BUREAU OF STANDARDS  
MICROCOPY RESOLUTION TEST CHART

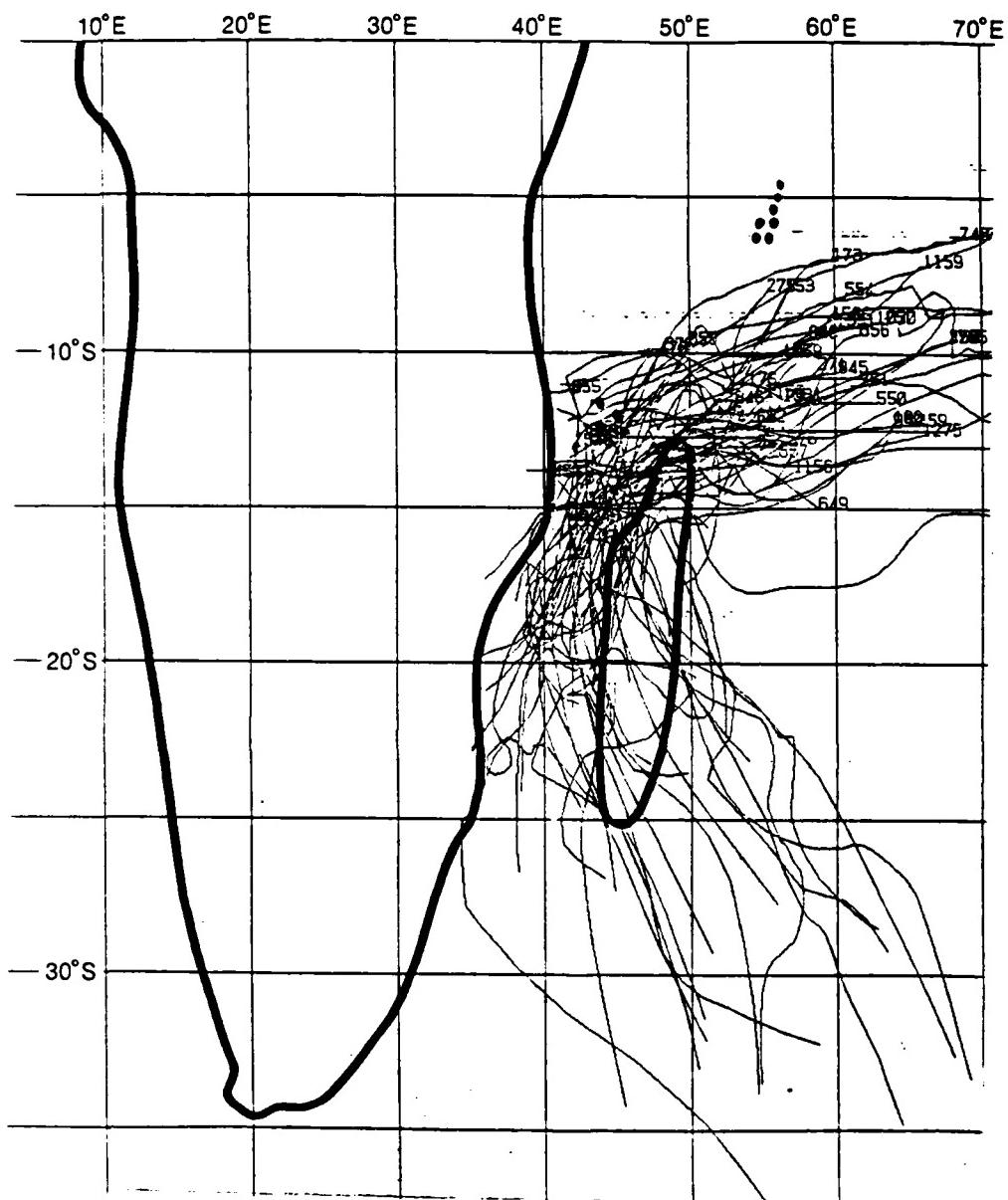


Fig. 4.2. Density Plot of Tropical Cyclone Tracks Affecting the Northern Mozambique Channel (i.e., passing through area: 41°E-49°E, 11°S-16°S)

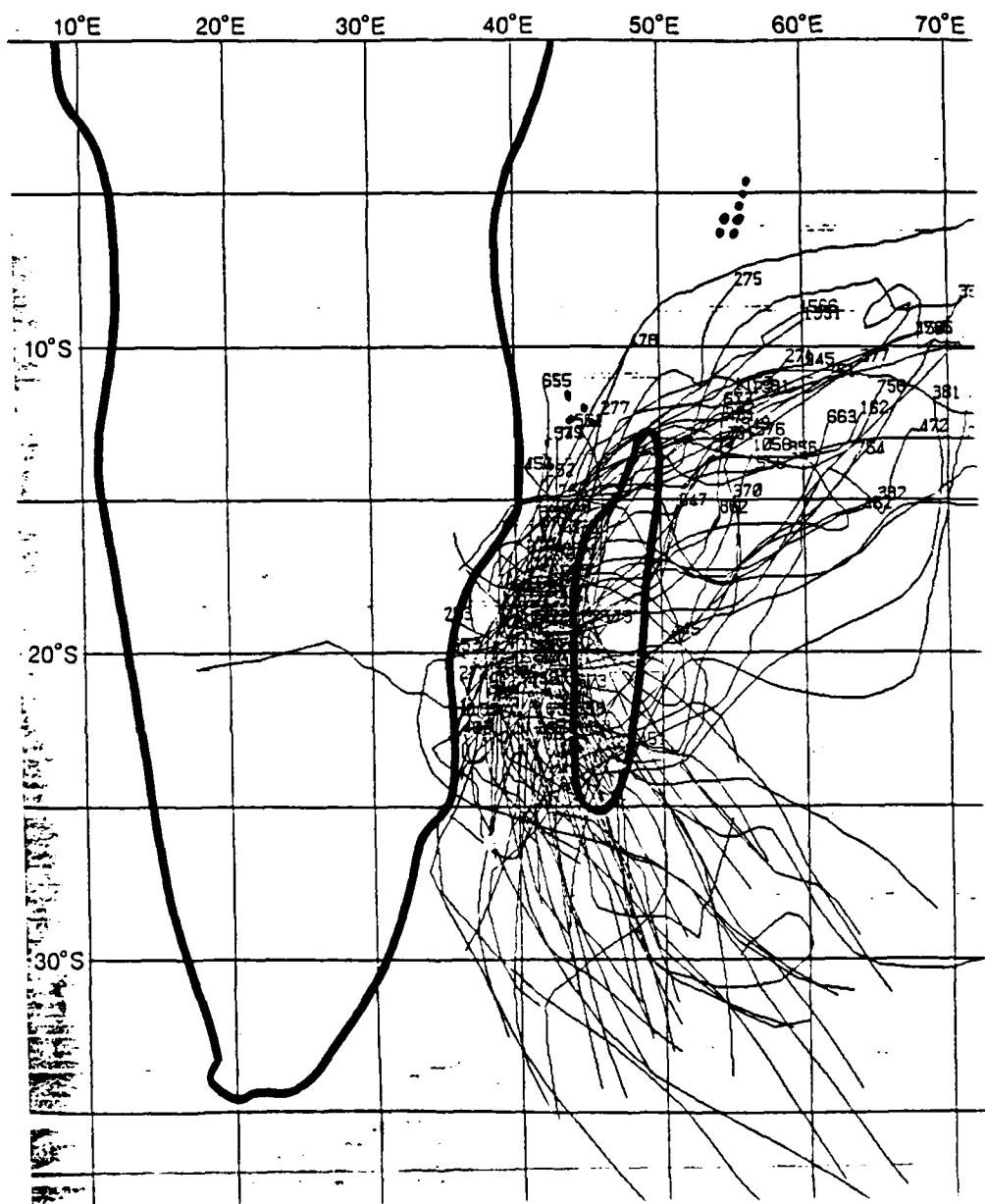


Fig. 4.3. Density Plot of Tropical Cyclone Tracks Affecting the Southern Mozambique Channel (i.e., passing through area: 35°E-45°E, 16°S-25°S)

During the tropical cyclone season, strong high pressure cells are migrating eastward across the south Indian Ocean, south of the Malagasy Republic. If a tropical cyclone advances (relatively) toward one of these migrating anticyclones, surface winds between the two systems are increased significantly. Strong gradient winds (20-30 kt) are likely to be extended in the direction of the high cell. An example is shown in Figs. 4.4 and 4.5 in which 20-30 kt winds extend over 600 n mi south-southeast of the tropical cyclone center. Figure 4.6 is a mosaic from the polar orbiting NOAA-4 satellite which passed near the Malagasy Republic at approximately 0600 GMT (six hours before the analysis time of Fig. 4.5).

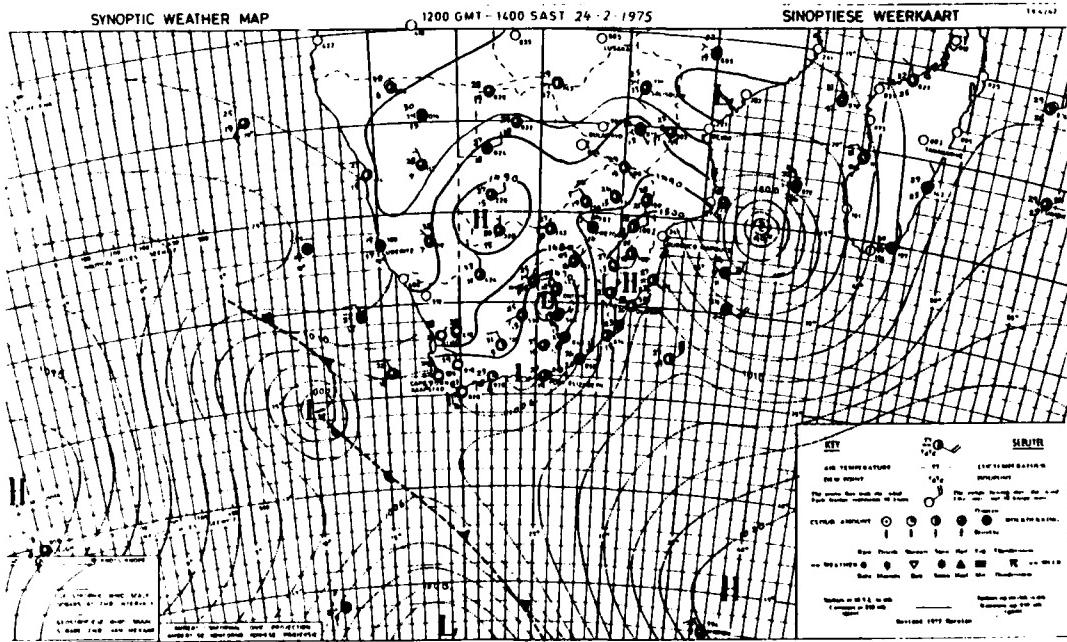


Fig. 4.4. Republic of South Africa Weather Bureau Surface (over Ocean) and 850 mb (over Continent) Analysis: 1200 GMT 24 February 1975

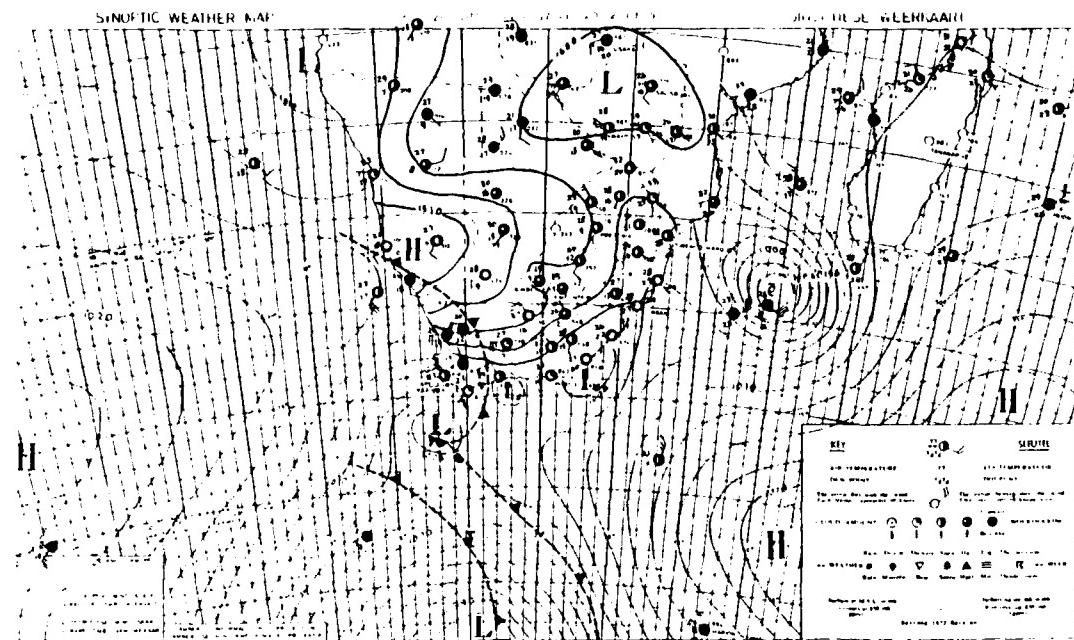


Fig. 4.5. Same as Fig. 4.4 except for 1200 GMT 25 February 1975

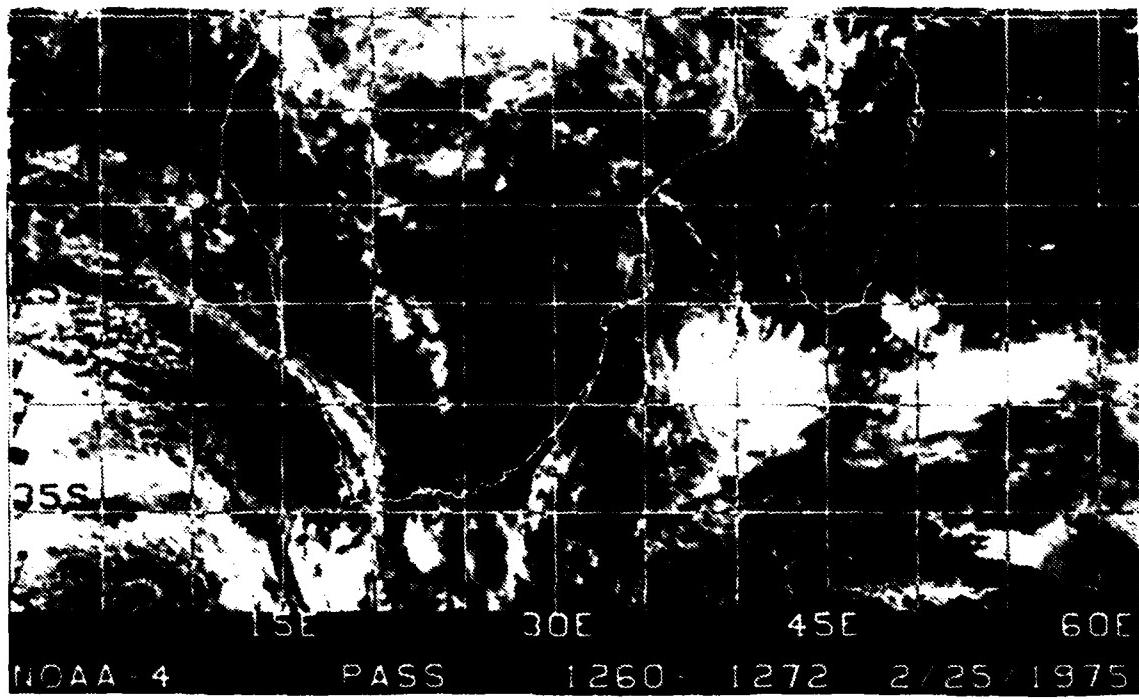


Fig. 4.6. NOAA 4 Visible Satellite Imagery (at approx. 0600 GMT at 45°E) 25 February 1975

## 4.2 WEATHER ASSOCIATED WITH TROPICAL CYCLONES

Weather phenomena over Mozambique, the Malagasy Republic and the surrounding south Indian Ocean vary significantly, depending on the track and intensity of the system.

### 4.2.1 Tropical Cyclones East of the Malagasy Republic

The following discussion is a case study of tropical cyclone Danae (Figs. 4.7 - 4.11). Winds\* on the Malagasy Republic's north and central east coast become moderate southeasterly as the tropical cyclone approaches from the northeast (Figs. 4.7 and 4.8). As the weather system continues southwestward, the northeast and central coasts of the Malagasy Republic experience south to southeasterly winds, broken to overcast clouds and developing rain showers prior to the cyclone passage. As the storm crosses into the island's northern and central interior (Figs. 4.9 and 4.10), northeasterly winds dominate over most of the east coast (except southerly winds found in the southern quadrant of the storm). Overcast clouds and rain also develop over most of the east coastal regions (heavier rains south of the system due to orographic lifting of onshore flow). Wind over the southwest coast becomes moderate southerly, while moderate westerly wind develops over the west coast north of the tropical cyclone. Overcast conditions and rain showers (frequently heavy) develop over the west coast north of the system. Rain shower activity decreases south of the center. After the tropical cyclone passes into the Mozambique Channel, coastal winds south of the system become moderate to strong northeasterly (Fig. 4.11). North of the system coastal wind is moderate northwesterly.

---

\* Discussions of wind and other weather phenomena over coastal Mozambique and the Malagasy Republic make use of observations from land-based stations. Wind speeds mentioned as 'typical' represent conditions ashore. Conditions over the coastal waters are likely to be more severe.

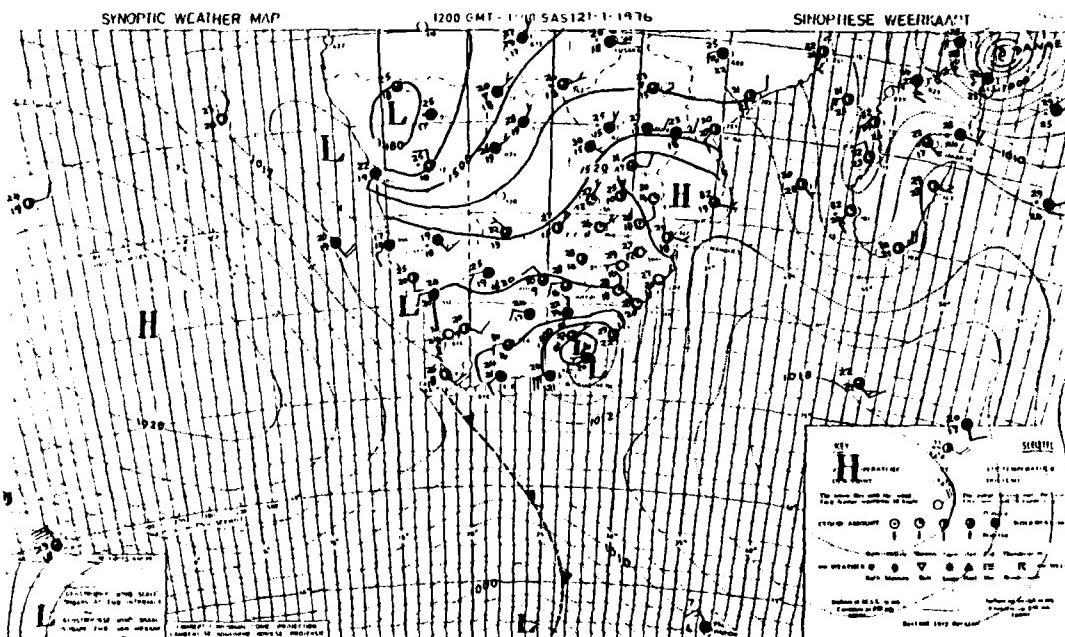


Fig. 4.7. Republic of South Africa Weather Bureau Surface (over Ocean) and 850 mb (over Continent) Analysis: 1200 GMT 21 January 1976

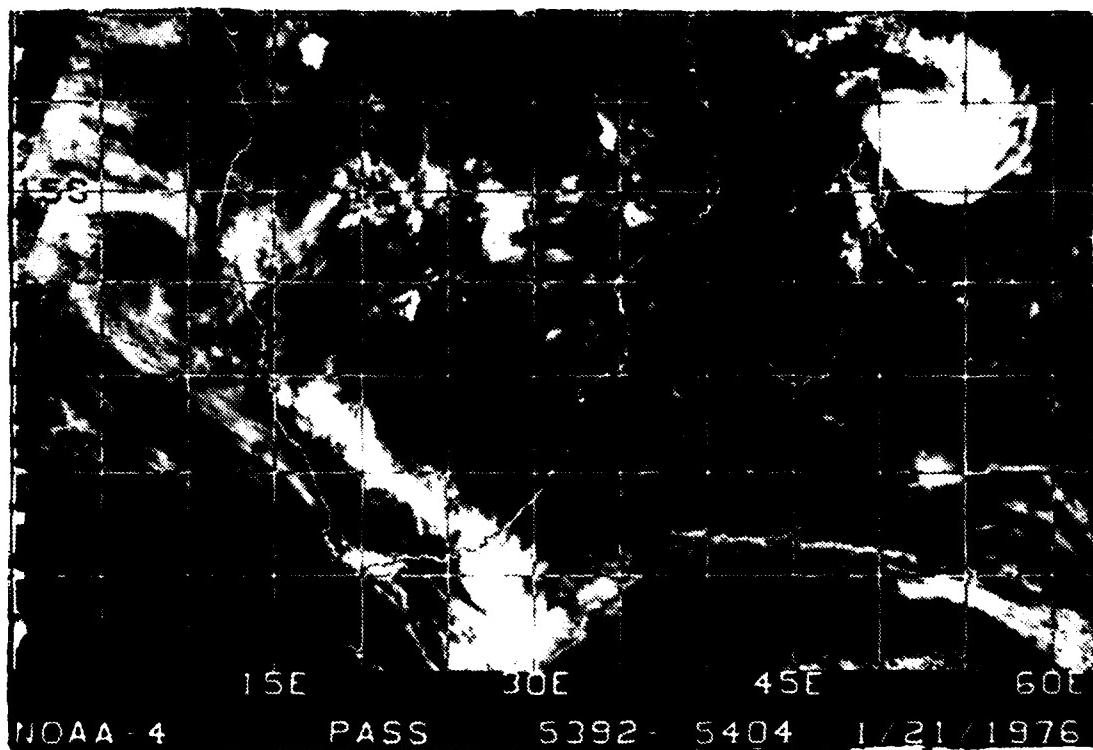


Fig. 4.8. NOAA 4 Visible Satellite Imagery (at approx. 0600 GMT at 45°E) 21 January 1976

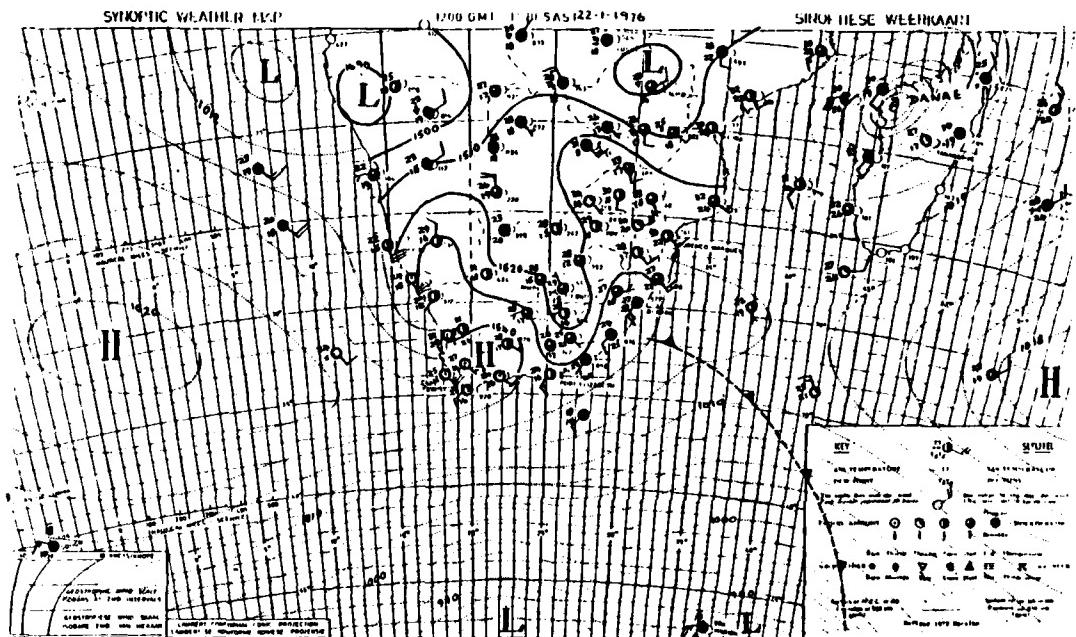


Fig. 4.9. Republic of South Africa Weather Bureau Surface (over Ocean) and 850 mb (over Continent) Analysis: 1200 GMT 22 January 1976



Fig. 4.10. NOAA 4 Visible Satellite Imagery (at approx. 0600 GMT at 45°E) 22 January 1976

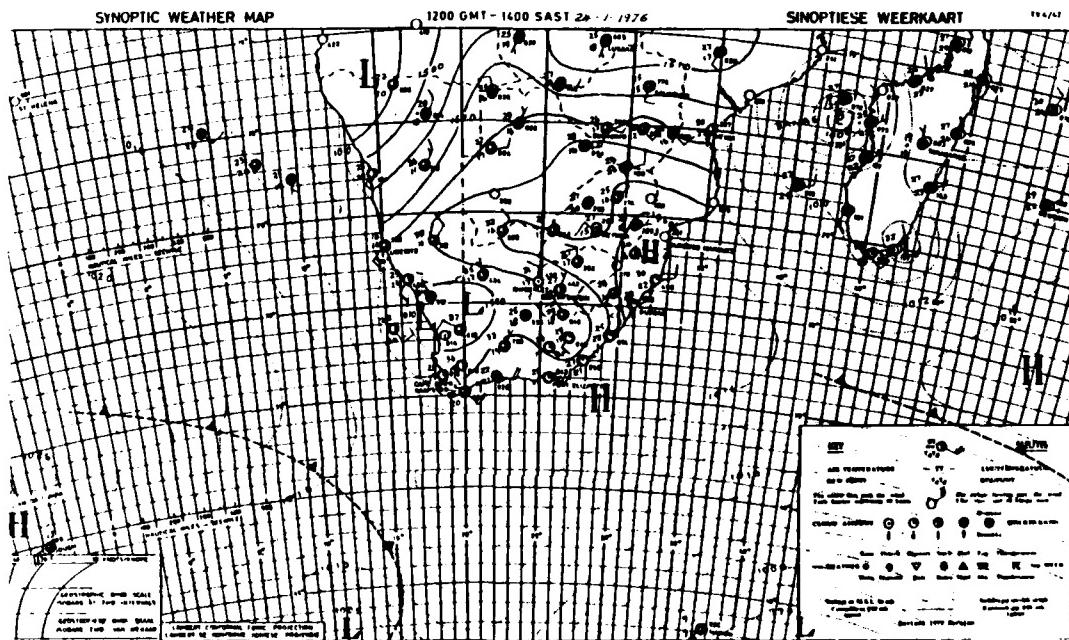


Fig. 4.11. Republic of South Africa Weather Bureau Surface (over Ocean) and 850 mb (over Continent) Analysis: 1200 GMT 24 January 1976

#### 4.2.2 Tropical Cyclones in the Mozambique Channel

##### a. Weather in Mozambique

Tropical cyclones moving into the channel from the north are frequently in the developing stage. Wind over northern coastal Mozambique is likely to become moderate southwesterly or southerly (Figs. 4.12 - 4.16). Broken to overcast cloud conditions and light to moderate rains develop. If the tropical cyclone moves to the east side of the Mozambique Channel, the system will have little effect over Mozambique. Storms developing or moving into the northern portion of the Mozambique Channel seldom continue southward on the west side. More frequently the storms move down the east side of the Channel and occasionally a system crosses over the Malagasy Republic into the Indian Ocean.

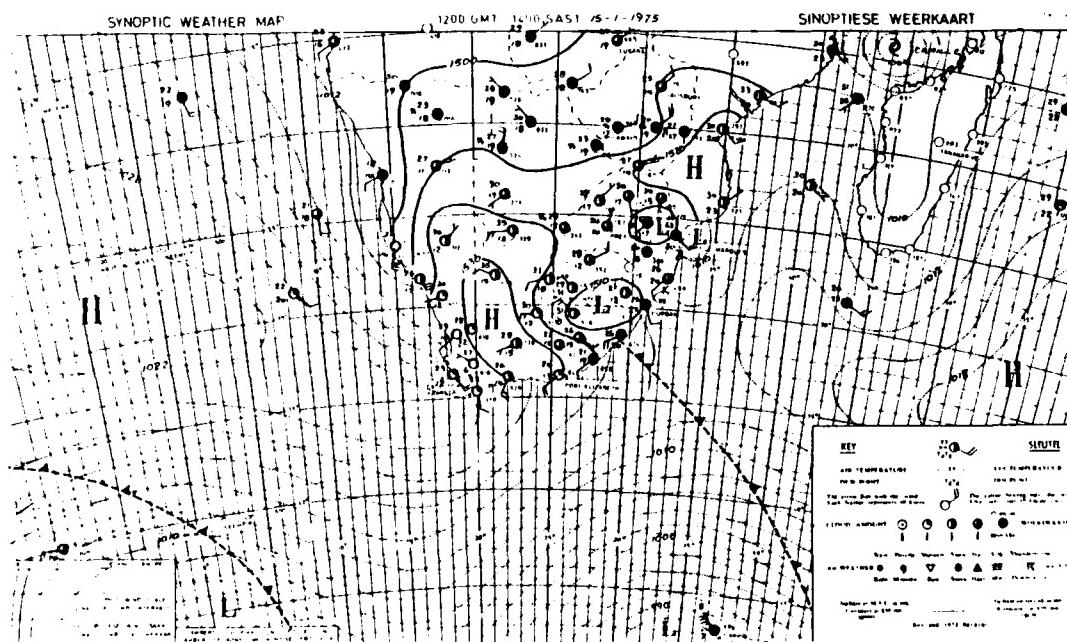


Fig. 4.12. Republic of South Africa Weather Bureau Surface (over Ocean) and 850 mb (over Continent) Analysis: 1200 GMT 15 January 1975

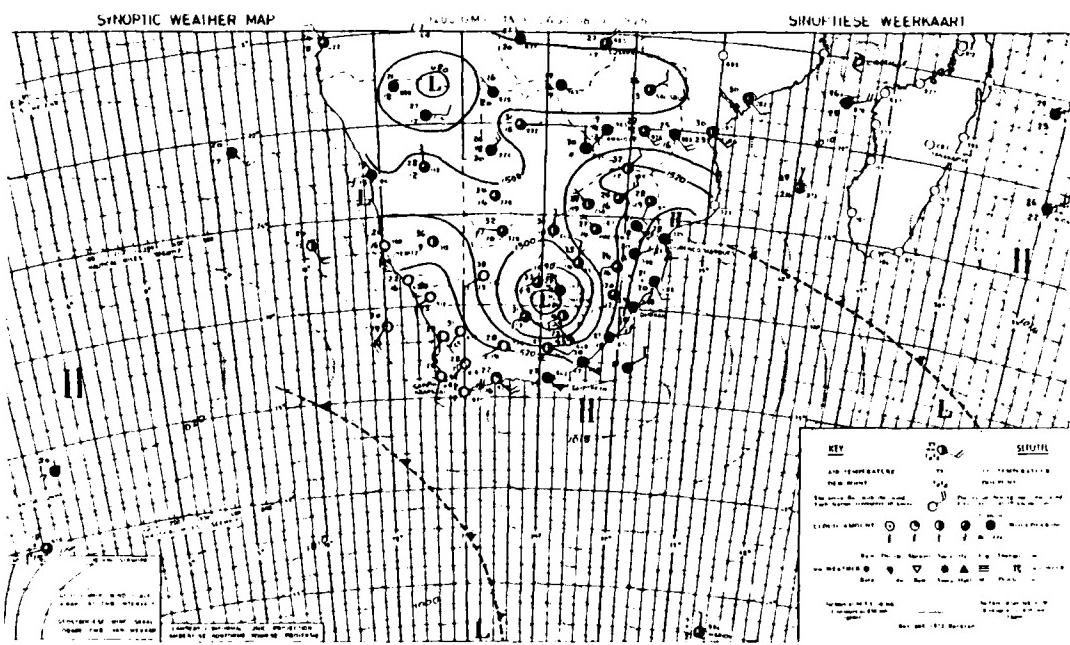


Fig. 4.13. Same as Fig. 4.12 except for 1200 GMT 16 January 1975

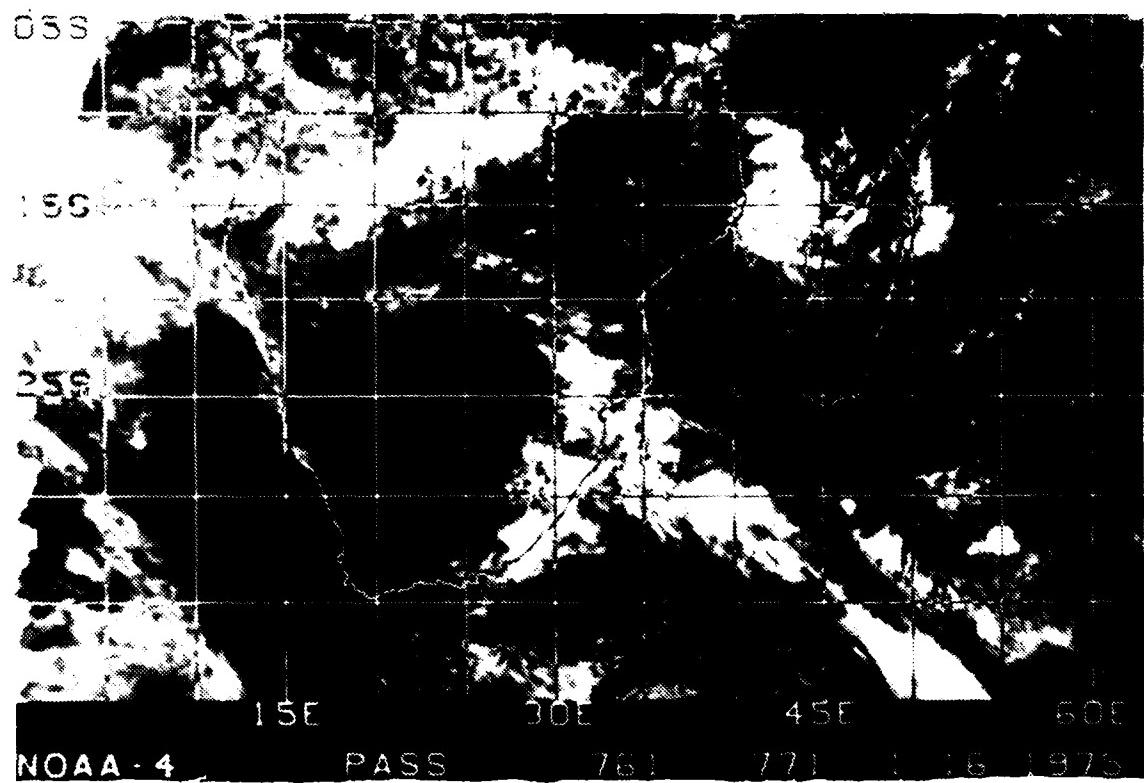


Fig. 4.14. NOAA 4 Visible Satellite Imagery (at approx. 0600 GMT at 45°E) 16 January 1975

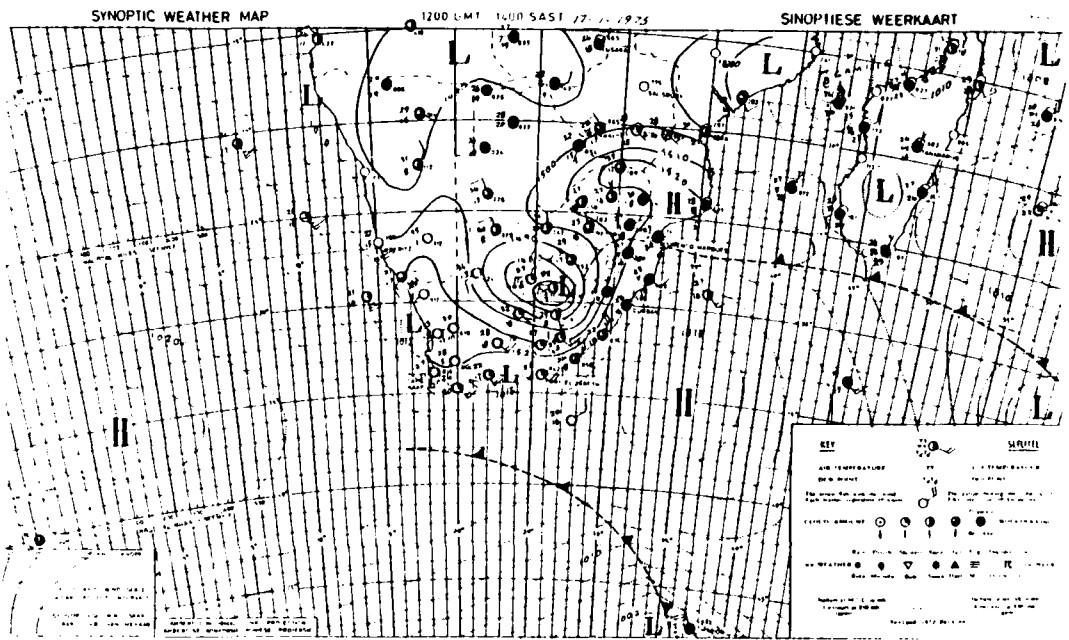


Fig. 4.15. Republic of South Africa Weather Bureau Surface (over Ocean) and 850 mb (over Continent) Analysis: 1200 GMT 17 January 1975

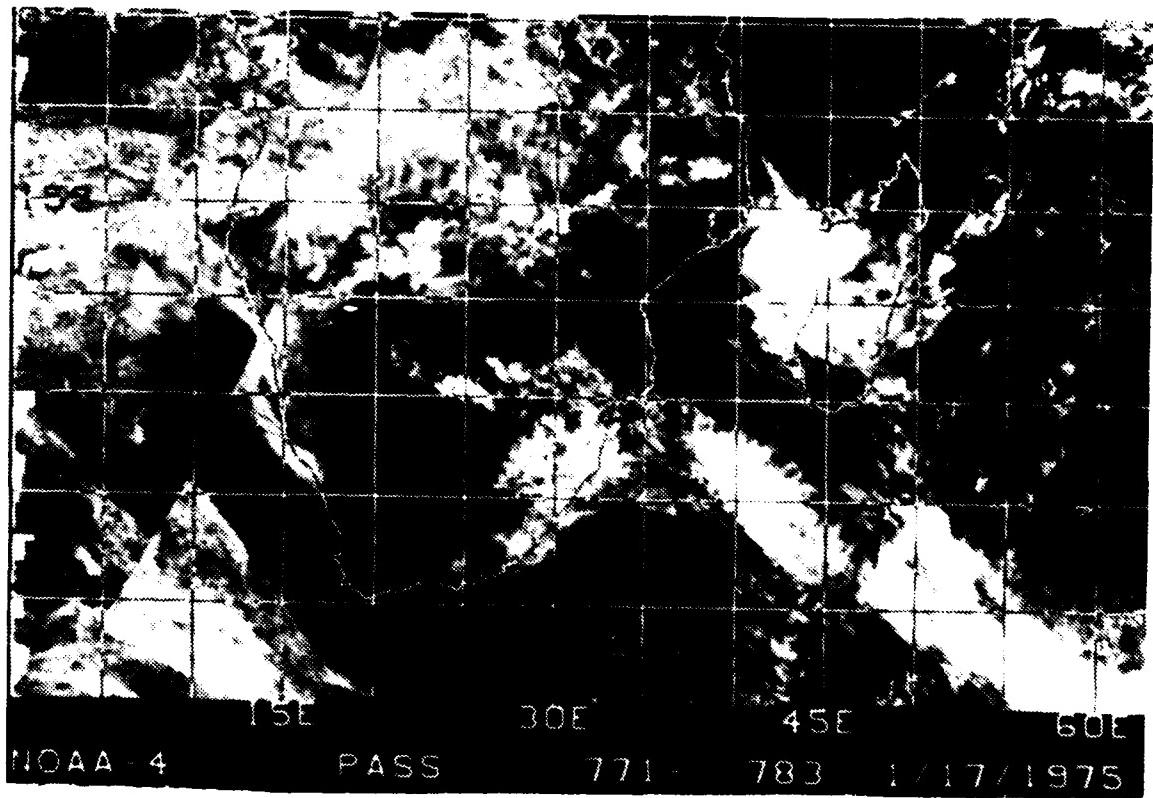


Fig. 4.16. NOAA 4 Visible Satellite Imagery (at approx. 0600 GMT at 45°E) 17 January 1975

A continuation of Danae's track is shown in Figs. 4.11, 4.17 - 4.19) to illustrate weather associated with the occasional cyclone tracking to the west side of the Channel. As the storm moves southwestward, winds over the northern coast of Mozambique are likely to become southwesterly. Heavy rain showers develop. Winds over the central coastal region of Mozambique become moderate to strong from the southeast (onshore) then southwest as the storm passes. Heavy rains develop along the central coast north and south of the tropical cyclone center. The winds over the south coastal region become south to southeast and begin to strengthen as the tropical cyclone continues southward (Figs. 4.17, 4.18). Winds over the northeast coast develop an offshore component. If landfall occurs over the central or southern Mozambique coast the system dissipates rapidly and winds weaken to the north and south (Fig. 4.19). Heavy rainfall and flooding are likely over large portions of the coast and interior of Mozambique. If landfall does not occur the system is likely to pass southward out of the Mozambique Channel. Weather over the central and southern coasts clears. Wind over the southern coastal region shifts to southwesterly and weakens. Recurvature of the cyclone to the southeast occurs rapidly.

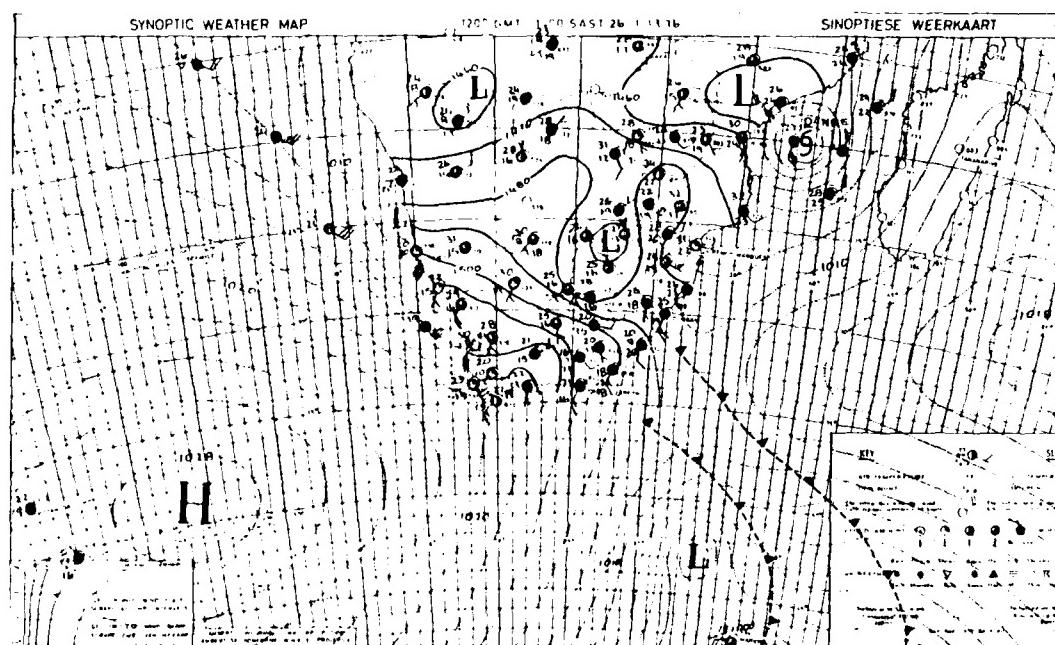


Fig. 4.17. Republic of South Africa Weather Bureau Surface (over Ocean) and 850 mb (over Continent) Analysis: 1200 GMT 26 January 1976

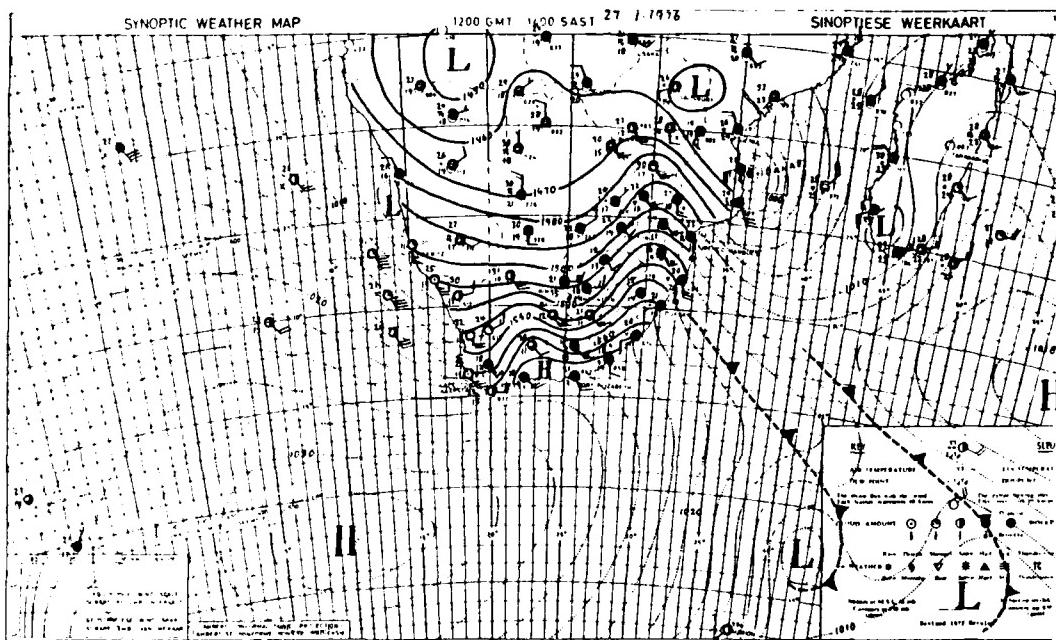


Fig. 4.18. Republic of South Africa Weather Bureau Surface (over Ocean) and 850 mb (over Continent) Analysis: 1200 GMT 27 January 1976

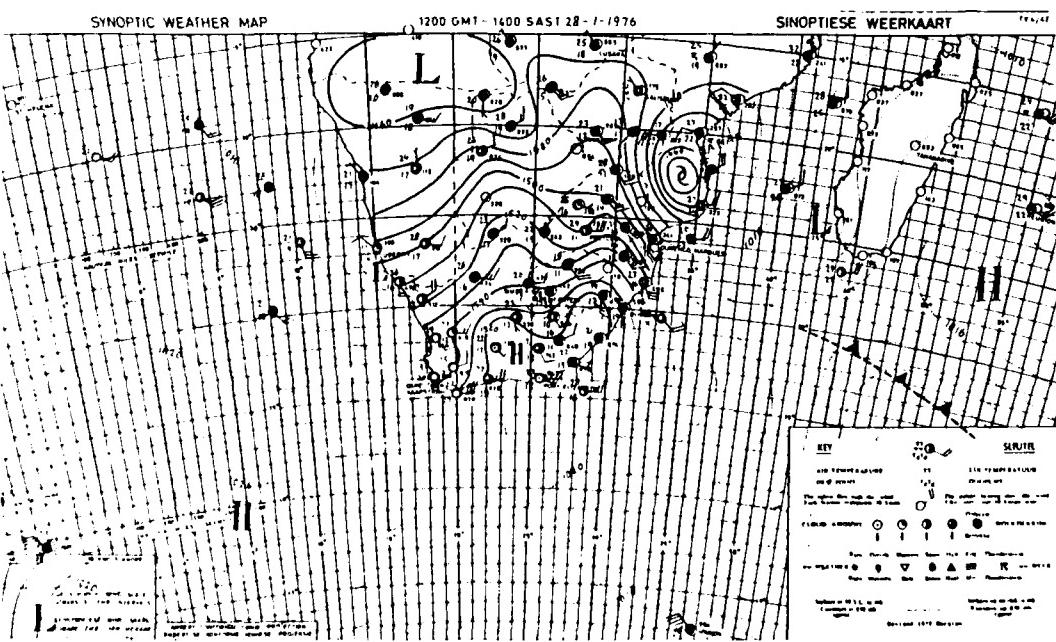


Fig. 4.19. Same as Fig. 4.18 except for 1200 GMT 28 January 1976

Tropical cyclones frequently re-intensify when moving from the Malagasy Republic into the Mozambique Channel. Motion of storms in the Mozambique Channel is occasionally slow and erratic as in the case of tropical cyclone Caroline (Figs. 4.20 - 4.22) (i.e., tropical cyclone Caroline meandered *northward* for several days before dissipating over southern Mozambique). However, storms generally move southward out of the channel then rapidly recurve southeastward into the Indian Ocean.

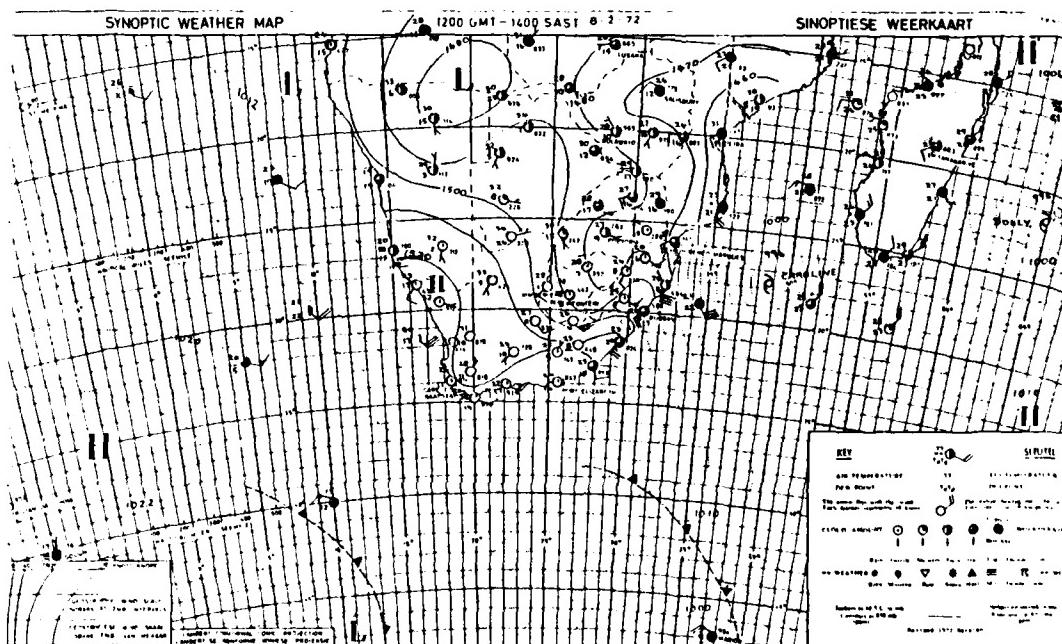


Fig. 4.20. Same as Fig. 4.18 except for 1200 GMT 8 February 1972

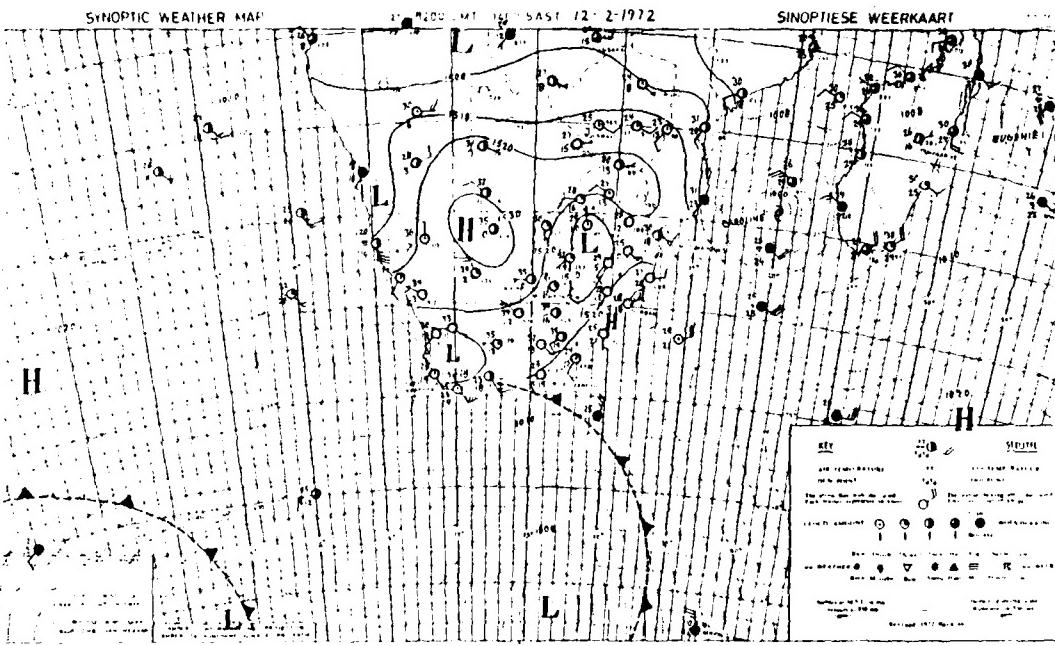


Fig. 4.21. Republic of South Africa Weather Bureau Surface (over Ocean) and 850 mb (over Continent) Analysis: 1200 GMT 12 February 1972

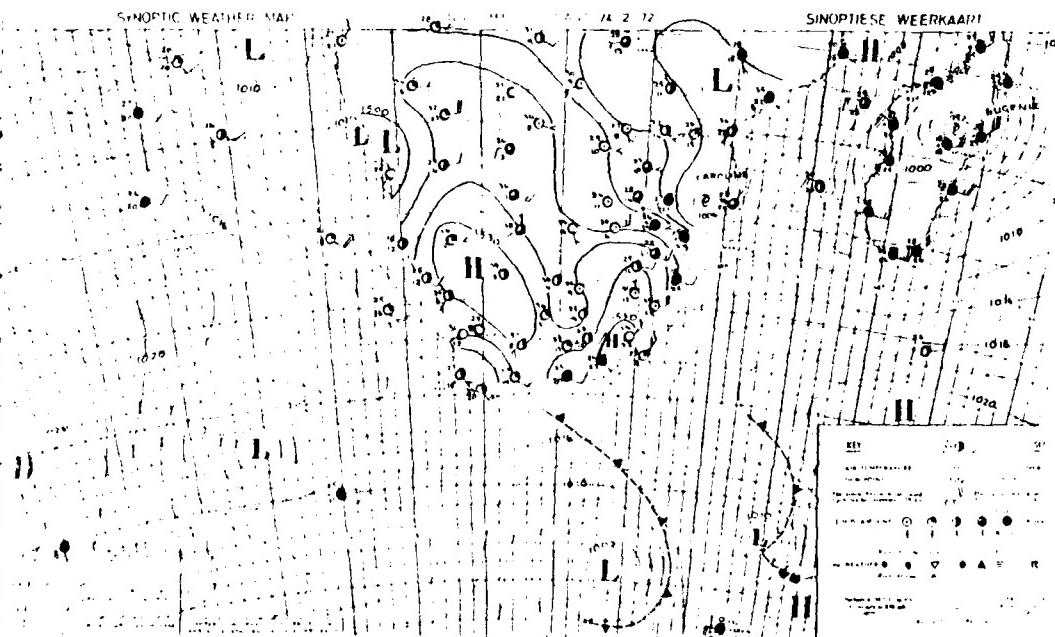


Fig. 4.22. Same as Fig. 4.21 except for 1200 GMT 14 February 1972

### b. Weather over the Malagasy Republic

Tropical cyclones which move to the east side of the Mozambique Channel significantly affect the weather of the Malagasy Republic. Occasionally, storms entering the northern Mozambique Channel move southeastward over the northwest coast of the Malagasy Republic. Storms crossing the Malagasy Republic from west to east follow various and sometimes erratic paths, and the weather associated with these systems varies. A brief case study follows on tropical cyclone Charlotte (Figs. 4.23 - 4.26). Tropical cyclone Charlotte appears to be representative of a typical storm passage over the island. Winds on the northwest coast become strong northerly as the system approaches, and heavy rainfall ensues (Fig. 4.23). Over the central western coast, southwesterly winds develop as the system moves across the island (Fig. 4.24). Broken/overcast clouds and rain showers develop on the west coast. As the storm advances toward the east side of the Malagasy Republic, winds over the central and southwest coasts become westerly (Fig. 4.25). Rains (frequently heavy) are likely to develop over the southeast coast. When the system moves over the Indian Ocean, winds on the east coast north of the system develop an offshore component, while winds over the southeast coast become southeasterly (Fig. 4.26). The likelihood of offshore winds over the northern and central east coast increases with the horizontal dimensions of the tropical cyclone. Tropical cyclones often re-intensify when moving from the Malagasy Republic to the Indian Ocean. The radius of 30 kt winds will increase significantly.

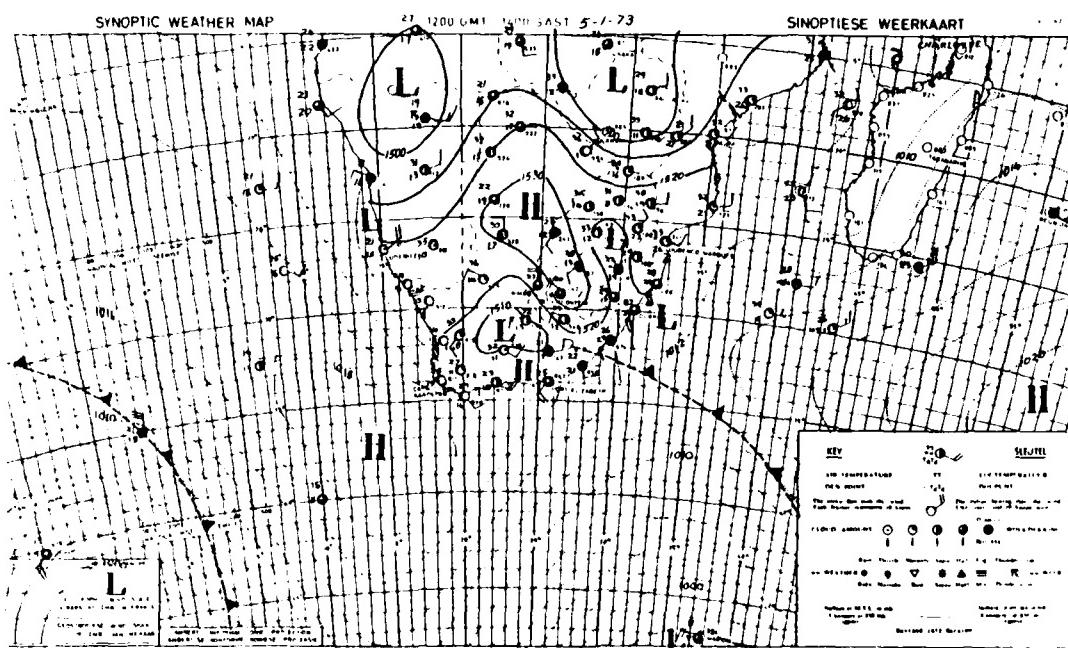


Fig. 4.23. Republic of South Africa Weather Bureau Surface (over Ocean) and 850 mb (over Continent) Analysis: 1200 GMT 5 January 1973

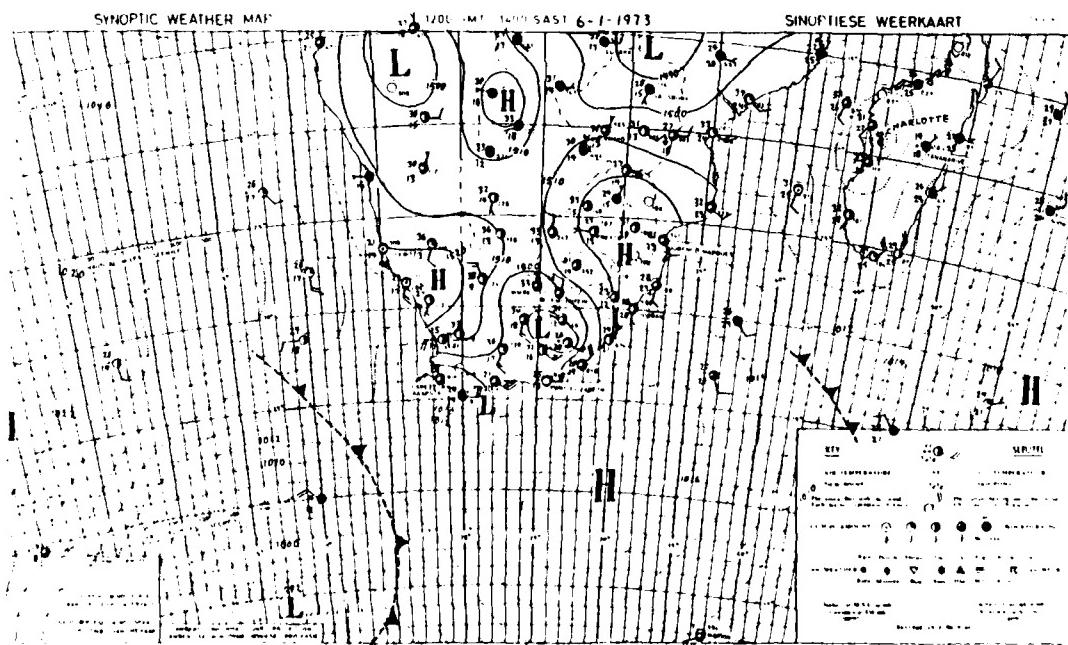
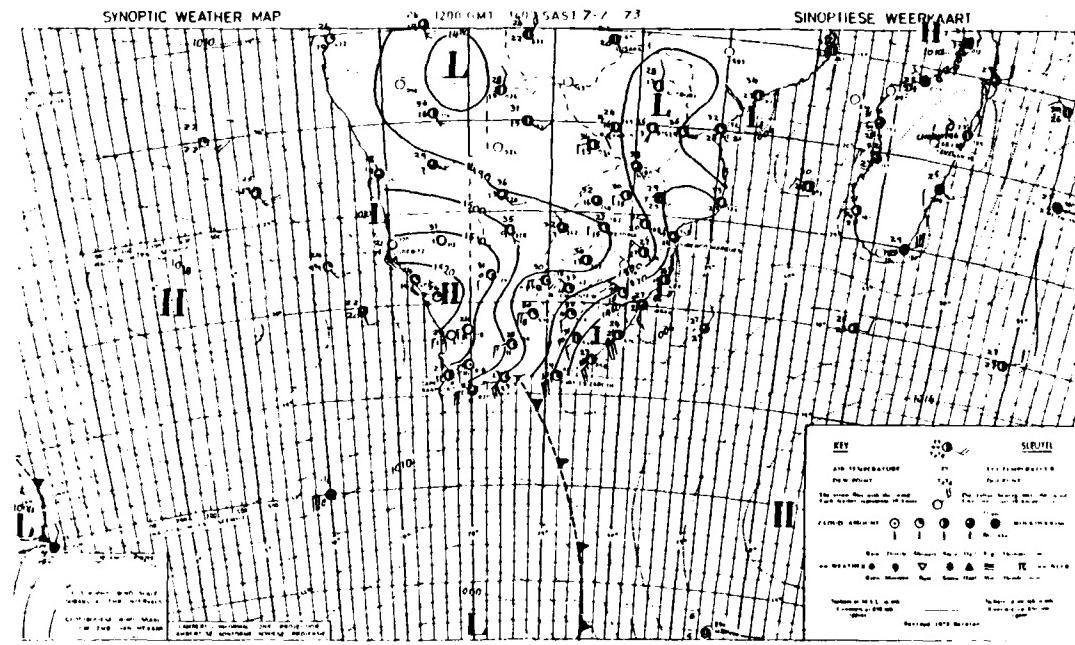


Fig. 4.24. Same as Fig. 4.23 except for 1200 GMT 6 January 1973



Tropical cyclones occasionally cross the southern Malagasy Republic from the Mozambique Channel. As tropical cyclone Camille approaches the southwest coast, winds over most of the central northwest coast become moderate northwesterly (Fig. 4.27). This wind is strengthened if ridging occurs over the Mozambique Channel from the north. Wind south of the system becomes moderate easterly (offshore). Rain and overcast conditions develop over the central west coast in advance of landfall. Winds shift to westerly on the west coast, and northerly on the east coast, as the system passes over the southern Malagasy Republic (Fig. 4.28). On the southeast coast (south of the system) wind becomes northeasterly with overcast conditions and rain showers (Fig. 4.28). Rain showers decrease northward from the system and terminate over the central east coast. When the system moves out over the Indian Ocean the winds over the southeast coastal region become southerly and decrease (Fig. 4.29).

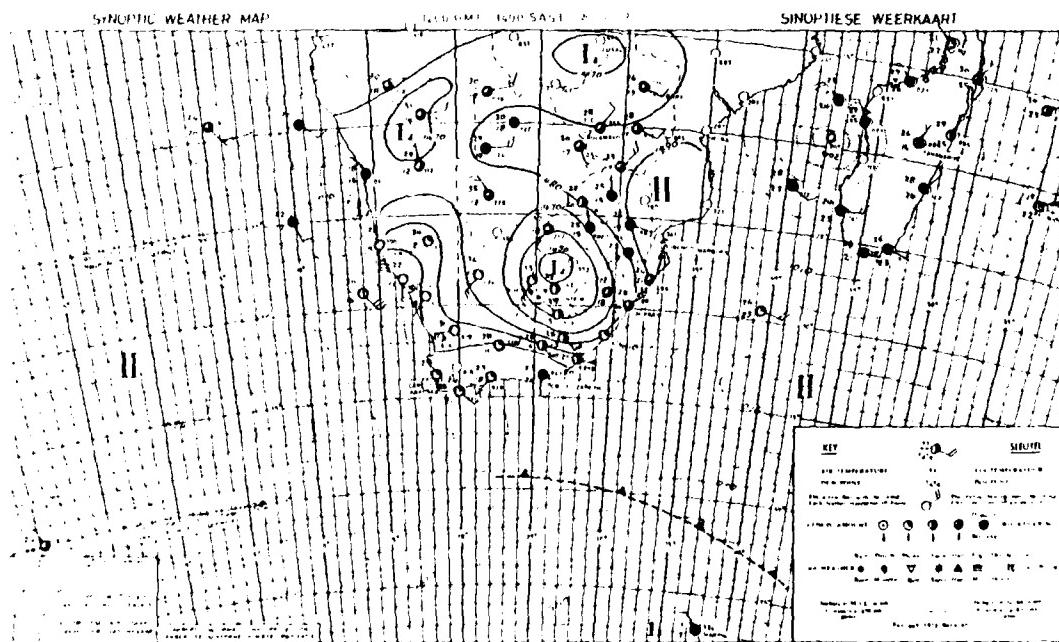


Fig. 4.27. Republic of South Africa Weather Bureau Surface (over Ocean) and 850 mb (over Continent) Analysis: 1200 GMT 18 January 1975

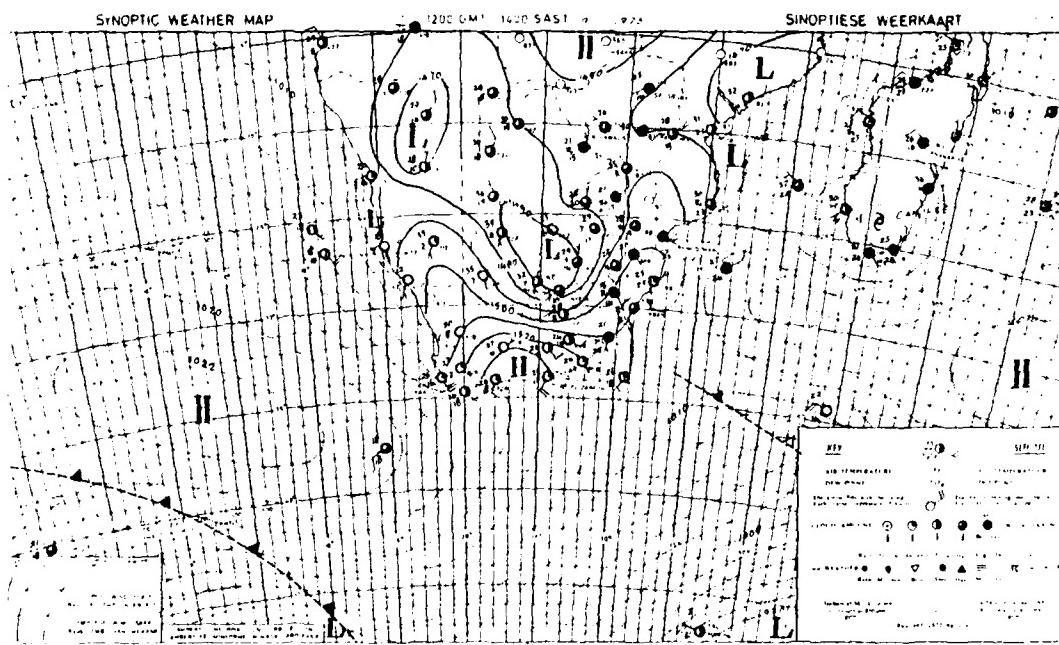


Fig. 4.28. Same as Fig. 4.27 except for 1200 GMT 19 January 1975

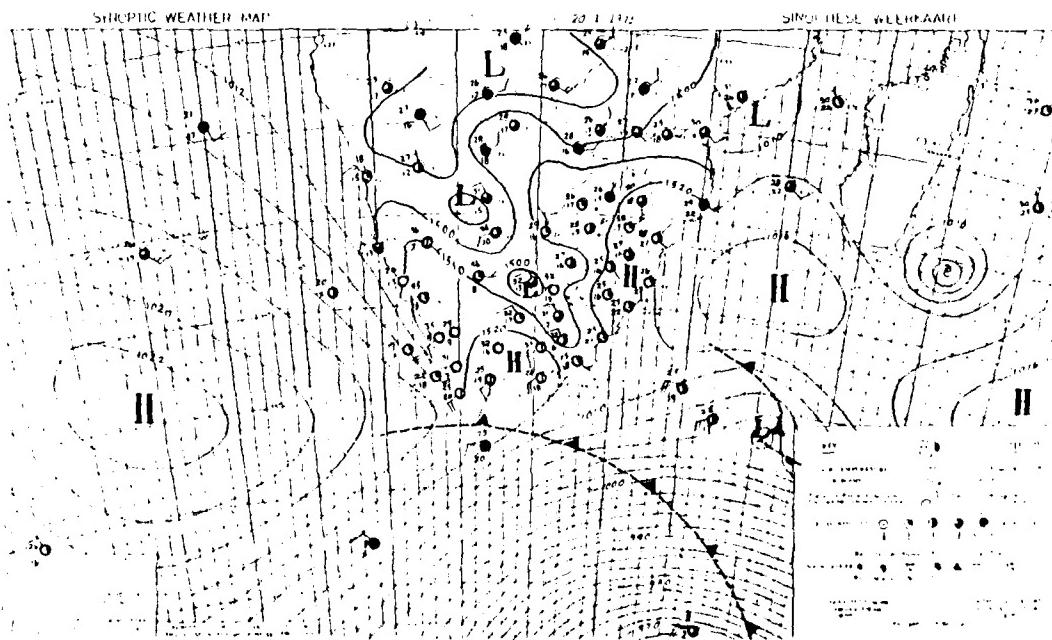


Fig. 4.29. Same as Fig. 4.27 except for 1200 GMT 20 January 1975

## 4.3 THE ISLANDS OF MAURITIUS AND REUNION, AND THE SEYCHELLES

### 4.3.1 Mauritius and Reunion (*Islands east of Malagasy Republic*)

The geographical locations of Mauritius and Reunion are shown in Fig. 1.1. Mauritius has a weather service and issues weather forecasts. Weather over Mauritius and Reunion falls into one of two basic patterns. Most of the year these islands are influenced by strong or moderate southeasterly winds and associated cool and dry conditions. This weather occurs in association with the strong Indian Ocean anticyclone. The anticyclone (and associated southeasterly flow) is most intense from June through September. During the period from September through March the southeasterlies are often interrupted when the subtropical anticyclone weakens sufficiently or withdraws from this portion of the Indian Ocean. Southeasterly flow is replaced by northerly flow of warm moist tropical air into the area. When the subtropical ridge is reestablished over the area, the southeasterlies are restored. The cool air from polar and mid-southern latitudes flows under and lifts the tropical air. Associated cloud development and rain shower activity is extensive and sometimes lasts for several days. Southeasterly flow can become strong in these situations (25 - 35 kt over water) if westward ridging of the subtropical anticyclone is intense. The second of the two basic patterns occurs when the anticyclone is replaced by a tropical depression south of Mauritius. This occurs most frequently from December through March. Weak northerly flow over the area is associated with these situations, and cumulonimbus clouds and convective rain shower activity is likely to develop in the afternoon. Occasionally thunderstorm activity develops in this situation (Naval Environmental Prediction Research Facility, 1980a).

#### a. Precipitation

Several types of rainfall affect Mauritius and Reunion at different times of the year. Orographic rains are light and most prevalent over these islands when strong southeasterlies are present. From November to April the islands come under the influence of weak tropical depressions and occasionally tropical cyclones. Rains associated with these systems are sometimes heavy but seldom steady. Heavy rain shower activity occurs for short periods (several hours), separated by periods of light rain. This kind of activity may continue for two to three days. Another type of rainfall occurs in association with frontal activity. This is convective rainfall, occasionally with thunderstorm activity (Naval Environmental Research Facility, 1980a).

The Mauritian rainy season lasts from December through April. Most of the rainfall occurs from January through March and is associated with passing tropical cyclones. The rainy season at Reunion occurs from November through April. Most of the rain falls from December through March, also in association with passing tropical cyclones. A significant portion of the rainfall on Reunion is orographically induced. The island's mountain range (maximum elevation - 8000 ft) is perpendicular to the southeasterly flow. Therefore, the east side of the island receives frequent rain showers in southeasterly flow while the west side

remains relatively dry. Rain shower activity over Reunion is generally discontinuous and seldom heavy (Naval Environmental Prediction Research Facility, 1980a).

#### 4.3.2 Seychelles Islands (Islands northeast of Malagasy Republic)

The Seychelles Islands are positioned close enough to the equator (Fig. 1.1) so that they are under the influence of tropical air year round. Weather over the Seychelles Islands is dominated by east and southeasterly monsoonal winds from mid-April to mid-November. Sustained wind of 10 kt is typical during this period. Strongest flow (occasionally sustained wind 25 - 35 kt) occurs in July and August when the Indian Ocean subtropical high is strongest. The northwest monsoon (derived from the Northern Hemisphere northeast monsoon) moves over the islands in mid-November and dominates regional weather through mid-April. Winds associated with the northeast monsoon are light (mean flow 5 kt) and calms are frequent (November - January) (Naval Environmental Prediction Research Facility, 1980a).

##### a. Precipitation

The wet season is from November to March and the highest rainfall occurs in December and January. The driest period of the year is July and August. Rainfall gradually increases in September and October but in November there is a large increase in rainfall. This increase occurs in association with squall activity. Squalls occur over the Seychelles from November through January and are associated with low level turbulence and heavy rain showers. Winds are likely to increase rapidly to 25 - 35 kt (over land) with the approach of a squall. Despite the existence of the wet season from November to April during the northwest monsoon, Mahe, the largest of the Seychelles Islands, has experienced the maximum 24-h rainfall during the month of September while southeasterly flow still dominates (Naval Environmental Prediction Research Facility, 1980a).

#### 4.3.3 Thunderstorms (Mauritius, Reunion and the Seychelles)

Thunderstorms occur only occasionally over Mauritius and Reunion. Over Mauritius the highest frequency of occurrence is from November to May. The maximum mean of five thunderstorms per month occurs in March. The most severe storms occur in association with nearby, passing tropical cyclones. During the months of December through March, unstable conditions occasionally develop in association with converging unstable northerly (warm moist) flow. Thunderstorm activity occasionally persists for two to three days when such flow develops. Over Reunion an average of ten thunderstorms are observed annually and virtually all of the activity occurs between November and April.

Thunderstorms over the Seychelles Islands are also infrequent. The maximum frequency of occurrence is from December through May (two to three per month). Activity is most likely associated with squalls and with tropical depressions passing south of the islands.

#### 4.3.4 Tropical Cyclones Affecting the Islands

Tropical cyclones occur most frequently from November through April. Early in the season storms generally track east of the Malagasy Republic near Mauritius and Reunion or farther east. The storms develop farther west in December through March (see Table 4.1) (Naval Environmental Prediction Research Facility, 1980a). In April tropical cyclones generally develop and track a considerable distance east of Mauritius and Reunion. The Seychelles Islands seldom experience heavy weather (other than rain showers) in association with tropical cyclones as these systems generally pass well south of the islands before developing significantly. Information concerning these systems in the form of warning and bulletins is made available by the United States Navy/Air Force Joint Typhoon Warning Center, Guam (JTWC) and by the Mauritian Weather Service.

## Section 5

### KENYA AND TANZANIA

#### 5.1 TOPOGRAPHY

The most significant topographical features are the mountainous highlands of western Kenya and northeastern Tanzania (Figs. 1.1, 1.2 and 5.1). The interior mountains ascend to 6000 m (Griffiths, 1972). The mountains extend almost to the ocean at the Kenya-Tanzania border. The eastern portions of Kenya and southeastern Tanzania are mostly lowlands and plains with elevations between sea level and 500 m. The western interior of Tanzania is mostly plateau (1000 m) ascending toward the west, northwest and toward the mountainous northeast (over 2000 m) (Editions Jenne Afrique, 1973). Lake Victoria extends over a large portion of northern Tanzania and also into western Kenya.

Kenya and Tanzania are positioned geographically such that weather is dominated year round by monsoonal flow. Northeast monsoons dominate from December through March (Northern Hemisphere winter monsoon) and the southeast/southwest monsoon dominates from June through September (Northern Hemisphere summer monsoon). Both monsoon flows are shallow, averaging only 2 km in depth, and are capped by inversion and dry subsiding air. Stratus/stratocumulus overcasts occur frequently over Nairobi and the surrounding region in association with this inversion. Additionally, flow in both of the monsoons is divergent over the eastern portions of Kenya and northern Tanzania. The associated rainfall over these regions is light or insignificant except during the transition periods. A semipermanent heat low over southwestern Kenya is a cause for intense thunderstorm activity over the Rift Valley region and the surrounding west Kenyan highlands during the winter and summer monsoons. Other significant synoptic features include the low-level jet which develops over the Kenya/Somali coast during the austral (southern) winter months, and the strong low-level southeasterly jet present year round between the Kenyan and Ethiopian highlands.



Fig. 5.1. Station Locations of Kenya and Tanzania  
(After Griffiths, 1972)

## 5.2 SURFACE WINDS

### 5.2.1 Kenya

The mean surface wind is less than 10 kt over most of Kenya and calms occur frequently at night. An exception to this rule is in Equator, Kenya (Fig. 5.1) where the mean wind is 16-17 kt during the austral summer. The strongest winds occur in association with thunderstorm activity which occurs mostly over the western plateau throughout the year. Convection and thunderstorm activity occur over the eastern plains in March and April. Strong winds also occur frequently over the coastal region. Diurnal variation of the winds is greatest over the coastal region and in the vicinity of Lake Victoria. On the coast at Mombasa (Fig. 5.1) the annual mean wind varies from 5 kt at 0600 to 13 kt at 1200 (LST). There is little seasonal change in the diurnal variation. Over most of the western plateau there is no diurnal variation in surface wind velocities.

### 5.2.2 Tanzania

Surface winds over Tanzania vary little from one location to another and are generally weak (mean winds less than 10 kt over most of the country) during the entire year. As in Kenya, the strongest winds occur in association with convection and thunderstorm activity, which is most prevalent in the vicinity of the western lakes. The weakest winds occur over the northeast interior. The monthly mean maximum winds at Morogoro, Tanzania (Fig. 5.1) do not exceed 6 kt. Over the coastal region south of 5°S, southeasterlies during the month of June are often 10-20 kt and occasionally strengthen to 25 to 35 kt (United States Naval Weather Service Command, 1974). The extreme south coast is likely to experience strong (greater than 20 kt) southeasterly winds in January and February in association with tropical cyclones to the south. From June to September occasionally strong (greater than 20 kt) winds may occur in association with frontal passages to the south and east. The strongest winds over most of Tanzania occur from July through September, although seasonal variation is small. Diurnal variation of the wind is strongest over the coastal regions and in the vicinity of the lakes. The annual mean wind on the coast at Dar es Salaam (Fig. 5.1) varies from 2.5 kt at 0600 to 5 kt at 1200 (LST). Over the central interior there is virtually no diurnal wind variation (Griffiths, 1972).

### 5.3 TEMPERATURE

The annual temperature variation over Kenya and Tanzania is six degrees Celsius or less. The annual mean maximum temperature in Mombasa and Dar es Salaam is 30°C (86°F), and monthly mean maximum temperatures fluctuate within three degrees (Mombasa) and within one degree (Dar es Salaam) of this value. Spatial variation of temperature over the region is small and is due almost entirely to changes in elevation. The western highlands are five to ten degrees cooler than the coastal region. The hottest portion of the region is the interior lowlands where temperatures often climb above 32°C (90°F). The coldest period of the year is in July-August. The warmest period is in March over most of Kenya and northern Tanzania. In south and central Tanzania, November and December are the warmest months. The diurnal temperature variation is 10 to 13°C over most of the region. The exceptions to this are the coastal region and in the vicinity of the lakes where the diurnal temperature variation is seven to nine degrees Celsius. Diurnal temperature ranges do not vary significantly from summer to winter (Griffiths, 1972).

## 5.4 SIGNIFICANT WEATHER SYSTEMS

### 5.4.1 Austral Summer

#### a. Kenya

Northeasterly flow is present over Kenya in austral summer months (Fig. 5.2) due to the influence of the Arabian anticyclone. The low-level large scale flow diverges over the east Kenyan plains. Part of the flow continues south, drawn by the heat low over Mozambique and the other portion branches westward toward the heat low over the Rift Valley. The large scale flow is strongest in January. The flow is warm moist and unstable but also shallow and meridional. The northeasterly monsoon is associated with frequent rains over the western highlands. Surges of tropical westerly flow over western Kenya are associated with occasionally intense rainfall. The east Kenyan plains are hot and dry in winter due to the effect of low-level diverging winds (Trewartha, 1981).

#### b. Tanzania

Shallow (low-level) northeast monsoonal flow dominates weather over Tanzania in summer (Fig 5.2). The shallow monsoonal flow diverges over the northeastern portion of the country and is associated with hot rainless weather over the region. The flow over the south travels a greater distance over water than the flow over northern Tanzania and is more moist. The low-level flow converges over the south and southwest portions of the country as it flows toward the southwest African low. Rain shower activity over south and southwestern Tanzania is greatest in the summer period. This is also the rainy season over north central Tanzania east of Lake Victoria (Griffiths, 1972). Much convection occurs over the western interior and mountains in association with convergence of highly unstable westerly flow with the tropical northeasterlies.

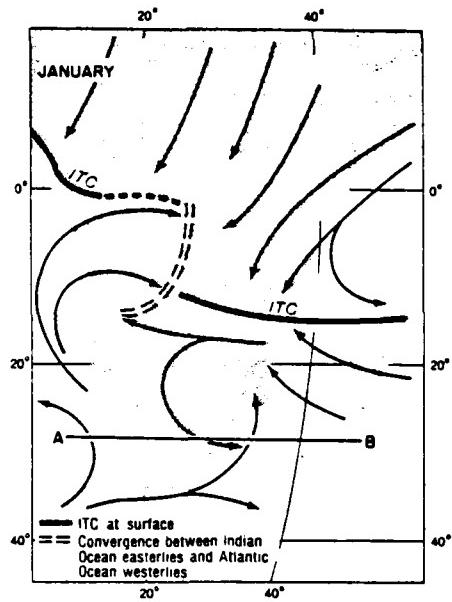


Fig. 5.2. Mean Northeasterly Monsoon Flow at lower levels over eastern and southern Africa: January (Trewartha, 1981)

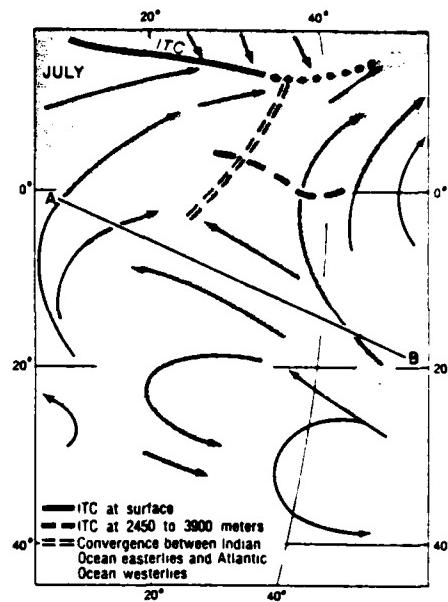


Fig. 5.3. Mean Southwesterly or Southeasterly Monsoon Flow at lower levels over eastern and southern Africa: July (Trewartha, 1981)

#### 5.4.2 Austral Winter

##### a. Kenya

Southeasterly/southwesterly flow dominates weather over Kenya in the winter months (Fig. 5.3). This flow is shallow but increases in depth to 2400 m to 3600 m (above sea level) near the equator. The flow is strongest in May and June. In June the winds over the Kenya coastal waters generally exceed 16 kt and sometimes strengthen to 25-35 kt (Naval Environmental Prediction Research Facility, 1980b). The anticyclone over the southwest Indian Ocean has made its farthest penetration northward. Additionally, the semipermanent low center over southwest Asia is at its northernmost position. The southerly flow over eastern Kenya is divergent. The major flow continues northward towards the low over southwest Asia while a minor flow branches westward into the heat low over the Rift Valley. Divergent flow over eastern Kenya is associated with hot, dry weather during the winter months. However, the west Kenyan highlands experience frequent heavy rainfalls during the winter months. The southerly monsoon flow is more unstable and less meridional than the northeasterly (summer) monsoon. The associated rainfalls over the western highlands are frequent and occasionally heavy.

Occasionally, in the winter months, belts of rain shower activity develop over the coastal ocean waters. The belts are oriented from north-northeast to south-southwest and advance toward the coast after formation. A possible cause for such a development is surging in the southeast monsoonal flow. The likelihood of this kind of rain shower activity increases in September (Trewartha, 1981). Fog (associated with upwelling) is likely when strong southeasterlies develop over the coastal waters.

#### b. Tanzania

The winter southeast monsoon flow divides over Tanzania, one major flow continuing northward and the other flowing northwestward (Fig. 5.3). The southeasterly flow is strongest in June when winds are often 10-20 kt (sometimes up to 35 kt) over the Tanzania coastal water (Naval Weather Service, 1974). The flow is also shallow (less than 2 km deep) (Trewartha, 1981). Weather over most of Tanzania is hot and rainless in winter in association with the low-level divergence. The southwest African low, present during the summer period, is replaced by a low-level anticyclone in winter. Aloft (500 mb), strong convergence and subsidence is present over much of Tanzania (Anyamba and Kiangi, 1983). Rain shower activity is infrequent over most of the country. Even in the vicinity of the western lakes thunderstorm activity is reduced significantly. Over the coastal region fog is likely when the southerly flow is strong. The fog occurs in association with upwelling of the coastal waters.

### 5.4.3 Transition Periods (April-May and October-November)

#### a. Kenya

During the transition periods wind flow is weaker and easterly. This is the most unstable flow occurring over Kenya and is associated with increased rain shower activity over the eastern lowlands. Converging easterlies and rain shower activity are most likely when an equatorial duct develops over the country. The duct develops when anticyclones are present on both sides of the equator, positioned on a north-south axis (Fig. 5.4) (Trewartha, 1981). Cross contour flow and convergence occurs at the entry point on the east side of the duct. Extensive cloud development and rain shower activity is likely to develop in this region. At the exit on the west side of the duct the flow is decelerating and diverging (World Meteorological Organization, 1964). The likelihood of rain shower activity increases over eastern Kenya if either or both of the anticyclones intensify. The equatorial duct is occasionally displaced four to five degrees of latitude away from the equator. The rains which occur in October - November are much less significant than those in April - May over the eastern lowlands. Occurrence of the duct is critical to the development of rains in the October - November period. If the Southern Hemisphere subtropical high recedes southward early in the transition period or if the anticyclone north of the equator is slow in establishing itself, rains in October and November will be light or insignificant over the east.

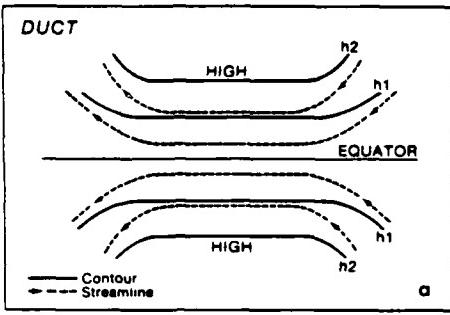


Fig. 5.4. Equatorial Duct (Trewartha, 1981)

#### b. Tanzania

During the transition periods the flow over Tanzania is weak and easterly. This flow is similar to the warm, moist and highly unstable air present over Kenya during the same period. Rain shower activity is maximum in the northeast portion of the country in March and April. In Dar es Salaam and Morogoro, between 50 and 60% of the mean annual rain falls from March through May. Rain shower activity does occur, though much less frequently, in the other (October-November) transition period. Frequent and occasionally heavy rain shower activity is likely over northeast and north central Tanzania when the equatorial duct develops. Intensification of either anticyclone (north or south of the duct) in such a situation increases the likelihood of heavy rain shower activity.

#### 5.4.4 Thunderstorms

##### a. Kenya

Thunderstorms occur during summer and winter months with high frequency over the western Kenyan highlands. The eastern lowlands experience little thunderstorm activity except in March and April because flow at low-levels in this region is generally divergent. During the austral summer months showers develop frequently when unstable tropical westerly flow frequently penetrates over the Kenyan highlands, converging with the northeasterly flow (Trewartha, 1981). Convective cloudiness occurs mostly over the western slopes of the mountains. The probability of penetrating westerlies is increased if the subtropical anticyclone over northwest Southern Africa is intense or building.

The austral winter southeast monsoon has greater heat, moisture and instability than the northeast monsoon (United States Air Force Air

Weather Service, 1980), and is associated with frequent convective and thunderstorm activity over the western highlands. Thunderstorm activity is likely to increase, especially over the southwest highlands, with intensification of the heat low over the Rift Valley region.

During the transition months highly unstable easterly flow dominates. The air has a long trajectory over warm tropical waters before passing over eastern Kenya. Over the eastern lowlands this flow is associated with convective rain shower and thunderstorm activity. In Nairobi thunderstorm activity is highest in April (mean of five thunderstorm days). Enhanced convection and thunderstorm activity over eastern Kenya is likely when the easterly flow is strong and increasing.

#### b. Tanzania

Convection and thunderstorm activity occur with highest frequency over the western and southwestern portions of Tanzania, during the summer months (December - March). The summer maximum over the extreme western portions of the country is associated with surges in the tropical westerlies penetrating over the western mountains. As in Kenya, most of the convective activity occurs over the western facing slopes as the unstable westerly flow converges with the northeast monsoon (Trewartha, 1981).

Thunderstorm activity, though significant during the transition months, occurs with much lower frequency than in summer. Convective activity over most of Tanzania during the winter is minimal. Thunderstorm activity is almost nonexistent over the west and southwest portions of the country. Even over the western mountains and lakes the frequency of convective activity is low. Divergent southeasterly flow at the surface and convergent flow at 500 mb are associated with reduced convective activity over most of the country in the austral winter (Anyamba and Kiangi, 1983). Additionally, the semipermanent low over southwest Africa is replaced with an anticyclone from June through September. The associated low-level subsidence is an additional factor in the suppression of convection.

### 5.5 UPPER-AIR WINDS AND TURBULENCE

#### 5.5.1 Kenya

The significant features in the flow aloft are the Somali (low-level) Jet and a low-level southeasterly jet present year round between the Kenyan and Ethiopian highlands. The Somali Jet is present during the winter months at elevations up to 1-1.5 km off the Kenya-Somali coast. The jet migrates northwest from south of the equator during the months of February to June and then remains stationary from June through August (see Fig. 3.14). In September the jet axis begins migration back to the southeast. Fig. 3.15 (Krishnamurti, 1979) shows the mean position of the wind speed maxima in August. The mean wind maxima occur northeast and southeast of Kenya, however strong (mean 15-25 kt) winds are still observed over the Kenyan coast. Stronger wind velocities occur when the jet is intensified. The Somali Jet develops on

the west side of the southerly/southwesterly monsoon flow. The Somali Jet has a diurnal variation in its elevation and intensity. The jet is at its highest elevation (1-1.5 km) during the night-time hours between midnight and dawn. After sunrise the wind velocities aloft begin weakening and the jet builds toward the surface. The jet descends to elevations as low as 250 m during daylight hours. At dusk the low-level winds begin to decrease and the jet begins its evening ascent. Strongest winds at night occur near the 750 m level (United States Air Force Air Weather Service, 1980). The strength of the Somali Jet is also affected by synoptic disturbances to the south in the Southern Hemisphere westerlies. Clear air turbulence is likely near the surface during daylight hours and at elevations near one kilometer at night in the vicinity of the jet. Low-level turbulence is most likely and most severe in the afternoon, while upper-level (one kilometer) turbulence is most likely in the morning hours.

The strong low-level southeasterly flow between the Kenyan and Ethiopian highlands (referred to as the Turkana Channel Jet, see Fig. 3.15) is present throughout the year. The jet occurs at and below an elevation of 0.75 km (above ground) and is strongest near the 0.6 km level. The flow increases in intensity from the ground to 0.5 km and weakens above 0.8 km. Wind velocities in the jet often exceed 60 kt and occasionally exceed 100 kt. There is a diurnal variation in the jet intensity with the strongest winds occurring in the morning hours. Clear air turbulence, occasionally severe, is likely in the vicinity of the jet flow (Kinuthia and Asnani, 1983).

Wind<sup>9</sup> at high elevations (e.g., 300 mb, 200 mb) over Kenya is weak throughout the year. The mean flow is south-southeasterly (10-20 kt) over northern Kenya and southeasterly over southern Kenya in the austral summer becoming east-northeasterly (5-20 kt) during the winter months (see Figs. 2.27, 2.28). At 500 mb, weak (5-15 kt) east-northeasterly flow dominates over Kenya throughout the year (see Figs. 2.29, 2.30). Northeasterly (5-15 kt) flow is present at low level (700 mb) in summer, and in the winter months weak (5-15 kt) south-southwesterly winds dominate (see Figs. 2.31, 2.32) (Dean, 1972).

Clear air turbulence is associated with the low-level jets mentioned earlier. Areas affected are limited to northeastern and coastal Kenya, and the Kenyan-Ethiopian Highlands. Additionally, turbulence occurs in association with thunderstorm and convective activity over the western highlands in winter and summer, and over the eastern lowlands in March and April. Turbulence associated with these thunderstorms occurs at all levels and can be severe.

---

<sup>9</sup> See footnote 4 on page 2-24 regarding upper-air wind analyses.

### 5.5.2 Tanzania

The significant low-level feature over Tanzania is the low-level jet, found often in close proximity to the eastern coast. This low-level jet migrates northwest from February to June (see Fig. 3.14). The jet remains quasi-stationary from June through August and is most likely to affect the Tanzanian coast starting in May. Fig. 3.15 shows the mean low-level jet flow for the month of August. Although the speed maxima are not close to the Tanzanian coast, strong (15-25 kt) wind occurs frequently. Stronger winds occur over the northern coast when the jet and surrounding wind field are intensified. This strong flow is part of a larger scale low-level flow which includes the Somali Jet described earlier in this section. Turbulence is likely in the vicinity of the jet at low-levels in the afternoon and near the one kilometer elevation before sunrise.

At the upper levels (200 mb) the summer mean winds are south-easterly (15-25 kt) over Tanzania while during the winter mean winds are primarily easterly (Figs. 2.27, 2.28). The 500 mb flow is light (5-15 kt) and variable in summer and light southeasterly in winter (see Figs. 2.29, 2.30). At 700 mb the mean flow is weak northeasterly during the summer months and 5-15 kt southerly/southeasterly in the winter (see Figs. 2.31, 2.32).

Turbulence, occasionally severe, is also likely in the vicinity of intense convection and thunderstorm activity in western and southwestern Tanzania. Such weather is most likely in winter and during the transition periods.

## Section 6

### CASE STUDIES AND OCEANIC WEATHER

#### 6.1 CASE I - EASTERLY WAVES (24 - 28 AUGUST 1983)

##### 6.1.1 General Discussion

Meteorologists have devoted much discussion and research to waves in the westerlies and waves in the easterlies. In recent years scientists have increasingly studied easterly waves because of their link with tropical storms and cyclones.

Waves in the easterlies have been observed in many parts of the tropics; their origin is believed to be near the 700 mb level over east central Africa. The waves have a synoptically observed wavelength of 2000 km and a period of 3.2 days, although a statistical study gave a larger wavelength and period (Burpee, 1972). They are predominant from June to October with a maximum frequency over Dakar, Senegal (extreme west Africa) near the first of August (Frank, 1970).

Easterly waves, over North Africa, are hard to detect on both weather analyses and satellite imagery. However, Frank (1969) has shown that some easterly waves are recognizable over oceanic areas in satellite imagery as "inverted V" cloud patterns (see Fig. 6.1). Fett et al. (1973) detailed the structure of oceanic easterly waves and proposed a modification of Frank's schematic model (see Fig. 6.2). This model coupled with the characteristic satellite "inverted V" cloud signature makes it possible for forecasters to track easterly waves in data sparse oceanic areas and to keep watch for possible development into tropical storms/cyclones.

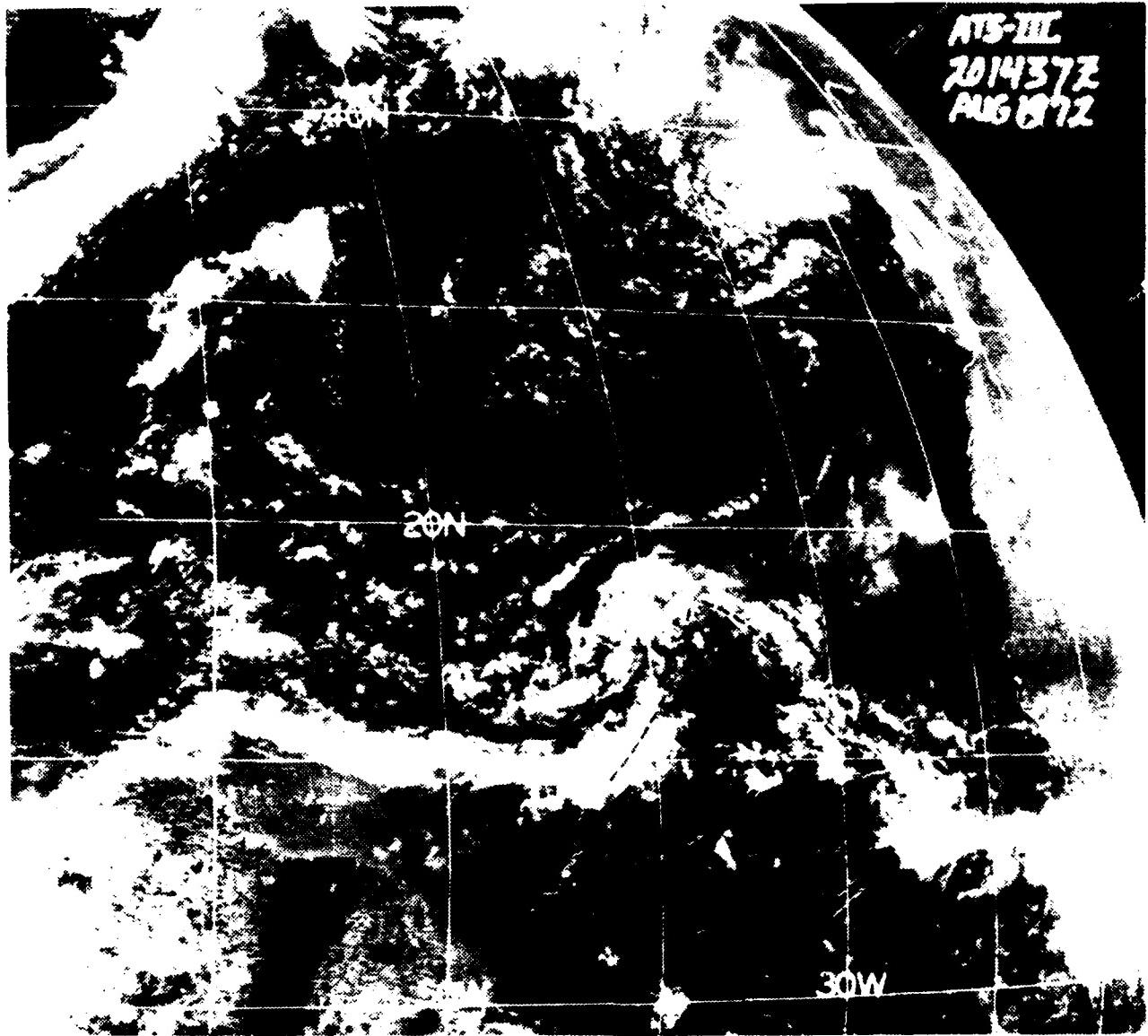


Fig. 6.1. An ATS-3 (Applications Technology Satellite) view of an inverted V cloud pattern in the Atlantic on 20 August 1972 at 1437 GMT (Fett et al., 1973)

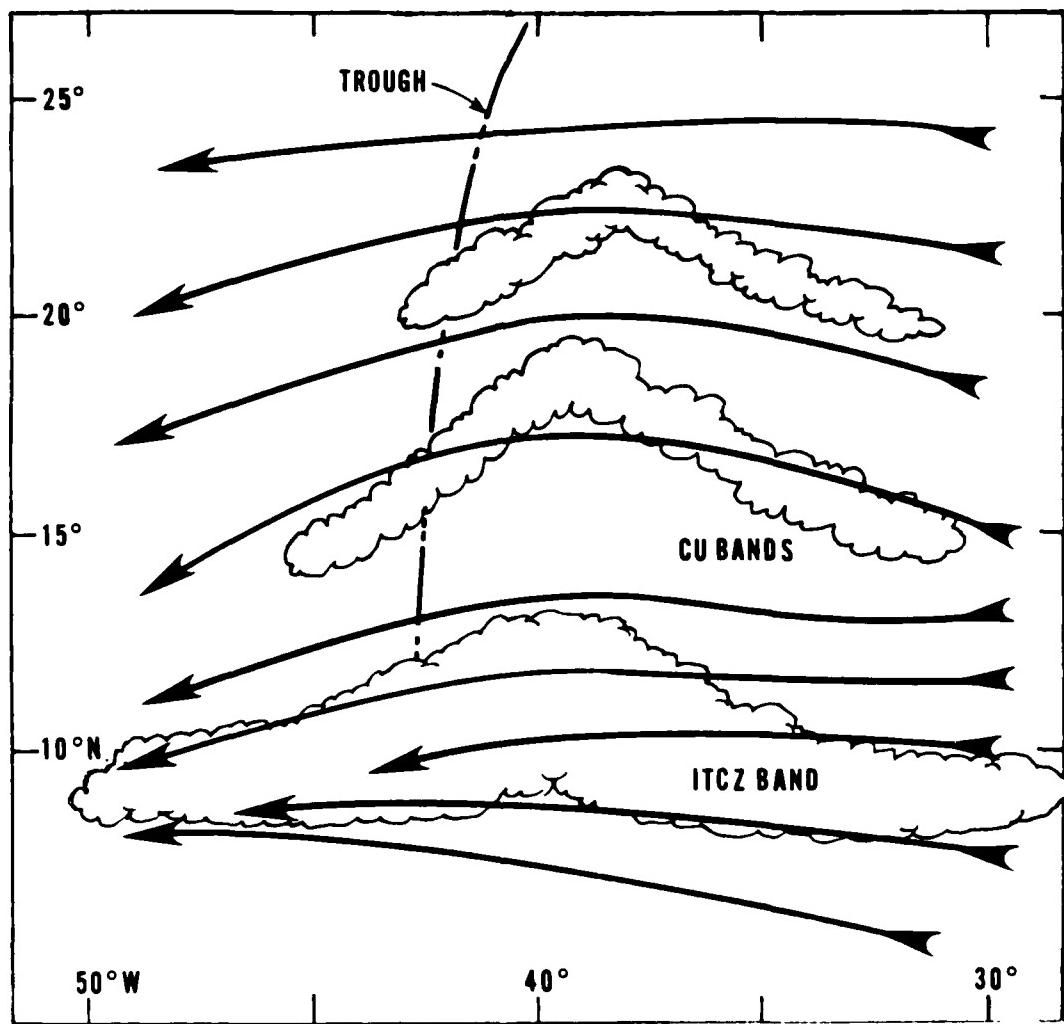


Fig. 6.2. Proposed modification of Frank's schematic relationship between lower tropospheric flow and the inverted V pattern (After Fett et al., 1973)

### 6.1.2 Synoptic Description

The source region of easterly waves appears to be the region between Ft. Lamy, Chad ( $15^{\circ}$ E) and Khartoum, Sudan ( $32^{\circ}$ E) with the horizontal and vertical shear of the mean zonal wind acting as equal sources of energy for the perturbations. Potential vorticity is at a maximum equatorward of the mid-tropospheric jet between  $5^{\circ}$ E to  $35^{\circ}$ E from June to October in both the same season and region that easterly waves are first observed. The mean zonal flow may therefore become unstable because of the potential vorticity between these longitudes (Burpee, 1972). The instability is then propagated westward in the low zonal flow.

Evaluation of the temperature, specific humidity and geopotential height of the waves reveals little significant scientific evidence as to their structure. However, Carlson (1969) found that the largest sea-level pressure variations occurred in the northern sector of the wave in the vicinity of a major cyclonic eddy near  $20^{\circ}$ N which moved with the disturbance. Fett's (1973) vorticity analysis (Fig. 6.3) depicts these eddies.

Soundings taken near  $15^{\circ}$ N show that the waves are relatively warm in the high troposphere and cold near the surface. Since easterly waves are cold core, this implies an indirect circulation. The cold air must be replenished or warming occurs and the circulation weakens. In the vertical, soundings show that the wave axis slopes eastward with height in the lower troposphere.

Synoptic observations and satellite pictures show that cloudiness becomes an organized part of the wave only after they have reached western Africa. Convective instability increases as the wave moves westward, especially after crossing  $5^{\circ}$ W with the greatest intensity found between  $10^{\circ}$ W and  $20^{\circ}$ W. Here along the African coast there is a great abundance of moist, unstable air embedded in a favorable large-scale regime. The inverted V cloud pattern suffers disintegration as it moves westward of  $20^{\circ}$ W.

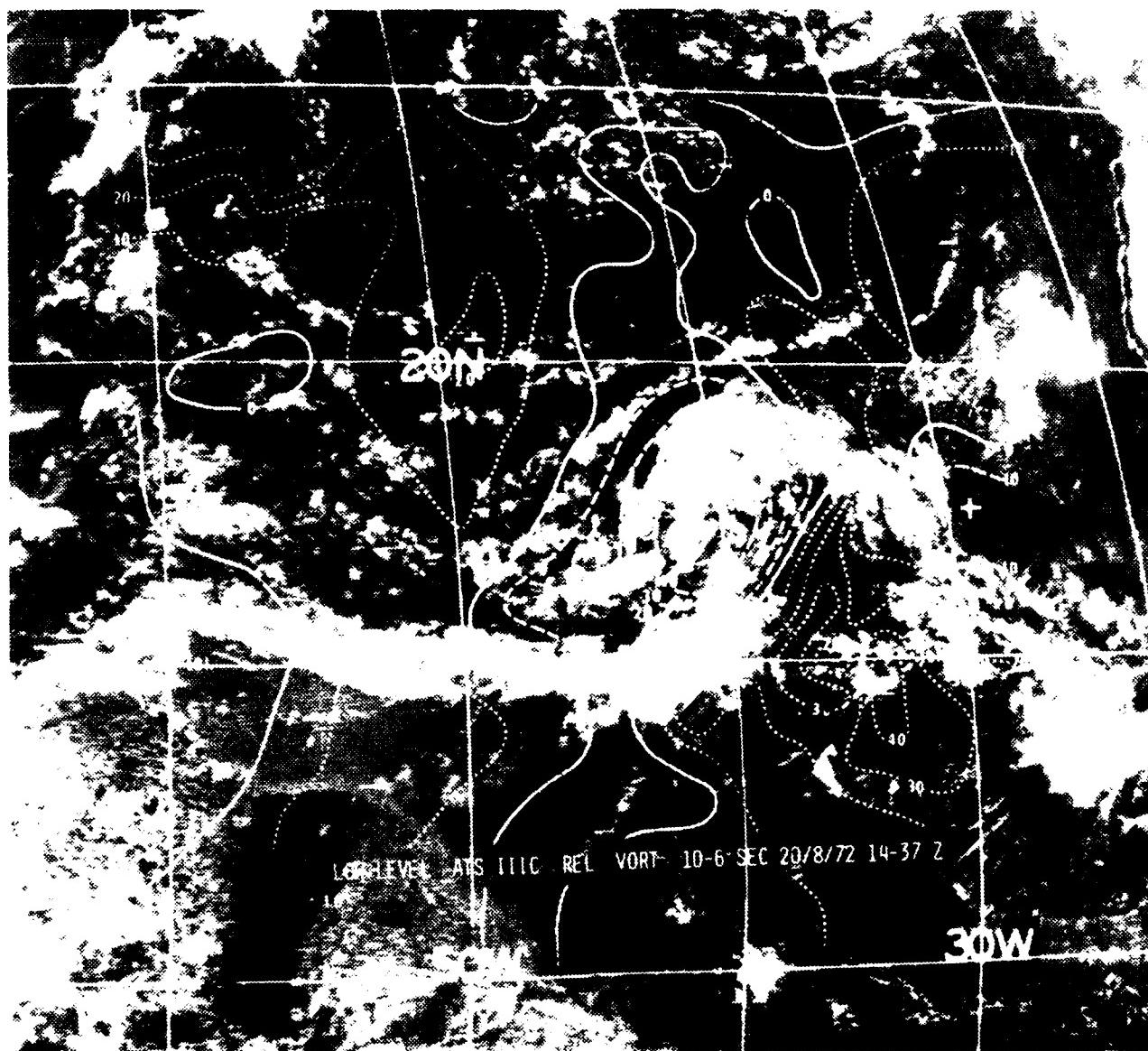
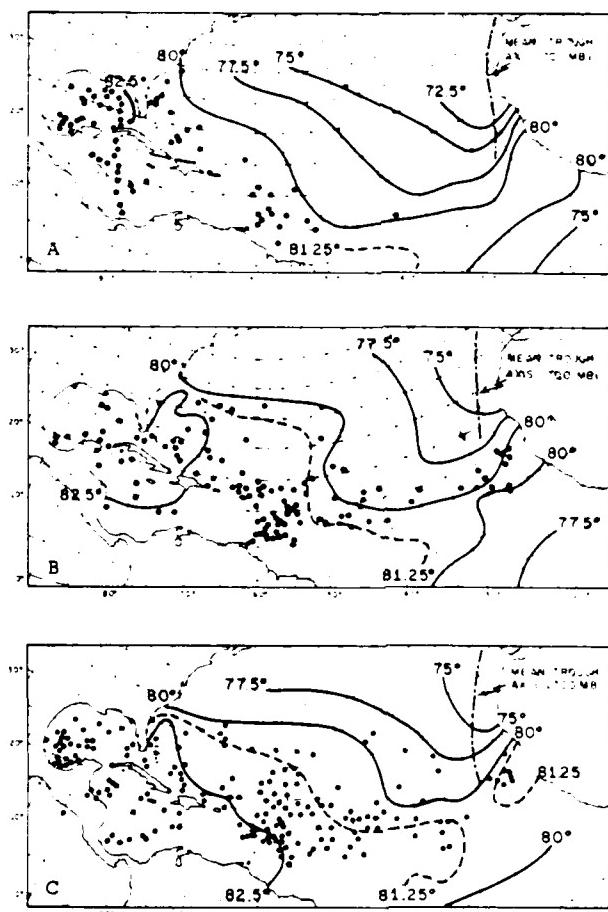


Fig. 6.3. An analysis of the field of relative vorticity (units  $10^{-6}$  sec $^{-1}$ ) for the 20 August 1972 inverted V example (Fett et al., 1972)

Figure 6.4 depicts the mean sea-surface isotherms for the months favorable for easterly wave Atlantic transits. It is interesting to note the effects of the relatively cold tongue in the sea-surface temperature (SST) field on tropical storm formation. Formation is sensitive to the location of the  $80^{\circ}\text{F}$  ( $26.7^{\circ}\text{C}$ ) isotherm, with little development occurring when the SST is below that temperature. Similarly the disintegration of easterly waves ("inverted V" cloud patterns) seems to be associated with the colder SST.

The speed of movement of easterly waves is faster over oceans than over the continent with overall acceleration greater after reaching  $22^{\circ}\text{W}$ , (Carlson, 1969). At  $22^{\circ}\text{W}$  a large scale 700 mb level trough (see Fig. 6.4) exists as a semipermanent feature along the Euro-African landmass (U. S. Weather Bureau, 1952). The mean position of the upper ridge is located near  $45^{\circ}\text{W}$ . The speed of the waves is affected by the presence of these features in that they decelerate east of the trough and accelerate west of the trough (Carlson, 1969).



**Fig. 6.4.** Mean sea-surface isotherms ( $^{\circ}$ F), the distribution of initial tropical storm fixes, 1901 - 1967 (filled circles), and the mean position of the 700-mb wave axis for (A) June and July, (B) August and (C) September (Carlson, 1969)

Interestingly the waves have their greatest intensity near longitudes ( $10^{\circ}\text{W}$  -  $20^{\circ}\text{W}$ ) when they decelerate ahead of the trough. They weaken and dissipate after they accelerate west of the trough. Figures 6.5-6.9, from METEOSAT, the geostationary satellite of the European Space Agency, track an easterly wave from Africa to the central Atlantic.

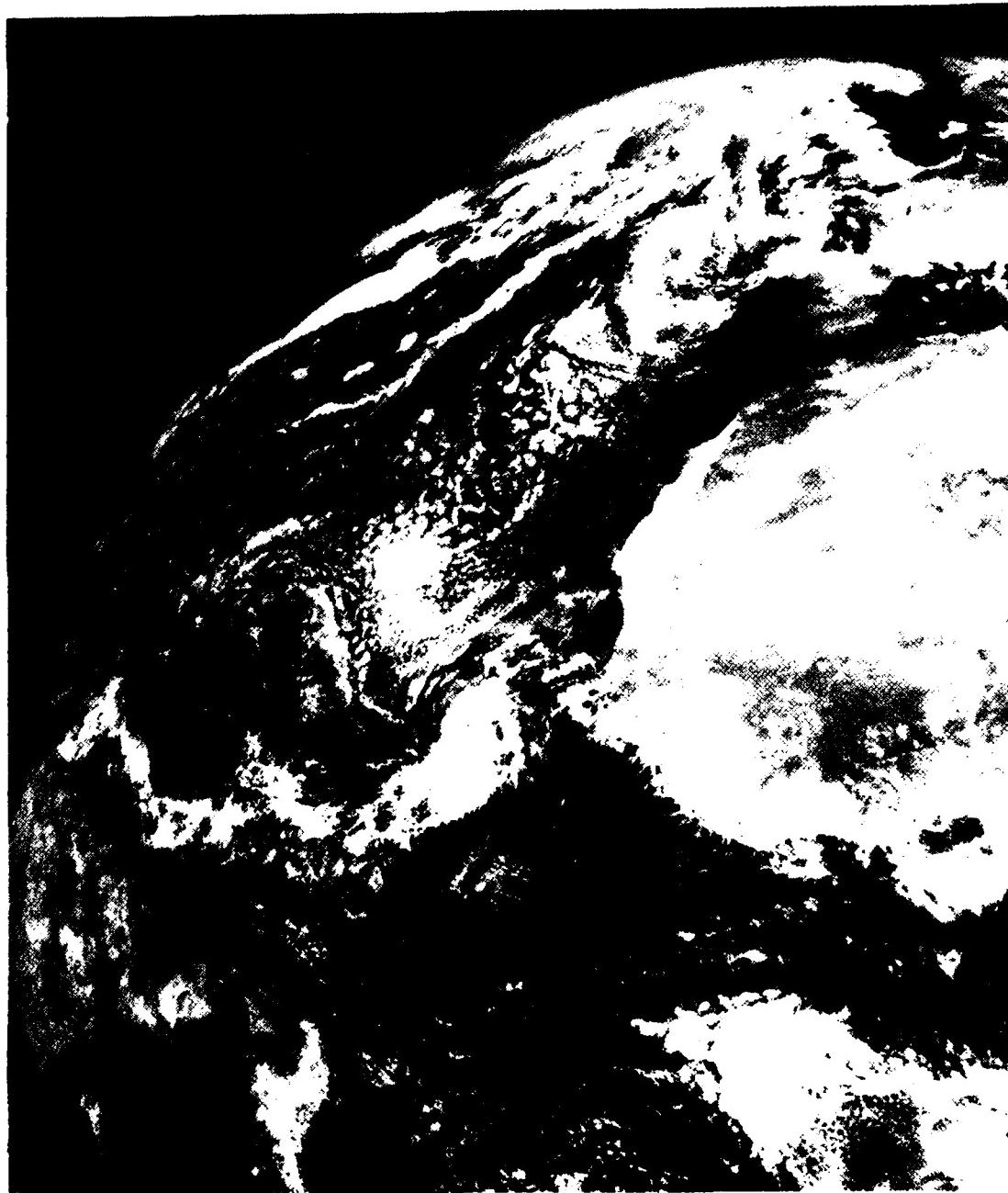


Fig. 6.5. Visible imagery of an Easterly Wave (inverted V) propagating from Africa to the central Atlantic Ocean as viewed from METEOSAT on 24 August 1983

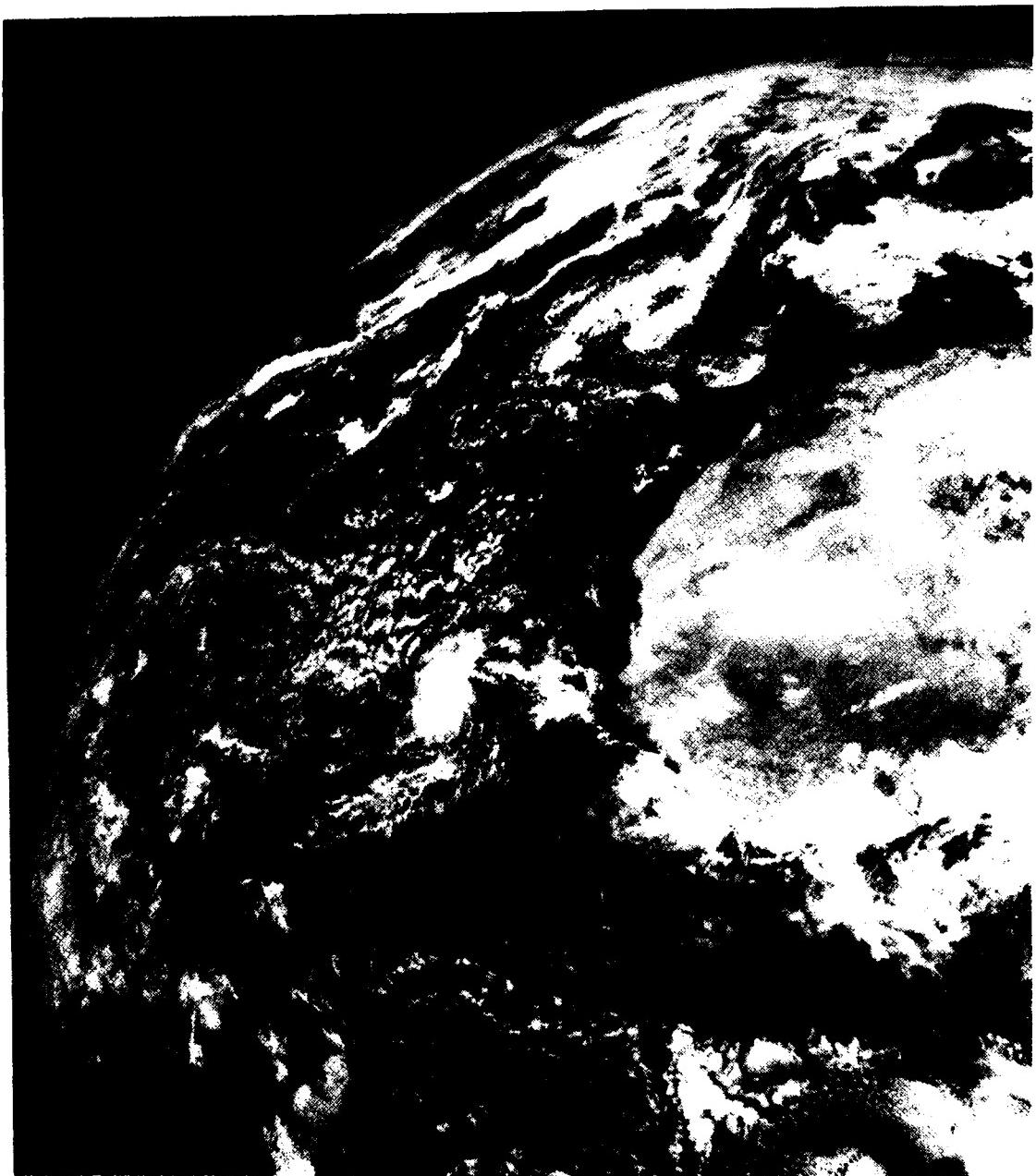


Fig. 6.6. Same as Figure 6.5. except for 25 August 1983



Fig. 6.7. Same as Figure 6.5, except for 26 August 1983



Fig. 6.8. Same as Figure 6.5, except for 27 August 1983

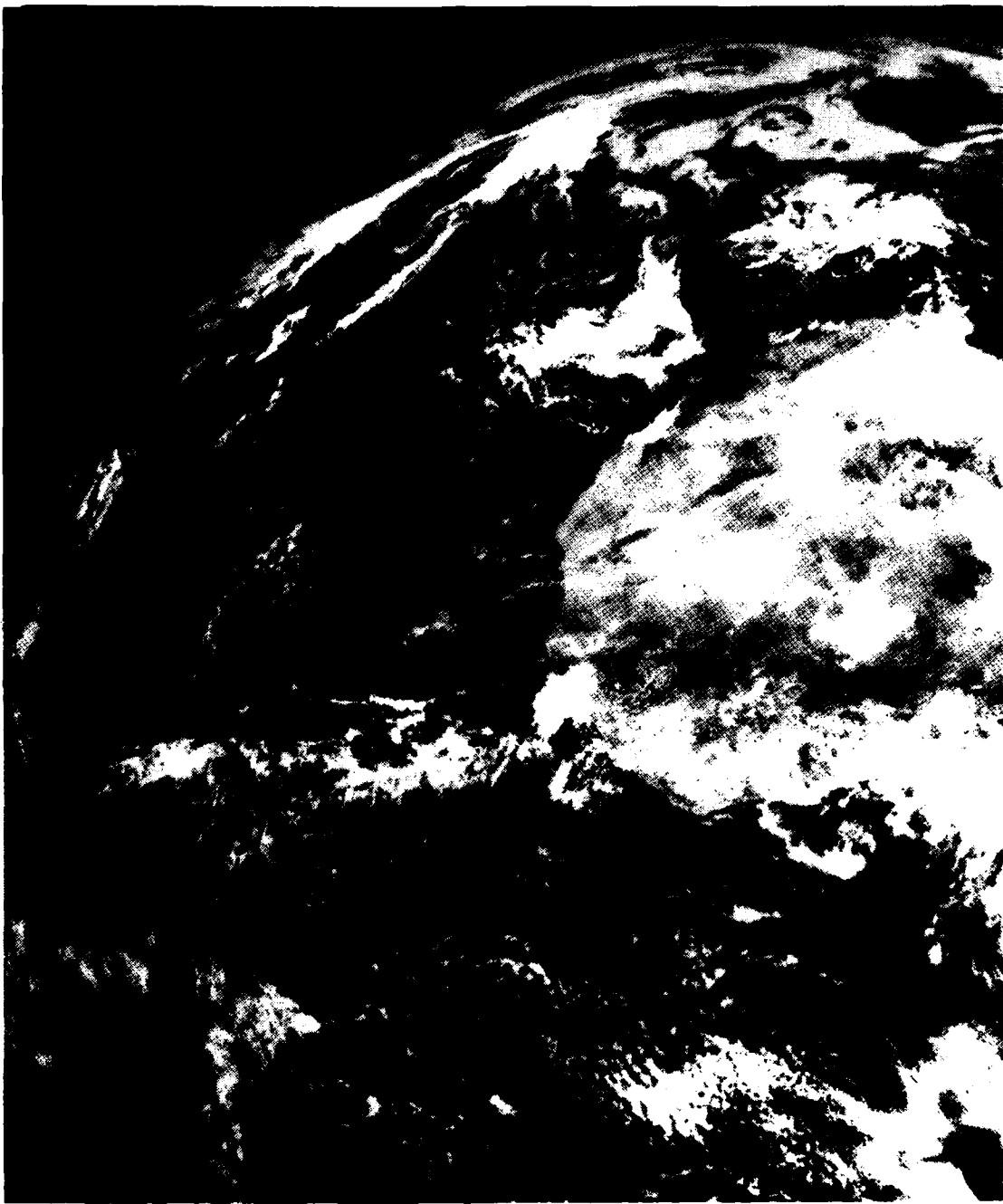


Fig. 6.9. Same as Figure 6.5, except for 28 August 1983

### **6.1.3 Forecast Rules/Aids**

1. Surface charts are poor indicators of the position of easterly waves. The waves first appear between 5°E to 35°E over North Africa at 700 mb from June through October.
2. An area of maximum positive relative vorticity usually precedes the wave near 20°N and can be identified on satellite imagery as a cloud mass ahead of the inverted V.
3. The waves are cold core and must resupply the cold air or the circulation will weaken.
4. Convective instability is greatest between 10°W and 20°W in the area of southeasterly flow aloft.
5. Forecast increase speed of movement and disintegration after the wave passes west of 22°W.

### **6.1.4 Satellite Imagery 'Clues'**

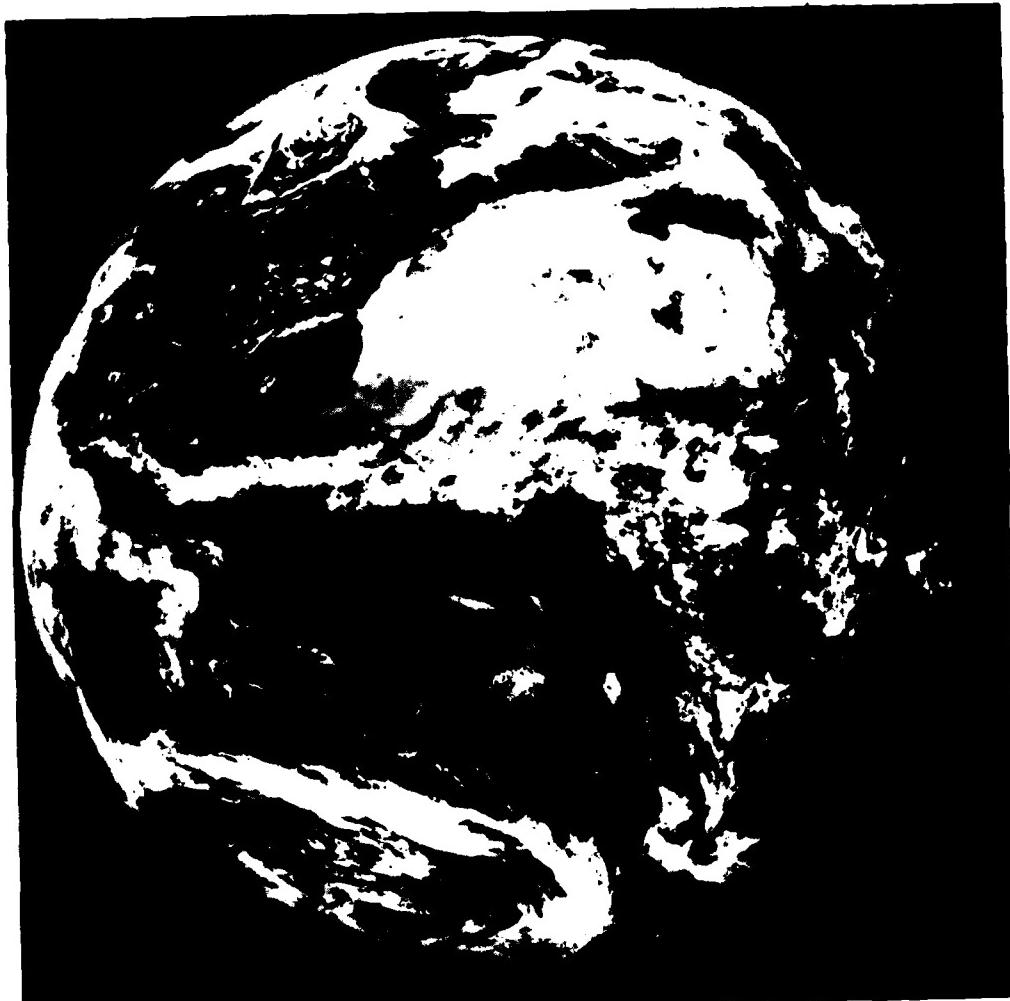
1. A tropical wave disturbance is usually found ahead of the "inverted V" cloud formation.
2. Cloudiness becomes organized only after the wave reaches Western Africa.
3. The "inverted V" cloud pattern disintegrates as it moves westward but still can be identified on satellite imagery as it crosses the tropical Atlantic to the Antilles.

## **6.2 CASE II - SAHARAN DUST OUTBREAKS (2 - 3 MAY 1983)**

### **6.2.1 General Discussion**

Navy forecasters are not usually attuned to forecasting dust aloft in the lower layers of the atmosphere, especially when operations are distant from dust source areas. However, shipboard forecasters crossing the equatorial Atlantic should be aware that the internal prolonged heating of air over the Sahara during late spring, summer and fall forms a deep mixed layer which occasionally contains large amounts of dust due to the abrasive action of strong winds at ground level. Figures 6.10 and 6.11 are METEOSAT imagery of a Saharan dust outbreak occurring in May 1983. This dust-laden heated layer emerges from West Africa within large scale anticyclonic eddies imbedded in the tropical easterlies. The dust, residing in the layer between 5,000 and 15,000 ft., overrides the trade-wind moist layer and can be advected westward to the Caribbean. As the dust proceeds westward, the continuous fallout of the particulate matter and convective mixing causes the dust to

be transferred to the lower levels where concentrations may become sufficient to produce haze at the surface. Because the dusty Saharan air leaves Africa in a layer between 850-550 mb, these pulses are not easily recognizable on surface or upper air charts. However, the dust is apparent in high quality satellite imagery as a distinct gray-shade, appearing as a lighter-toned value in comparison to adjacent dust-free regions. Navy forecasters can learn to interpret this condition by becoming familiar with the characteristic Saharan dusty-air signature.



**METEOSAT**

2 MAY 1983 0000Z TIME 1255 GMT NORTH ATLANTIC  
NORTH AFRICA DUST OUTBREAK

Fig. 6.10. Visible imagery of a Saharan dust outbreak as viewed from METEOSAT on 2 May 1983. (Note extent of dust outbreak lying from North Africa to the central Atlantic with an intense dust plume located south of Dakar, Senegal imbedded in the larger dust outbreak.)



**METEOSAT**

1983 MONTH 5 DAY 3 TIME 1155 GMT (NORTH) CM. VIS 2  
HORIZONTAL SCANNING DATA SLOT 24 COPYRIGHT - ESA -

Fig. 6.11. Visible imagery on a Saharan dust outbreak as viewed from METEOSAT on 3 May 1983. (Dust stretches from North Africa to nearly South America. Anticyclonic turning is visible in the northern leading edge of the outbreak over the central Atlantic.)

### 6.2.2 Saharan Air Characteristics

As a layer of air flows across the North African deserts it becomes intensely heated. This heating produces dry convection throughout the layer. Because of the vastness of the African arid terrain the layer remains in contact with the ground for several days and acquires a uniform potential temperature. Typically the potential temperature ranges from 40°C to 45°C in July with this layer extending to 500 mb (Carlson and Ludlam, 1965). The layer of air acquires a considerable amount of sensible heat but little moisture. Therefore, the Saharan air is especially warm and very dry in the lower layers.

Above 500 mb, the temperatures are cooler than the surrounding tropical air mass. Relative humidity increases rapidly with height within the dust layer, with possible saturation at the top (Fig. 6.12).

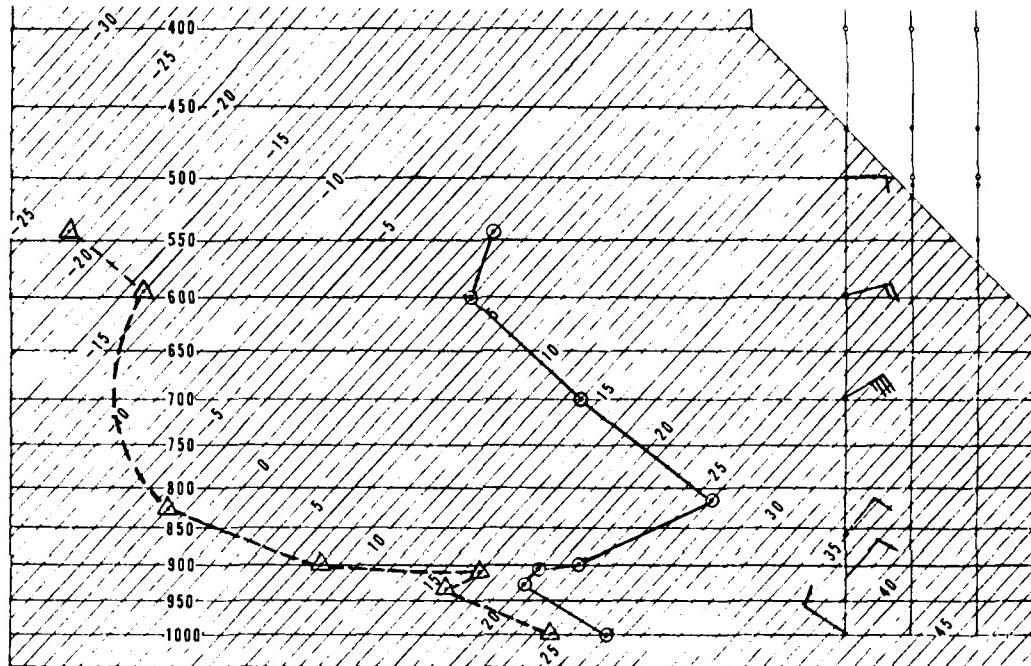


Fig. 6.12. Idealized Skew T, Log P sounding for dust-laden Saharan air outbreak. Saharan air is located approx. between 820 and 600 mb. A wind maximum is located at 700 mb. Temperature and dewpoint temperature converge from 700 to 600 mb, indicating increasing relative humidity due to mixing of maritime tropical air. The Saharan layer is nearly isentropic. The lower (cooler and more moist) portion of the sounding is attributed to the northerly maritime flow along the African coast.

Wind speed within the dusty Saharan layer is linked to the temperature contrast between the warm dry Saharan air and the relatively cooler surrounding tropical air. The Saharan air is warmer at the base of the isentropic segment and cools with height usually disappearing near the 650 mb level. Wind speed also diminishes with height especially above the 700-600 mb wind maximum. The presence of Saharan air can be recognized on conventional meteorological soundings as an isentropic layer with a potential temperature of approximately  $40^{\circ}\text{C}$ , with a wind maximum of 35-50 kt usually between 700 and 600 mb, and increasing relative humidity near the top of the layer.

### 6.2.3 Large Scale Movement of Saharan Air Dust

The onset of dusty Saharan air outbreaks seem to be associated with weak tropical waves moving off the western North African coast. These waves can be identified on satellite imagery ahead of inverted V cloud patterns (Fett et al., 1973) which were described in Case I. A serrated line can be drawn, to the east of the axis of the inverted V cloud pattern, separating areas of large stratocumulus cells to the west from smooth, small-celled stratocumulus with clearing weather to the east (see Fig. 6.13). When Saharan air overrides maritime cloud cover, the latter becomes suppressed and could, in some cases vanish entirely if a strong inversion is formed (Carlson and Prospero, 1971). This overriding creates a light uniform grey shade in the satellite imagery. This discontinuity identifies the leading edge of the Saharan air dust plume on visible satellite imagery. Generally, the plume over the ocean can be identified in the visible imagery only in the first few days of transit across the Atlantic. By the time the plume has entered the central and western Atlantic, estimates of position using satellite imagery should be verified by soundings, using the above mentioned characteristics as guidance.

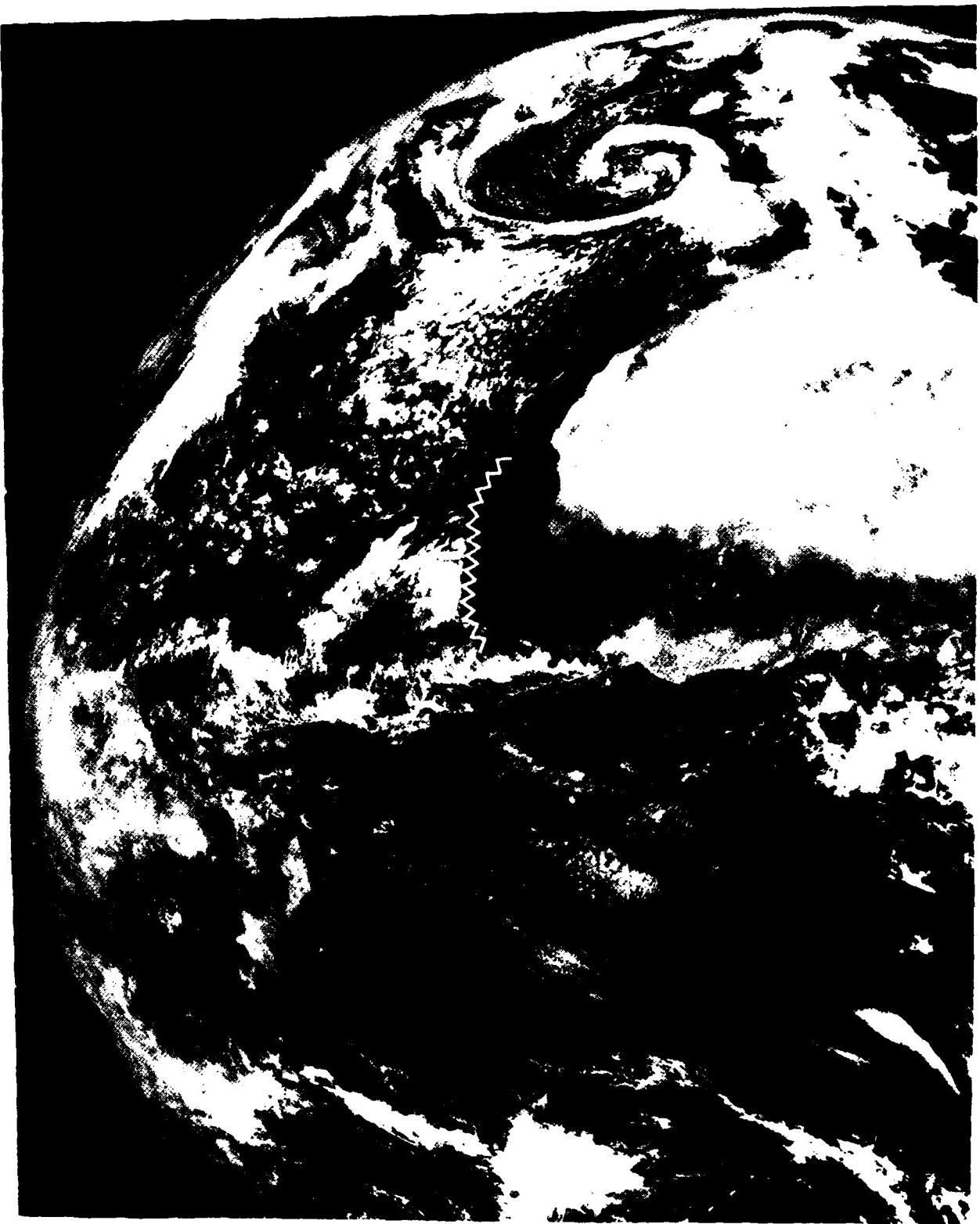


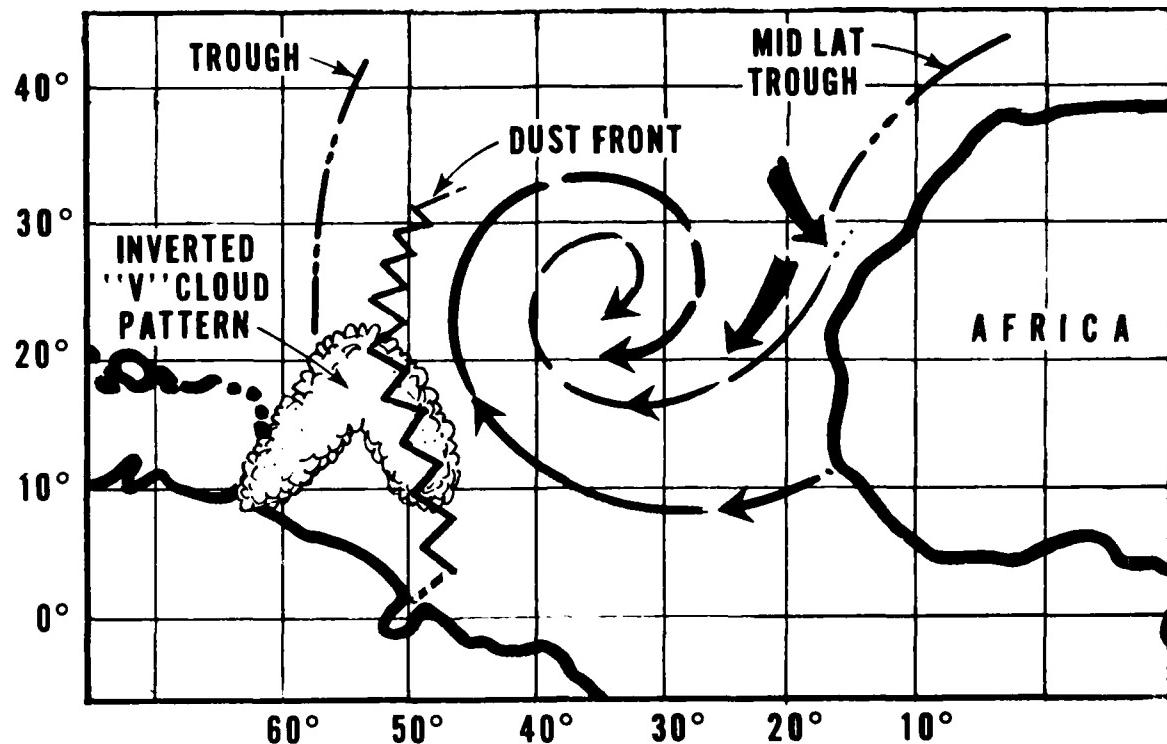
Fig. 8-13. Superimposed serrated line indicating dust front to the east of (trailing) the axis of an inverted V cloud pattern as seen on METEOSAT visible imagery. (In other cases, the dust front (serrated line) may overlie the trailing (eastward) segment of the inverted V cloud pattern.)

Satellite imagery depicts a clockwise turning of the Saharan air toward the north along the west coast of Africa. This anticyclonic flow is associated with the warm Saharan anticyclone and semi-permanent upper trough which lies along the coast of Europe and Africa during the Northern Hemisphere summer. Figure 6.14 is a schematic model of a dust plume moving off Africa during the summer months (Carlson & Prospero, 1971) (Fett et al., 1973). The model depicts the following features:

1. African wave disturbance often visible in satellite imagery ahead of the "inverted V" cloud pattern.
2. Dust front located over the suppressed stratocumulus clouds of the "inverted V" cloud pattern.
3. Large scale anticyclonic eddies behind the dust front.
4. Trajectories of dust-laden air near 700 mb.
5. Upper-level winds from the Sahara overriding the tropical low level winds along the coast.

There is evidence of a seasonal trend for transportation of dust-laden Saharan air. Climatology shows favorable conditions for westward transport during the Northern Hemisphere summer months between May and October. During that time, easterly winds dominate from the surface to over 500 mb. During the winter, the easterly winds diminish and are restricted to about 850 mb and below, with westerly winds ("counter trade winds") prevailing. Therefore, there is a maximum transport in summer and a minimum in winter over the eastern tropical Atlantic.

The latitudinal extent ranges from 5°N to 25°N. This range can be explained by the northward migration of the ITCZ in summer which confines the dust between 15°N to 25°N, while in winter the dust layer extends toward the southwest and is located between 5°N and 15°N (Semmelhack, 1934). Figure 6.15 portrays this seasonal shift of the dust layer.



#### LEGEND

- ← TRAJECTORIES OF DUST-LADEN AIR NEAR 700MB
- ← LOW-LEVEL AIR FLOW ALONG COAST

Fig. 6.14. Schematic model of a dust plume moving off Africa during summer months (After Carlson and Prospero, 1951 and Fett et al., 1973)

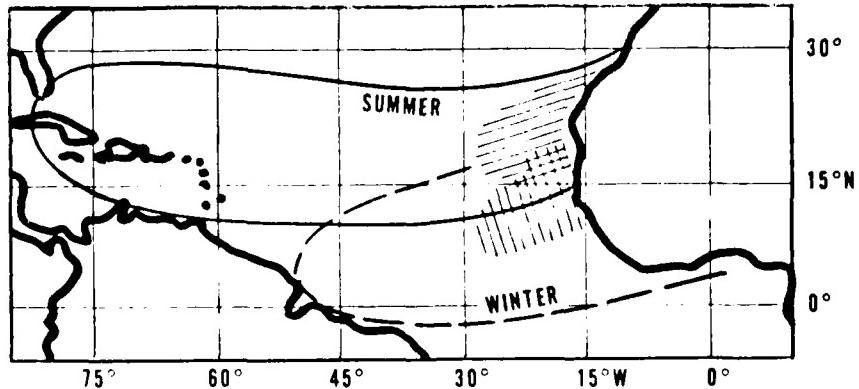


Fig. 6.15. Saharan dust plume fallout over Atlantic during N. H. summer and winter. Hatched areas represent the mean extension of dust fallout regions (After Semmelhack, 1934).

#### **6.2.4 Forecast Rules/Aids**

1. Westward transport of the dust is greater in summer.
2. Dust outbreaks are usually preceded by large amplitude disturbances (easterly waves) by one or two days. However, not all disturbances indicate dust outbreaks.
3. On plotted soundings the dusty Saharan air has a potential temperature near 40°C. A wind maximum of 35 - 50 kt is found within the air layer, usually near 600 mb.
4. The Saharan air aloft is usually found between 850 - 550 mb.

#### **6.2.5 Satellite Imagery 'Clues'**

1. A tropical Wave disturbance is usually found ahead of an "inverted V" cloud formation.
2. The inverted V cloud pattern associated with the outbreak can be divided into two features, with large-size cloud cells to the west and smooth, small-celled clouds to the east. The small cells are suppressed by the strong inversion at the base of the Saharan air outbreak.
3. Overriding Saharan air usually appears as anticyclonic flow with a light uniform grey shade tonality typifying the dust area as opposed to much darker-toned conditions indicative of a dust-free atmosphere.
4. The dust plume can only be identified the first few days of transit across the Atlantic.

### 6.3 CASE III - CAPE ROLLERS (ABNORMAL WAVES) (21 - 26 SEPT. 1973)

### 6.3.1 General Discussion

With increasing shipping traffic, primarily super tankers too large for the Suez Canal, considerable interest has been generated in the unusually high swells, sometimes in excess of 40 feet, in the area off southeast Africa from Durnford Point to Port Elizabeth (see Fig. 6.16). These huge swells have been named "Cape Rollers" by the seamen who sail around the African Cape. Ships returning from the Persian Gulf/Indian Ocean take advantage of the rapid southwest flowing Agulhas Current (4 to 5 kt) to shorten their travel time. The course of the Agulhas Current runs "head on" into large swells from the southern ocean during the austral winter.

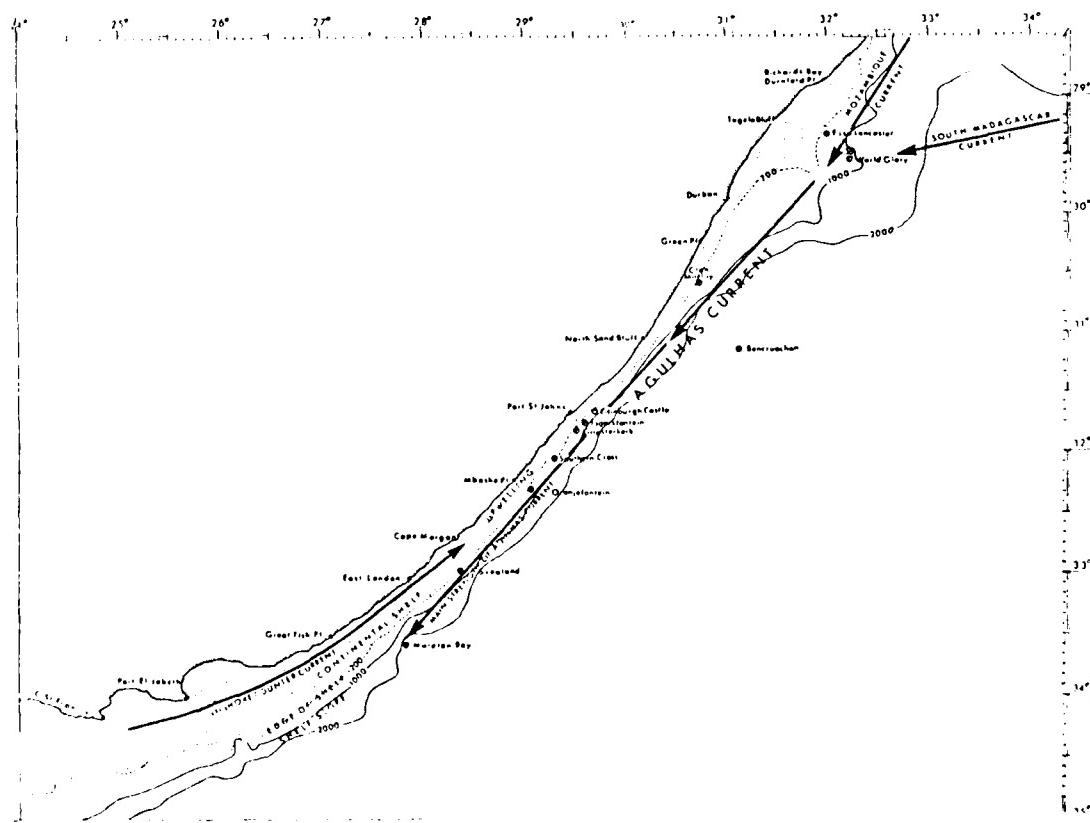


Fig. 6.16. Chart of southeast coast of the Republic of South Africa showing the continental shelf, shelf edge and continental slope, Agulhas Current and coastal upwelling, with positions of ships which have encountered an abnormal wave (depths in meters) (Mallory, 1974).

Davies (1972) computed Fig. 6.17 which depicts trajectories of swells generated at 55°S. These large swell trains can be generated by more than one source, each swell group having its own wavelength and frequency. These northeast traveling swells are affected by the counterflowing Agulhas Current off southeast Africa which shortens the wavelength, raises the height of the swell waves and steepens their slope. Locally produced wind waves can momentarily superimpose themselves upon these swell thereby increasing the height. Mallory (1974) determined the typical incoming northeast moving swell arriving along the southeast coast of Africa from the southern ocean as having a wavelength of 660 ft (201 m) and a steepness of .08 in the open ocean. Using these figures, Smith (1976) calculated the crest to trough wave height as high as 52.8 ft (16.1 m) with the possibility of wind waves superimposing another 16.5 ft (5 m) on the giant swell. Obviously, such giant waves are extremely dangerous to shipping and the task force meteorologist must be aware of the synoptic situation that generates them.

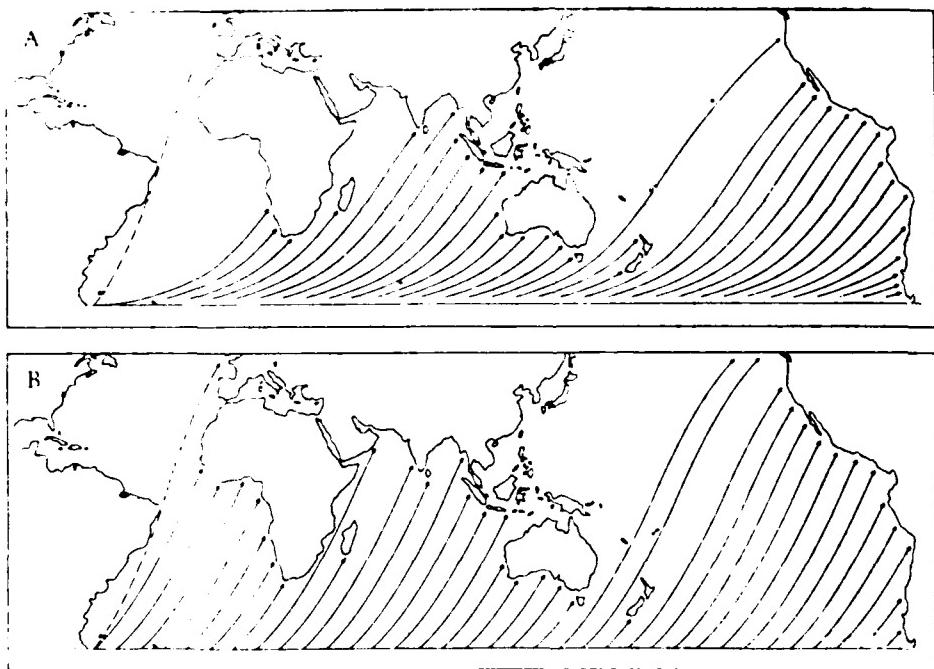


Fig. 6.17. Typical great circle paths followed by swell generated at Latitude 55°S by (A) Westerly and (B) Southwesterly gales, according to J. L. Davies. Note the paths parallel to the southeast coast of Southern Africa.

### 6.3.2 Geophysical Background

Further description and statistics concerning Cape Rollers are given in paragraph 7.4 under Coastal Oceanographic Influences. Because of its depth, the main core of the Agulhas Current is found outside of the continental shelf but within 100 n m of the shoreline (see Fig. 7.24).

During the austral winter (May - October), cyclones following the normal storm track usually pass near Marion Island ( $47^{\circ}\text{S}$ ,  $38^{\circ}\text{E}$ ), creating a southwesterly fetch of over 1200 miles behind the front (see Fig. 6.18). Hence, the swell generated by the southwesterly winds behind the front will be fully developed and will have reached maximum height and length when they reach the southeast African coast. It must be remembered that even if the coastal winds are light, the southerly swell is nonetheless fully developed. The local wind however may superimpose wind waves over the fully developed swell. These abnormally high waves will be preceded by correspondingly deep troughs described by the expression "a hole in the sea". The effect of the Agulhas Current is much weaker as the large swells encounter lower current speeds. Mallory (1974) speaks of the current as being strongest near the 100 fathom line where the maximum height and steepness of the giant waves are found during the austral winter. In Mallory's investigation of 10 ship disasters caused by the giant waves none occurred shoreward of the 100 fathom line.

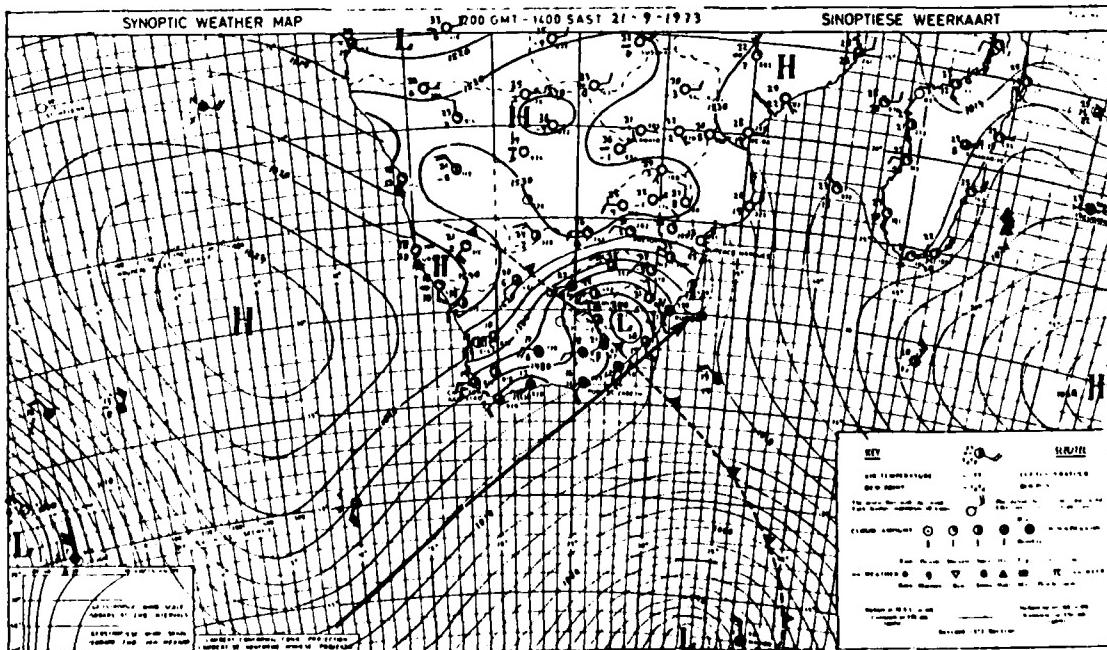


Fig. 6.18. Republic of South Africa Weather Bureau Surface (over Ocean) and 850 mb (over Continent) Analysis: 1200 GMT 21 September 1973

### 6.3.3 Case History

At 1647 L, on 25 September 1973, the 258,000-ton tanker SVEALAND, fully loaded, steaming southwestward suffered damage and casualties when she plunged into a long deep trough which appeared ahead of the ship. The ship reported 30-40 ft (6-13 m) waves with gale force winds prior to the mishap. SVEALAND was steaming one mile seaward of the 100 fathom line, 23 miles east from Hood Point, South Africa at a reduced speed. SVEALAND's position at the time of encountering the giant waves is plotted in Fig. 6.16, east of East London.

The Republic of South Africa Weather Bureau 1200 GMT surface charts from 21 September 1973 through 26 September 1973, encompassing the time of SVEALAND's calamity, are reproduced as Figs. 6.18 - 6.23.

On 21 September (see Fig. 6.18) a cold front is moving northeast along the southeastern coast of Southern Africa with southwesterly gales in the cold air mass. The long arrow marks the fetch from which the large swell waves propagate. The fetch is approximately 1200 miles long.

At 1200 GMT on 22 September (Fig. 6.19) the cold front has penetrated north of Lourenco Marques. The fetch is reduced to 800 - 900 miles as an anticyclone follows the cold front around the cape.

By 1200 GMT 23 September (Fig. 6.20) the anticyclone is dominant over the coastal waters of southeast Africa. The associated northeasterly winds produce a reduced fetch from the opposite direction and accentuate the Agulhas Current. A second cold front is approaching Cape Town from the southwest.

Near Port Elizabeth on 24 September (Fig. 6.21) a sudden change of wave direction takes place ahead of the cold front. The 989 mb low tracks eastward toward Marion Island.

The surface weather chart of 25 September (Fig. 6.22) shows the cold front north of Durban with an unlimited fetch behind it. Southwesterly winds continue through 1200 GMT on 26 September (Fig. 6.23). The anticyclone following the cold outbreak is centered further south than the anticyclone of 22/23 September. The SVEALAND suffered damage and casualties on 25 September.

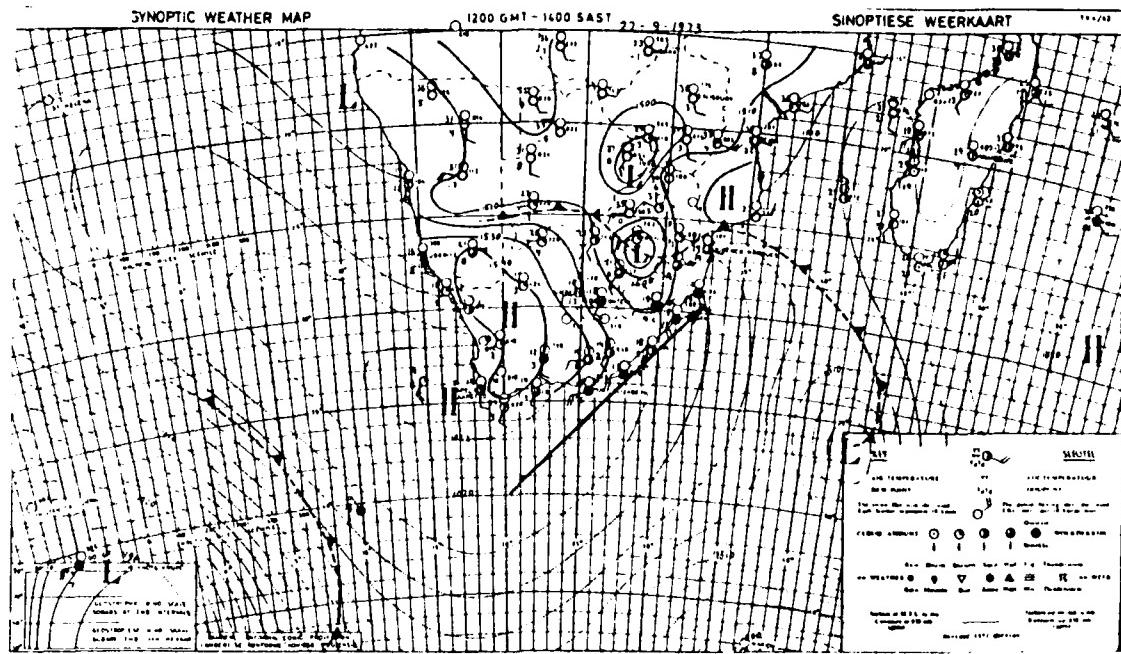


Fig. 6.19. Republic of South Africa Weather Bureau Surface (over Ocean) and 850 mb (over Continent) Analysis: 1200 GMT 22 September 1973

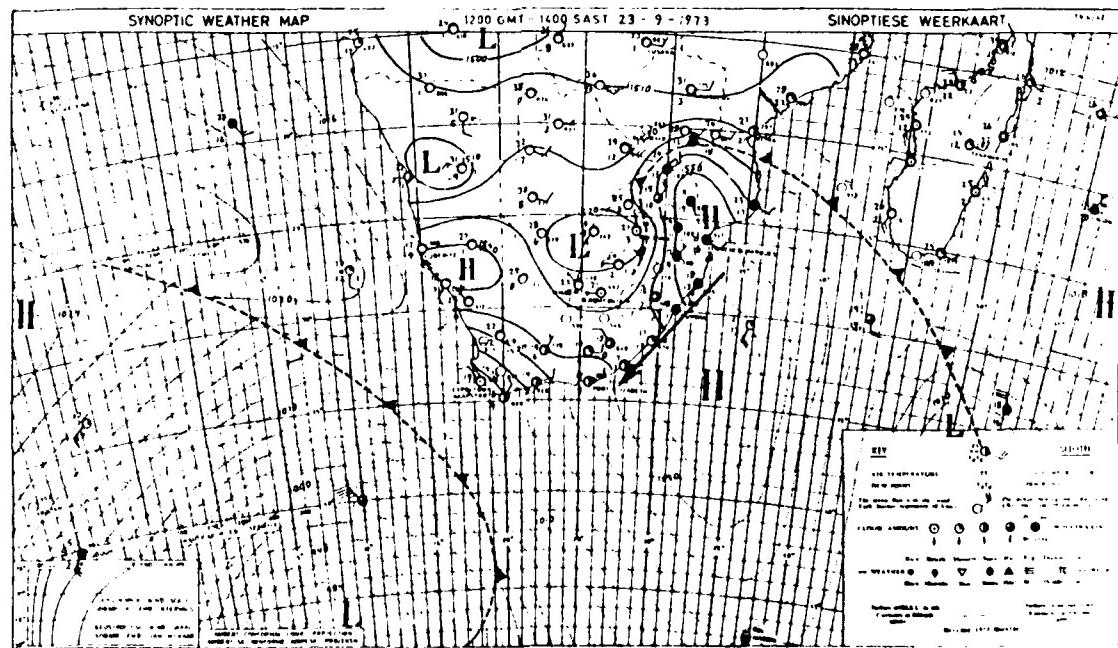


Fig. 6.20. Same as Figure 6.19 except for 1200 GMT 23 September 1973

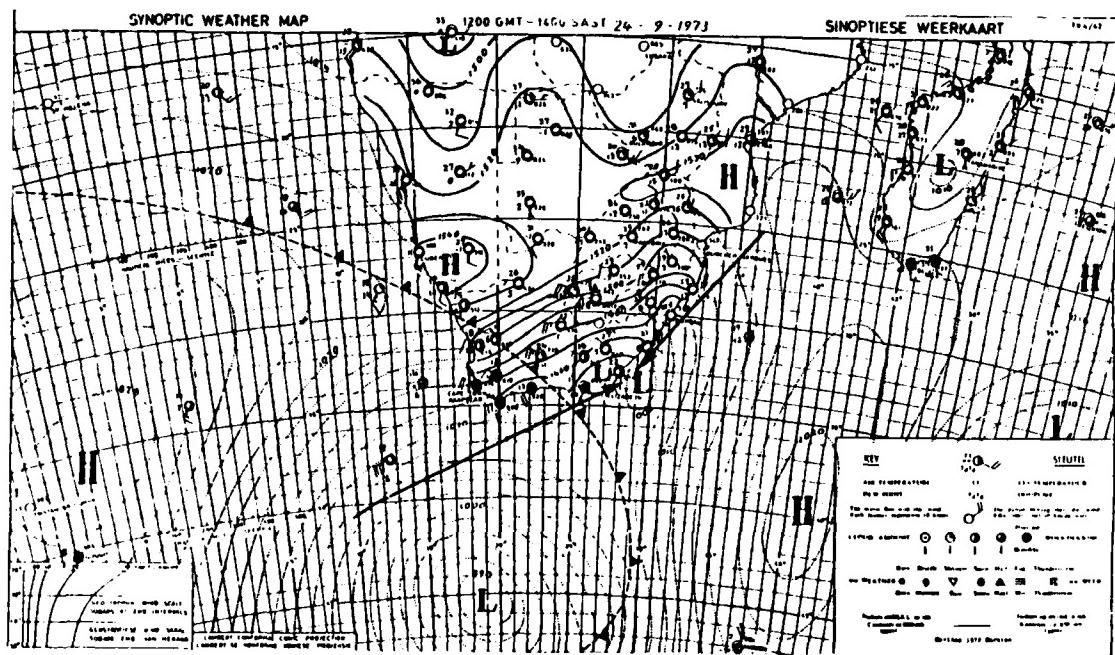


Fig. 6.21. Republic of South Africa Weather Bureau Surface (over Ocean) and 850 mb (over Continent) Analysis: 1200 GMT 24 September 1973

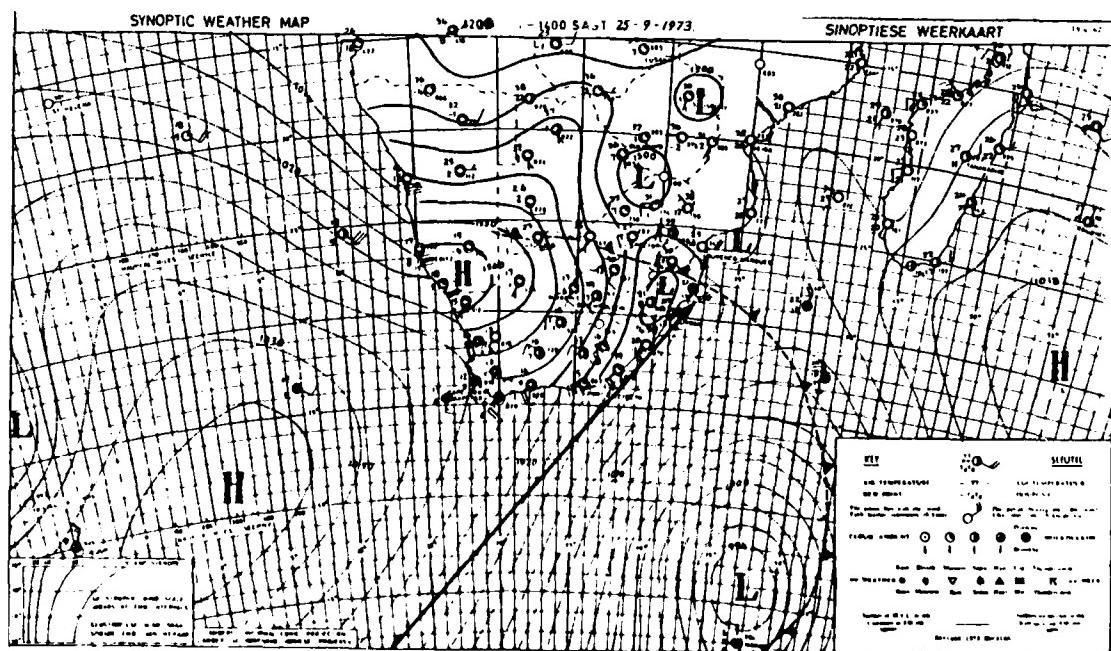


Fig. 6.22. Same as Figure 6.21 except for 1200 GMT 25 September 1973

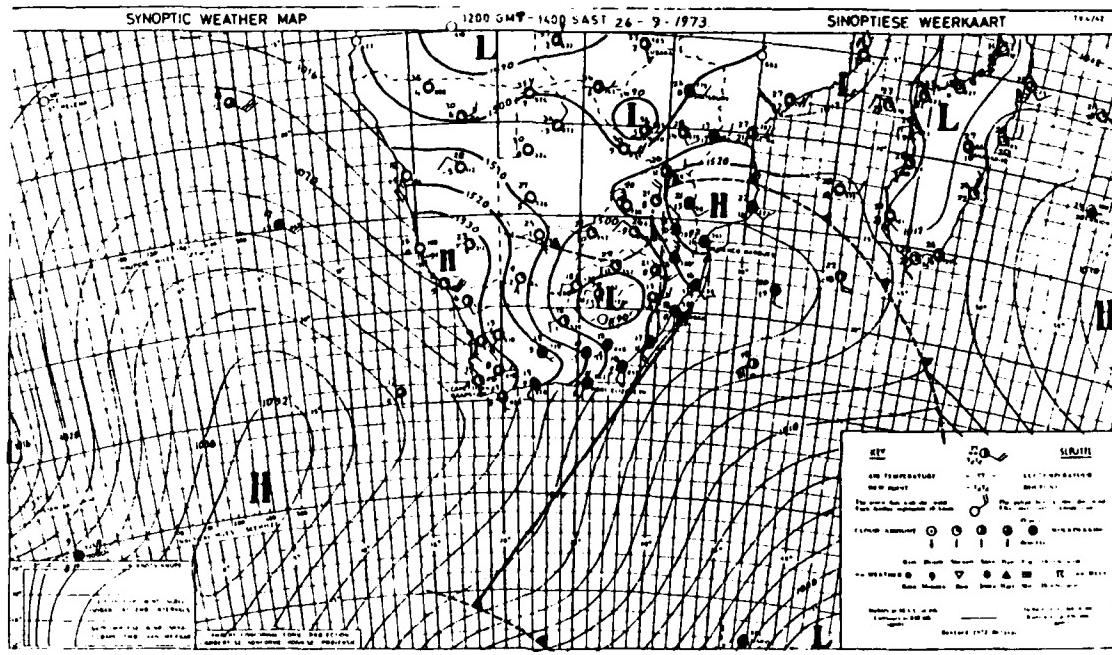


Fig. 6.23. Same as Figure 6.21 except for 1200 GMT 26 September 1973

#### 6.3.4 Forecast Rules

1. If strong southerly waves/swell are expected,<sup>10</sup> recommend a track as close to the RSA shore as safe navigation permits, especially if the ship is on a southerly heading. If not feasible, stay well offshore (outside the 100 fathom line) (Hubert et al., 1983).
2. If expected waves are slight to moderate from any direction, the effect of the Agulhas Current on speed made good is probably the most important factor in track selection (Hubert et al., 1983).
3. Prior to passages of cold fronts along the southeast African coast, northeasterly winds accentuate the speed of the Agulhas current.

<sup>10</sup> See Subsection 7.4 for additional recommendations concerning avoidance of Cape Rollers by ships proceeding in the Agulhas Current.

4. A rapid change of wind direction occurs with frontal passage over these coastal waters, backing from NE Force 6 (22-27 kt) to SW Force 6/7 (22-33 kt) in about 4 hours.
5. The effect of southwesterly winds is immediate, creating local rough seas. These rough seas occur within one hour and create 10 ft (3 m) waves with lengths of 200 ft (60 m) and a 6-7 second period. The Agulhas Current shortens the wavelength to 175 ft (53 m) with a height of 12 ft (4 m).
6. Fully developed swells from the southwest accentuate the height of the locally generated waves.
7. A correspondingly abnormally deep trough occurs ahead of the giant wave.

## 6.4 CASES IV, V AND VI - WINTER STORMS (JULY/AUGUST 1983)

### 6.4.1 Introduction

The primary purpose of this subsection is to familiarize prospective forecasters/users with the behavior of *Southern Hemisphere* migratory cyclones. Recognizing the more equatorward penetration of storm tracks (see Fig. 1.9 in Section 1) during the *winter* months, the studies span periods in July and August 1983. The three sequences consist of several days when particularly active cyclones and fronts are approaching the southern coastal regions of Africa. This number of cases is presented to *condition* the prospective forecaster to feel comfortable with the *clockwise* rotation of Southern Hemisphere cyclones and *coun-terclockwise* rotation of anticyclones, as well as to expose the prospective forecaster to typical movement of these migratory systems. An additional purpose of the subsection is to compare analyses of the U. S. Navy with those of other agencies. While the initial examination is conducted using regional surface analyses by the Weather Bureau of the Republic of South Africa (RSA) and METEOSAT imagery from the geostationary satellite of the European Space Agency, a cursory comparison will be made between RSA *regional* surface analyses and *global* surface analyses<sup>11</sup> provided by the Fleet Numerical Oceanography Center (FNOC). Additionally, examples of imagery from polar orbiting satellites (both NOAA 7 and the Defense Meteorological Satellite Program (DMSP)), which are more readily available to naval operating units than METEOSAT imagery, are included. A comparison will also be made of 500 mb analyses produced by the U. S. National Meteorological Center (NMC) and by FNOC. Finally, a few summary forecast rules/hints are presented.

---

<sup>11</sup> The reader must keep in mind that the manually enhanced RSA analyses often include features gleaned from recently received satellite imagery or data not included within the global FNOC analysis. However, such features will often be added by the regional naval oceanography centers, such as Norfolk and Guam in their preparation of subsequent forecasts. Also note that this discussion is restricted to analyses only, i.e., no *prognoses* (forecast charts) are presented or discussed.

#### 6.4.2 Case Study IV (5 - 9 July 1983)

5 July 1983

Fig. 6.24 provides an introduction for this case study on 5 July, depicting a cold air mass penetrating over southern RSA with a cold front extending from a frontal wave cyclone near 40°S, 33°E. With the limited resolution available for such a large area, the METEOSAT imagery (Fig. 6.25) generally supports the frontal position, but clearly shows extensive open cellular cloudiness associated with the cold air advection and unstable conditions within the cold air mass over the ocean south of the continent. Note that the RSA *manual* analysis<sup>12</sup> (Fig. 6.24) includes a vortex at point A (37°S, 25°E) whose existence was identified by the satellite imagery. The automated FNOC surface analysis (Fig. 6.26) portrays a strong *frontal* trough in agreement with Fig. 6.24, but has no indication of the coastal vortex at point A or the possible frontal wave analyzed in Fig. 6.24 at 40°S, 33°E.

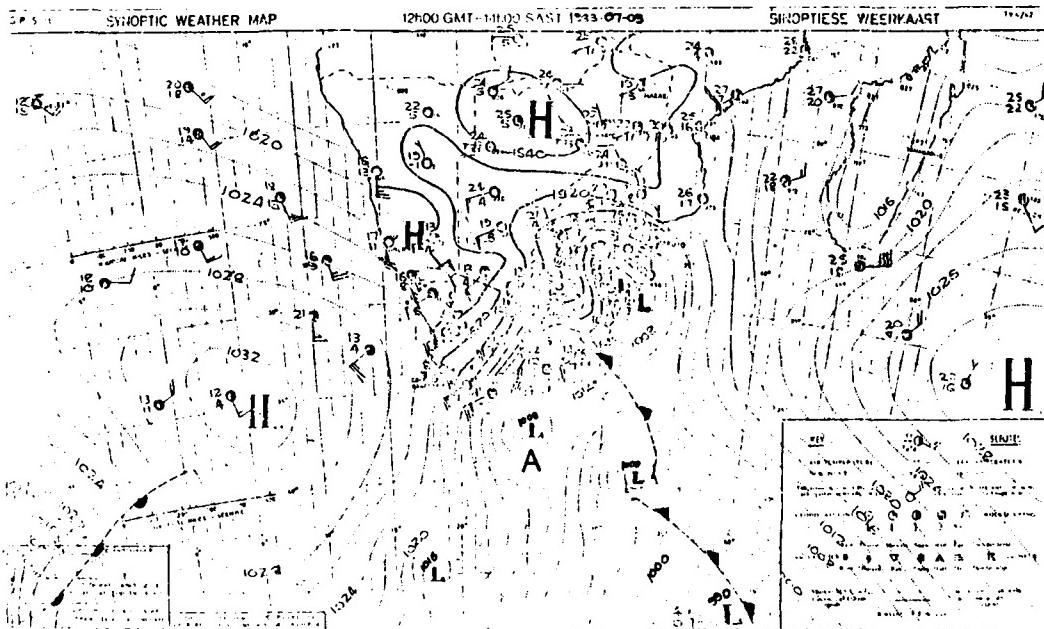
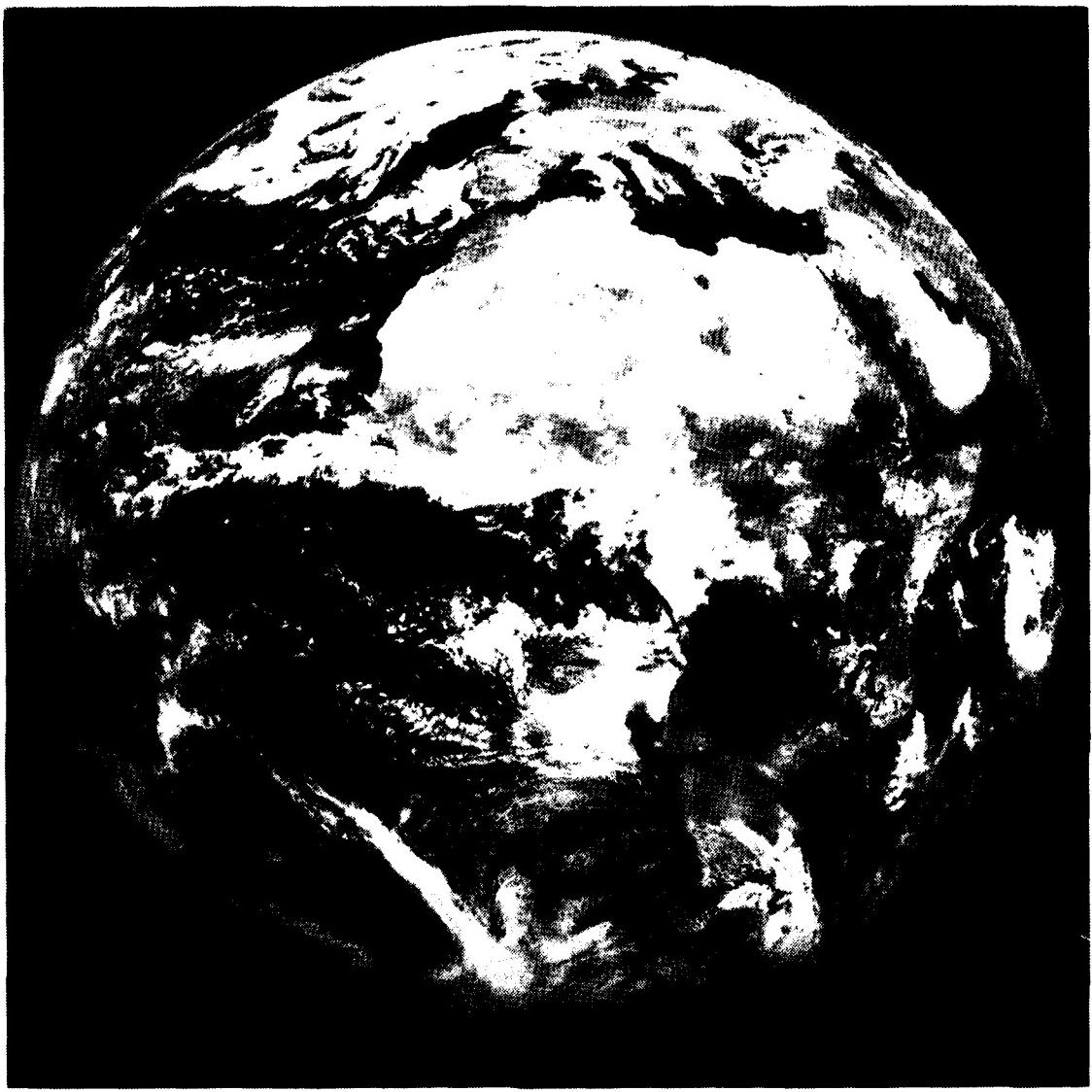


Fig. 6.24. Republic of South Africa Weather Bureau Surface (over Ocean) and 850 mb (over Continent) Analysis: 1200 GMT 5 July 1983

<sup>12</sup> The author apologizes for the poor copies of the RSA analyses for Cases IV and V.



**METEOSAT**

1983 MARCH 7 10 5 TIME 1155 GMT NORTH CH WIC E  
001100 - 1000 0000 DATA 0007 04 LAIRIGHT + ECR +

Fig. 6.25. Visible METEOSAT imagery, 1155 GMT on 5 July 1983

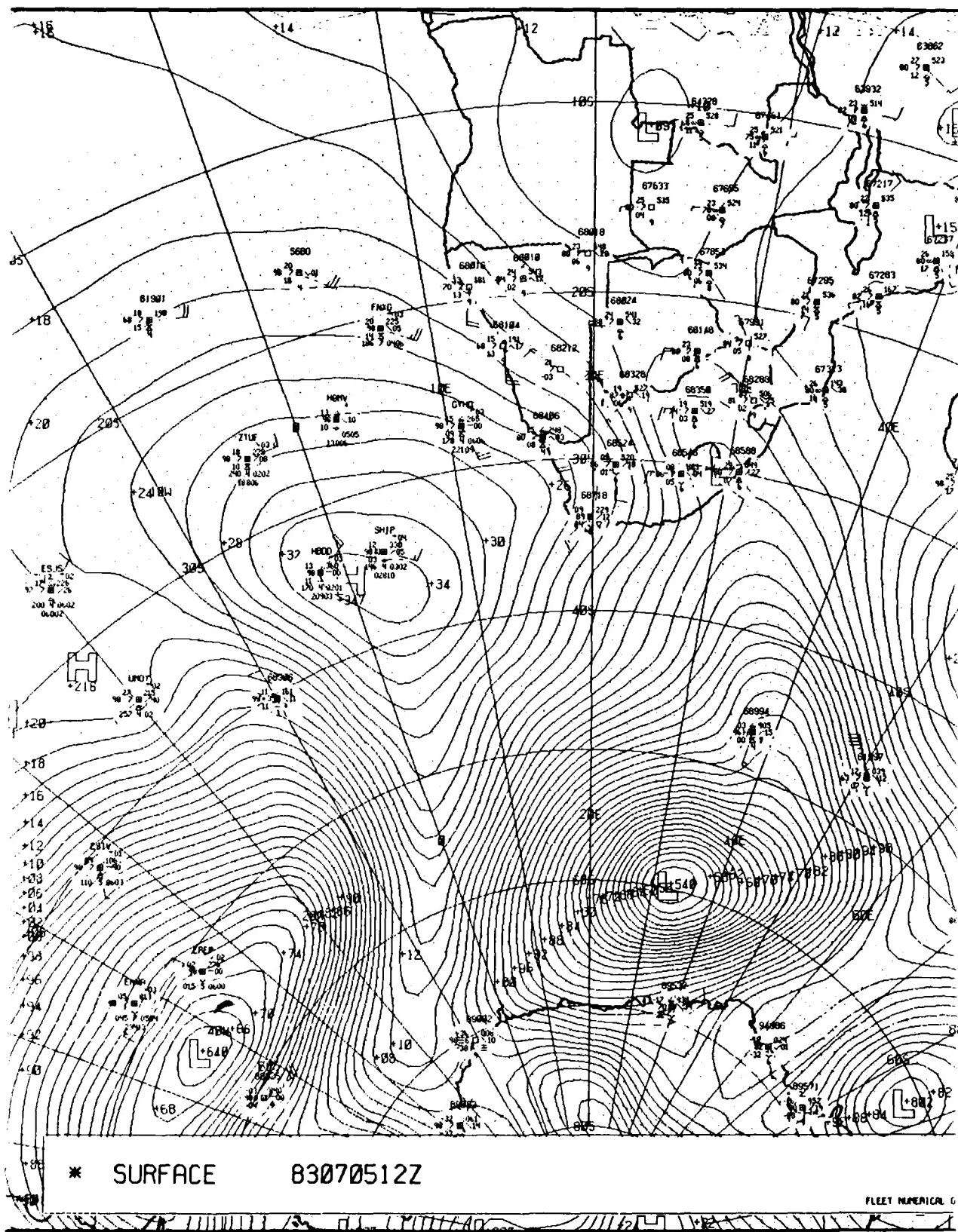


Fig. 6.26. FNOC sea-level pressure analysis, 1200 GMT on 5 July 1983

6 July 1983

On this date (Fig. 6.27), the RSA analysis depicts the cold front of the previous day having moved at ~25 kt and approaching the southern tip of the Malagasy Republic. The vortex at 37°S, 25°E on 5 July has moved eastward at the same speed to 38°S, 38°E and now has a cold front extending northwestward to Port Elizabeth. The METEOSAT imagery (Fig. 6.28) supports both fronts and still has an extensive area of open cells behind the trailing front. In the FNOC surface analysis (Fig. 6.29), the *frontal* trough toward the Malagasy Republic, associated with the leading front of the RSA analysis, is well depicted (note the ship reporting 30-kt SW wind with 6 ft seas (code 04) and 11 ft swell (code 07) at 29°S, 41°E behind the trough (front)). However, the vortex at 38°S, 38°E is absent, and there is only a faint hint of a trough extending toward the southeastern coast of RSA to compare with the new front on Fig. 6.27. Fig. 6.30 is a swath of visible imagery from the NOAA 7 polar orbiting satellite, taken between 1238 and 1243 GMT, and available for receipt aboard ship. Again the open cellular convection is readily apparent behind (to the west of) the trailing front, while stronger convective activity is apparent where the leading front is just reaching the southwest coast of the Malagasy Republic.

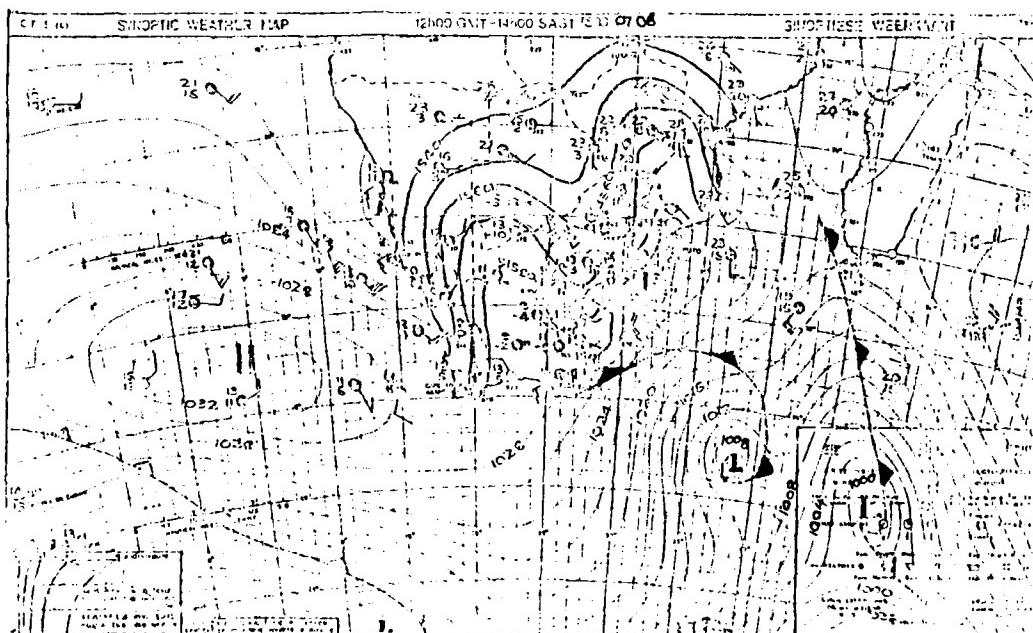
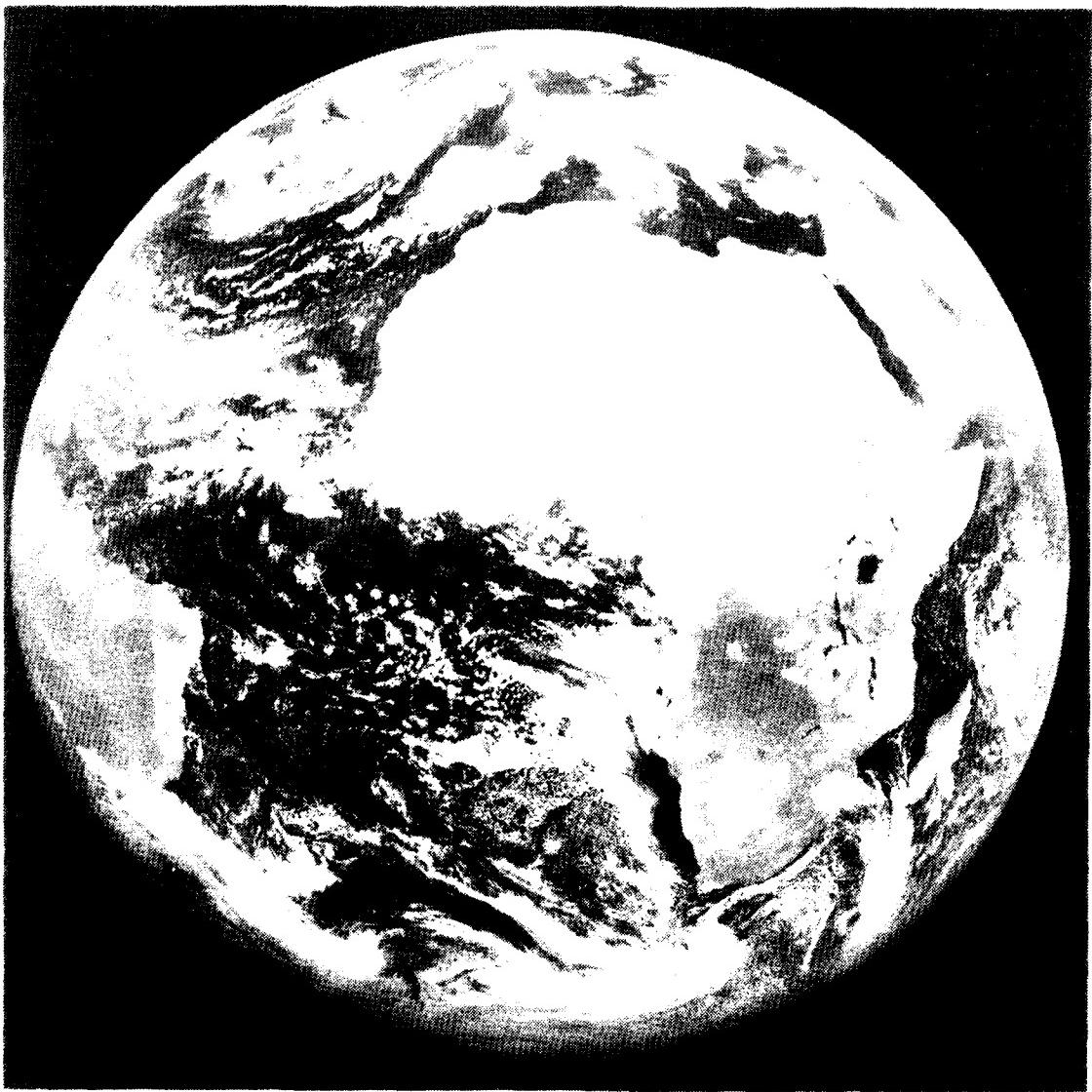


Fig. 6.27. Republic of South Africa Weather Bureau Surface (over Ocean) and 850 mb (over Continent) Analysis: 1200 GMT 6 July 1983



METEOSAT

Fig. 6.28. Visible METEOSAT imagery, 1155 GMT on 6 July 1983

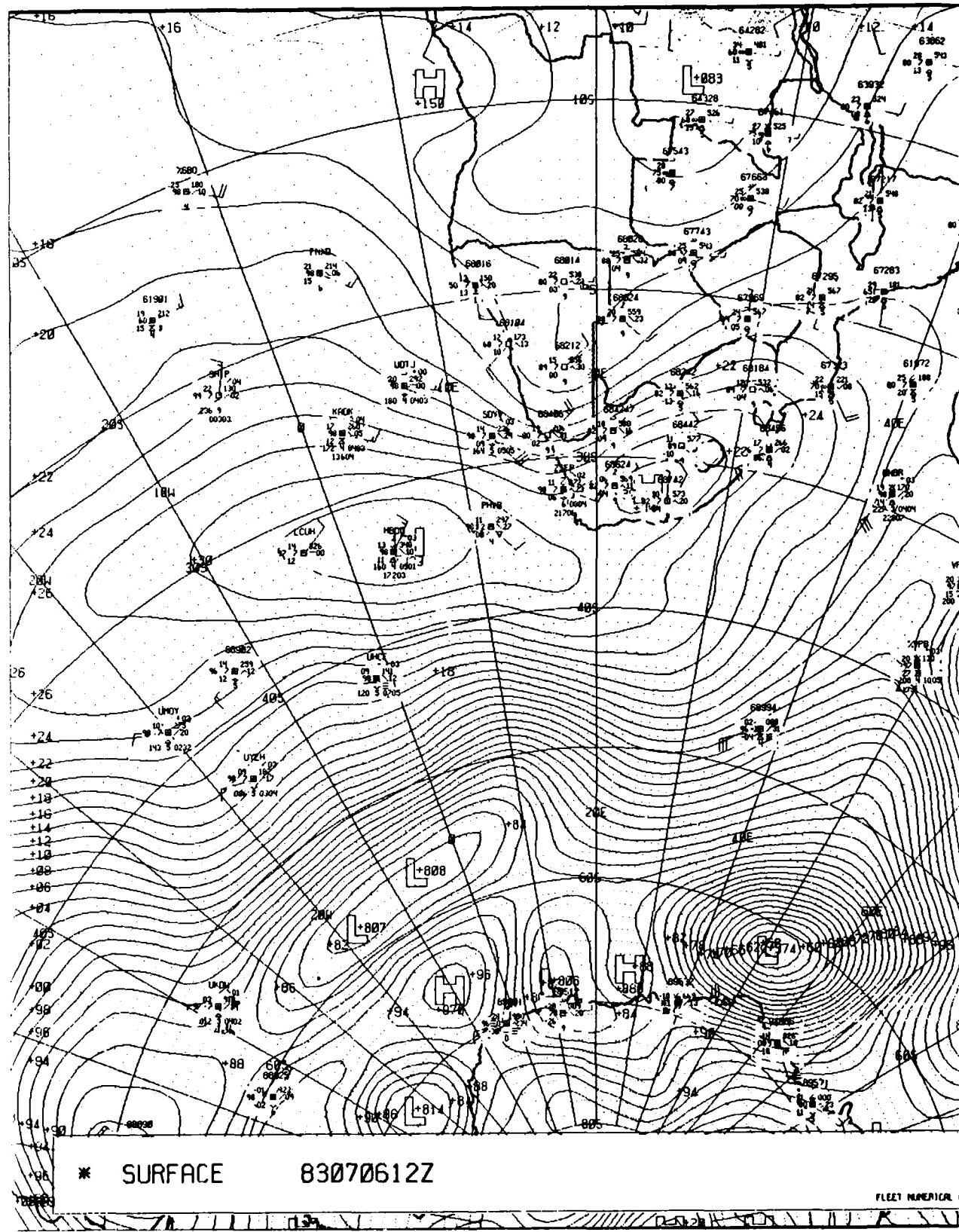


Fig. 6.29. FNOC sea-level pressure analysis, 1200 GMT on 6 July 1983

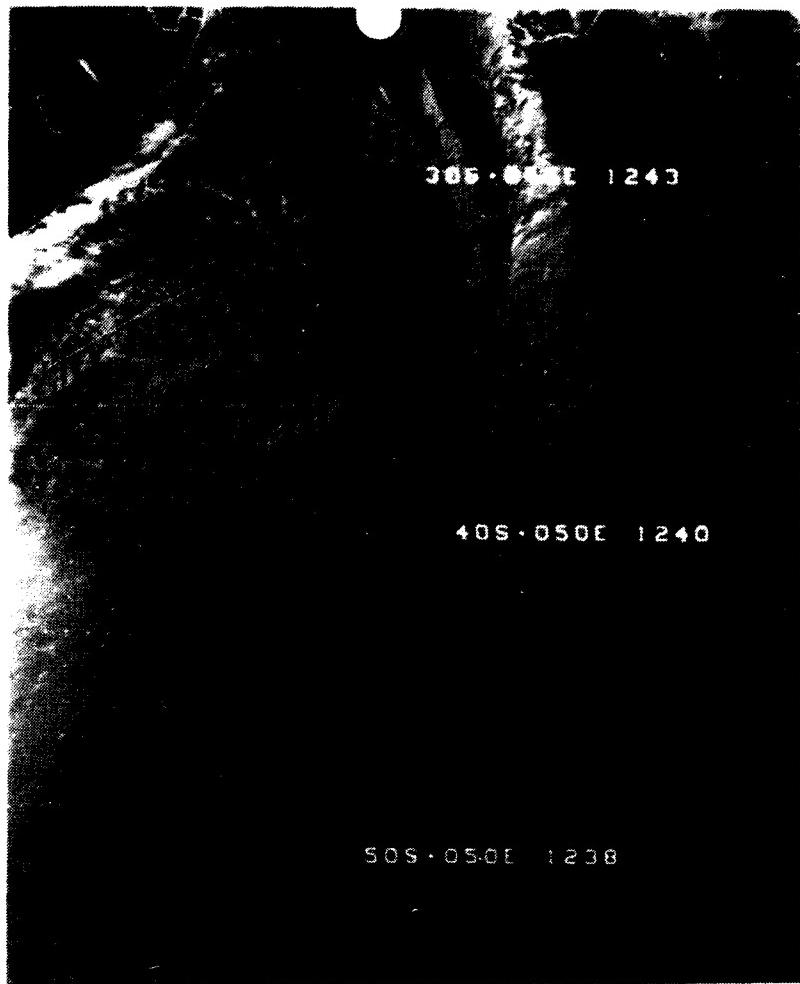
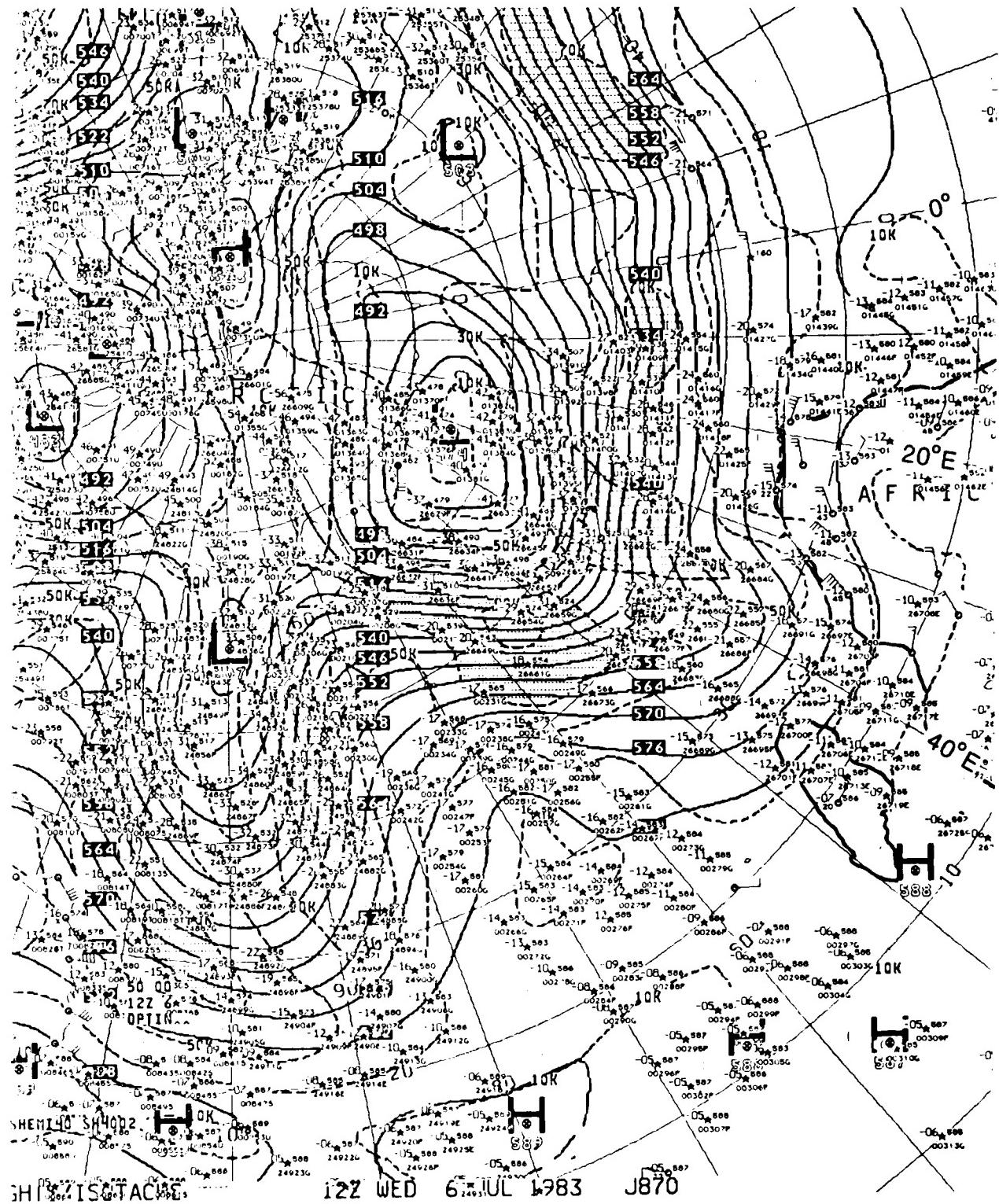


Fig. 6.30. NOAA 7 visible imagery, 1238-1243 GMT on 6 July 1983

The 500 mb analyses from NMC<sup>13</sup> and FNOC (Figs. 6.31 and 6.32, respectively) both show a large amplitude trough vertically consistent with (i.e., trailing to the west of) the surface frontal trough approaching the Malagasy Republic.

---

<sup>13</sup> Note that on Fig. 6.31, and all subsequent NMC 500 mb analyses, Africa is heavily outlined and rotated to the right side of the figure.



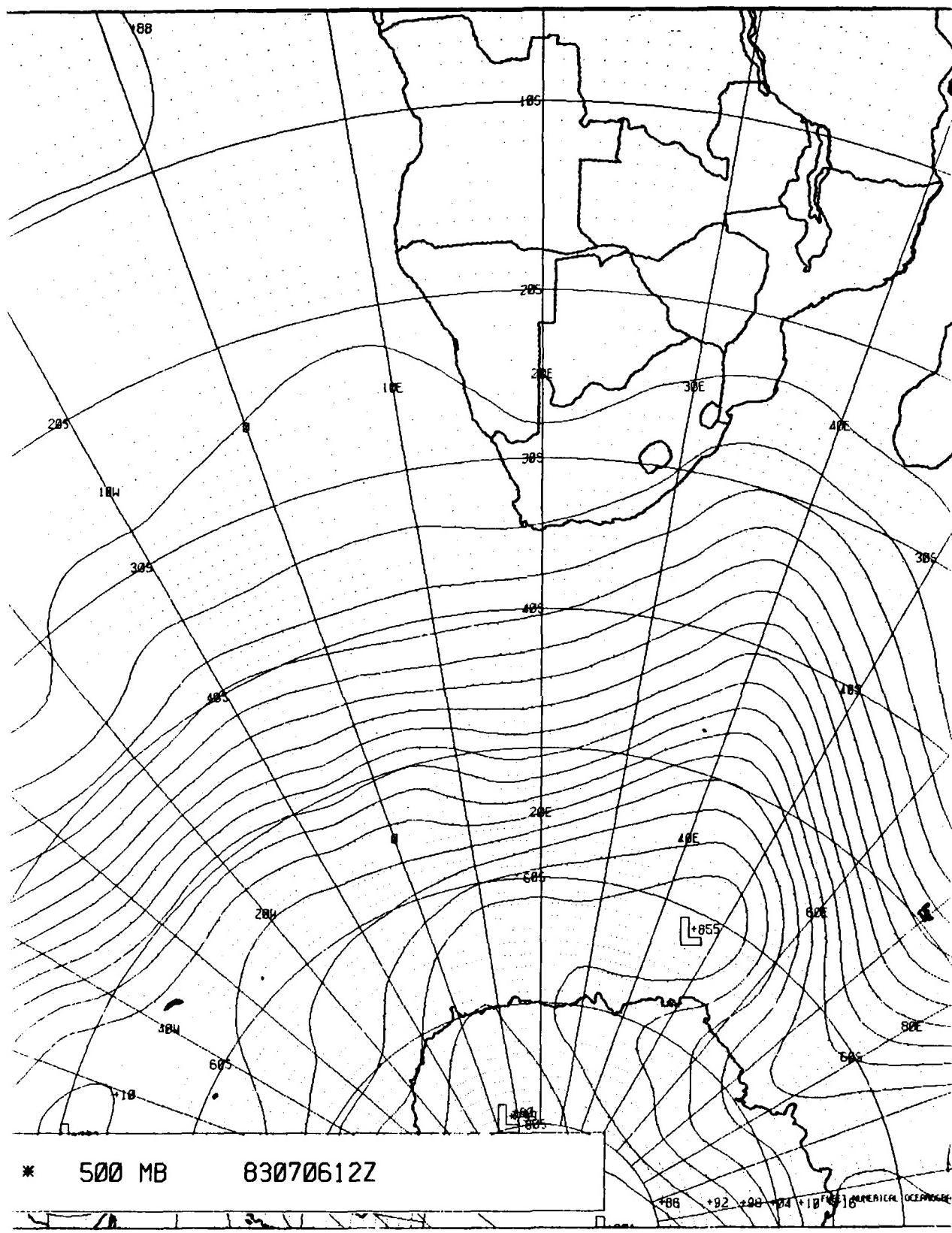


Fig. 6.32. FNOC 500 mb analysis (contours only), 1200 GMT on 6 July 1983

7 July 1983

On this date the cold front is departing the southeastern coast of the Malagasy Republic while the RSA analysis (Fig. 6.33) depicts a new frontal wave cyclone (1009 mb at 39°S, 15°E) approaching southwestern RSA; the cold front is ~150 n mi off Cape Town. The visible and infrared imagery of METEOSAT (Figs. 6.34 and 6.35) strongly support the frontal wave analyzed by the RSA, and open cells (Fig. 6.34) are again present within the cold air advection following the approaching cold front. As might be expected from a global analysis, the FNOC surface analysis (Fig. 6.36) depicts only a trough southwest of RSA with no frontal wave cyclone. However, the FNOC surface trough southeast of the Malagasy Republic (Fig. 6.36) does closely agree with the position of the front in the RSA analysis (Fig. 6.33).

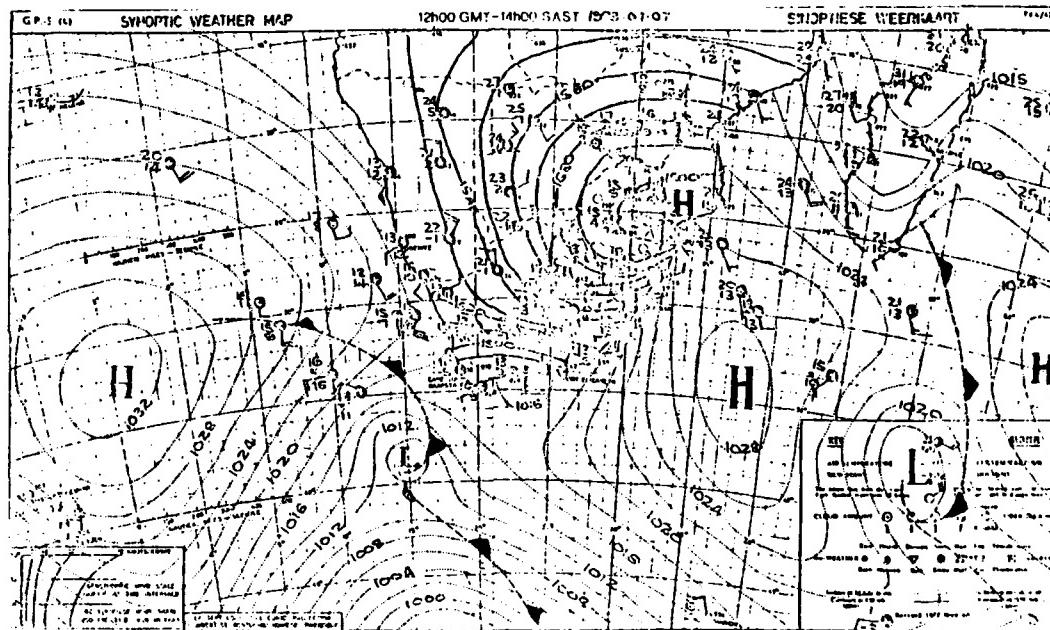
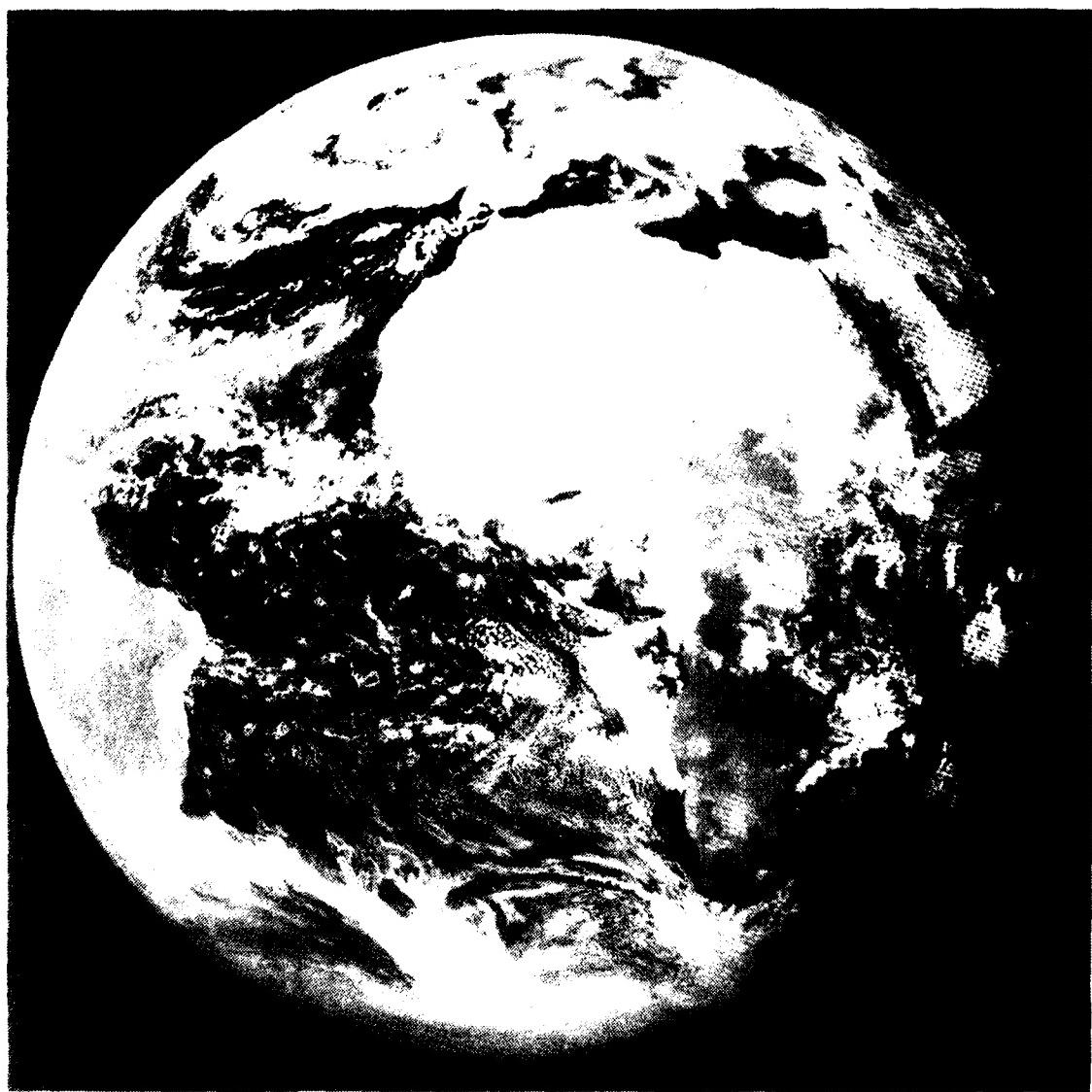


Fig. 6.33. Republic of South Africa Weather Bureau Surface (over Ocean) and 850 mb (over Continent) Analysis: 1200 GMT 7 July 1983



METEOSAT

Fig. 6.34. Visible METEOSAT imagery, 1255 GMT on 7 July 1983



**METEOSAT**

1983 MONTH 7 DAY 7 TIME 1255 GMT (NORTH) CH. IR 1  
NOMINAL SCAN PAW DATA SLOT 26 COPYRIGHT - ESA -

Fig. 6.35. Infrared METEOSAT imagery, 1255 GMT on 7 July 1983

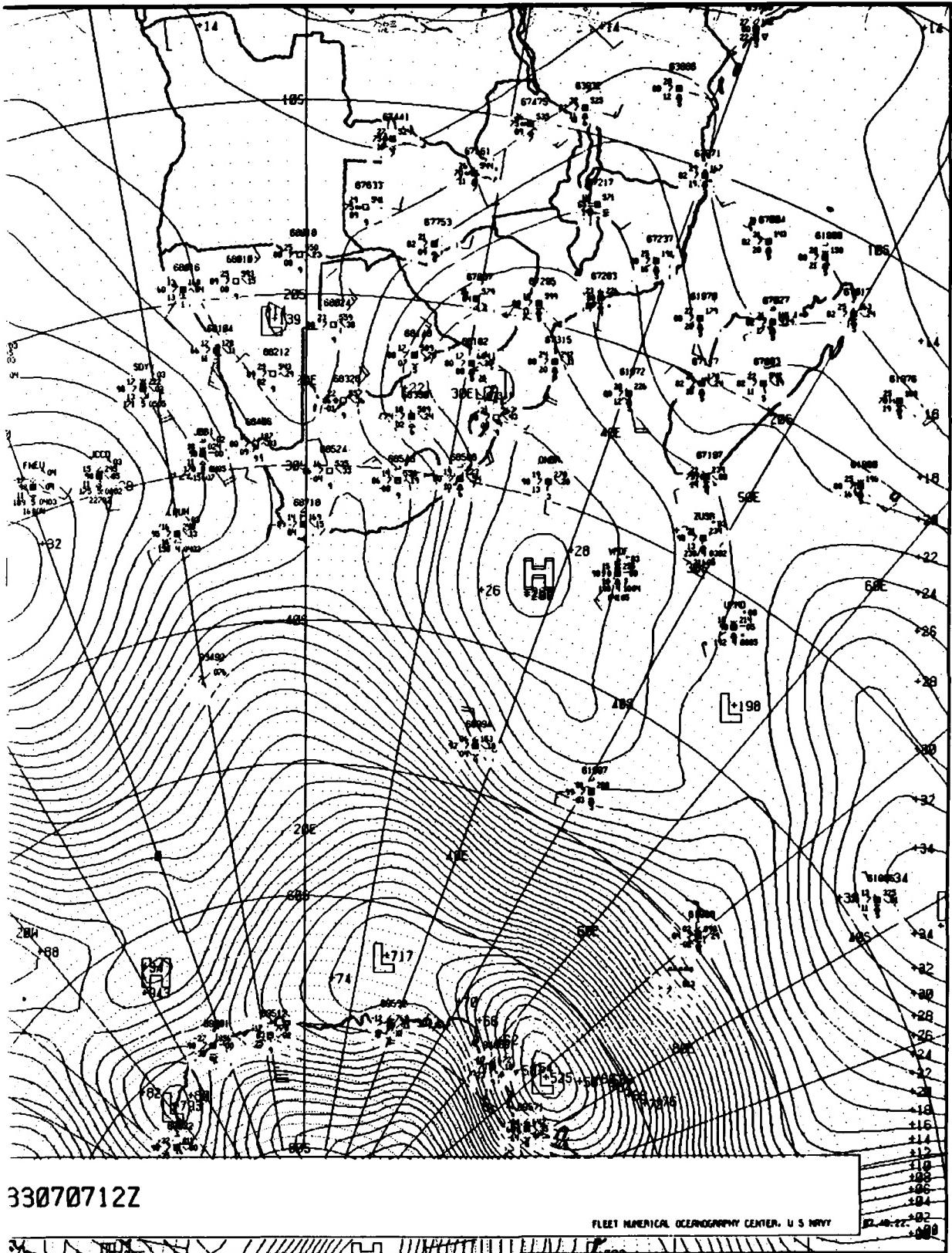


Fig. 6.36. FNOC sea-level pressure analysis, 1200 GMT on 7 July 1983

Fig. 6.37 displays the FNOC 500 mb analysis which satisfactorily depicts both upper-air troughs (i.e., the 500 mb trough at ~12°E (west of Cape Town) and another trough depicted on the margin of the figure south of the Malagasy Republic) associated with the surface fronts.

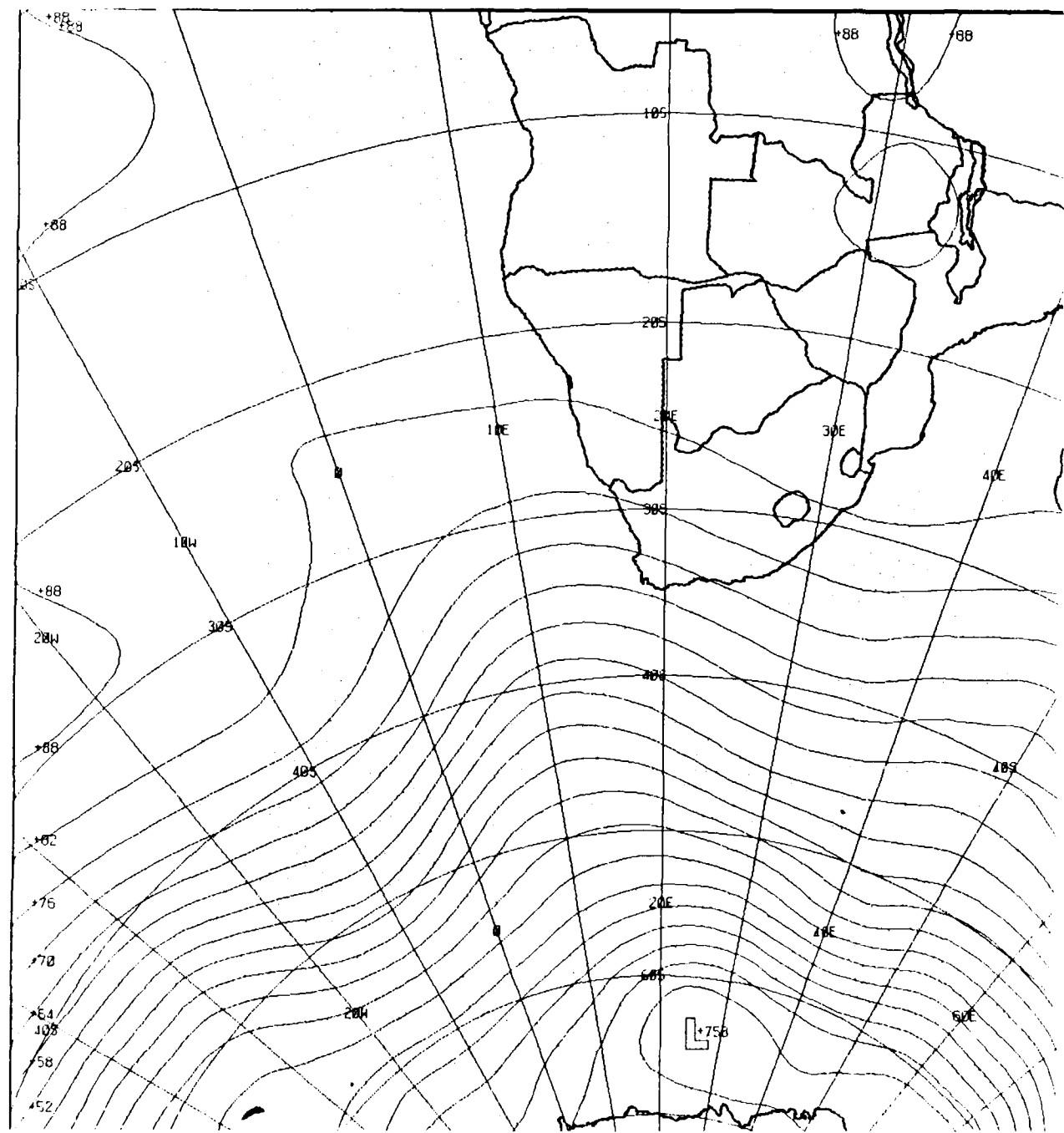
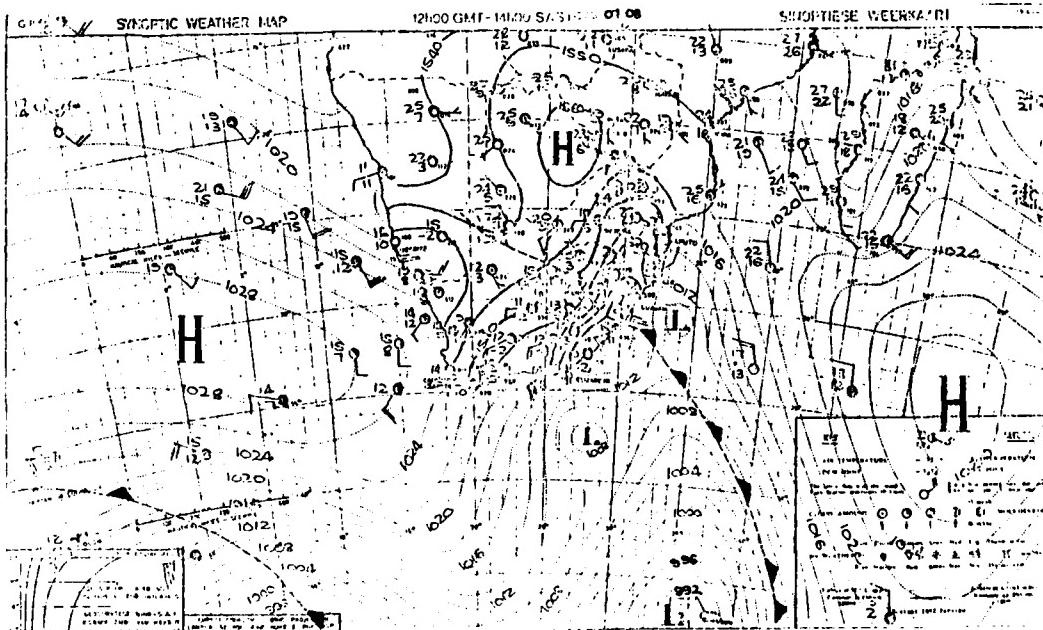
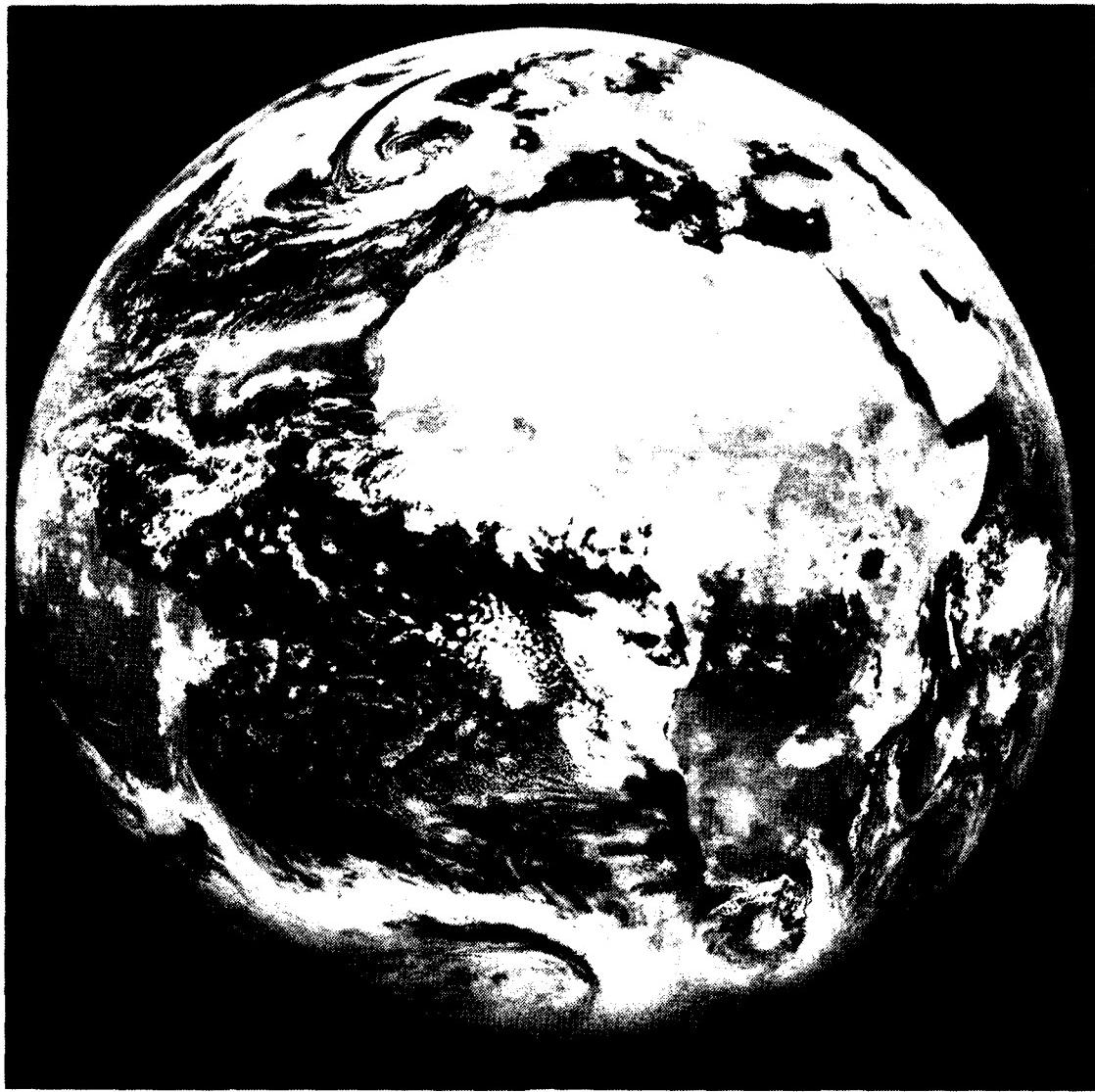


Fig. 6.37. FNOC 500 mb analysis (contours only), 1200 GMT on 7 July 1983

8 July 1983

On the following day, the RSA surface analysis (Fig. 6.38) depicts the cold front having advanced eastward and now approaching Durban on the southeast coast of the RSA. A new low center (1007 mb) is shown south-southeast of Port Elizabeth near 37°S, 28°E within the cold air mass. Additionally, another cold front is depicted far to the southwest (crossing latitude 40°S at 2°W). The METEOSAT imagery (Fig. 6.39) shows all of these features quite well. The FNOC surface analysis (Fig. 6.40) depicts a large amplitude trough entering RSA near 30°S, 32°E (near Durban) coinciding with the RSA frontal trough, although, as expected, there is no low in the cold air mass at 37°S, 28°E, nor is there the *coastal closed low*, depicted in the RSA analysis (Fig. 6.38) at 31°S, 34°E. The FNOC analysis (Fig. 6.40) does display a very strong pressure gradient poleward (i.e., toward the south) of 40°S within the cold air mass behind the new cold front approaching from the South Atlantic (e.g., note the ship reporting a 35-kt westerly wind at 42°S, 2°W).





**METEOSAT**

1115 HRS 8 JULY 1983 TIME 1155 GMT NORTHERN HEMISPHERE  
METEOSAT-2 INFRARED 10.8 MICRONS

Fig. 6.39. Visible METEOSAT imagery, 1155 GMT on 8 July 1983

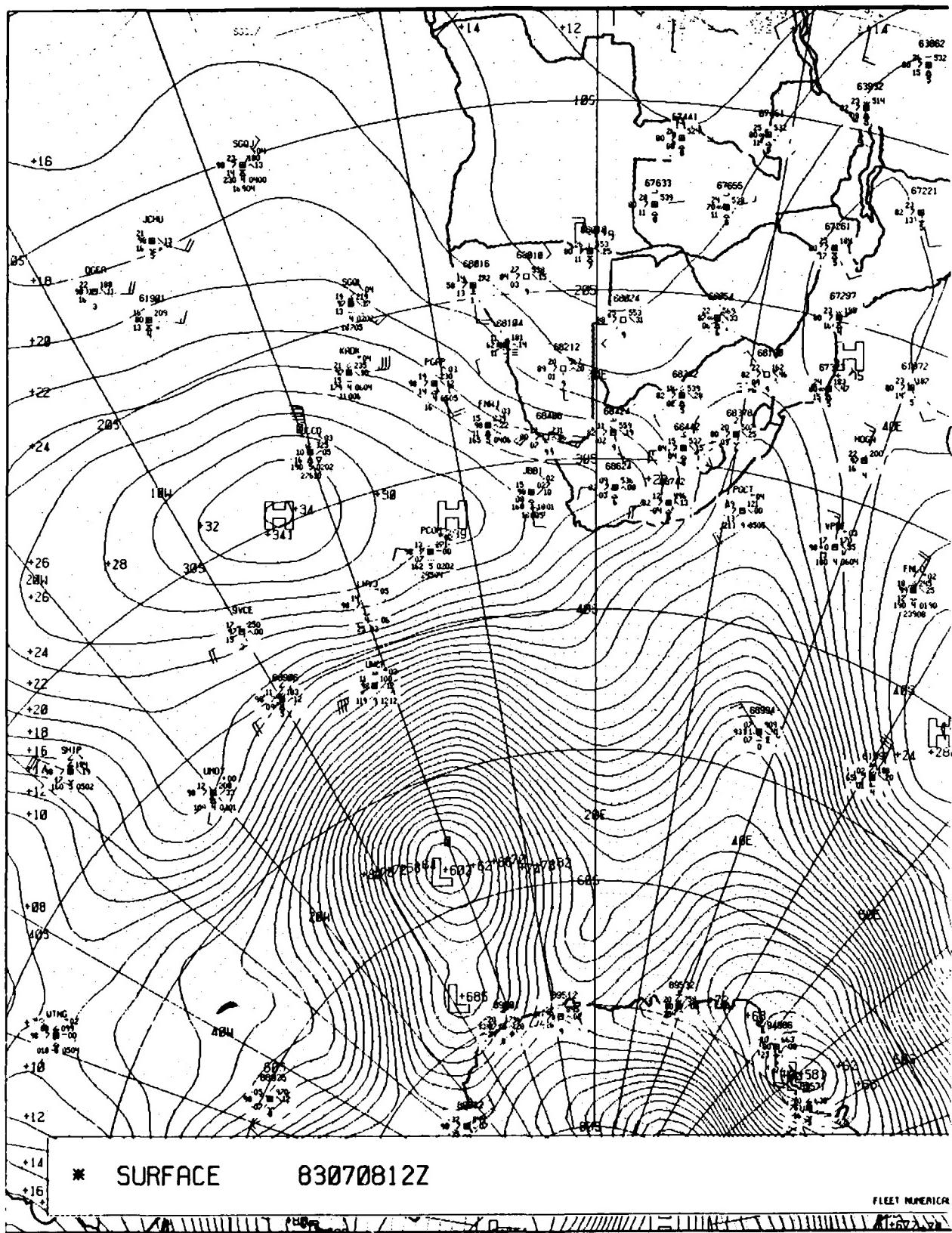


Fig. 6.40. FNOC sea-level pressure analysis, 1200 GMT on 8 July 1983

The front currently approaching Durban has moved at an average speed of ~30 kt during the past 24 hours along the RSA coast. This is not surprising since both Figs. 6.41 and 6.42 depict large 500 mb gradients over the RSA coast with Fig. 6.41 having a 70-kt isotach currently over the southeast coast of RSA. Both 500 mb analyses depict a short wave 500 mb trough near 25°E over the RSA, vertically consistent, i.e., trailing the surface front.

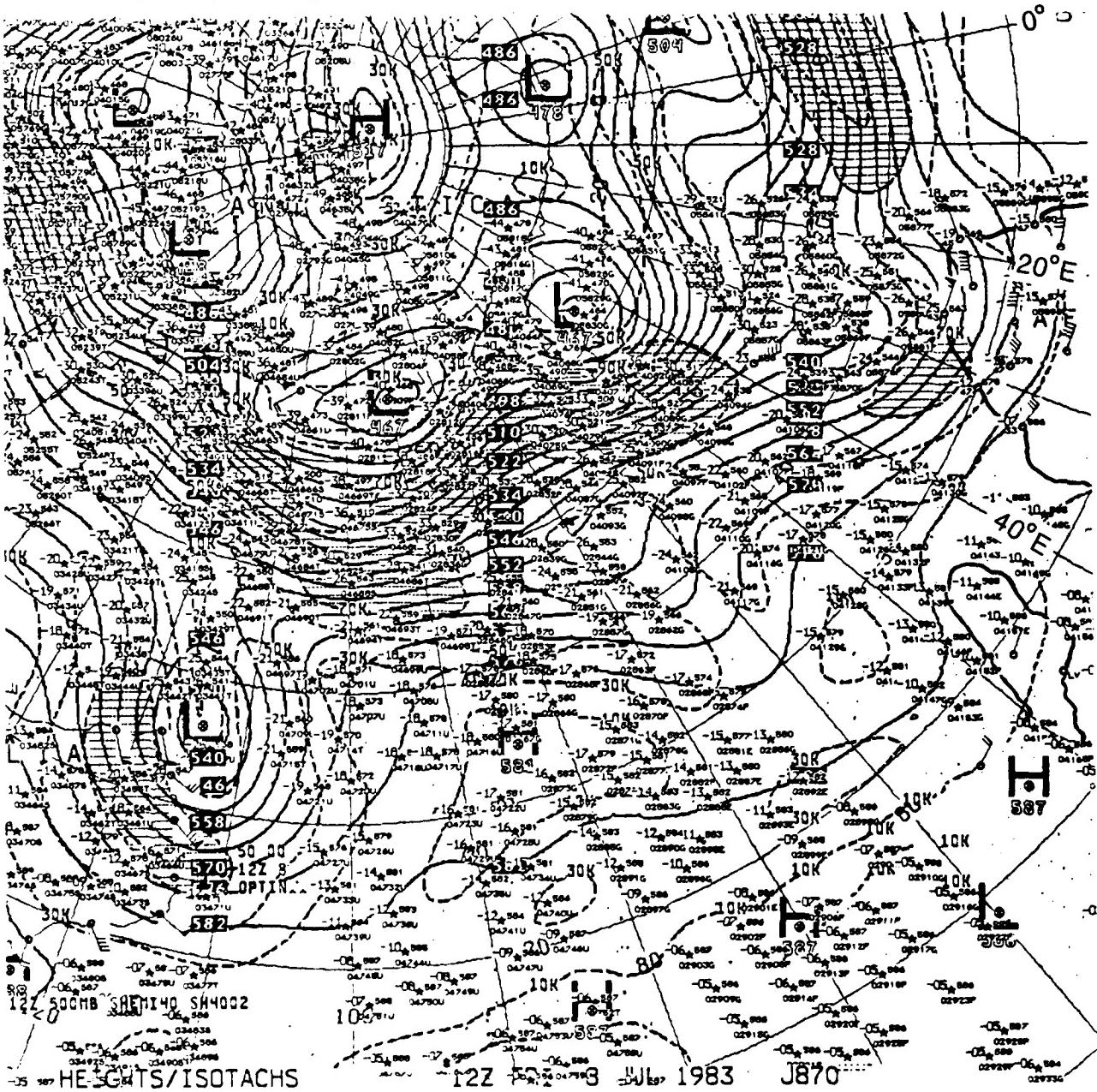


Fig. 6.41. NMC 500 mb analysis (contours and isotachs), 1200 GMT on 8 July 1983 (Note that Africa is outlined on right side of figure)

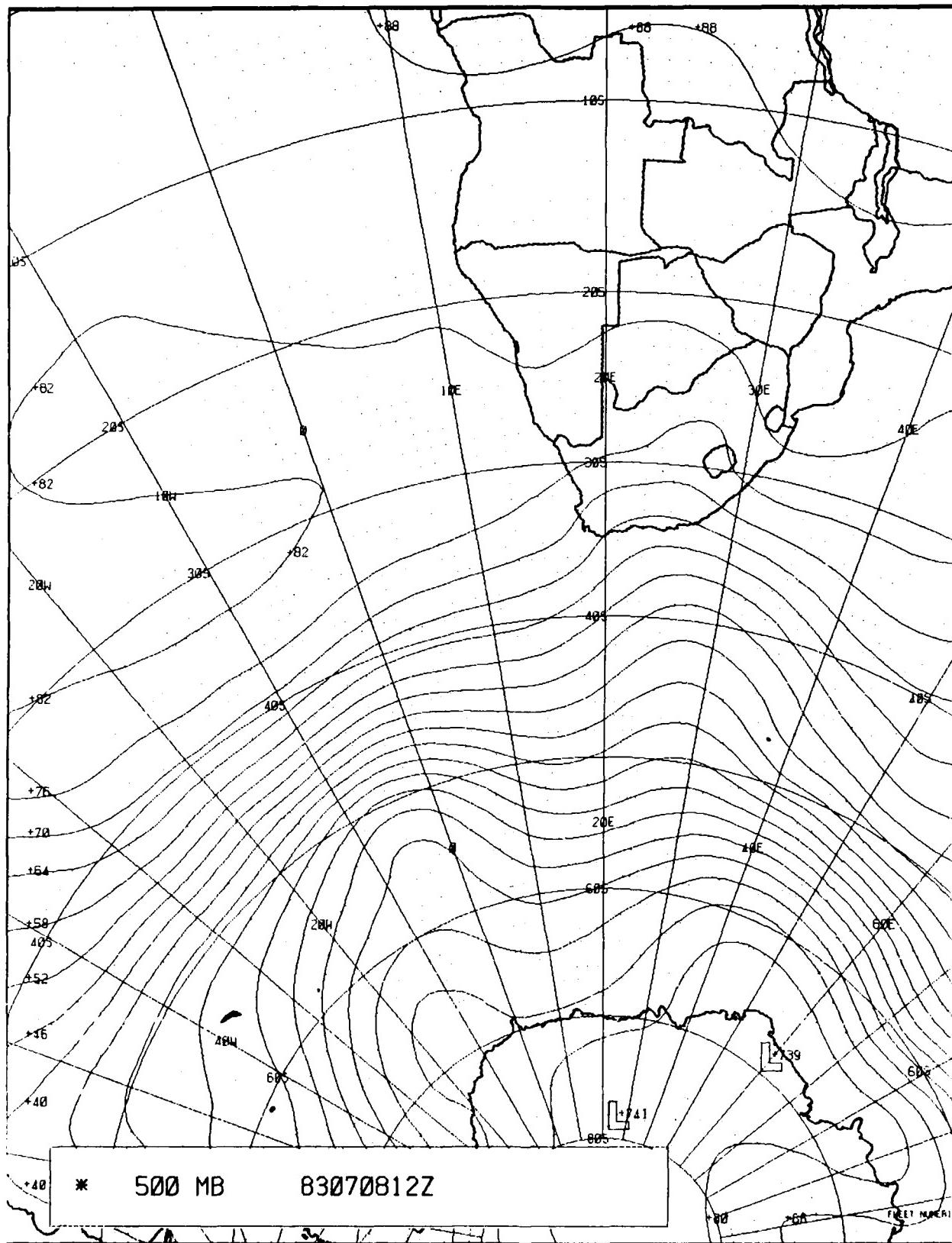


Fig. 6.42. FNOC 500 mb analysis (contours only), 1200 GMT on 8 July 1983

9 July 1983

The last day in this case (Fig. 6.43) finds the incipient low (just off Port Elizabeth on the previous day) having moved southeastward and developing into a strong frontal wave cyclone (1007 mb, at 39°S, 41°E) on the RSA analysis. Its associated front extends northwestward to the southern coast of Mozambique. The front approaching from the South Atlantic is now 250 n mi southwest of Cape Town with a frontal wave cyclone (1017 mb) near 36°S, 1°E. The features on the METEOSAT imagery (Fig. 6.44) support the RSA analysis, including both frontal waves. The FNOC surface analysis (Fig. 6.45) displays a frontal trough extending toward the Mozambique Channel, in agreement with the RSA analysis. (However, Fig. 6.46, presenting the visible imagery available from NOAA 7 of the frontal wave south of the Malagasy Republic at 1204 GMT, indicates a better agreement with the low position analyzed by the RSA than with the FNOC low center position far south near 48°S). FNOC (Fig. 6.45) does depict advancement of the intense surface pressure gradient (to near 40°S, 20°E) associated with the approaching front, but location of the front requires reference to satellite imagery.

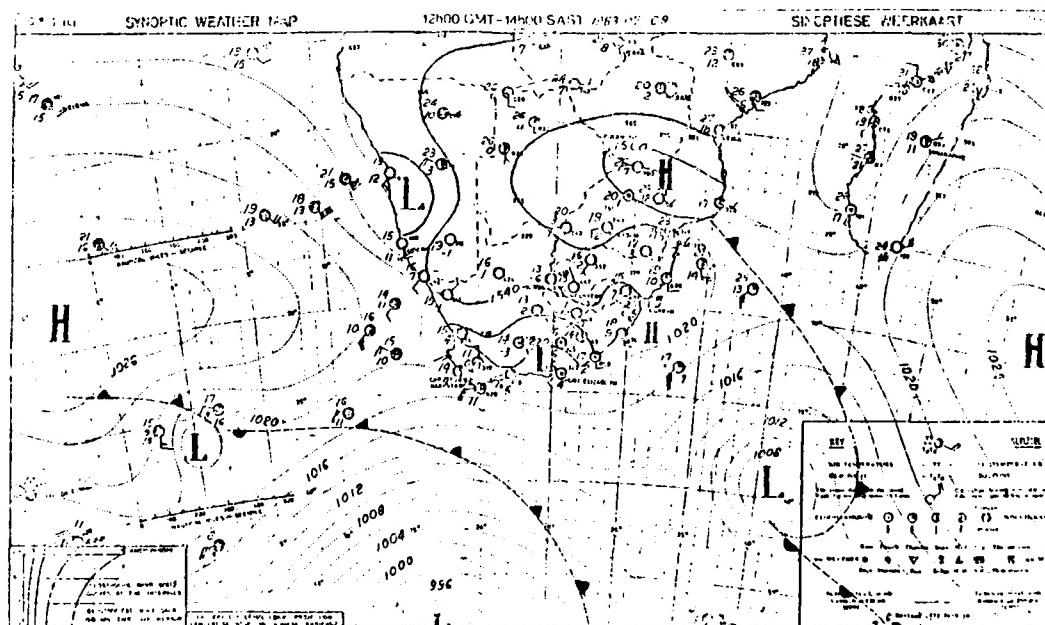
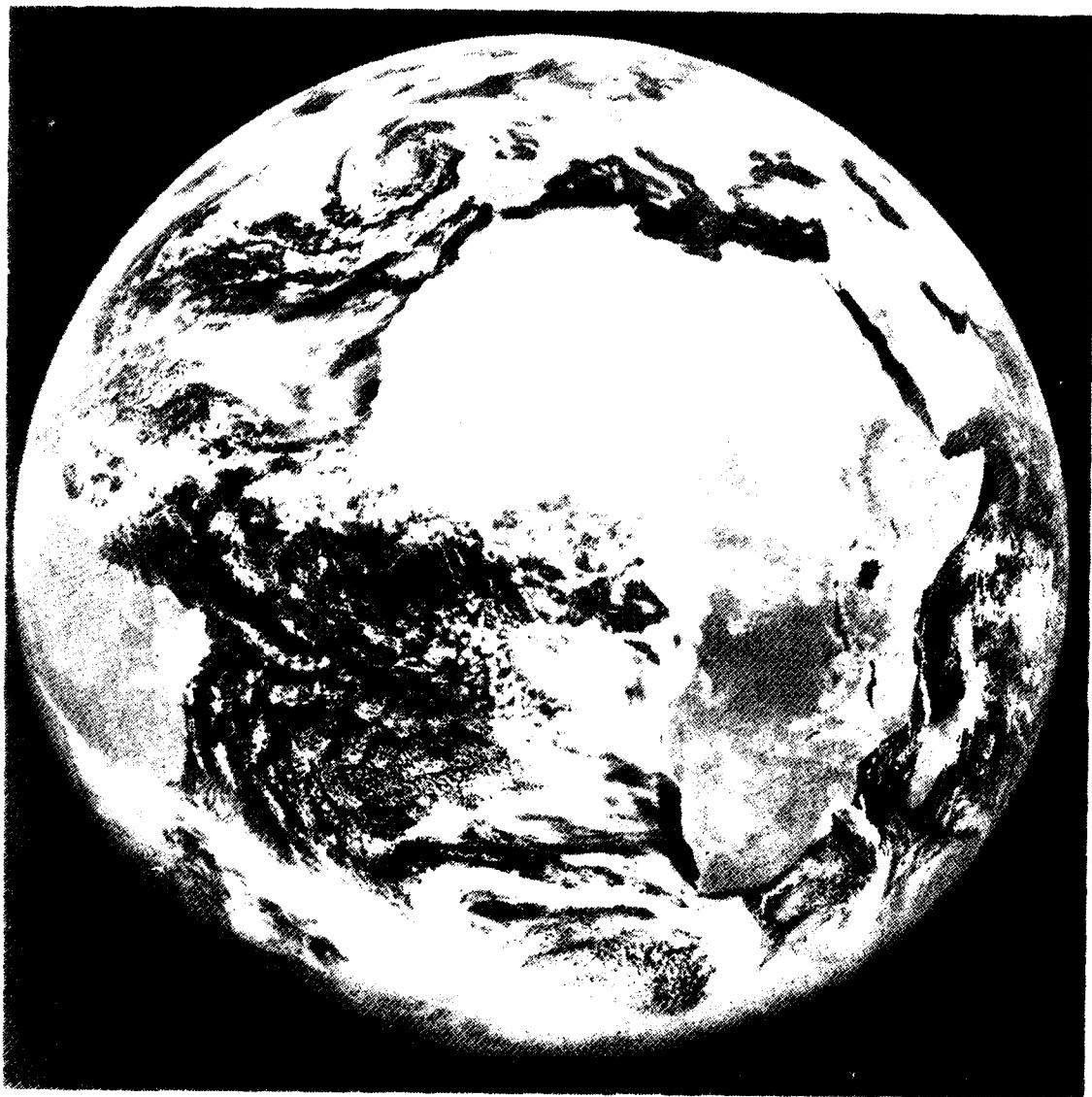


Fig. 6.43. Republic of South Africa Weather Bureau Surface (over Ocean) and 850 mb (over Continent) Analysis: 1200 GMT 9 July 1983



METEOSAT

Fig. 6.44. Visible METEOSAT imagery, 1155 GMT on 9 July 1983

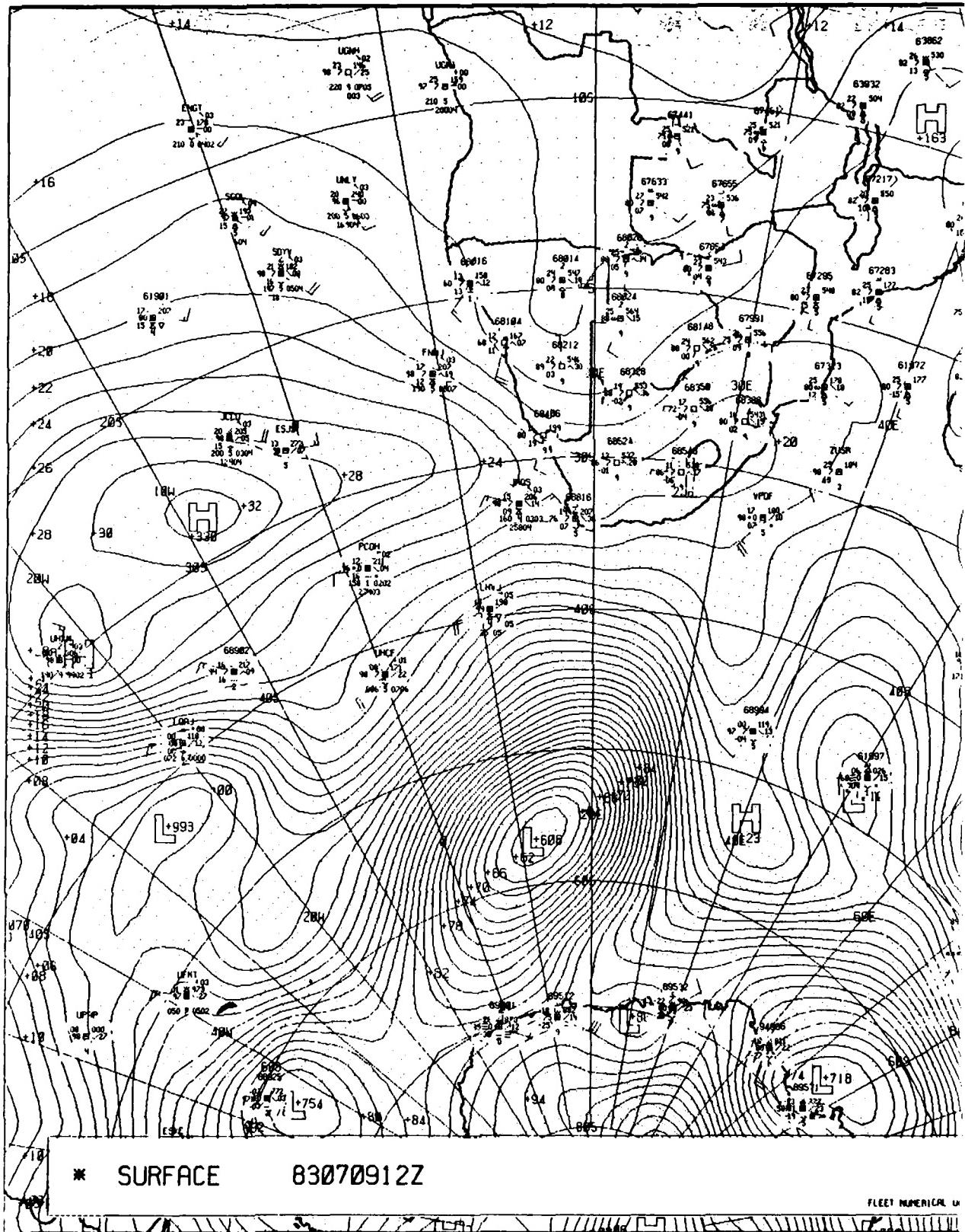


Fig. 6.45. FNOC sea-level pressure analysis, 1200 GMT on 9 July 1983

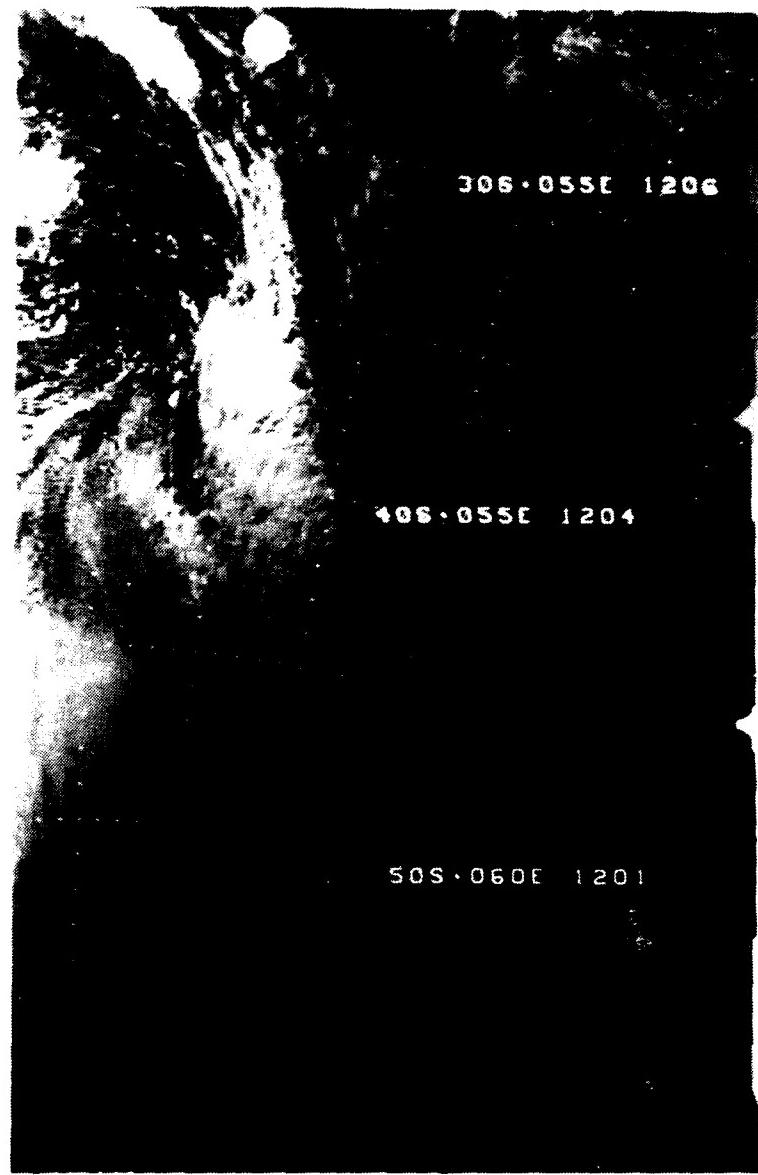


Fig. 6.46. NOAA 7 visible imagery, 1201-1206 GMT on 9 July 1983

Both the NMC and FNOC 500 mb analyses (Figs. 6.47 and 6.48) depict a trough oriented north-south near  $42^{\circ}\text{E}$  associated with the front south of the Malagasy Republic, as well as a strong gradient in the vicinity of  $45^{\circ}\text{S}$ ,  $10^{\circ}\text{E}$  ( $\geq 90$  kt on Fig. 6.47) associated with the front approaching Cape Town.

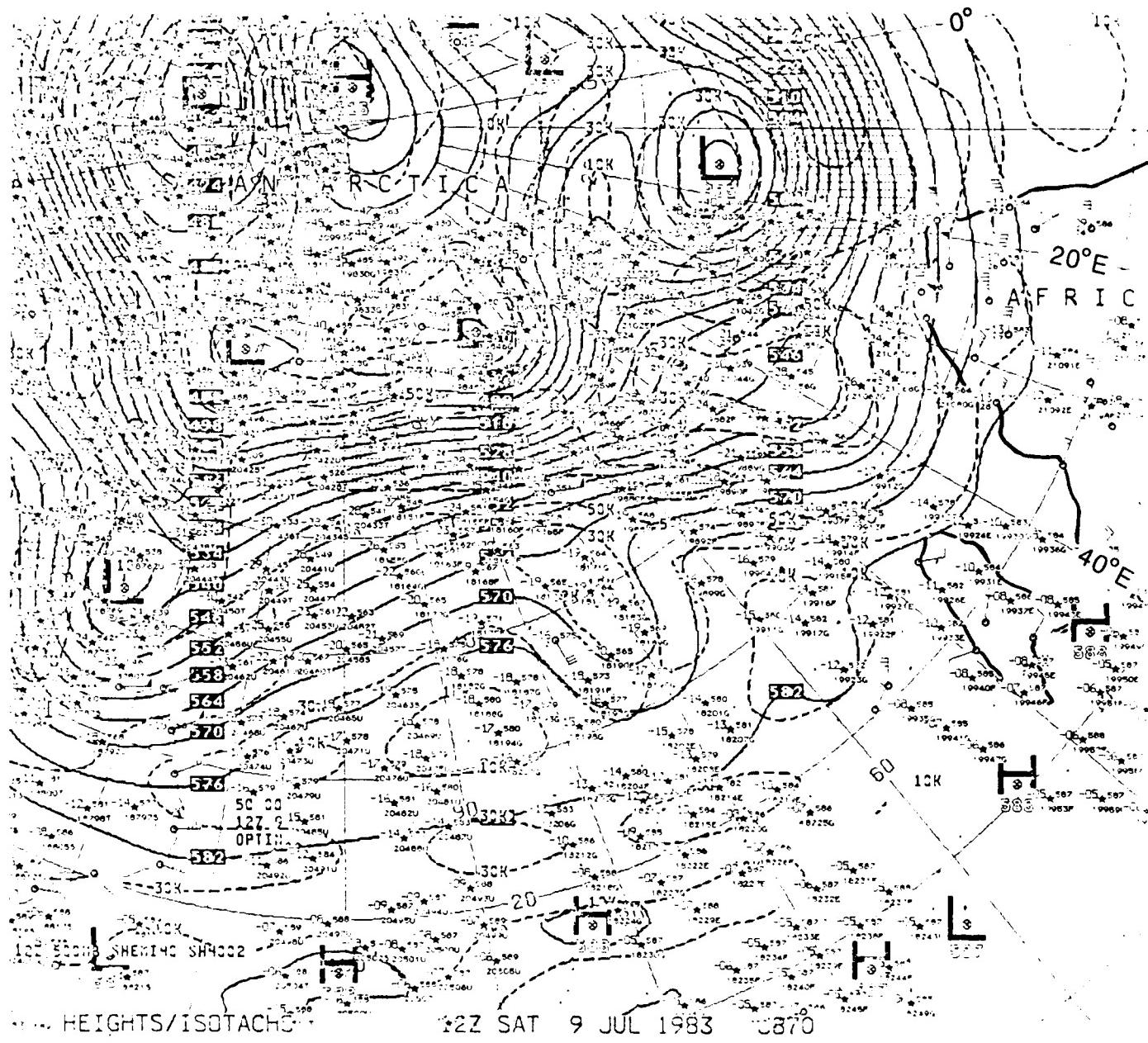


Fig. 6.47. NMC 500 mb analysis (contours and isotachs), 1200 GMT on 9 July 1983 (Note that Africa is outlined on right side of figure)

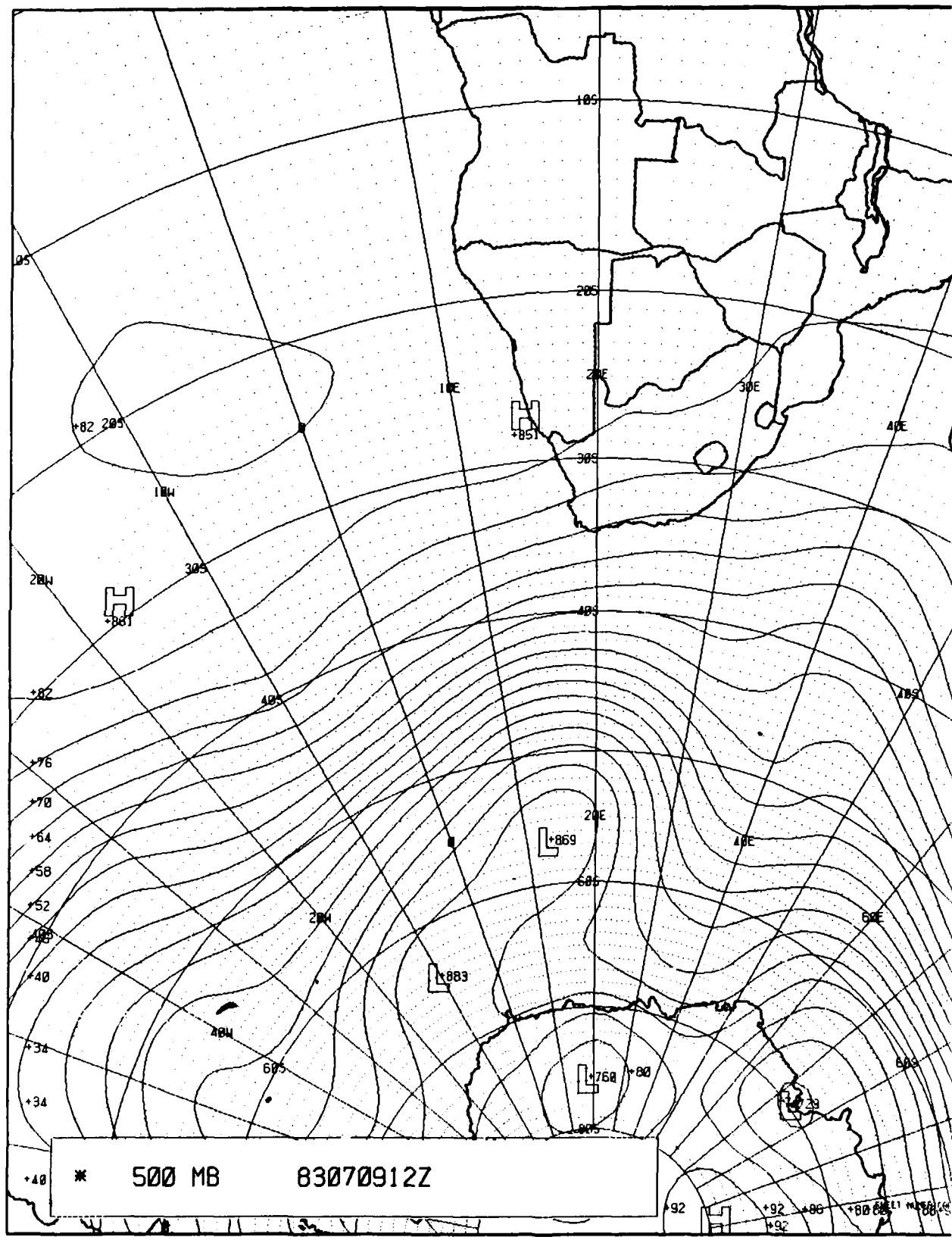


Fig. 6.48. FNOC 500 mb analysis (contours only), 1200 GMT on 9 July 1983

### 6.4.3 Case Study V (19 - 23 July 1983)

19 July 1983

This case study commences 10 days later on 19 July 1983 when one cold front extends from a coastal low (1007 mb) near Cape Town northward to southern Namibia while another frontal system associated with a low center (997 mb) at 39°S, 6°W (near Gough Island) is moving rapidly eastward (Figs. 6.49 and 6.50).

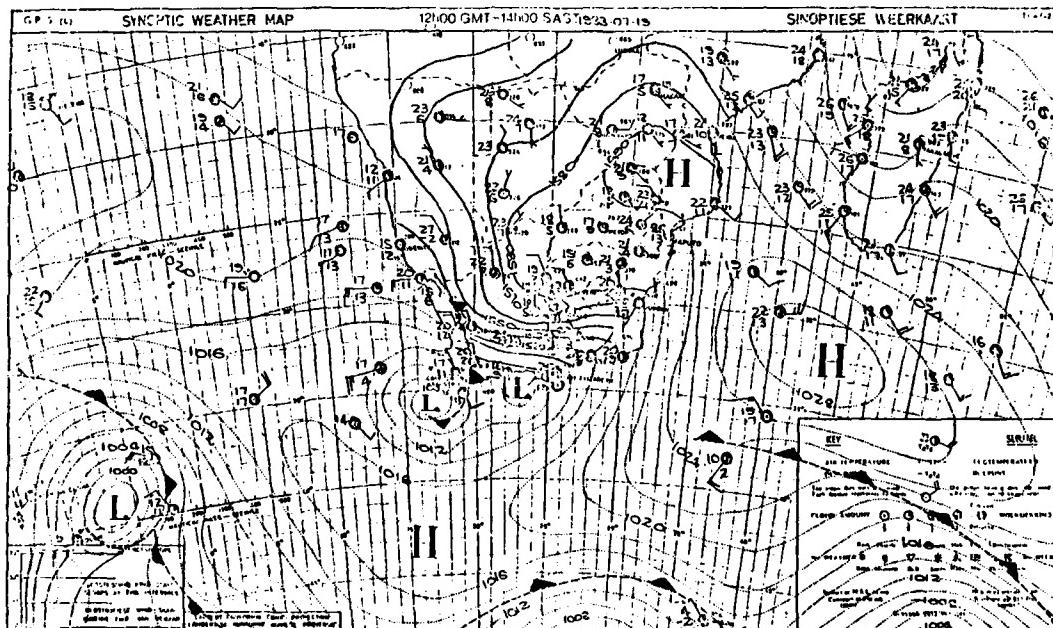
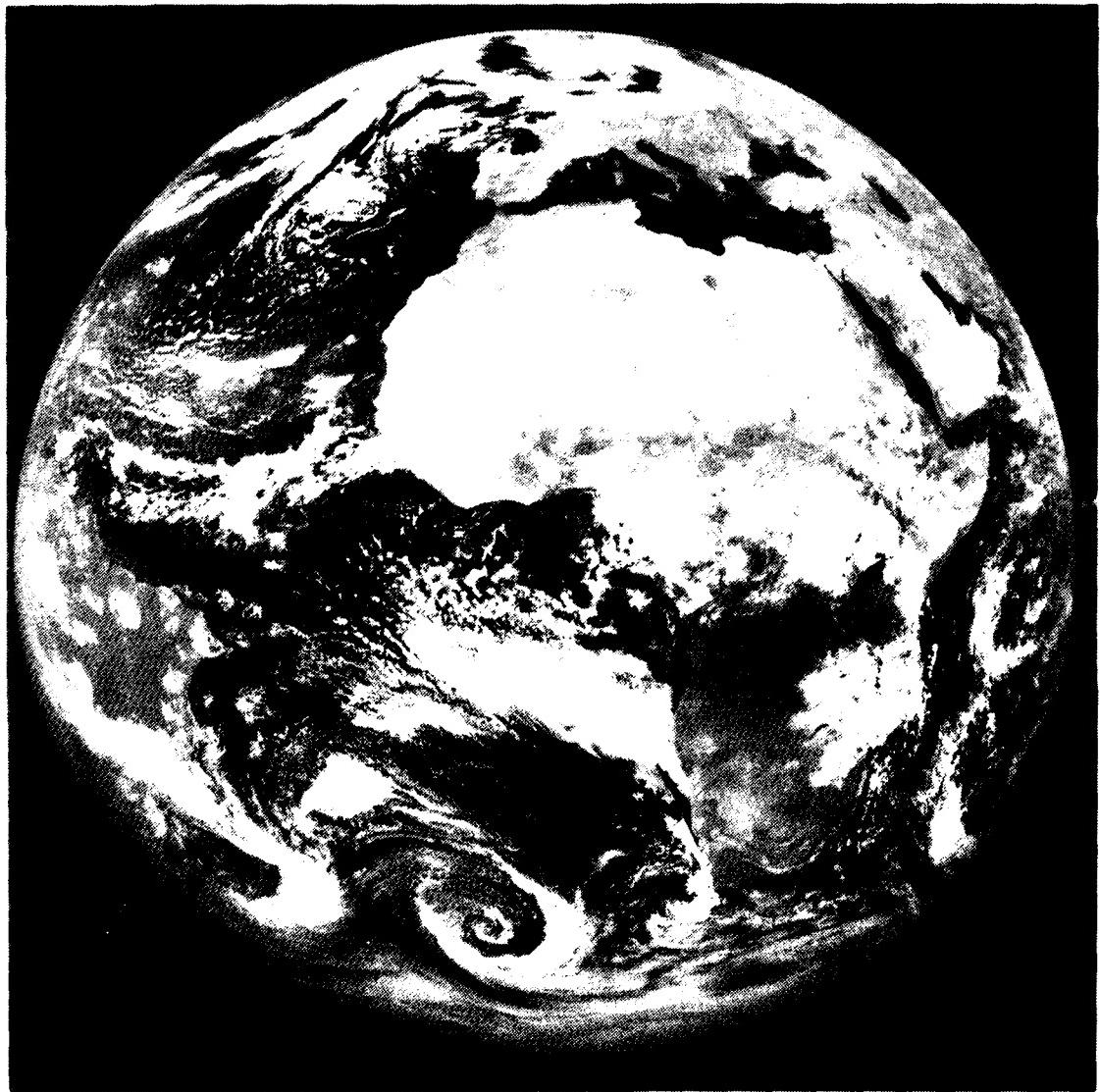


Fig. 6.49. Republic of South Africa Weather Bureau Surface (over Ocean) and 850 mb (over Continent) Analysis: 1200 GMT 19 July 1983



METEOSAT

Fig. 6.50. Visible METEOSAT imagery, 1155 GMT on 19 July 1983

20 July 1983

The cold front approaching from the South Atlantic has advanced along latitude 35°S at a speed of ~27.5 kt during the past 24 hours, while its associated low pressure center has deepened from 997 mb to 983 mb and moved southeastward at ~26 kt<sup>14</sup> to 43°S, 7°E (according to the RSA analysis (Fig. 6.51)). This analysis is well supported by the METEOSAT imagery (Fig. 6.52). The FNOC surface analysis (Fig. 6.53) frontal trough is a bit broader, but agrees in general configuration with the RSA analysis, although the central pressure of the low center is ~10 mb higher (993.5 mb) on the FNOC analysis. There is close agreement in the position of the small closed low near 38°S, 32°E on both analyses (Figs. 6.51 and 6.53); this low may be a redevelopment of the low center off Cape Town on the 19th. Fig. 6.54 displays the NOAA 7 imagery showing that formation of frontal cloudiness is commencing by 1311 GMT.

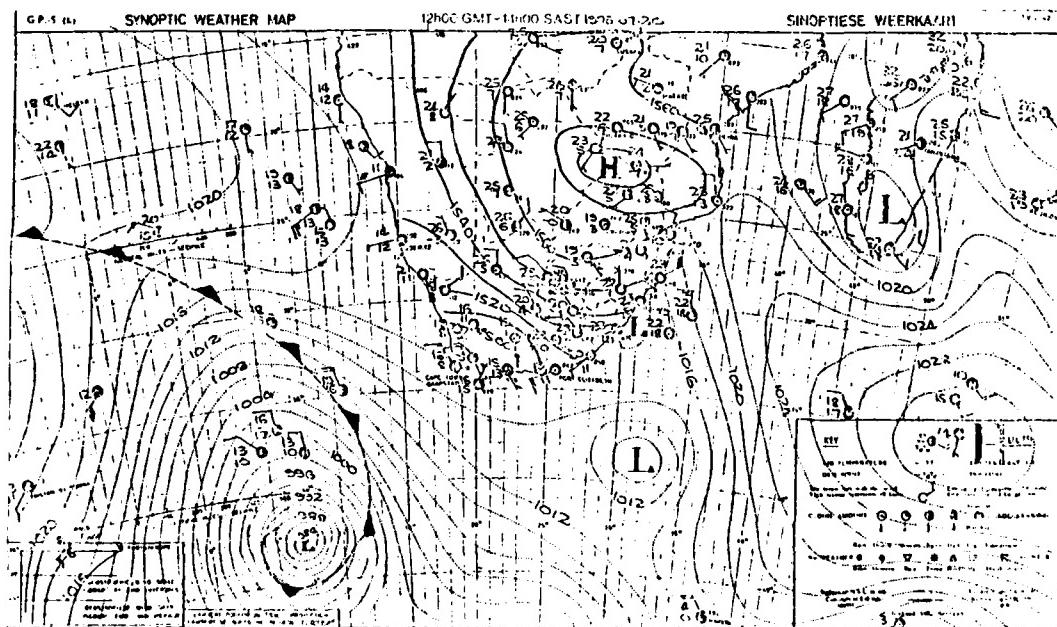
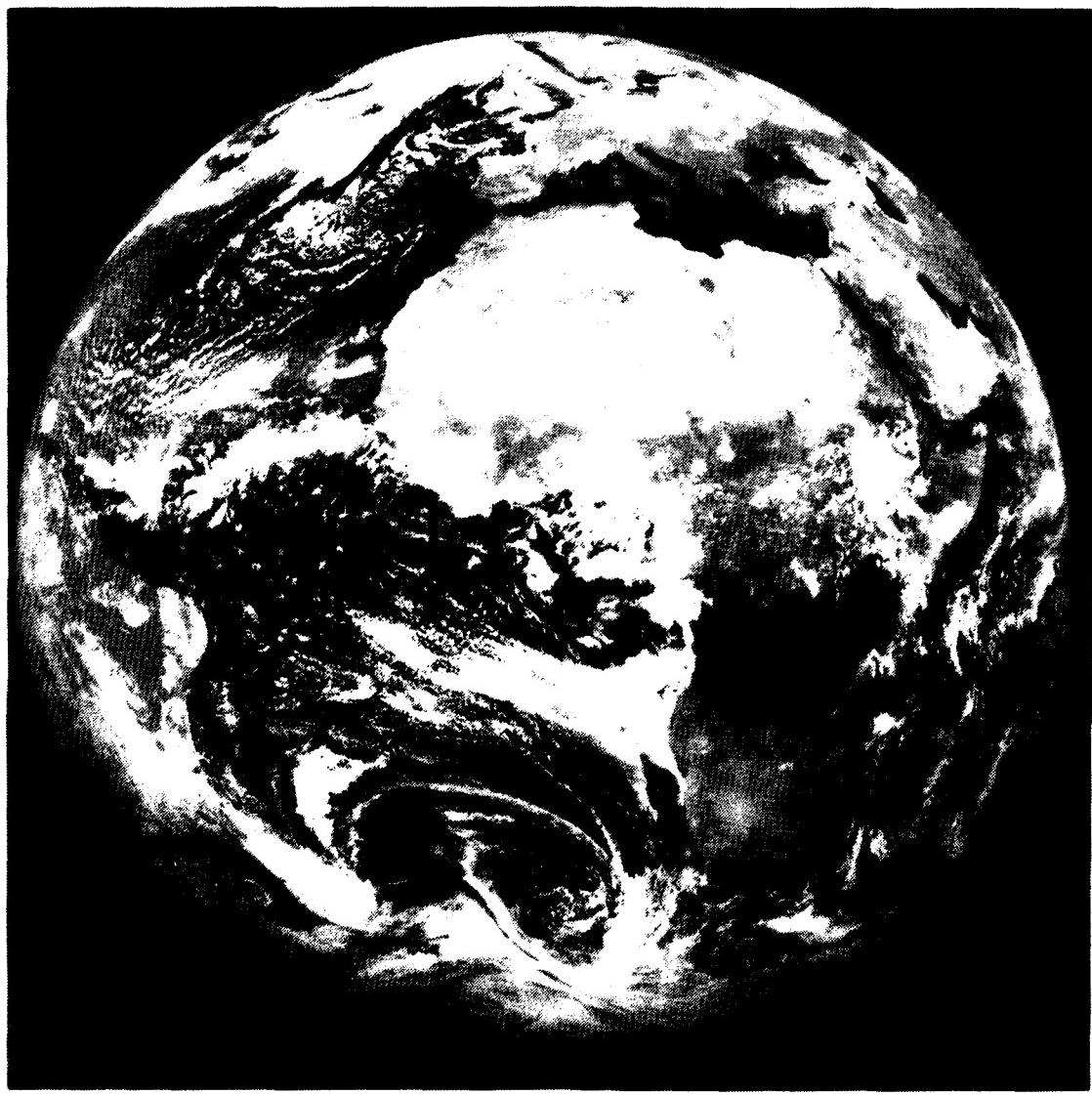


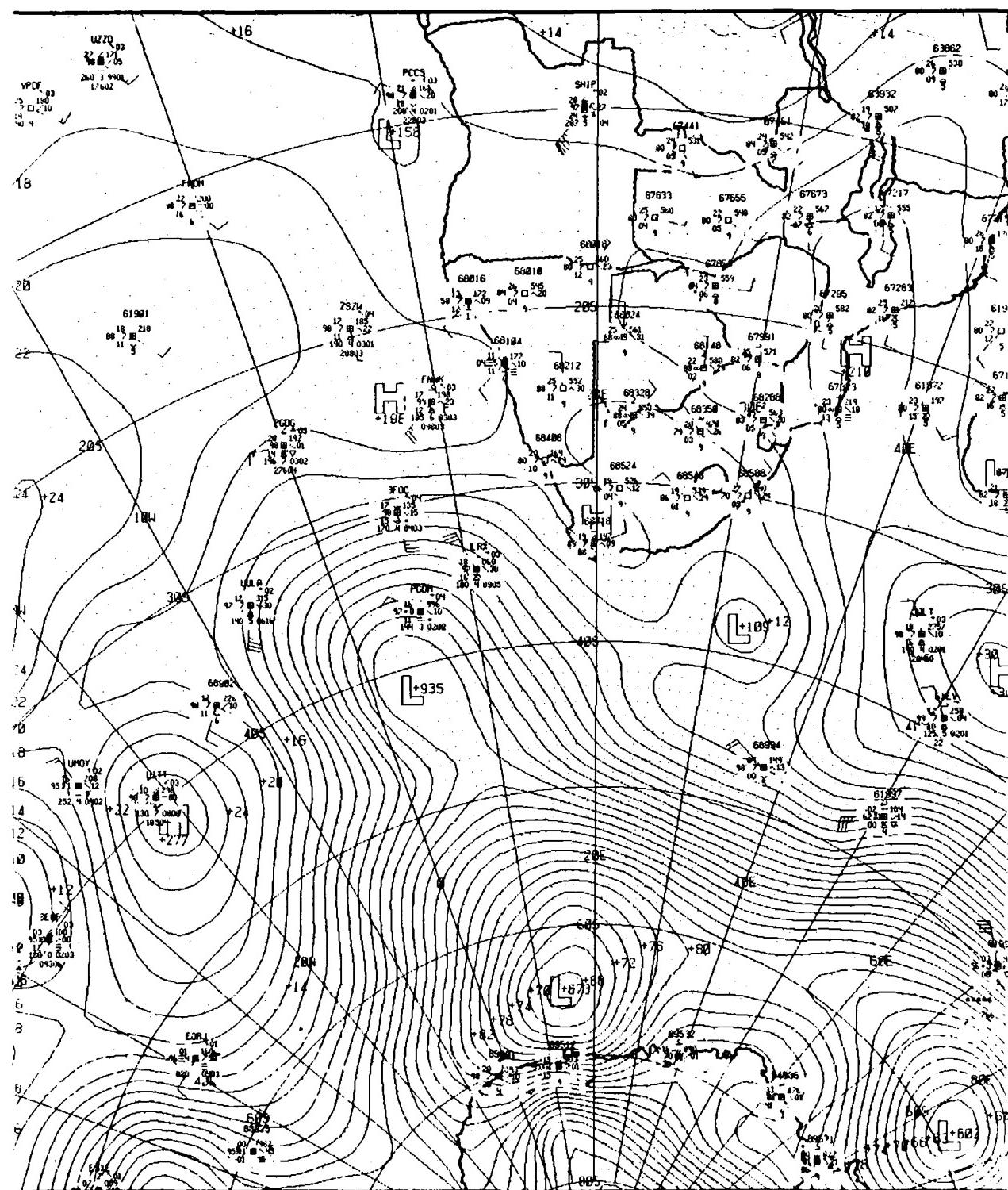
Fig. 6.51. Republic of South Africa Weather Bureau Surface (over Ocean) and 850 mb (over Continent) Analysis: 1200 GMT 20 July 1983

<sup>14</sup> This speed agrees well with the statistical results of van Loon (1967) describing the speed of movement of lows in the latitude band 40°S - 50°S (see Fig. 1.25 in Section 1).



METEOSAT

Fig. 6.52. Visible METEOSAT imagery, 1155 GMT on 20 July 1983



\* SURFACE 83072012Z

FLEET NUMERICAL OCEAN

Fig. 6.53. FNOC sea-level pressure analysis, 1200 GMT on 20 July 1983

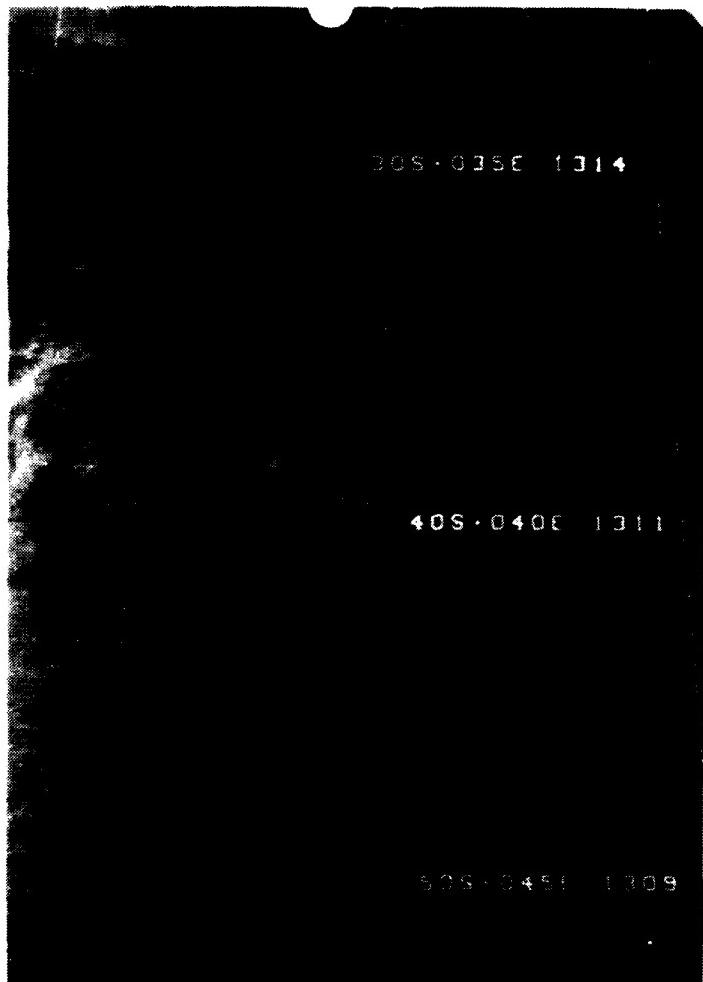


Fig. 6.54. NOAA 7 visible imagery, 1309-1314 GMT on 20 July 1983

The NOAA 7 imagery (Fig. 6.55) on the following orbit (1450 - 1458 GMT) depicts the *meridional* orientation of the front as it approaches Cape Town ~3 hours after the analysis of Fig. 6.51. Fig. 6.55 clearly depicts the active convection along the front as its leading edge is crossing  $35^{\circ}$ S at  $\sim 12.5^{\circ}$ E, having moved at a speed of  $\sim 30$  kt during the past three hours. Especially note the enhanced convective vortex trailing the front, centered near  $36^{\circ}$ S,  $4^{\circ}$ E, which manifests itself on the following day (see Fig. 6.56) as a new low at  $36^{\circ}$ S,  $16^{\circ}$ E.

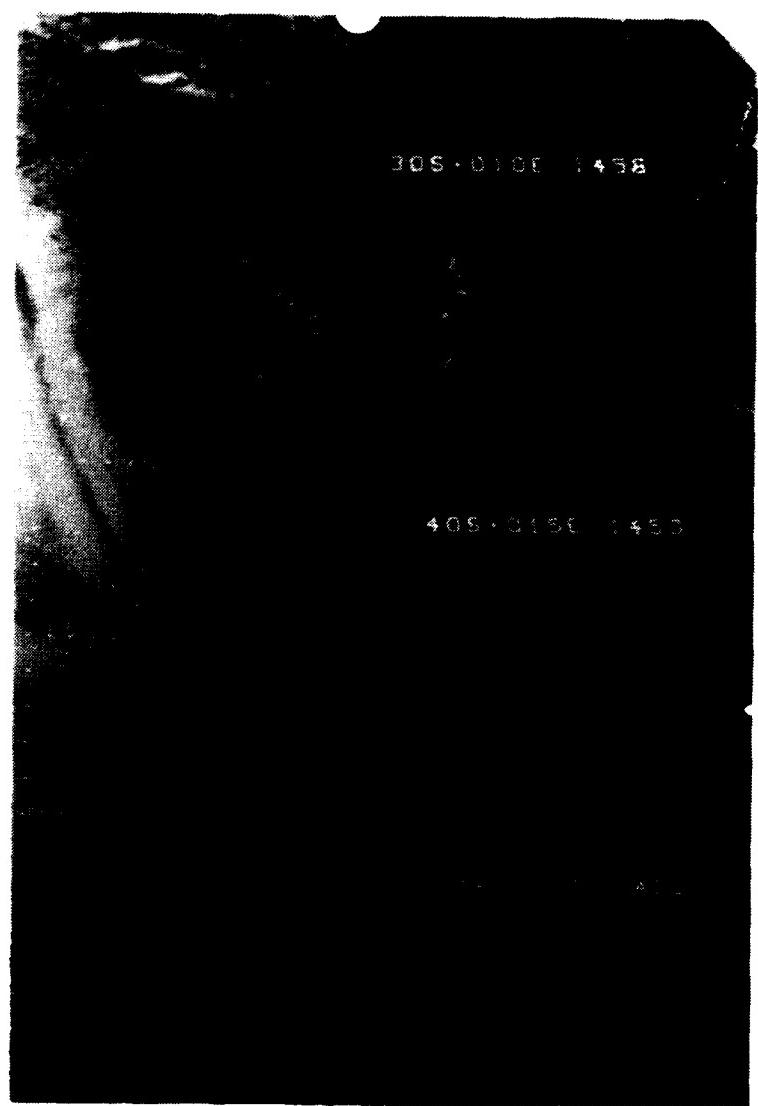


Fig. 6.55. NOAA 7 visible imagery, 1450-1458 GMT on 20 July 1983

21 July 1983

The parent low, with its front now east of Cape Town, has moved rapidly east-southeastward (~29 kt) and deepened to 977 mb at 46°S, 23°E (Fig. 6.56). The formation of a low off Cape Town on the 20th is confirmed as it now has moved to 36°S, 16°E with an associated front extending toward the northwest. The small low southeast of Port Elizabeth on the 20th has moved to 41°S, 41°E and deepened to 1005 mb, and now has an associated cold front, which was seen forming in Fig. 6.54 on the 20th. The METEOSAT imagery (Figs. 6.57 and 6.58) support the existence of the three fronts depicted by the RSA analysis described above. Although the FNOC surface analysis (Fig. 6.59) depicts a large amplitude (frontal) trough extending equatorward just west of RSA, *none* of the three low centers displayed on the RSA regional analysis is depicted. In fact, the FNOC frontal trough emanates from a low near the Antarctic continent at 66°S, 27°E!

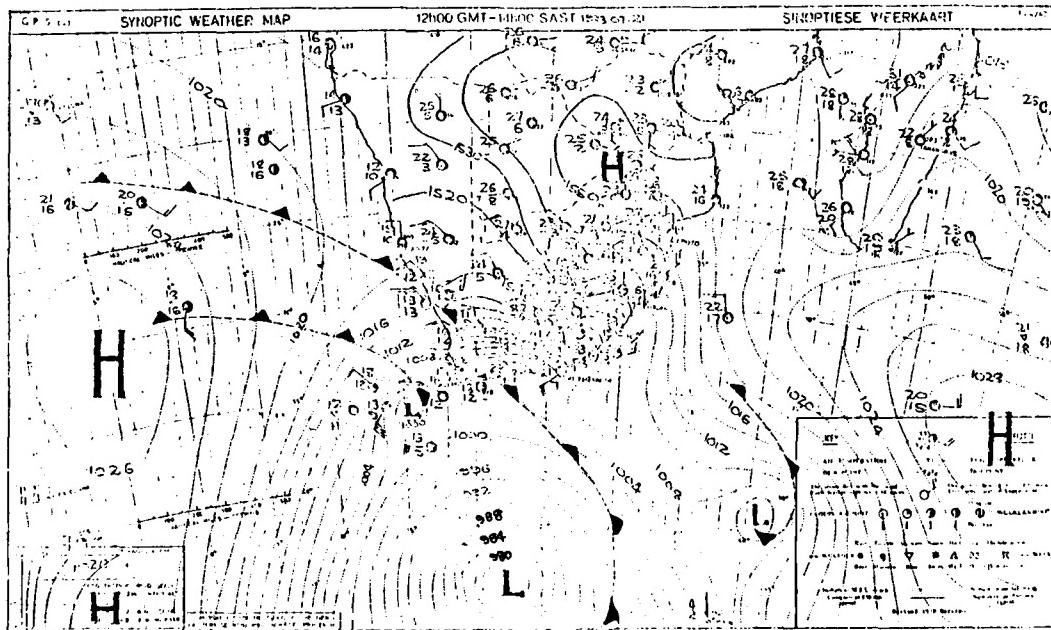
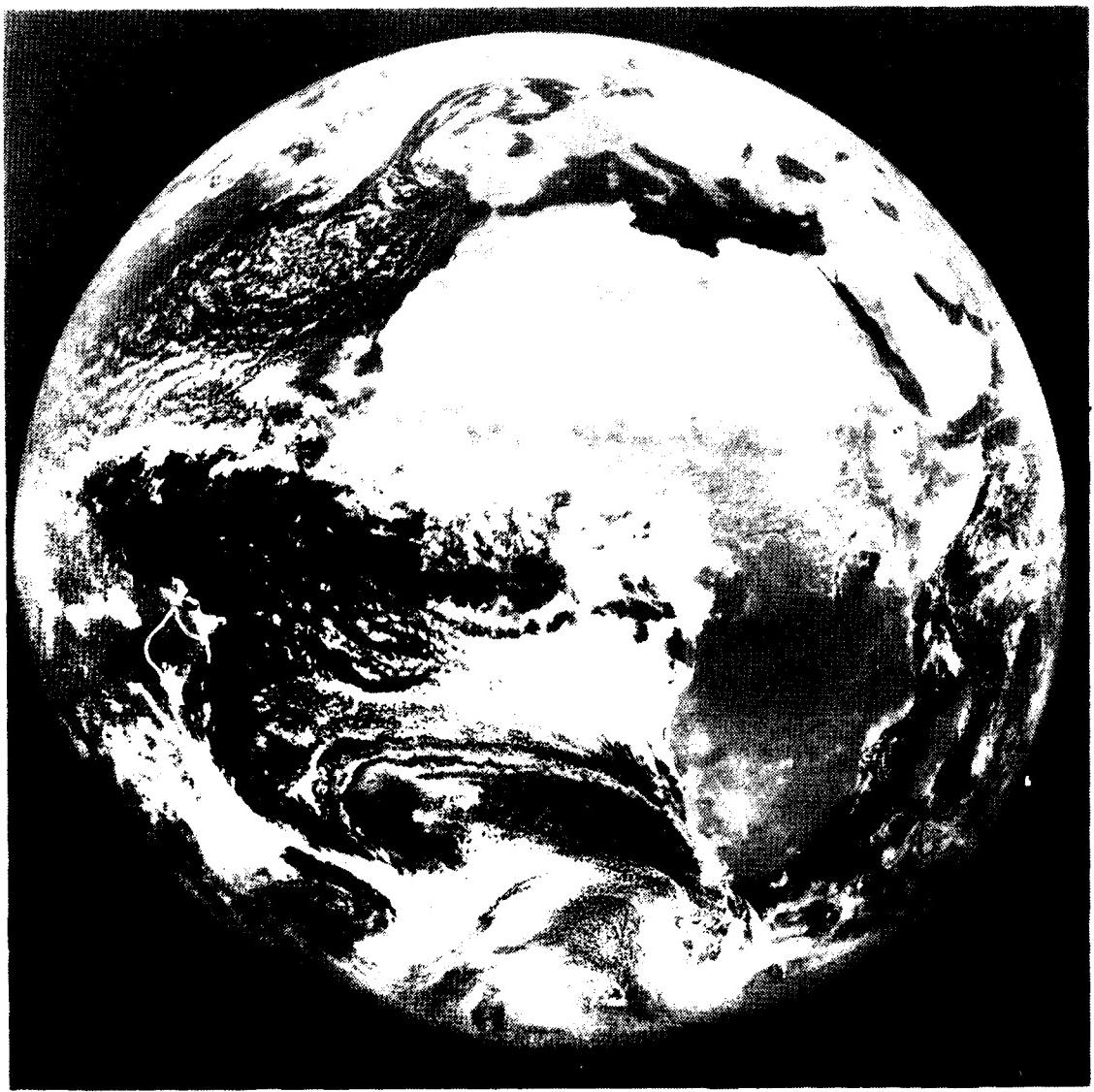


Fig. 6.56. Republic of South Africa Weather Bureau Surface (over Ocean) and 850 mb (over Continent) Analysis: 1200 GMT 21 July 1983



METEOSAT

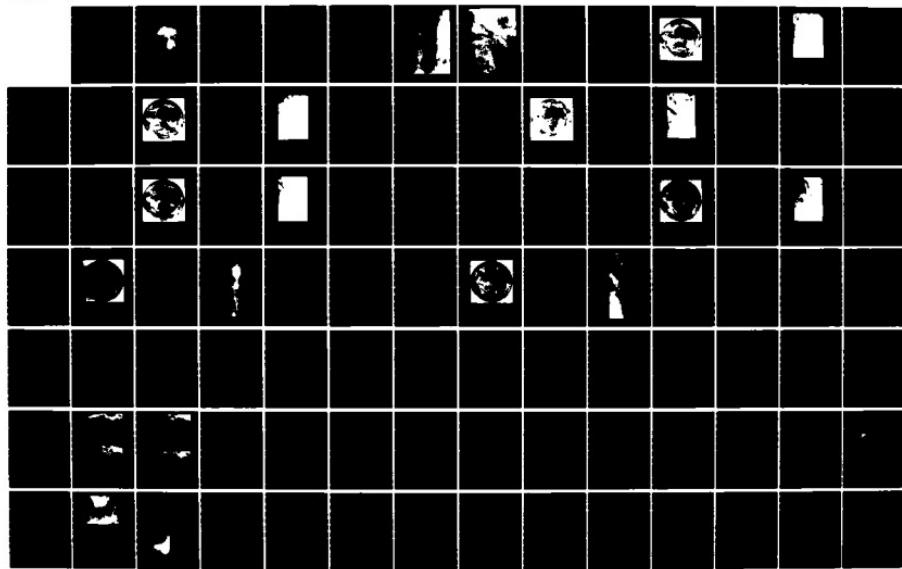
Fig. 6.57. Visible METEOSAT imagery, 1155 GMT on 21 July 1983

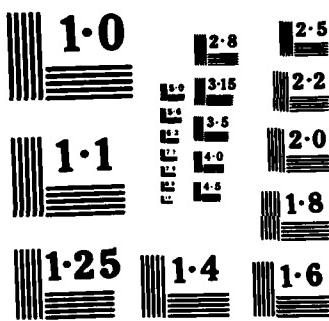
RD-R163 196 FORECASTERS HANDBOOK FOR THE SOUTHERN AFRICAN CONTINENT 3/4  
AND ATLANTIC/INDI. (U) NAVAL ENVIRONMENTAL PREDICTION  
RESEARCH FACILITY MONTEREY CA. F R WILLIAMS ET AL.  
NOV 84 NEPRF-TR-84-08

UNCLASSIFIED

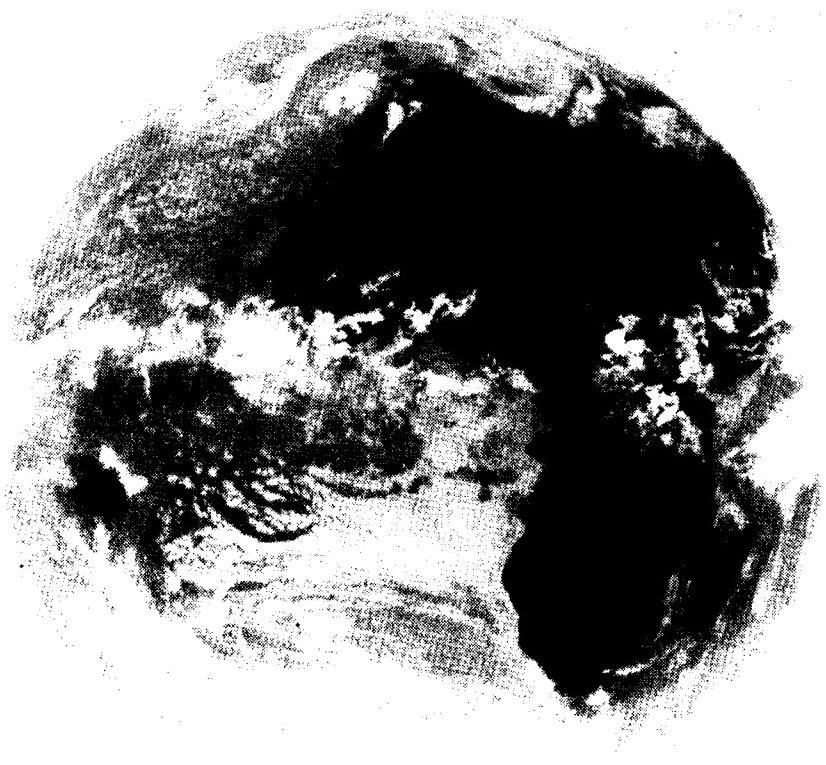
F/G 4/2

NL





NATIONAL BUREAU OF STANDARDS  
MICROCOPY RESOLUTION TEST CHART



**METEOSAT**

1983 MONTH 7 DAY 21 TIME 1155 GMT (NORTH) CH. IR 1  
NOMINAL SCAN/RAW DATA SLOT 24 COPYRIGHT - ESA -

Fig. 6.58. Infrared METEOSAT imagery, 1155 GMT on 21 July 1983

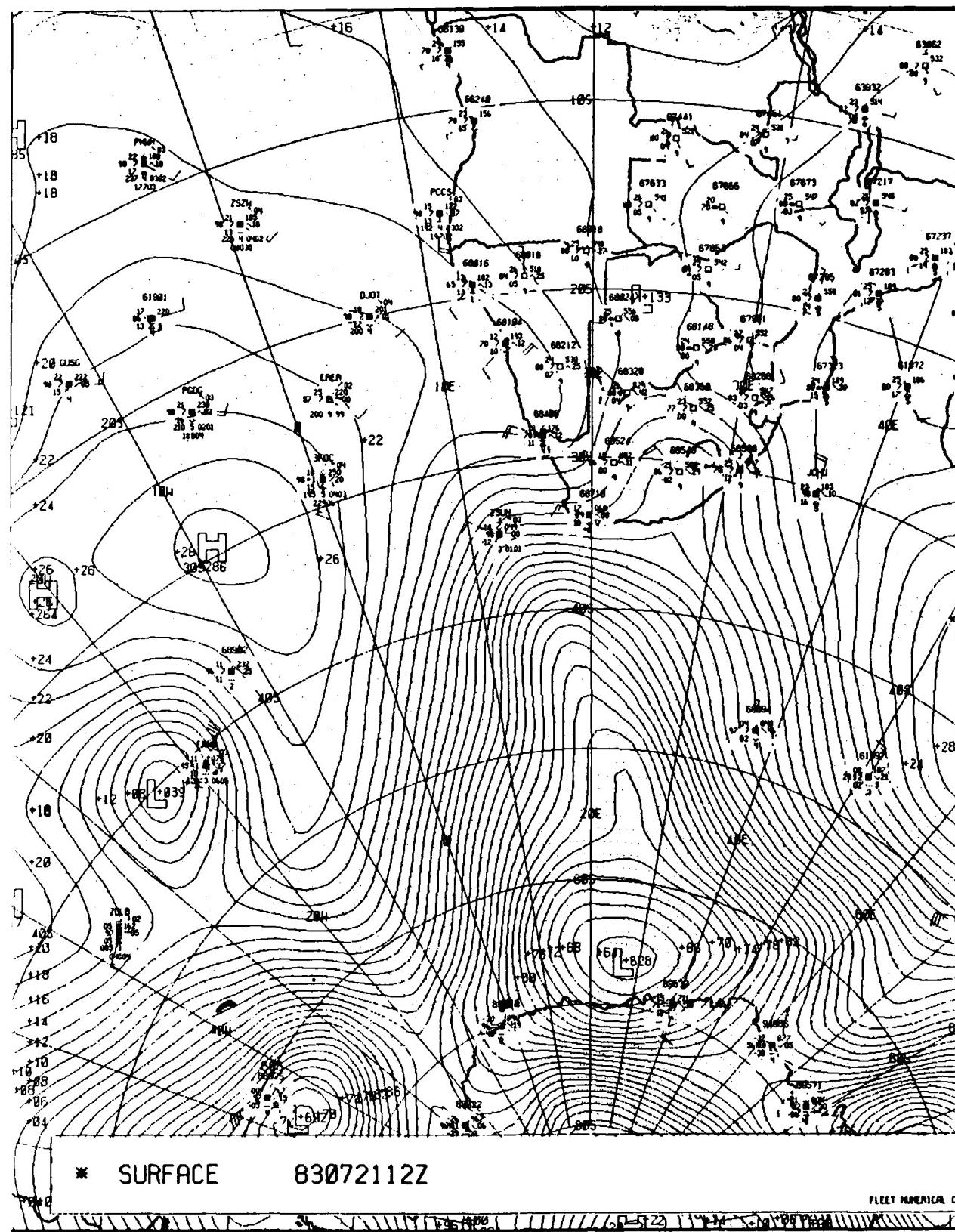


Fig. 6.59. FNOC sea-level pressure analysis, 1200 GMT on 21 July 1983

The upper-air analyses of NMC and FNOC (Figs. 6.60 and 6.61) both depict a large amplitude 500 mb trough just west of RSA near 12-13°E in some vestige of support of the complex double frontal system near the southwest coast of RSA. However, it appears that the weak 500 mb short wave troughs displayed by both analyses (near 43°E) have insufficient westward tilt from the newly formed low near 41°S, 41°E on Fig. 6.56. Of course this is a moot argument concerning the FNOC surface analysis (Fig. 6.59) which has no low center at 41°S, 41°E!

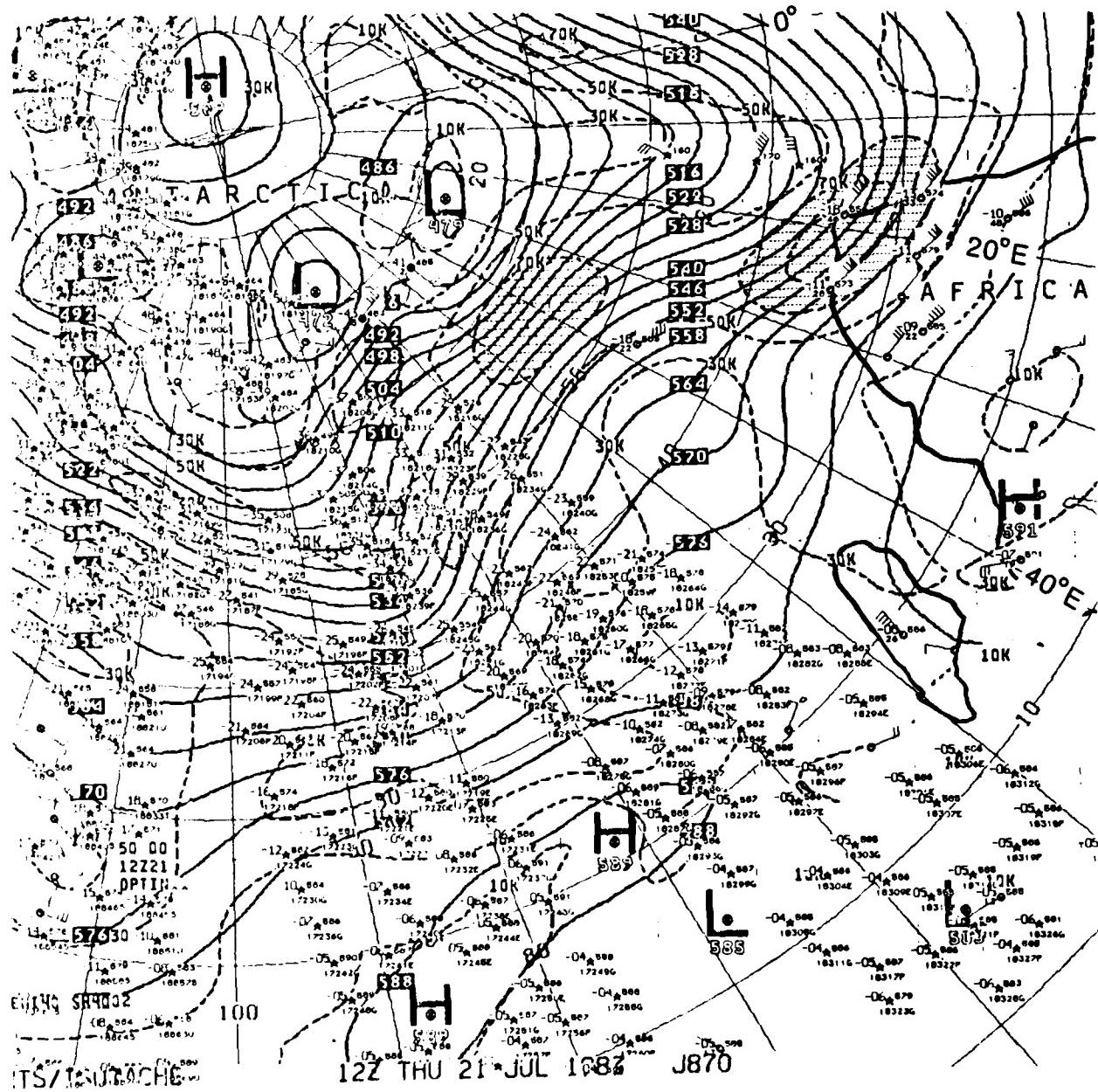


Fig. 6.60. NMC 500 mb analysis (contours and isotachs), 1200 GMT on 21 July 1983 (Note that Africa is outlined on right side of figure)

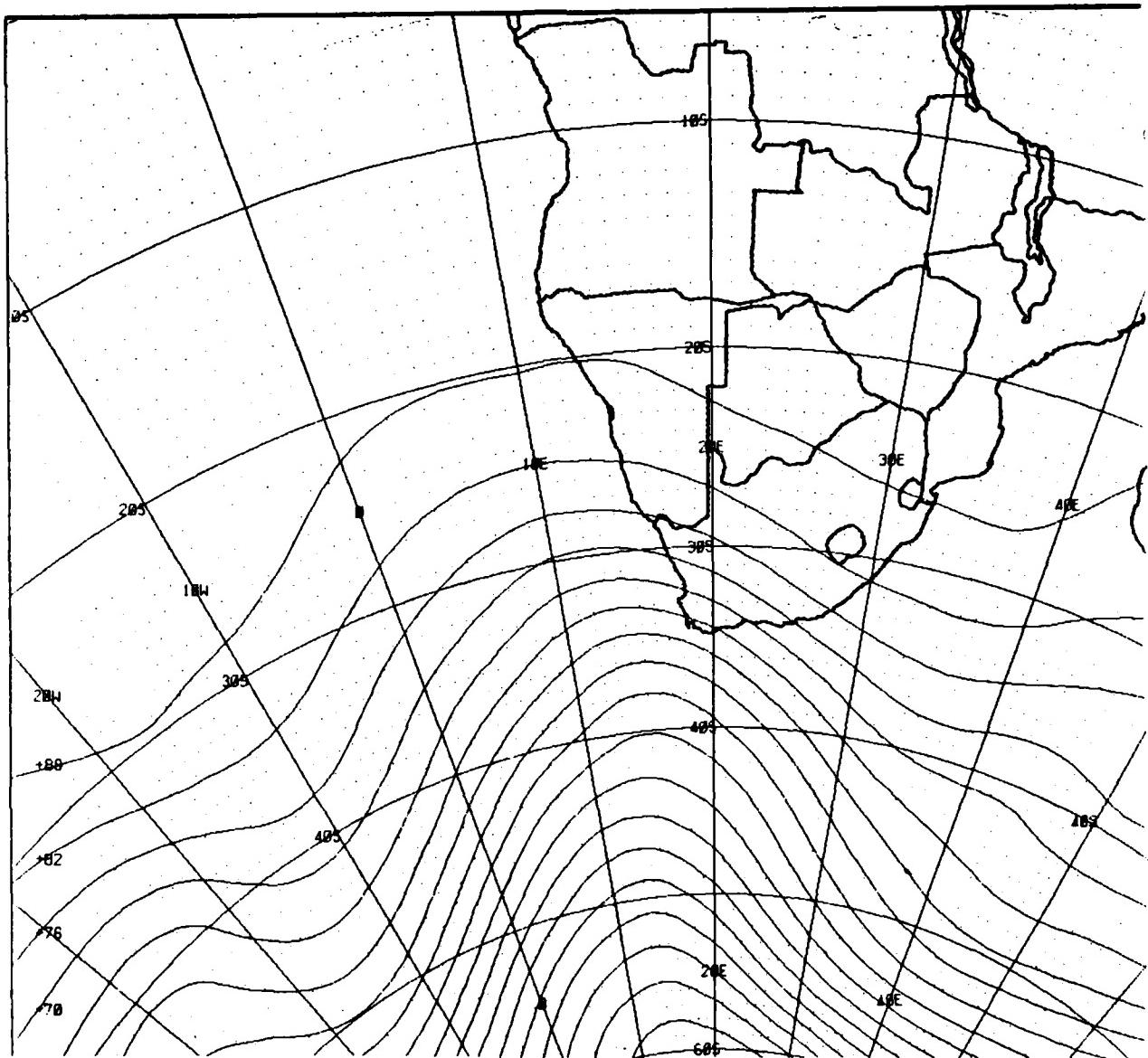


Fig. 6.61. FNOC 500 mb analysis (contours only), 1200 GMT on 21 July 1983

Figs. 6.62 and 6.63 are examples of visible and infrared (IR) high resolution imagery available aboard most U. S. aircraft carriers from the Defense Meteorological Satellite Program (DMSP). These images depict conditions four and one-half hours after the analysis time for Fig. 6.56, as the trailing cold front is approaching Cape Town. The more vigorous convective activity is readily identified by the whiter (brighter) images in both the frontal cloudiness and the open cell cloudiness within the cold air mass displayed in the IR image (Fig. 6.63).

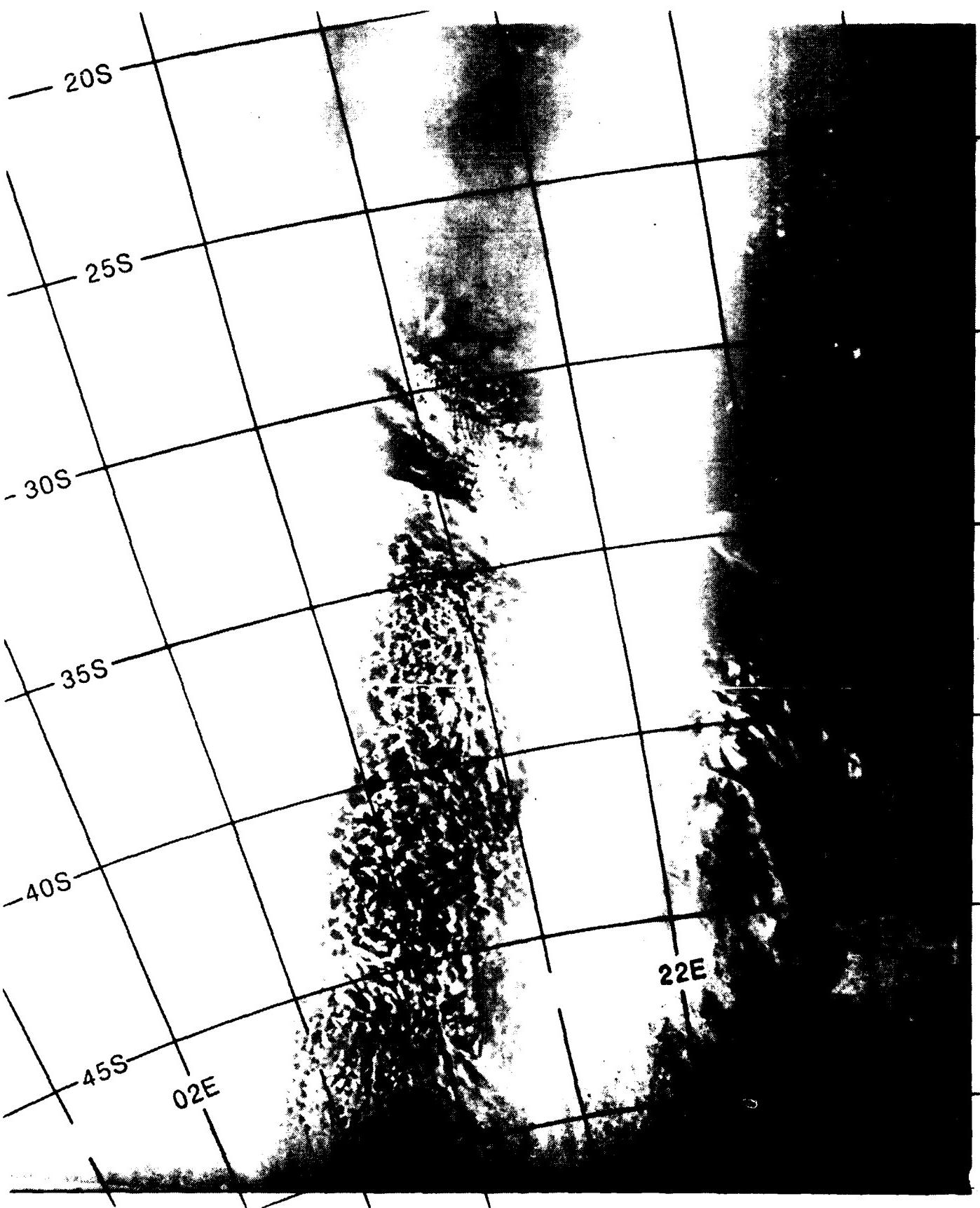


Fig. 6.62. DMSP visible imagery, 1635 GMT 21 July 1983

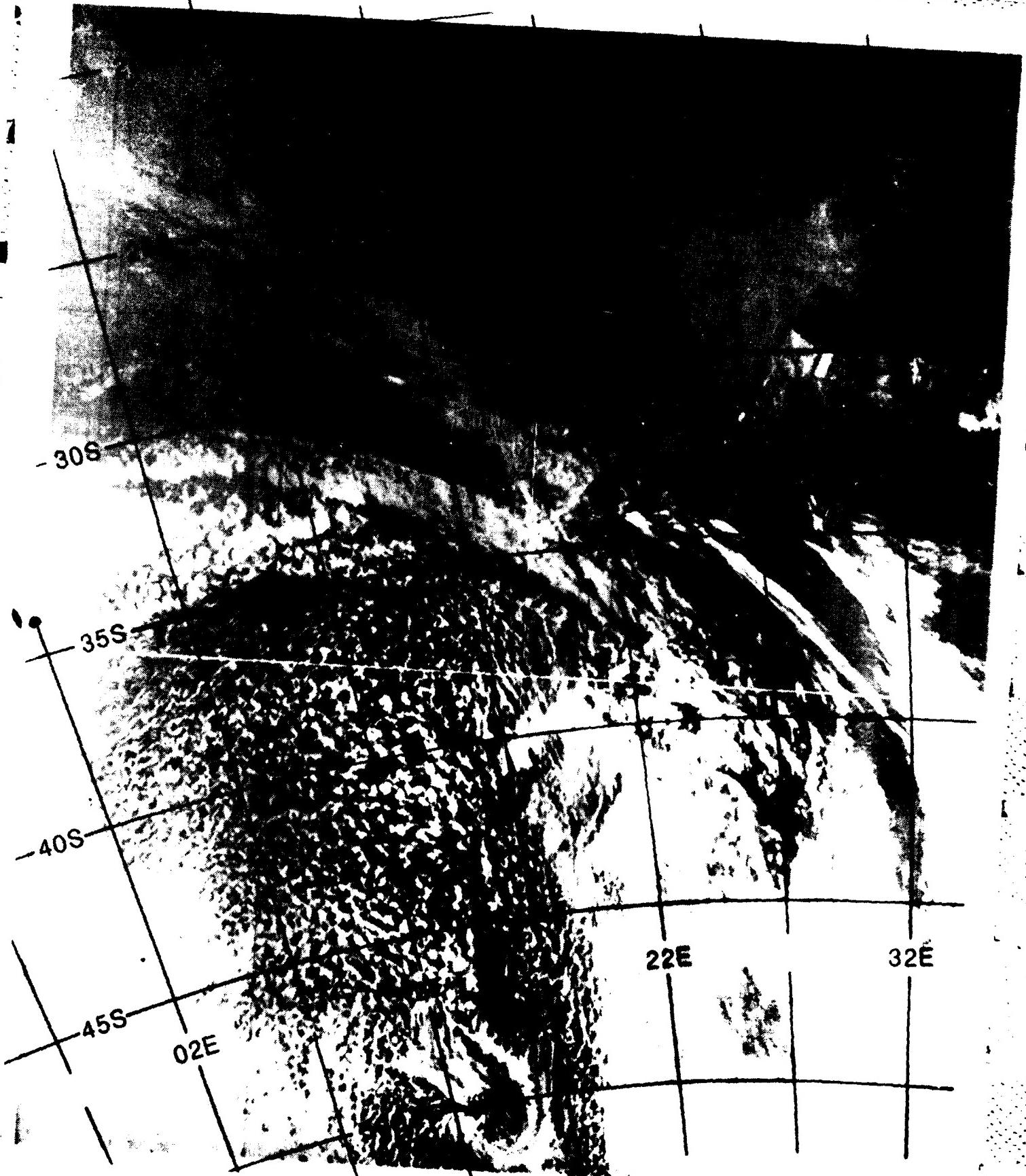


Fig. 6.63. DMSP infrared imagery, 1635 GMT 21 July 1983

22 July 1983

The parent low near  $46^{\circ}\text{S}$ ,  $23^{\circ}\text{E}$  on the 21st has moved off the RSA analysis area (Fig. 6.64), i.e., the low is now poleward (south) of the 50-kt northwest wind reported from Marion Island (station 68994 at  $47^{\circ}\text{S}$ ,  $38^{\circ}\text{E}$ , see Fig. 6.66). However, the associated cold front from this low is displayed extending far northwestward, reaching the RSA coast between Port Elizabeth and Durban (Fig. 6.64). The weak vortex (1011 mb) near  $42^{\circ}\text{S}$ ,  $23^{\circ}\text{E}$  may be a remnant of the short wave disturbance which was nearing Cape Town on the 21st (see Fig. 6.56). While the low at  $41^{\circ}\text{S}$ ,  $41^{\circ}\text{E}$  on the 21st appears to have moved rapidly southeastward (and is now off the RSA analysis area), there is a new low (1011 mb) approaching from the South Atlantic at  $44^{\circ}\text{S}$ ,  $11^{\circ}\text{W}$ . The METEOSAT imagery (Fig. 6.65) depicts all three of the lows described above on the RSA analysis. The FNOC surface analysis (Fig. 6.66) does have a trough crossing  $45^{\circ}\text{S}$  at  $10^{\circ}\text{W}$  supporting the existence of the low approaching from the South Atlantic; however, there is no *closed* center on the FNOC surface analysis. The FNOC frontal trough, crossing  $40^{\circ}\text{S}$  near  $36^{\circ}\text{E}$ , is in good agreement with the RSA surface trough in Fig. 6.64. Although, as expected, the global analysis does not include the weak vortex near  $42^{\circ}\text{S}$ ,  $23^{\circ}\text{E}$ , there is a strong pressure gradient supporting the 50-kt wind at Marion Island ( $47^{\circ}\text{S}$ ,  $38^{\circ}\text{E}$ ) on the trough in the cold air. Fig. 6.67 (visible imagery from NOAA 7 taken between 1244 and 1250 GMT) strongly supports the frontal position depicted earlier at 1200 GMT by the RSA analysis (Fig. 6.64). Fig. 6.67 also has a circular cloud mass centered near  $52^{\circ}\text{S}$ ,  $35^{\circ}\text{E}$  which is more supportive of the *implied* closed low center just south of the RSA analysis area than of the FNOC analysis which has no low pressure center (i. e., only a trough) until far poleward adjacent to Antarctica.

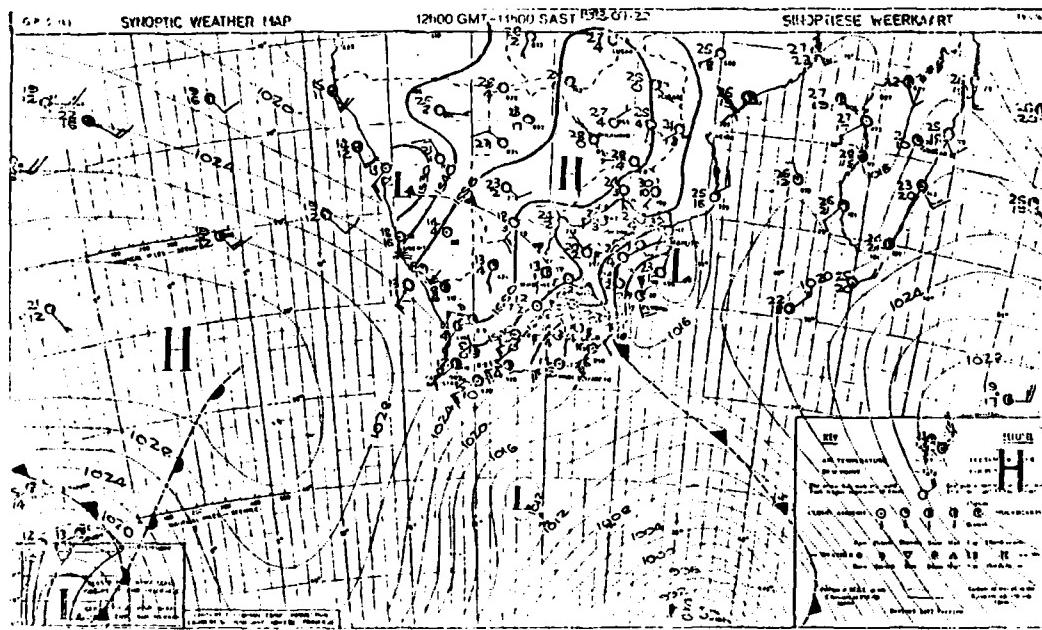
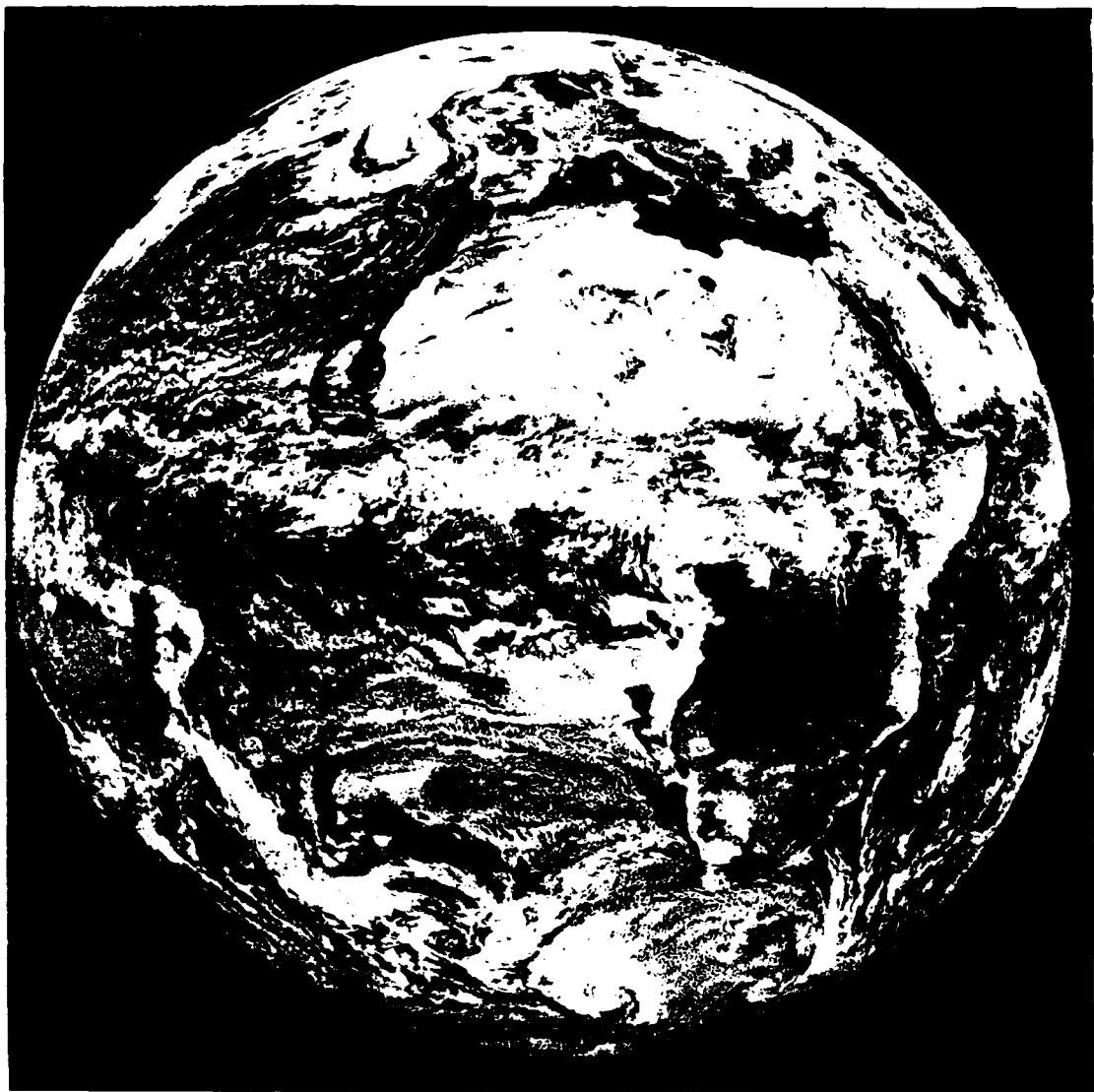


Fig. 6.64. Republic of South Africa Weather Bureau Surface (over Ocean) and 850 mb (over Continent) Analysis: 1200 GMT 22 July 1983



**METEOSAT**

1983 MONTH 7 DAY 22 TIME 1155 GMT NORTH CH. VIS 2  
NOMINAL SCAN PAN DATA SLOT 24 COPYRIGHT - ESR -

Fig. 6.65. Visible METEOSAT imagery, 1155 GMT on 22 July 1983

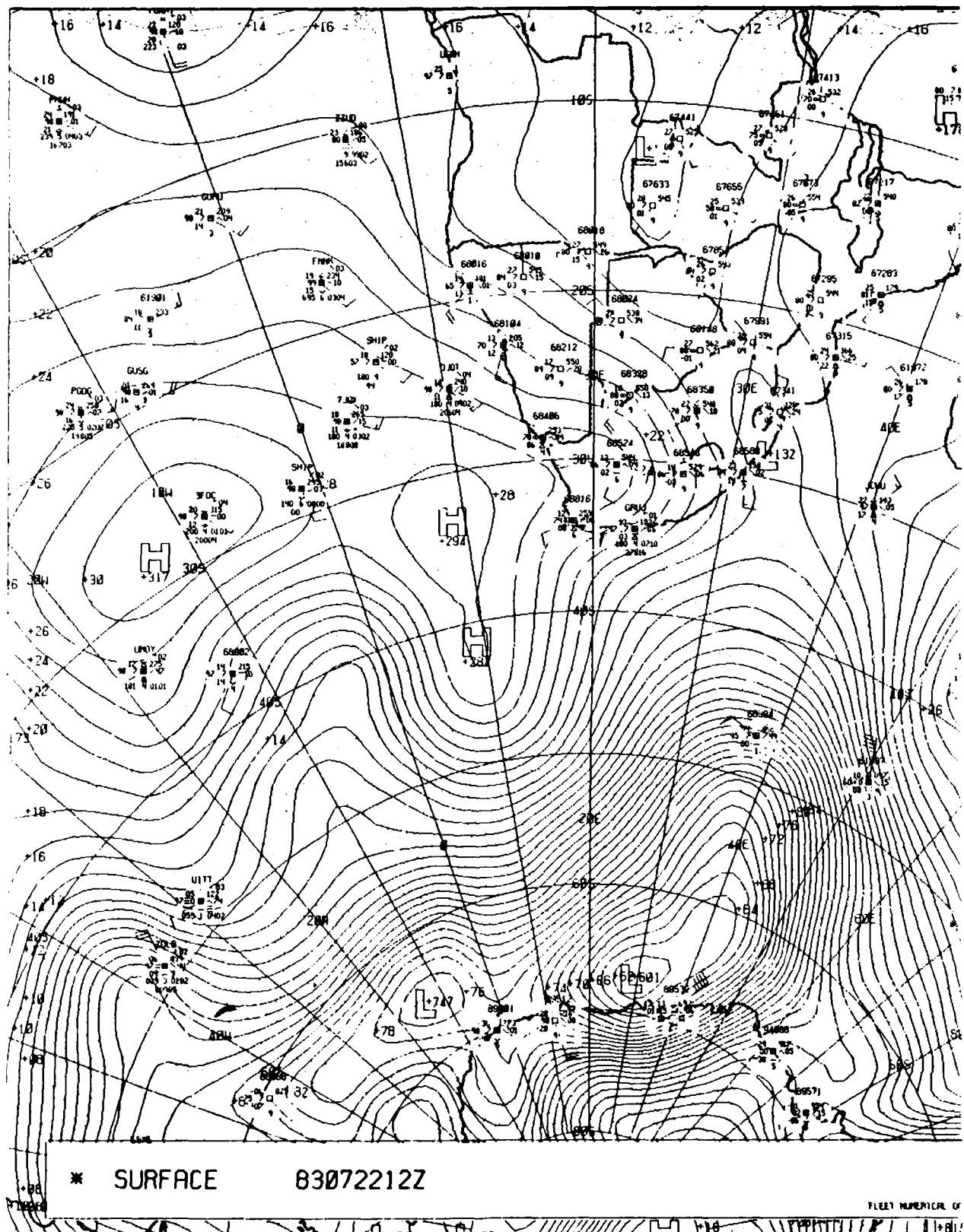


Fig. 6.66. FNOC sea-level pressure analysis, 1200 GMT on 22 July 1983

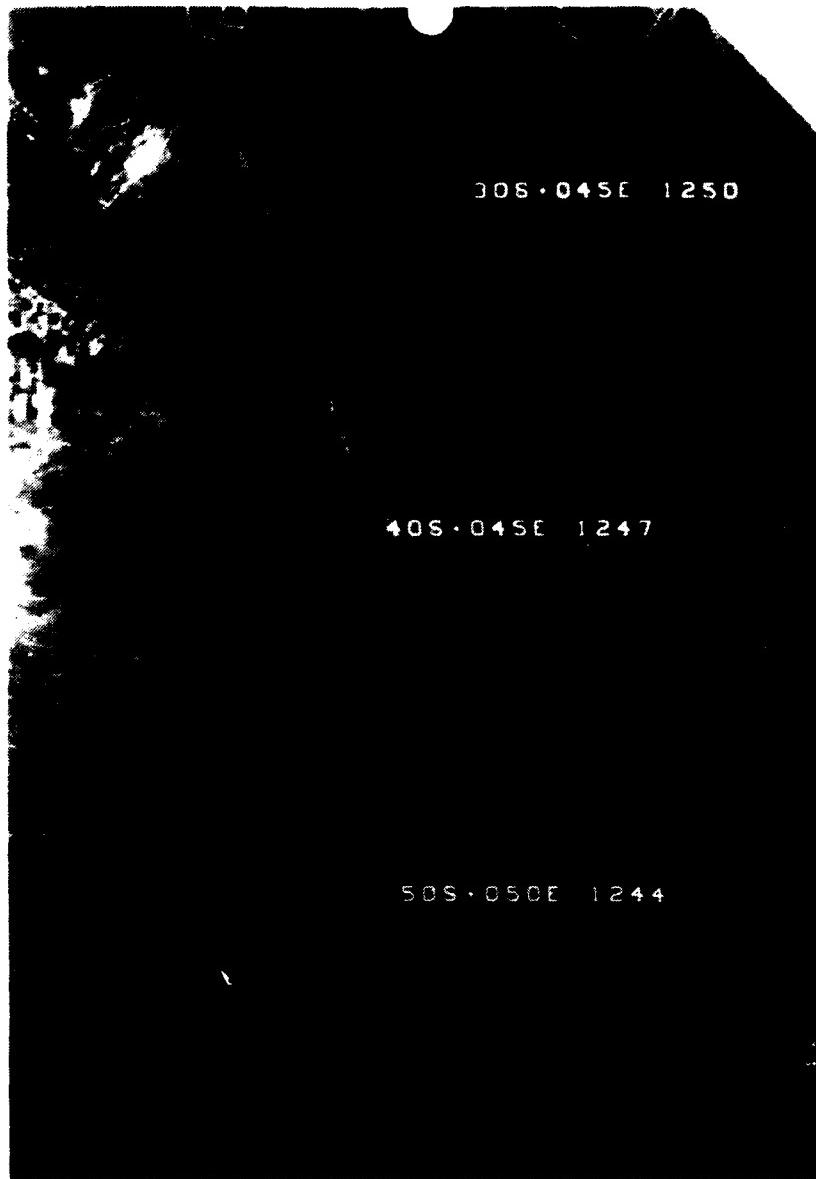


Fig. 6.67. NOAA 7 visible imagery, 1244-1250 GMT on 22 July 1983

Both Figs. 6.68 and 6.69 have a large amplitude trough crossing  $40^{\circ}\text{S}$  near  $25^{\circ}\text{E}$  which is vertically consistent with the surface trough to the east. The upper-air short wave trough depicted near  $10^{\circ}\text{W}$  on both analyses displays very little tilt toward the west from the surface low, but may be reasonable since the RSA surface analysis contains an occlusion and does have a cold front crossing  $40^{\circ}\text{S}$  near  $7^{\circ}\text{W}$ .

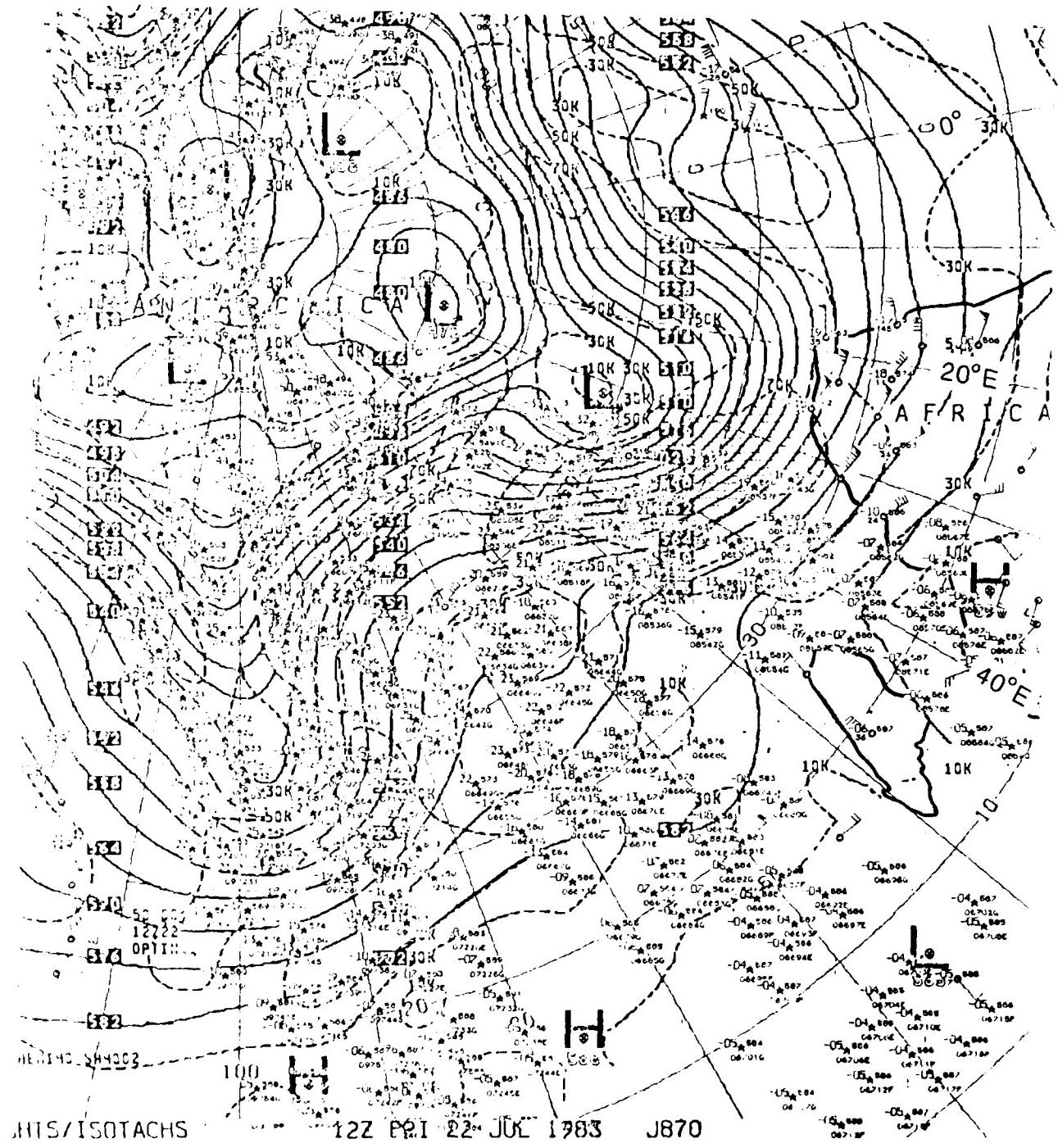


Fig. 6.68. NMC 500 mb analysis (contours and isotachs), 1200 GMT on 22 July 1983 (Note that Africa is outlined on right side of figure)

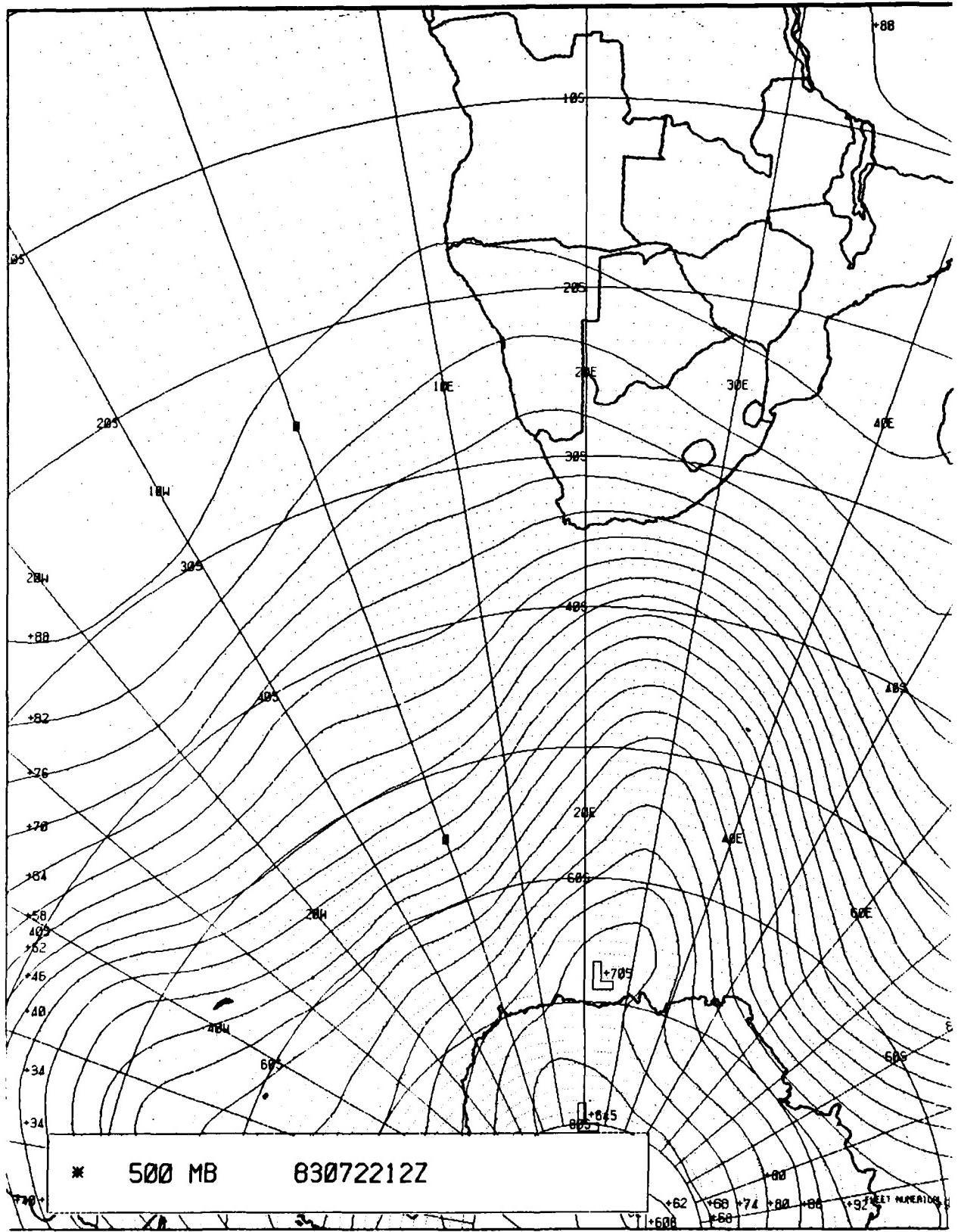


Fig. 6.69. FNOC 500 mb analysis (contours only), 1200 GMT on 22 July 1983

23 July 1983

On the final day of this case, the RSA analysis (Fig. 6.70) depicts a 1013 mb low center at 39°S, 43°E with a cold front extending into southern Mozambique and a second trailing cold front striking the RSA coast near Port Elizabeth. METEOSAT imagery (Fig. 6.71) supports the RSA analysis; also note the extensive open cell convection in the southwesterly flow within the cold air. Although the FNOA analysis (Fig. 6.72) shows a trough (frontal) near 38°S, 48°E, with a hint of a trough to Port Elizabeth, the low near 39°S, 43°E is *missing!* The NOAA 7 swath (Fig. 6.73) sharply defines the frontal cloudiness and open cells taken at 1231 - 1237 GMT. In particular, note the possible visible imagery support for the RSA low center near 39°S, 43°E, i.e., the NOAA 7 imagery at 1234 GMT depicts a nearly circular area of clearing (west of the frontal cloudiness) near 39°S, 44°E.

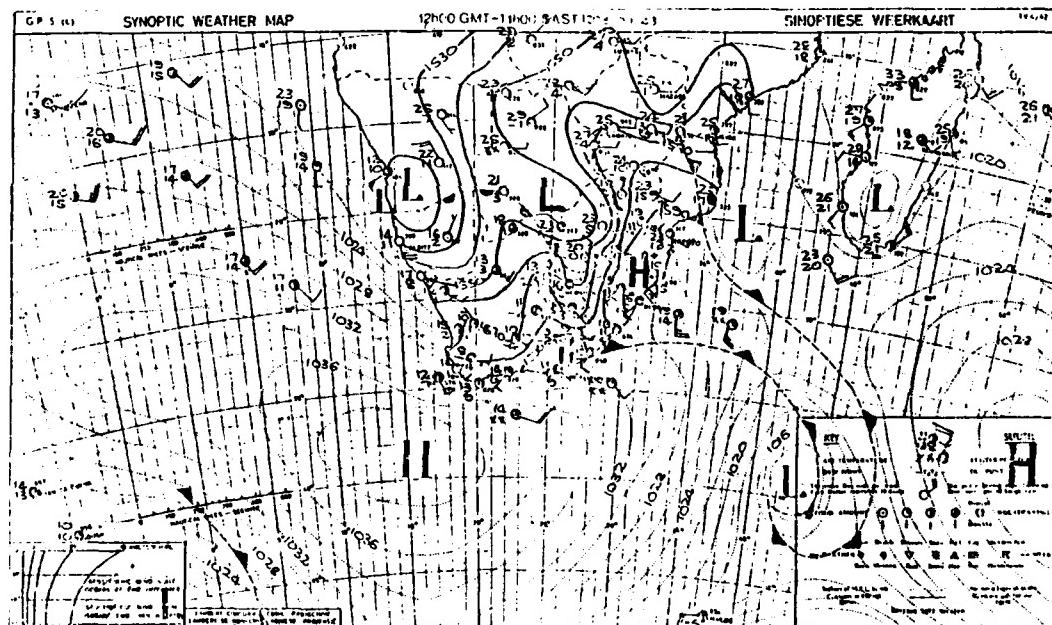
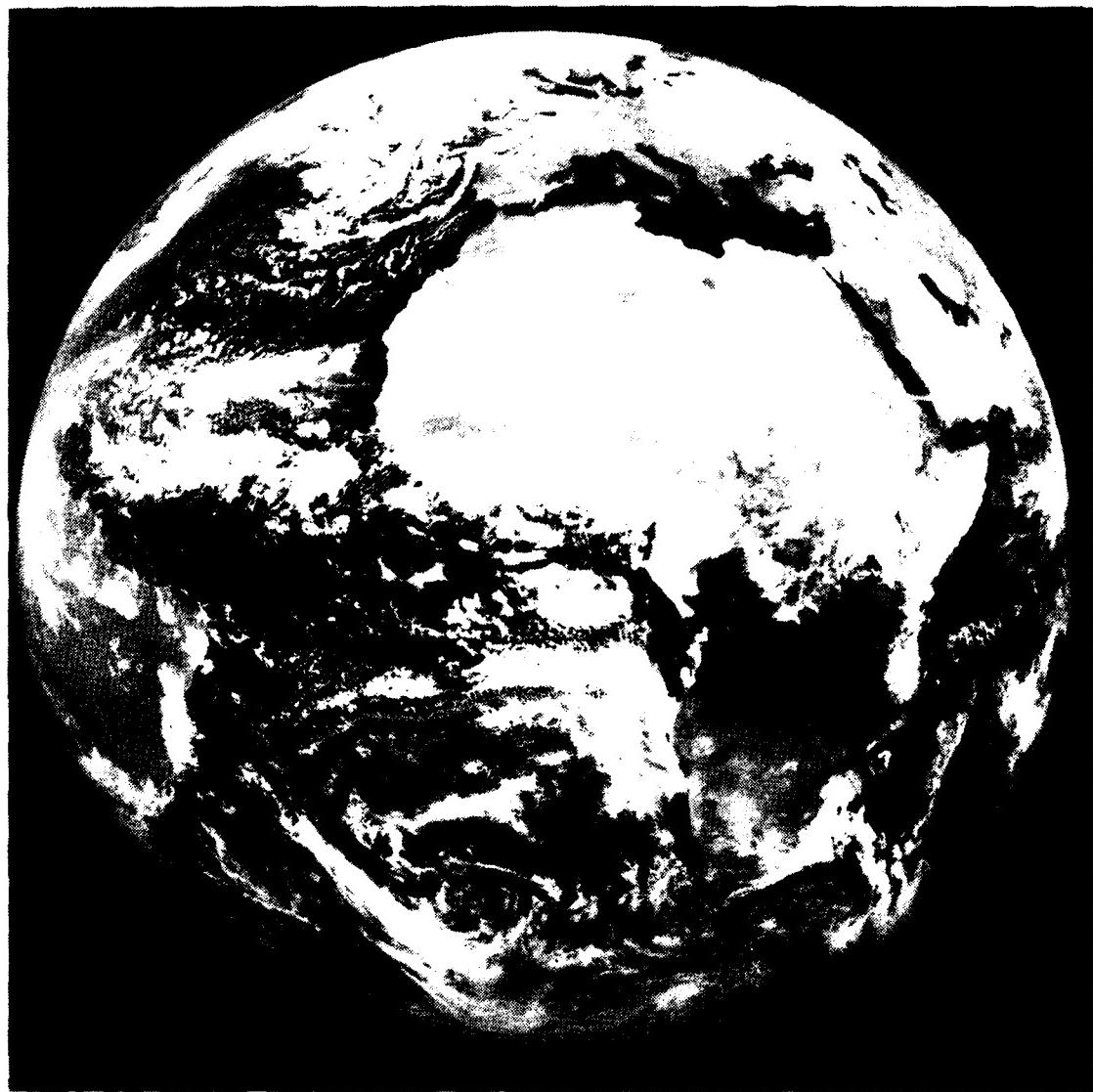


Fig. 6.70. Republic of South Africa Weather Bureau Surface (over Ocean) and 850 mb (over Continent) Analysis: 1200 GMT 23 July 1983



METEOSAT

19-7-1983 1155 1155 1155 1155 1155 1155  
NORTH 1155 1155 1155 1155 1155 1155 1155  
NOMINAL 1155 1155 1155 1155 1155 1155 1155  
1155 1155 1155 1155 1155 1155 1155

Fig. 6.71. Visible METEOSAT imagery, 1155 GMT on 23 July 1983

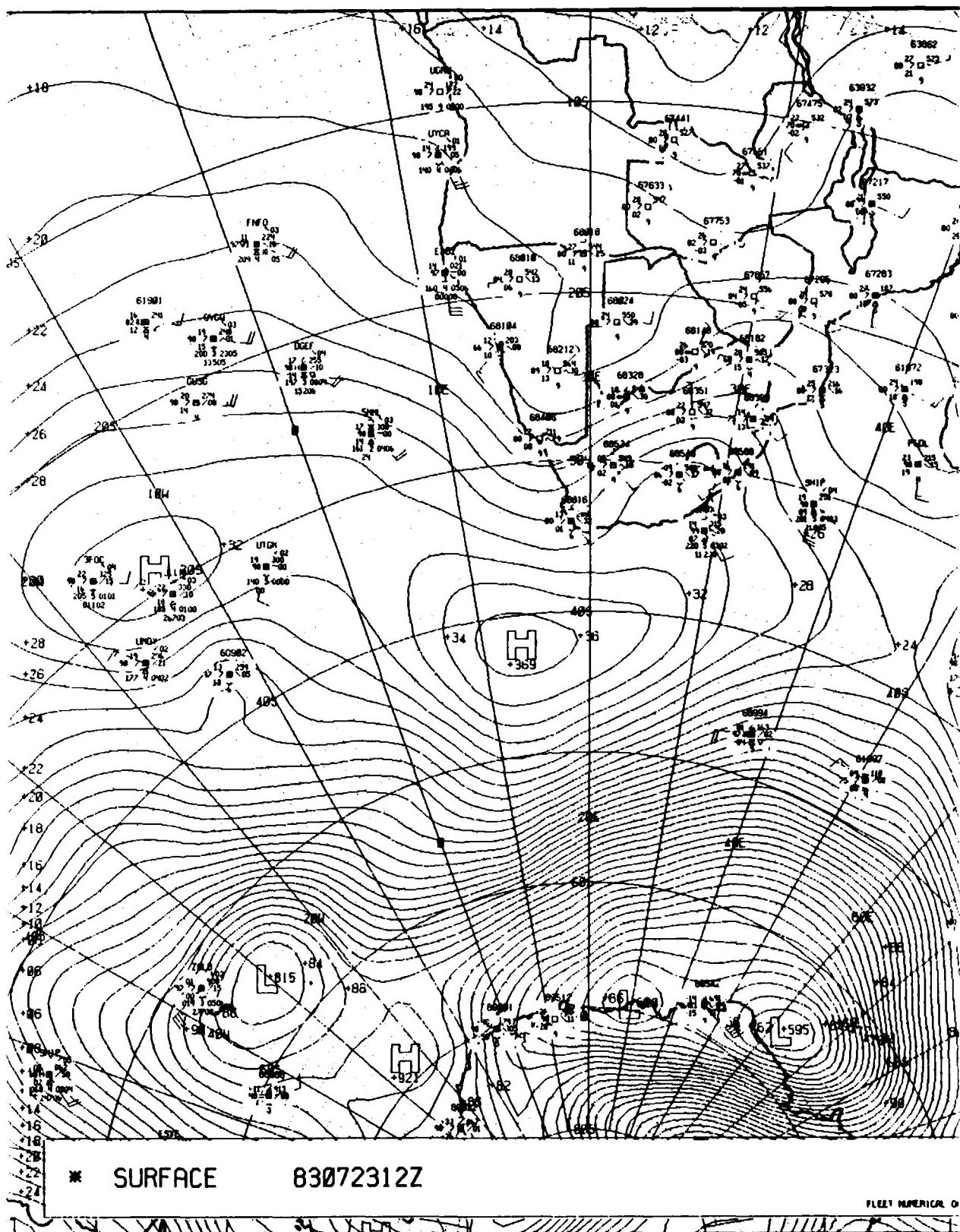


Fig. 6.72. FNOC sea-level pressure analysis, 1200 GMT on 23 July 1983

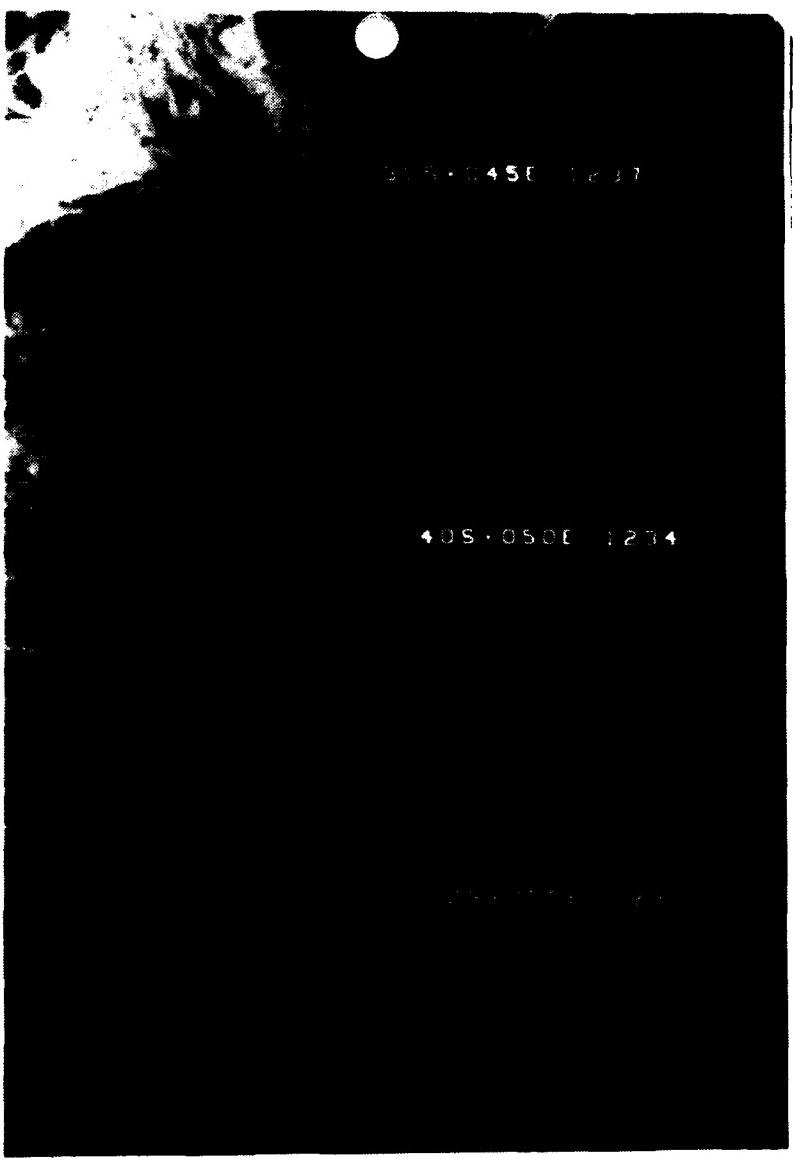


Fig. 6.73. NOAA 7 visible imagery, 1231-1237 GMT on 23 July 1983

Both 500 mb analyses (Figs. 6.74 and 6.75) have a trough crossing 40°S at 38°E (~5520 geopotential meters (gpm)) vertically consistent with the surface trough (or low) to the east.

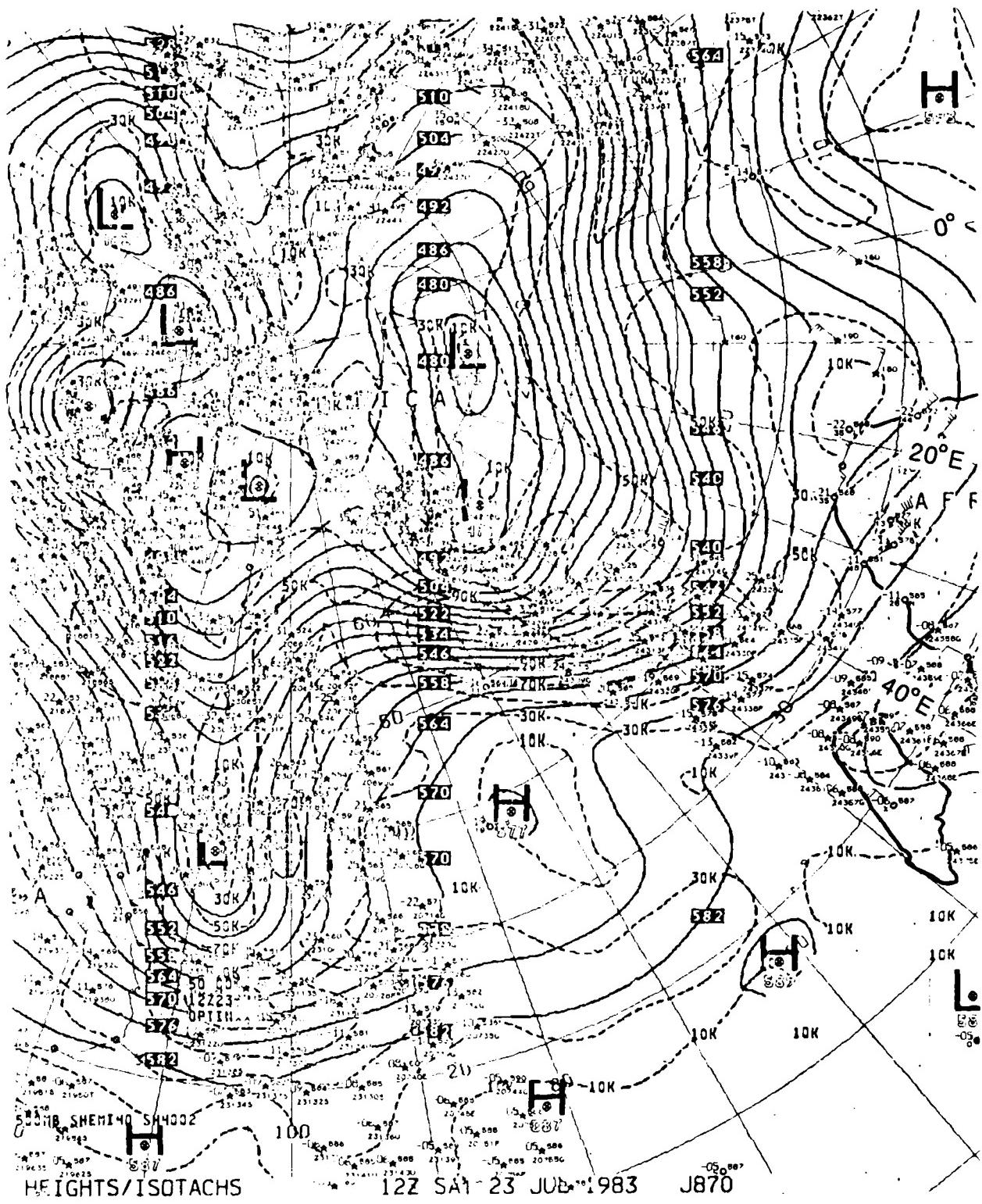


Fig. 6.74. NMC 500 mb analysis (contours and isotachs), 1200 GMT on 23 July 1983 (Note that Africa is outlined on right side of figure)

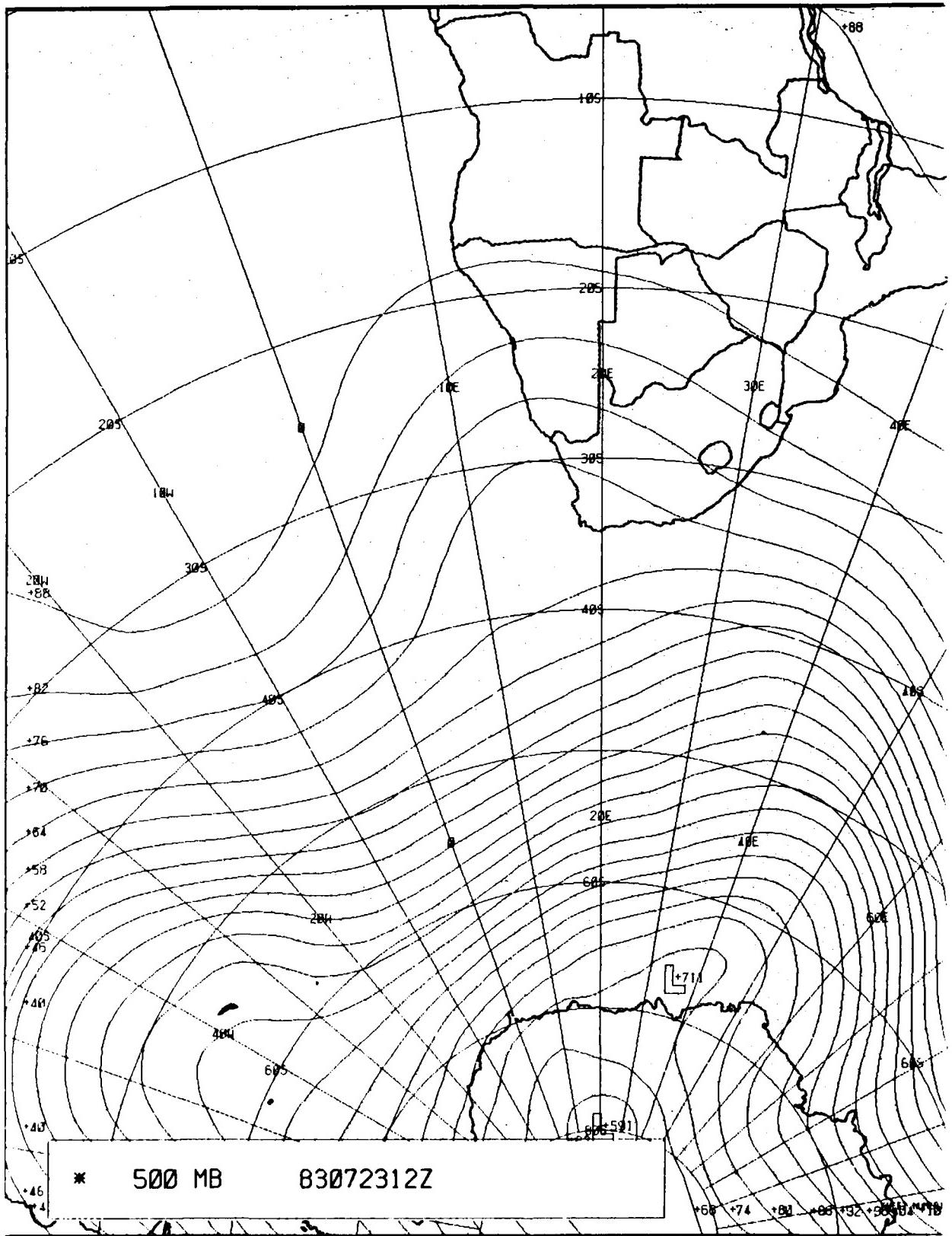
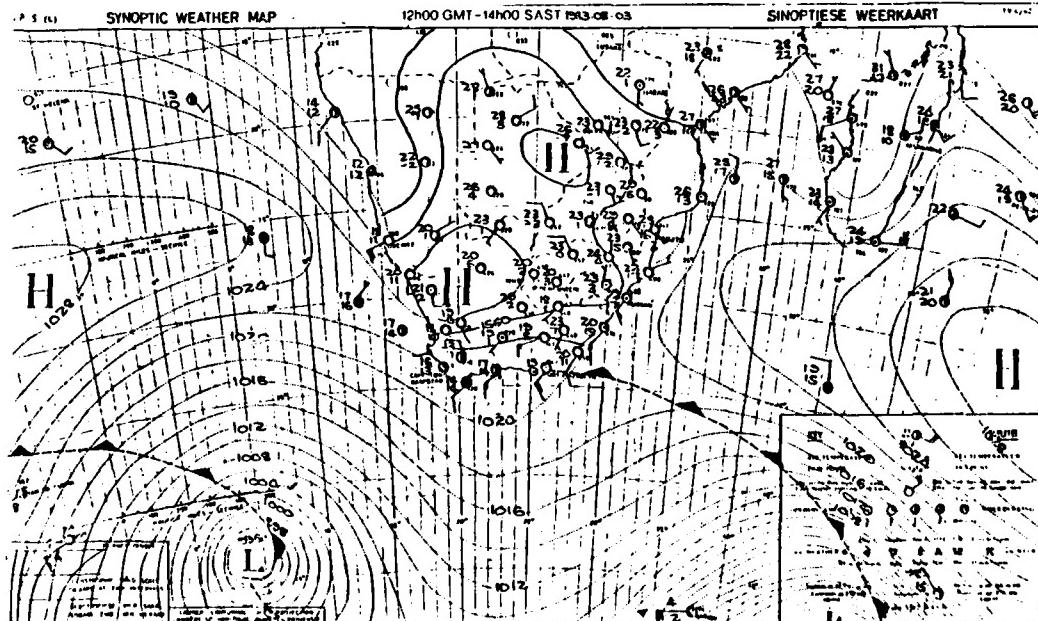


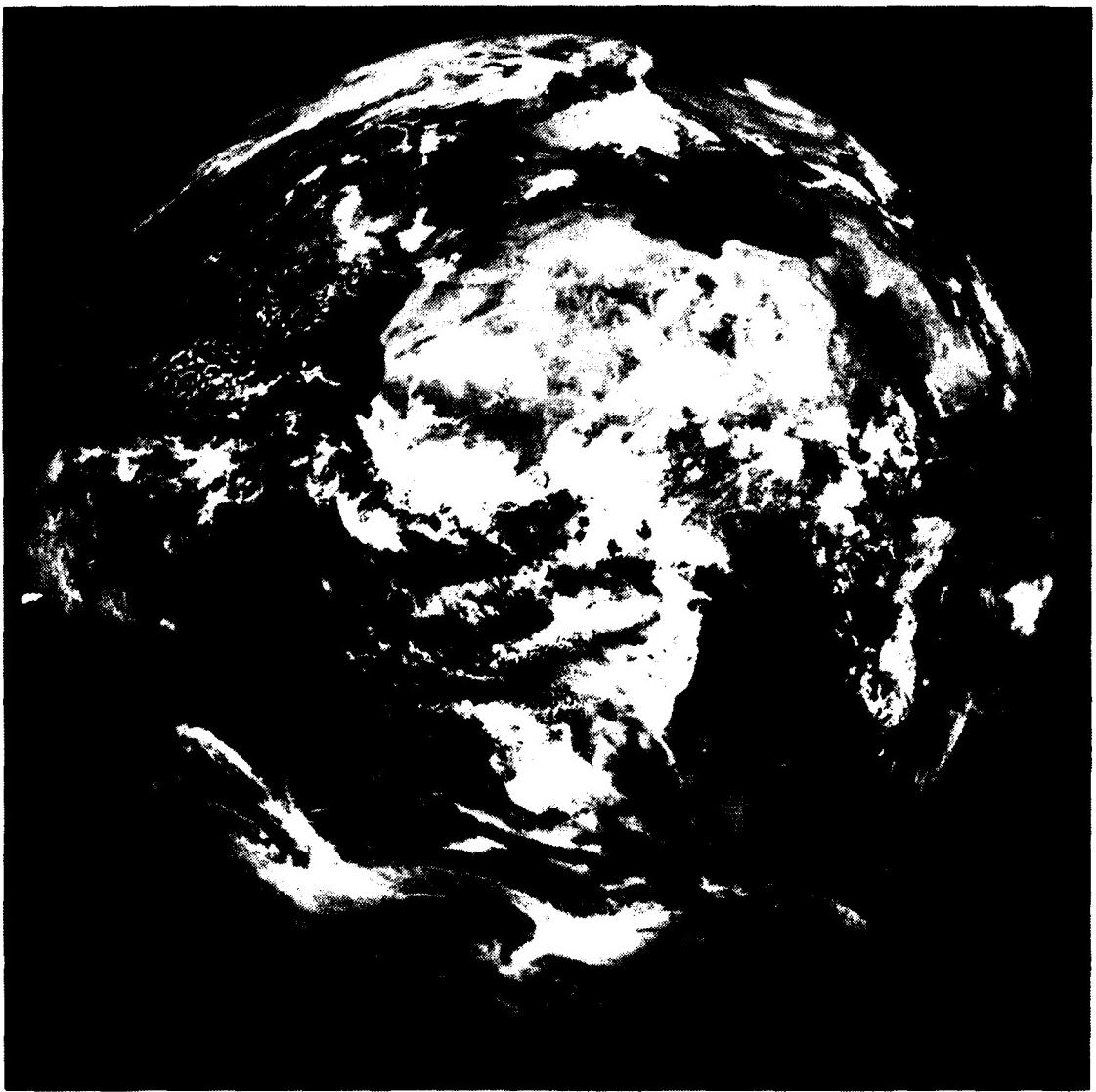
Fig. 6.75. FNOC 500 mb analysis (contours only), 1200 GMT on 23 July 1983

#### 6.4.4 Case VI (3 - 7 August 1983)

3 August 1983

The RSA surface analysis (Fig. 6.76) displays two frontal systems, with one extending to Port Elizabeth from a low east of Marion Island. An approaching, and intensifying, low (995 mb) near  $43^{\circ}\text{S}$ ,  $4^{\circ}\text{E}$  has an attendant cold front extending northwestward. METEOSAT imagery (Fig. 6.77) supports the low approaching from the South Atlantic and also displays remnants of the receding front which had affected Cape Town on the previous day. The concurrent FNOC surface analysis (Fig. 6.78), as expected without the extensive embellishment of regional satellite information, shows no vortex (low) but only a trough crossing  $40^{\circ}\text{S}$  at  $3^{\circ}\text{W}$ . (In particular, note that the FNOC analysis places a broad trough near  $43^{\circ}\text{S}$ ,  $3^{\circ}\text{W}$  contrasted to the RSA low position at  $43^{\circ}\text{S}$ ,  $4^{\circ}\text{E}$ . Note also that the global FNOC automated analysis has not drawn precisely to the pressure (1015.4 mb) reported at Gough Island (station 68906 at  $40^{\circ}\text{S}$ ,  $10^{\circ}\text{W}$ ) which was easily accommodated by the regional RSA manual analysis.) Fig. 6.79 displays the NOAA 7 polar orbiting imagery available aboard ship. From this information, the RSA analysis (Fig. 6.76) positioned the Indian Ocean front crossing  $40^{\circ}\text{S}$  at  $46^{\circ}\text{E}$  at precisely 1200 GMT.





**METEOSAT**

1983 MONTH 8 DA 3 TIME 1155 GMT (NORTH CH. HIS 2  
NOMINA, JOHN FAY INT'L. SIGHT 24) COPYRIGHT - ESR -

Fig. 6.77. Visible METEOSAT imagery, 1155 GMT on 3 August 1983

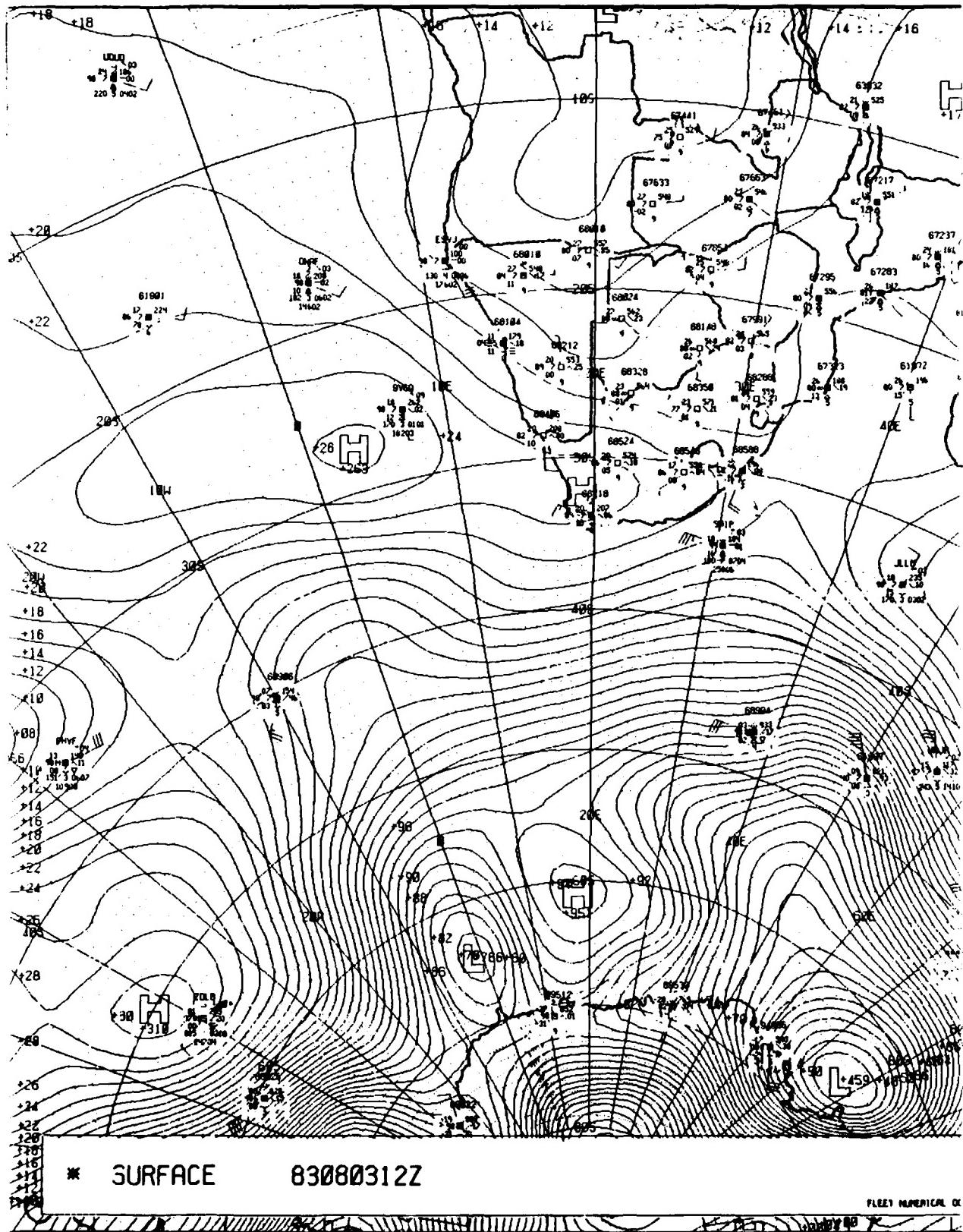


Fig. 6.78. FNOC sea-level pressure analysis, 1200 GMT on 3 August 1983

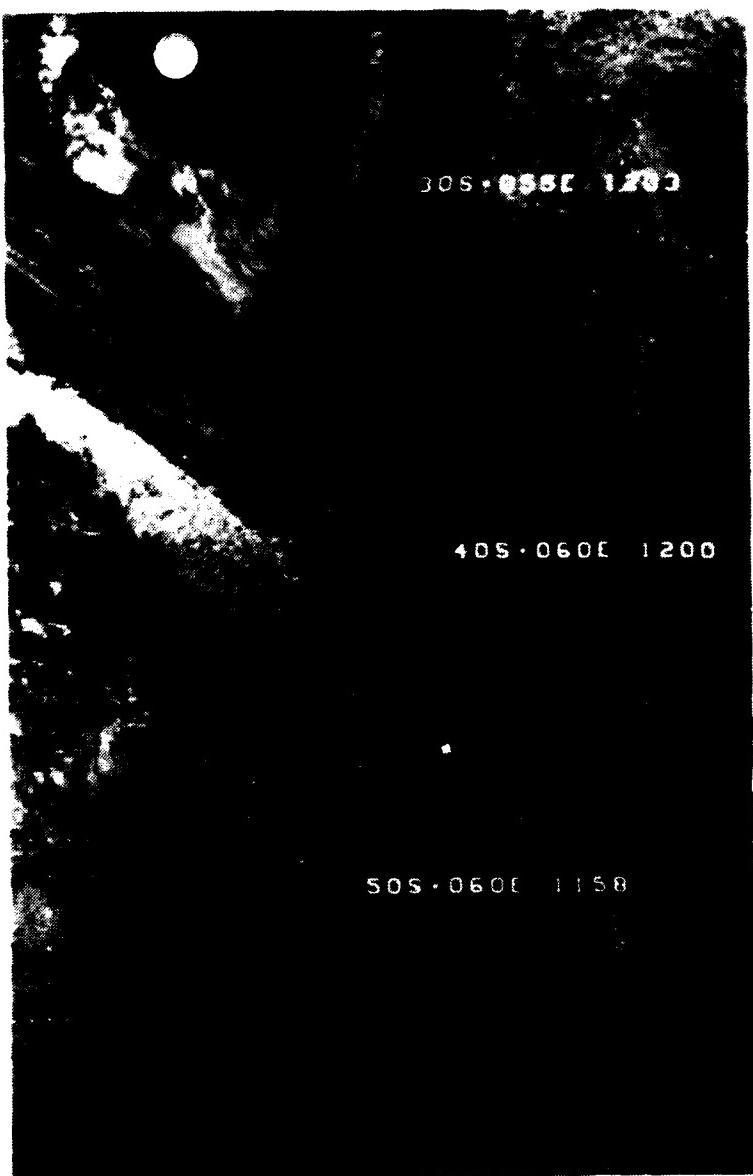


Fig. 6.79. NOAA 7 visible imagery, 1158-1203 GMT on 3 August 1983

Both the NMC and FNOC 500 mb analyses (Figs. 6.80 and 6.81) show the short wave trough crossing  $40^{\circ}\text{S}$  near  $6^{\circ}\text{W}$  associated with the developing surface system approaching from the southwest.

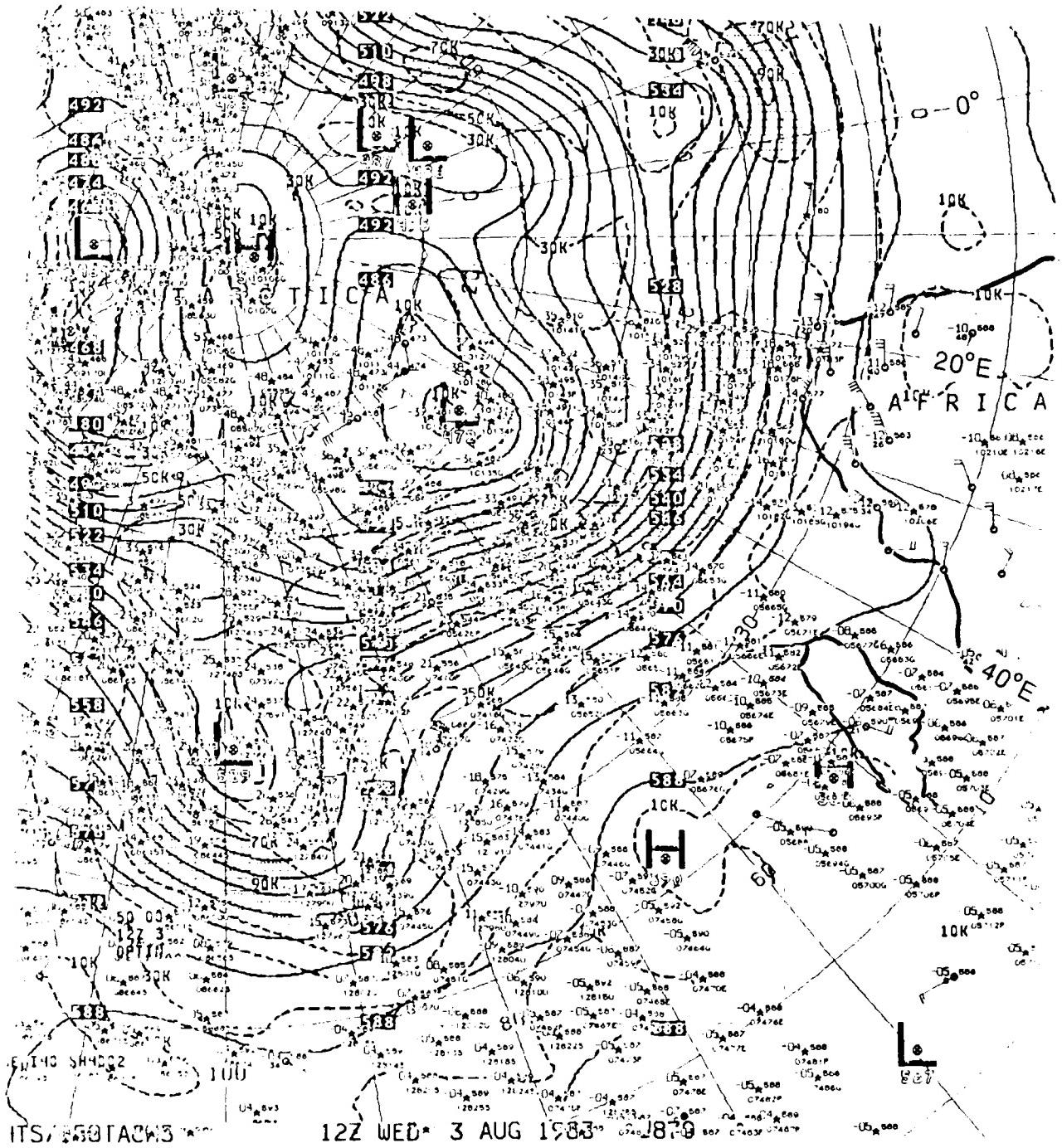


Fig. 6.80. NMC 500 mb analysis (contours and isotachs), 1200 GMT on 3 August 1983 (Note that Africa is outlined on right side of figure)

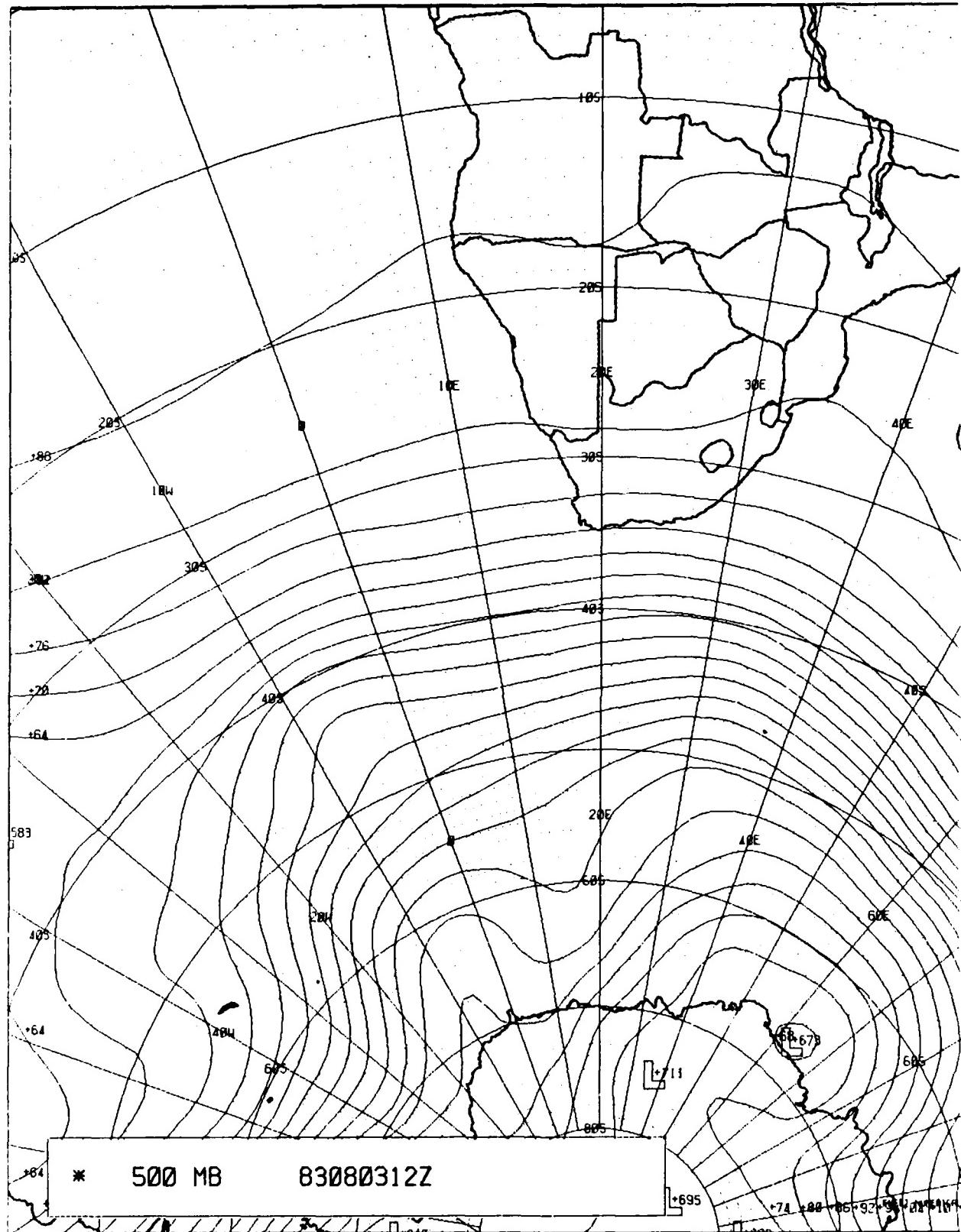


Fig. 6.81. FNOC 500 mb analysis (contours only), 1200 GMT on 3 August 1983

(Blank)

4 August 1983

On the second day of this case study (Fig. 6.82), the RSA regional surface analysis depicts the low approaching from the Atlantic on 3 August having moved (at ~31 kt) to 45°S, 22°E and deepened considerably to 973 mb. (Note that the speed of advance of the front along latitude 40°S during the past 24 hours is ~39 kt!). This analysis is in concurrence with the METEOSAT imagery (Fig. 6.83) which shows the classic vortex with its front extending northwestward to Cape Town and beyond. Also depicted by METEOSAT is the enhanced convection (NVA)<sup>15</sup> forming *within* the cold air mass (depicted as a 997 mb low center at 41°S, 12°E with a newly formed cold front; see Fig. 6.82). The FNOC surface analysis (Fig. 6.84) satisfactorily depicts the parent low near 45°S, 22°E (albeit at a central pressure of 982.8 mb -- 10 mb higher than the RSA analysis); however, without the advantage of regional satellite data, there is no hint of the low forming within the cold air mass at 41°S, 12°E. Fig. 6.85, from the polar orbiting NOAA 7 clearly displays the parent low and front, with considerable convection, south of RSA at 1330 GMT. Attention also should be addressed to the FNOC analysis (Fig. 6.84) which appears to have injected a spurious low center near 25°S, 55°E, southeast of the Malagasy Republic. Although there may be *additional observations* available for the FNOC analysis, the area appears to be described satisfactorily by the RSA analysis, i.e., simply on the periphery of the Indian Ocean anticyclone (see Fig. 6.82).

---

<sup>15</sup> Note that the terminology so familiar to Northern Hemisphere meteorologists must be adapted to Southern Hemisphere dynamics which define both a *negative* Coriolis Parameter (*f*) as well as *negative* relative vorticity for *cyclonic* circulations. Thus the phrase 'Positive Vorticity Advection' (PVA), associated with upper-air divergence and lower-level convergence and convection in the Northern Hemisphere, becomes 'Negative Vorticity Advection' (NVA) in the Southern Hemisphere! Moreover, note that use of the phrase, 'Cyclonic Vorticity Advection', is acceptable in both hemispheres.

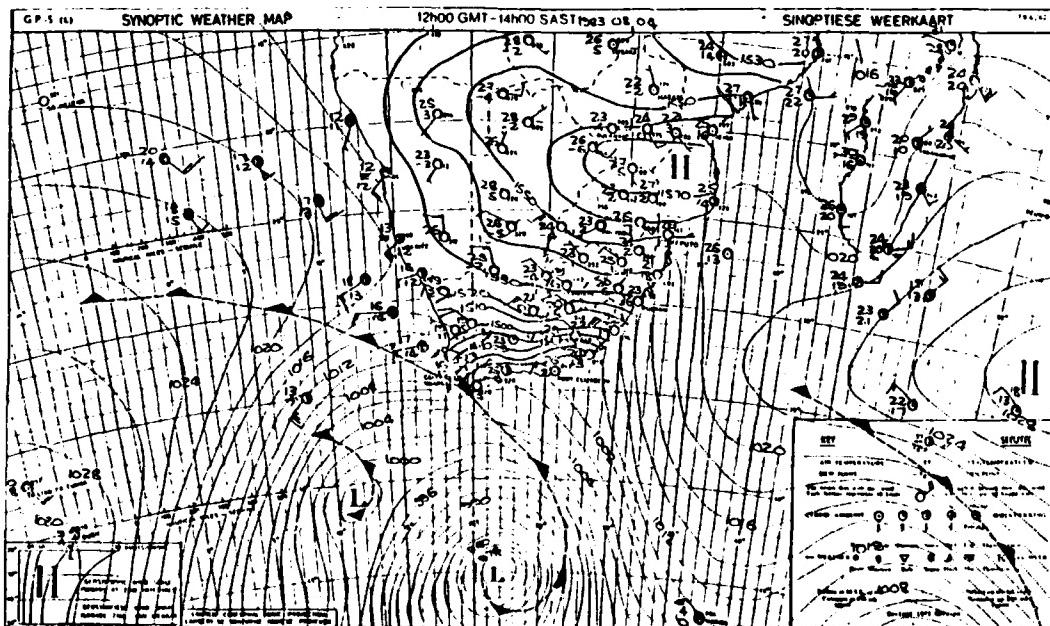
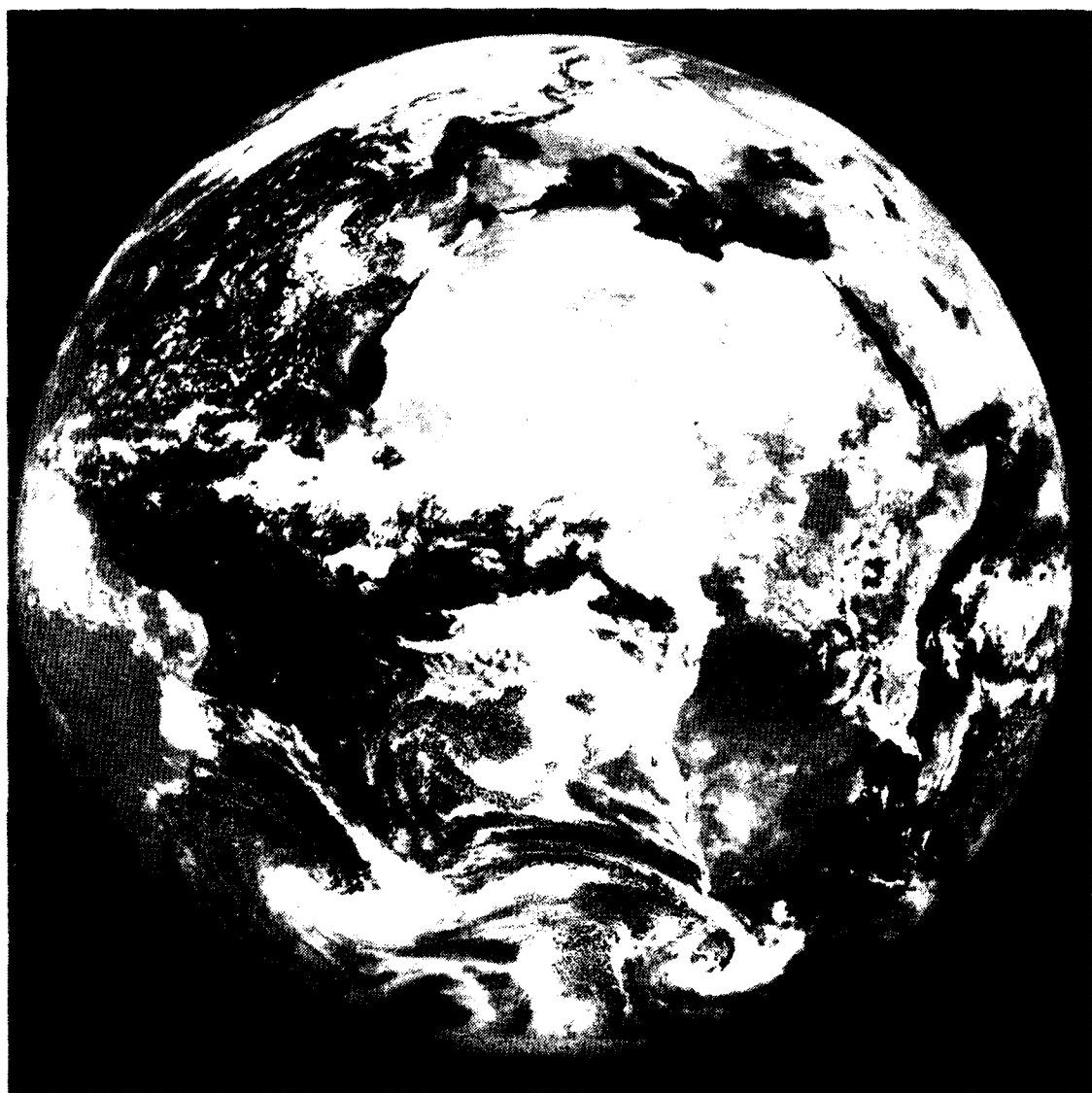


Fig. 6.82. Republic of South Africa Weather Bureau Surface (over Ocean) and 850 mb (over Continent) Analysis: 1200 GMT 4 August 1983



METEOSAT

Fig. 6.83. Visible METEOSAT imagery, 1155 GMT on 4 August 1983

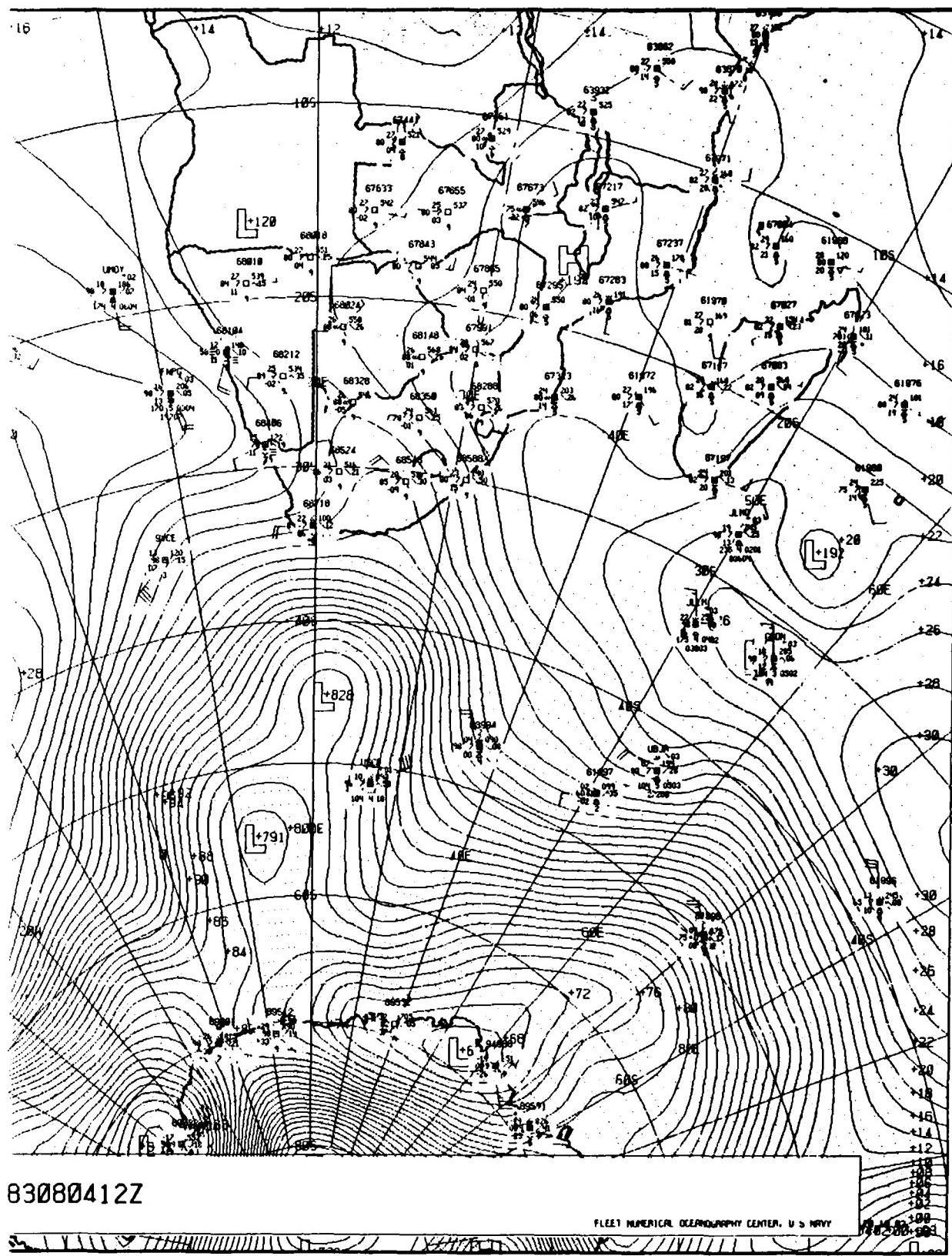


Fig. 6.84. FNOE sea-level pressure analysis, 1200 GMT on 4 August 1983

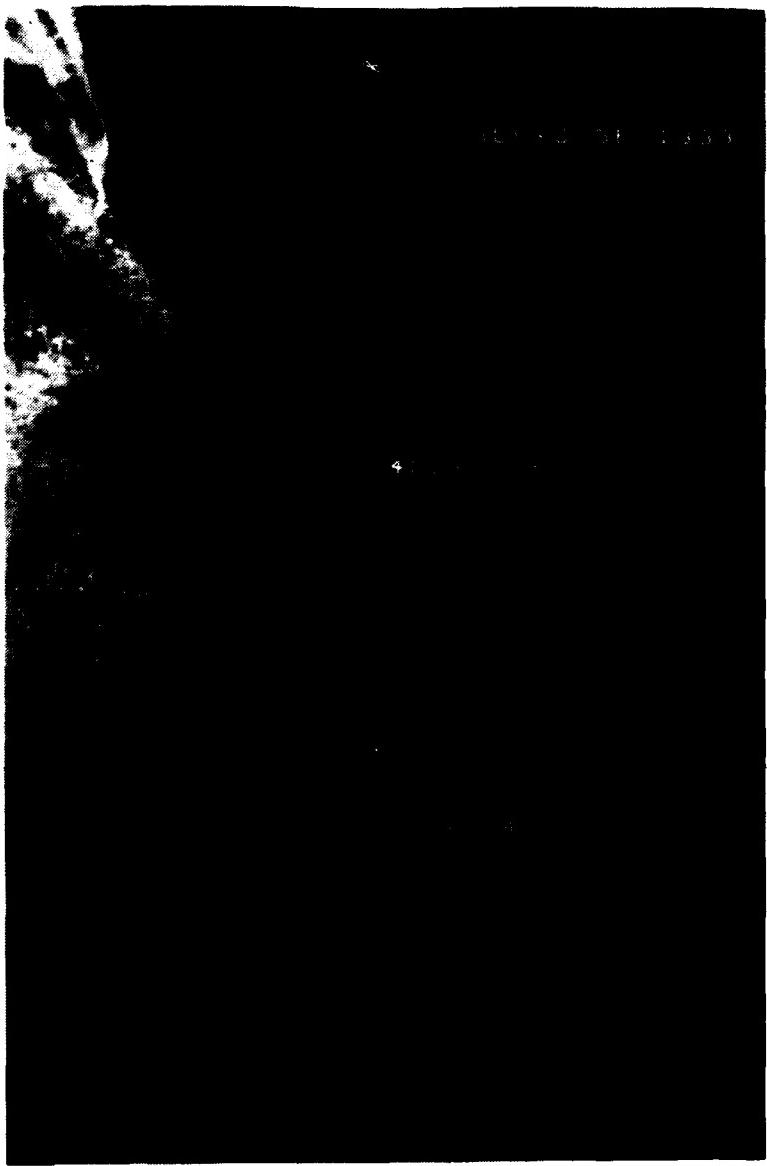


Fig. 6.85. NOAA 7 visible imagery, 1327-1333 GMT on 4 August 1983

The two 500 mb analyses (Figs. 6.86 and 6.87) depict a trough with considerable magnitude crossing 40°S near 15°E supporting the surface trough (front) just penetrating RSA.

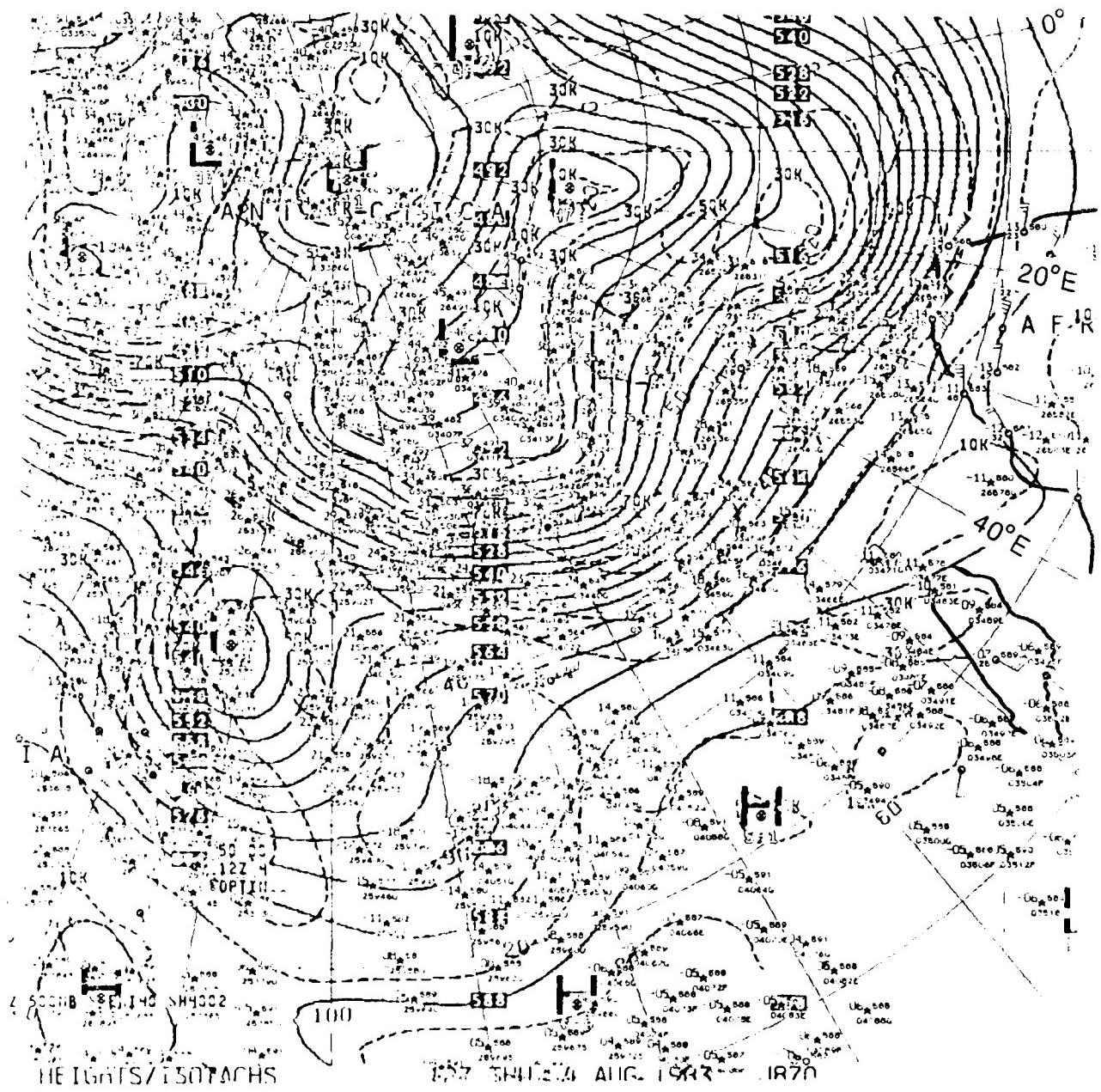


Fig. 6 86. NMC 500 mb analysis (contours and isotachs), 1200 GMT on 4 August 1983 (Note that Africa is outlined on right side of figure)

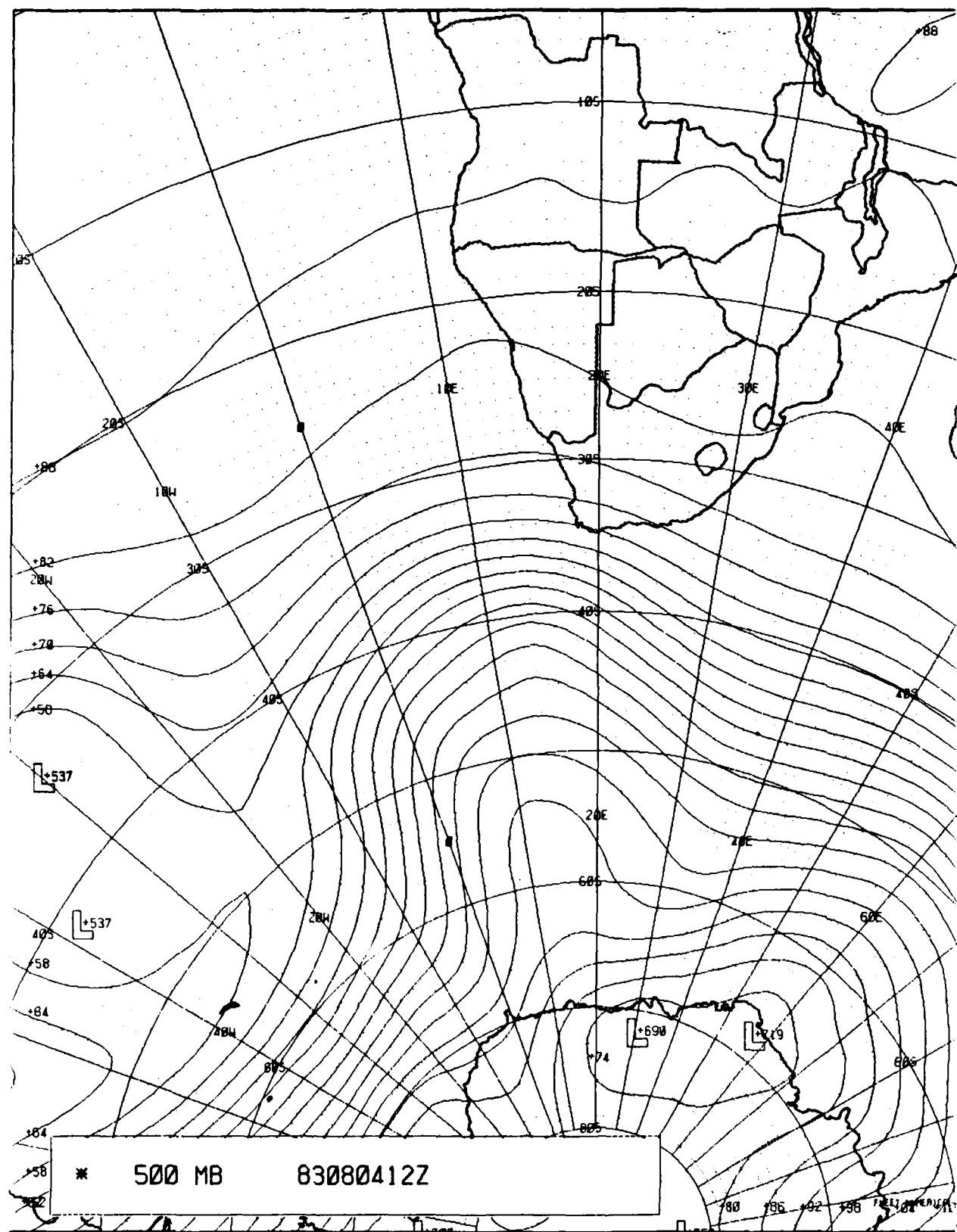


Fig. 6.87. FNOC 500 mb analysis (contours only), 1200 GMT on 4 August 1983

(Blank)

## 5 August 1983

On the next day, the RSA analysis (Fig. 6.88) depicts the low, first noted 4 August in the cold air mass (at 41°S, 12°E), as having moved (at ~37 kt)<sup>16</sup> to 42°S, 33°E, deepened to a central pressure of 991 mb and having nearly overtaken the original front. This rapid speed of advance of the newly formed low is supported by the strong 'steering' flow at 500 mb above the low on 4 August (~70 kt on Fig. 6.86) and the continuing, even stronger, 500 mb cyclonic flow depicted above the vortex in Fig. 6.92 on 5 August. Additionally, another new polar low, with an associated front, has formed within the original cold air mass and is found at 42°S, 21°E, also with a central pressure of 991 mb (Fig. 6.88). The METEOSAT imagery (Fig. 6.89) shows a configuration with the fronts reaching the southeast RSA coast between Port Elizabeth and Durban; note that the leading low center, to the east, displays the 'inverted comma' configuration while open cell cloudiness abounds in the cold air southwest of Cape Town. On this date, the FNOC surface analysis (Fig. 6.90) shows a trough in the general area of the fronts analyzed by RSA, as well as a low center at 30°S, 30°E, near Durban, as analyzed by RSA. However, no closed low centers are depicted south of the continent *near* 42°S, although there is a closed low far poleward, at 54°S, 38°E, no doubt the original, parent low which was located in the South Atlantic at 43°S, 4°E (995 mb) on 3 August (see Fig. 6.76). Fig. 6.91, NOAA 7 imagery from 1315 - 1320 GMT, depicts the cloudiness of the two fronts striking the coast. The NOAA 7 imagery may also support the RSA vortex position if a low center is perceived in the clear area near 43°S, 33°E at Point B, with a large convective cloud mass just poleward.

<sup>16</sup> Fig. 1.25 (van Loon, 1967) indicates that (within the 40 - 50°S latitude band) ~29% of the low centers move at speeds 30 - 40 kt.

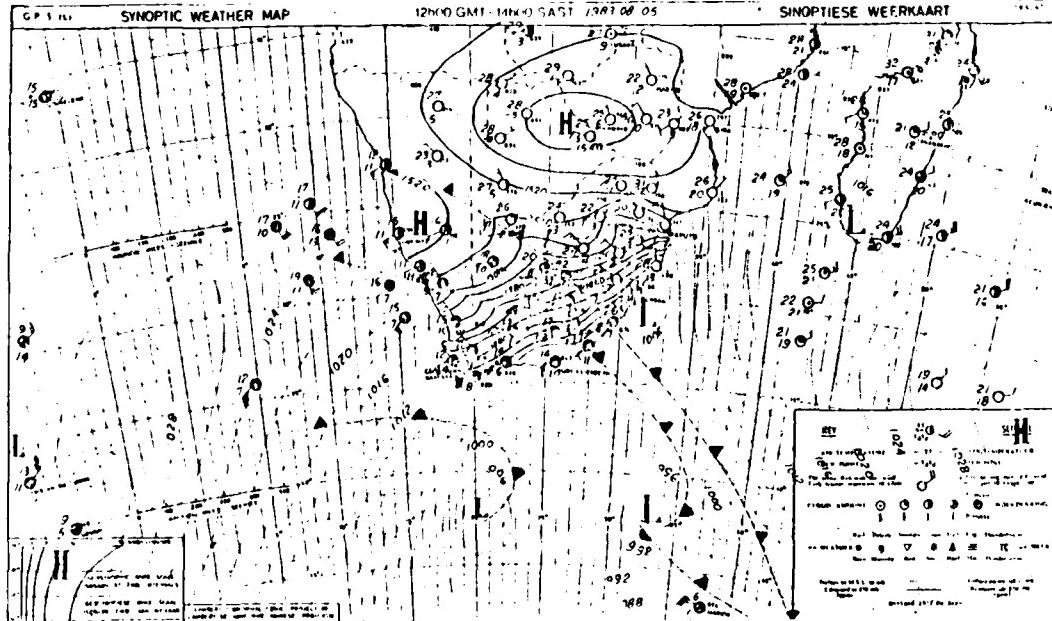
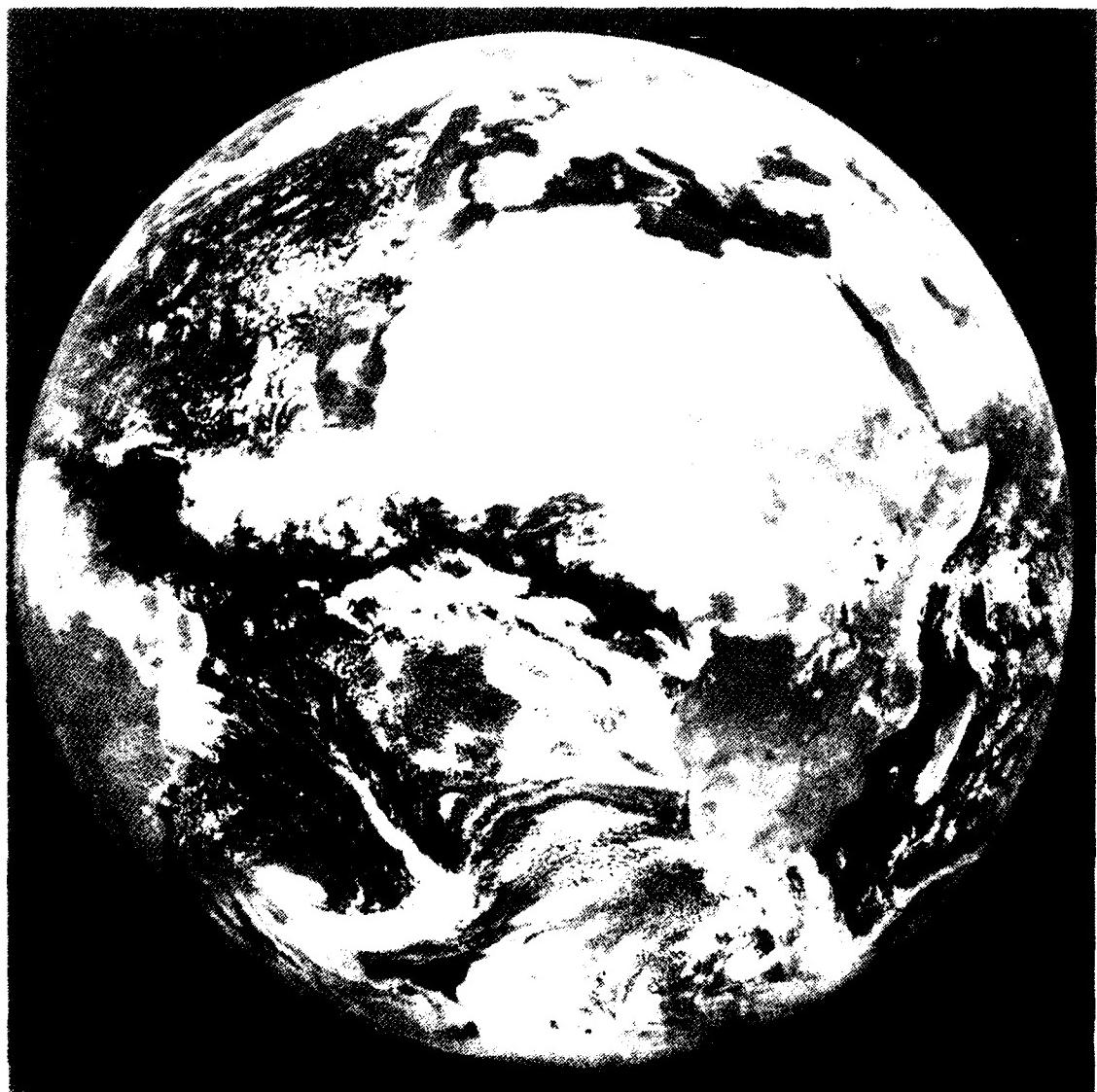


Fig. 6.88. Republic of South Africa Weather Bureau Surface (over Ocean) and 850 mb (over Continent) Analysis: 1200 GMT 5 August 1983



METEOSAT

Fig. 6.89. Visible METEOSAT imagery, 1155 GMT on 5 August 1983

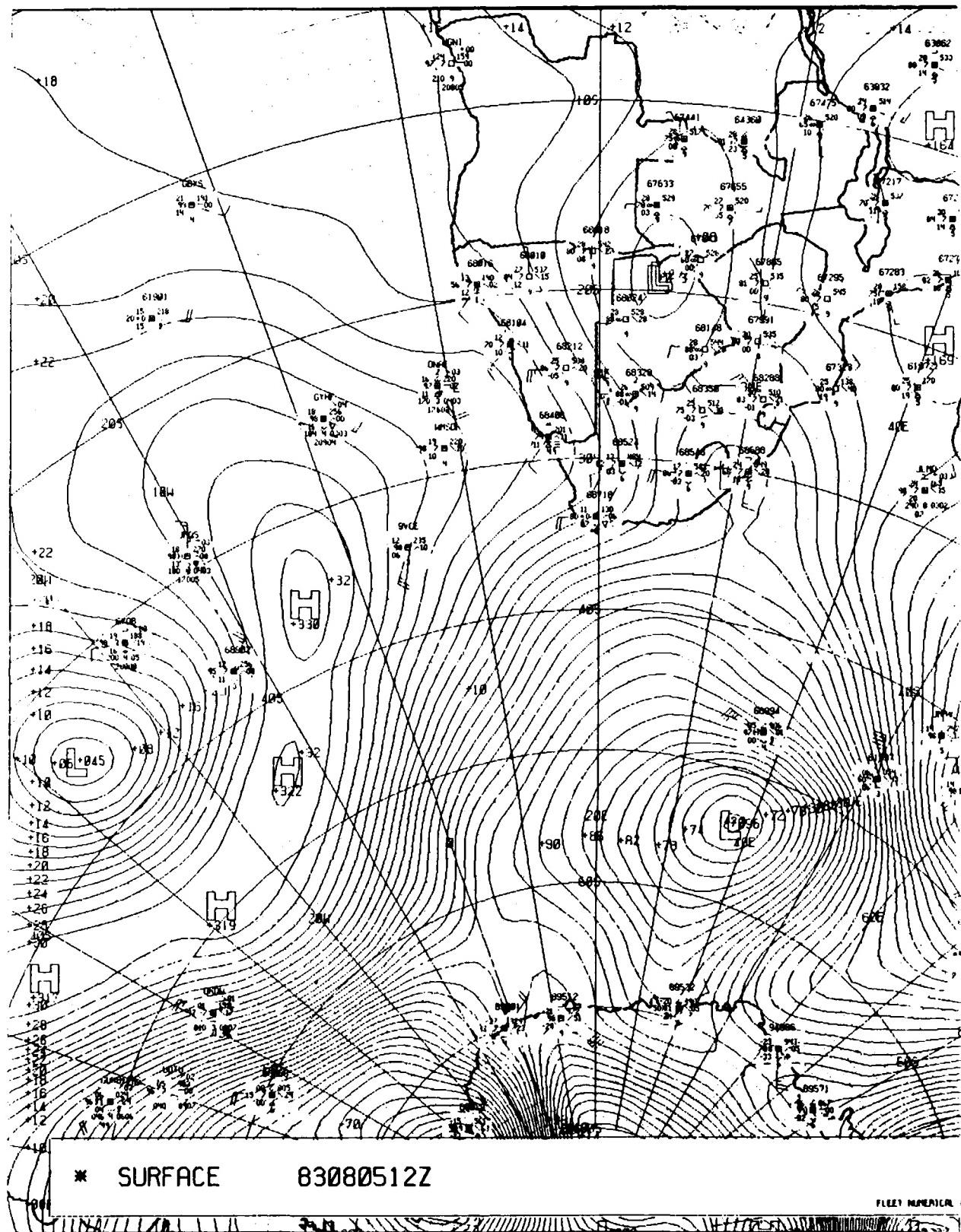


Fig. 6.90. FNOC sea-level pressure analysis, 1200 GMT on 5 August 1983

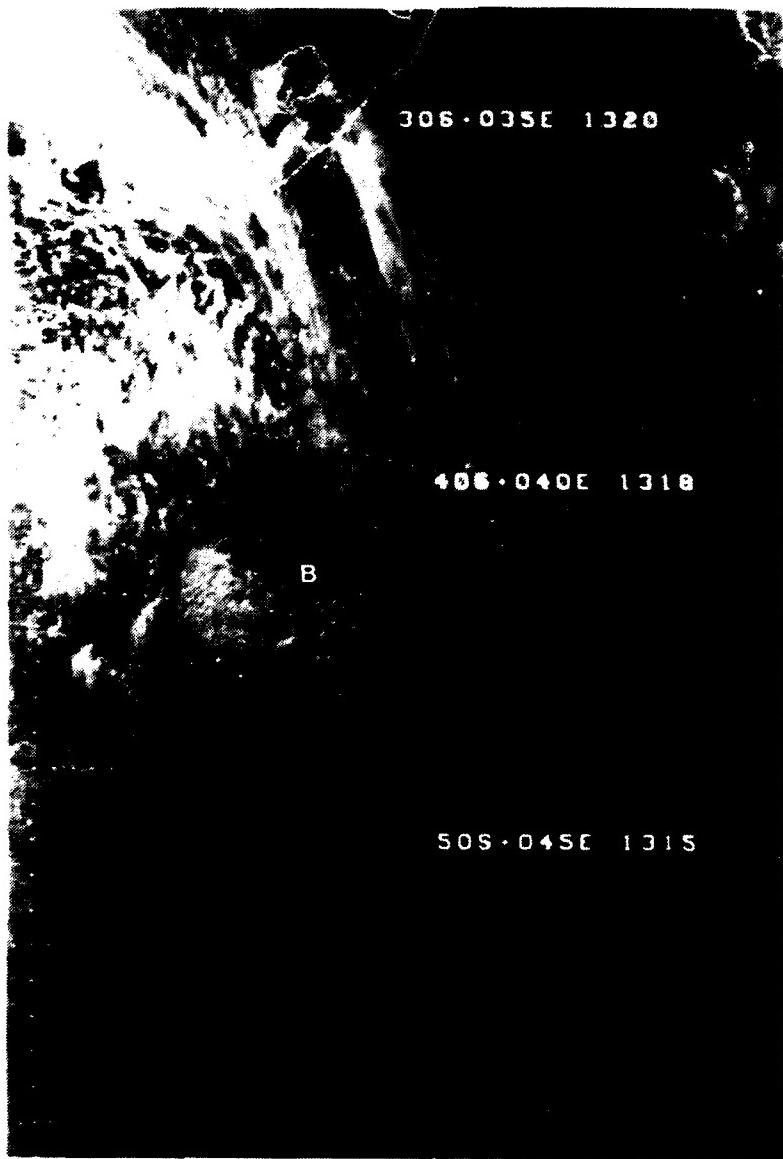


Fig. 6.91. NOAA 7 visible imagery, 1315-1320 GMT on 5 August 1983

Fig. 6.92 from FNOC displays continuity in advancing the 500 mb trough eastward to cross 40°S near 21°E.

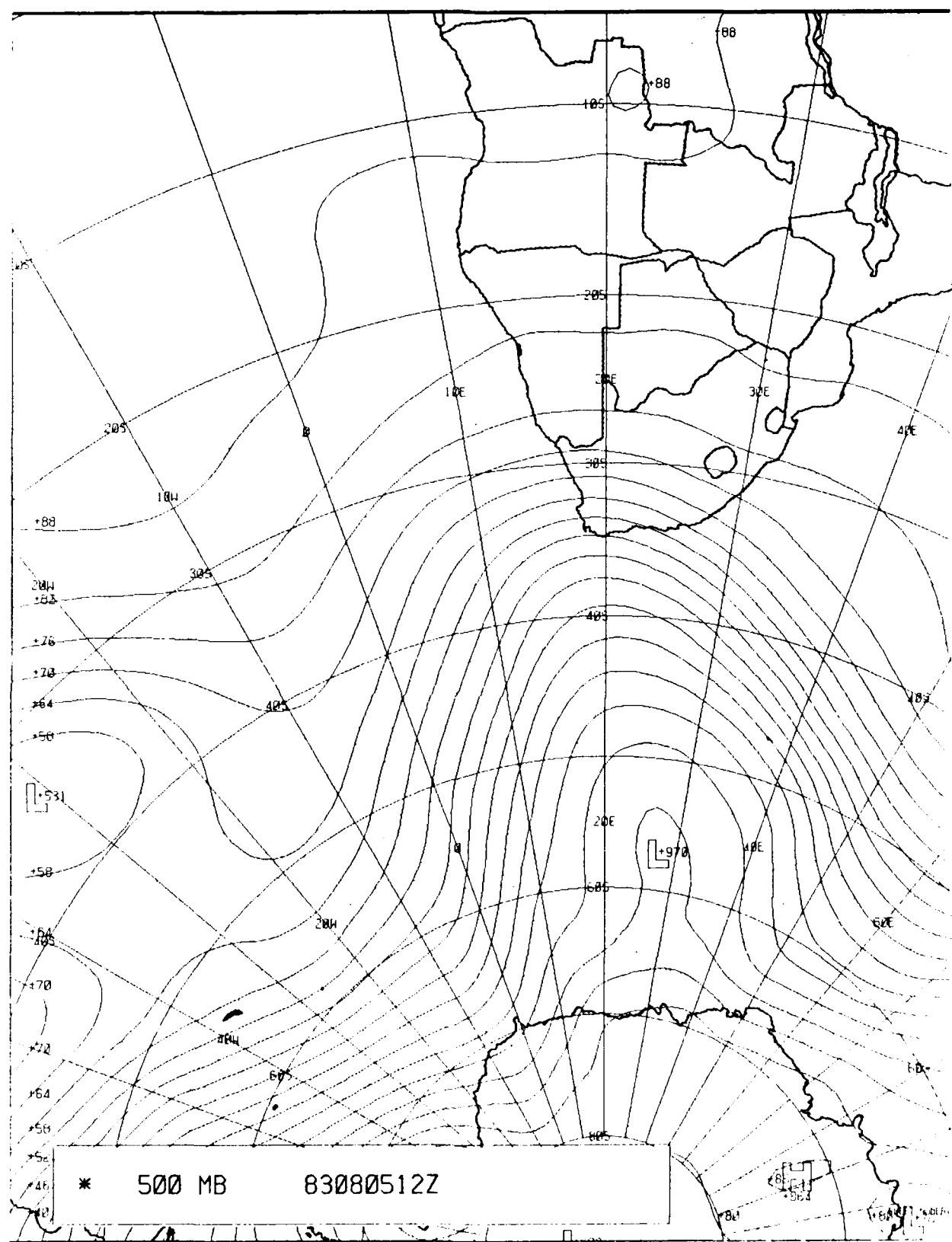


Fig. 6.92. FNOC 500 mb analysis (contours only), 1200 GMT on 5 August 1983

6 August 1983

On the following day, the RSA surface analysis (Fig. 6.93) shows the polar low, first noted south of Cape on the 5th, having moved eastward, at only ~16 kt,<sup>17</sup> to 42°S, 29°E (note that the surface low is now under a rather broad trough and only 30-kt flow at 500 mb; see Fig. 6.97); while the front, to the east, extends from east of Marion Island to Durban and beyond. The METEOSAT visible imagery (Fig. 6.94) suggests general support of the front nearing Durban, but its resolution does not permit precise location of the front south of Port Elizabeth. However, visible imagery from DMSP (see Fig. 6.96) tends to support the front south of Port Elizabeth despite the imagery being from an orbit at 1602 GMT. As expected, the FNOC surface analysis (Fig. 6.95) does not depict the low near 42°S, 29°E, but does have a trough extending to southern Mozambique in agreement with Fig. 6.93.

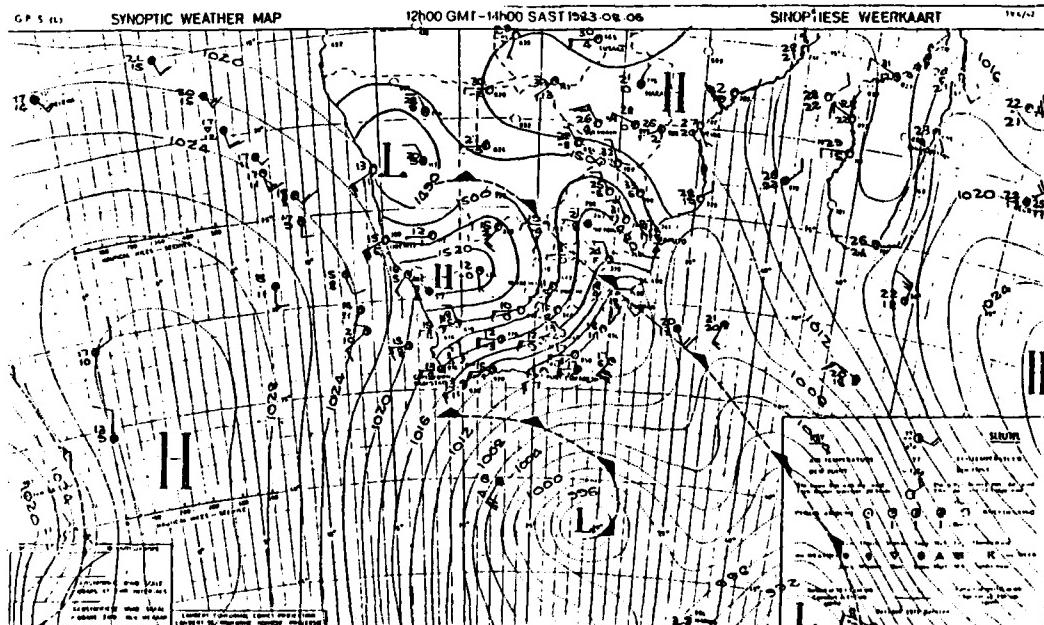
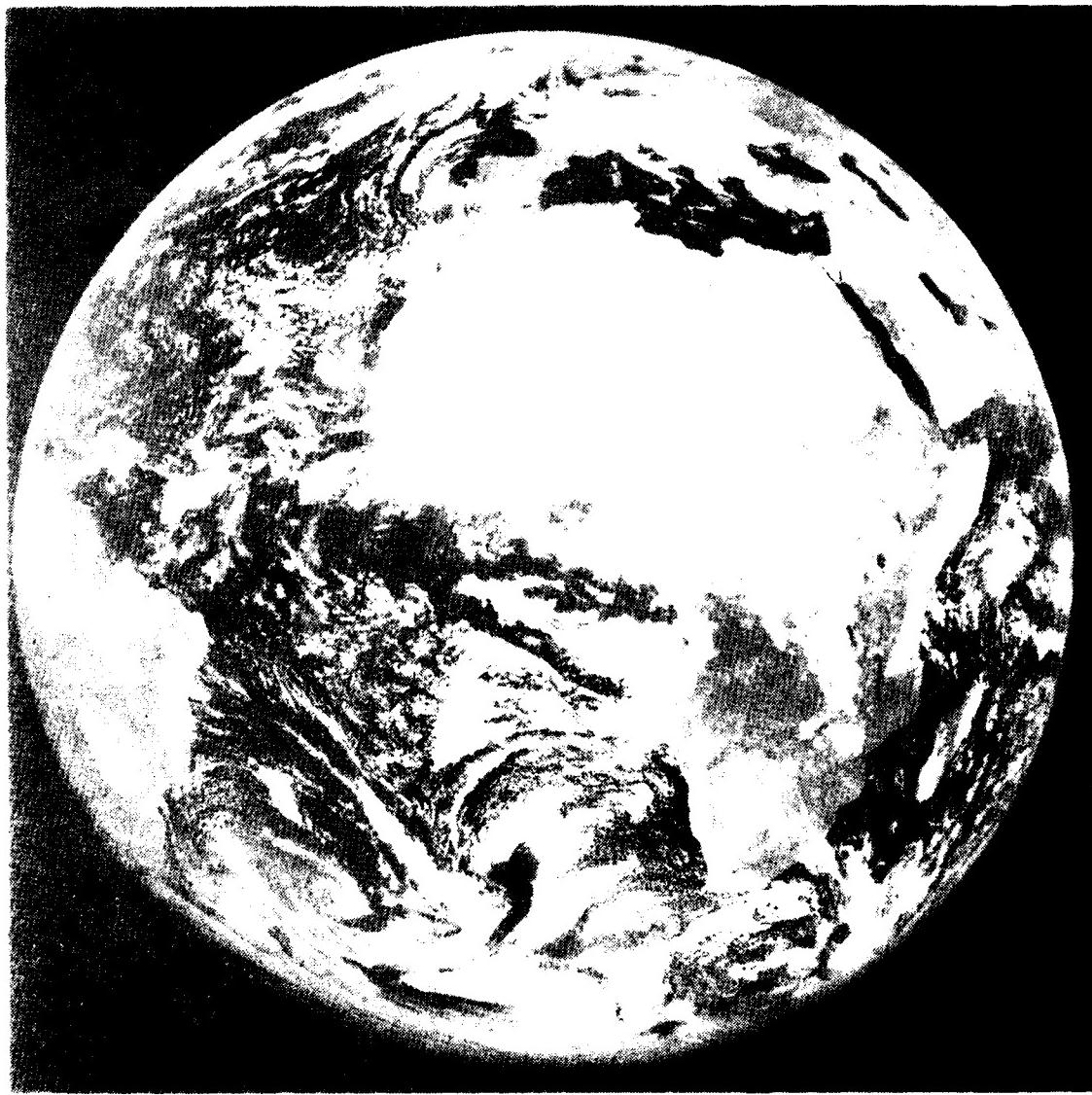


Fig. 6.93. Republic of South Africa Weather Bureau Surface (over Ocean) and 850 mb (over Continent) Analysis: 1200 GMT 6 August 1983

<sup>17</sup> Again reference to Fig. 1.25 reveals that, within the 40 - 50°S latitude band, only 16% of the low centers move at the relatively slow speeds of 10 - 20 kt.



METEOSAT

Fig. 6.94. Visible METEOSAT imagery, 1155 GMT on 6 August 1983

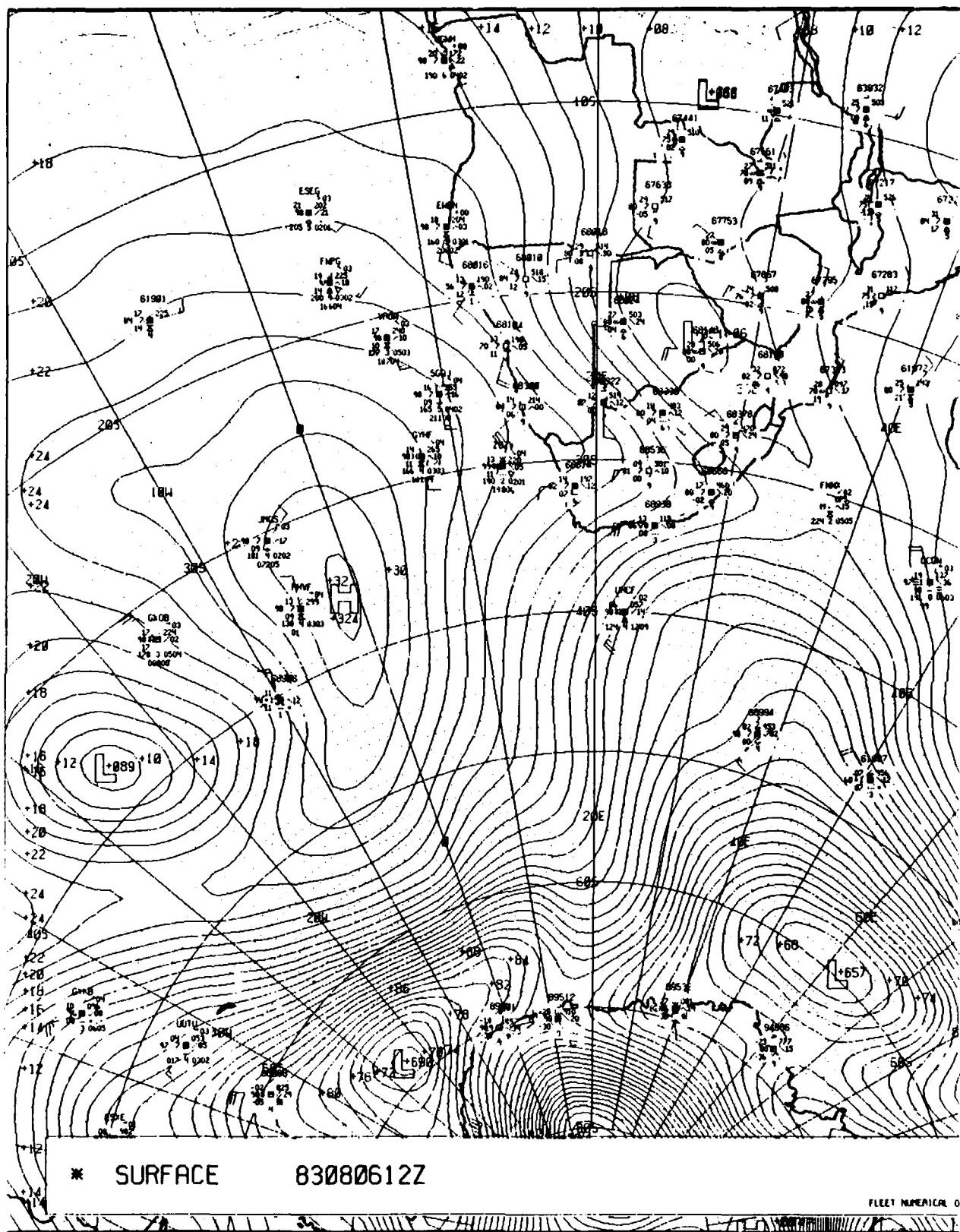


Fig. 6.95. FNOC sea-level pressure analysis, 1200 GMT on 6 August 1983

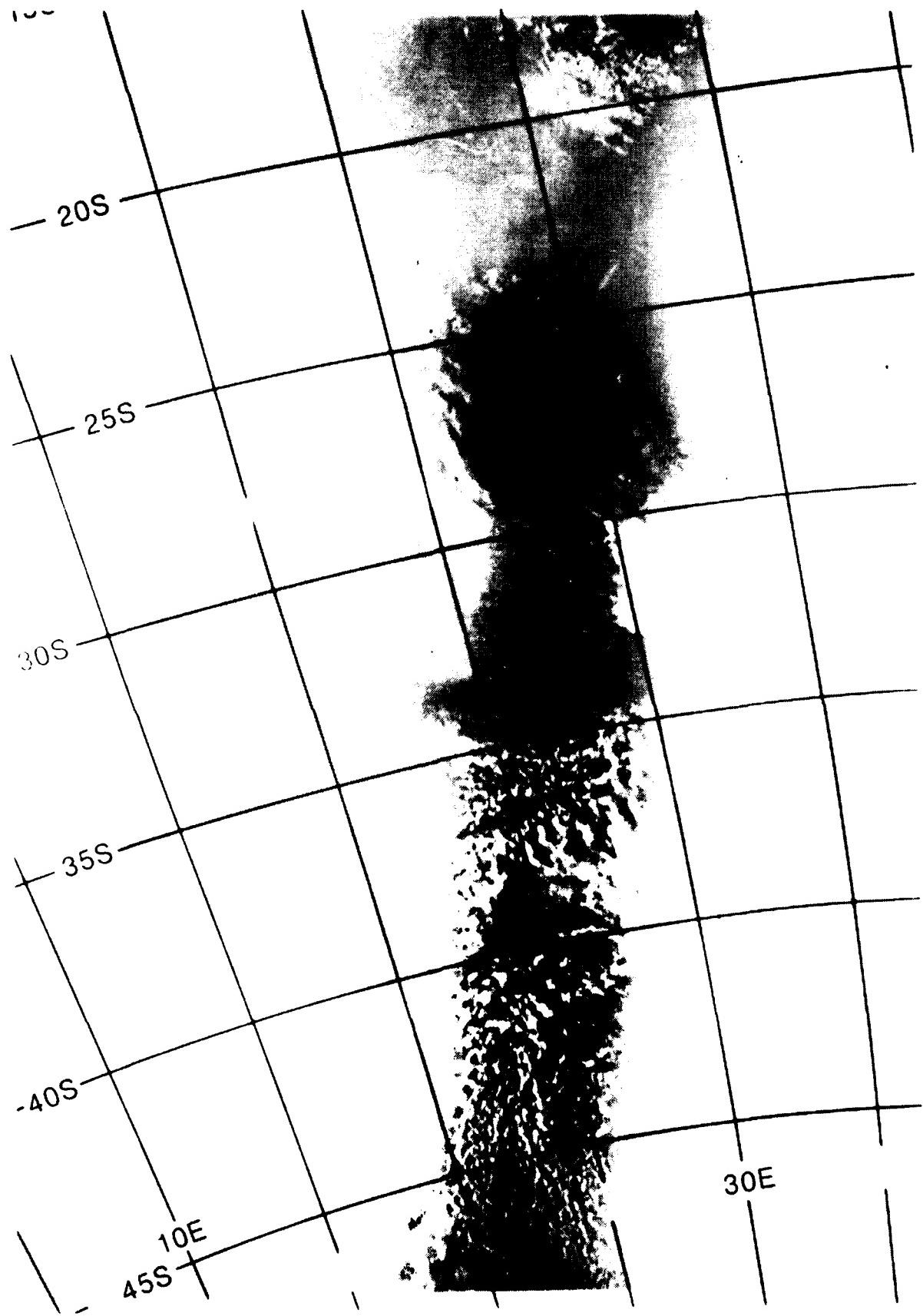


Fig. 6.96. DMSP visible imagery, 1602 GMT 6 August 1983

The 500 mb analyses (Figs. 6.97 and 6.98) both display a deep trough, intersecting the RSA coast at  $\sim 25^{\circ}\text{E}$ , vertically consistent with (i.e., trailing) the surface front, which is nearing Durban at  $\sim 30^{\circ}\text{E}$ . Note that both analyses depict the height of the 500 mb trough over RSA at  $30^{\circ}\text{S}$  as  $\sim 5640$  gpm.

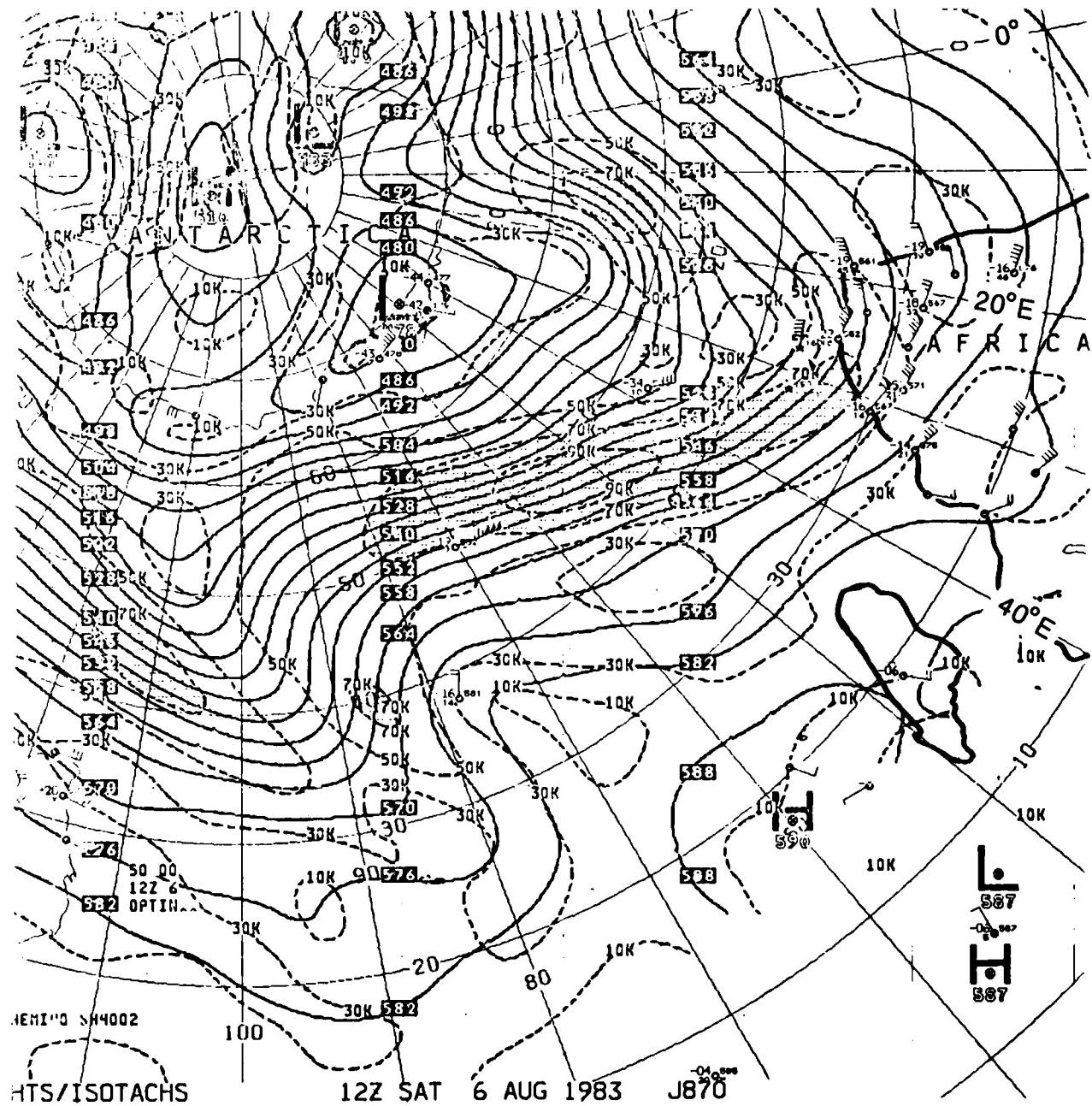


Fig. 6.97. NMC 500 mb analysis (contours and isotachs), 1200 GMT on 6 August 1983 (Note that Africa is outlined on right side of figure)

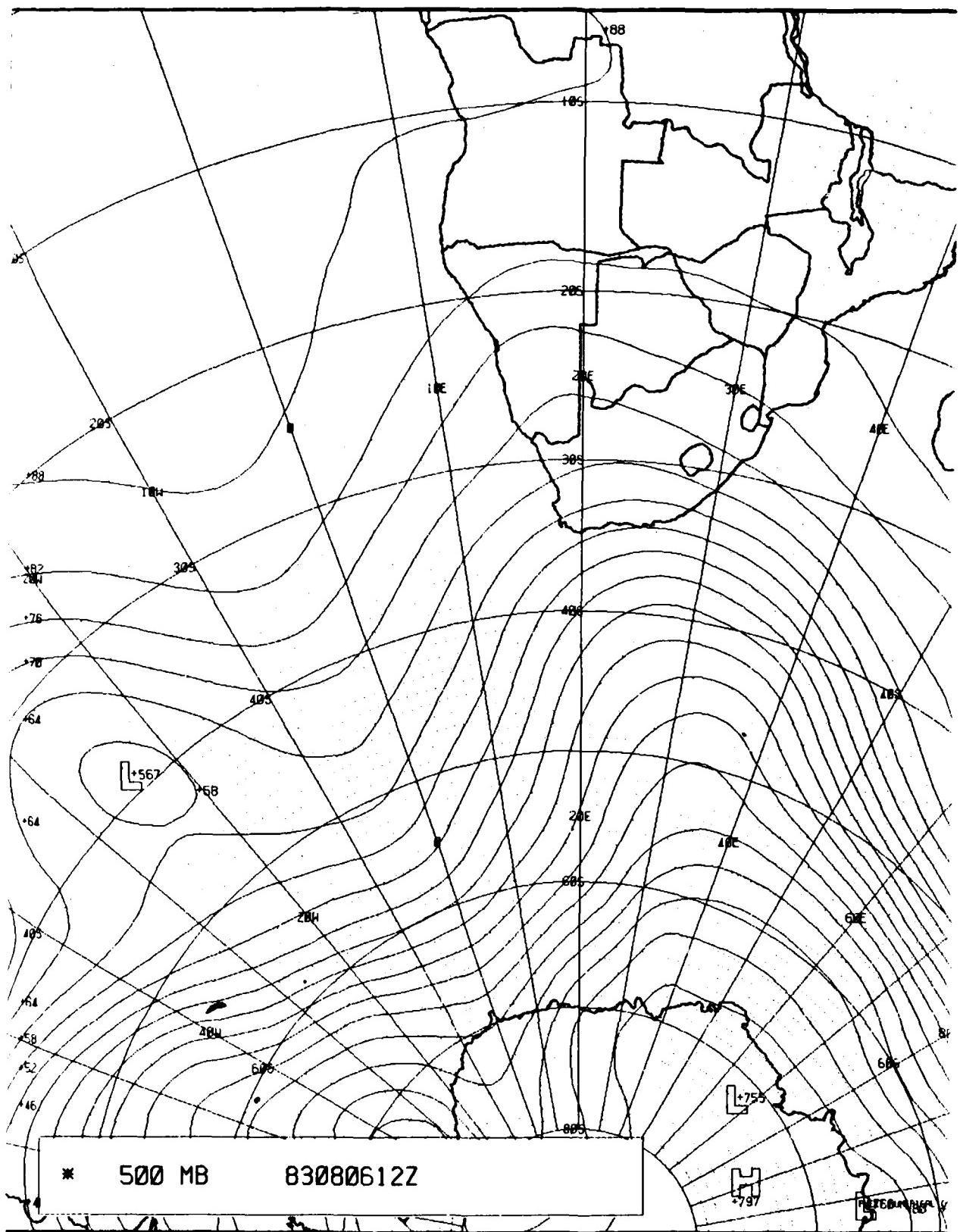
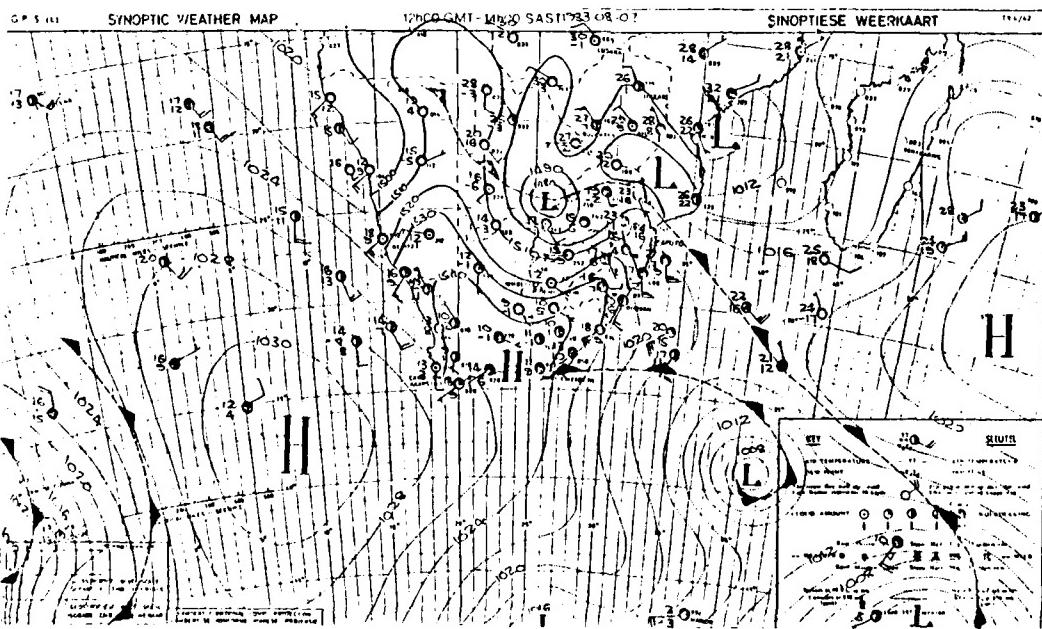
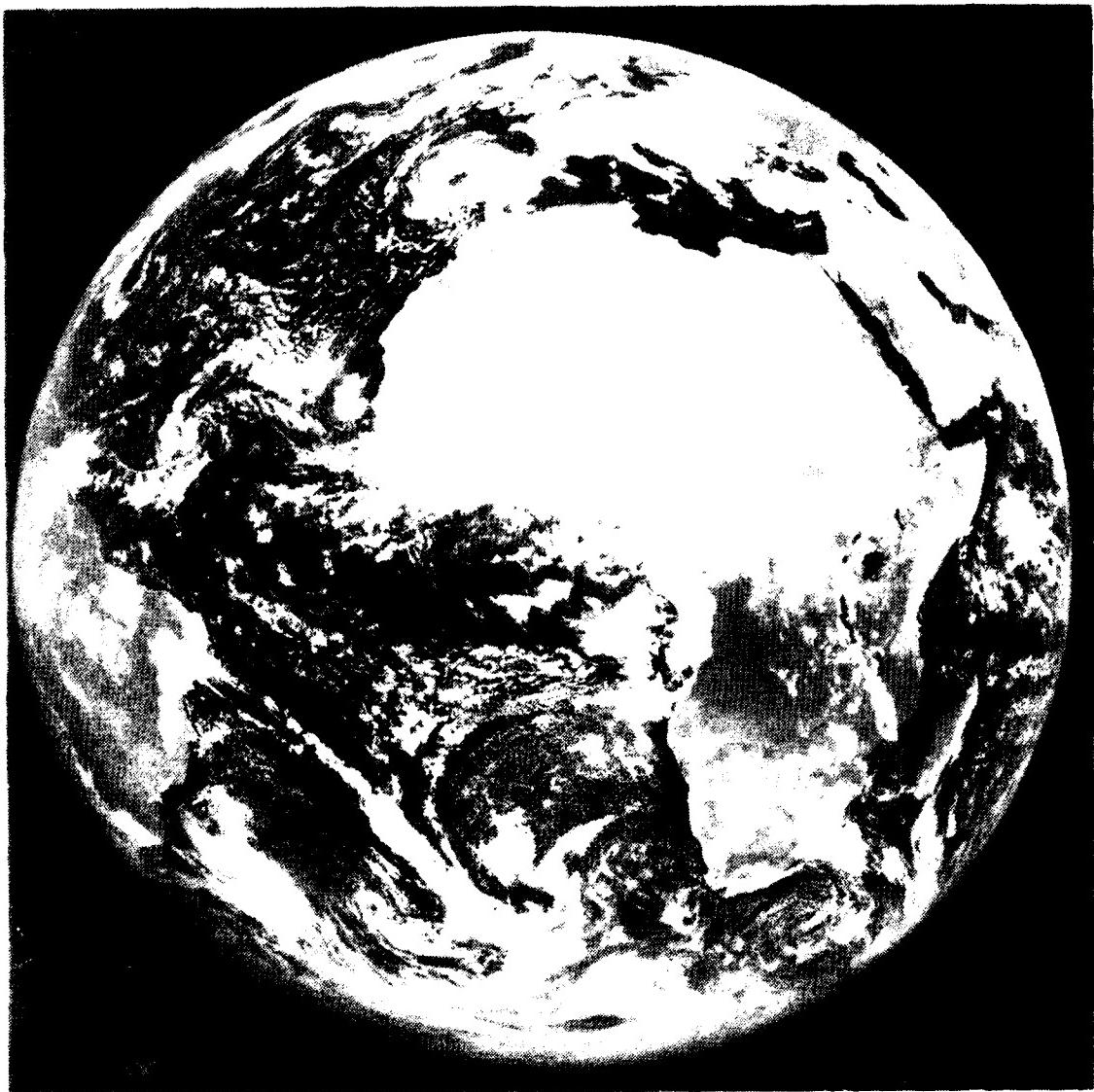


Fig. 6.98. FNOC 500 mb analysis (contours only), 1200 GMT on 6 August 1983

7 August 1983

The RSA analysis (Fig. 6.99), on the last day of this case study, shows an anticyclone dominating the Atlantic coast of RSA while a low, central pressure 1005 mb, is located at 39°S, 41°E, with an associated front extending northwestward to Port Elizabeth. This front has almost overtaken the front to the east which has moved very slowly during the past 24 hours. Fig. 6.100, the visible METEOSAT imagery, provides general support for the position of the vortex at 39°S, 41°E, whose position is also in good agreement with the FNOC surface analysis (Fig. 6.101), although the FNOC central pressure is 1012.5 mb compared to the RSA pressure of 1005 mb. The FNOC surface analysis depicts a (frontal) trough extending into southern Mozambique in agreement with the RSA analysis, as well as a hint of a weak trough back toward Port Elizabeth. Fig. 6.102, from DMSP (although taken during an orbit ~7.5 hours before the RSA surface analysis (Fig. 6.99)) sharply depicts the front extending toward southern Mozambique as well as the vortex associated with the secondary front. Note the shadows cast westward as the sun is rising. However, the ship plot (41°S, 19°E) on the FNOC surface analysis (Fig. 6.101) appears to have an erroneous wind direction (the 25-kt wind from the north should be southerly, i.e., Southern Hemisphere anticyclonic flow is counterclockwise). The same ship (International Code, UHCF) indicates an acceptable wind, 25 kt from the southwest, on the previous day (see Fig. 6.95).





**METEOSAT**

Fig. 6.100. Visible METEOSAT imagery, 1155 GMT on 7 August 1983

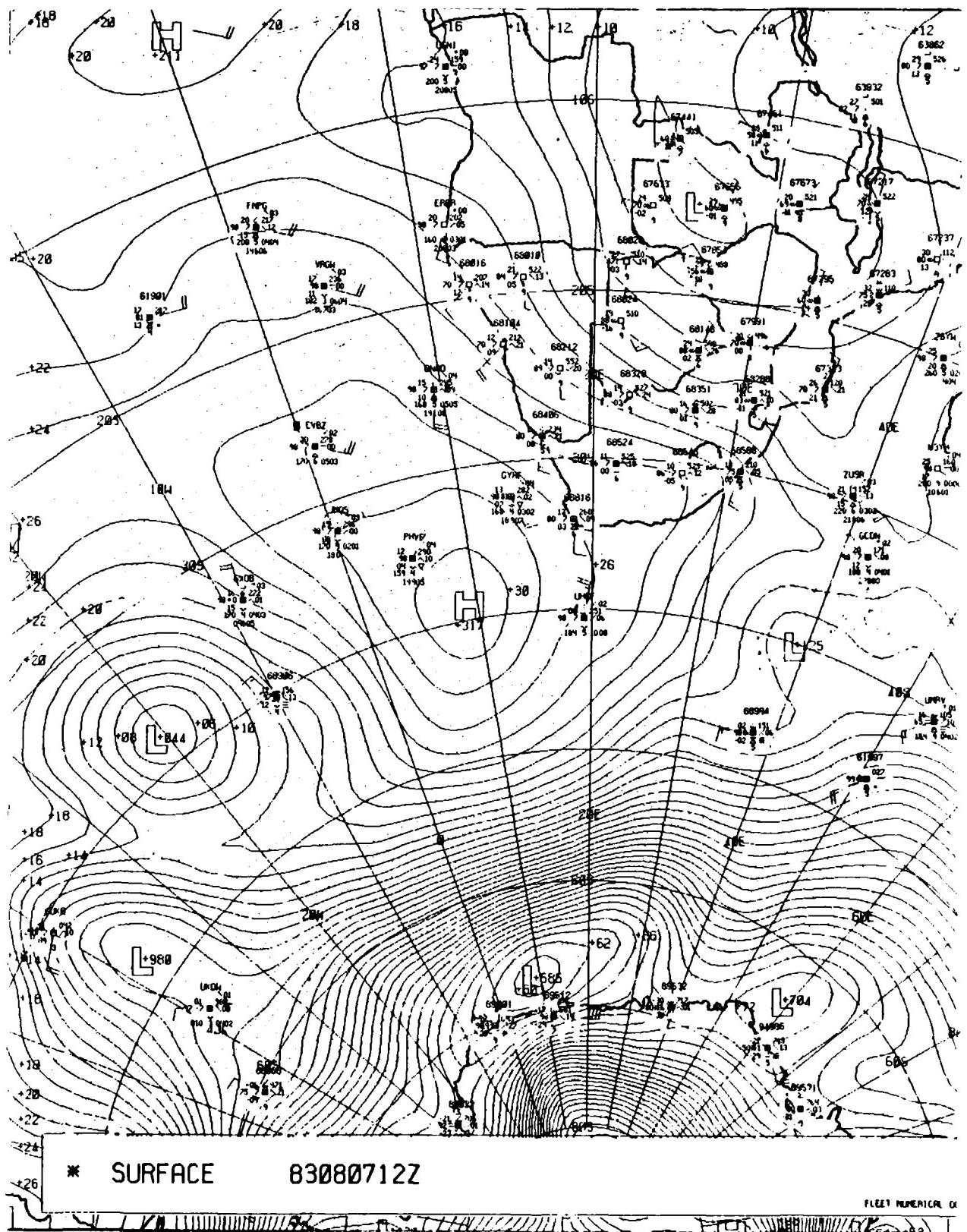


Fig. 6.101. FNOC sea-level pressure analysis, 1200 GMT on 7 August 1983

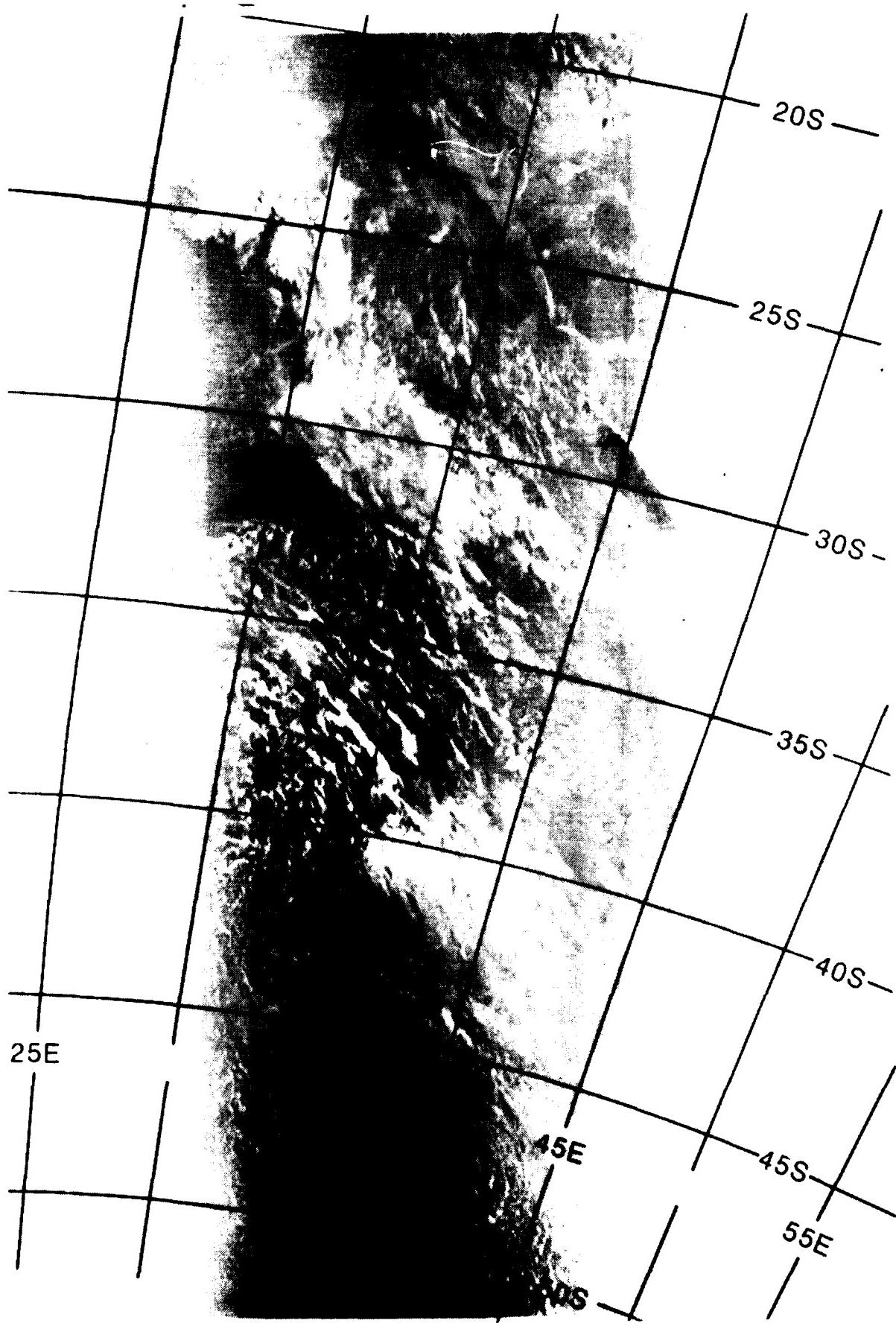
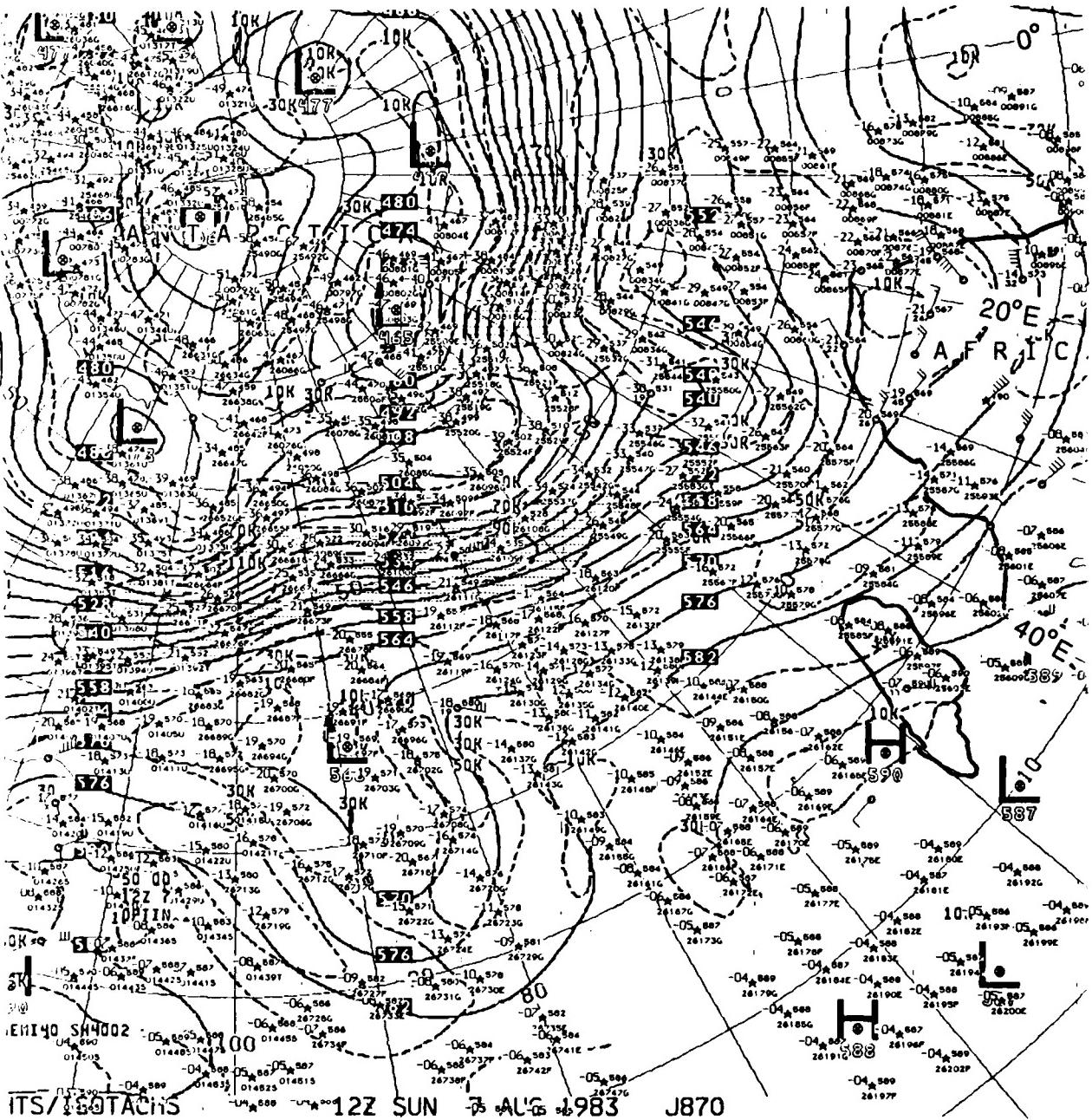


Fig. 6.102. DMSP visible imagery, 0423 GMT 7 August 1983

While the 500 mb analyses (Figs. 6.103 and 6.104) show similar synoptic scale patterns (i.e., a broad weak trough over the Southern African Continent and a short wave trough crossing 40°S near 35°E (NMC) and 39°E (FNOC)), it appears that the FNOC 500 mb trough position represents less westward tilt, with height, of the frontal zone.



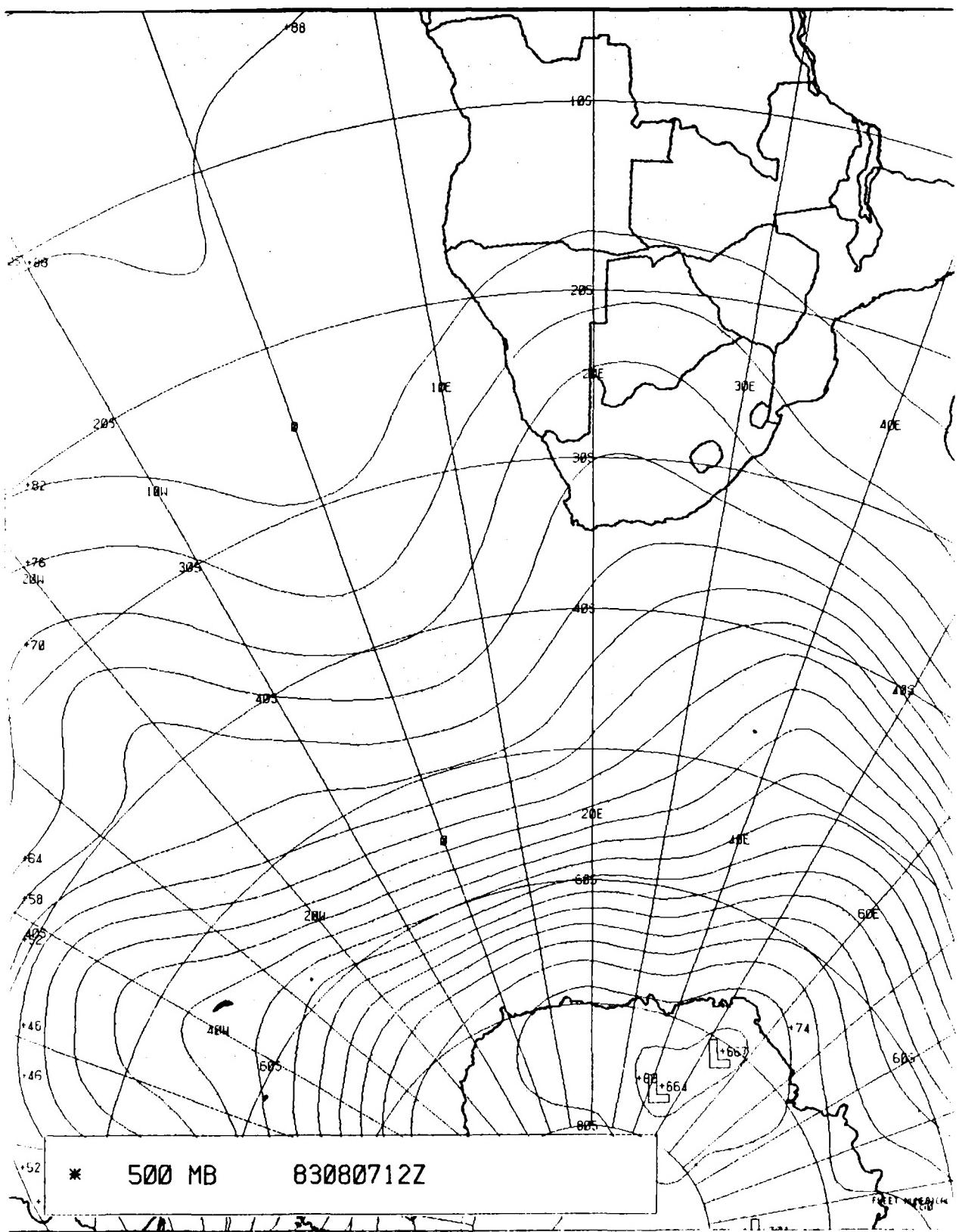


Fig. 6.104. FNOC 500 mb analysis (contours only), 1200 GMT on 7 August 1983

#### 6.4.5 Forecast Rules/Hints

1. The FNOC *global* analyses, while providing a good estimate of the location of surface troughs, often omit closed lows (vortices) within these troughs.
2. Satellite imagery must be used to determine the location of closed lows.
3. Satellite imagery is the best tool for locating cold fronts. Cold fronts predominate; warm fronts seldom exist.
4. Close scrutiny of satellite imagery will often permit early detection of forming vortices (low centers), especially within the cold air mass behind existing cold fronts. These incipient centers manifest themselves as enhanced convective clusters, often circular, on both visible and infrared satellite imagery.
5. While the movement of surface cyclones lies within a broad spectrum of speeds, the speed of movement of low centers can approach and even exceed 40 kt when the center lies beneath a strong 500-mb steering current ( $\geq 70$  kt).
6. The FNOC *global* 500-mb analyses depict large amplitude troughs, vertically consistent with (i.e., trailing) the associated surface fronts. However, the positions of newly forming short wave troughs are sometimes questionable.

(Blank)

## 6.5 AVERAGE OCEANIC WEATHER

### 6.5.1 Introduction

This subsection presents climatological data concerning the oceanic areas surrounding the South African Continent. While subsection 6.4 provided three case studies describing the daily migration of cyclones over the South Atlantic and southwest Indian Oceans during the austral winter, this subsection describes climatological winds, air and sea-surface temperature, etc. during the entire year. The information is from Atlases of Pilot Charts prepared by the United States Defense Mapping Agency.

### 6.5.2 Atlantic (Equator - 35°S and 15°W - West African Coast)

Weather over the subtropical Atlantic Ocean is dominated by the Southern Hemisphere subtropical anticyclone throughout the year. In the summer months (December - March), the ITCZ occasionally affects the northern South Atlantic Ocean with disturbed weather. During the period from May - October, Southern Hemisphere mid-latitude frontal systems influence the southern portions of the region (see subsection 6.4). These frontal systems and the low cloudiness and fog associated with the Benguela Current are the only significant synoptic-scale weather phenomena which affect the region.

#### a. Winds

Winds over most of the region are southeasterly throughout the year. The exception is found in the coastal area, from Angola northward where south and southwest winds dominate. The wind speeds vary from a low of 5-15 kt in February to May (higher near the axis of the Benguela Current) to a high of 10-20 kt in June to December. However, between 30°S and 35°S, west of 5°E, the wind is distributed more equally among directions, with components from the west predominant in the western section of the area. Here, the wind speeds vary from a low of 10-15 kt in January to May to a high of 10-30 kt in June to November (United States Defense Mapping Agency, 1981).

Gales, with winds equaling or exceeding 35 kt, are a significant problem (probability exceeding 5%) only in the area 30-35°S, especially 5-15°W during the months of May to October. In May and June, the frequency of occurrence exceeds 10% in at least part of the area specified, while gales are reported by 13-16% of the ships just poleward of the southern boundary (35°S) of this ocean area in June (Fig. 6.105). However, inadequate sampling likely leads to a low frequency bias in gale distributions described in this, as well as the other two, ocean areas.

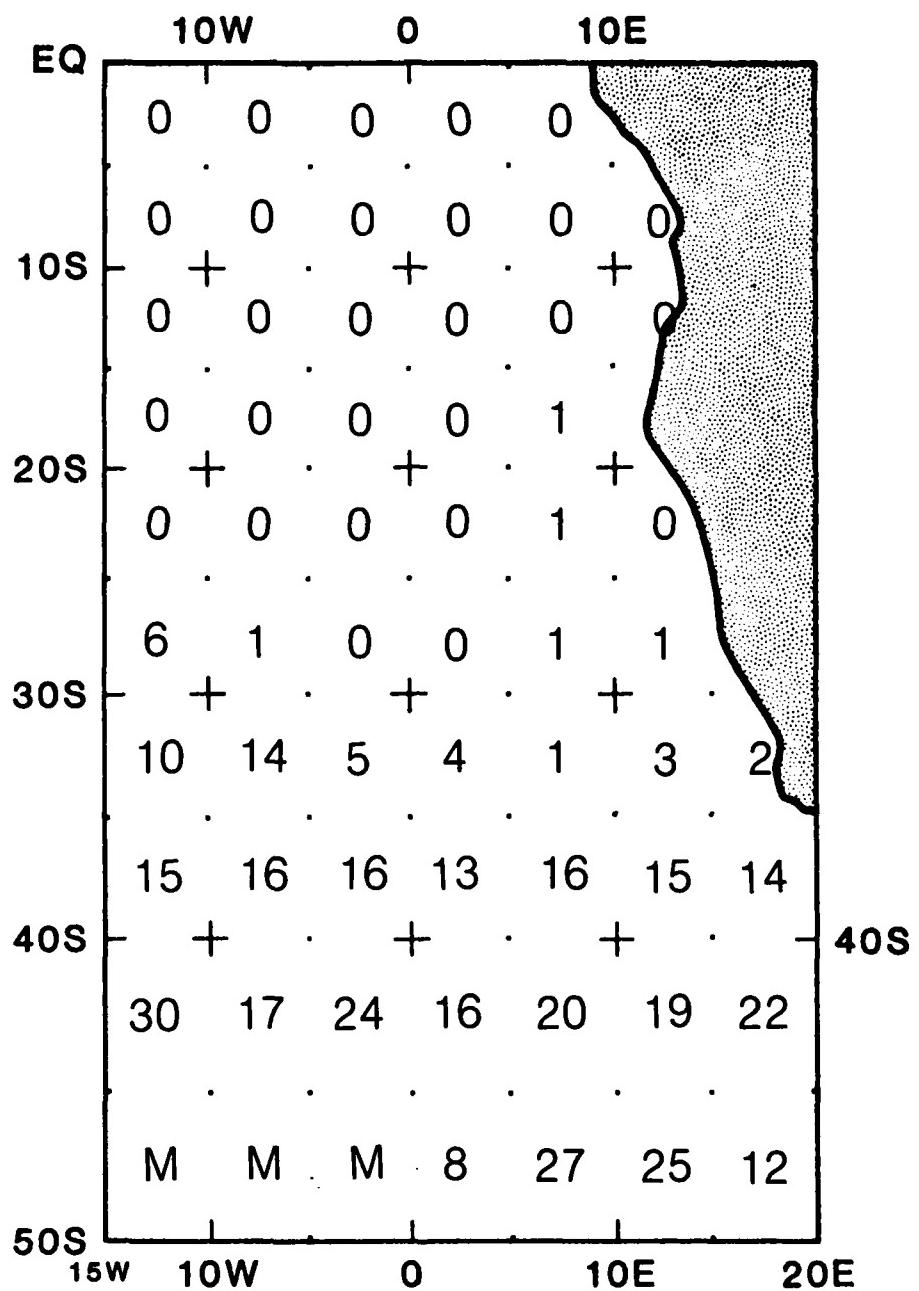


Fig. 6.105. Gales, June - Average percentage of ship reports with wind speed  $\geq 35$  kt. In areas where observation count is low, the gale frequency may be nonrepresentative. Where "0" is given, gales may have been recorded, but too infrequently to give a percentage value. "M" has been inserted in the three areas left blank in the reference document (United States Defense Mapping Agency, 1981).

### b. Temperature

Air and sea-surface temperatures are similar and vary slowly together according to season, with some exception. For example, in September the air temperatures range from 14°C near the coast south of 20°S, to 24°C near the Equator (Fig. 6.106). Due to upwelling the sea-surface temperature is as low as 12°C in September in the coastal area just cited. By March the air temperatures are 18°C near Cape Town increasing to 27°C near the Equator (Fig. 6.107), with sea-surface temperatures near the Namibian coast at only 18°C (not shown).

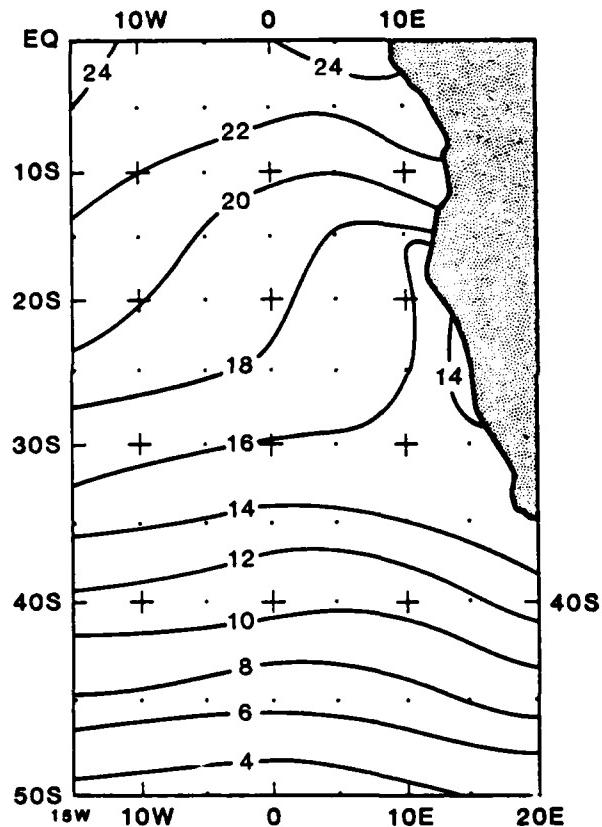


Fig. 6.106. Air Temperature, September - The mean air temperature ( $^{\circ}\text{C}$ ) is shown for every 2 degrees (United States Defense Mapping Agency, 1981).

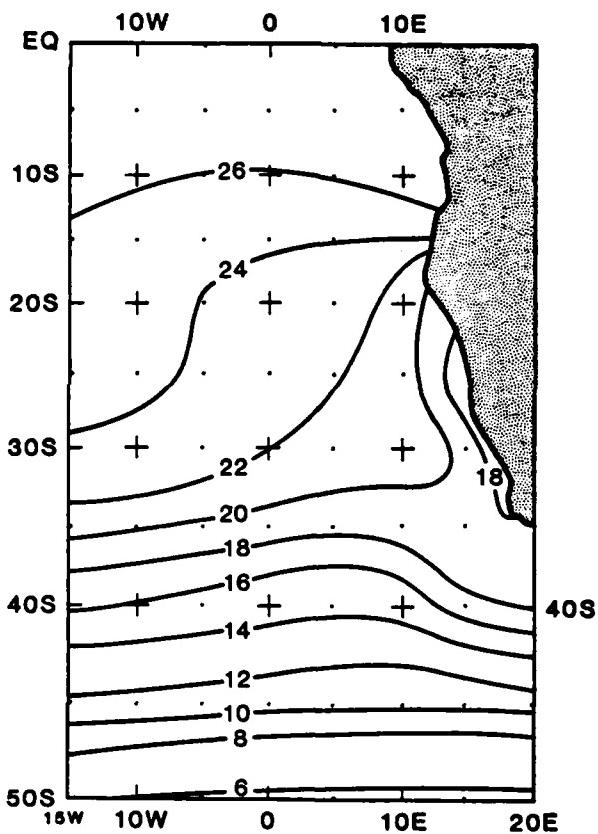


Fig. 6.107. Air Temperature, March - The mean air temperature ( $^{\circ}\text{C}$ ) is shown for every 2 degrees (United States Defense Mapping Agency, 1981).

### c. Coastal fog

Fog and low stratus occurs often over the Namibian coastal waters and over the waters off the southwest and south RSA coasts. Figs. 2.21 through 2.24 shows the percentage frequency of occurrence of fog over the Southern African coastal waters (see discussion in subsection 2.3.1). While Fig. 2.23 indicates a *maximum* frequency of fog occurrence along the Namibian coast during January (austral summer), to the contrary, Fig. 1.15 A indicates a *minimum* of cloudiness west of Namibia during the austral summer.

### d. Wave Heights

Increased wave heights will accompany migratory cyclones in the poleward portion of the South Atlantic Ocean area (see subsection 6.4). However, for planning purposes, Fig. 6.108 depicts the average frequency of wave height equal to or greater than 12 feet during August (United States Defense Mapping Agency, 1981). A similar equatorward extension of the 20% isopleth exists for the months of June, November, January and March in association with the Benguela Current, described in subsection 7.6.

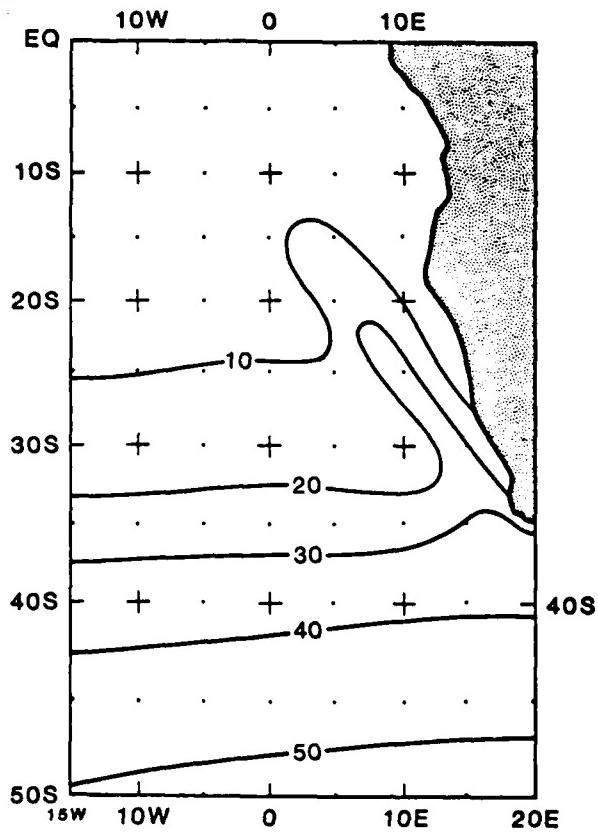


Fig. 6.108. Frequency of Wave Height, August - Percentage frequency of wave height  $\geq 12$  feet. When both sea and swell were reported, the higher value was used in the reference document (United States Defense Mapping Agency, 1981).

### 6.5.3 Atlantic & Indian Oceans ( $35^{\circ}\text{S}$ - $50^{\circ}\text{S}$ and $15^{\circ}\text{W}$ - $60^{\circ}\text{E}$ )

The subject South Atlantic and Indian Ocean areas are subject to significant risk of gale winds and heavy weather throughout the year. Migratory anticyclones and mid-latitude frontal low centers dominate the weather all months (see subsection 6.4). Such systems are most intense and travel farthest north through the area during the austral winter (June - September). Glaciated ice may extend into this area even to within a hundred miles of the RSA coast, especially in late winter.

#### a. Winds

##### (1). Atlantic Ocean, $15^{\circ}\text{W}$ to $20^{\circ}\text{E}$

In the area  $35^{\circ}\text{S}$  -  $50^{\circ}\text{S}$ , winds predominate from westerly directions with coastal summer season directions favoring south and southwest. Speeds average 10-30 kt south of  $35^{\circ}\text{S}$ , the area of the famous roaring forties, except in summer when winds 5-15 kt are favored in the  $35\text{-}40^{\circ}\text{S}$  belt. Gales (wind speed 35 kt or higher) are a hazard all year in the area. Summer season frequencies of gale occurrence near the coast are approximately 5% rising to 15-25% in the southwest section of the South Atlantic Ocean area; while winter figures for the same area range from ~15% near the RSA coast to 30% in the western portion of the area (see Fig. 6.105). Other months yield transitional values of frequency, however, the five-degree square in the SW corner (near  $50^{\circ}\text{S}$ ,  $15^{\circ}\text{W}$ ) records a maximum of 57% of ships reporting gale force wind during August (not shown) (United States Mapping Agency, 1981).

##### (2). Indian Ocean, $20^{\circ}\text{E}$ to $60^{\circ}\text{E}$

The roaring forties have their best manifestation on the Indian Ocean side of this latitude belt. Wind speeds generally average 10-30 kt, with lightest values in December. Prevailing directions are consistent one month to another, with the NW quadrant predominant, although SW wind directions are a close second. The percentage of SW components generally increases toward the eastern section of the area. Gales are a problem every month of the year, with frequency of occurrence generally increasing southward over the area and maximizing both at extreme west (directly south of the RSA) and east longitudes. Least likelihood of gales occurs in the period November through April, with probabilities ranging from 5% to 15-20% in the area noted above. Gales in other months are more hazardous, maximizing in the period May through July, when probabilities range from 10-15% to <30% (Fig. 6.109). However note that there is one square, south of Port Elizabeth with 42% gale reports. (United States Defense Mapping Agency, 1979).

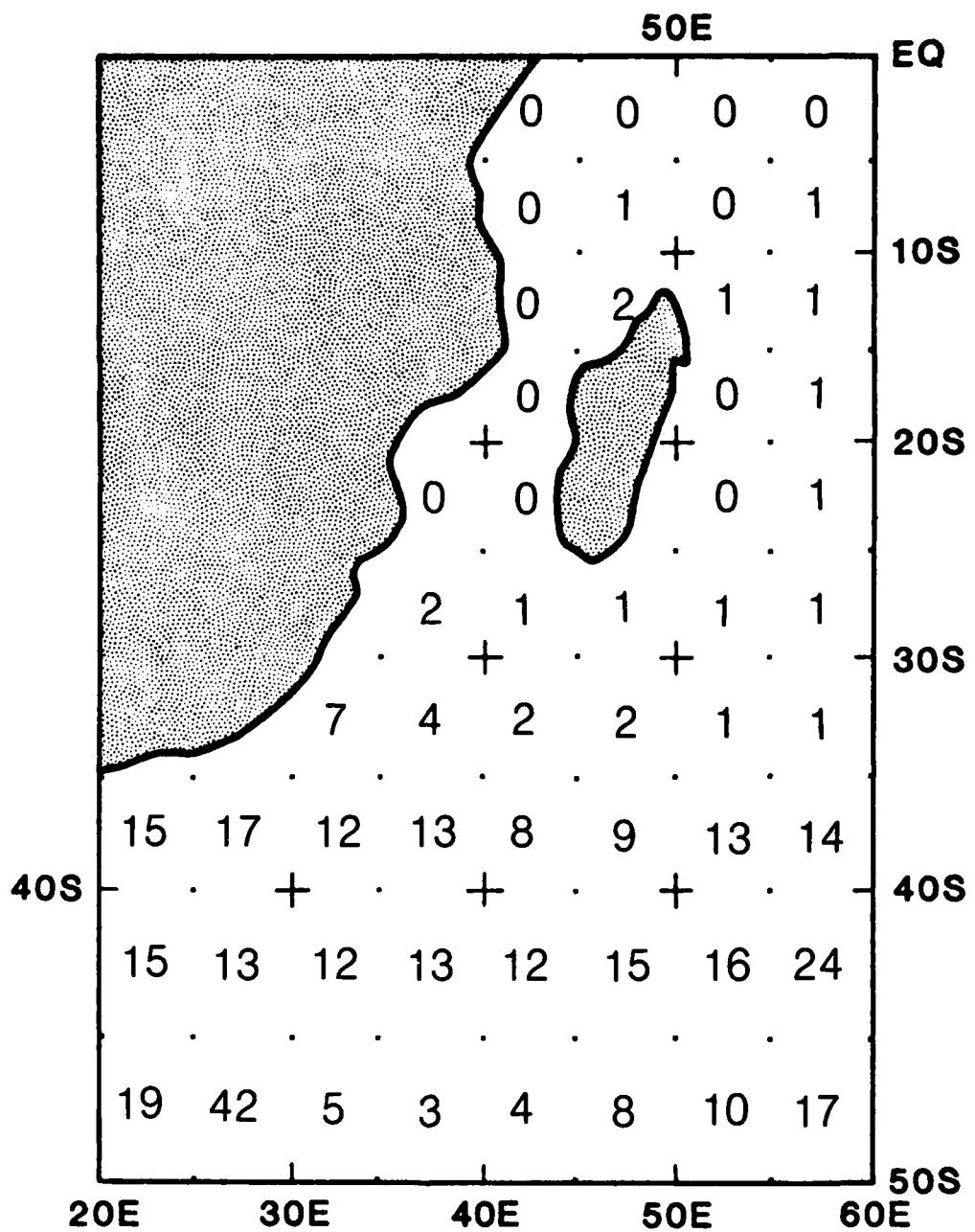


Fig. 6.109. Gales, July - Average percentage of ship reports with wind speed  $\geq 35$  kt. In areas where observation count is low, the gale frequency may be nonrepresentative. Where "0" is given, gales may have been recorded, but too infrequently to give a percentage value. (United States Defense Mapping Agency, 1979)

b. Temperature

(1). Atlantic Ocean, 15°W to 20°E

The mean air and sea-surface temperature patterns are quite similar from one month to another. Zonal orientation of isotherms is the best description. Winter air temperatures range from near 3°C at 50°S, to 15°C near the coast of RSA (Fig. 6.110) with summer values 2°C higher near 50°S to 6°C higher near the RSA coast. Sea-surface temperatures are generally within a degree of the air temperature value (United States Defense Mapping Agency, 1981).

(2). Indian Ocean, 20°E to 60°E

Like the South Atlantic area in this latitude belt, temperatures change slowly month to month. Isotherm orientation is generally east/west, except near RSA due to the south-flowing warm Agulhas Current, where both air and sea-surface temperatures bulge poleward. Air temperature minima occur in the August/September period, ranging from 18°C near the coast at 35°S, to 3°C near 50°S (Fig. 6.111). For sea-surface temperatures, these numbers become 19.5°C and 3°C (not shown). The season peaks in February with an air temperature range 6°C-23°C, while sea-surface temperatures range 4°C-23.5°C (United States Defense Mapping Agency, 1979).

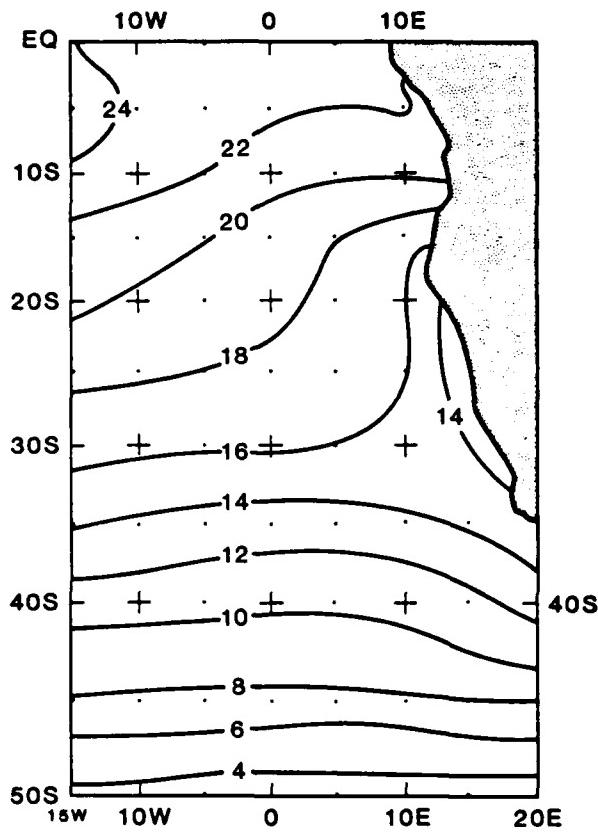


Fig. 6.110. Air Temperature, August - The mean air temperature ( $^{\circ}\text{C}$ ) is shown for every 2 degrees (United States Defense Mapping Agency, 1981).

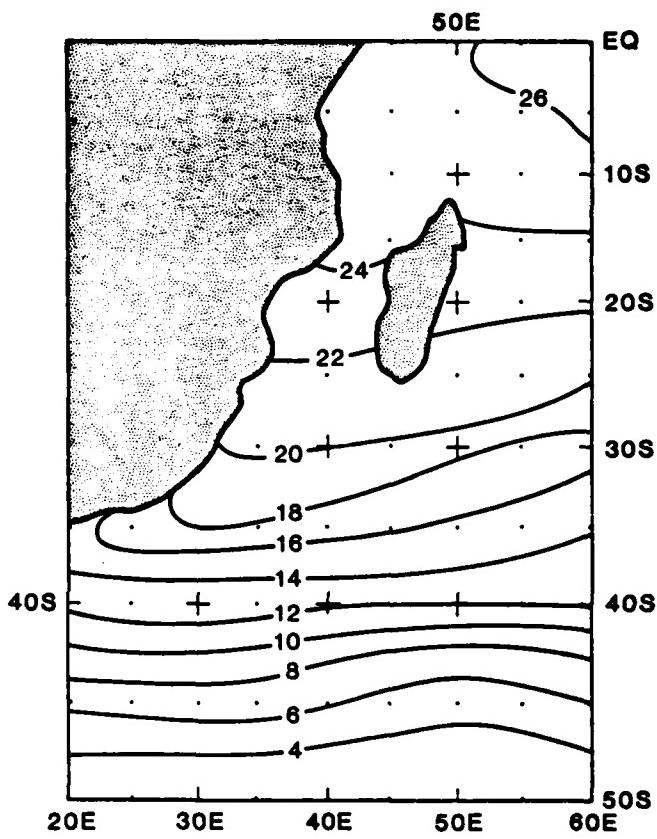


Fig. 6.111. Air Temperature, August - The mean air temperature ( $^{\circ}\text{C}$ ) is shown for every 2 degrees (United States Defense Mapping Agency, 1979).

### c. Wave Heights

Increased wave height will accompany migratory cyclones described in the case studies of subsection 6.4. However, for planning purposes, Fig. 6.112 (with Fig. 6.108) depicts the average frequency of wave height equal to or greater than 12 feet during the winter (August).

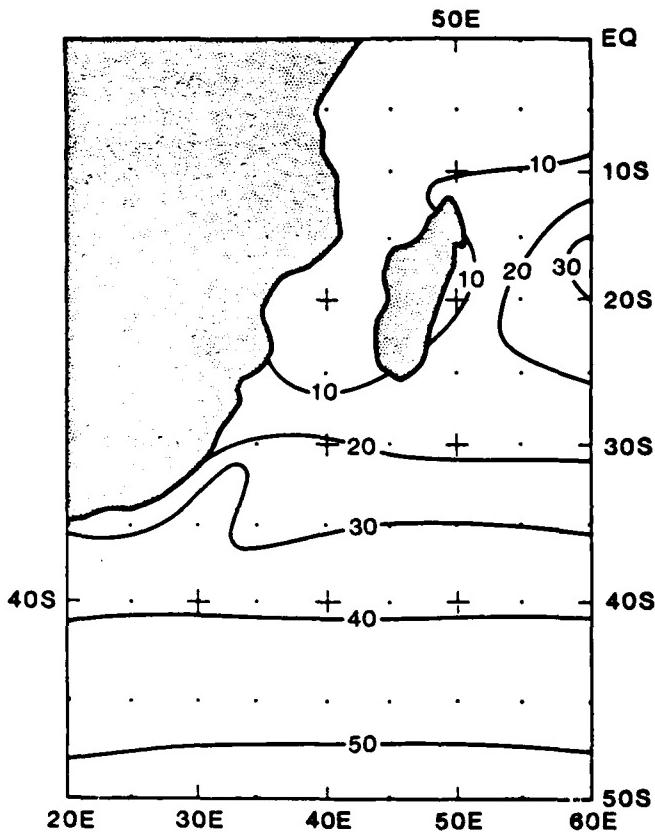


Fig. 6.112. Frequency of Wave Height, August - Percentage frequency of wave height  $\geq 12$  feet. When both sea and swell were reported, the higher value was used in the reference document (United States Defense Mapping Agency, 1979).

#### 6.5.4 Indian Ocean (Equator - 35°S and 20°E - 60°E)

Weather over this portion of the south Indian Ocean fluctuates significantly between winter and summer months. The subtropical high migrates northward and intensifies in the winter months. Southeasterly trades are strongest in winter. Deep low centers and associated fronts track farther north (equatorward) and are more intense in winter than in summer.

##### a. Winter (May-October)

###### (1). Winds

During the winter period, the belt of southeasterlies extends from near the equator to approximately 28°S, just poleward of the Malagasy Republic. Average winds in the area are typically 10-20 kt. Other than the changes affected by migrating systems, exceptions are few. For example, wind directions off the coast of RSA are predominantly parallel to the coastline, i.e., northeasterly or southwesterly, while variable wind directions are found in the area south and southwest of the Malagasy Republic. Other exceptions are easterly winds in the area east of the Malagasy Republic, while in May through August southerly winds dominate near the equator in the northwest corner of this ocean area.

The frequency of gale force winds ( $\geq 35$  kt) is largest along the southern boundary of the area where, in July, the frequency of gales is ~7% at the coast of RSA diminishing along the southern boundary of the area to ~1% at the southeast corner near 35°S, 60°E (see Fig. 6.109). A 10% gale frequency is found in the five-degree area south of the Malagasy Republic near 35°S in June, whereas in the area north of the Malagasy Republic gales are possible, but generally are too infrequent to provide reliable climatology (United States Defense Mapping Agency, 1979).

###### (2). Temperature

Air and sea-surface temperature are similar and vary slowly together according to season, with some exception. For example, the average air temperature southeast of the Malagasy Republic, near 35°S, 60°E, decreases from 16°C in May to 14°C in August (see Fig. 6.111), while the average air temperature near the RSA coastline decreases from a May value of 20°C to 18°C in August (see Fig. 6.111). North of the Malagasy Republic near the equator, the average air temperature cools from 28°C to 26°C by August. Sea-surface temperatures are similar to air temperatures although normally 1-2°C warmer in the area southeast of the Malagasy Republic (United States Defense Mapping Agency, 1979).

##### b. Summer (November-April)

Southeasterly trade wind flow is weaker in the summer period. The south Indian Ocean anticyclone moves south and weakens, and the north-south extent of the southeasterlies shrinks. Northwesterly flow

often penetrates over the waters north and northwest of the Malagasy Republic. This flow is likely when the Arabian anticyclone builds and ridges southward. Frontal lows continue to affect the southwest Indian Ocean but the low centers are weaker than those of the winter period.

### (1). Winds

The dominance of the southeasterly flow is broken as the Northern Hemisphere northeast monsoon brings predominantly north or northeast flow, 10-15 kt, to the equatorial waters off Kenya from December through March. Northerly flow also dominates in the northern Mozambique Channel from December through February, except during incursions of tropical cyclones (see subsections 4.1 and 4.2). Easterly flow, 15-20 kt, dominates in the southwestern portion of this ocean area except immediately adjacent to RSA where the wind remains predominantly parallel to the coast, i.e., northeasterly or southwesterly 15-20 kt. The eastern portion of this ocean area experiences mostly easterly components except from December through March in the northeast portion where winds are frequently north-northwesterly 5-20 kt (United States Defense Mapping Agency, 1979).

As in winter, the frequency of gale reports is largest along 35°S bordering the roaring forties, but smaller than during winter months. Gale frequencies of slightly over 5% off the coast of RSA diminish to less than 5% during the January-March period, while the frequency of gales in the southeastern corner of the area, near 35°S, 60°E, is even smaller. Also, as in winter, gales are generally too infrequent north of the Malagasy Republic to provide reliable statistics although the area east of the Malagasy Republic experiences nearly a 5% gale frequency during the month of February (United States Defense Mapping Agency, 1979). Of course, this minimal frequency of gale reports from shipping must not prevent the forecaster from being alert for tropical cyclones during the austral summer.

### (2). Temperature

As during the winter, this ocean area spanning from the tropics to the poleward boundary of the subtropics experiences slowly-varying and similar air and sea-surface temperatures. On the southern (poleward) boundary, November mean air temperatures of 20°C along the RSA coastline and 15°C near 35°S, 60°E, warm to 24°C and 20°C respectively by February. The equatorial mean air temperature returns to 28°C by January. The sea-surface temperature generally matches the air temperature but, as during the winter, sea-surface temperature is 1-2°C warmer than the air temperature to the southeast of the Malagasy Republic (United States Defense Mapping Agency, 1979).

### c. Wave Heights

Increased wave height will accompany tropical cyclones (see subsections 4.1 and 4.2) from November through May. They will also accompany migratory cyclones (see subsection 6.4) in the poleward portion of this ocean area, with especially hazardous wave heights present during Cape Roller episodes off the southeast coast of RSA (see sub-

sections 6.3 and 7.4). Additionally, increased wave height will accompany the low-level southeasterly jet, equatorward (north) of the Malagasy Republic (see paragraph 3.2.1.d.(1)), although the major effect of the low-level jet, on wave height, is felt in the Northern Hemisphere off Somalia. For planning purposes, see Fig. 6.112 which depicts the average frequency of wave height equal to or greater than 12 feet during the winter (August) (United States Defense Mapping Agency, 1979).

## Section 7

### COASTAL OCEANOGRAPHIC INFLUENCES

#### 7.1 INTRODUCTION

Attention will be focused on the nearshore ocean areas of the Southern African Continent, extending from 5°N to 35°S latitude. The primary interest is in describing those ocean features which may influence the dynamic character of weather disturbances.

The continental shelf and slope are indicated along the African Continent by the location of the 2,000-fathom contour in Figure 7.1 (U. S. Naval Oceanographic Office, 1968). The 2000-fathom curve lies close to Somalia (eastern equatorial Africa), spreads away from the coastline in the vicinity of Kenya and Tanzania, and encompasses the island of the Malagasy Republic. An underwater southward extension occurs from the Malagasy Republic, which may provide some explanation for the behavior of current patterns there.

The 2000-fathom curve encompasses one basin to the southwest of the Malagasy Republic (the Madagascar Basin), and the contour is irregular to the southeast of the continent. Then toward the south of the continent there is the Agulhas Plateau, which appears to participate in the directing of the Agulhas Current termination and retroflection (i.e., its turning toward the east, south of the continent).

Along the Atlantic side of Africa, the 2000-fathom contour extends further from the continental landmass at Capetown up to the juncture with the undersea Walvis Ridge at about 25°S, although there has been progressive narrowing of the shelf/slope from the south to this point. Northward, the shelf/slope widens to a slightly greater width at the equator. The Atlantic side off Africa shows a narrower continental shelf/slope than does the Indian Ocean side in the southern hemisphere.

The ocean circulation adjacent to the African continent in the southern hemisphere depends on a variety of influences. Ocean-wide circulation patterns, resulting from a time-integration of windstress, ocean density fields and Coriolis effects, provide the general characteristics for several of the currents which approach the African continent. Thus the Agulhas Current along the southeastern African coastline has the general character of a *western boundary* current, which it indeed represents in the south Indian Ocean. Characteristics of western boundary currents, as well as for other major current types, are listed in table 7.1 from Gross (1982). The Benguela Current along southwestern Africa is the *eastern boundary* current in the South Atlantic Ocean. At several degrees of latitude south of the Cape of Good Hope the northern boundary of the West Wind Drift ocean circulation is encountered as it moves around Antarctica in response to the westerlies in the southern hemisphere storm belt of middle latitudes.

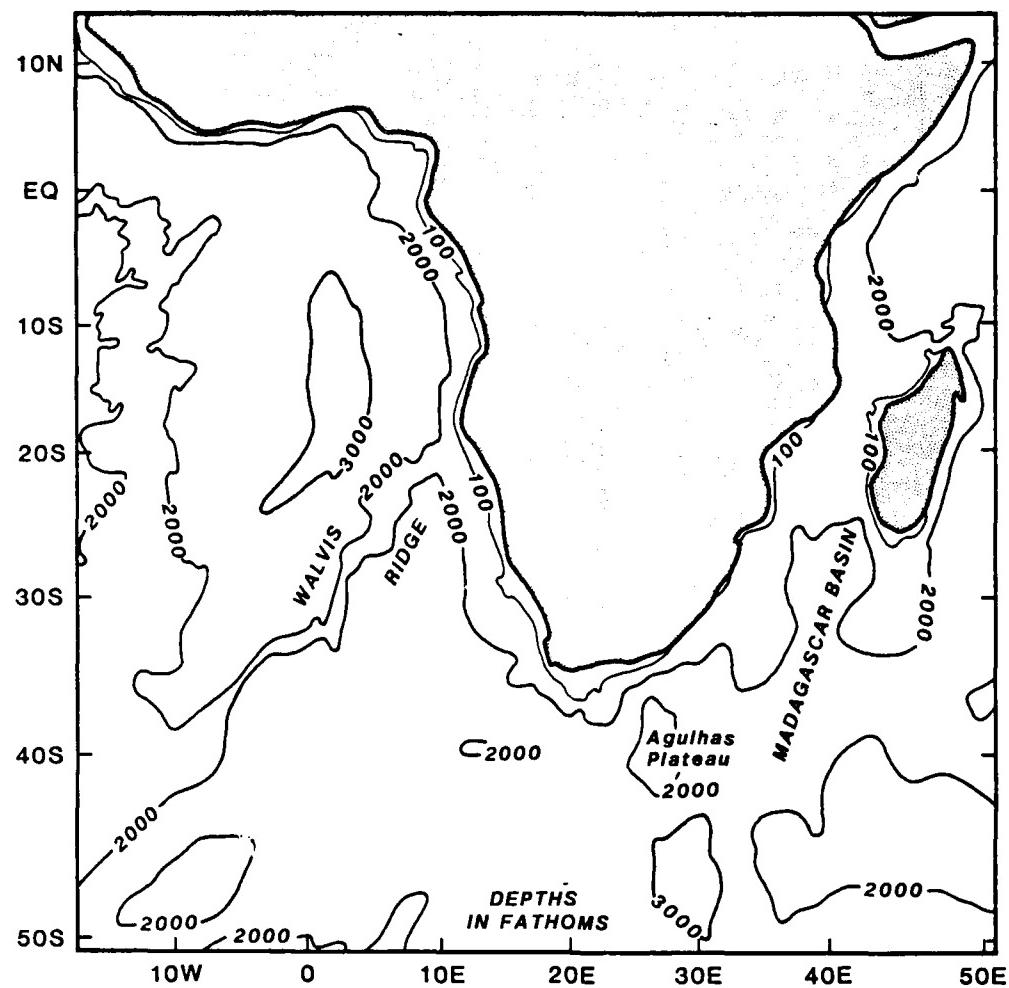


Fig. 7.1. Southern portion of the African continent and adjacent ocean areas; the 100-fathom and 2000-fathom contours below sea level are indicated. (After U. S. Naval Oceanographic Office, 1968)

There are additional influences imposed on these broad general flows which are regional in nature. *Coastal character* and *bottom topography* provide forcing to localize upwelling centers or to turn the currents away from the upstream direction. The *seasonal reversal in wind direction* (and strength) over equatorial and northern hemisphere areas of the Indian Ocean (*Monsoon influence*) has consequences far downstream for the ocean circulation along the southeastern African coasts.

Finally, there are influences from relatively small areas along the shore which may assume overwhelming importance in extreme cases. The interaction between ocean current and storm-waves can destroy

TABLE 7.1  
COMPARISON OF BOUNDARY CURRENT SYSTEMS (Gross, 1982)

TYPE OF CURRENT (example)	GENERAL FEATURES	SPEED	TRANSPORT (millions of cubic meters per second)	SPECIAL FEATURES
Eastern boundary currents	Broad, ~1000 km Shallow, ≤ 500 m	Slow, tens of km per day	Small, typically 10 - 15	Diffuse boundaries separating from coastal currents Coastal upwelling common Waters derived from West Wind Drift
California Current Canaries Current				
Western boundary currents	Narrow, ≤ 100 km Deep - substantial transport to depths of 2 km	Swift, hundreds of km per day	Large, usually 50 or greater	Sharp boundary with coastal circulation system Little or no coastal upwelling: waters tend to be depleted in nutrients, unproductive Waters derived from Trade Wind belts
Gulf Stream Kuroshio				

ships under certain conditions along the southeastern African coastal area. The location and synoptic conditions for this destructive situation will be described in detail in a later subsection.

Temperature of the ocean adjacent to the African continent varies during the year as indicated in Figures 7.2-7.5 from Tchernia (1980a) for the months of February, May, August and November.

For the Indian Ocean, the thermal equator intersects Africa about 10°S in February; moves to 12°N in May; returns to 3°S in August and to 6°S in November. Temperatures are greatest in February (>28°C) along the thermal equator and are elevated correspondingly (by some 4°C) in the southern hemisphere along Africa compared to the cooler temperatures observed in August.

On the Atlantic Ocean side, cool temperatures occur along the African coast associated with upwelling inshore from the Benguela Current. Temperatures in the upwelling region vary seasonally, reaching extremes less than 15°C during February-August, temperatures are some 3-5°C higher in November. The northern extent of the strong upwelling migrates as well; it reaches about 23°S in February, 18°S in May, 14°S in August and 22°S in November. The southern boundary of upwelling is near Cape Town the year round.

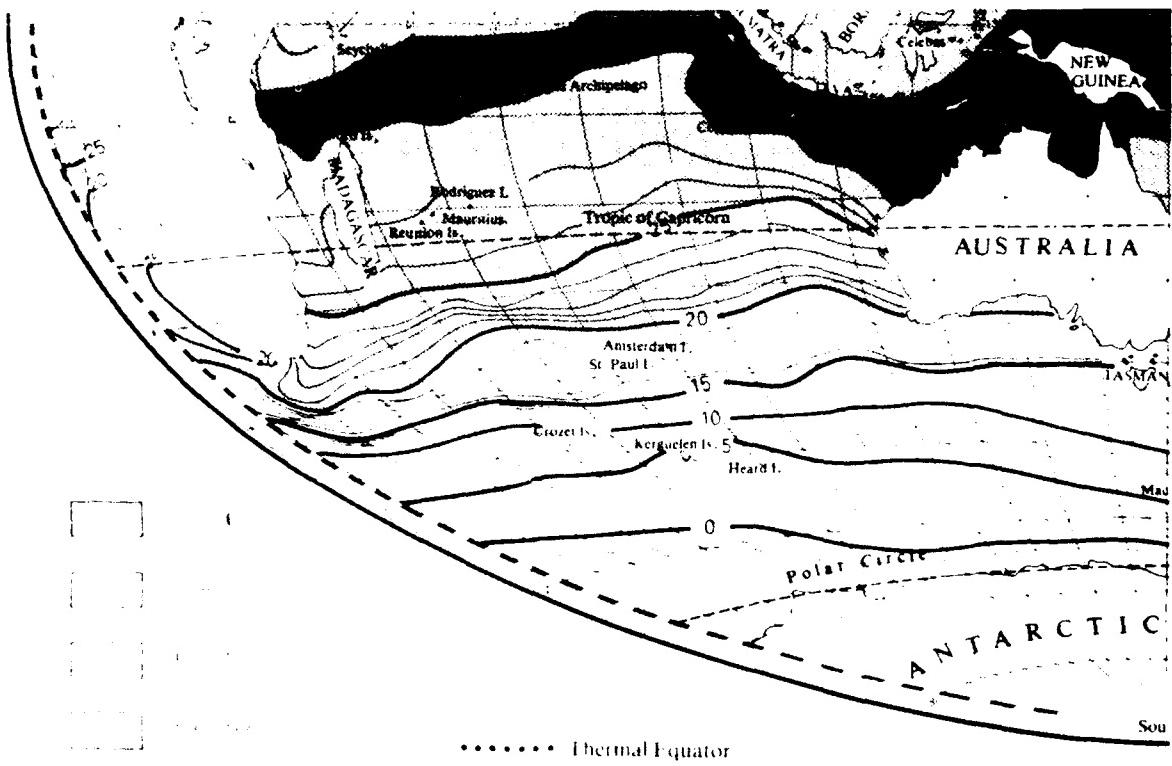


Fig. 7.2. Distribution of Surface Isotherms, February (Tchernia, 1980a, Plate 15)

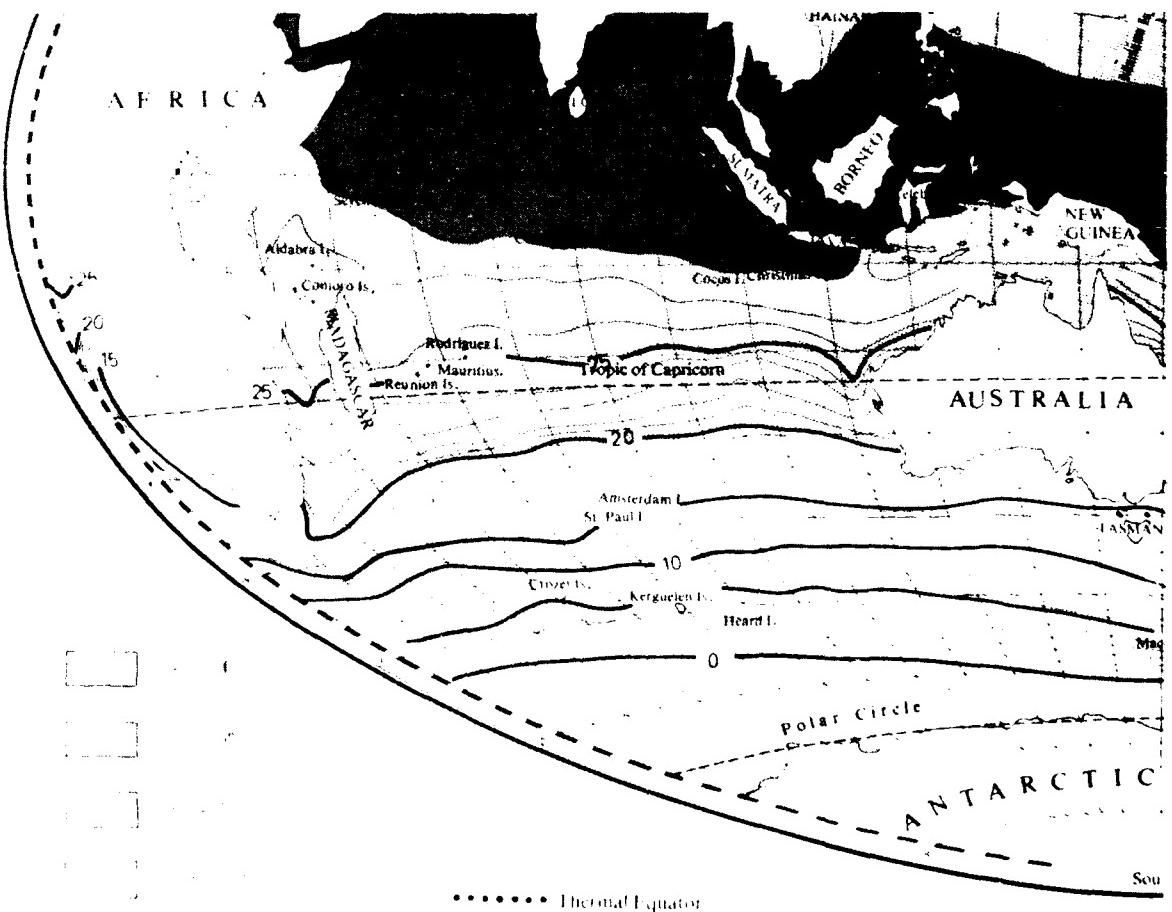


Fig. 7.3. Distribution of Surface Isotherms, May (Tchernia, 1980a, Plate 16)

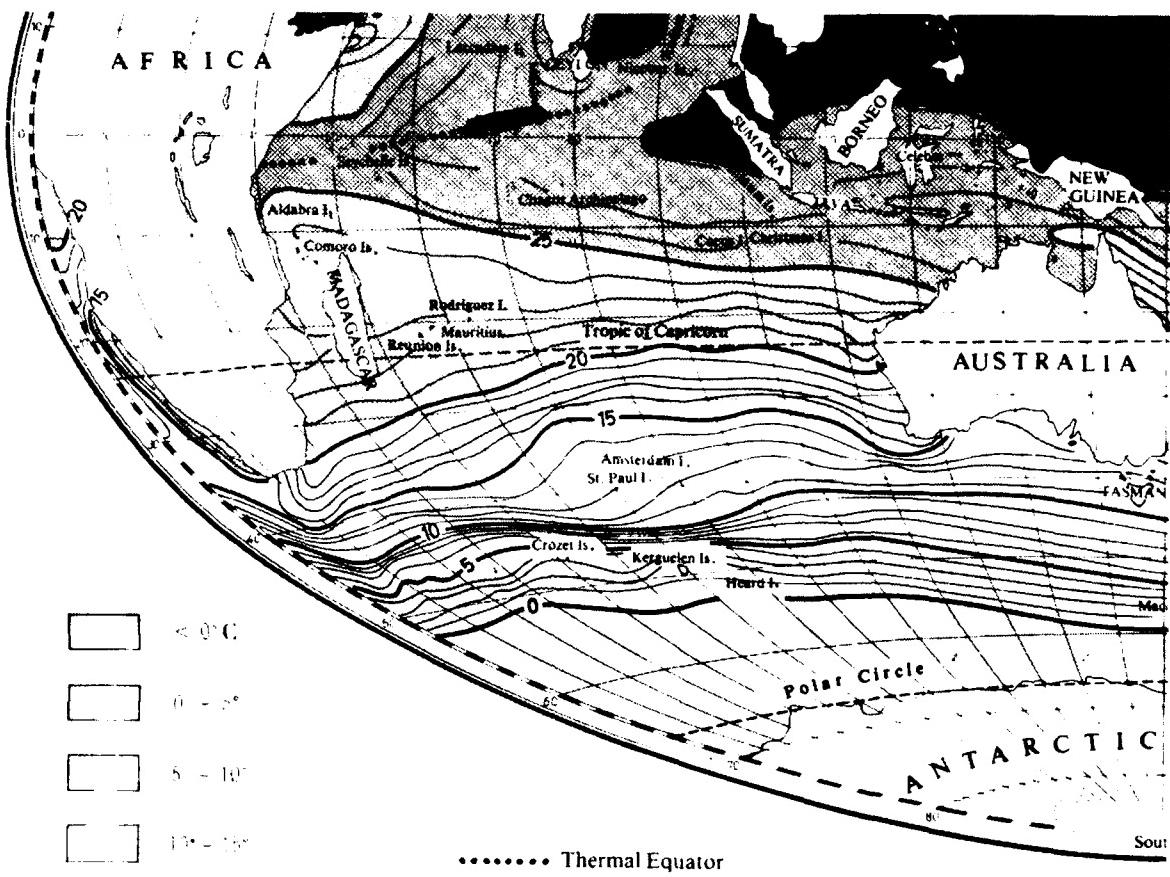


Fig. 7.4. Distribution of Surface Isotherms, August (Tchernia, 1980a, Plate 17)

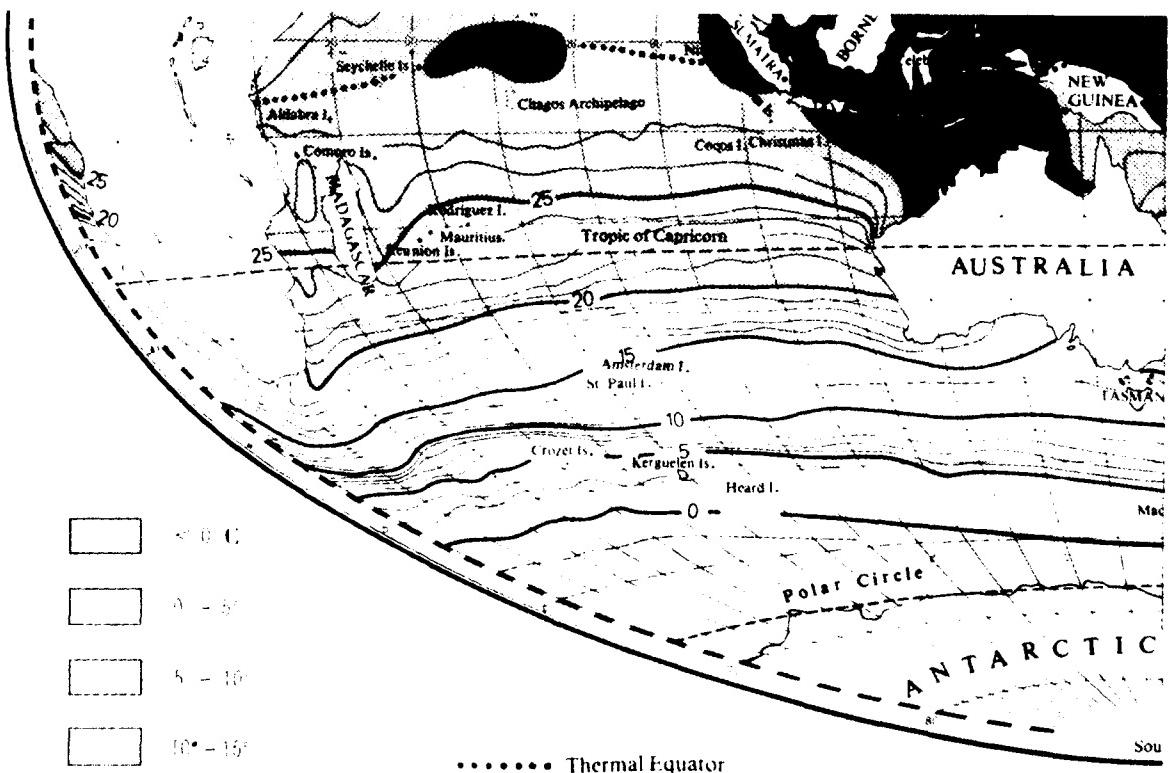


Fig. 7.5. Distribution of Surface Isotherms, November (Tchernia, 1980a, Plate 18)

Salinities at the sea surface undergo seasonal variation along the Indian Ocean coast of Africa, north of 10°S. The salinities there become less than 35‰ in northern hemisphere summer, associated with the southwest monsoon and upwelling along the equatorial Somalia coast. In northern winter, the salinities north of 10°S are higher, reaching almost 36‰ along the coast from 10°S-28°S, with offshore salinities there from 35.0-35.5‰ (see Fig. 7.6 from Tchernia (1980a)).

On the Atlantic Ocean side, salinities less than 35.0‰ occur inshore from the Benguela Current, associated with the upwelling regions along the southern hemisphere Atlantic coastline of Africa.

It seems appropriate to start in the western Indian Ocean for the more detailed coverage of nearshore ocean conditions adjacent to southern hemisphere Africa; the equatorial area there is strongly responsive to the Indian Ocean Monsoon. The seasonal reversal of wind direction of the monsoon has its influence felt most strongly in the *northern* hemisphere of the western Indian Ocean. As suggested above, however, equatorial regions within the southern hemisphere also are profoundly affected by the Monsoon; since western boundary currents carry equatorial effects poleward, we find that the Agulhas Current shows a response to these Monsoonal influences.

Thus, our regional coverage will begin with a brief discussion of Monsoon influences in the equatorial Indian Ocean, followed by subsections centered on the Agulhas Current, on the South Capes region and finally on the Benquela Current and equatorial Atlantic regions.

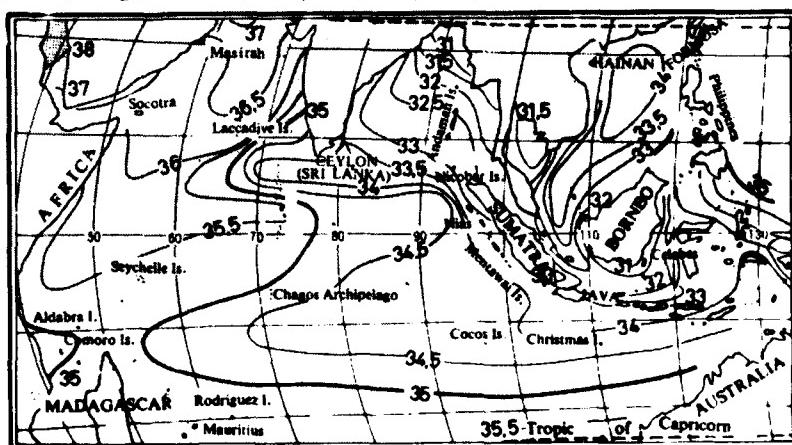
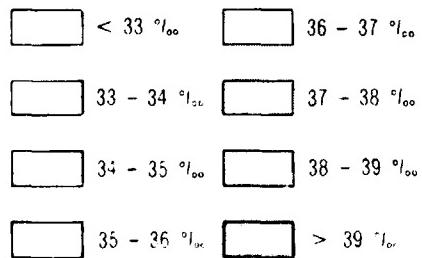


Fig. 7.6 Distribution of Surface Isohalines, Northern Summer. Inset, Northern Winter. (Tchernia, 1980a, Plate 19)

## 7.2 MONSOON CIRCULATION PATTERNS, WESTERN INDIAN OCEAN

Because the great Asian landmass of the northern hemisphere becomes very cold in winter and very warm in summer compared to adjacent ocean waters, the atmospheric circulation pattern reverses annually. The large high (sea level atmospheric) pressure over the cold land surface of Asia in (northern hemisphere) winter has associated a clockwise wind circulation pattern approximately parallel to the isobars of Figure 7.7 (January) from Tchernia (1980a). In (northern hemisphere) summer, a strong low (sea level atmospheric) pressure pattern replaces the winter high pressure pattern, with its center displaced southward over the Persian Gulf and Pakistan. The sense of wind circulation about this summer low pressure center has become counterclockwise (see July, Fig. 7.7).

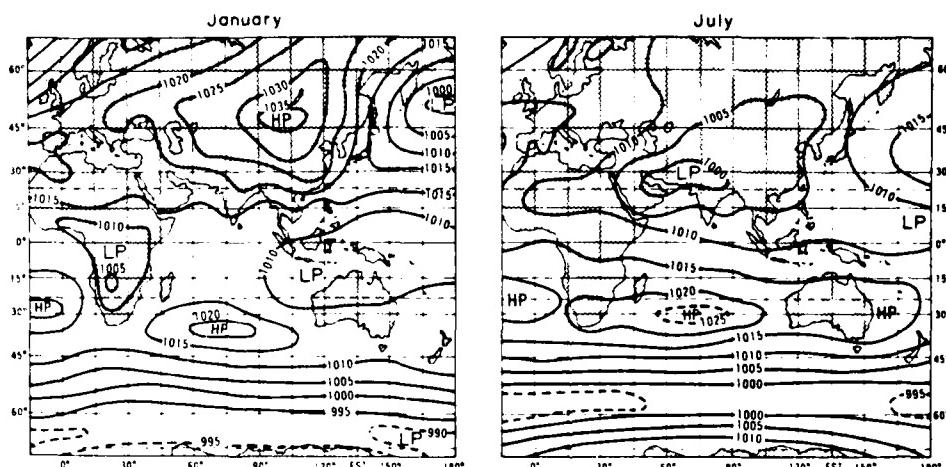


Fig. 7.7. Distribution of high and low pressures in the two opposite seasons (January & July). (Tchernia, 1980a)

The extent of this monsoon wind pattern is shown in Figure 7.8 from Tchernia (1980a); north of the indicated boundary line a seasonal monsoonal reversal occurs in the wind pattern. This clearly shows monsoon influences extending to about 18°S along the African coastline, and across the northern extremity of the island of Madagascar.

January winds are from the east or northeast in the Monsoon region (in the northern hemisphere). The winds reverse and are from the southwest in July (in the northern hemisphere).

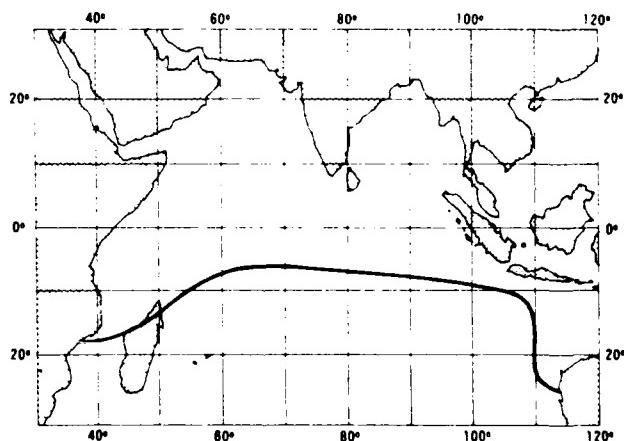


Fig. 7.8. Limit of the monsoon system (Tchernia, 1980a)

Figure 7.9 (a), from Gross (1982) indicates more clearly the nature of the surface wind pattern in August, not only for the Monsoon region, but all over the Indian Ocean. The resulting ocean current pattern is indicated in Figure 7.9 (b) for August. A pronounced clockwise circulation pattern exists for the ocean currents from 20°S northward. The South Equatorial Current splits as it impinges on Madagascar. The northward-directed branch reaches the African coast at about 15°S where it divides once more. The branch toward the north feeds the strong Somali Current along the Somali coast during (northern hemisphere) summer. The branch toward the south feeds the Agulhas Current, which originates between Madagascar and the Mozambique coast of mainland Africa (see Fig. 7.10 for added details including upwelling regions and tropical convergences).

In February, the surface winds of the Monsoon region have reversed and are directed from the northeast and north (near the equator) (see Fig. 7.9 (c)). The resulting surface current pattern in the Indian Ocean is shown in Fig. 7.9 (d). In the northwestern part of the Indian Ocean the circulation has reversed to *countrerclockwise*. A North Equatorial Current, from the northeast and east, has replaced the Southwest Monsoon Current. An Equatorial Counter Current, from west to east, is present from 5°S to 10°S. The Somali Current likewise does not occur in February.

Along the African coastline between the equator and about 10°S there has been a reversal in the current direction in response to the monsoon influence. The current is directed northward in August; it reverses and is directed southward in February (see Fig. 7.11 for added detail). On time scales shorter than the seasonal reversal of the monsoon winds (and resulting currents) there is also variability in these ocean features. This is indicated for the ocean currents (Figs. 7.10 and 7.11 from Tchernia (1980a)) by the arrow length to indicate "Regularity of the Current"; the longest arrows represent currents present in that direction more than 50% of the time while the shortest arrows indicate that currents in that direction occur less than 25% of the time.

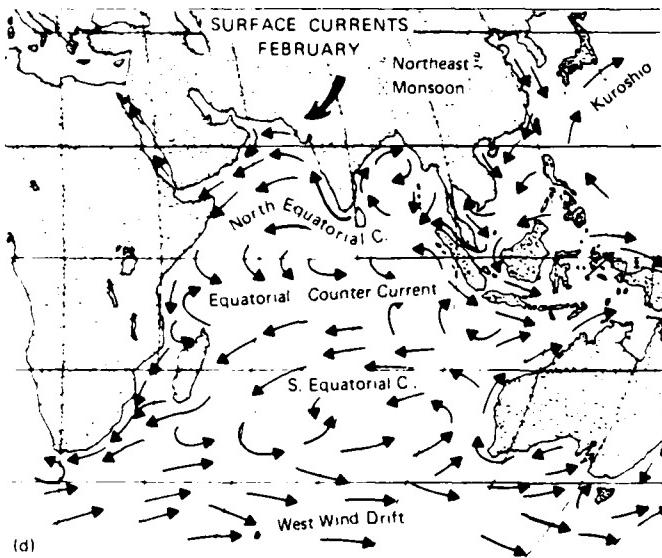
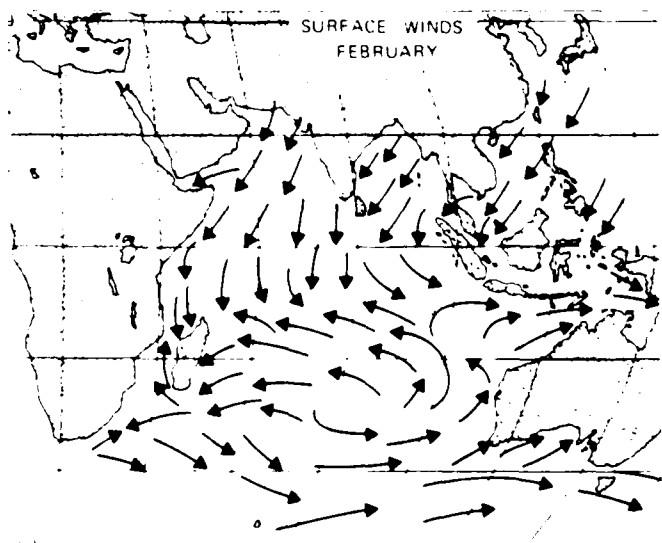
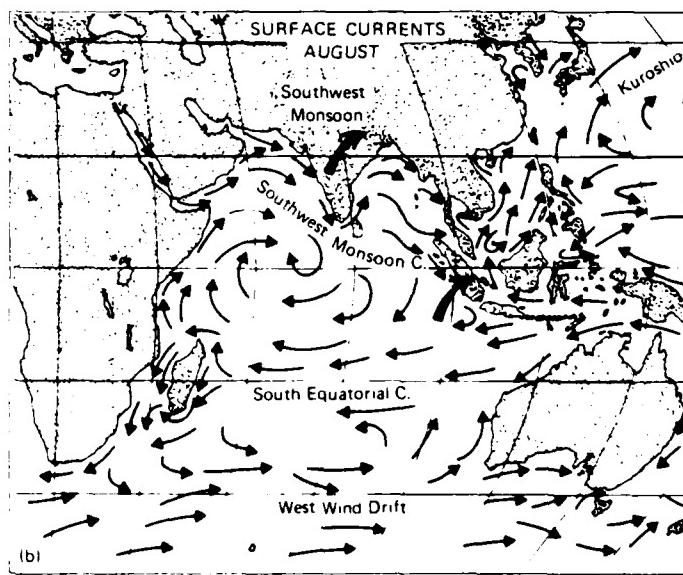
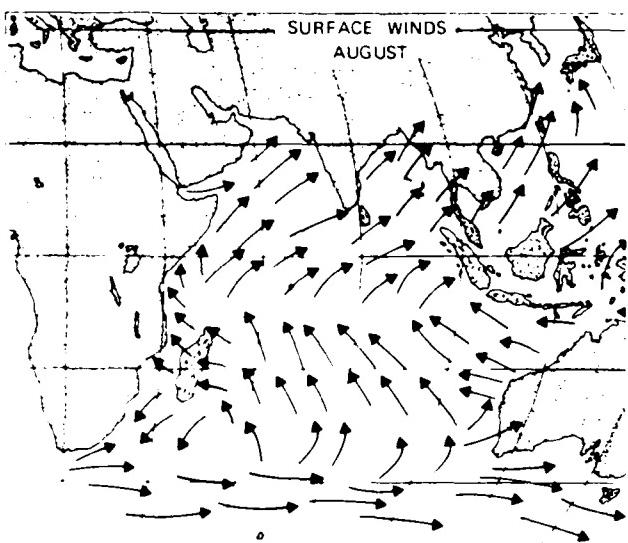


Fig. 7.9 (a) Surface Winds and (b) Monsoon Currents, Southwest Monsoon;  
 (c) Surface Winds and (d) Monsoon Currents, Northeast Monsoon (Gross, 1982)



+ + + Tropical Convergence  
 - - - Subtropical Convergence  
 — Antarctic Convergence  
 △ △ △ Limit of drift ice during southern winter  
 ▨ ▨ ▨ Limit of close pack-ice during southern winter  
 × × × Upwelling Zone

#### REGULARITY OF THE CURRENT

- > 50 %
- 25 to 50 %
- < 25 %

#### CURRENT VELOCITY

- 12 to 30 n.m. per 24 hours
- < 12 n.m. per 24 hours

Fig. 7.10. Surface Currents, Indian Ocean, Northern Summer (August-September) (Tchernia, 1980a, Plate 14)



Fig. 7.11. Surface Currents, Indian Ocean, Northern Winter  
(February-March) (Tchernia, 1980a, Plate 13)

### 7.3 THE AGULHAS CURRENT

In an earlier study of the Agulhas Current area, Darbyshire (1964) concentrates on the region from 30°S-40°S, extending from the southeastern African coastline out some 2 degrees of longitude.

Figure 7.12 indicates the offshore bathymetry for the region adjacent to Africa from 15-55°S. In this figure the sharp gradient of bottom surface as it drops from the coastline offshore is clearly shown in the Agulhas Current region. Two shallower regions offshore are indicated as well:

1. In the Mozambique Channel between Africa and Malagasy, the depths reach somewhere between 1,000-2000 fathoms, with a broad extension southwestward, inshore from the Natal Basin;
2. The Agulhas Plateau to the south of the continent is less than 2,000 fathoms; it appears to provide topographic guidance to the retroreflection character of the Agulhas Current.

Note also the Madagascar (undersea) ridge extending southward from Malagasy, shallower than 100 fathoms in places. The complexities of the bathymetry of this region contribute to the variability in the current distributions of the region.

Darbyshire concentrates on vertical temperature and salinity sections that extend outward from the coastline across the strongest portion of the Agulhas Current. Current velocities were calculated from dynamic height values, since no direct current measurements were made on the six cruises reviewed. Darbyshire notes the following items:

1. The main features that control the Agulhas Current are the South Equatorial Current and the West Wind Drift;
2. In southern winter (May-October) the South Equatorial Current is deflected mostly to the north of the equator (jointly by the Southeast Trade Winds of the southern hemisphere and by the Southwest Monsoon in the northern hemisphere), and the part of the Southern Equatorial Current deflected *southward* is very small;
3. This leads to a weak Agulhas Current in southern hemisphere winter;
4. In southern summer, the effect of the (northern hemisphere) Northeast Monsoon *increases* the Agulhas Current by increasing the portion of the South Equatorial Current deflected southward;
5. At the southern extremity, the west wind drift moves northward in southern winter, and limits the southward extension of the Agulhas Current in April-July;
6. In January, the Agulhas Current warm tongue extends far westward;

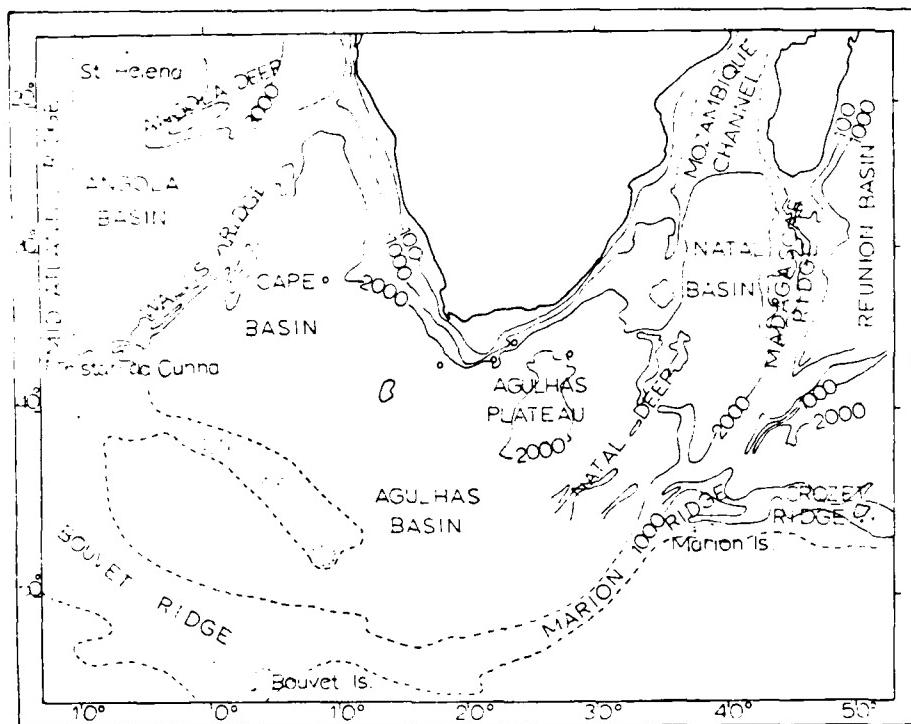


Fig. 7.12. Broad outline of bottom topography of Southern Ocean area  
(Darbyshire, 1964)

7. The Agulhas Current flow returns northeastward offshore, well to the east of the Cape of Good Hope;
8. Local winds have little effect on the Agulhas Current system;
9. There are a large number of eddies inside the Agulhas Current system.

(Darbyshire concludes, incorrectly in view of more recent evidence shown below, that the large eddies found south and west of the Cape of Good Hope did not appear to have any strong association with the Agulhas Current system.)

Harris (1972) studied the sources for the Agulhas Current water for the spring of 1964. Figure 7.13 shows several eddies between Madagascar and the African coast, and eddy D to the southwest at about 30°S just off the African coast and in the Agulhas Current region. He concludes that these are deep anticyclonic vortices, of the order of 200 miles in diameter and with associated transports of 10-20 Sverdrups ( $Sv$ ,  $10^6 m^3/sec$ ) and analyzes the volume transported by the *Agulhas Current* to be 67  $Sv$  in the upper layers (and estimates the intermediate and deeper water transported southward as 5  $Sv$ ).



Fig. 7.13. On Sigma-t surface 25.1, isolines are shown for: (a) salinity, ‰ (first two digits omitted), (b) oxygen, ml/l, (c) acceleration potential, dyn m. (Harris, 1972)

Sources for the 72 Sv total southward transport are (Harris, 1972):

1. South Equatorial (Current) water passing the south end of Madagascar and entering the Agulhas Current . . . . . 35-Sv
  2. Mozambique Current through Mozambique Channel . . . . . 10-Sv
  3. Agulhas Return Current, recycled west of the Madagascar Ridge . . . . . 15-Sv
  4. Agulhas Current recycled in Vortex D (see Figure 7.13) . . . . 12-Sv

Total . . . . . 72-Sv

Harris and van Foreest (1978) analyzed data from a multiship survey over essentially the whole length of the Agulhas Current in March 1969. An important tributary to the current (from the east) just south of Durban ( $30^{\circ}$ S) was identified. Offshore deflections of the Agulhas Current occurred just north of Durban, and also near East London ( $\sim 33^{\circ}$ S) and Port Elizabeth ( $\sim 34^{\circ}$ S), as shown in Figure 7.14 from Harris and van Foreest (1978). Note the apparent relation between bottom topography and current pattern in Figure 7.14. More detailed bottom topography for the southern African offshore region is shown in Figure 7.15 from Harris and van Foreest (1978) along with identifying names for the features.

The retroflection of the Agulhas Current occurs at about  $20^{\circ}$ E, where the Agulhas Current reverses direction and flows parallel to the main current for 500 n miles, before undergoing a sharp wave-like oscillation after encountering the Agulhas Plateau. Figure 7.16 shows the relationship between the dotted-line-path of a satellite-tracked buoy (EOLE) and the configuration of dynamic topography, with associated ocean current directions. Compare with Figure 7.14, which shows the dotted path of satellite-tracked buoy 1116 in the northern part of the region.

Grundlingh (1979) describes a large meander in the Agulhas Current which was observed in May 1973 by a shipboard cruise from  $32\text{--}35^{\circ}$ S; this meander occurred in a region where the Agulhas Current ordinarily adheres closely to the coastline. This loop in the current has a form and position similar to one observed by satellite three years later (August 1976) shown in Figure 7.17 from Grundlingh (1979). The loop appeared to contain a cyclonic eddy about 50 km in diameter, with evidence of upwelling in the center (cold surface and no mixed layer). In comparing two successive satellite images from 1976, the meander appeared to be moving toward the southwest at 20 cm/sec. In reviewing results of cruises from April, May and June through the 1973 meander, it appeared that the meander also was moving in a similar manner, and it was amplifying as it advected southwestward.

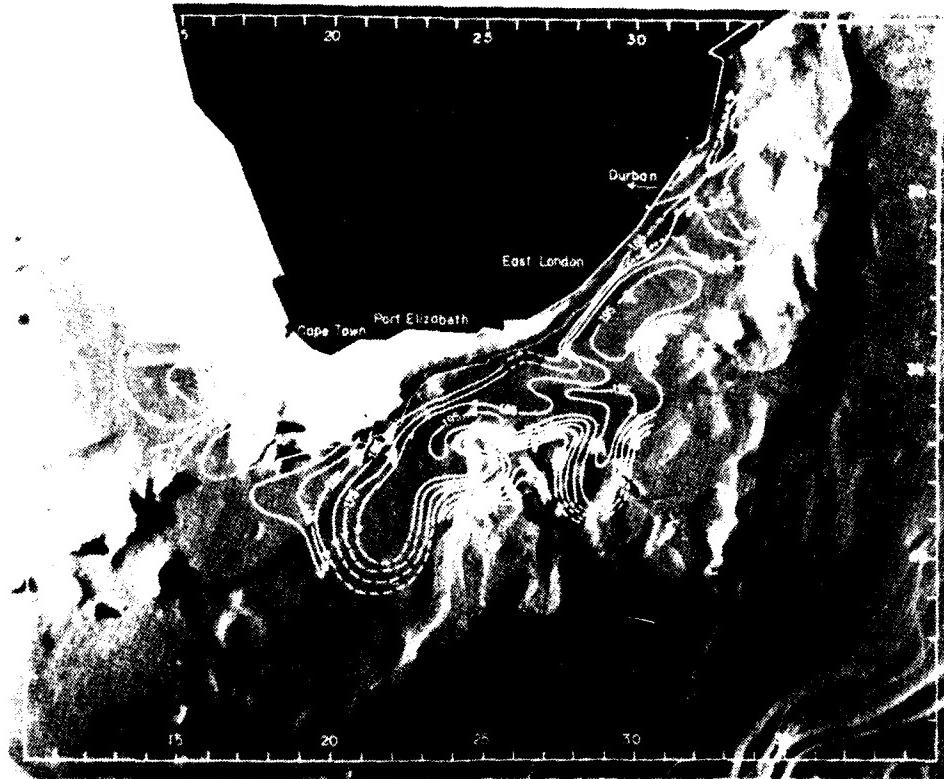


Fig. 7.14. Surface dynamic height (in dynamic meters) with reference to the 1000-dbar level. Contoured at intervals of 10 dyn. cm. Measured surface current vectors are inserted on the Durban line (1 cm = 2 knots). Heavy dots indicate part of the track of satellite tracked buoy 1116. The lightly dotted line corresponds to the 1000-m isobath. (Harris and van Foreest, 1978)

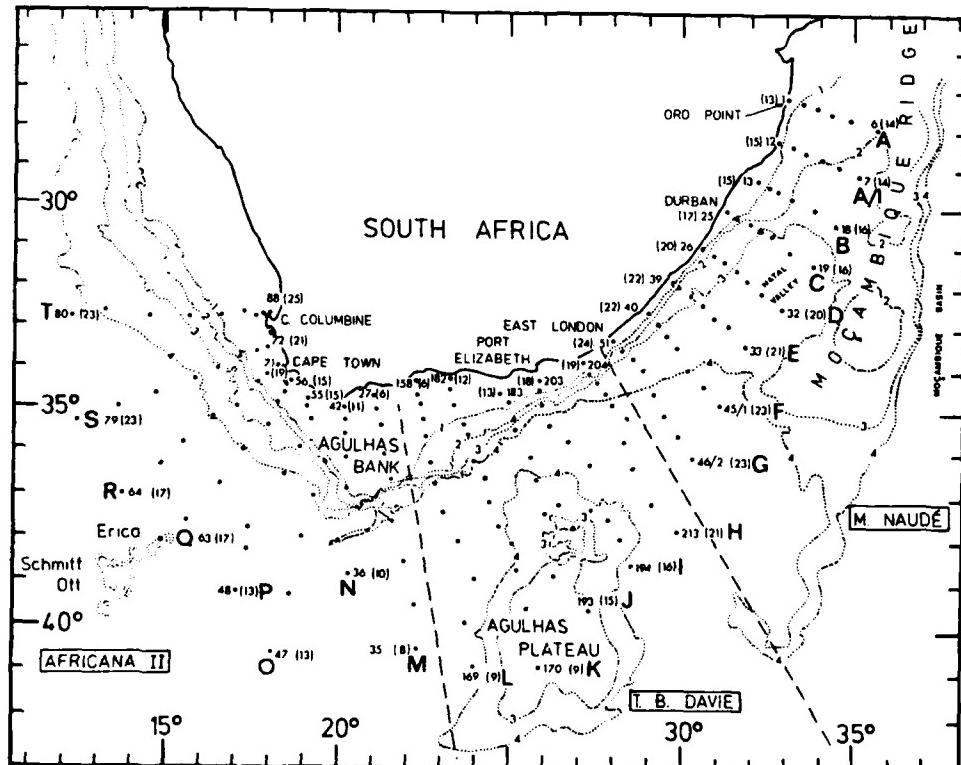
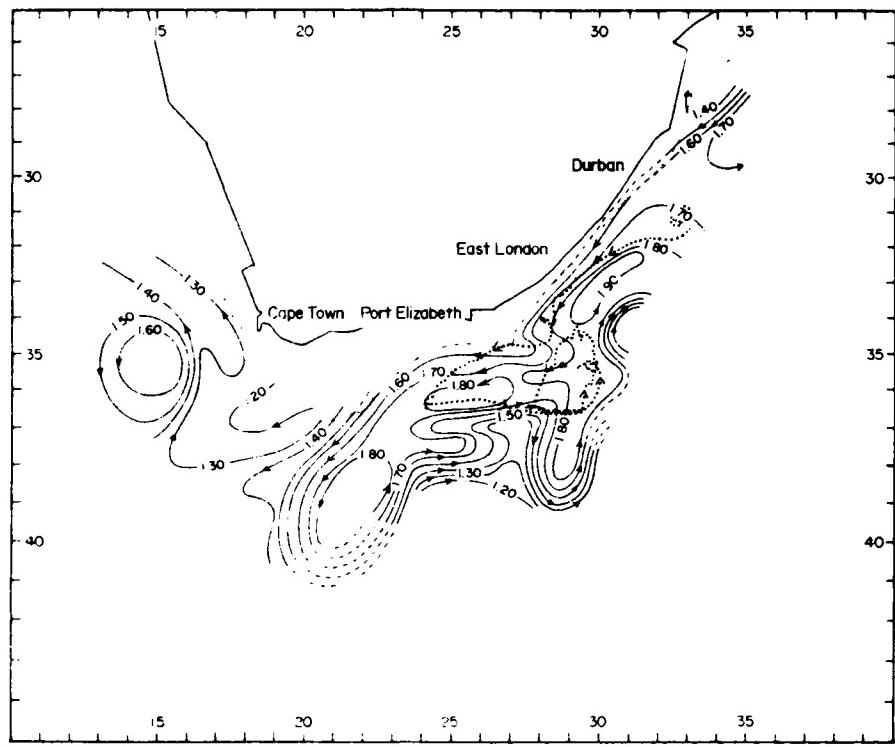


Fig. 7.15. Station dispositions superimposed on the bathymetry (contour interval 1000 m) off southern Africa. (Harris and van Foreest, 1978)



The volume transport of the Agulhas Current was reviewed and new estimates produced by Grundlingh (1980) through careful procedures applied to data from eight cruises through the region (1 from September 1966; 7 from August 1975-April 1976). On five of these, direct current vertical profiles were measured from a drifting ship whose position was accurately tracked continuously with a DECCA Navigator system.

Geostrophic transports relative to 1,000 meters were calculated from each cruise. In five of the cruises, the measured current was matched to the geostrophic current and the resulting transports were calculated to 1,000 meters. Figure 7.18 from Grundlingh (1980) shows the locations for the sections studied on these cruises. Table 7.2 tabulates earlier geostrophic transport estimates in part (a); these range from 19 to 137 Sv. Table 7.2 part (b) shows results from the study based on the eight cruises of Grundlingh (1978). While values vary from 20-38 Sv for the geostrophic transports relative to 1,000 m, the values for similar transports that are matched to observed currents vary only between 60-64 Sv.

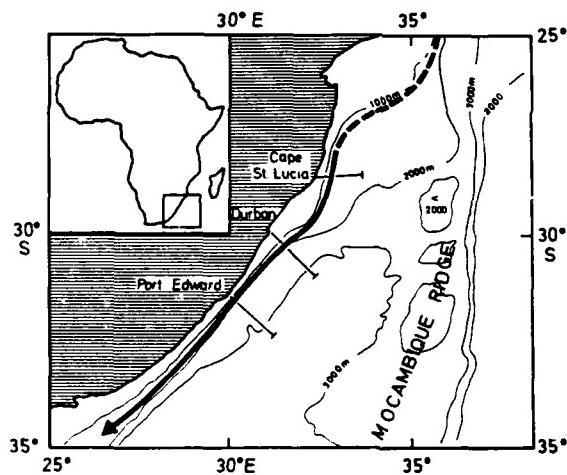


Fig. 7.18. Location chart of the sections across the Agulhas Current at Cape St. Lucia, Durban and Port Edward with an indication of the Agulhas Current path. (Grundlingh, 1980)

TABLE 7.2  
Volume Transport ( $10^6 \text{m}^3 \text{s}^{-1}$ ) of the Agulhas Current (Grundlingh, 1980)

(a) *Historic data*

Source	Location	Geostrophic transport rel. to 1000 m	Total geostrophic transport
DIETRICH (1935)	Durban	19	
DUNCAN (1970)	Cape Agulhas	22	
LUTJEHARMS (1972)	SW Indian Ocean	24-33	67-91
VERONIS (1973)	Durban		56
HARRIS (1972)	Theoretical model		72
DARBYSHIRE (1972)	SW Indian Ocean		67
JACOBS and GEORGI (1977)	Durban		9-63
HARRIS and VAN FOREEST (1978)	Durban	37 (to 1300 m)	137
	Cape Agulhas		
	Port Edward	30	

(b) *Present investigation*

Cruise date	Location	Geostrophic transport rel. to 1000 m	Matched transport to 1000 m	Transport extrapolated to bottom
27-31 August 1975	Durban	20		
4- 6 November 1975	Port Edward	29	64	67
17-22 January 1976	Port Edward	23	62	75
9-10 August 1976	Port Edward	36	61	73
8-10 February 1977	Port Edward	22	62	75
5- 6 April 1977	Port Edward	37		
14-15 September 1966	Port Edward	31	60	72
7- 9 April 1978	Cape St Lucia	38		

If one compares the total transport (extrapolated to the bottom) at Port Edward, about 75 Sv, with that derived for Cape Agulhas by Jacobs and Georgi, 137 Sv from Table 7.2 (a), an increase in volume transport of about 6 Sv per 100 km is obtained as one moves southward from near Port Elizabeth to Cape Agulhas off the Continent's southern tip.

Pearce and Grundlingh (1982) consider the conflicting evidence pertaining to seasonal variability in the Agulhas Current speed and volume transport. Figure 7.19 from Pearce and Grundlingh (1982) indicates no appreciable seasonal trend in *mean* current speeds; there is a suggestion of a maximum in *peak* current speeds in November-December and a minimum in August-October.

For volume transports by the Agulhas Current, *geostrophic* calculations alone suggests that a seasonal variation occurs (as indicated by Column 3 in Table 7.2 (b) of Grundlingh (1980): largest transport in April-August; lowest in January-February. However, when volume transports are calculated from data based on (calculated) currents

matched to observed currents, seasonal transport variation is observed. Pearce and Grundlingh (1982) note that wind fields are strongly varying with season in equatorial regions, but this seasonal variation weakens progressively toward higher latitudes over the Agulhas Current region. The authors suggest this wind field variation may contribute to these conflicting results.

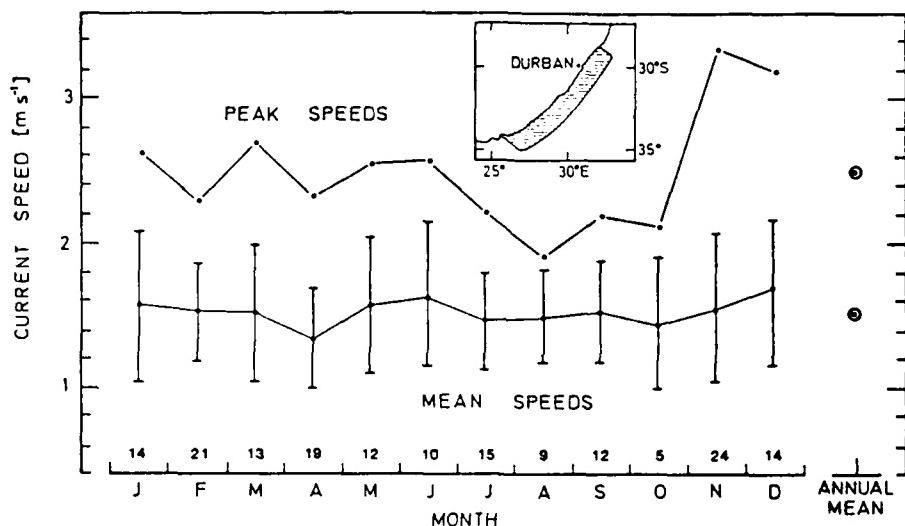


Fig. 7.19. Monthly mean (with standard deviation) and peak (individual) speeds in the core of the Agulhas Current based on direct current measurements off the Southern African coast. The number of observations for each month is shown. (Pearce and Grundlingh, 1982)

Schumann (1982) considers the relation between the bathymetry of the continental shelf and slope and the varied flow regimes along the coast for the inshore edge of the Agulhas Current. The studied region is off Durban (Figure 7.20) where the offshore terrace is wider to the north and becomes very narrow at Port Edward. The maximum speed of the Agulhas Current is just offshore from the shelf break in the north, off Richards Bay. Along the terraced bathymetry off Durban, a variable current regime occurs; further south, off Port Edward, the current core is more stable in position once again, within 10-15 km of the coastline.

Within 6 km of the shore off Richards Bay measured currents are variable; there is a *northward* flow off Durban, and a *southward* flow off Port Edward. The postulated semipermanent cyclonic gyre off Durban (from the measured current results) has been confirmed by satellite. The gyre has a diameter of about 30 km.

The sea surface temperature chart (Figure 7.21), based on airborne radiation thermometer (ART) measurements, shows the presence of a cold surface isotherm near Durban which may be associated with the postulated cyclonic gyre, and, in turn, Schumann relates this to the bottom topography of Figure 7.20. Indeed, this temperature pattern is evident on all ART flights along this coast (Lutjeharms 1980). The strong nearshore temperature gradient in Figure 7.21 reflects the location of the inshore edge of the Agulhas Current.

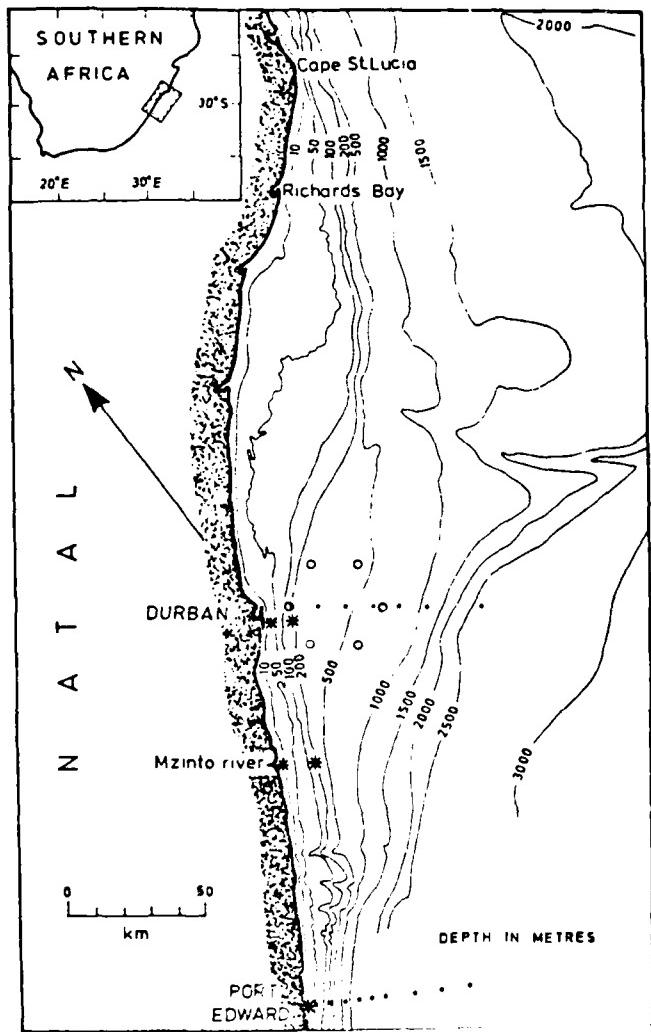


Fig. 7.20. The coastal bathymetry off Natal, with the inset map showing the location of the area. (Schumann, 1982)

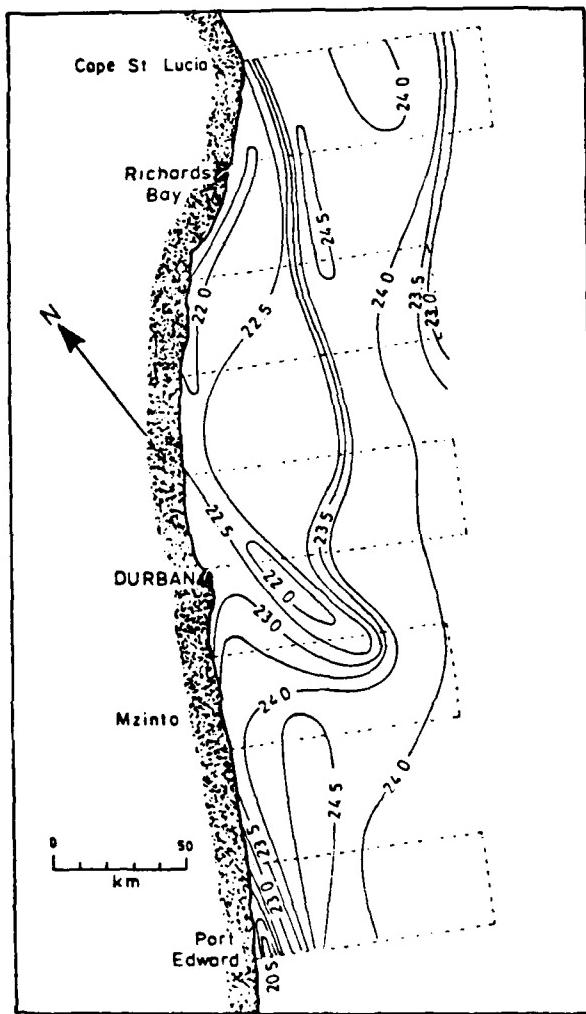


Fig. 7.21. Sea surface temperatures from an airborne radiation thermometer (ART) flight on 30 November 1967. Temperatures are given in degrees Celsius, while the aircraft flight pattern is also shown. (Schumann, 1982)

#### 7.4 CAPE ROLLERS, UNUSUALLY HIGH SWELL OFF SOUTH AFRICA

Figure 7.22 from Quayle (1974a) focuses attention on the sea portion of Marsden Square (MS) 441 ( $30^{\circ}$ - $40^{\circ}$ S,  $20$ - $30^{\circ}$ E) where unusually high swell occur and occasionally seriously damage shipping moving to the southwest through this region. Five ship disasters are reviewed by Quayle (1974a), and one each in Quayle (1974b) and Schumann (1976a). Figure 7.23 from Quayle (1974b) shows the synoptic weather chart associated with one shipping accident; it shows the *large atmospheric pressure gradient* between a low pressure center southeast of the region and a high pressure center over the Cape area. Winds from the southwest generate waves and swell that move north and northeastward along the African coastline. The waves and swell in MS 441 reach unusually large heights; these are tabulated in Table 7.3 from Quayle (1974a) in terms of the frequency of occurrence (once in 5, 10,...100 years) for significant and for extreme wave heights. Table 7.4 from Quayle (1974a) shows that there are unusual numbers of high waves in this region compared with other ocean areas in the world with similar or greater gale wind frequencies. Schumann (1976a) focuses attention on the conditions which appear necessary for freak waves of 20 m (66 ft.) or higher that are preceded by a *very deep trough* in the sea surface:

1. Seaward edge of continental shelf off east coast of South Africa between East London (see Fig. 7.15) and Richards Bay (see Fig. 7.20). This is a *narrow continental shelf* region, with a *steep bathymetric gradient* in the *continental slope* area.
2. A swift current (the Agulhas Current) runs alongshore from northeast toward southwest.
3. An area of low pressure moves east-northeastward (Fig. 7.23) to produce a strong wind from the southwest blowing against the flow of the Agulhas Current. Waves of 7 to 8 m, with a period of about 10 seconds and length 60-90 m are generated by this wind; these waves are superimposed on swell (16-second period and much longer wave length) moving northeastward from storm centers further south.

Coinciding wave crests can create a short-lived freak wave of 20 m or more, that extends only over about 200-500 yds.

Oceanroutes (1978) reviews conditions that precede freak waves: A strong southwest wind of Force 6 (22-27 kt) or more blowing for 24 hours or more is present; the wind has not built up slowly, but has veered from the northeast to the southwest. Caution is advised (ship slowed) if

1. The ship is steaming southwest between Richards Bay and East London in a rough sea, on a course line *within the area* which is 20 miles seaward of the continental shelf;
2. The barometer is low; and
3. southwesterly wind has blown for at least 24 hours.

Schumann suggests that ships should keep *inshore* of the 200 m (100-fathom) bathymetric contour when the above conditions occur. This contour marks the approximate inshore boundary of the Agulhas Current (see Fig 7.24).

Schumann (1976b) investigates the interaction between current and wave energy and concludes that energy transfer can occur from a current to ocean waves under certain circumstances. He notes the Agulhas Current meets these conditions on most occasions. Kenyon (1971) also indicates that waves will be refracted toward higher current velocities when waves and currents interfere at an angle and that it is possible for certain waves (and their energy) to be trapped along the peak of a current.

Schumann (1980) also refers to the energy transfer between current and opposing waves. Also the steepening effect on waves by the opposing current is noted, as well as the steepening effect of the ship steaming into opposing wave trains. He notes the dominant wave periods in the Agulhas Current are 10-15 seconds, with occasional waves with 20-second periods observed off the Cape.

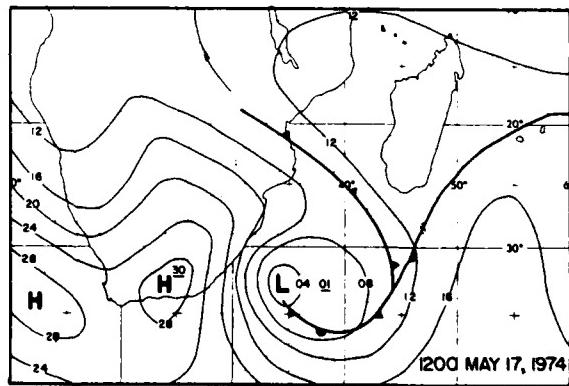
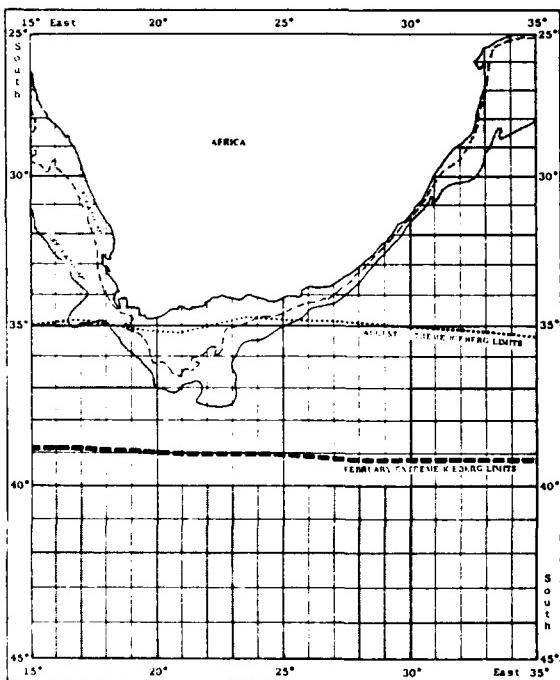


TABLE 7.3

Wave height return values (Quayle, 1974 a)

<u>Years</u>	<u>Significant Height (ft)</u>	<u>Extreme Height (ft)</u>
5	56	100
10	61	109
25	67	121
50	73	131
100	79	142

TABLE 7.4

Percentage frequency of observations of waves with gentle breeze or calmer, and gales (Quayle, 1974 a)

Area	Gentle breeze or calmer (Winds $\leq$ 10 kt with wave reports)	Gales (Winds $\geq$ 34 kt with wave reports)	Waves			
			$\geq 8$ ft	$\geq 12$ ft	$\geq 17$ ft	$\geq 23$ ft
M.S. 441 (30° - 40°S, 200°-300°E)	43.0	3.0	42.7	18.5	4.7	1.1
Bermuda (30° - 34°N, 63°-67°W)	40.4	3.0	18.4	7.1	1.9	0.8
Tokyo (34° - 37°N, 139°-142°E)	33.4	4.6	20.1	7.0	1.3	0.3
Azores (36° - 40°N, 24°-32°W)	34.7	6.0	29.9	12.9	2.9	0.9

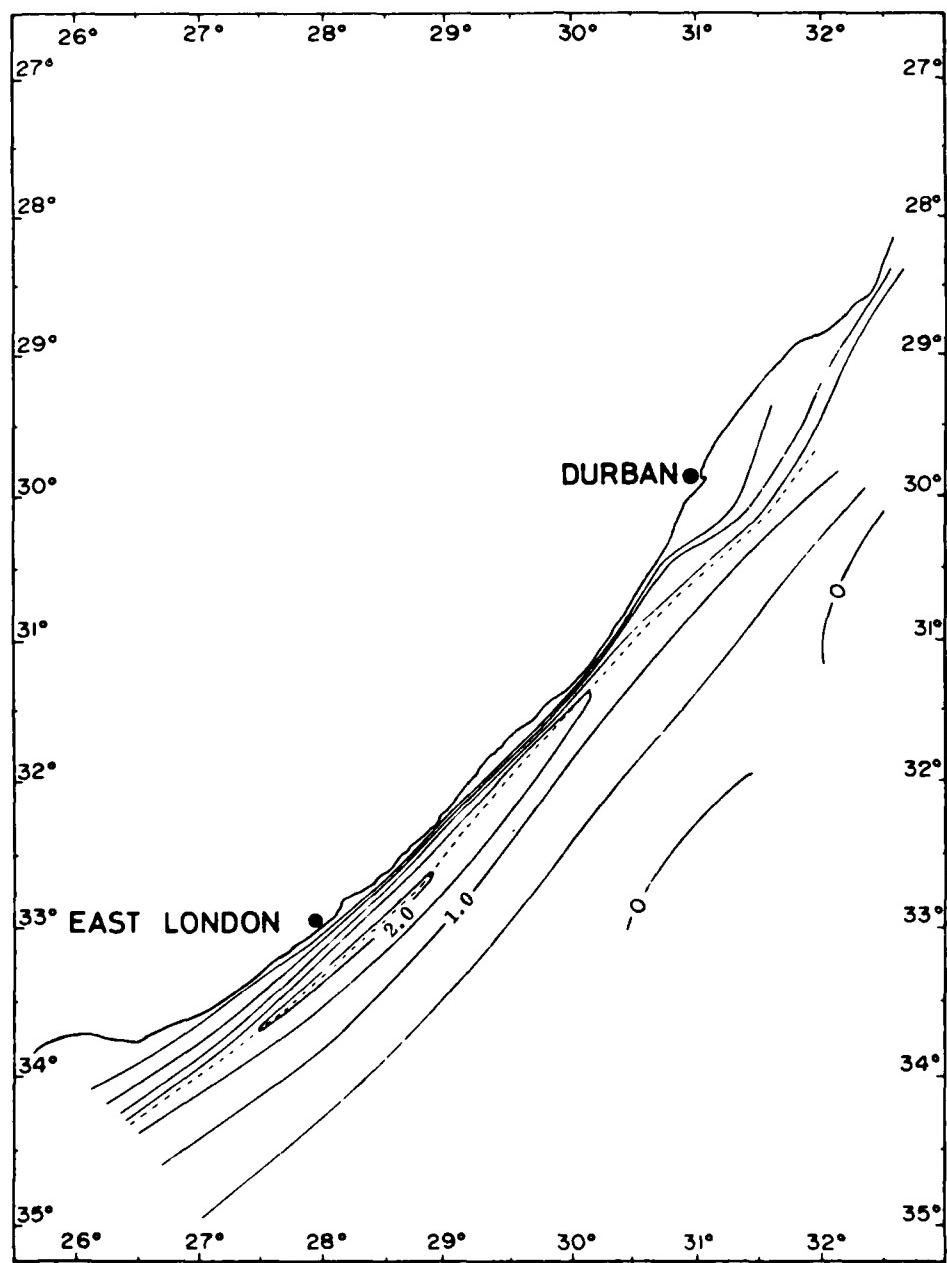


Fig. 7.24. Mean southerly current speed parallel to the coast in m/s.  
(Schumann, 1976a)

## 7.5 SOUTHERN OCEAN AREA

(Capetown, Cape Agulhas to Port Elizabeth,  
and Adjacent Coastal Areas 30 to 45°S; 10 to 45°E)

The Subtropical Convergence region off South Africa separates the warmer waters of the South Atlantic and Indian Ocean counterclockwise gyres from the colder waters further south that move as a part of the West Wind Drift circling the Antarctic Continent. Nearshore, along the southwestern African coastline, is the Benguela Current which will be described in the following section; it is a cool, complex current associated with upwelling waters along the shelf. In the preceding subsection, a detailed description of the Agulhas Current has been given; this warm current originates at lower latitudes in the Indian Ocean and represents a strong, western boundary current along the southeastern coast of Africa.

To the south of Africa, between the coastline (~34°S) and the Subtropical Convergence (~39°S), there is an intermediate zone between the strong Agulhas Current of the Indian Ocean and the Benguela Current of the Atlantic Ocean that is marked by slower water speeds, eddies from the Agulhas Current, and by the Agulhas Return Current directed eastward as the outflow from this region that compensates the volume from the inflowing Agulhas Current. In Fig. 7.25 Lutjeharms (1981a) shows a schematic rendition of these features; notice that both warm core (G) and cold core (K) eddies may be present in the region. The warm core eddies may drift west and north into the region off southwestern Africa and make the watermass characteristics extremely complex there. Darbyshire probably was observing effects of these eddies in describing the presence of "Agulhas water" associated with the upwelling region of the Benguela Current (Darbyshire, 1966a, pp. 70-71).

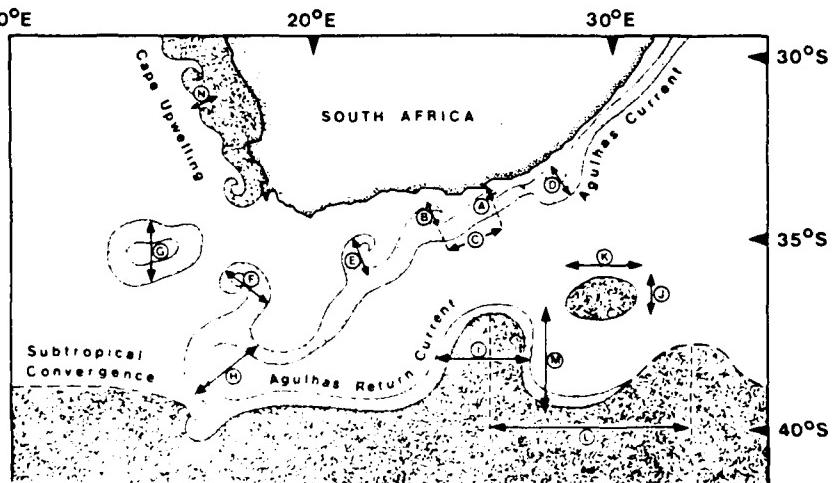


Fig. 7.25. A conceptual image of the main features of the circulation in the ocean areas adjacent to South Africa. Specific features, of which the spatial scales have been investigated, are lettered. Four distinct circulation regimes can be distinguished, namely a western boundary regime (A-E), a retroflexion regime (F-H) that includes part of the Agulhas Return Current (I-M) and an upwelling regime (N). (Lutjeharms, 1981a)

In Grundlingh's study of free-drifting buoys that were tracked by satellite in this area (Grundlingh, 1978), the influence of shallower bottom features on the buoy drift pattern was indicated (Fig. 7.26). There is an abrupt direction change of the Agulhas Current at 39°S, 14°E when the Agulhas Return Current is formed, that moves west-to-east. There is an abrupt deceleration of the Return Current (130 cm/sec at 20°E to 80 cm/sec at 40°E to 40 cm/sec at 60°E). Equatorward deflections of the Return Current are observed at the Agulhas Plateau, at the Mozambique Ridge and at the Madagascar Ridge.

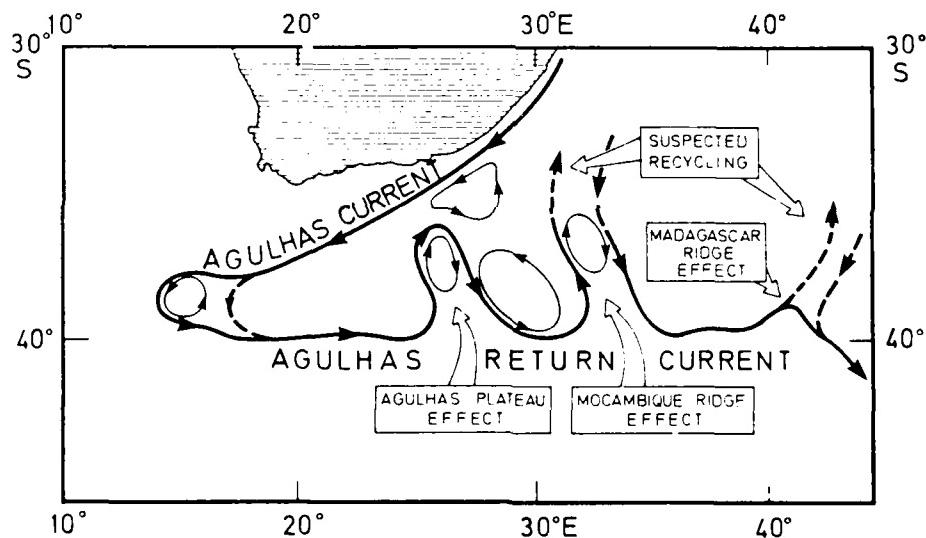
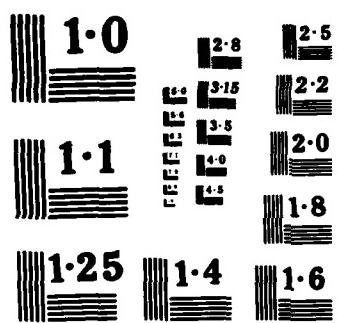


Fig. 7.26. Conceptual representation of the circulation in the Agulhas Current and Agulhas Return Current, derived for the time of the buoy drift. Bold line indicates observed current paths, bold dashed lines possible current courses and faint lines observed vortices. (Grundlingh, 1978)

AD-A163 196 FORECASTERS HANDBOOK FOR THE SOUTHERN AFRICAN CONTINENT 4/4  
AND ATLANTIC/INDI. (U) NAVAL ENVIRONMENTAL PREDICTION  
RESEARCH FACILITY MONTEREY CA. F R WILLIAMS ET AL.  
UNCLASSIFIED NOV 84 NEPRF-TR-84-08 F/G 4/2 NL

END  
FILMED  
IN  
UTC



NATIONAL BUREAU OF STANDARDS  
MICROCOPY RESOLUTION TEST CHART

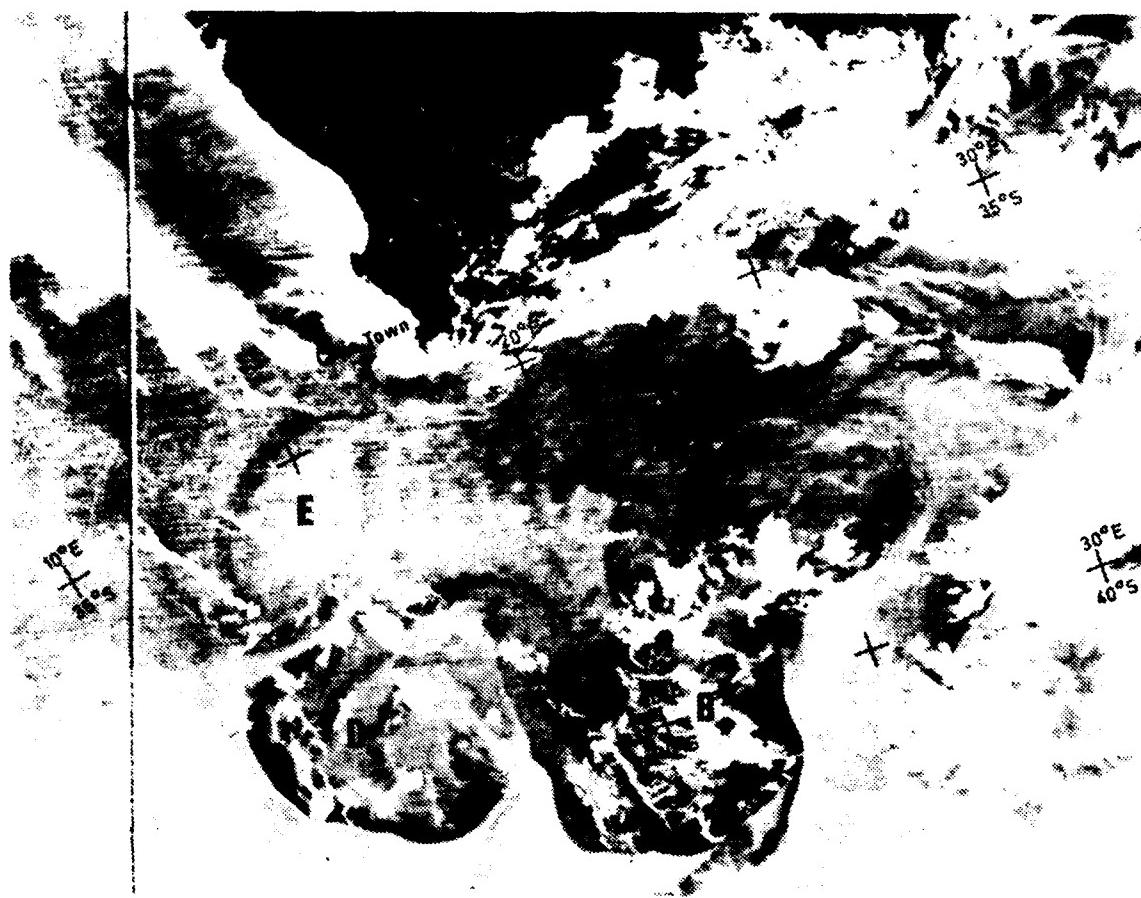


Fig. 7.27. The terminal region of the Agulhas Current south of South Africa. The thermal infrared image is from the VHRR of the NOAA-5 satellite for 9 February 1977 and shows the warm Agulhas Current water (A) impinging on the Subtropical Convergence, retroreflecting (B) and then flowing north-eastwards as the Agulhas Return Current (C). One retroflection loop (D) has been cut off at an earlier date and is evident west of the present retroflection point (B) while the faint surface evidence of a previous retroflection ring is visible northwest of these (E). A number of other eddy-like disturbances at the convergence are noticeable, having a range of diameters. (Lutjeharms and Baker, 1980)

In a dramatic infrared image of this region from the VHRR (Very High Resolution Radiometer) of the NOAA 5 satellite on 9 February 1977, taken from Lutjeharms and Baker (1980), the warm Agulhas Current water is shown in Figure 7.27 as region (A), retroflection (B) as it impinges on the Subtropical Convergence, and flows northeastward as the Agulhas Return Current (C). One cutoff eddy is present (D) that has drifted westward from the present retroflection point (B), and a faint image further northwest suggests an even older ring is present (E). This set of processes was fully understood only since they were described by Nils Bang in 1969 when he analyzed results from concurrent cruises by three research vessel in this region. It then became

evident that earlier individual cruise results, going back to 1851, 1865 and 1935, supported the idea of retroflection in the Agulhas Current. A second item shown by all earlier studies (that the Agulhas Current had a second branch that rounded the Cape of Good Hope and flowed northward off Africa's southwestern coast) was proven false, as described by Lutjeharms (1980a) (see Figure 7.28).

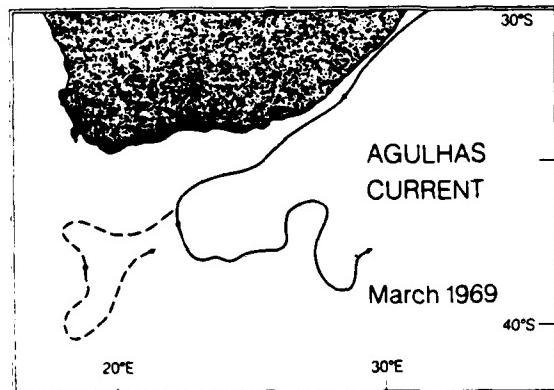


Fig. 7.28. The Agulhas Current, an enormous southerly flow of water, abruptly reverses off Africa's tip and heads eastward, a phenomenon oceanologists call "retroflection"-(Catherine Conner). (Lutjeharms, 1980a)

In his review of the drift of the disabled steamer, the WAIKATO, in the Agulhas Return Current in 1899, Pearce (1983) demonstrates in Figure 7.29 the close similarity between the track of the drifting WAIKATO, solid line, (starting on Agulhas Bank on 5 June 1899) and the trajectory of a satellite-tracked buoy (1975-1976, dotted line). The Waikato was obviously influenced by eddies and planetary waves in the Agulhas Return Current in 1899.

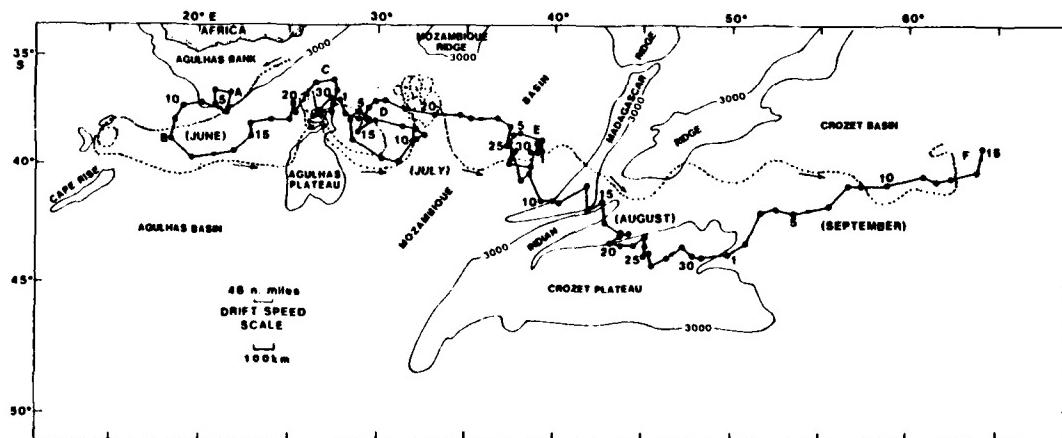


Fig. 7.29. The 1899 track of the WAIKATO (solid line) with every fifth date shown, and the trajectory of a recent satellite tracked buoy (Grundlingh, 1978, dotted). The 3000 m depth contours are included with the names of the major bathymetric features. The scale of 48 n mi (i.e., a day's drift at 2 kt.) is given. (Pearce, 1983)

Lutjeharms (1981a) separates the region into three circulation regimes (Fig. 7.30): The Upwelling Regime shows the lowest circulation intensity, while the Retroflexion Regime shows the highest circulation intensity with spatial scales of perturbation in the flow similar to those in the adjacent Southern Ocean (west-wind drift). He suggests these perturbations are propagated by the drift of warm "spin-off" rings in the Agulhas Current and Return Current, as well as by shifts or deformations in the larger-scale circulation patterns. Eddies in the thermal front of the upwelling region have a mean diameter of 120 km; in the retroflexion region, the eddies have diameters from 150-200 km.

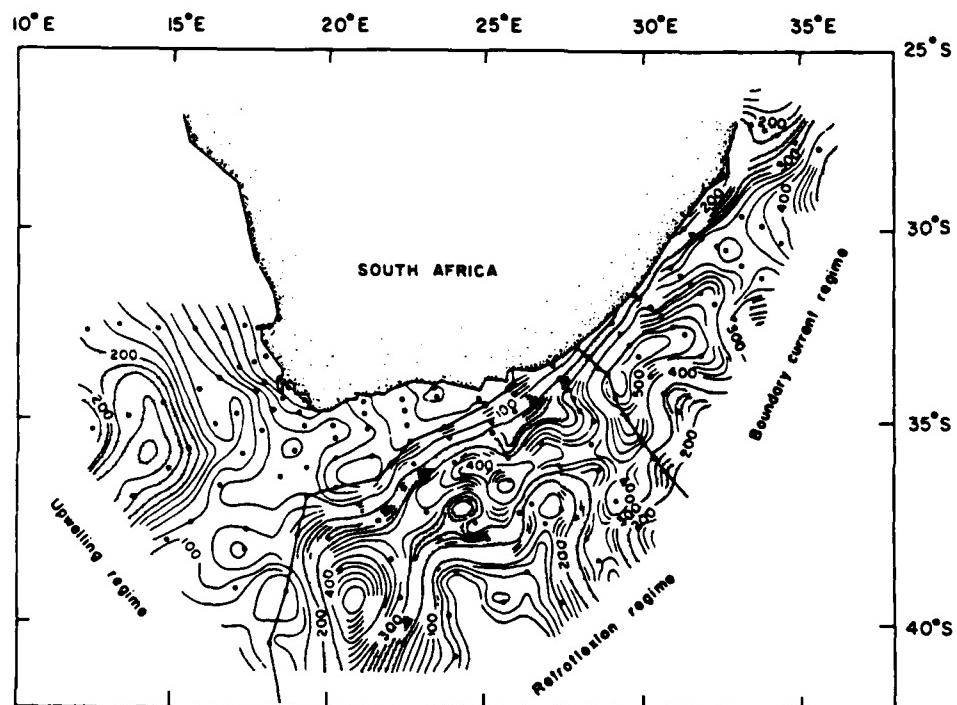


Fig. 7.30. Depth of the 26.20 sigma-t surface during March 1969 for the ocean areas adjoining South Africa. Water movement theoretically takes place parallel to these isobaths. Heavy contours are at intervals of 100 m, lighter lines at intervals of 20 m. Depths between 200 and 300 m have been stippled to accentuate the location of the Agulhas Current and the Agulhas Return Current. The boundaries selected for the three defined oceanic regimes are shown by heavy lines. (Lutjeharms, 1981a)

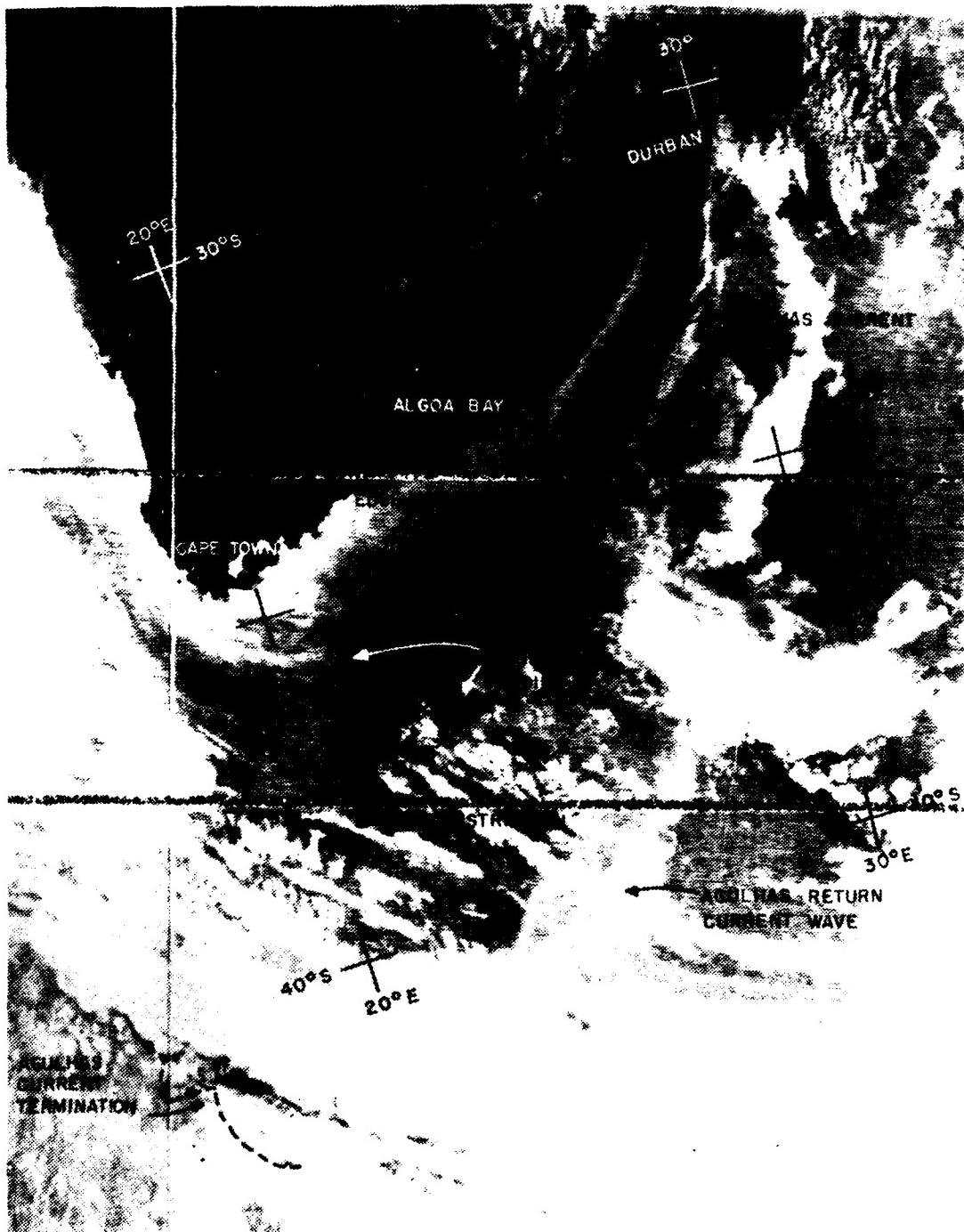


Fig. 7.31. The disposition of clouds and ocean currents in the vicinity of South Africa on 16 December 1977, as portrayed by an infrared temperature sensor on the NOAA-5 satellite. The warm landmass is black, while cold clouds are the main white features. The dark ribbon of Agulhas Current water with its attendant eddies is noticeable. (Lutjeharms, 1980b)

Satellite images illustrate the complexity of this region. Figure 7.31 from Lutjeharms (1980b) shows a view taken by the infrared sensor of the NOAA 5 satellite on 16 December 1977 with notations indicating the Agulhas Current, eddies, the termination of the Agulhas Current and the Agulhas Return Current. Figure 7.32 from Lutjeharms (1981b) shows the relation between the location of the Agulhas Retroflection, Agulhas rings, and the upwelling zone off southwest Africa indicated by the NOAA 5 infrared image taken 9 February 1977. Figure 7.33 from Cheney et al. (1983) indicates the variability in sea height measured by the SEASAT satellite altimeter from 15 September - 10 October 1978. The region off southern Africa is a center of maximum variability which must be associated with the changing watermasses associated with eddies within the region. Cheney et al. (1983) indicates this is the region of greatest variability of sea height within the southern hemisphere, with the magnitude and horizontal scale of variability similar to that in the Gulf Stream region of the northern hemisphere.

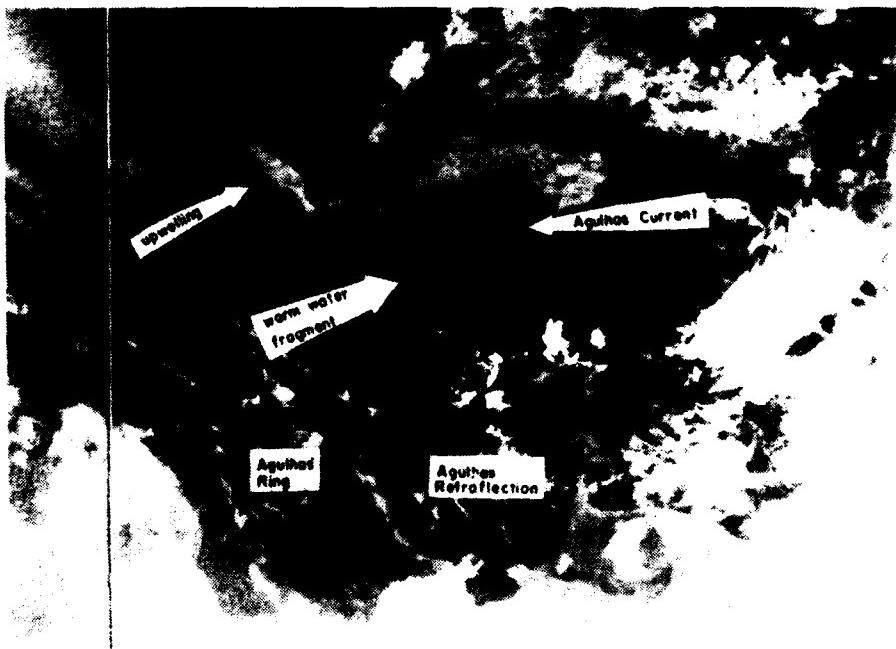


Fig. 7.32. The advection of warm (darker) water masses of Agulhas Current origin into the South Atlantic as inferred from an infrared satellite image from the NOAA-5 satellite for 9 February 1977. Note the warm water moving close, and directly parallel to, the upwelling front off the west coast of the Cape of Good Hope. (Lutjeharms, 1981b)

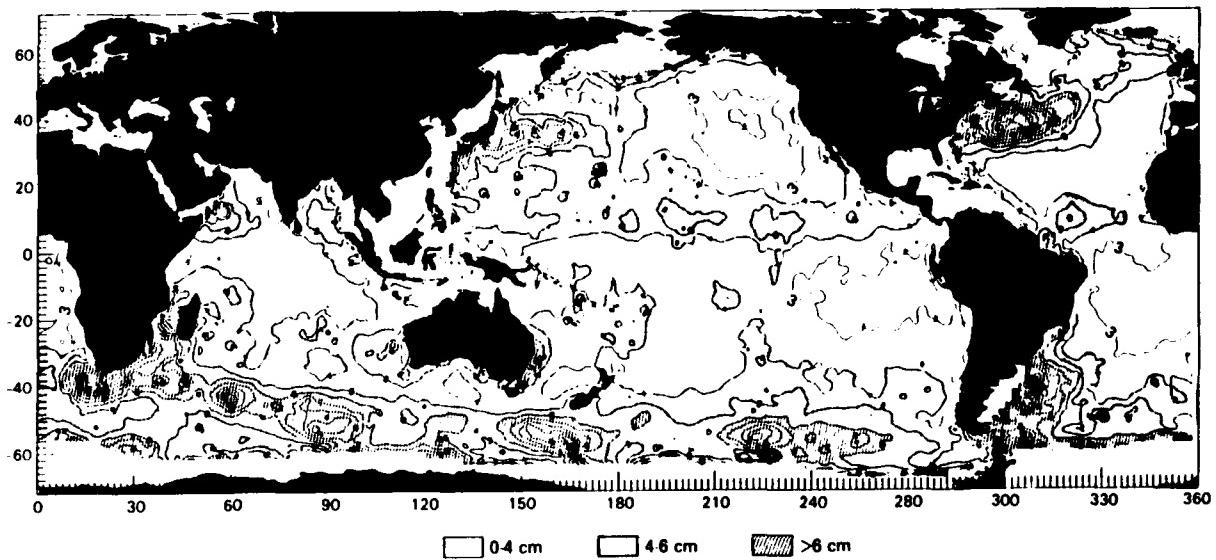


Fig. 7.33. Global mesoscale sea height variability measured by the SEASAT altimeter, 15 September to 10 October 1978. This map was constructed from 110,000 globally distributed variability values determined every 7 km along the satellite tracks. A gridding routine was then used to obtain smoothed values at regular  $2^{\circ}$  intervals of latitude and longitude. These were contoured to reveal large-scale variability patterns due to current systems. The North Atlantic and North Pacific are dominated by the energetic Gulf Stream and Kuroshio systems that extend 4000 km. In the southern hemisphere the Agulhas Current below Africa and the Falkland/Brazil Current confluence off South America are clearly apparent. High variability due to the Antarctic Circumpolar Current extends in a nearly continuous band around the polar oceans, with isolated maxima coinciding with major topographic ridges and plateaus. Owing to the predominance of values less than 4 cm in mid-ocean, the north equatorial current systems in both the Atlantic and Pacific can be seen as zonal bands of higher variability. (Cheney et al., 1983)

## 7.6 THE BENGUELA CURRENT REGION, 15°S TO 35°S

The Benguela Current is a slow-moving, eastern boundary current in the South Atlantic Ocean adjacent to the west coast of Africa; it is the northward - directed portion of the counterclockwise current gyre at the surface in the South Atlantic. Similar to conditions associated with eastern boundary currents elsewhere in the world's oceans, the Benguela Current is relatively slow ( $\leq 25$  cm/sec, (Darbyshire, 1963)), shallow, broad, and associated with one of the most important coastal upwelling regions in the world.

Within this region there is active upwelling which undergoes a seasonal cycle; strong upwelling is observed when strong southeasterly winds blow during (southern hemisphere) summer months in the southern portions of this region. Active upwelling is most pronounced in early summer; it may be present but not actively maintained later in the summer (Darbyshire, 1966a).

During (southern hemisphere) winter, the area dominated by the southeast trade winds shifts northward, and the areas of active upwelling along the coast also shift northward; in the winter season a westerly wind regime occurs over the most southern part of this region, and active upwelling ceases there at this time.

There are at least 3 watermasses involved in the upwelling areas. The surface water overlies the South Atlantic Central water in this region, which in turn overlies the Antarctic Intermediate (AAI) water. Remnants of surface water of the southwestern Indian Ocean (Agulhas Current water) may also appear in the region, especially in the southern latitudes in (southern hemisphere) summer (Darbyshire, 1966a).

Characteristic values associated with these water masses are:

- Surface: T values  $> 15^{\circ}\text{C}$ ; S values  $> 35.35^{\circ}/\text{oo}$ .
- Central (mixing between surface & AAI):  $15^{\circ}\text{C} \geq T \geq 6^{\circ}\text{C}$ ;  $35.35^{\circ}/\text{oo} \geq S \geq 34.5^{\circ}/\text{oo}$ .
- AAI (core at 600-800 m depth):  $5^{\circ}\text{C} \geq T \geq 4^{\circ}\text{C}$ ;  $S \sim 34.33^{\circ}/\text{oo}$  (Jones, 1971).
- Agulhas Current Water:  $27^{\circ}\text{C} \geq T \geq 16^{\circ}\text{C}$ ;  $35.4^{\circ}/\text{oo} \geq S \geq 35.2^{\circ}/\text{oo}$  (Darbyshire, 1966a).
- Subtropical water:  $24^{\circ}\text{C} \geq T \geq 16^{\circ}\text{C}$ ;  $35.7^{\circ}/\text{oo} \geq S \geq 35.5^{\circ}/\text{oo}$  (Darbyshire, 1966a).

Seasonal variation in upwelling in the Benguela Current region is described by Darbyshire (1966a). Uniform surface temperature is found in the stable winter (July) conditions, with Central Water not far below the surface. In September or October (spring) upwelling of subsurface water commences, bringing Central Water to the surface over a wide area. This produces a (horizontal) surface temperature gradient which increases during the following (summer) months. Later in the summer the upwelled water remains at the surface and changes considerably due to the surface influences of direct radiation, precipitation and river

runoff; some time is required to bring about effects from these influences, however. Early summer appears to be the time of active upwelling, and this diminishes and becomes static by late summer. When winter arrives, uniform conditions occur, with extremes in surface salinities and temperatures having disappeared.

The upwelling seems to result from action of wind at the sea surface along the African coastline; these winds along Africa's South Atlantic coastal area are controlled largely by the atmosphere's subtropical high pressure system over the South Atlantic Ocean; the continental high pressure system over Africa also has some influence along the coast.

In summer (December) the Trade Winds blow from the southeast about 80% of the time. In winter (July) the area south of 30°S is influenced by the Westerlies wind belt which has moved northward and brings low pressure systems and associated winter rainfall into the southern portion of this coastal region. When southeast trade winds are present (over the entire region in summer and in the northern portion in winter) there are diurnal variations present in the winds as well. Winds blow onshore (from south or southwest) in the afternoon and evening, and offshore at night and in the morning. The southeast winds are strongest in the Cape area in early summer. These trade winds produce upwelling which brings colder, fresher (Central) water to the surface. Darbyshire (1966b) states that the presence of water having the character of the Agulhas Current occurs in the Benguela Current region and is associated with upwelling to the north of 30°S. Agulhas water is withdrawn partially or completely from the Benguela Current region during winter and this withdrawal is associated with lack of upwelling in the winter in this area.

Subtropical Water is carried toward the coast during cessation of upwelling, and is partly responsible for reducing the (horizontal) surface temperature gradient.

In a detailed study of upwelling in the southernmost significant upwelling site in the Benguela Current, Andrews and Hutchings (1980) concentrate attention on the southern one of two upwelling locations, off the Cape (of Good Hope) peninsula (at ~34°30'S); the other is off Cape Columbine (at ~33°S). Fig. 7.34 from Andrews and Hutchings (1980) indicates the surface temperatures on 14 January 1973 and shows that the upwelling there occurs along the most prominent coastline feature in the region.

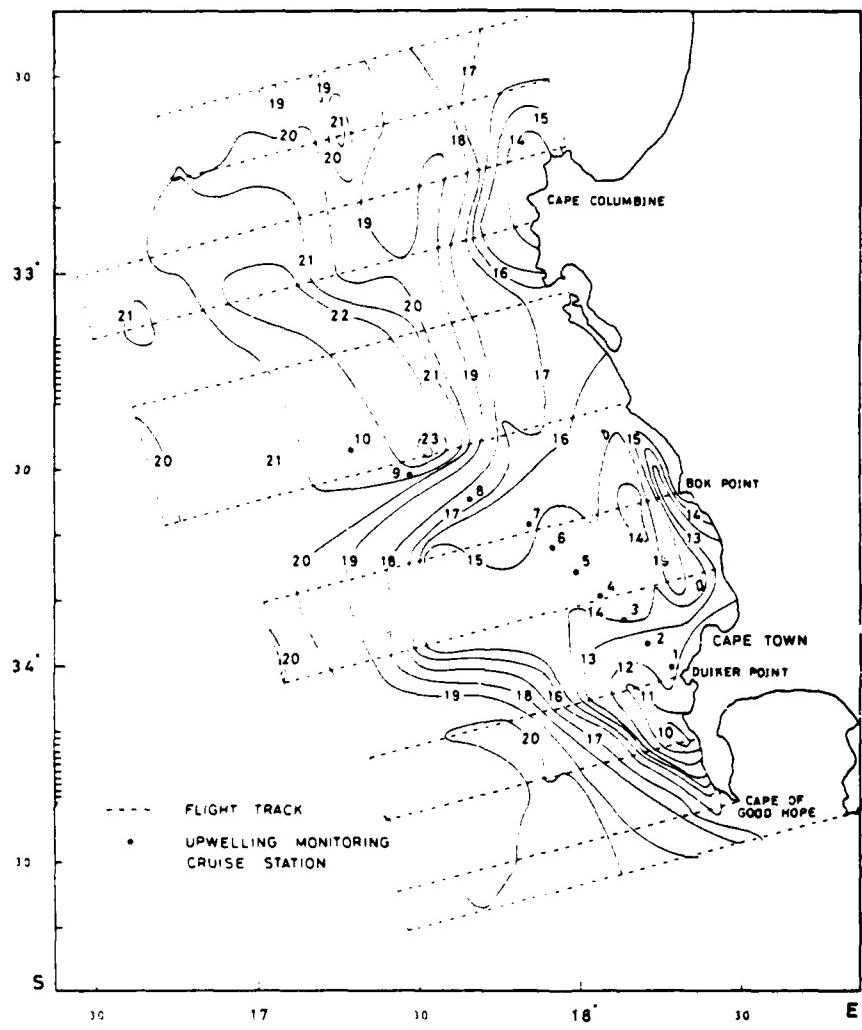


Fig. 7.34. Surface temperature ( $^{\circ}\text{C}$ ) distribution (from ART data) of the southern Benguela Current during upwelling on 14 January 1973 with positions of Upwelling-Monitoring Cruise stations marked. (Andrews and Hutchings, 1980)

Synoptic weather charts for typical summer (Fig. 7.35) conditions show pronounced SE winds along the Benguela Current region ( $35\text{--}25^{\circ}\text{S}$ ). In spring, summer and autumn, the subtropical high pressure cell, a permanent feature in the South Atlantic Ocean, periodically ridges eastward south of the African continent, causing southeasterly winds along the coast to predominate (50-70% of the time). Peak frequencies occur in spring and late summer with a lull in midsummer of strong winds ( $>8$  m/sec). Southeasterly "blows", (winds of 18-25 m/sec) last 4 to 5 days before a depression passes, weakening the pressure ridge; then winds diminish and reverse. Once or twice a year exceptional gales will last for 8-12 days. Typical winter conditions (Fig. 7.36) show onshore flow from the NW-W in this area. Upwelling would be expected here in summer, and no upwelling in winter.

In winter, low pressure cyclones move west to east across southern Cape Province with NW winds dominating (although not as persistent as SE winds in summer.) SE winds in winter occur, but less than 10% of the time.

Andrews and Hutchings (1980) indicate that a cold plume (front) goes NW from Cape Peninsula and is a semipermanent feature in summer months, and disappears during the winter months.

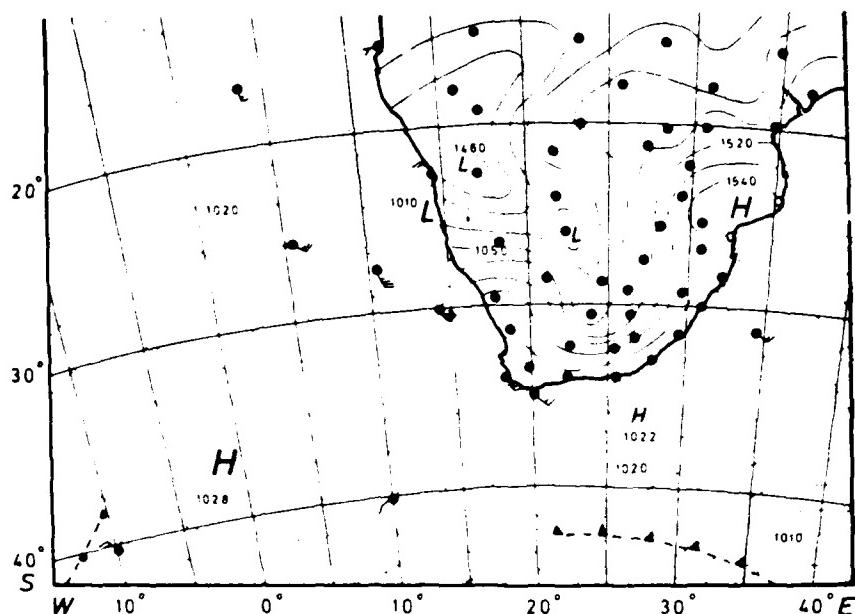


Fig. 7.35. Synoptic weather map of southern Africa showing typical summer atmospheric pressure system. (Andrews and Hutchings, 1980)

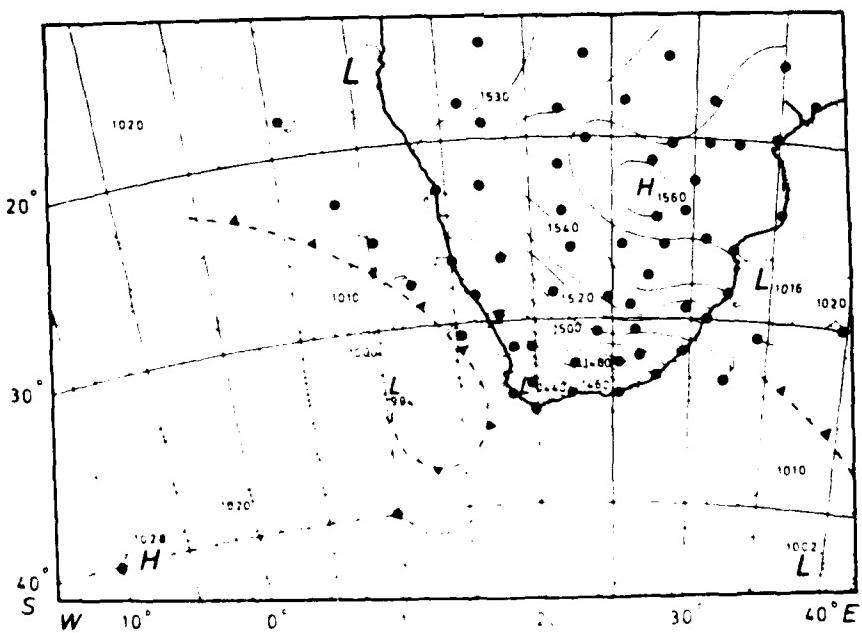


Fig. 7.36. Synoptic weather map of Northern Africa showing typical winter atmospheric pressure system (Andrews and Hutchings, 1980).

Four water types are described in Andrews and Hutchings (1980):

1. Ocean Water -- lying outside the oceanic front and above the thermocline.
2. Upwelling Water -- water upwelling into the photic zone.
3. Mixed Water -- formed by mixing between oceanic and upwelled water.
4. Shelf Water -- lying under upwelled water.

Table 7.5 gives temperature, salinity and oxygen characteristics during five different upwelling seasons off the Cape (of Good Hope) Peninsula. Fig. 7.37 relates these water types in a vertical section off the coastline during upwelling.

Estimates of the upwelling velocities in this region were made by three methods. Upwelling was estimated to be 21 m/day; 22 m/day; and 32 m/day maximum.

TABLE 7.5

Characteristics of Three Water Types off the Cape \* (Andrews and Hutchings, 1980)

Property	Season	Oceanic Water			Upwelling Water			Shelf Water		
		Mean	S.D.	n	Mean	S.D.	n	Mean	S.D.	n
Temperature (°C)	1968-69	—	—	—	9.20±0.52	257	7.59±0.34	13		
	1969-70	18.73±0.45	214		8.97±0.56	526	7.57±0.37	182		
	1970-71	—	—	—	9.03±0.53	115	7.86±0.11	5		
	1971-72	20.05±1.17	21		9.05±0.55	164	7.25±0.83	21		
	1972-73	18.80±0.59	11		9.17±0.48	167	7.20±0.61	11		
Salinity (per mille)	1968-69	—	—	—	34.69±0.06	257	34.57±0.07	13		
	1969-70	35.42±0.07	214		34.69±0.09	503	34.56±0.07	170		
	1970-71	—	—	—	34.68±0.07	110	34.58±0.10	5		
	1971-72	35.37±0.11	21		34.69±0.08	162	34.51±0.11	17		
	1972-73	35.22±0.16	11		34.72±0.07	166	34.50±0.07	10		
Oxygen (ml l⁻¹)	1968-69	—	—	—	4.65±0.39	146	4.57±0.30	10		
	1969-70	5.54±0.34	211		4.53±0.37	522	4.56±0.22	177		
	1970-71	—	—	—	4.19±0.50	111	3.89±0.14	4		
	1971-72	5.36±0.18	21		4.19±0.57	160	4.36±0.48	19		
	1972-73	6.51±0.75	11		4.35±0.76	166	4.73±0.20	8		

\*Data for 1968-69 season from November 1968 Upwelling Cruise (ANDREWS and CRAM, 1969), for 1969-70 from December 1969 Upwelling Cruise; for 1970-71 from January 1971 Upwelling-Monitoring Cruise; for 1971-72 from Upwelling-Monitoring Cruises in November and December 1971 and January and February 1972, and for 1972-73 from Upwelling-Monitoring Cruises in November and December 1972 and January and February 1973.

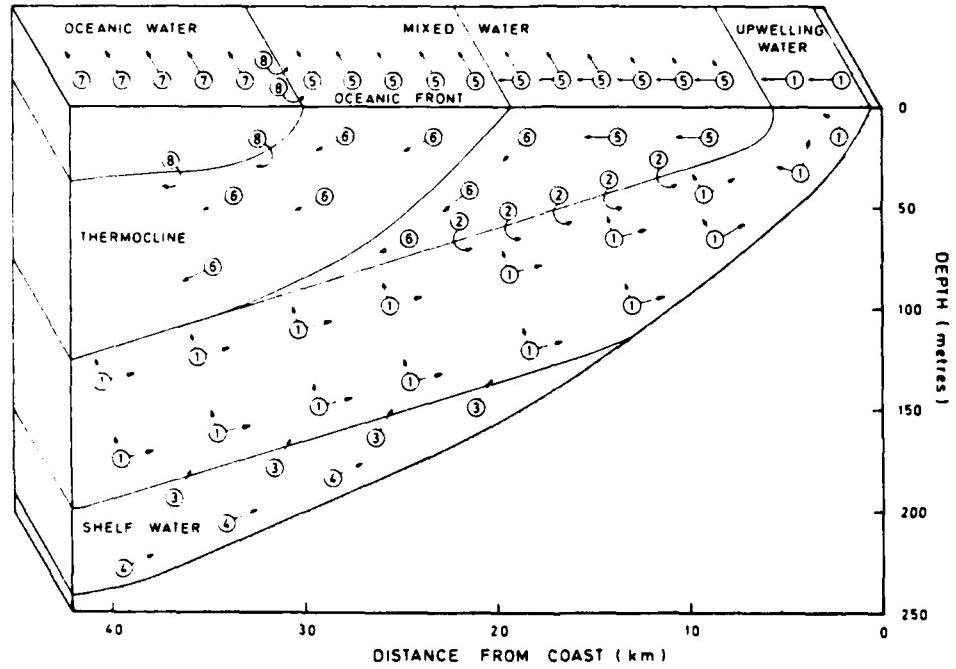


Fig. 7.37. A diagram of the relation of the water types found off the Cape Peninsula during upwelling. (Andrews and Hutchings, 1980)

More detailed studies of the southern Benguela Current region made by Jones (1971) and Bang (1971) indicate that the region exhibits considerable complexity, even showing the surface divergence regions associated with upwelling to be separated over wider shelf regions into an area of nearshore upwelling and a second area at the continental shelf edge (Fig. 7.38). Between these upwelling regions (Bang, 1971) is a region of convergence and downwelling. An oceanic front is present at the surface over the shelf edge separating warmer water further offshore from that upwelled near the shelf edge. A countercurrent (directed southward) along the immediate coastline occurs during active inshore upwelling. A jet current flows northward above and just offshore from the edge of the shelf, beneath and within the thermocline and surface front.

It appears that the inshore zone upwelling area (region a in Fig. 7.38, from Bang (1971)) is a result of direct, short-term windstress at the sea surface, producing "spasmodic and discontinuous" upwelling. The offshore upwelling area (region d in Fig. 7.38) is a flow northward warmer than the "true Benguela system" of region a, inshore. It is suggested by Bang (1971, p. 222) that in region a, *inshore*, oceanic processes are dominated by short-term atmospheric interactions; while in region d, at and beyond the shelf edge, the driving force lies within the ocean itself ("the climatic flywheel of southeast Atlantic deep sea circulations"). This author (Bang, 1971) suggests the two regions of upwelling may operate in unison, and then the discontinuities along the shelf may tend to disappear. At other times, the two upwelling regions *may operate in opposition*, when strong current shears, internal disturbances and eddy formations occur associated with surface divergence and vertical motion in the shelf waters.

Bang also visualized a *wave-like deformation* upstream from a "pivot" along the shelf in describing time changes that occur in the locations of the surface front which separates warmer water offshore from the colder upwelled nearshore along the southwest African coast (Fig. 7.39 from Bang (1971)).

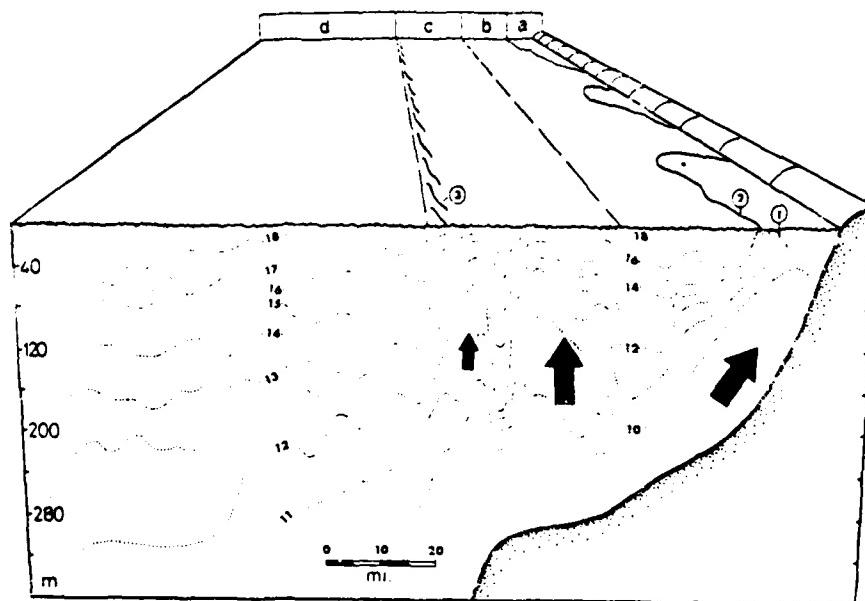


Fig. 7.38. Idealization of main structural features of the Benguela region between  $29^{\circ}$  and  $32^{\circ}$ S. (Bang, 1971)

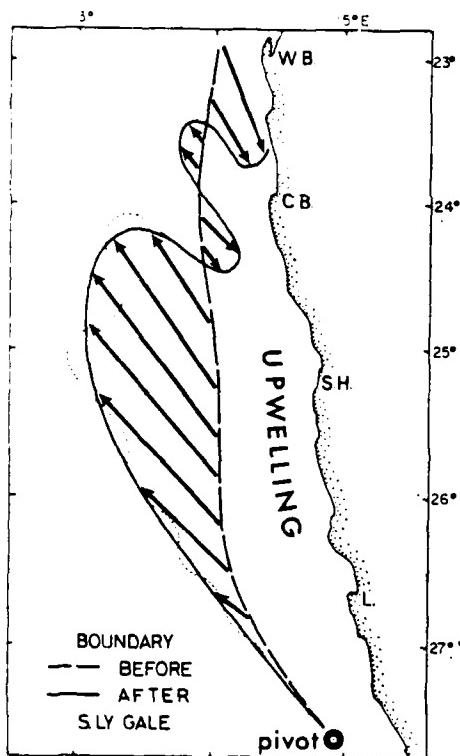


Fig. 7.39. Idealization of frontal behaviour in the development of a 'centre of upwelling'. (Bang, 1971)

## 7.7 EQUATORIAL ATLANTIC REGION (in the area nearshore to Africa from 5°N to 15°S)

The region is influenced by the Guinea Current (see Fig. 7.40 from (Gross, 1982)) in the northernmost extremity as it flows from west to east, north of the equator; this makes up the equatorial countercurrent in the Atlantic Ocean. Its position changes although it always remains north of the equator (Plutchak, 1966). In northern hemisphere winter, it moves southward between 7°N and 3°N at 20°W, and extends westward only to 25°W. In northern summer, it broadens and occupies the region from 15°N to 3°N, extending west to 40°W. The water carried by the Guinea Current has higher salinity (34.5 to 37.0‰) relative to the fresher water of the Gulf of Guinea that originates from the Niger and Congo rivers emptying into the general area (Tchernia, 1980b). The current carries warm water (25°C-28°C) with lowest temperatures in September (Tchernia, 1980c). It is a shallow current, with speeds of 13 to 22 n mi/day extending to only 180-200 meters below the surface, and quite variable in nature, probably associated with the wind variability. There is also an undercurrent, just below and opposite in direction to the Guinea Current, suggested by some researchers (Plutchak, 1966).

The South Equatorial Current occupies the region along the Atlantic coastline of central Africa from 3°N to 15°S. The flow is directed toward the northwest along this coastal region of Africa. Temperatures here are warm, 20°C to 27°C for annual mean values, with the temperatures increasing from south to north along the coast, and the maximum occurring at the northern extremity of this region.

The width of the continental shelf (200 meters and less below sea level) is generally narrow along this coastal region, widening slightly in the Niger and Congo delta regions. The shelf is narrowest along Angola, in the vicinity of 15°S.

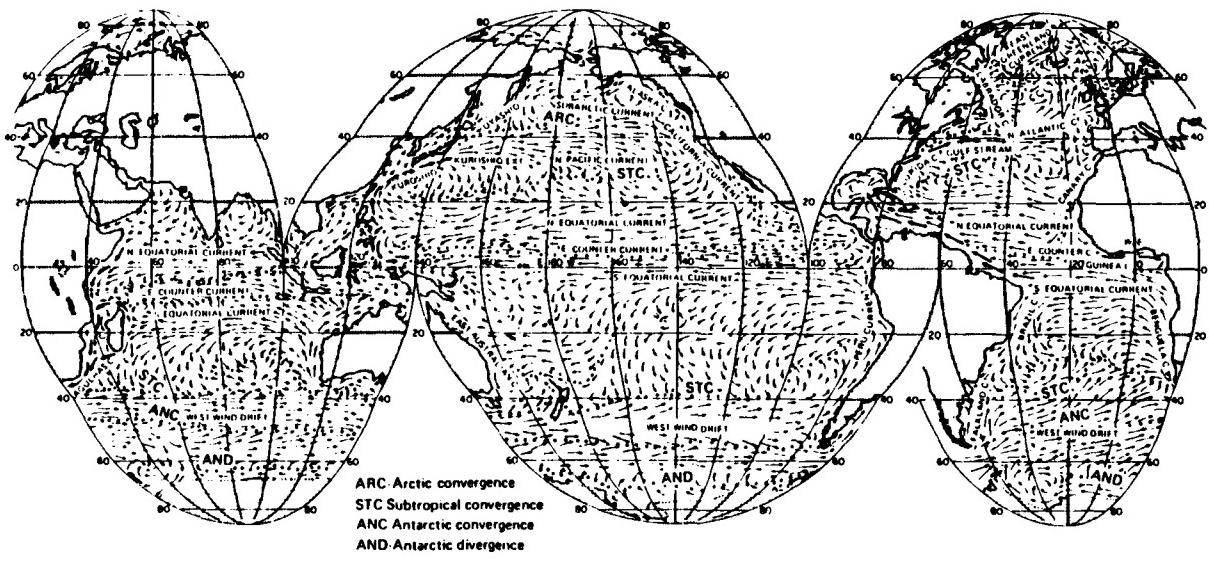


Fig. 7.40. Ocean surface currents in February-March. The thick arrows indicate especially strong currents. (Gross, 1982)

## Section 8

### REFERENCES

- American Meteorological Society, 1959: *Glossary of Meteorology* (R. E. Huschke, ed.), Boston, Massachusetts, 638 pp.
- Andrews, W. R. H. and L. Hutchings, 1981: Upwelling in the Southern Benguela Current. *Progress in Oceanography*, 9, 1-81.
- Anyamba, Ebby K. and Kiangi, P.M.R., 1983: The Tropospheric Mean Wind Flow Patterns over East Africa during the Northern Summer. *Preprints 1st International Conf. on Southern Hemisphere Meteorology*, July 31 - August 6, 1983, Sao Jose dos Campos, Brazil. American Meteorological Society, Boston, Massachusetts, 371-376.
- Bang, N. D., 1971: The southern Benguela Current in February, 1966: Part II. Bathymetry and air-sea interactions. *Deep-Sea Research*, 18, 209-224.
- Burpee, R. W., 1972: The Origin and Structure of Easterly Waves in the Lower Troposphere of North Africa. *J. Atmos. Sci.*, 29, 77-90.
- Carleton, A. M., 1979: A Synoptic Climatology of Satellite-Observed Extratropical Cyclone Activity for the Southern Hemisphere. *Arch. Met. Geoph. Biokl.*, Ser. B, 27, 265-279.
- Carlson, T. N., 1969: Some Remarks on African Disturbances and Their Progress Over the Tropical Atlantic. *Mon. Wea. Rev.*, 97, 716-726.
- , and F. H. Ludlam, 1965: Research On Characteristics and Effects Of Severe Storms. Annual Summary Rept. No. 1, Grant AF-EOAR-64-60, Imperial College London.
- , and J. M. Prospero, 1971: The Large-Scale Movement Of Saharan Air Outbreaks Over the Northern Equatorial Atlantic. *J. Appl. Meteor.*, 11, 283-297.
- Cheney, R. E., J. G. Marsh and B. D. Beckley, 1983: Global Mesoscale Variability from Collinear Tracks of SEASAT altimeter data. *Journal of Geophysical Research*, 88, 4343-4354.
- Darbyshire, J., 1964: A hydrological investigation of the Agulhas Current area. *Deep-Sea Research*, 11, 781-815.
- Darbyshire, M., 1963: Computed Surface Currents off the Cape of Good Hope. *Deep-Sea Research*, 10, 623-632.

- , 1966a: The Surface Waters near the Coasts of Southern Africa. *Deep-Sea Research*, 13, 57-81.
- , 1966b: Benguela Current. *The Encyclopedia of Oceanography* (R. W. Fairbridge, ed.), Reinhold Publishing Co., New York, 123-129.
- Davies, J. L., 1972: Geographical variation in coastal development. Oliver & Boyd, Edinburgh, 34-35.
- Dean, G. A., 1972: The Three Dimensional Temperature and Wind Structure over Africa in 1970. Dept. of Meteorology, Florida State University, Tallahassee, FL, 41 pp.
- Editions Jenne Afrique, 1973: *The Atlas of Africa* (Regine Van Chi-Bonnardel, ed.), Paris France, 335 pp.
- Fett, R. W., R. E. Nagle and W. F. Mitchell, 1973: The Low Level Structure of Weak Tropical Waves. Environmental Prediction Research Facility Tech. Paper No. 3-73, Monterey, CA, 26 pp.
- Findlater, J., 1969: A Major low-level air current near the Indian Ocean during the northern summer. *Quart. J. Roy. Meteor. Soc.*, 95, 362-380.
- , 1971: Mean monthly air flow at low levels over the western Indian Ocean. *Geophys. Memo. No. 115*, Her Majesty's Stationery Office, London, 53 pp.
- Frank, N. L., 1969: The "inverted-V" cloud pattern - An Easterly Wave? *Mon. Wea. Rev.*, 97, 130-140.
- , 1970: Atlantic Tropical Systems of 1969. *Mon. Wea. Rev.*, 98, 307-314.
- Griffiths, J. F., 1972: Eastern Africa and Mozambique. *World Survey of Climatology* (J. F. Griffiths, ed.), Vol X, Elsevier Publishing Company, Amsterdam, The Netherlands, 313-347 and 389-408.
- and R. Ranaivoson, 1972: Madagascar. *World Survey of Climatology* (J. F. Griffiths, ed.), Vol X, Elsevier Publishing Company, Amsterdam, The Netherlands, 461-499.
- Gross, M. G., 1982: *Oceanography, A View of the Earth*, Third Edition, Prentice-Hall, New Jersey, Figs. 7-3 & 7-16, Table 7-1, 183-199.
- Grundlingh, M. L., 1978: Drift of a satellite-tracked buoy in the southern Agulhas Current and Agulhas Return Current. *Deep-Sea Research*, 25, 1209-1224.
- , 1979: Observation of a Large Meander in the Agulhas Current. *Journal of Geophysical Research*, 84, 3776-3778.

- , 1980: On the Volume Transport of the Agulhas Current. *Deep-Sea Research*, 27, 557-563.
- Harangozo, S. A. and M. S. J. Harrison, 1983: On the Use of Synoptic Data in Indicating the Presence of Cloud Bands over Southern Africa. Informal Technical Report, Climatology Research Group, University of Witwatersrand, Johannesburg, Republic of South Africa, 8 pp.
- Harris, T. F. W., 1972: Sources of the Agulhas Current in the spring of 1964. *Deep-Sea Research*, 19, 633-650.
- and D. van Foreest, 1978: The Agulhas Current in March 1969. *Deep-Sea Research*, 25, 549-561.
- Harrison, M. S. J., 1983: The Southern Oscillation, Zonal Equatorial Circulation Cells and South African Rainfall. *Preprints 1st International Conf. on Southern Hemisphere Meteorology*, July 31 - August 6, 1983. Sao Jose dos Campos, Brazil. American Meteorological Society, Boston, Massachusetts, 302-305.
- Hayward, L. G. and E. E. Steyn, 1967: *Aeronautical Climatological Summaries*. Descriptive Memoranda for Five South African Airports, WB 31. Weather Bureau, Dept. of Transport, Pretoria, South Africa, 73 pp.
- Hoflich, O., 1984: Climate of the South Atlantic Ocean. *Climates of the Oceans* (H. van Loon, ed.) Vol XV, Elsevier Publishing Company, Amsterdam, The Netherlands, 1-191.
- Hubert, W. E., A. N. Hull, D. R. Morford and R. E. Englebretson, 1983: *Forecasters Handbook for the Middle East/Arabian Sea*. Naval Environmental Prediction Research Facility Contractor Report 83-06, 3-40 through 3-44.
- Jones, P. G. W., 1971: The southern Benguela Current in February, 1966: Part I. Chemical Observations with particular reference to upwelling. *Deep-Sea Research*, 18, 193-208.
- Kenyon, K. E., 1971: Wave Refraction in Ocean Current. *Deep-Sea Research*, 18, 1023-1034.
- Kinuthia, J. H. and G. C. Asnani, 1983: A Newly Found Jet in North Kenya (Turkana Channel). *Preprints 1st International Conf. on Southern Hemisphere Meteorology*, July 31 - August 6, 1983, Sao Jose dos Campos, Brazil. American Meteorological Society, Boston, Massachusetts, 377 - 380.
- Krishnamurti, T. N., 1979: *Compendium of Meteorology*, Vol. II, Part 4 - *Tropical Meteorology*. WMO No. 364. Secretariat of the World Meteorological Organization, Geneva, Switzerland, 261-303.

- , Philip Ardanuy, Y. Ramanathan and Richard Pasch, 1981: On the Onset Vortex of the Summer Monsoon. *Mon. Wea. Rev.*, 109, 344-363.
- Lutjeharms, J. R. E., 1980a: Retroflection When the Current Turns. *Oceans*, July, p. 31.
- , 1980b: Drift of the VENOIL in the Agulhas Current. *Mariners Weather Log*, 24, 1-6.
- , 1981a: Spatial scales and intensities of circulation in the ocean areas adjacent to South Africa. *Deep-Sea Research*, 28A, 1289-1302.
- , 1981b: Satellite Studies of the South Atlantic Upwelling System. *Oceanography from Space* (J. R. F. Gower, ed.), Plenum Press, New York, 195-199.
- and D. J. Baker, Jr., 1980: A Statistical Analysis of the Mesoscale Dynamics of the Southern Ocean. *Deep-Sea Research* 27, 145-160.
- Mallory, J. K., 1974: Abnormal waves on the southeast coast of South Africa, *The International Hydrographic Review*, Vol. LI No. 2, 99-129.
- Meinardus, W., 1928: Deutsche Sudpolar-Expedition 1901-1903. *Meteorologie*, Band III, Berlin, Walter de Gruyter, 133-307.
- , 1929: Die Luftdruckverhaltnisse und ihre Wandlungen sudlich von 30° sndl. Breite. *Meteor. Z.*, 46, 41-49 and 86-96.
- Naval Environmental Prediction Research Facility, 1980a: Weather in the Indian Ocean to Latitude 30°S and Longitude 95°E Including the Red Sea and Persian Gulf, Vol II, Local Information Part 8, The South Indian Ocean to Latitude 30°S. Reprint of handbook originally issued by the Meteorological Office, Air Ministry, London, England during 1940-1944, 74 pp.
- , 1980b: Weather in the Indian Ocean to Latitude 30°S and Longitude 95°S Including the Red Sea and Persian Gulf, Vol II, Local information Part 9, Coast of East Africa from the Equator to Cape Delgado. Reprint of handbook originally issued by the Meteorological Office, Air Ministry, London, England during 1940-1944, 38 pp.
- Naval Weather Service, 1974: Summary of Synoptic and Meteorological Observations. East African and Selected Island Coastal Marine Areas, Vol. 4, National Climatic Center, Asheville, N. C., 553 pp.
- , 1978: Study of Worldwide Occurrence of Fog, Thunderstorms, Supercooled Low Clouds and Freezing Temperatures, NAVAIR 50-1C-60 CH-1. Published for Director, Naval Oceanography and Meteorology, 144 pp.

- Oceanroutes, Inc., 1978: Memorandum on "Freak Waves" (Unpublished Manuscript). Palo Alto, CA. 2 pp.
- Pearce, A., 1983: Adrift in the Agulhas Return Current. *Deep-Sea Research* 30, 343-347.
- and M. L. Grundlingh, 1982: Is there a seasonal variation in the Agulhas Current? *Journal of Marine Research* 40, 177-184.
- Plutchak, N. B., 1966: Guinea Current. *The Encyclopedia of Oceanography* (R. W. Fairbridge, ed.) Reinhold Publishing Co., New York, 311-312.
- Quayle, R. G. 1974a: Cape Rollers - Unusually High Swells off the South African Coast. *Mariners Weather Log* 18, 145-148.
- , 1974b: Important Notice, Freak Waves off South Africa. *Mariners Weather Log* 18, 297-298.
- Schulze, B. R., 1972: South Africa. *World Survey of Climatology* (J. F. Griffiths, ed.) Vol. X, Elsevier Publishing Company, Amsterdam, The Netherlands, pp. 501-555.
- Schumann, E. H., 1976a: High Waves in the Agulhas Current; Duncan, C. P., Additional Comment. *Mariners Weather Log* 20, 1-5.
- , 1976b: Changes in energy of surface gravity waves in the Agulhas Current. *Deep-Sea Research* 23, 509-518.
- , 1980: Giant Wave. Anomalous Seas of the Agulhas Current. *Oceans*, July, 27-30.
- , 1982: Inshore Circulation of the Agulhas Current off Natal. *Journal of Marine Research* 40, 43-55.
- Semmelhack, N., 1934: Die Staubfalle Im Nordwest-Afrikanischen Gebiet Des Atlantischen Ozeans. *Ann. Hydrol.* 62, 273.
- Smith, R., 1976: Giant Waves. *J. Fluid Mech.* Vol. 77, Part 3, 417-431.
- Streten, N. A., 1973: Some Characteristics of Satellite-Observed Bands of Persistent Cloudiness Over the Southern Hemisphere. *Mon. Wea. Rev.*, 101, 486-495.
- and W. R. Kellas, 1973: Aspects of Cloud Pattern Signatures of Depressions in Maturity and Decay. *J. Appl. Met.*, 12, 23-27.
- and A. J. Troup, 1973: A Synoptic Climatology of Satellite-Observed Cloud Vortices Over the Southern Hemisphere. *Quart. J. Roy. Meteor. Soc.*, 99, 56-72.

- Taljaard, J. J., 1972: *Synoptic Meteorology of the Southern Hemisphere*. *Meteorology of the Southern Hemisphere* (C. W. Newton, ed.), Meteorological Monographs 13, 139-213.
- , 1984: Unpublished Correspondence. Department of Transport, Weather Bureau, Pretoria, Republic of South Africa, 18 May 1984, 3 pp.
- and H. van Loon, 1962: Cyclogenesis, cyclones and anticyclones in the Southern Hemisphere during the winter and spring of 1957. *Notos*, 11, 3-20.
- , H. van Loon, H. L. Crutcher and R. L. Jenne, 1969: *Climate of the Upper Air: Southern Hemisphere. Vol I, Temperature, Dew Points and Heights at Selected Pressure Levels*. NAVAIR 50-1C-55, Chief of Naval Operations, Washington, D. C., 135 pp.
- Tchernia, P., 1980a: *Descriptive Regional Oceanography*, Pergamon Press, New York, Plates 10, 11, 13-19; Figs. 6.1, 6.4, 6.5, 6.8 and 6.9, pp. 178, 187 and 211.
- , 1980b: Distribution of Surface Isohalines. *Descriptive Regional Oceanography*, Pergamon Press, New York, Plate 9.
- , 1980c: Distribution of Surface Isotherms, Annual Mean. *Descriptive Regional Oceanography*, Pergamon Press, New York, Plate 8.
- Trewartha, Glen T., 1981: *The Earth's Problem Climates*, 2nd ed. The University of Wisconsin Press, 371 pp.
- Union of Soviet Socialist Republics Ministry of Defense, 1979: *World Ocean Atlas Vol. II Atlantic and Indian Oceans*, Pergamon Press, Oxford, England, 306 pp.
- United States Air Force Air Weather Service, 1980: Forecaster Memo AWS-FM-100-006. U. S. Air Force, 34 pp.
- United States Defense Mapping Agency, 1979: *Atlas of Pilot Charts Indian Ocean*, Pub. 109, First edition. Defense Mapping Agency, Hydrographic/Topographic Center, Washington, D. C. 12 pp.
- , 1981: *Atlas of Pilot Charts South Atlantic Ocean*, Pub. 105, First edition. Defense Mapping Agency, Hydrographic/Topographic Center, Washington, D. C. 12 pp.
- United States Naval Oceanographic Office, 1968: H. O. Chart 1262A, Revised 1968.
- United States Weather Bureau, 1952: *Normal Weather Maps for the Northern Hemisphere*. Technical paper N. 21, Washington, D. C. 74 pp.

- van Loon, H., 1956: Description of a blocking situation in the central South Atlantic Ocean (April 29 to May 11, 1956). *Notos*, 5, 117-119.
- , 1965: A climatological study of the atmospheric circulation in the Southern Hemisphere during the IGY, part I. *J. Appl. Meteor.*, 4, 479-491.
- , 1967: A climatological study of the atmospheric circulation in the Southern Hemisphere during the IGY, Part II. *J. Appl. Meteor.*, 6, 803-815.
- , (editor), 1984: *Climates of the Oceans*. World Survey of Climatology, Vol XV. Elsevier Publishing Company, Amsterdam, The Netherlands, 716 pp.
- World Meteorological Organization, 1964: High Level Forecasting for Turbine-Engined Aircraft Operations over Africa and the Middle East, Technical Note No. 64, WMO-No. 159, TP. 77. Secretariat of the World Meteorological Organization, Geneva, Switzerland, 201 pp.

**ROUTINE REPLY, ENDORSEMENT, TRANSMITTAL OR INFORMATION SHEET**

 OPNAV 5216/158 (Rev. 7-78)  
 SN 0107 LF 052 1691

 A WINDOW ENVELOPE MAY BE USED  
 Formerly NAVFEXOS 3789

 CLASSIFICATION (UNCLASSIFIED when  
 detached from enclosures, unless otherwise  
 indicated)

**UNCLASSIFIED**

FROM (Show telephone number in addition to address)

 Commanding Officer, Naval Environmental Prediction Research  
 Facility, Monterey, CA 93943-5006 AV 878-2837

DATE

4 December 1985

SUBJECT

FORWARDING OF NAVENVPREDRSCHFAC TECHNICAL PUBLICATION

SERIAL OR FILE NO.

5600 NEPRF/SBB:sb

Ser 350

REFERENCE

TO

ENCLOSURE

**Distribution**

[Encl (1), pp D-1--6]

VIA

ENDORSEMENT ON

 FORWARDED

 RETURNED

 FOLLOW UP, OR  
TRACER

 REQUEST

 SUBMIT

 CERTIFY

 MAIL

 FILE

## GENERAL ADMINISTRATION

FOR APPROPRIATE ACTION

UNDER YOUR COGNIZANCE

**XX INFORMATION & retention**

APPROVAL RECOMMENDED

YES

NO

APPROVED

DISAPPROVED

COMMENT AND OR CONCURRENCE

CONCUR

DATED RETURN BY

SIGN RECEIPT &amp; RETURN

REPLY TO THE ABOVE BY

REFERENCE NOT RECEIVED

SUBJECT DOCUMENT FORWARDED TO

SUBJECT DOCUMENT RETURNED FOR

 SUBJECT DOCUMENT HAS BEEN  
 REQUESTED AND WILL BE  
 FORWARDED WHEN RECEIVED

 COPY OF THIS CORRESPONDENCE  
 WITH YOUR REPLY

ENCLOSURE NOT RECEIVED

ENCLOSURE FORWARDED AS REQUESTED

 ENCLOSURE RETURNED FOR  
 CORRECTION AS INDICATED

CORRECTED ENCLOSURE AS REQUESTED

REMOVE FROM DISTRIBUTION LIST

REDUCE DISTRIBUTION AMOUNT TO

## CONTRACT ADMINISTRATION

 NAME & LOCATION OF SUPPLIER  
 OF SUBJECT ITEMS

SUBCONTRACT NO OF SUBJECT ITEM

 APPROPRIATION SYMBOL, SUBHEAD,  
 AND CHARGEABLE ACTIVITY

SHIPPING AT GOVERNMENT EXPENSE

YES

NO

 A CERTIFICATE, VICE BILL  
 OF LADING

 COPIES OF CHANGE ORDERS,  
 AMENDMENT OR MODIFICATION

CHANGE NOTICE TO SUPPLIER

 STATUS OF MATERIAL ON  
 PURCHASE DOCUMENT

## PERSONNEL

REPORTED TO THIS COMMAND

DETACHED FROM THIS COMMAND

OTHER

## REMARKS (Comment - if any)

Enclosure (1) describes the analysis and forecasting of atmospheric and oceanic conditions important to air and sea operations over and near the southern African continent. Climatological data are given for Southern Hemisphere tropical cyclones occurrences. Atmospheric and oceanic case studies are provided.

SIGNATURE &amp; TITLE

WAYNE S. SHIVER, By direction

 CLASSIFICATION (UNCLASSIFIED when  
 detached from enclosure, unless otherwise  
 indicated)

**UNCLASSIFIED**

COPY TO

DISTRIBUTION

COMMANDER IN CHIEF  
U.S. ATLANTIC FLEET  
ATTN: FLT METEOROLOGIST  
NORFOLK, VA 23511

COMMANDER IN CHIEF  
U.S. ATLANTIC FLEET  
ATTN: NSAP SCIENCE ADVISOR  
NORFOLK, VA 23511

COMMANDER IN CHIEF  
U.S. PACIFIC FLEET  
CODE 02M  
PEARL HARBOR, HI 96860-7000

COMMANDER IN CHIEF  
U.S. NAVAL FORCES, EUROPE  
ATTN: METEOROLOGICAL OFFICER  
FPO NEW YORK 09510

CINCUSNAVEUR  
ATTN: NSAP SCIENCE ADVISOR  
BOX 100  
FPO NEW YORK 09501

COMMANDER SECOND FLEET  
ATTN: METEOROLOGICAL OFFICER  
FPO NEW YORK 09501-6000

COMSECONDFLT  
ATTN: NSAP SCIENCE ADVISOR  
FPO NEW YORK 09501-6000

COMTHIRDFLT  
ATTN: FLT METEOROLOGIST  
PEARL HARBOR, HI 96860

COMTHIRDFLT  
ATTN: NSAP SCIENCE ADVISOR  
PEARL HARBOR, HI 96860

COMSIXTHFLT  
ATTN: FLT METEOROLOGIST  
FPO NEW YORK 09501-6002

COMSIXTHFLT/COMFAIRMED  
ATTN: NSAP SCIENCE ADVISOR  
FPO NEW YORK 09501-6002

COMMANDER  
U.S. NAVAL FORCES, AZORES  
APO NEW YORK 09406

COMMANDER  
U.S. NAVAL FORCES, JAPAN  
FPO SEATTLE 98762

COMMANDER  
U.S. NAVAL FORCES, MARIANAS  
FPO SAN FRANCISCO 96630

COMMANDER  
U.S. NAVAL FORCES, PHILIPPINES  
BOX 30/N3  
FPO SAN FRANCISCO 96651

COMMANDER  
U.S. NAVAL FORCES, KOREA  
APO SAN FRANCISCO 96301

COMMANDER  
MIDDLE EAST FORCE  
FPO NEW YORK 09501-6008

COMMANDER NAVAL AIR FORCE  
U.S. ATLANTIC FLEET  
NORFOLK, VA 23511-5188

COMMANDER NAVAL AIR FORCE  
U.S. ATLANTIC FLEET  
ATTN: NSAP SCIENCE ADVISOR  
NORFOLK, VA 23511-5188

COMNAVPAIRPAC  
ATTN: NSAP SCIENCE ADVISOR  
NAS, NORTH ISLAND  
SAN DIEGO, CA 92135

COMMANDER  
NAVAL SURFACE FORCE  
U.S. ATLANTIC FLEET  
NORFOLK, VA 23511

COMNAVSURFLANT  
ATTN: NSAP SCIENCE ADVISOR  
NORFOLK, VA 23511

COMNAVSURFPAC  
NAVAL AMPHIB. BASE, CORONADO  
SAN DIEGO, CA 92155

COMNAVSURFPAC  
(005/N6N)  
ATTN: NSAP SCIENCE ADVISOR  
SAN DIEGO, CA 92155

COMMANDER  
MINE WARFARE COMMAND  
ATTN: NSAP SCIENCE ADVISOR  
CODE 007  
CHARLESTON, SC 29408

COMSUBFORLANT  
ATTN: NSAP SCI. ADV. (013)  
NORFOLK, VA 23511

SUBMARINE FORCE  
U.S. PACIFIC FLEET (009)  
PEARL HARBOR, HI 96860

COMMANDER  
AMPHIBIOUS GROUP 2  
ATTN: METEOROLOGICAL OFFICER  
FPO NEW YORK 09501

COMMANDER  
AMPHIBIOUS GROUP 1  
ATTN: METEOROLOGICAL OFFICER  
FPO SAN FRANCISCO 96601

COMMANDER  
OPTEVFOR  
NAVAL BASE  
NORFOLK, VA 23511

COMMANDER  
OPTEVFOR  
ATTN: NSAP SCIENCE ADVISOR  
NORFOLK, VA 23511

DEPUTY COMMANDER  
OPTEVFOR, PACIFIC  
NAS, NORTH ISLAND  
SAN DIEGO, CA 92135

COMMANDING OFFICER  
OCEANOGRAPHIC UNIT FIVE  
USNS HARKNESS (T-AGS 32)  
FPO NEW YORK 09573-7105

COMMANDER  
U.S. NAVAL SUPPORT FORCE,  
ANTARCTICA  
FPO SAN FRANCISCO 96601-6010

COMMANDER  
SURFACE WARFARE DEV. GROUP  
NAVAMPHTB BASE, LITTLE CREEK  
NORFOLK, VA 23521

COMMANDER  
NAVAL SURFACE GROUP  
MEDITERRANEAN, BOX 35  
FPO NEW YORK 09521

COMMANDING OFFICER  
USS AMERICA (CV-66)  
ATTN: MET. OFFICER, OA DIV.  
FPO NEW YORK 09531-2790

COMMANDING OFFICER  
USS CORAL SEA (CV-43)  
ATTN: MET. OFFICER, OA DIV.  
FPO NEW YORK 09550-2720

COMMANDING OFFICER  
USS D. D. EISENHOWER (CVN-69)  
ATTN: MET. OFFICER, OA DIV.  
FPO NEW YORK 09532-2830

COMMANDING OFFICER  
USS FORRESTAL (CV-59)  
ATTN: MET. OFFICER, OA DIV.  
FPO MIAMI 34080-2730

COMMANDING OFFICER  
USS INDEPENDENCE (CV-62)  
ATTN: MET. OFFICER, OA DIV.  
FPO NEW YORK 09537-2760

COMMANDING OFFICER  
USS J. F. KENNEDY (CV-67)  
ATTN: MET. OFFICER, OA DIV.  
FPO NEW YORK 09538-2800

COMMANDING OFFICER  
USS NIMITZ (CVN-68)  
ATTN: MET. OFFICER, OA DIV.  
FPO NEW YORK 09542-2820

COMMANDING OFFICER  
USS SARATOGA (CV-60)  
ATTN: MET. OFFICER, OA DIV  
FPO MIAMI 34078-2740

COMMANDING OFFICER  
USS CONSTELLATION (CV-64)  
ATTN: MET. OFFICER, OA DIV  
FPO SAN FRANCISCO 96635-2780

COMMANDING OFFICER  
USS ENTERPRISE (CVN-65)  
ATTN: MET. OFFICER, OA DIV.  
FPO SAN FRANCISCO 96636-2810

COMMANDING OFFICER  
USS KITTY HAWK (CV-63)  
ATTN: MET. OFFICER, OA DIV.  
FPO SAN FRANCISCO 96634-2770

COMMANDING OFFICER  
USS MIDWAY (CV-41)  
ATTN: MET. OFFICER, OA DIV.  
FPO SAN FRANCISCO 96631-2710

COMMANDING OFFICER  
USS RANGER (CV-61)  
ATTN: MET. OFFICER, OA DIV.  
FPO SAN FRANCISCO 96633-2750

COMMANDING OFFICER  
USS CARL VINSON (CVN-70)  
ATTN: MET. OFFICER, OA DIV.  
FPO SAN FRANCISCO 96629-2840

COMMANDING OFFICER  
USS IOWA (BB-61)  
ATTN: MET. OFFICER, OA DIV.  
FPO NEW YORK 09546-1100

COMMANDING OFFICER  
USS NEW JERSEY (BB-62)  
ATTN: MET. OFFICER, OA DIV.  
FPO SAN FRANCISCO 96688-1110

COMMANDING OFFICER  
USS MOUNT WHITNEY (LCC-20)  
ATTN: MET. OFFICER  
FPO NEW YORK 09517-3310

COMMANDING OFFICER  
USS GUADALCANAL (LPH-7)  
ATTN: MET. OFFICER  
FPO NEW YORK 09562-1635

COMMANDING OFFICER USS INCHON (LPH-12) ATTN: MET. OFFICER FPO NEW YORK 09529-1655	COMMANDING OFFICER USS PUGET SOUND (AD-38) ATTN: METEOROLOGICAL OFFICER FPO NEW YORK 09544-2520	COMFLTAIR, MEDITERRANEAN ATTN: NSAP SCIENCE ADVISOR CODE 03A FPO NEW YORK 09521
COMMANDING OFFICER AIR TEST & EVAL. SQDN 1-VX-1 NAVAL AIR STATION PATUXENT RIVER, MD 20670-5305	AVIATION SUP. DEPT. OFFICER NSFA, DET. CHRISTCHURCH ANTARCTIC DEV. SQDN 6-VXE-6 FPO SAN FRANCISCO 96690	OFFICER IN CHARGE DET. POINT MUGU ANTARCTIC DEV. SQDN 6-VXE-6 NAVAL AIR STATION POINT MUGU, CA 93042
COMMANDING GENERAL (G4) FLEET MARINE FORCE, ATLANTIC ATTN: NSAP SCIENCE ADVISOR NORFOLK, VA 23511	USCINCPAC BOX 28 CAMP SMITH, HI 96861	USCINCLANT NAVAL BASE NORFOLK, VA 23511
USCINCPAC BOX 13 STAFF CINCPAC J37 CAMP SMITH, HI 96861	COMMANDER IN CHIEF U.S. CENTRAL COMMAND ATTN: CCJ2-T MACDILL AFB, FL 33608	SACLANT ASW RESEARCH CENTER APO NEW YORK 09019
ASST. FOR ENV. SCIENCES ASST. SEC. OF THE NAVY (R&D) ROOM 5E731, THE PENTAGON WASHINGTON, DC 20350	CHIEF OF NAVAL RESEARCH (2) LIBRARY SERVICES, CODE 784 BALLSTON TOWER #1 800 QUINCY ST. ARLINGTON, VA 22217-5000	OFFICE OF NAVAL RESEARCH CODE 422AT ARLINGTON, VA 22217-5000
OFFICE OF NAVAL RESEARCH CODE 420 ARLINGTON, VA 22217-5000	OFFICE OF NAVAL RESEARCH CODE 422 CS ARLINGTON, VA 22217-5000	OFFICE OF NAVAL RESEARCH CODE 422 ARLINGTON, VA 22217-5000
OFFICE OF NAVAL RESEARCH CODE 422 PO ARLINGTON, VA 22217-5000	OFFICE OF NAVAL RESEARCH CODE 422 MM ARLINGTON, VA 22217-5000	CHIEF OF NAVAL OPERATIONS (OP-952) U.S. NAVAL OBSERVATORY WASHINGTON, DC 20390
CHIEF OF NAVAL OPERATIONS NAVY DEPT., OP-622C WASHINGTON, DC 20350	CHIEF OF NAVAL OPERATIONS NAVY DEPT. OP-986G WASHINGTON, DC 20350	CHIEF OF NAVAL OPERATIONS U.S. NAVAL OBSERVATORY DR. R. W. JAMES, OP-952D1 34TH & MASS. AVE., NW WASHINGTON, DC 20390
CHIEF OF NAVAL OPERATIONS U.S. NAVAL OBSERVATORY DR. RECHNITZER, OP-952F 34TH & MASS AVE. WASHINGTON, DC 20390	CHIEF OF NAVAL OPERATIONS OP-952D U.S. NAVAL OBSERVATORY WASHINGTON, DC 20390	CHIEF OF NAVAL OPERATIONS OP-953 NAVY DEPARTMENT WASHINGTON, DC 20350
COMMANDANT OF THE MARINE CORPS HQ, U.S. MARINE CORPS WASHINGTON, DC 20380	DET. 2, HQ, AWS THE PENTAGON WASHINGTON, DC 20330	OFFICER IN CHARGE NAVOCEANCOMDET AFGWC OFFUTT AFB, NE 68113

OFFICER IN CHARGE U.S. NAVOCEANCOMDET FPO SAN FRANCISCO 96685-2905	COMMANDING OFFICER NAVAL RESEARCH LAB ATTN: LIBRARY, CODE 2620 WASHINGTON, DC 20390	COMMANDING OFFICER OFFICE OF NAVAL RESEARCH 1030 E. GREEN ST. PASADENA, CA 91101
OFFICE OF NAVAL RESEARCH SCRIPPS INSTITUTION OF OCEANOGRAPHY LA JOLLA, CA 92037	COMMANDING OFFICER NAVAL OCEAN RSCH & DEV ACT NSTL, MS 39529-5004	COMMANDING OFFICER FLEET INTELLIGENCE CENTER (PACIFIC) PEARL HARBOR, HI 96860
COMMANDER NAVAL OCEANOGRAPHY COMMAND NSTL, MS 39529-5000	COMMANDING OFFICER NAVAL OCEANOGRAPHIC OFFICE BAY ST. LOUIS NSTL, MS 39522-5001	COMMANDING OFFICER FLENUMOCEANCEN MONTEREY, CA 93943-5005
COMMANDING OFFICER NAVWESTOCEANCEN BOX 113 PEARL HARBOR, HI 96860	COMMANDING OFFICER NAVEASTOCEANCEN MCADIE BLDG. (U-117), NAS NORFOLK, VA 23511-5399	COMMANDING OFFICER U.S. NAVOCEANCOMCEN BOX 12, COMNAVMARIANAS FPO SAN FRANCISCO 96630-2926
COMMANDING OFFICER U.S. NAVOCEANCOMCEN BOX 31 (ROTA) FPO NEW YORK 09540-3200	CHAIRMAN OCEANOGRAPHY DEPT. U.S. NAVAL ACADEMY ANNAPOLIS, MD 21402	DIRECTOR OF RESEARCH U.S. NAVAL ACADEMY ANNAPOULS, MD 21402
SUPERINTENDENT NAVPGSCOL MONTEREY, CA 93943-5000	NAVAL POSTGRADUATE SCHOOL METEOROLOGY DEPT. MONTEREY, CA 93943-5000	NAVAL POSTGRADUATE SCHOOL OCEANOGRAPHY DEPT. MONTEREY, CA 93943-5000
LIBRARY NAVAL POSTGRADUATE SCHOOL MONTEREY, CA 93943-5002	PRESIDENT NAVAL WAR COLLEGE GEOPHYS. OFFICER, NAVOPS DEPT. NEWPORT, RI 02841	COMMANDER (2) NAVAIRSYSCOM ATTN: LIBRARY (AIR-723D) WASHINGTON, DC 20361-0001
COMMANDER NAVAIRSYSCOM (AIR-330) WASHINGTON, DC 20361-0001	COMMANDER SPACE & NAVAL WARFARE SYSTEMS COMMAND ATTN: CODE 06G, NAVY DEPT. WASHINGTON, DC 20363	COMMANDER NAVSURFWEACEN, WHITE OAKS NAVY SCIENCE ASSIST. PROGRAM SILVER SPRING, MD 20910
COMMANDER PACMISTESTCEN GEOPHYSICS OFFICER PT. MUGU, CA 93042	COMMANDING GENERAL WEATHER SERVICE OFFICE MARINE CORPS AIR STATION CHERRY POINT, NC 28533	COMMANDER AWS/DN SCOTT AFB, IL 62225
USAFETAC/TS SCOTT AFB, IL 62225	SUPERINTENDENT ATTN: USAFA (DEG) USAF ACADEMY, CO 80840	3350TH TECH. TRNG GROUP TTGU/2/STOP 623 CHANUTE AFB, IL 61868

AFGWC/DAPL  
OFFUTT AFB, NE 68113

3 WW/DN  
OFFUTT AFB, NE 68113

AFGL/LY  
HANSOM AFB, MA 01731

OFFICER IN CHARGE  
SERVICE SCHOOL COMMAND  
DET. CHANUTE/STOP 62  
CHANUTE AFB, IL 61868

HQ 1ST WEATHER WING/DN  
HICKAM AFB, HI 96853

DET 4 HQ AWS/CC  
APO SAN FRANCISCO 96334

COMMANDER  
ARMY DEFENSE & READINESS COM  
ATTN: DRCLDC  
5001 EISENHOWER AVE.  
ALEXANDRIA, VA 22304

COMMANDING OFFICER  
U.S. ARMY RESEARCH OFFICE  
ATTN: GEOPHYSICS DIV.  
P.O. BOX 12211  
RESEARCH TRIANGLE PARK, NC  
27709

COMMANDER & DIRECTOR  
ATTN: DELAS-AS  
U.S. ARMY ATMOS. SCI. LAB  
WHITE SANDS MISSILE RANGE,  
NEW MEXICO 88002

COMMANDER/DIRECTOR  
US ARMY ATMOS. SCIENCE LAB.  
ATTN: DELAS-AT-0  
WHITE SANDS MISSILE RANGE, NM  
88002

DIRECTOR (12)  
DEFENSE TECH. INFORMATION  
CENTER, CAMERON STATION  
ALEXANDRIA, VA 22314

DIRECTOR, ENV. & LIFE SCI.  
OFFICE OF UNDERSECRETARY OF  
DEFENSE FOR RSCH & ENG E&LS  
RM. 3D129, THE PENTAGON  
WASHINGTON, DC 20505

CENTRAL INTELLIGENCE AGENCY  
ATTN: OCR STANDARD DIST.  
WASHINGTON, DC 20505

DIRECTOR, TECH. INFORMATION  
DEFENSE ADV. RSCH PROJECTS  
1400 WILSON BLVD.  
ARLINGTON, VA 22209

COMMANDANT  
DEFENSE LOGISTICS STUDIES  
INFORMATION EXCHANGE  
ARMY LOGISTICS MANAGEMENT  
CENTER  
FORT LEE, VA 23801

COMMANDING OFFICER  
USCGC GLACIER (WAGB-4)  
FPO SAN FRANCISCO 96601

NOAA-NESDIS LIAISON  
ATTN: CODE SC2  
NASA-JOHNSON SPACE CENTER  
HOUSTON, TX 77058

DIRECTOR  
NATIONAL METEORO. CENTER  
NWS, NOAA  
WB W32, RM 204  
WASHINGTON, DC 20233

DIRECTOR  
NATIONAL EARTH SAT. SERV/SEL  
FB-4, S321B  
SUITLAND, MD 20233

FEDERAL COORD. FOR METEORO.  
SERVS. & SUP. RSCH. (OFCM)  
11426 ROCKVILLE PIKE  
SUITE 300  
ROCKVILLE, MD 20852

UNIVERSITY OF HAWAII  
METEOROLOGY DEPT.  
2525 CORREA ROAD  
HONOLULU, HI 96822

MR. W. G. SCHRAMM/WWW  
WORLD METEOROLOGICAL  
ORGANIZATION  
CASE POSTALE #5, CH-1211  
GENEVA, SWITZERLAND

DIRECTOR, JTWC  
BOX 17  
FPO SAN FRANCISCO 96630

BUREAU OF METEOROLOGY  
BOX 1289K, GPO  
MELBOURNE, VIC, 3001  
AUSTRALIA

LIBRARY, AUSTRALIAN NUMERICAL  
METEOROLOGY RESEARCH CENTER  
P.O. BOX 5089A  
MELBOURNE, VICTORIA, 3001  
AUSTRALIA

DIRECTOR OF NAVAL  
OCEANO. & METEOROLOGY  
MINISTRY OF DEFENCE  
OLD WAR OFFICE BLDG.  
LONDON, S.W.1. ENGLAND

MINISTRY OF DEFENCE  
NAVY DEPARTMENT  
ADMIRALTY RESEARCH LAB  
TEDDINGTON, MIDDX  
ENGLAND

INSTITUTE FOR MARITIME TECH.  
P.O. BOX 181  
SIMONSTOWN, 7995  
REPUBLIC OF AFRICA

CHIEF ATMOS. SCIENCES DIV.  
WORLD METEORO. ORGANIZATION  
P.O. BOX 5  
GENEVA 20, SWITZERLAND

NAVAL POSTGRADUATE SCHOOL (6)  
ATTN: DR. R. J. RENARD  
DEPT. OF METEOROLOGY  
MONTEREY, CA 93943

NAVAL POSTGRADUATE SCHOOL (6)  
ATTN: FORREST R. WILLIAMS  
DEPT. OF METEOROLOGY  
MONTEREY, CA 93943

NAVAL POSTGRADUATE SCHOOL (2)  
ATTN: DR. G. H. JUNG  
DEPT. OF OCEANOGRAPHY  
MONTEREY, CA 93943

USS LEXINGTON (AVT-16)  
ATTN: LT R. D. TOMKINS, USN  
FPO MIAMI 34088

NATIONAL CENTER FOR  
ATMOSPHERIC RESEARCH  
ATTN: DR. HARRY VAN LOON  
BOULDER, CO 80307

UNIVERSITY OF VIRGINIA  
ATTN: DR. MICHAEL GARSTANG  
CHARLOTTESVILLE, VA 22903

NATIONAL CENTER FOR  
ATMOSPHERIC RESEARCH  
ATTN: DR. H. VAN DE BOOGAARD  
BOULDER, CO 80307



## SUNDAY, FEBRUARY 2

8:30 am **CHEESEBORO CANYON:** "Cheeseboro Canyon Hike" A 5 - 6 mile moderate to strenuous hike to learn about the pristine area. Wear sturdy shoes and bring water and lunch. Reservations required. Call (818) 888-3770. 4 hrs

10:00 am **FRANKLIN CANYON RANCH:** "Mountains for All Your Senses" See, hear, smell, taste and touch the natural wonders of Franklin Canyon in all her diverse beauty. Docent led hike. 2 hrs.

10:00 am **MALIBU SPRINGS:** "Tcu-mac" Learn about the Indians that made the Santa Monica Mountains their home. Reservations required (818) 888-3770 2½ hrs.

11:00 am **COLDWATER CANYON PARK:** "Park Tour" Tour of Coldwater Canyon Park - TreePeople headquarters. Come explore the trails, gardens, tree nursery, education center, and bee hives. 1 hr.

11:00 am -3:00 pm **LEO CARRILLO STATE BEACH:** "Whale Watch" A naturalist will be on site to answer questions and provide information on the Gray whale and other marine life. Binoculars will be available to borrow, and visitors can enter sightings into an observation log.

1:00 pm **ROCKY OAKS:** "Picnic Under the Oaks" Join a ranger in the amphitheater for an update on the Santa Monica Mountains National Recreation Area. Learn about new park areas, trails and programs. Bring a picnic lunch and beverage. 1 hr.

1:30 pm **TOPANGA STATE PARK:** "Nature Walk" Join a docent for an easy paced walk suitable for the whole family. 2 hrs.

1:30 pm **PETER STRAUSS RANCH (LAKE ENCHANTO):** "Nature Walk" Join a docent for an easy paced walk suitable for the whole family. 2 hrs.

## MONDAY, FEBRUARY 3

10:00 am **FRANKLIN CANYON RANCH:** "Babes in the Woods" This walk is for babies (3 years and under) and their parents 2 hrs. Reservations required. Contact (213) 858-3834

## TUESDAY, FEBRUARY 4

7:30 pm **COLDWATER CANYON PARK:** "Thriving in L.A." An entertaining and educational program about TreePeople's activities each month, highlighting an aspect of the Los Angeles environment. Orientation about TreePeople's history. 7:00 pm Refreshments 1½ hrs.

## WEDNESDAY, FEBRUARY 5

11:00 am **FRANKLIN CANYON:** "Babes in the Woods" This walk is for babies (3 years and under) and their parents 2 hrs. Reservations required. Contact (213) 858-3834

## SATURDAY, FEBRUARY 8

9:00 am **TOPANGA STATE PARK:** "Winter Stroll" Easy ranger-led hike through chaparral, oak woodlands, and riparian areas on the beautiful Musch Trail. 2½ hrs

9:30 am **RANCHO SIERRA VISTA/SATWIWA:** "Nature Jog" Jog along some of the old ranch roads to a scenic view of Sycamore Canyon. Stops along the way. For the beginner. 1 hr

10:00 am **FRANKLIN CANYON RANCH:** "Canyon Ecology" Take an easy paced walk along a canyon bottom and learn about the plant-animal-land relationships. 2 hrs.

11:00 am -3:00 pm **POINT DUME STATE RESERVE:** "Whale Watch" A naturalist will be on site to answer questions and provide information on the Gray whale and other marine life. Binoculars will be available to borrow, and visitors can enter sightings into an observation log

1:00 pm **STUNT HIGH TRAIL:** "Through the Woods and Along the Stream" Join a ranger for a morning walk through chaparral, oak woodland, and riparian area on an easy trail in the mountains. 2½ hrs.

## SUNDAY, MARCH 9

9:00 am **CASTRO CREST:** "Ranger's Choice" Join an interpreter on a hike focusing on the park's natural history. Bring snack and water. 3 hrs

10:00 am **MALIBU LAGOON STATE BEACH:** "Outdoor Sketching: Lagoon Life" Learn about fresh and salt water estuaries through sketch exercises. Ranger led. Bring a large pad, utensils, and seating. For reservations call (818) 888-3770. 2 - 3 hrs

10:00 am **FRANKLIN CANYON RANCH:** "Babes in the Woods" This walk is for babies (3 years and under) and their parents 2 hrs. Reservations required. (213) 858-3834

10:00 am **RANCHO SIERRA VISTA/SATWIWA:** "SLOW?" Discover the natural and cultural resources of the area. Hike. 2½ hrs

11:00 am **COLDWATER CANYON PARK:** "Park Tour" Tour of Coldwater Canyon Park - TreePeople headquarters. Come explore the trails, gardens, tree nursery, education center, and bee hives. 1 hr

11:00 am -3:00 pm **LEO CARRILLO STATE BEACH:** "Whale Watch" A naturalist will be on site to answer questions and provide information on the Gray whale and other marine life. Binoculars will be available to borrow, and visitors can enter sightings into an observation log

1:00 pm **FRANKLIN CANYON RANCH:** "Map and Compass Hike" Come and learn the basics of map and compass, while enjoying a walk through Franklin Canyon. Bring a compass if you have one. Docent led. 2 hrs

1:30 pm **PARAMOUNT RANCH:** "Nature Walk" Join a docent for an easy paced walk suitable for the whole family. 2 hrs.

1:30 pm **ROCKY OAKS:** "Nature Walk" Join a docent for an easy paced walk suitable for the whole family. 2 hrs

2:00 pm **PARAMOUNT RANCH:** "Western Town Tour" Learn about the history of Western Town and Paramount Pictures, film techniques and how movies affect our lives. Ranger led. Bring a camera! 1½ hrs

## MONDAY, MARCH 10

10:00 am **FRANKLIN CANYON RANCH:** "Babes in the Woods" This walk is for babies (3 years and under) and their parents 2 hrs. Reservations required. Contact (213) 858-3834

## WEDNESDAY, MARCH 12

8:00 pm **COLDWATER CANYON PARK:** "The Tropical Rainforest: Epicenter of Life on Earth" Arnold Newman naturalist and rainforest explorer, will talk about the richest ecosystem in the world. Slides, refreshments \$2.00 donation requested. 1½ hrs

## THURSDAY, MARCH 13

11:00 am **FRANKLIN CANYON RANCH:** "Babes in the Woods" This walk is for babies (3 years and under) and their parents 2 hrs. Reservations required. Contact (213) 858-3834

## SATURDAY, MARCH 15

8:30 am **CHEESEBORO CANYON:** "Cheeseboro Canyon Hike" A 5 - 6 mile moderate to strenuous hike to learn about the pristine area. Wear sturdy shoes and bring water and lunch. Reservations required. Call (818) 888-3770. 4 hrs

10:00 am **FRANKLIN CANYON RANCH:** "Chaparral Ecotour" Learn about the inter-relationship of plants and animals in the chaparral. Discover why fire is necessary and how plants and animals adapt to it. 2 hrs

10:00 am **MALIBU SPRINGS:** "Sharing Nature" A walk for younger children and their parents. Introduction to using your senses in the outdoors. Reservations required, please call (818) 888-3770. 1½ hrs

11:00 am -3:00 pm **POINT DUME STATE RESERVE:** "Whale Watch" A naturalist will be on site to answer questions and provide information on the Gray whale and other marine life. Binoculars will be available to borrow, and visitors can enter sightings into an observation log

1:00 pm **CHARMLEE COUNTY REGIONAL PARK:** "Nature Jog" Join a ranger as we jog to a scenic vista of the Malibu coastline and Channel Islands. Easy-paced, stops along the way. 1½ hrs

**END**

**FILMED**

**2-86**

**DTIC**